

IDŐJÁRÁS

QUARTERLY JOURNAL
OF THE HUNGARIAN METEOROLOGICAL SERVICE

CONTENTS

- Editorial I
Dr. György Major's scientific career II
I. Laszlo and R. T. Pinker: Shortwave radiation budget of the Earth: Absorption and cloud radiative effects 189
M. Ostrožlík and F. Smolen: Effect of the atmospheric boundary layer on the radiative fluxes 207
K. Behrens and K. Gericke: A comparison between measured and calculated values of atmospheric long-wave radiation 219
É. Borbás, P. Menzel and J. Li: A space-based GPS meteorological application 231
F. Miskolczi: High accuracy skin temperature retrieval from spectral data of multichannel IR imagers 243
I. A. Csizsár: On the use of satellite-derived climatological data sets to map global land surface temperature range 253
T. Várnai and A. Marshak: Observations of three-dimensional radiative effects that influence satellite retrievals of cloud properties 265
M. Diószeghy: Operative cloud classification using Meteosat images 279
I. Szunyogh, Gy. Gyarmati and D. Dévényi: Using observed data for testing the statistical consistency of initial ensemble perturbations 293

http://omsz.met.hu/irodalom/firat_ido/ido_hu.html

IDŐJÁRÁS

Quarterly Journal of the Hungarian Meteorological Service

Editor-in-Chief
TAMÁS PRÁGER

Executive Editor
MARGIT ANTAL

EDITORIAL BOARD

- | | |
|--|---|
| AMBRÓZY, P. (Budapest, Hungary) | MÉSZÁROS, E. (Veszprém, Hungary) |
| ANTAL, E. (Budapest, Hungary) | MIKA, J. (Budapest, Hungary) |
| BARTHOLY, J. (Budapest, Hungary) | MARACCHI, G. (Firenze, Italy) |
| BOZÓ, L. (Budapest, Hungary) | MERSICH, I. (Budapest, Hungary) |
| BRIMBLECOMBE, P. (Norwich, U.K.) | MÖLLER, D. (Berlin, Germany) |
| CZELNAI, R. (Budapest, Hungary) | NEUWIRTH, F. (Vienna, Austria) |
| DÉVÉNYI, D. (Budapest, Hungary) | PINTO, J. (R. Triangle Park, NC, U.S.A) |
| DUNKEL, Z. (Brussels, Belgium) | PROBÁLD, F. (Budapest, Hungary) |
| FISHER, B. (London, U.K.) | RENOUX, A. (Paris-Créteil, France) |
| GELEYN, J.-Fr. (Toulouse, France) | ROCHARD, G. (Lannion, France) |
| GERESDI, I. (Pécs, Hungary) | S. BURÁNSZKY, M. (Budapest, Hungary) |
| GÖTZ, G. (Budapest, Hungary) | SPÁNKUCH, D. (Potsdam, Germany) |
| HANTEL, M. (Vienna, Austria) | STAROSOLSZKY, Ö. (Budapest, Hungary) |
| HASZPRA, L. (Budapest, Hungary) | SZALAI, S. (Budapest, Hungary) |
| HORÁNYI, A. (Budapest, Hungary) | SZEPESI, D. (Budapest, Hungary) |
| HORVÁTH, Á. (Siófok, Hungary) | TAR, K. (Debrecen, Hungary) |
| IVÁNYI, Z. (Budapest, Hungary) | TÄNCZER, T. (Budapest, Hungary) |
| KONDRATYEV, K. Ya. (St. Petersburg,
Russia) | VALI, G. (Laramie, WY, U.S.A.) |
| MAJOR, G. (Budapest, Hungary) | VARGA-HASZONITS, Z. (Moson-
magyaróvár, Hungary) |

*Editorial Office: P.O. Box 39, H-1675 Budapest, Hungary or
Gilice tér 39, H-1181 Budapest, Hungary
E-mail: prager.t@met.hu or antal.e@met.hu
Fax: (36-1) 346-4809*

Subscription by

*mail: IDŐJÁRÁS, P.O. Box 39, H-1675 Budapest, Hungary
E-mail: prager.t@met.hu or antal.e@met.hu; Fax: (36-1) 346-4809*



Dr. György Major is 60

Dr. György Major celebrated his 60th birthday in 2001. However a little late, Időjárás, the journal in which a significant part of his excellent scientific papers was published, and for which he had been acting as Editor-in-Chief for four years wishes to celebrate his anniversary with a number containing nine articles written by his friends, colleagues and apprentices, working in Hungary and abroad. The authors dedicate their papers to him as a sign of appreciation for the help and friendship they received and continue to receive from Dr. Major.

Dr. Major is a really honourable and sympathetic main personality of the Hungarian meteorological scientific community and also of the much broader international scientific communities of atmospheric physicists: radiation experts and satellite meteorologists, astronomers, etc. In the name of the Editorial Board, which comprises members from the above communities, and—feeling obliged to do so—in the name of the mentioned communities in the whole, we would like to send you, dear Gyurka, our best regards, and wish you continuing successes in your work and personal life.

Dr. György Major's scientific career

Dr. György Major was born in Beregszász, in 1941. He finished his studies at the Eötvös Loránd University of Budapest in 1964, and received two diplomas, one as teacher of mathematics and physics, and one as meteorologist. Dr. Major started to work at the Hungarian Meteorological Service (HMS) just after finishing the university, where he held various researchers and then leading positions. He achieved his PhD (CSc) degree in 1975, and then the DSc degree in 1981. He published about 80 scientific articles, most of them in English in leading scientific periodicals. He remained faithful to the Service throughout his whole scientific career as an active researcher, until his recent retirement. However, he is active in the HMS even now, fulfilling the position of President of the Scientific Council of the Service.

His scientific interest was always concentrated on the field of atmospheric physics, and especially, atmospheric radiation and satellite meteorology. His major scientific achievements were connected with the methodology of solar radiation measurements, the estimation of circum-solar radiation, the analysis of radiation budget of the Earth-atmosphere system, radiation climatology of Hungary, and industrial-engineering applications of solar radiation. The development of meteorological satellite technology turned his interest more and more to satellite radiation measurements and applications. A basic scientific result of a research team led by him was the compilation of monthly and yearly insolation maps of the Earth's surface that was then published by the World Meteorological Organization.

Beside his scientific activities he had been taking a significant share in the university education of meteorologists for a long time at his mother university and he is one of the authors of the current university text-book on atmospheric physics. One of his successes has been the establishment of a scientific school in atmospheric radiation and satellite meteorology where generations of young scientists received excellent postgraduate education during the years passed. In recent years he has been very active in promoting talented young scientists to achieve academic degrees/titles.

He plays an active role in both domestic and international scientific organizations and societies. In 1993 he was elected a corresponding member and in 1998 a regular member of the Hungarian Academy of Sciences. From 1990 to 1996 he served also as the Chairman of the Meteorological Scientific Committee of the Academy. From 1993 he has been serving as Secretary-General of the Hungarian Meteorological Society, he acted as Secretary-General of the Hungarian Astronautical Society in the period 1985–1993, and as President of the same society in the years 1997–2000. He also worked as the Editor-in-Chief of the present 106 years old scientific periodical from 1995 to 1998. As regards his memberships in international organizations, he is a Member of the International Radiation Commission, a commission of ICSU/IUGG/IAMAS, and also the Commission for Atmospheric Sciences of the WMO. He had been working for a long period as the Director of the Regional Radiation Centre in Budapest, which is a part of the Baseline Surface Radiation Network (a WMO/ICSU organization).

IDŐJÁRÁS

Quarterly Journal of the Hungarian Meteorological Service
Vol. 105, No. 4 — Vol. 106, No. 1, October 2001 — March 2002, pp. 189–205

Shortwave radiation budget of the Earth: Absorption and cloud radiative effects

Istvan Laszlo¹ and Rachel T. Pinker²

¹NOAA/NESDIS/Office of Research and Applications; Camp Springs, MD 20746, USA;

²Department of Meteorology, University of Maryland, College Park, MD 20742, USA

E-mails: Istvan.Laszlo@noaa.gov; pinker@atmos.umd.edu

(Manuscript received October 29, 2001; in final form December 31, 2001)

Abstract—The University of Maryland, Global Energy and Water Cycle Experiment, Shortwave Radiation Budget algorithm was used with satellite data from the D1 product of the International Satellite Cloud Climatology project to estimate monthly values of the shortwave top of atmosphere (TOA) and surface fluxes for the period of July 1983–June 1994. Based on this data set, regional, zonal and global averages of absorption and cloud radiative effects are examined in the total shortwave spectrum. Absorption of radiation varies significantly both regionally and with latitude. Out of the 342 W m^{-2} of radiation arriving annually from the Sun at the top of the atmosphere 240 W m^{-2} is absorbed by the Earth. Annual global mean atmospheric and surface absorption are larger by 11 and 34 W m^{-2} , respectively, for land than for ocean. The top of atmosphere radiation budget is in good agreement with those from the ERBE and ScaRaB missions. The global annual average SW flux absorbed at the surface from this study is 165 W m^{-2} , and agrees well with other satellite studies. However, this value is about 20 W m^{-2} larger than the absorption indicated by studies that employ radiation data measured at ground sites. SW cloud radiative forcing at the TOA and the surface from this study is -46 W m^{-2} and -49 W m^{-2} , respectively.

Key-words: cloud radiative forcing, GEWEX/SRB algorithm, shortwave radiation budget, solar absorption, solar net flux, solar radiation

1. Introduction

The planet Earth receives energy from space in the form of solar radiation. Part of this energy is reflected back to space and part of it is absorbed by the atmosphere and the surface. Part of the absorbed solar energy is then re-radiated back to space in the form of thermal (infrared) radiation, and part of it will drive the weather and determine the climate. The measure of this energy

exchange between the planet Earth and space is the planetary radiation budget. A similar budget is defined to measure the energy exchange between the atmosphere and the surface.

Clouds play a key role in shaping the energy exchange both at the planetary and surface level. Because of their generally higher albedo, they reflect more solar radiation to space than a cloudless atmosphere would, and thus reduce the energy available for absorption by the atmosphere and the surface. On the other hand, they reduce the heat lost to space by reemitting part of the thermal radiation towards the surface. The physical mechanism and the effect of this cloud-induced change on the interaction between radiation and climate are rather complex, and in some cases not yet fully understood. For example, recent studies of the top of atmosphere radiation budget observed by satellites show decadal variations at the level of 4 W m^{-2} in shortwave (SW) and longwave (LW) fluxes, and about 1 W m^{-2} in total net flux across the entire tropics. This variability is caused by changes in cloudiness, an observational fact that current climate models cannot capture (*Wielicki et al.*, 2002). The decadal variations in the radiative fluxes are consistent with other meteorological fields and show a decadal change in the strength of the Hadley and Walker circulations (*Chen et al.*, 2002). Data from the CERES (Clouds and the Earth's Radiant Energy System) instrument on the TRMM (Tropical Rainfall Measuring Mission) satellite showed dramatic changes in the effect clouds have on the SW and LW radiation in early 1998. These changes were caused by a factor of two drop in the median cloud altitude over the western Pacific Ocean Warm Pool. The cloud height changes were shown to be related to the total shutdown of the tropical Walker Cell circulation. Preliminary studies show that climate models are not currently capturing this signal very well (*Cess et al.*, 2001).

Early studies of the radiation budget calculated the flux components from estimates of the radiative properties of the atmosphere and the surface (e.g., *Budyko*, 1974). Satellite data offer improvements over the early estimates of the planetary budget in two ways: 1) they provide a more accurate observation of atmospheric and surface properties, and 2) the planetary radiation budget is directly observed. The surface radiation budget is usually obtained from the planetary budget using models, since surface radiation is not observed directly from space. However, even for the surface budget, satellite data clearly present advantages by providing a constraint at the top of atmosphere via the requirement of conservation of energy in the total surface-atmosphere system. Over the past decade or so, there have been a number of studies that employ various satellite data to infer the radiation budget, or at least some component of it. For example, SW radiation budget parameters were estimated from the International Satellite Cloud Climatology Project (ISCCP) data by *Bishop and Rossow* (1991), *Darnell et al.* (1992), *Pinker and Laszlo* (1992), *Rossow and*

Zhang (1995), and from the Earth Radiation Budget Experiment (ERBE) data by Li and Leighton (1993).

In the current paper, only the shortwave (SW) component of the radiation budget is presented. We define shortwave as the electromagnetic spectrum between 0.2 and 4.0 μm . The SW radiation budget was obtained from the D1 product of the ISCCP using Version 2.1 of the University of Maryland (UMD), Global Energy and Water Cycle Experiment (GEWEX), Shortwave Radiation Budget (SRB) algorithm (Pinker and Laszlo, 1992; Laszlo and Pinker, 1997). Downward and upward radiative fluxes at the top of the atmosphere and at the surface were calculated for 6596 equal-area cells covering the entire globe at every three hours for a period of about 11 years (July 1983–August 1994). Each cell represents an area of about 280×280 km. Selected daily and monthly SW fluxes from this data set are also available on a CD-ROM (*University of Maryland Shortwave Radiation Budget Daily and Monthly Data Set, July 1983–August 1994, D1 Product Version 1.0, June 2000*) upon request from the Department of Meteorology, University of Maryland, College Park, MD 20742, USA (e-mail: srb@atmos.umd.edu). The new data set represents an improvement over the previous radiation budget data provided in the *First WCRP Surface Radiation Budget Global Data Sets, Short-wave Radiation Parameters March 1985–December 1988 (Version 1.1)*, and distributed by the NASA Earth Observing System Distributed Active Archive Center at NASA Langley Research Center, Hampton, VA, USA (Whitlock *et al.*, 1995). The latter data set used the C1 data of ISCCP, while the current data are based on the D1 product. The ISCCP D1 product is an improved version of the C1 product (Rossow and Schiffer, 1999); the improvements, among others, are related to a new cloud screening methodology that resulted in a better cloud detection over snow, in particular, in the polar regions. Differences of D1 and C1 estimates of the surface downward flux were found to be large ($\sim 100 \text{ W m}^{-2}$) on a regional scale at high latitudes, but zonal average differences were less than 10 W m^{-2} for tropical and middle latitude regions (Laszlo *et al.*, 1997). In addition to using the D1 data of ISCCP, the UMD/GEWEX/SRB algorithm applied in the new data set is an improved version of the one used in Version 1.1 of the WCRP/SRB data. Following Ramaswamy and Freidenreich (1992), Version 2.1 of the algorithm employs a more accurate parameterization of water vapor absorption as described in Laszlo and Pinker (1997).

In Section 2, we briefly describe the UMD/GEWEX/SRB algorithm and the ISCCP D1 satellite data that are used to obtain the SW radiation budget data set. Next, in Section 3, we present results on the radiation budget, concentrating on absorption and radiative effects of clouds. A brief analysis of the same data set has already been presented by Pinker *et al.* (2000). In the current

paper, we expand on that work, and present a more comprehensive analysis of global fluxes. Finally, in Section 4, we offer some conclusions and a summary of the main results.

2. Flux retrieval method and input data set

2.1 The UMD/GEWEX/SRB algorithm

Version 2.1 of the UMD/GEWEX/SRB algorithm (hereafter referred to as the UMD algorithm) determines the upward and downward shortwave fluxes at the top of the atmosphere and at the surface from satellite-derived clear and cloudy radiances, clear-sky composite radiance, cloud cover fraction, as well as the total amount of water vapor and ozone (*Pinker and Laszlo, 1992; Laszlo and Pinker, 1997*). The radiative fluxes are calculated in five spectral intervals, 0.2–0.4, 0.4–0.5, 0.5–0.6, 0.6–0.7, and 0.7–4.0 μm , by determining the atmospheric transmission and reflection and surface albedo pertaining to a particular satellite observation. This is done by comparing the satellite-measured top of atmosphere (TOA) shortwave reflectance to a radiative model of the surface-atmosphere system. The former is estimated from the narrowband radiance observed by the satellite, using spectral and angular transformations between narrowband radiance and shortwave reflectance. The radiative model accounts for absorption by the radiatively most important gases (water vapor and ozone), and multiple scattering by cloud and aerosol. Absorption by ozone and water vapor is parameterized following *Lacis and Hansen (1974)* and *Ramaswamy and Freidenreich (1992)*, respectively. Optical properties and vertical distribution of the concentration of aerosols are from the Standard Radiation Atmospheres (WCP-55, 1983). Extinction properties of clouds are derived from the parameterization of *Stephens (1978)* and *Stephens et al. (1984)*. A single cloud layer placed between 2 and 5.5 km is assumed. The radiative transfer in this plane parallel, vertically inhomogeneous, scattering and absorbing atmosphere is solved by the delta-Eddington method based on the numerical algorithm of *Wiscombe (1977)*. To ensure fast performance on a global scale, the radiative model is made available for the flux retrieval in the form of a pre-calculated look-up table. The look-up table describes the relationship between reflectance and transmittance for a representative (discrete) set of water vapor and ozone amounts, aerosol and cloud optical depths, and solar zenith angles.

In deriving the fluxes, first the surface albedo is estimated from the clear-sky composite reflectance by correcting it for Rayleigh scattering, aerosol extinction and absorption by ozone and water vapor. In this step, the amount of

aerosol is specified according to the Standard Radiation Atmospheres (WCP-55, 1983). Next, two sets of atmospheric transmittance-reflectance pairs are selected from the look-up table according to the input solar zenith angle, water vapor and ozone amount, and combined with the surface albedo to yield shortwave TOA reflectances. The two sets are for clear and cloudy conditions with varying values of the aerosol and cloud optical thickness, respectively. Finally, clear-sky and cloudy-sky transmittances and fluxes are obtained by adjusting the model aerosol and cloud optical thickness until the clear and cloudy TOA reflectances match, respectively, the shortwave reflectances derived from the satellite-observed clear-sky and cloudy-sky radiances. The clear-sky and cloudy-sky fluxes are then weighted according to the cloud cover fraction to yield the all-sky flux. In addition to the all-sky flux, the clear-sky flux is also saved, thus making it possible to quantify the radiative effects of clouds. Although fluxes are calculated in the five spectral intervals listed above, in the final product, they are summed up to provide values in three broad intervals: visible (VIS: 0.4–0.7 μm), near infrared (NIR: 0.7–4.0 μm) and shortwave (SW: 0.2–4.0 μm).

The key features of the UMD algorithm that set them apart from similar algorithms are:

- fully physical (the relationship between surface and top of the atmosphere radiative fluxes are obtained from radiative transfer theory);
- spectral and solar zenith angle dependence of the surface reflectance are included;
- cloud optical depth dependent on cloud type (effective radius of droplets changes);
- aerosol absorption explicitly included, even under cloudy conditions;
- direct and diffuse components of fluxes are separated (improved modeling of radiative interaction with vegetation and oceans is possible);
- modular (improvements in the representation of physics in the algorithm can easily be incorporated; different sets of satellite data can be used).

The various elements of the UMD/GEWEX/SRB algorithm have been tested in a number of different ways. The radiative transfer component was evaluated in the framework of the Intercomparison of Radiation Codes in Climate Models (ICRCCM). The UMD fluxes were in good agreement with those from high-resolution radiative transfer models (Fouquart *et al.*, 1991). The differences in atmospheric absorption, when compared to high-resolution computations, are about 2% and 7% for the clear and the cloudy cases, respectively. A validation of satellite-estimated monthly-mean downward fluxes at the surface against ground measurements showed that, on the average, biases

are less than 20 W m^{-2} (Whitlock *et al.*, 1995). However, the satellite-estimated fluxes are less accurate in regions of intense biomass burning and heavy aerosol concentrations (Konzelmann *et al.*, 1996).

The UMD algorithm estimates a relatively large number of SRB parameters (spectral upward and downward, total and diffuse fluxes at the top of atmosphere and at the surface for clear-sky and all-sky conditions). Among these, for the current study, we selected parameters that quantify the absorption of solar radiation and the radiative effects of clouds.

The amount of radiation absorbed by the earth-atmosphere system is measured by the difference of the incoming and exiting radiative fluxes, and is referred to as the net flux (NF). The net flux at TOA is obtained from the satellite data, and is considered measured. The net flux at the surface is measured directly only at a limited number of sites; on a global scale, it is usually derived from the TOA net flux using a relationship between TOA and surface values. This relationship is either estimated empirically or obtained from modeling. In the UMD algorithm, the connection between TOA and surface net fluxes is established from radiative transfer simulations, and essentially amounts to the following relationship (Laszlo and Pinker, 1994):

$$\begin{aligned} n_{SRF}(\mu_0) &= A + B n_{TOA}(\mu_0), \\ B &= (1 - \tilde{r}) / \tilde{t}, \\ A &= t_0(\mu_0) - B(1 - r_0(\mu_0)), \end{aligned} \tag{1}$$

where n_{TOA} and n_{SRF} are the fractional TOA and surface net fluxes, respectively, t_0 , \tilde{t} , r_0 and \tilde{r} are the planar and spherical transmissivity and reflectivity of the atmosphere, and μ_0 is the cosine of the solar zenith angle. Since, as it was shown in Laszlo and Pinker (1994), A and B varies relatively weakly with changing atmospheric condition, the above relationship is very closely linear.

Clouds modulate the radiative energy exchange between the atmosphere and its boundaries (space and the surface). Since the albedo of clouds is usually larger than that of the cloudless sky, they reflect more radiation to space and transmit less radiation to the surface, and thus reduce the shortwave radiation absorbed by the atmosphere-surface system. This ability of clouds to force changes in the source and sink terms of the energy budget is referred to as cloud radiative forcing (CRF). A measure of this forcing is the difference between the all-sky and clear-sky net fluxes (NF_{all} and NF_{clear}) (e.g., Ramanathan *et al.*, 1989), and is defined as

$$CRF = NF_{all} - NF_{clear}. \tag{2}$$

2.2 Input data

The input data used in this study for the UMD algorithm are from the D1 product of the International Satellite Cloud Climatology Project (ISCCP) (Rossow and Schiffer, 1999). ISCCP is a project of the World Climate Research Programme (WCRP) with the objective of collecting and analyzing satellite radiance measurements to infer the spatial and temporal distribution of cloud radiative properties on a global scale. It began its collection of visible and infrared radiances from the imaging radiometers onboard an array of operational weather satellites in July 1983. The array consists of the NOAA polar orbiters and the geostationary satellites, GOES, METEOSAT and GMS. First, the radiances are sampled to reduce data volume, then radiometrically calibrated and navigated, and finally placed in a common format.

The visible ($\approx 0.6 \mu\text{m}$) and infrared ($\approx 11 \mu\text{m}$) radiances common to all satellites are normalized to those of the Advanced Very High Resolution Radiometer (AVHRR). The normalization procedure attempts to create a uniform radiance set for the whole globe. The calibration of the AVHRR is monitored and the calibration standard is transferred from one satellite to the next in the NOAA series. The radiances are sorted according to whether they correspond to clear or cloudy scenes. The analyzed radiances are merged with the TIROS Operational Vertical Sounder (TOVS) daily analysis product produced by the National Oceanic and Atmospheric Administration (NOAA) and the weekly snow/ice cover data from the NOAA/National Environmental Satellite Data and Information Service (NESDIS) and NAVY/NOAA Joint Ice Center. The D1 data have a nominal spatial resolution of about 280 km, 6596 equal-area grid cells make up the whole globe. The data are provided at a nominal temporal resolution of 3 hours. The D1 product differs from the earlier C1 product (Schiffer and Rossow, 1985), in that the analysis method used to produce it was changed to improve cirrus cloud detection over land, low-level cloud detection over snow and ice by using $3.7\text{-}\mu\text{m}$ radiances, etc.

The D1 parameters used as input to the UMD algorithm are the mean visible clear, cloudy and clear-sky composite radiances, column amount of ozone and precipitable water amount, solar and satellite zenith and relative azimuth angles at every three hours. The fluxes retrieved at this temporal resolution are summed over a day to obtain daily values, and over a month to get monthly values. Fluxes for all three temporal resolutions are saved in the UMD/SRB product. In the next section, we present an analysis of the monthly results.

3. Results

Using the ISCCP D1 data in the UMD algorithm leads to SRB parameters at the three-hourly, daily and monthly time scales, however in the current study, we present results only for the monthly means.

3.1 Regional distribution

Mean values of the shortwave radiation absorbed by the atmosphere-surface system and those at the surface (TOA and surface net fluxes) for all-sky and clear-sky conditions were calculated for each of the 6596 equal-area ISCCP grid cell by averaging the 132 monthly values covering the period between July 1983 and June 1994. The regional distribution of the mean values for all-sky conditions is presented in *Fig. 1*. The comparison of the two fields reveals a high degree of similarity. This similarity suggests a strong correlation between TOA and surface net fluxes, a fact that has been exploited to retrieve surface solar absorption from satellite-measured TOA albedo, as mentioned in the previous section. Both fields show strong solar zenith angle dependence that is mainly modified only by persistent cloud cover. The largest absorption ($> 300 \text{ W m}^{-2}$) by the system occurs over tropical oceanic regions with relatively low cloud cover. Poleward of 70° latitude, the absorbed energy is less than about 100 W m^{-2} . The surface absorption in the tropics is about 100 W m^{-2} less than the system absorption and it is generally $50\text{--}100 \text{ W m}^{-2}$ less over land than over ocean. On a global scale, the smallest surface absorption occurs in the polar regions, as expected, due to the high surface albedo and low surface irradiance available for absorption there. The largest absorption is in the equatorial Pacific Ocean between the longitudes of about 120°W and 150°W .

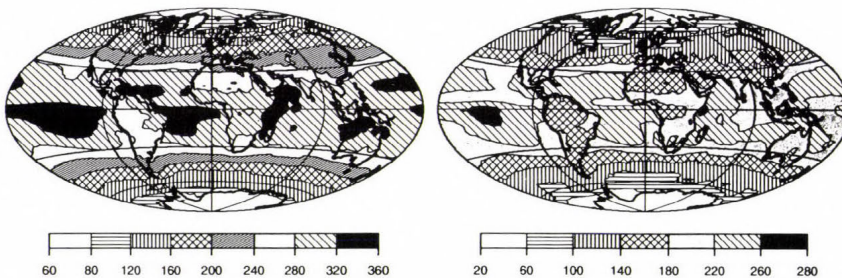


Fig. 1. Geographical distribution of annual mean shortwave energy absorbed by the earth-atmosphere system (left panel) and that by the surface (right panel) for all-sky conditions. Units are W m^{-2} .

The difference between the TOA and surface net flux is the flux absorbed by the atmosphere. The regional distribution of its ratio to the TOA solar irradiance is shown in *Fig. 2* for all-sky conditions. Atmospheric absorption varies between 18% and 28% regionally. The smallest absorption occurs over relatively clear oceanic regions, while the largest absorption is over the tropical land areas of South America, equatorial Africa, most of the Sahara and the Arabian Peninsula, Pakistan and northeast India. A somewhat enhanced absorption, relative to clear regions, is observed in the cloudy Intertropical Convergence Zone (ITCZ), just north of the equator. Because of the markedly different optical depths of clouds and aerosols over ocean and land, the gradient of absorption is the largest along the coastlines. This large gradient is, however, not necessarily realistic everywhere, since the aerosol optical depth field was initialized by a rather rudimentary climatology that assumed a visible optical depth of 0.1 over ocean and 0.23 over land. The clear-sky atmospheric absorption (not shown) varies over a somewhat larger range than that of the all-sky; it ranges from 17% to 32%. The low values are concentrated over the Southern-Hemisphere oceans between the latitudes of about 30°S and 60°S. Large values of absorption can be observed over the equatorial land areas, similar to that seen for all-sky.

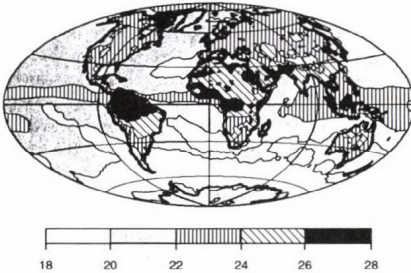


Fig. 2. Geographical distribution of annual mean shortwave radiation absorbed by the all-sky atmosphere in percent of the TOA irradiance.

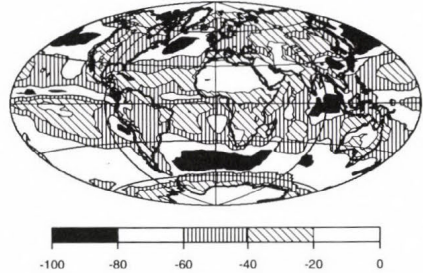


Fig. 3. Geographical distribution of annual mean shortwave cloud radiative forcing at the surface. Units are $W m^{-2}$.

The effect of clouds on the annual surface shortwave radiative energy budget is shown in *Fig. 3*. All forcing values are negative, indicating that clouds reduce the energy available for absorption at the surface in the shortwave spectrum (SW cooling). The largest forcing is observed over the northern Atlantic and Pacific oceans, to the south of the African continent and over the Asian monsoon region to the south of India. It is the result of the persistent

cloud cover in these regions and the high albedo of clouds compared to the dark ocean surface. Somewhat weaker shortwave cloud forcing is associated with the deep convective regions over central Africa and the Amazon. Similarly, a significant cloud forcing is evident off the west coast of Africa, in the regions of stratocumulus clouds off the coast of California and Chile and near the Philippines and over the ITCZ. Low shortwave cloud forcing values are found over the Sahara, the Arabian Peninsula, most of Australia, to the south of the ITCZ, over Greenland and for the snow/ice covered Polar regions. Cloud forcing at the TOA (not shown) is similar to that at the surface, except its magnitude is somewhat smaller.

3.2 Zonal averages

Total column SW absorption, that is the absorption by the atmosphere-surface system, varies significantly with latitude (*Fig. 4*). It is about 40% in the polar latitude bands, while it reaches about 75% in the tropics. Most of the SW absorption occurs at the surface. It is also the surface absorption that defines the latitudinal variation of the column absorption, since the atmospheric absorption varies only very slightly with latitude as shown in the lower panel of *Fig. 4*. There is a slight asymmetry between the northern (NH) and southern hemisphere (SH) atmospheric absorption; the northern-hemisphere atmospheric absorption is slightly larger (22.3%) than that of the southern hemisphere (20.9%). Surface SW absorption is, however, somewhat larger over the southern hemisphere, and almost balances the larger northern hemisphere atmospheric absorption in the hemispheric column absorptions, leading to SW column absorptions of 68.4% (NH) and 67.9% (SH).

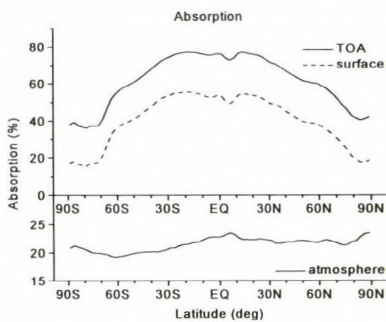


Fig. 4. Zonal mean of annual mean absorption by the atmosphere-surface system, by the atmosphere and by the surface under all-sky conditions.

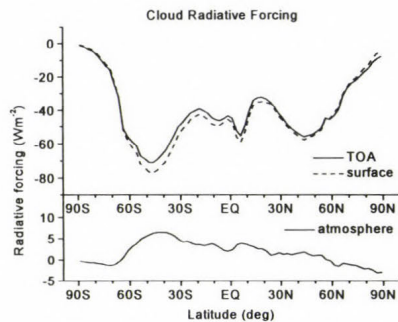


Fig. 5. Zonal mean of annual mean cloud radiative forcing at TOA, at the surface and of the atmosphere.

The SW cloud radiative forcing also exhibits a strong latitudinal dependence (Fig. 5). The largest forcing (more negative) values occur in the northern and southern hemisphere storm tracks (around 45°N and 45°S), and the smallest forcing is at high latitudes. At high latitudes, a large part of the radiation is already reflected back by the bright snow/ice cover even under clear skies, and the presence of clouds does not change this significantly. Except for zones of high latitudes, surface cloud forcing is stronger than the TOA forcing.

3.3 Global annual mean

Annual mean net fluxes of the 6596 equal-area cells were averaged to obtain global mean values. Because of the lack of satellite observations at certain high latitudes, some cells have no fluxes reported. To reduce the effect these missing cells might have on the global average, monthly average of the TOA downward flux was calculated both analytically and numerically from the available cells, and all fluxes were multiplied by the ratio of numerical to analytical TOA flux. To facilitate comparisons with other studies, we assumed a solar constant of 1367 W m⁻² for the analytical TOA downward flux, although in the UMD algorithm the solar constant is 1372.6 W m⁻². This led to a global annual mean SW irradiance of 342 W m⁻² at the TOA. Global annual mean radiation budget parameters at the top of atmosphere and at the surface are summarized in Table 1. The parameters listed in this table include the all-sky downward flux, net flux, albedo and cloud radiative forcing. The global average of the SW radiation absorbed at the surface is 165 W m⁻². The atmosphere absorbs an additional 75 W m⁻², bringing the total solar energy absorbed by the system to 240 W m⁻². Global annual SW cloud radiative forcing at the surface is 3 W m⁻² larger than at the TOA.

Table 1. Global annual mean all-sky downward flux (DF), net flux (NF), albedo (A), and cloud radiative forcing (CRF) at the top of atmosphere (TOA), at the surface and of the atmosphere. Fluxes and cloud radiative forcing are in W m⁻²

Global annual mean shortwave radiation budget parameters									
TOA				Surface				Atmosphere	
DF	NF	A	CRF	DF	NF	A	CRF	NF	CRF
342	240	0.298	-46	188	165	0.122	-49	75	3

Table 2 presents a comparison between global annual mean SW radiation budget parameters in the present study and those obtained from other studies. The comparison is admittedly not comprehensive, however the selected studies do represent different approaches for estimating the solar radiation budget.

Some of these studies are concerned with only the surface or the TOA radiation budget, but four of them address both the TOA and the surface absorption. All studies, except one, employ satellite data. *Ohmura and Gilgen (1993)* use radiation data directly observed at the ground along with estimates of the surface albedo, and report a global annual value of surface-absorbed solar radiation (net flux (NF) at surface) of 142 W m^{-2} . *Major (1998)* finds a value of 146 W m^{-2} for the same quantity in two earlier studies. In one of these studies, *Major (1976)* used a limited sample of Nimbus-3 satellite data and surface radiation data, and obtained an annual mean global surface-absorbed solar radiation of 43%. Subsequently, combining an extended number of surface data with global satellite observation of cloudiness, *Major et al. (1981)* received a value of 146 W m^{-2} for the surface-absorbed solar flux. The latter value is in close agreement with that of *Ohmura and Gilgen (1993)*. *Li et al. (1997)*, who used satellite data from the Earth Radiation Budget Experiment (ERBE) along with a highly parameterized form of the radiative transfer, received a value that is 15 W m^{-2} larger than that of *Ohmura and Gilgen (1993)*. *Rossow and Zhang (1995)* applied the C1 data of ISCCP and a modified version of the NASA/Goddard Institute for Space Studies (GISS) radiative transfer model, and arrived at the same value of surface absorption as the one found in the current study, which is 23 W m^{-2} higher than the one by *Ohmura and Gilgen (1993)*. The highest surface absorption (168 W m^{-2}) reported in this comparison is from *Kiehl and Trenberth (1997)*, who used model calculations constrained by satellite observations at TOA. Although the surface absorption is the same in the *Rossow and Zhang (1995)* study and in the current (UMD) study, the shortwave radiation absorbed by the atmosphere differs in the two studies; the UMD model atmosphere absorbs 10 W m^{-2} more radiation. The UMD atmospheric absorption is in the middle of the range listed in *Table 2*; in which the highest atmospheric absorption (83 W m^{-2}) is obtained by *Li et al. (1997)*. Both *Rossow and Zhang (1995)* and the current study use the ISCCP satellite data, however, the former is based on the C1 product while the latter employs the more recent D1 data. The water vapor data in these products are different, and this difference contributes to the difference observed in the atmospheric absorption in the two studies. The TOA albedo is also higher in the *Rossow and Zhang (1995)* study; this means more radiation is reflected back to space and less is available for absorption in the atmosphere. The difference in cloud cover in the two ISCCP products contributes to the difference seen in TOA albedos. In addition, the two studies employ different methods to derive fluxes. *Rossow and Zhang (1995)* take the cloud optical depth and surface reflectance directly from the ISCCP product and calculate surface and TOA radiation budget parameters from these. The UMD algorithm, on the other hand, uses the ISCCP radiances and retrieves the cloud optical depth and surface re-

flectance independently of ISCCP. In the process, the UMD algorithm uses angular and spectral transformations of the radiance to TOA albedo that are derived from the ERBE data. This results in an annual mean global TOA albedo of 30% that is in agreement with the value obtained from ERBE, and independently from the more recent French-Russian-German Scanner for Radiation Budget (ScaRaB) project (*Kandel et al.*, 1998). The global annual mean value of the shortwave TOA cloud radiative forcing (CRF) ranges from -46 W m^{-2} to -54 W m^{-2} . It is interesting to note that the two extreme values come from the two studies that use the ISCCP data. The CRF value from *Kiehl and Trenberth* (1997) is in the middle of this range. The ERBE and the ScaRaB data sets, which are considered two of the best TOA radiation budget data sets today, lead to a CRF value of -48 W m^{-2} . (The same CRF value of *Li et al.* (1997) is not independent from the ERBE value, since at the TOA, it only represents a direct application of the clear and all sky data from the ERBE.)

Table 2. Comparison of global annual mean SW radiation budget parameters (solar constant, all-sky flux reflected at TOA (UF), net flux (NF) at the surface and of the atmosphere and cloud radiative forcing (CRF) at TOA). The parameters listed are from *Major et al.* (1981), *Ohmura and Gilgen* (1993) (OG), *Li et al.* (1997) (LMA), *Kiehl and Trenberth* (1997) (KT), *Rossow and Zhang* (1995) (RZ), the ERBE and the ScaRaB satellite experiments, and the present study (UMD). Fluxes and cloud radiative forcing are in W m^{-2} . TOA albedos in percent are also given (in parenthesis)

Comparison of global annual mean SW radiation budget parameters								
	<i>Major et al.</i> (1981)	OG	LMA	KT	RZ ISCCP C1	UMD ISCCP D1	ERBE Mar 85– Feb 89	ScaRaB Mar 94– Feb 95
Solar constant			1365	1367	1366	1367		
UF at TOA			101 (30)	(31)	112 (33)	102 (30)	101 (30)	102 (30)
NF of atm			83	67	65	75		
NF at surface	146	142	157	168	165	165		
CRF at TOA			-48	-50	-54	-46	-48	-48

Ohmura and Gilgen (1993) used data from the Global Energy Balance Archive (GEBA) to evaluate the global surface solar radiation budget. The main source of the radiation data in GEBA is the data collected by the World Radiation Data Center in St. Petersburg, Russia. *Major* (1976) and *Major et al.* (1981) also used radiation data from the same network of stations. The above studies use relationships based on radiation data at these stations and conventional or satellite data to extrapolate the SRB to a global scale. These stations are concentrated on land areas, and it is not obvious if and how they can be used to estimate SRB on a global scale. To estimate the differences between SRB parameters for different scenes, we calculated averages sepa-

rately from the land, ocean and costal ISCCP grid cells. The result for all-sky conditions is summarized in *Table 3*. Because the average land surface albedo is about three times that of the ocean, surface absorption for land is expected to be smaller than the oceanic value of 175 W m^{-2} . The annual surface-absorbed solar radiation averaged for land cells is 141 W m^{-2} ; this, incidentally, is almost exactly the same value that *Ohmura and Gilgen (1993)* obtained for the global average. Although the cloud cover averaged for land cells is smaller than that averaged for ocean cells, the amount of radiation available for absorption at the surface is less because the average optical depth is about three times larger over land than over ocean. In spite of the larger cloud optical depth over land, the TOA shortwave cloud radiative forcing over land is 16 W m^{-2} weaker than that over ocean. The atmosphere over land areas absorbs 10 W m^{-2} more SW radiation than the atmosphere over the oceans. SRB values for coastal cells lie between the values for land and ocean cells.

Table 3. Global annual mean SW all-sky net flux at the top of atmosphere (TOA), at the surface (SRF) and of the atmosphere (ATM) for land, ocean, coastal and all ISCCP-D1 cells. SW TOA cloud radiative forcing (CRF), cloud fraction (CF) and cloud optical thickness (τ) are also listed along with all-sky SW TOA and surface albedos (A_{TOA} , A_{SRF}). Net fluxes and CRF are in W m^{-2}

SW radiation budget parameters for various scene types								
	TOA	SRF	ATM	CRF	CF	τ	A_{TOA}	A_{SRF}
All	240	165	75	-46	0.67	10.6	0.298	0.122
Land	224	141	83	-34	0.60	21.7	0.345	0.250
Ocean	247	175	72	-50	0.70	6.5	0.278	0.074
Coast	236	160	76	-42	0.67	14.5	0.310	0.140

4. Summary and conclusions

We used the ISCCP D1 data as input to the UMD/GEWEX/SRB algorithm to estimate monthly values of the shortwave TOA and surface net fluxes for the period of July 1983–June 1994 (132 months). Shortwave radiation absorbed by the atmosphere-surface system has a strong regional and zonal variability. Annual global mean atmospheric and surface absorption for land and ocean areas differ by 11 and 34 W m^{-2} , respectively. The global annual average SW flux absorbed at the surface from this study is 165 W m^{-2} ; this agrees with the value reported by *Rossow and Zhang (1995)*, but it is 19 W m^{-2} larger than the value reported by *Major (1998)* and 23 W m^{-2} larger than the average obtained by *Ohmura and Gilgen (1993)*. The latter studies used direct observations of the downward SW irradiance; however, the surface albedo was estimated indirectly with a potentially large uncertainty. An additional source of uncertainty

in the latter estimates is the uneven spatial coverage of station data. Sources of errors in the UMD/SRB parameters are also numerous. For example, misclassification of scenes in the satellite data results in erroneous spectral and angular transformations. Even if the scene identification is correct, the spectral and angular transformations applied to three-hourly radiances are valid only in a statistical sense. Moreover, the surface albedo retrieval assumes only a very rudimentary aerosol climatology, which in turn affects the flux retrievals. The radiative transfer and the inversion procedure assume plane parallel clouds and account for the current state of knowledge about cloud-radiation interactions. Several recent studies (e.g., *Cess et al.*, 1995) suggest that clouds may absorb about 20–25 W m⁻² more SW radiation than is calculated by models, including the one used in the current study. The additional absorption would reduce the surface absorbed flux reported in this study to 145 W m⁻², bringing it into agreement with the values reported by *Ohmura and Gilgen* (1993) and by *Major* (1998). At the same time, atmospheric absorption would increase to 95 W m⁻², which would make this the highest value in *Table 2*. However, the existence of this “anomalous” cloud absorption is not universally accepted. It is argued that although an increased absorption may exist in the tropics, it is more likely caused by underestimation of the aerosol absorption in that region (e.g., *Li et al.*, 1997).

SW cloud radiative forcing at the TOA and at the surface from this study is -46 W m⁻² and -49 W m⁻². Cloud forcing over ocean is 16 W m⁻² larger than over land. It is noted, that cloud forcing does not uniquely measure the radiative effect of clouds since it is calculated relative to the clear sky. In other words, the same cloud would have a larger effect on a dark oceanic scene than on a brighter land scene.

Acknowledgements—This work was supported by grant NAG59634 from the National Aeronautical and Space Administration (NASA) Research Division, Office of Earth Science, MDAR Code Y (*Dr. D. Anderson*, Project Manager), by grant NAG56667 from the NASA PATHFINDER Mission to Planet Earth (MTPE) Program Science Division (*Dr. J. Dodge*, Program Manager), and by grant NAG11831 from the NASA Radiation Sciences Program Office of MTPE Code YS (*Dr. R. Curran*, Project Manager). The ISCCP D1 data were obtained from the NASA Langley Research Center Atmospheric Sciences Data Center. We thank *Dr. B. Zhang* for the help with the calculations.

References

- Bishop, J.K.B. and Rossow, W.B.*, 1991: Spatial and temporal variability of global surface solar irradiance. *J. Geophys. Res.* 96, 16839-16858.
- Budyko, M.I.*, 1974: *Climate and Life* (ed.: *D.H. Miller*). Academic Press, San Diego, California, 508 pp.
- Cess, R.D., Zhang, M.H., Minnis, P., Corsetti, L., Dutton, E.G., Forgan, B.W., Garber, D.P., Gates, W.L., Hack, J.J., Harrison, E.F., Jing, X., Kiehl, J.T., Long, C.N., Morcrette, J.J.*,

- Potter, G.L., Ramanathan, V., Subasilar, B., Whitlock, C.H., Young, D.F., and Zhou, Y., 1995: Absorption of solar-radiation by clouds – Observations versus models. *Science* 267, 496-499.
- Cess, R.D., Zhang, M.G., Wang, P.H., and Wielicki, B.A., 2001: Cloud structure anomalies over the tropical Pacific during the 1997/98 El Niño. *Geophys. Res. Lett.* 28, 4547-4550.
- Chen J, Carlson, B.E., and Del Genio, A.D, 2002: Evidence for strengthening of the tropical general circulation in the 1990s. *Science* 295, 838-841.
- Darnell, W.L., Staylor, W.F., Gupta, S.K., Ritchey, N.A., and Wilber, A.C., 1992: Seasonal variation of surface radiation budget derived from International Satellite Cloud Climatology Project C1 data. *J. Geophys. Res.* 97, 15741-15760.
- Fouquart, Y., Bonnel, B., and Ramaswamy, V., 1991: Intercomparing shortwave radiation codes for climate studies. *J. Geophys. Res.* 96, 8955-8968.
- Kandel, R, Viollier, M., Raberanto, P., Duvel, J.Ph., Pakhomov, L.A., Golovko, V.A., Trishchenko, A.P., Mueller, J., Raschke, E., Stuhlmann, R., and the International ScaRaB Scientific Working Group (ISSWG), 1998: The ScaRaB earth radiation budget dataset. *Bull. Amer. Meteor. Soc.* 79, 765-783.
- Kiehl, J.T. and Trenberth, K.E., 1997: Earth's annual global mean energy budget. *Bull. Amer. Meteor. Soc.* 78, 197-208.
- Konzelmann, T., Cahoon, D.R., and Whitlock, C.H., 1996: Impact of biomass burning in equatorial Africa on the downward surface shortwave irradiance: Observations versus calculations. *J. Geophys. Res.* 101, 22833-22844.
- Lacis, A.A. and Hansen, J.E., 1974. A parameterization for the absorption of solar radiation in the earth's atmosphere. *J. Atmos. Sci.* 31, 118-132.
- Laszlo, I. and Pinker, R.T., 1997: Impact of changes to water vapor parameterization on surface short-wave radiative fluxes. In *IRS '96: Current Problems in Atmospheric Radiation*. A. Deepak Publishing, Hampton, Virginia, USA, 526-529.
- Laszlo, I. and Pinker, R.T., 1994: On the relationship between shortwave net radiative fluxes at the top of the atmosphere and at the surface. Preprints *Eighth Conference on Atmospheric Radiation*. Nashville, TN, January 23-28, 1994. *Amer. Meteor. Soc.*, 532-533.
- Laszlo, I., Pinker, R.T., and Whitlock, C.H., 1997: Comparison of short-wave fluxes derived from two versions of the ISCCP products. In *IRS '96: Current Problems in Atmospheric Radiation*. A. Deepak Publishing, Hampton, Virginia, USA, 762-765.
- Li, Z. and Leighton, H.G., 1993: Global climatologies of solar radiation budgets at the surface and in the atmosphere from 5 years of ERBE data. *J. Geophys. Res.* 98, 4919-4930.
- Li, Z., Moreau, L., and Arking, A., 1997: On solar energy disposition: A perspective from observation and modeling. *Bull. Amer. Meteor. Soc.* 78, 53-70.
- Major, G., 1976: Absorption of short-wave solar radiation in the atmosphere. *Országos Meteorológiai Szolgálat Kisebb Kiadványai* 40, Budapest, 49 pp.
- Major, G., 1998: On surface-absorbed solar radiation. *Bull. Amer. Meteor. Soc.* 79, 92-93.
- Major, G., Miskolczi, F., Putsay, M., Rimóczi-Paál, A., Takács, O., and Tárkányi, Zs., 1981: World maps of relative global radiation. Annex to WMO Tech. Note 172. [Available from *World Meteorological Organization, C. P. 2300, Geneva 2, Switzerland.*]
- Ohmura, A. and Gilgen, H., 1993: Re-evaluation of the global energy balance. *Interactions between Global Climate Systems, The Legacy of Hann. Geophys. Monogr.* No. 75. *Amer. Geophys. Union*, 93-110.
- Pinker, R.T. and Laszlo, I., 1992: Modeling surface solar irradiance for satellite applications on a global scale. *J. Appl. Meteor.* 31, 194-211.
- Pinker, R.T., Laszlo, I., and Zhang, B., 2001: Pathfinder large scale radiative fluxes: Data availability and their use in climate research. In *IRS 2000: Current Problems in Atmospheric Radiation* (eds.: W.L. Smith and Yu.M. Timofeyev). A. Deepak Publishing, Hampton, Virginia, 481-484.
- Ramaswamy, V. and Freidenreich, S.M., 1992: A study of broadband parameterizations of the solar radiative interactions with water vapor and water drops. *J. Geophys. Res.* 97, 11,487-11,512.

- Rossow, W.B. and Schiffer, R.A., 1999: Advances in understanding clouds from ISCCP. *Bull. Amer. Meteor. Soc.* 80, 2261-2287.
- Rossow, W.B. and Zhang, Y.-C., 1995: Calculation of surface and top of atmosphere radiative fluxes from physical quantities based on ISCCP data sets 2. Validation and first results. *J. Geophys. Res.* 100, 1167-1197.
- Schiffer, R.A. and Rossow, W.B., 1985: ISCCP global radiance data set: A new resource for climate research. *Bull. Amer. Meteor. Soc.* 66, 1498-1505.
- Stephens, G.L., 1978: Radiation profiles in extended water clouds, II. Parameterization schemes. *J. Atmos. Sci.* 35, 2123-2132.
- Stephens, G.L., Ackerman, D., and Smith, E.A., 1984: A shortwave parameterization revised to improve cloud absorption. *J. Atmos. Sci.* 41, 687-690.
- WCP-55, 1983: World Climate Research Report of the experts meeting on aerosols and their climatic effects. Williamsburg, Virginia, 28-30 March 1983, (eds.: A. Deepak and H.E. Gerber), 107 pp.
- Whitlock, C.H., Charlock, T.P., Staylor, W.F., Pinker, R.T., Laszlo, I., Ohmura, A., Gilgen, H., Konzelman, T., DiPasquale, R.C., Moats, C.D., LeCroy, S.R., and Ritchey, N.A., 1995: First Global WCRP Shortwave surface Radiation Budget Data Set. *Bull. Amer. Meteor. Soc.* 76, No. 6, 1-18.
- Wielicki, B.A., Wong, T., Allan, R.P., Slingo, A., Kiehl, J.T., Soden, B.J., Gordon, T., Miller, A. J., Yang, S.-K., Randall, D.A., Robertson, F., Susskind, J., and Jacobowitz, H., 2002: Evidence for large decadal variability in thertropical mean radiative energy budget. *Science* 295, 841-844.
- Wiscombe, W.J., 1977: The delta-Eddington approximation for a vertically inhomogeneous atmosphere. *NCAR Technical Note TN-121+STR*.

IDŐJÁRÁS

Quarterly Journal of the Hungarian Meteorological Service
Vol. 105, No. 4 — Vol. 106, No. 1, October 2001 — March 2002, pp. 207–218

Effect of the atmospheric boundary layer on the radiative fluxes

Marian Ostrožlík and František Smolen

*Geophysical Institute of Slovak Academy of Sciences
Dúbravská cesta 9, 842 28 Bratislava, Slovak Republic
E-mail: geofostr@savba.sk*

(Manuscript received September 27, 2001; in final form January 8, 2002)

Abstract—Based on the short- and long-wave radiative fluxes in the high-mountain positions Skalnaté Plešo and Stará Lesná the influence of the atmospheric boundary layer on the radiative fields in the High Tatras is studied. Besides the time and space variability of the radiative fluxes the attention to the emissivity, radiative cooling and heating in the investigated atmospheric layer as well as the influence of the low clouds on the long-wave radiation balance is paid.

Key-words: global radiation, diffuse radiation, short- and long-wave radiative fluxes, radiation balance, atmospheric emissivity, radiative cooling

1. Introduction

Present knowledge on the radiative fields distribution in the atmosphere shows that the atmospheric boundary layer plays an important role at the transfer and the transformation of the radiant energy. Its physical conditions are characterized by the large time and spatial variability which depends not as on the general and local circulation but as on the proper radiative processes which take place in the atmospheric boundary layer. An explanation of the complicated processes is possible on the basis of the theoretical knowledge on radiant energy transfer as well as from a detailed analysis of experimental data, obtained by means of the radiative fluxes measurement in the atmosphere.

Thermal energy obtained by the transformation of the short-wave radiation in the Sun-Earth-atmosphere system is a main source of energy for the meteorological processes in the lower atmospheric layers. The long-wave

radiative fluxes enable to obtain some information about transport of thermal energy in the atmospheric boundary layer. Wide range of shapes, sizes, and microphysical properties of clouds in a substantial measure influence the transformation of the radiative fluxes.

2. Data and methods

To propose to explain some regularities of the atmospheric boundary layer as well as the influence of the low clouds on the time and space variability of the short- and long-wave radiative fluxes, and the radiative processes in the atmospheric boundary layer between Stará Lesná and Skalnaté Pleso the measurements at the meteorological observatories Skalnaté Pleso ($\varphi=49^{\circ}12'N$, $\lambda=20^{\circ}14'E$, $h=1778$ m a.s.l.) and Stará Lesná ($\varphi=49^{\circ}09'N$, $\lambda=20^{\circ}17'E$, $h=810$ m a.s.l.) were used.

The vertically different position of both sites approximately 1000 m and their small horizontal distance (about 3000–4000 m) make suitable conditions to study the following properties of the atmosphere: atmospheric transmissivity, absorption ability, emissivity and radiative cooling or heating. Using of the analogical measurement technique and method at the both sites provide us the opportunity to a certain measure to eliminate mistakes which could be occurred by the quantitative evaluation of the investigated layer influence on the radiative fluxes.

3. Results and discussion

Based on the 5-year data set of continuous measurements of the radiative fluxes at the both observatories (*Ostrožlík and Janičkovičová, 1992–1995*) some results in the short-wave and long-wave spectral ranges are presented.

3.1 Global solar radiation – G

Vertical change of the global solar radiation we expressed by the parameter δ , which is given as a ratio of differences of the global solar radiation at Stará Lesná and Skalnaté Pleso to the global solar radiation at Skalnaté Pleso in %. Annual course of this parameter at the clear sky, overcast sky and at the average cloud conditions is presented in *Fig. 1*. Decrease of the flux density of the global solar radiation with altitude is expressed by the negative sign of the δ value.

Obtained results have shown that at the clear sky the flux density of the global solar radiation increases with altitude during the whole year up to 6% in average. The most vertical changes of the flux density occur in the months

April, May, June (approximately 9–10%). On the other side, the smallest changes of the global solar radiation are in November. In this month the flux densities are practically the same at the both localities.

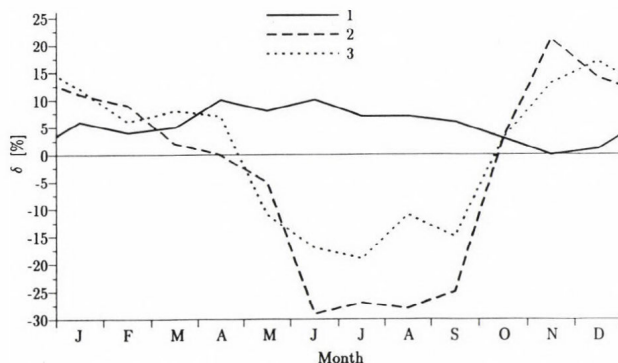


Fig. 1. Variability of the global solar radiation (δ) in the atmospheric layer between Skalnaté Pleso and Stará Lesná: 1 – clear sky, 2 – overcast sky, 3 – average conditions during the period 1991–1995.

A quite different situation of the annual course of the vertical change of the global solar radiation is at the overcast sky as well as at the average cloud conditions. In these cases in the summer months the flux density of global solar radiation is lower at Skalnaté Pleso than at Stará Lesná. It confirms that in this period of the year the cloudiness more attenuates the global solar radiation at Skalnaté Pleso than at Stará Lesná. Obtained results were compared with results of measurement in Hungary (*Major and Takács, 1974*), where it is stated that the growing values of global radiation are compensated by cloudiness only in summer.

3.2 Diffuse radiation – *D*

Fig. 2 illustrates the annual change of the diffuse radiation at Stará Lesná and at Skalnaté Pleso in dependence on cloudiness. It can be seen that at the clear sky the diffuse irradiance decreases with altitude in all months of the year. However, at the average cloud conditions it is remarkable that the diffuse irradiance in the spring months—from February to April—is higher at Skalnaté Pleso than at Stará Lesná. It means that in this part of year the diffuse irradiance increases with altitude. The mentioned anomaly in the diffuse radiation distribution is connected with the interaction of the snow cover reflectance, the

multiple reflection in a complex terrain, cloudiness, and the short-wave radiation backscattering.

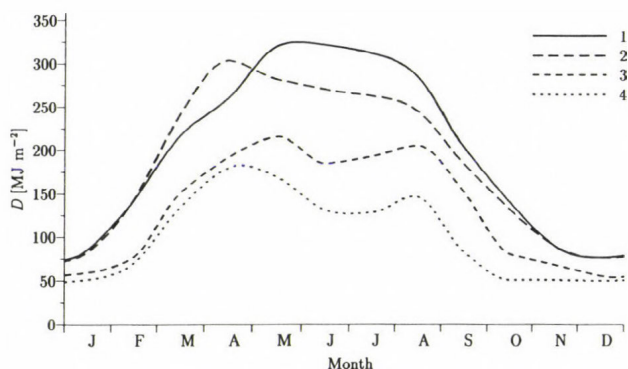


Fig. 2. Annual course of the mean monthly sums of diffuse radiation (D) at Skalnáté Pleso (2 – average conditions, 4 – clear sky) and at Stará Lesná (1 – average conditions, 3 – clear sky) during the period 1991–1995.

Effect of the atmospheric boundary layer on the short-wave radiation can be also characterized by the ratio of diffuse radiation (D) to global solar radiation (G). This ratio indirectly expresses the scattering ability of the investigated atmospheric layer. Obtained results have shown that the ratio D/G is 0.22 at Skalnáté Pleso and 0.28 at Stará Lesná in annual mean at the clear sky. Scattering ability varies greatly both in space and time depending upon the atmospheric conditions. The smallest value of the scattering occurs in February. The difference of D/G values at Skalnáté Pleso and at Stará Lesná is only 0.015. The largest scattering of this layer occurs in warming period and the corresponding difference between D/G values at both observatories is 0.122. During the day the largest scattering falls on 4 till 5 hours and on the other side the lowliest scattering occurs as a rule at noon or at the afternoon hours. A low scattering of the considered atmospheric layer in February shows on the low turbidity in the atmospheric boundary layer. The small values of Linke's turbidity factor (T_p) also confirm this fact. Mean value of T_p is 1.75 in February in the layer Skalnáté Pleso and Stará Lesná (Smolen, 1961).

We must emphasize that in the high-mountain positions the values of diffuse radiation are in a great measure influenced by the backscattering and the multiple reflection of the short-wave radiation in the atmosphere (Möller, 1965; Smolen and Ostrožlík, 1998a). A numerical comparison of the calculated data of the intensification factor (G_r/G_0) or (D_r/D_0) with the backscattering coefficient (d) shows that while in the highest positions of the mountain massif

the diffuse radiation flux density is influenced by the backscattering and multiple reflectance, the reason of short-wave radiation flux density increase in the lower positions is mainly the backscattering (G_r and D_r are the global and diffuse radiation at the high albedo of snow cover, G_0 and D_0 are the global and diffuse radiation in July at the same Sun's elevation as the G_r and D_r). The mentioned factors will influence not as the short-wave radiation balance (B_K) but as the total radiation balance (B) in the final consequence.

3.3 Short-wave radiation balance – B_K

More detailed analysis of the B_K values has shown that in case of the clear sky to the more expressive vertical change of B_K value comes as it exists at the mean cloud conditions. Its value in a great measure depends on the seasonal period (Pjatkovskaja, 1975). The difference between the short-wave radiation balance at Skalnaté Pleso and Stará Lesná (ΔB_K) enables to determine the magnitude of the radiative flux divergence in the atmospheric boundary layer. We must emphasize, that the ΔB_K value in a great measure depends on the vertical change of the reflecting ability of the active surface. Functional dependence of the short-wave radiation balance differences ΔB_K on the corresponding differences of surface albedo ΔA in the short-wave spectral range can be expressed by polynomial of degree 3 (Fig. 3).

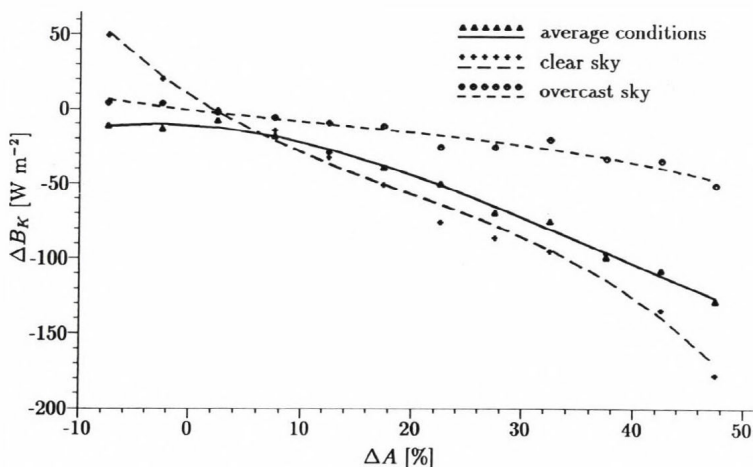


Fig. 3. Dependence of the short-wave radiative flux differences (ΔB_K) upon the differences of surface albedo (ΔA) in the atmospheric layer between Skalnaté Pleso and Stará Lesná during the 1991–1995 period.

Some another results about the time variability of the radiative receipt or radiative loss of heat in a consequence of the interaction of the short-wave radiation fluxes in the layer between Skalnáté Pleso and Stará Lesná in case of clear sky, low clouds as well as average cloud conditions are presented in the paper of authors *Smolen* and *Ostrožlík* (1999a).

3.4 Long-wave radiation balance – L^*

The loss of thermal energy by active surface was expressed by means of long-wave radiation balance. It was shown that the loss of thermal energy increases with altitude in the investigated layer. It is especially remarked at the clear sky (*Smolen et al.*, 1996). The measure of the long-wave radiation balance decrease with altitude enables the vertical gradient of long-wave radiation balance γ_{L^*} . Daily course of the γ_{L^*} value at the overcast sky as well as at the clear sky are illustrated in *Fig. 4*. We can see an analogous course of the γ_{L^*} in both cases. The mean values of vertical gradient γ_{L^*} are substantially higher at the clear sky than at the overcast sky. We can also observe a sudden decrease of the γ_{L^*} value after 15 h. This is especially marked in case of overcast sky. In this case γ_{L^*} values obtain a negative sign in a time interval of 18 to 20 h. It means that L^* values are higher at Skalnáté Pleso than at Stará Lesná.

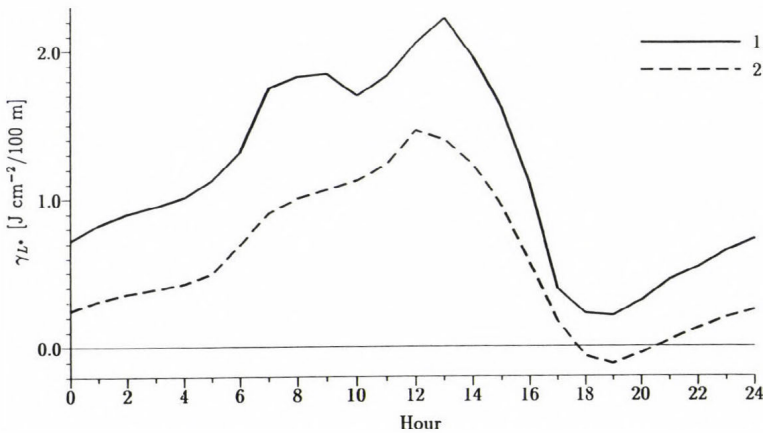


Fig. 4. Daily course of the long-wave radiation balance vertical gradient (γ_{L^*}) in the layer between Skalnáté Pleso and Stará Lesná during the 1991–1995 period (1 – overcast sky, 2 – clear sky).

3.5 Total radiation balance – B

Measurements of the short- and long-wave radiative fluxes at Skalnaté Pleso and Stará Lesná enabled to study the total radiation balance in the atmospheric boundary layer as well as its change with altitude. Time variability of the total radiation balance at the levels Skalnaté Pleso and Stará Lesná are illustrated in *Fig. 5*. Based on the 5-year measurement data it was shown that while the annual mean of radiation balance at Skalnaté Pleso is only 6.941 J cm^{-2} , the corresponding value at Stará Lesná represents up to 21.124 J cm^{-2} . It can be seen that radiation balance decreases with altitude in the investigated layer. This fact is remarkable during the day.

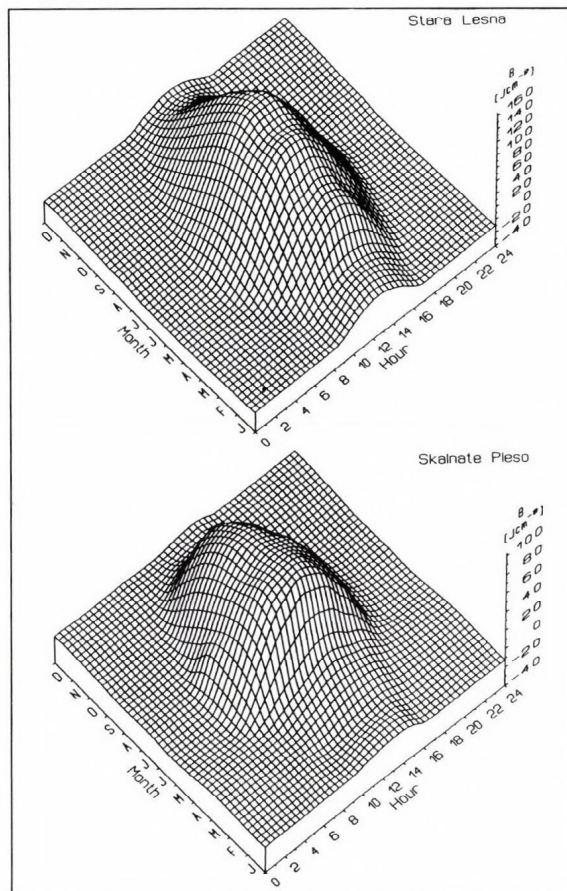


Fig. 5. Time variability of the total radiation balance at Skalnaté Pleso and at Stará Lesná at the average cloud conditions during the 1991–1995 period.

The vertical gradient of radiation balance (γ_B) served a measure of radiation balance decreasing in the layer between Skalnaté Pleso and Stará Lesná. Daily course of this gradient is demonstrated in Fig. 6. From the course of the curves we can see that γ_B has a pronounced daily course with maximum at noon. The most intensive decrease of radiation balance with altitude occurs in spring months. This expressive decrease of radiation balance with increasing altitude is due to the large reflecting ability of the active surface in the higher mountain localities.

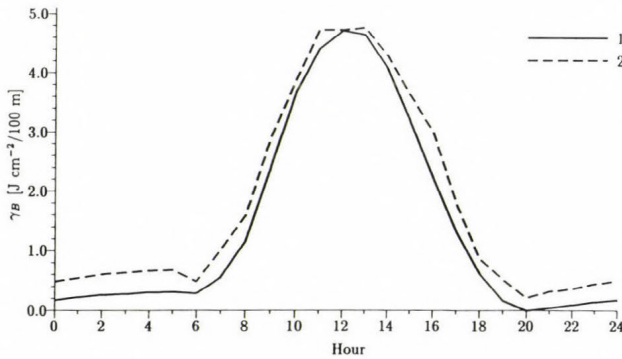


Fig. 6. Daily course of the radiation balance vertical gradient (γ_B) in the layer between Skalnaté Pleso and Stará Lesná during the 1991–1995 period (1 – average conditions, 2 – clear sky).

3.6 Atmospheric emissivity – ε_a

Daily course of the total atmospheric emissivity is presented in Fig. 7 at the clear sky. From the comparison of the individual curves we receive that the total atmospheric emissivity at Skalnaté Pleso is characterized by the higher daily amplitude than Stará Lesná. There is a question, what is the reason which causes such daily course of the total atmospheric emissivity? It is known that the atmospheric emissivity is directly dependent on optical depths of absorbing gases as well as on their temperature. The different daily course of total atmospheric emissivity at Skalnaté Pleso than at Stará Lesná will be probably caused by vertical change of the water vapour content.

In general, the atmospheric emissivity decreases with the altitude. This decrease at the clear sky in the investigated layer represents in average by 15% and depends on the vertical change of the water vapor content, and CO_2 as well as on the air temperature (Smolen and Ostrožlík, 2001). In spite of fact

that *Staley and Jurica* (1970) have shown on the smaller variability of the water vapor emissivity with temperature change, surely we must take into attention the air temperature change with altitude at the study of total atmospheric emissivity.

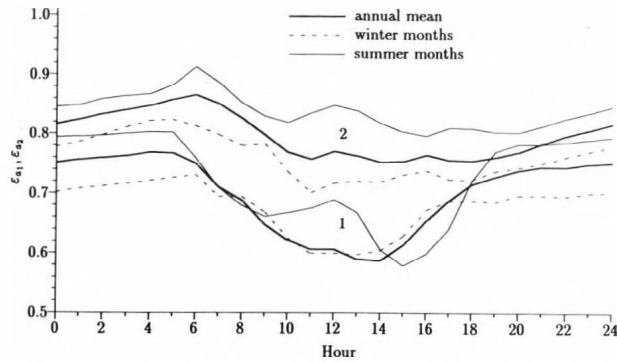


Fig. 7. Daily course of total atmospheric emissivity (ϵ_a) at Skalnáté Pleso (1) and at Stará Lesná (2) at the clear sky during the 1991–1995 period.

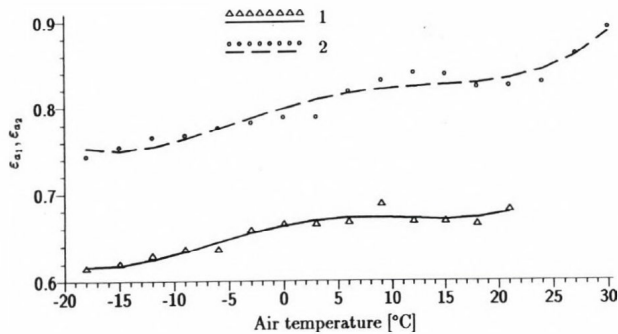


Fig. 8. Dependence of total atmospheric emissivity ($\epsilon_{a_1}, \epsilon_{a_2}$) on air temperature at Skalnáté Pleso (1) and at Stará Lesná (2) during the 1991–1995 period.

Fig. 8 demonstrates the dependence of total atmospheric emissivity on air temperature at the levels for the cases, when the optical depth of precipitated water vapor above these levels is from 0.300 to 2.500 g cm⁻². Such values correspond the mean meteorological conditions in the high-mountain regions. It is remarkable that the atmospheric emissivity at the clear sky at Skalnáté Pleso as well as at Stará Lesná slowly rises with the increasing air temperature. This

dependence of atmospheric emissivity on air temperature can be expressed with a relatively good accuracy by the polynomial function of 4. degree.

3.7 Radiative cooling and heating rate – $(\delta T / \delta t)_{\Delta F}$

Study of the relationships between the radiative temperature fluxes $(\delta T / \delta t)_{\Delta F}$ and the cloudiness in the atmospheric layer between Stará Lesná and Skalnaté Pleso has shown that the cloud cover decreases the radiative cooling rate. According to experimental data, the mean annual values of the radiative cooling rate are: at the average cloud conditions 0.070 K h^{-1} , at the clear sky 0.1218 K h^{-1} , and at the overcast sky 0.012 K h^{-1} . The most intensive radiative cooling rate is in December at the clear sky, and the mean value of $(\delta T / \delta t)_{\Delta F}$ is 0.171 K h^{-1} . On the other side the smallest values of the radiative cooling rate are in August. A some decrease of the radiative cooling rate in August can be probably caused by the development of the convective clouds in the high-land regions during the day.

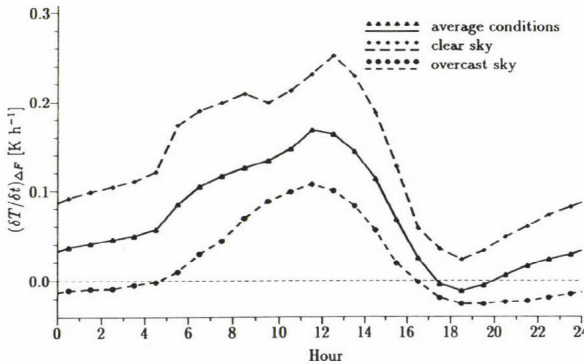


Fig. 9. Daily course of the radiative cooling rate $(\delta T / \delta t)_{\Delta F}$ in the layer between Skalnaté Pleso and Stará Lesná during the 1991–1995 period.

Fig. 9 presents daily variations of the radiative cooling rate in the investigated atmospheric layer in dependence on cloudiness. It can be seen that the daily course of the radiative cooling or heating rate has a pronounced daily course with midday maximum. The most intensive radiative cooling rate at noon occurs as a result of the mutual interaction of the long-wave radiative fluxes. In this part of day the mean values of $(\delta T / \delta t)_{\Delta F}$ is 0.228 K h^{-1} . The sudden change of radiative cooling rate occurs in the later afternoon hours. In evening hours after the sunset the radiative heating occurs (values have a

negative sign). Such radiative heating in the evening hours is especially pronounced at the overcast sky conditions.

Increasing of the low cloud amount very expressively contributes to the decrease of the radiative cooling rate. Separation of the atmospheric layer between Stará Lesná and Skalnaté Pleso to three sublayers by the low clouds has shown, that the most intensive radiative cooling exists in the sublayer over the clouds. The values of $(\delta T / \delta t)_{\Delta F}$ at the certain meteorological conditions can reach up to 1.591 K h^{-1} . A relatively small radiative cooling rate is observed in the cloudy sublayer, and below its. The radiative heating of the atmosphere very often occurs in the sublayer below the clouds. The values of the radiative heating rate can be up to -0.042 K h^{-1} and depend in a substantial measure from the low cloud extent. More detailed analysis of the radiative air temperature changes in the atmospheric boundary layer between Skalnaté Pleso and Stará Lesná is made in the papers *Smolen* and *Ostrožlík* (1998b, 1999b).

4. Conclusions

Evaluation of the experimental data of the short- and long-wave radiative fluxes in the atmospheric layer between Stará Lesná and Skalnaté Pleso has shown:

- investigated atmospheric layer attenuates of the global solar radiation flux density up to 6% but at the clear sky the flux density of the global solar radiation increases with altitude by 6% in average,
- while at Skalnaté Pleso the global solar radiation and diffuse irradiation are influenced by the backscattering and multiple reflectance, at Stará Lesná it is caused mainly by the backscattering,
- short-wave radiation balance depends in a great measure on vertical change of the reflecting ability of the active surface,
- the annual mean of the total radiation balance at Stará Lesná is 21.12 J cm^{-2} while at Skalnaté Pleso represents only 6.94 J cm^{-2} ,
- the atmospheric emissivity usually decreases with altitude and manifests the expressive time variability. This decrease represents 15% at the clear sky in the mentioned layer,
- emitted ability of atmosphere considerably varies during the year and the smallest values reaches in February,
- cloud cover in the atmospheric layer between Stará Lesná and Skalnaté Pleso decreases the radiative cooling rate. The mean values of the radiative cooling rate are: 0.070 at the average cloud conditions, 0.1218 K h^{-1} at the clear sky, and 0.012 K h^{-1} at the overcast sky.

Acknowledgement—The authors are grateful to the Grant Agency for Science (Grants No. 2/6041/01, 2/2093/22) for partially supporting this work.

References

- Major, G. and Takács, O., 1974: Change of sunshine duration and annual global radiation with altitude on the basis of data measured in Hungary (in Hungarian). *Időjárás* 78, 281-287.
- Möller, F., 1965: On the backscattering of global radiation by the sky. *Tellus* 17, 350-355.
- Ostrožlík, M. and Janičkovičová, L. (eds.), 1992–1995: *Results of Meteorological Measurements at the Observatories of the Geophysical Institute of the Slovak Academy of Sciences*. Geophysical Institute of SAS, Bratislava, 33.
- Pjatkovskaja, N. P., 1975: Radiation balance and short-wave radiative heat flux in the different climatic regions. *Trudy GGO*, 276, 43-61.
- Smolen, F., 1961: Atmospheric turbidity conditions in Carpathian region of Slovakia based on actinometric measurements (in Slovak). In *Príspevok k meteorológii Karpát*. Vydavateľstvo Slov. akadémie vied. Bratislava, 67-78.
- Smolen, F. and Ostrožlík, M., 1998a: Effect of albedo, atmospheric turbidity and cloudiness on the diffuse radiation in the high-mountain positions. *Contr. Geophys. Inst. SAS, Ser. Meteorol.* 18, 4-18.
- Smolen, F. and Ostrožlík, M., 1998b: Radiative cooling rate in the atmospheric boundary layer. *Időjárás* 102, 247-257.
- Smolen, F. and Ostrožlík, M., 1999a: Short-wave radiation balance and its vertical change in the atmospheric boundary layer in high-mountain conditions. *Meteorol. čas.* 2, 5-9.
- Smolen, F. and Ostrožlík, M., 1999b: Effect of clouds on the radiative temperature changes in the atmospheric boundary layer in the high-mountain conditions. *Contr. Geophys. Inst. SAS, Ser. Meteorol.* 19, 9-21.
- Smolen, F. and Ostrožlík, M., 2001: Emissivity of the atmospheric boundary layer in the high-mountain conditions. *Contrib. Geophys. and Geodesy.* 30, 495-508.
- Smolen, F., Ostrožlík, M., and Žák, B., 1996: Long-wave radiation fluxes in 200 m thick surface layer of atmosphere – the international experiment BOHUNICE '89. *Contrib. Geophys. Inst. SAS, Ser. Meteorol.* 16, 7-16.
- Staley, D. O. and Jurica, G. M., 1970: Flux emissivity tables for water vapor, carbon dioxide and ozone. *J. Applied Meteorol.* 9, 365-372.

IDŐJÁRÁS

Quarterly Journal of the Hungarian Meteorological Service
Vol. 105, No. 4 — Vol. 106, No. 1, October 2001 — March 2002, pp. 219–230

A comparison between measured and calculated values of atmospheric long-wave radiation

Klaus Behrens¹ and Klaus Gericke

Deutscher Wetterdienst, Meteorologisches Observatorium Potsdam,
Pf. 60 06 52, D-14405 Potsdam, Germany
E-mails: klaus.behrens@dwd.de; klaus.gericke@dwd.de

(Manuscript received December 3, 2001; in final form January 30, 2002)

Abstract—In the past 10 years an enormous progress was made in measuring long-wave radiation. In this study the measurements of atmospheric long-wave radiation, which have been carried out with different types of pyrgeometers at the German BSRN station at Lindenberg since October 1994, are compared with model calculations by LOWTRAN 7 at clear sky. It was found that since November 1996, the measurements have been matched the calculated values. Comparison of measured and modeled values is a good method to check the data quality.

Key-words: atmospheric long-wave radiation

1. Introduction

In the past 10 years an enormous progress was made in measuring long-wave radiation. The initial impulse came from the World Climate Research Program (WCRP), which initiated the Baseline Surface Radiation Network (BSRN) with goals which could only be reached by improvements of the instruments and corresponding calibration methods (*Ohmura et al.*, 1998).

Especially by investigations and developments, which were done at World Radiation Center (WRC) Physikalisch Meteorologisches Observatorium at Davos (PMOD) (Switzerland) with the characterization of pyrgeometers (*Philipona et al.*, 1995) and within the framework of the BSRN with the round-robin calibration experiment (*Philipona et al.*, 1998), important steps were gone. In recent time these efforts continued by the development of a sky-

¹ Corresponding author

scanning radiometer for absolute measurements of atmospheric long-wave radiation (*Philipona, 2001*) and an International Pyrgeometer and Absolute Sky-scanning Radiometer Comparison (IPASRC-I and II) (*Philipona et al., 2001*).

Since October 1994, at the German BSRN-Station the Meteorological Observatory at Lindenberg, measurements of atmospheric long-wave radiation have been carried out with the Precision Infrared Radiometer (PIR) pyrgeometer, developed by the Eppley Laboratory Inc. (USA), used different instruments and distinguished calculation formulas as well as with CG4 pyrgeometers, developed by Kipp & Zonen (Netherlands).

The goal of this investigation is to discuss the comparability of the atmospheric downward radiation measured and calculated both with different types of pyrgeometers and distinguished formulas within the previous seven years. Therefore, these measurements are compared with an independent method using the LOWTRAN 7 radiation code.

2. Instruments and data

The atmospheric long-wave radiation measured at Lindenberg is influenced by the above mentioned improvements. *Fig. 1* shows that downward long-wave radiation was measured by four different PIRs and two different CG4s partly in parallel during the past seven years between October 1994 and November 2001.

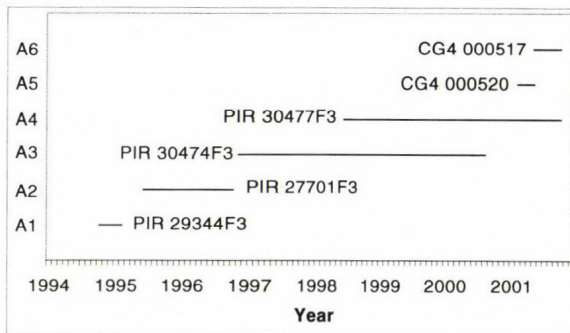


Fig. 1. Pyrgeometers used at the different periods (Ai) to measure atmospheric long-wave radiation at the BSRN station at Lindenberg (Germany).

Type and number of the pyrgeometers as well as the corresponding periods they were used are arranged in *Table 1*. Furthermore, because of a steadily improving knowledge about the PIRs, atmospheric long-wave radiation was

calculated by distinguished formulas, which are supplemented in an additional column together with those formulas applied to the CG4. All PIRs were shaded by a disc to prevent a heating of the dome by direct solar radiation. Additionally, during the first two measuring periods the remaining diffuse solar radiation, measured by CM 21 pyranometer, which was also shaded by a disc, was taken into account in Eq. (1) for correcting the downward long-wave radiation. Furthermore, the dome temperature of the PIRs was also measured because it was needed in the Eqs. (1) to (3) introduced in the formulas by *Albrecht et al.* (1974) and later by *Philipona et al.* (1995). These correction steps were applied to improve the determination of the atmospheric long-wave radiation, because of the known effects of the large dome absorptance of the PIRs (*Albrecht et al.*, 1974, *Enz et al.*, 1975).

Table 1. Pyrgeometers and measurement periods as well as the corresponding formulas for calculating atmospheric long-wave irradiance A

Pyrgeometer	Period	Formula
PIR 29344 F3	01.10.1994–01.03.1995	$A1 = \frac{U}{C} + \sigma T_b^4 - 4\sigma(T_d^4 - T_b^4) - 0.026D$ (1)
PIR 27701 F3	14.06.1995–15.11.1996	$A2 = \frac{U}{C} + \sigma T_b^4 - 4\sigma(T_d^4 - T_b^4) - 0.026D$ (1)
PIR 30474 F3	15.11.1996–22.08.2000	$A3 = \frac{U}{C} + \sigma T_b^4 - 3\sigma(T_d^4 - T_b^4)$ (2)
PIR 30477 F3	16.06.1998–31.10.2001	$A4 = \frac{U}{C}(1 + k_1\sigma T_b^3) + k_2\sigma T_b^4 - k_3\sigma(T_d^4 - T_b^4)$ (3)
CG4 000520	15.02.2001–08.05.2001	$A5 = \frac{U}{C} + \sigma T_b^4$ (4)
CG4 000517	08.05.2001–31.10.2001	$A6 = \frac{U}{C} + \sigma T_b^4$ (4)

A: atmospheric long-wave irradiance; the figures after “A” sign the period/instrument

U: voltage of the thermopile

C: sensitivity of the pyrgeometer

σ : Stefan-Boltzmann-constant

T: absolute temperature of the pyrgeometer

b: body

d: dome

k: correction factor

D: diffuse solar radiation

Because of the different construction, the measurement of the dome temperature is not necessary used in the CG4 for the determination of downwelling long-wave radiation. All pyrgeometers were ventilated with an air stream blowing around the pyrgeometer body and the dome.

The pyrgeometers used during the first two periods were calibrated with a black body at the Meteorological Observatory at Potsdam (MOP). The calibration factor of PIR 30474 F3 was derived comparing this instrument outdoors with MOP's reference pyrgeometer (PIR 30475 F3), which was calibrated at WRC PMO Davos. Also PIR 30477 F3 was calibrated at WRC Davos. The calibration factor of the CG4s were checked outdoors in comparison with the reference of the MOP with the result that no change of the factors was necessary.

Model calculation using LOWTRAN 7 (*Kneizys et al.*, 1988) are chosen to achieve the described goal. Profiles of height, pressure, temperature and relative humidity sampled by the radiosonde of the Lindenberg station are used as special input data of the model. LOWTRAN 7 restricts the number of atmospheric levels to be inserted of 34. This number of levels was distributed between the ground and 100 hPa which is the last level with information about relative humidity in a routine sounding. The input data were used at the 15 standard isobaric levels up to 100 hPa supplemented by significant levels mainly in the range up to 500 hPa. A higher resolution of the atmospheric profiles in the lower atmosphere is important because most information about long-wave downward radiation is generated in the first hectometers of the atmosphere (*Ohmura*, 2001). This fact is also important for the decision about the averaging time of the radiation measurements by the pyrgeometer comparing with calculated values by the model.

A balloon bearing the radiosonde is rising with a rate of ascent of between 5 and 8 m s⁻¹ (*WMO*, 1996). This means that in 15 minutes the radiosonde reaches a level of about 500 hPa and consequently the layer emitting the biggest share of the atmospheric long-wave radiation to the ground is explored. An extension of the averaging time up to 75 minutes, those time the radiosonde reaches the summit, does not bring more and better information but it will smooth the measured downwelling radiation.

Because every model reflects only a certain part of the reality, the investigations were concentrated on the only "simple" but well defined case of a cloudless sky. Furthermore, such selected homogeneous data make it easier to detect differences between the pyrgeometers. A clear sky was determined by the means of the hourly synoptic observations at the weather station. These conditions had to be fulfilled during the flight of the radiosonde that means at the main hours of observation and one hour before. At Lindenberg radiosondes are launched daily at 00, 06, 12 and 18 UTC. Therefore the measured data of atmospheric long-wave radiation are compared only with the calculated values by the model at these fixed times.

At BSRN Stations average, standard deviation as well as minimum and maximum values of the measured irradiance of all radiation quantities including the here investigated atmospheric long-wave radiation are calculated and

recorded every minute for the last 60 seconds. As discussed above, on the base of these measured data mean value (A_m), standard deviation, minimum and maximum were calculated over a time-span of 15 minutes beginning with the time of launching the radiosonde. These 15-minute-averages are going to be compared with the values received by the corresponding LOWTRAN 7 calculations (A_c). In every case a ratio A_m/A_c was calculated.

Table 2 gives overview about the number of measured values in the case of a cloudless sky. Related to the total more than 50% of the cases occurred at 00 UTC in the night.

Table 2. Number of the investigated cases at the different periods and the main hours of observation

	A1	A2	A3	A4	A5	A6	Total
00 UTC	32	136	187	186	29	17	587
06 UTC	16	71	87	73	3	13	263
12 UTC	7	33	34	24	0	2	100
18 UTC	10	41	44	46	3	6	150
Total	65	281	352	329	35	38	1100

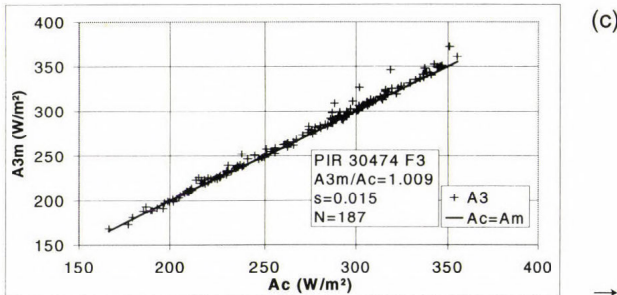
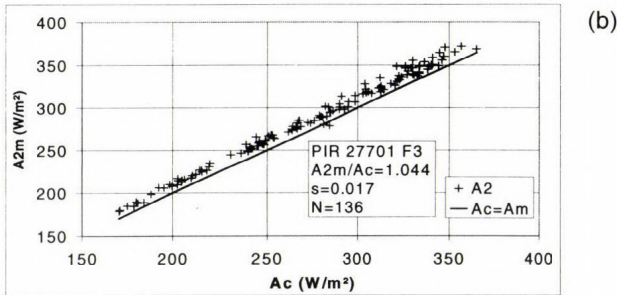
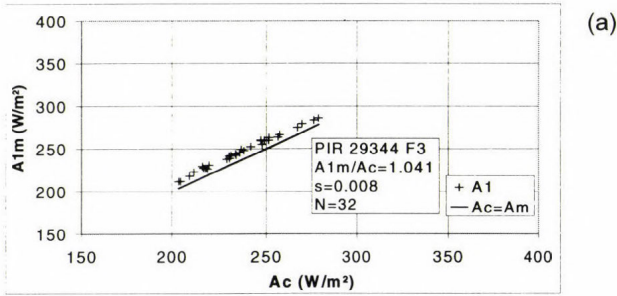
3. Results

The comparison of the measured atmospheric long-wave radiation A_m with the corresponding calculated values A_c by the LOWTRAN 7 model at 00 UTC is presented as an example at scatter diagrams in Figs. 2a-f. The short periods A1 and A6 cover only the cold and the warm season, respectively. Therefore, the plotted values in Figs. 2a and f are concentrated at the lower and the upper part of the range related to the corresponding sky temperatures, while the data of the other periods cover the full range.

The pictures of the first two periods (Figs. 2a and b) show a bias between measured and calculated values, because all crosses are remarkably clear about the line signing the equality of A_m and A_c . In both cases the measurements are about 4% higher than the calculations. The comparisons made later on (Figs. 2c-f) show a good correspondence between measurements and calculations. The mean ratios A_m/A_c are only slightly higher than 1.

Table 3 gives an overview about the mean ratios A_m/A_c as well as the standard deviations in different periods and at the different times of observations in detail. During the first two periods, the ratios between measured and calculated values A_m/A_c are about 1.04 with exception of 12 UTC in the second period, e.g., measurements and calculations are significantly different. As it is visible in Figs. 2c-f, ratios are close to 1 during all other periods for all

instruments. The measurements with the PIR 30474 F3 (period A3) are fitting best the modeled values. It seems that the downward long-wave radiation values measured by the CG4 are slightly higher than those measured in parallel by the PIRs and the calculated values. Because of the very small number of measurements made with the CG4 (see Table 2), clear sky did not occur at 12 UTC in period A5, and these facts should be considered as preliminary and not overrated. Furthermore, the comparison of night-time and daytime values shows no significant difference during all periods with exception of A2. This is a result of the permanent shading of the PIR's dome, because the solar radiation could not heat the dome.



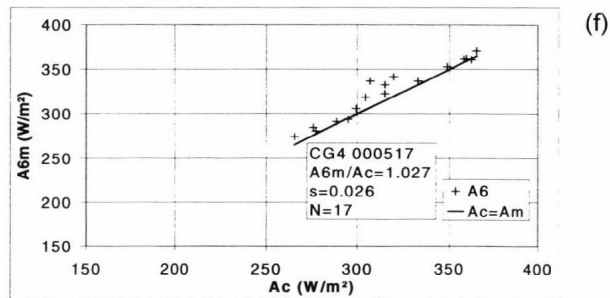
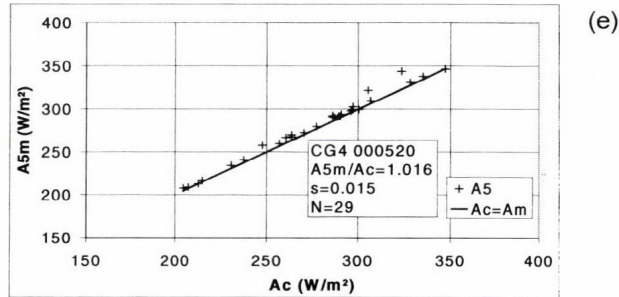
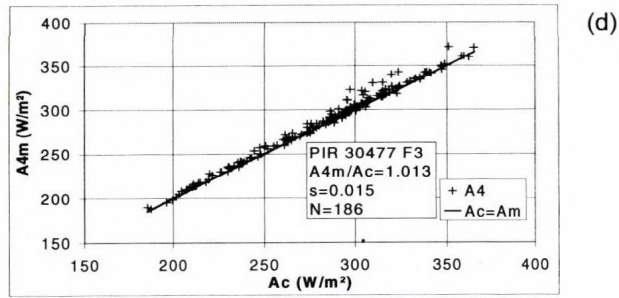


Fig. 2a-f. Comparisons of calculated irradiances of atmospheric long-wave radiation (A_c) by LOWTRAN 7 with measured irradiances (A_m) in different periods as well as with different pyrgeometers. In the box are given mean ratio (A_m/A_c), standard deviation (s) and number of measurements (N) at 00 UTC at Lindenberg, Germany.

Time series of the ratios between the measured and calculated values A_m/A_c at the four main hours of observation are given in Figs. 3a-d. The large deviations in the two first periods, already have been discussed, also attract attention in these pictures. The good correspondence of measured and calculated values at 12 UTC during the period A2 can not be explained up to now, especially because no changes in the measurements were documented.

The ratios at 00 UTC (Fig. 3a) seem to follow a yearly course. Therefore, the mean ratios are calculated for every period divided into winter and summer. Summer includes the months from April to September, while the remaining months are assigned to the winter. *Table 4* shows the results, which are similar to those of *Table 3*. The winter and summer ratios are close together. Standard deviations of these averages have the same magnitude as given in *Table 2*, which means that they are from the same population. Winter and summer ratios do not significantly differ. In some cases, e.g., in periods A5 and A6 at 06 UTC, the mean ratios have a small difference. This is caused by the small number of cases of these samples. They should be excluded from the assessment.

Table 3. Mean ratios Am/Ac and their standard deviations at the different periods and the main hours of observation

	Period	A1	A2	A3	A4	A5	A6
00 UTC	Mean (Am/Ac)	1.041	1.044	1.009	1.013	1.016	1.027
	Stdev	0.008	0.017	0.015	0.015	0.015	0.026
06 UTC	Mean (Am/Ac)	1.039	1.040	1.007	1.008	1.014	1.011
	Stdev	0.010	0.018	0.011	0.010	0.021	0.010
12 UTC	Mean (Am/Ac)	1.038	0.998	1.005	1.014	-	1.025
	Stdev	0.007	0.022	0.011	0.014	-	0.016
18UTC	Mean (Am/Ac)	1.040	1.043	1.005	1.014	1.021	1.015
	Stdev	0.007	0.015	0.012	0.014	0.019	0.008

Table 4. Mean ratios Am/Ac at the different periods and the main hours of observation separated for winter and summer season

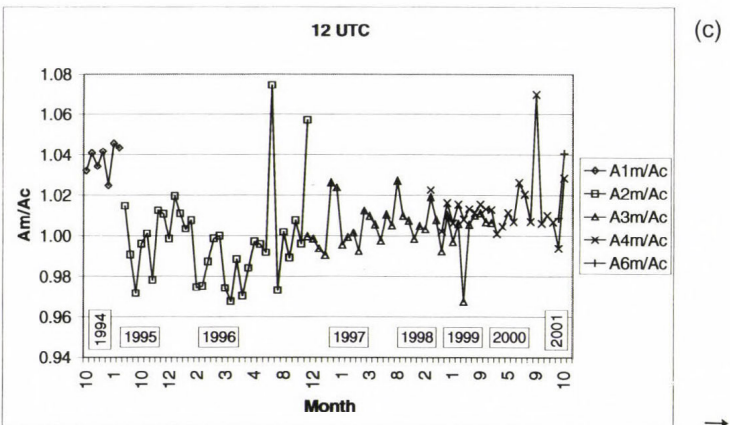
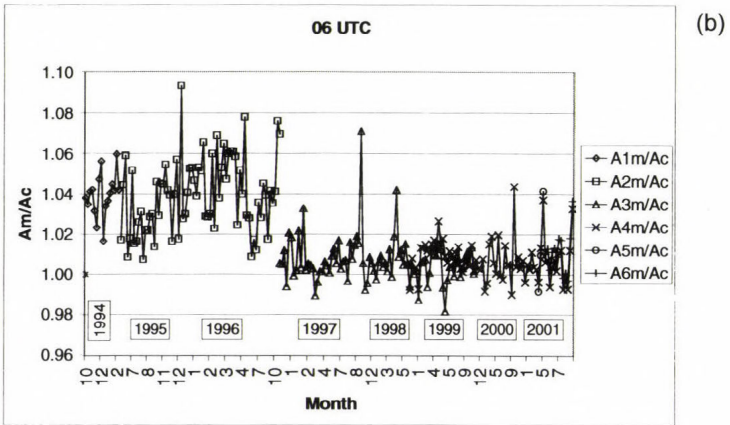
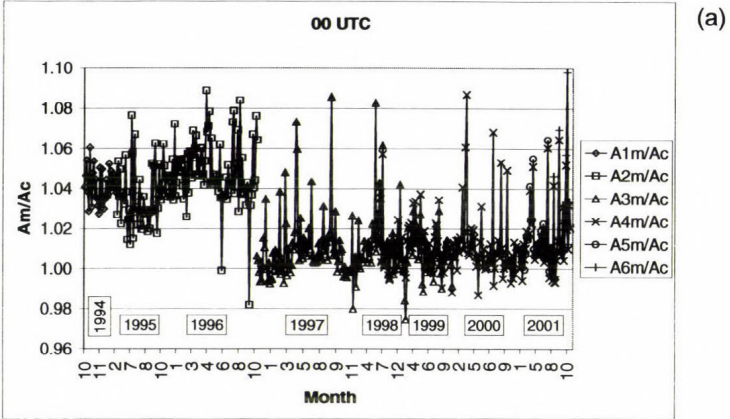
	Season	A1	A2	A3	A4	A5	A6
00 UTC	Winter	1.041	1.046	1.005	1.010	1.008	1.036
	Summer	1.038	1.042	1.012	1.014	1.017	1.020
06 UTC	Winter	1.039	1.046	1.005	1.007	1.001	1.028
	Summer	1.042	1.032	1.008	1.008	1.042	1.008
12 UTC	Winter	1.038	0.997	1.004	1.008	-	1.025
	Summer	-	0.999	1.007	1.018	-	-
18 UTC	Winter	1.040	1.044	1.002	1.011	1.004	1.019
	Summer	-	1.040	1.012	1.016	1.029	1.013

Time series of the ratios A_m/A_c (Figs. 3a–d) show also a number of outliers (about 5%) at every series, if an outlier is defined as a value which is outside of the range of mean ± 2 * standard deviation. Investigations have shown that the outliers are related to standard deviations of A_m , which are larger than in the normal case. One possible reason may be that these selected cloudless cases based on hourly synoptic observations were disturbed (no really clear cases) during the averaging time of the fundamental data. *Dutton (1993)* mentioned similar results and explained it by atmospheric variability and inhomogeneity as well as LOWTRAN 7 input variations. In these cases the given model conditions of a clear sky did not match the observed state of the atmosphere reflected by the measurements of the pyrgeometer. The recalculation of the ratios A_m/A_c and the corresponding averages, after cancelling the outliers, led only to marginal changes of the means and smaller standard deviations as one could expect, because of the normal distribution of the ratios.

Fig. 4 shows a relative frequency distribution of the differences $A_m - A_c$ after cancelling the outliers at 00 UTC for the periods A3 and A4, the periods with the largest number of observations. Nearly 30% of the data during the A3 period between $\pm 1 \text{ W m}^{-2}$ and about 60% lies within $\pm 3 \text{ W m}^{-2}$. The differences of A4 are slightly moved to higher values. The most frequent number of values (about 38%) are observed between 1 and 3 W m^{-2} . This underlines the very good agreement between measured and calculated atmospheric long-wave radiation after November 1996.

4. Conclusions

- This study showed that the comparison of atmospheric long-wave radiation measured by different types of pyrgeometers at different periods with independent calculations by means of a model, in this case LOWTRAN 7, is a good method to check the data quality under well defined conditions.
- The atmospheric long-wave radiation measured during the first two periods at a cloudless sky is about 4% too high and has to be corrected. Furthermore, a similar investigation is necessary to study this quantity at a totally covered sky including different types of clouds and to get further information in the case of broken clouds. Finally, on the base of this information a decision has to be made about the usage of one or more correction factors related to the clear or cloudy sky.
- The measurements carried out with PIRs or related to a PIR calibrated at the WRC PMO at Davos as well as with the CG4s are close to the independent calculations of LOWTRAN 7 at a clear sky.



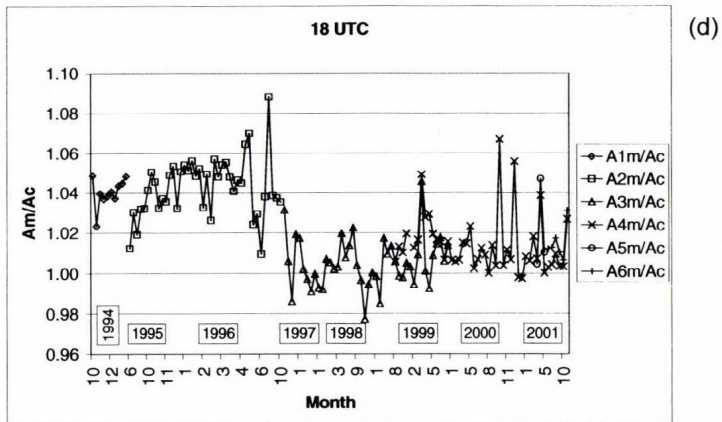


Fig. 3a-d. Ratios of measured (A_m) and calculated (A_c) values by LOWTRAN 7 of atmospheric long-wave radiation at Lindenberg, Germany.

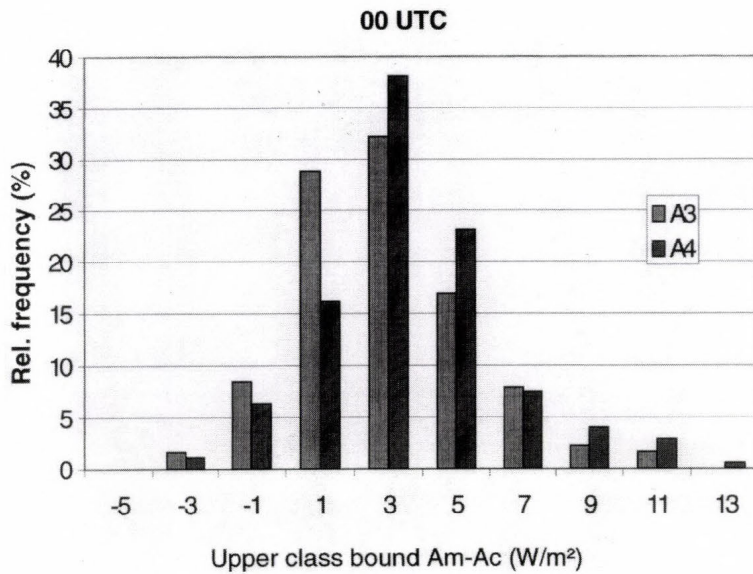


Fig. 4. Relative frequency distribution of the differences between measured (A_m) and calculated (A_c) irradiances of atmospheric long-wave radiation during the periods A3 and A4, after removing outliers at 00 UTC, at Lindenberg, Germany.

References

- Albrecht, B., Peollet, M., and Cox, S. K., 1974: Pyrgeometer measurements from aircraft. *Rev. Sci. Instrum.* **45**, 33-38.
- Dutton, E. G., 1993: An extended comparison between LOWTRAN 7 computed and observed broadband thermal irradiances: Global extreme and intermediate surface conditions. *J. Atmos. Oceanic Technol.* **10**, 326-336.
- Enz, J. W., Klink, J. C., and Baker, D. G., 1975: Solar radiation effects on pyrgeometer performance. *J. Appl. Meteor.* **14**, 1297-1302.
- Kneizys, F. X., Shettle, E. P., Abreu, L. W., Chetwynd, J. H., Anderson, G. P., Gallery, W. O., Selby, J. E. A., and Clough, S. A., 1988: Users guide to LOWTRAN 7, AFGL-TR-88-0177. Air Force Geophysics Laboratory, Hanscom AFB, MA 01731, USA, 137p.
- Ohmura, A., 2001: Physical basis for temperature-based melt-index method. *J. Appl. Meteor.* **40**, 753-761.
- Ohmura, A., Dutton, E. G., Forgan, B., Fröhlich, C., Gilgen, H., Hegner, H., Heimo, A., König-Langlo, G., McArthur, B., Müller, G., Philipona, R., Pinker, R., Whitlock, C. H., Dehne, K., and Wild, M., 1998: Baseline Surface Radiation Network (BSRN/WCRP): New precision radiometry for climate research. *Bull. Amer. Meteor. Soc.* **79**, 2115-2136.
- Philipona, R., 2001: Sky-scanning radiometer for absolute measurements of atmospheric longwave radiation. *Appl. Opt.* **40**, 2376-2383.
- Philipona, R., Fröhlich, C., and Betz, C., 1995: Characterization of pyrgeometers and the accuracy of atmospheric longwave radiation measurements. *Appl. Opt.* **34**, 1598-1605.
- Philipona, R., Fröhlich, C., Dehne, K., DeLuisi, J., Augustine, J., Dutton, E., Nelson, D., Forgan, B., Novotny, P., Hickey, J., Love, S. P., Bender, S., McArthur, B., Ohmura, A., Seymour, J. H., Foot, J. S., Shiobara, M., Valero, F. P. J., and Strawa, W., 1998: The Baseline Surface Radiation Network pyrgeometer round-robin calibration experiment. *J. Atmos. Oceanic Technol.* **15**, 687-696.
- Philipona, R., Dutton, E., Stoffel, T., Michalsky, J., Reda, I., Stifter, A., Wendling, P., Wood, N., Clough, A. S., Mlawer, E. J., Anderson, G., Revercomb, H. E., Shippert, T. R., and Timothy, R., 2001: Atmospheric longwave irradiance uncertainty: Pyrgeometers compared to an absolute sky-scanning radiometer, atmospheric emitted radiance interferometer and radiative transfer model calculations. *J. Geophys. Res.* **106**, 28,129-28,142.
- WMO, 1996: Guide to meteorological instruments and methods of observation. WMO-No. 8, 6th edition.

IDŐJÁRÁS

Quarterly Journal of the Hungarian Meteorological Service
Vol. 105, No. 4 — Vol. 106, No. 1, October 2001 — March 2002, pp. 231–242

A space-based GPS meteorological application

Éva Borbás¹, Paul Menzel² and Jun Li¹

¹*Space Science and Engineering Center, University of Wisconsin / Madison,
1225 West Dayton St., Madison, WI, 53706, USA; E-mail: eva.borb@ssc.wisc.edu*

²*NOAA/NESDIS Office of Research and Applications,
1225 West Dayton St., Madison, 53706, WI, USA*

(Manuscript received November 2, 2001; in final form December 12, 2001)

Abstract—The First Global Positioning System (GPS) satellite was launched in 1978, but the history of GPS meteorology (radio occultation) began in the 1960's with the beginning of the interplanetary flight. The studies of GPS meteorological applications appeared shortly after GPS system started to operate. In the literature many papers can be found about both the space-based and ground-based GPS applications; several papers discuss the opportunity of using GPS data for NWP and climatological applications. In this paper another GPS meteorological application is described. Radiances from current polar orbiting infrared (IR) and microwave (MW) sounders are used to derive temperature and moisture profiles in the troposphere in a physical retrieval algorithm. Specifications of the tropopause and the surface are necessary information in the profile retrieval. While the altitude of tropopause can be difficult to define in radiometric approaches, the GPS provides an opportunity to derive very accurate upper atmospheric temperature profiles by using radio occultation (RO) techniques. In this paper we show that the combination of radiometric (IR and MW) and geometric (RO) information yields improved tropospheric temperature and moisture profiles when compared to those inferred from either system alone.

Key-words: GPS occultation, ATOVS temperature and humidity retrieval

1. Introduction

Precise observations of the atmospheric water vapor and temperature with good temporal and spatial coverage are essential for weather prediction and climate research. The existing ground-based meteorological observing systems do not provide enough information about the state of the atmospheric temperature and especially rapidly changing variables like humidity. Currently

humidity observations that are operationally available for Numerical Weather Prediction (NWP) models are radiosonde data twice per day at about 200 km spatial resolution over land, and satellite data over clear sky regions. To get precise, timely and frequent information about humidity is one of the important problems of weather prediction. This would improve the accuracy of short-term cloud and precipitation forecasts by creating a better initial state for the NWP model. In satellite meteorology, because of the poor vertical resolution of the current observing systems, radiometric techniques are unable to distinguish the tropopause altitude. IR and MW sounders have limited skill in the stratosphere. The Global Positioning System is capable of deriving very accurate upper tropospheric and stratospheric temperature and moisture profiles by using radio occultation (RO) techniques. For climatological research long term, global, homogeneous and stable data sets are necessary. The GPS provides an opportunity to derive very accurate, long term, global coverage of atmospheric temperature and humidity profiles and total precipitable water (TPW) measurements.

This paper introduces the latest status in the space based GPS Meteorology as atmospheric sounding and shows some results of our own study in this field. In Section 2 the GPS meteorology will be defined and the short history of its development will be mentioned. Section 3 will highlight the advantages and disadvantages of this new method and discuss some solutions for its shortcomings. Future systems will be introduced in Section 4. Finally, in Section 5 the own results of a simulated study are described.

2. GPS meteorology

The Global Positioning System is a space based navigation system created by the United States (US) Department of Defense (DOD) originally for military purposes. The system consists of 24 GPS satellites orbiting the Earth at an altitude of 20,200 km in 6 orbit panels. The first GPS satellite was launched in 1978. The system description can be found in detail in *Hoffmann-Wellenhof et al.* (1993). A very similar Russian navigation system called Global Navigation Satellite System (GLONASS) (http://www.rssi.ru/SFCSIC/SFCSIC_main.html) has been operating since 1996. There are receivers able to receive signals from both systems (*Allan, 1996*) providing an opportunity to choose the best positioning satellite for processing purpose, however they are not well spread.

The history of GPS meteorology (*Lee et al., 2001*) started in the 1960's with the first days of the interplanetary flight. At that time the team of Jet Propulsion Laboratory (JPL) and Stanford University had the idea to probe the atmosphere of Mars and later other planets using the radio link between the

Earth and Marine 3 and 4 spacecrafts. Using RO techniques to investigate the neutral atmosphere, especially to measure the refractivity profiles of the planets, became possible after developing the two way coherent Doppler Tracking system and introducing the Abel transformation (*Fjeldbo and Eshleman, 1968*), the latter which converts the observed bending angle to refractivity. Using the radio occultation technique to investigate the neutral atmosphere of the Earth became realistic (less cost effective) with the appearance of the Global Positioning System. In 1988, GPS Geoscience Instrument (GGI) (JPL and the Stanford University) submitted the first GPS occultation proposal to NASA, and in 1995 NASA's first Low Earth Orbiting (LEO) satellite called MicroLab-1, carrying a small GPS receiver, was launched. This program called GPS/MET (*Ware et al., 1995*) and operated by the University Corporation for Atmospheric Research (UCAR) has successfully demonstrated active limb sounding of the earth's atmosphere using radio occultation technique. More than 70,000 occultation data were collected between April 1995 and February 1997 providing big data base for demonstrating purposes and for making statistical comparisons. *Ware et al. (1996)* and *Kursinski et al. (1996)* made the first validation of these data. An other comprehensive analysis and validation study (*Rocken et al., 1997*) showed that the agreement between refractivity profiles from GPS/MET data, Numerical Weather Prediction model analyses and radiosonde data are promising especially in the layer between 5 and 30 km. The standard deviation of the differences is about 2%. In July 15, 2000, after the success of the GPS/MET program, the German CHAMP (CHALLENGING Minisatellite Payload) LEO satellite was launched with the latest generation of JPL GPS receivers. The objective of this mission is almost the same of the GPS/MET program, i.e., to perform limb sounding of the Earth's neutral atmosphere and ionosphere and also to determine the Earth's gravity and magnetic fields. CHAMP has an improved antenna providing improved signal quality. Its capabilities enable sounding better into the lower troposphere than the GPS/MET system. The first validation result (*Wickert et al., 2001*) showed that the GPS-observed temperature bias (comparing to the NWP analyses) is less than 1 K above tropopause and less than 0.5 K in the 12 and 20 km at latitudes higher than 30 degree.

The meteorological applications of GPS are so widespread, that we can speak about separated branch of meteorology called GPS meteorology. These applications can be subdivided to space-based and ground-based GPS meteorology depending where the GPS receiver is placed. In this paper we focused on the space-based GPS meteorology, which uses the radio occultation technique to derive meteorological profiles (temperature or humidity) from the measured bending angle (refractivity) profiles. The equation relating the GPS

atmospheric refractivity (index of refraction) to atmospheric temperature and moisture was first expressed by *Smith and Weintraub* (1953):

$$N = 77.6 \frac{P}{T} + 3.73 * 10^5 \frac{P_w}{T^2}, \quad (1)$$

where P is the atmospheric pressure (hPa), P_w is the water vapor partial pressure (hPa) and T is the temperature (K) of the atmosphere. The first term is referred to as the dry or hydrostatic term, and the second one is the wet or moist term. The detailed description of the GPS radio occultation technique can be found in *Lee et al.* (2001).

A network of several ground based GPS receiver stations is also necessary for the navigation system. During the processing of GPS signals, the effect (time delay and curving of the signals) of the troposphere, called tropospheric delay were considered as a noise and a number of methods were developed to estimate and eliminate it (*Bevis et al.*, 1992). Using these methods the total precipitable water, which is the function of the tropospheric delay, can be determined for every GPS station. In spite of the fact that some of these methods have been available since 1970's, the data of the permanent GPS networks has been used for meteorological purposes only since 1990's related to getting precise enough ephemeris in a reasonable time for quazi-operational purposes. Since this time was shortened from 2 weeks to several hours, this application became promising for use in meteorological prediction. The number and size of these networks is growing very quickly (e.g., the Japanese GPS network already includes at least 1000 permanent GPS stations).

Another type of error in the GPS technique is the effect of the multipath signals, which may be also a new type data source in the future. It occurs when the GPS signals arrive at the receiver's antenna not only from the satellites, but from a nearby reflecting surface as well. *Komjathy et al.* (2000) demonstrated that GPS signals reflected from the ocean surface and received at an aircraft altitude of 3 to 5 km can be a remote sensing application to determine ocean surface wind speeds. This technique can be a new source of data for research of global ocean current circulation and global warning if similar results can be obtained using a GPS receiver on a LEO satellite.

3. Advantages and disadvantages of RO

One of the main advantages of the GPS occultation technique is that it does not require calibration, providing long-term stability of products near real-time in all weather conditions. Theoretically, one receiver carried on a LEO satellite

can measure 500 profiles per day with global coverage of the Earth in space and time. In practice, the GPS/MET system could measure about 250 occultations per day, and after filtering, about 150 occultations per day could be collected. This number can be higher in the case of the CHAMP satellite carrying a higher quality receiver and antenna. An 8 LEO satellite constellation could already provide 4000 soundings per day (see COSMIC mission, *Lee et al.*, 2001).

The system has a very high vertical resolution: 1.5 km in the stratosphere and 0.5 km in the lower troposphere. It is mainly limited by diffraction and horizontal atmospheric inhomogeneity (*Kursinski et al.*, 1997). The horizontal resolution is about 300 km, limited by the assumption of spherically symmetrical atmosphere in the Abelian transformation. Both resolutions can be improved by different methods like "backpropagation technique" (*Gorbunov and Gurvich*, 1998) or the holography method (*Hocke et al.*, 1999). Another method to avoid the error due to the spherical symmetry is the use of the bending angle profiles as GPS measurements via direct assimilation into the NWP model using variation method (*Healy and Eyre*, 2000). Using the GPS bending angle profiles directly also can be a solution for another disadvantage of the system: the ambiguity in separating the dry and moist contributions to the total refractivity. From the GPS refractivity profiles, derived from the bending angle profiles, the temperature profiles or the humidity profiles can be computed (see Eq. 1) if the other is known. Likewise, the temperature profiles can be computed from the dry area of the atmosphere. Another approach is to use the NWP temperature profiles as ancillary information to get the GPS humidity profiles.

The accuracy of the GPS products was estimated by *Kursinski et al.* (1997). The accuracy of the GPS refractivity profiles is the greatest (0.4%) or about 1 K for temperature in ranges from 5 km to 30 km. The accuracy became worse above and below this layer. Errors below 5 km are due to the variable water vapor content, multipath effect and the receiver itself, which can not always maintain phase lock in this region due to the low Signal to Noise ratio. Inconsistencies above 30 km are caused by measurement errors, calibration errors, and the effects of the solar and diurnal cycles in the ionosphere.

The RO retrieval method can still be improved in the future. In the lower troposphere the signal to noise ratio can be increased with higher gain antennas and lower-noise amplifiers as demonstrated by the now operating CHAMP satellite (*Wickert et al.*, 2001) carrying the latest version of JPL GPS flight receivers, since more than half of the selected profiles in the study reached the 1 km above the surface. An improved ionosphere calibration method would improve stratospheric retrievals and reduce the systematic errors that occur during the daytime retrievals because of the solar cycle maximum.

4. Future systems

After the successful GPS/MET project, the currently operating German CHAMP LEO satellite can provide an opportunity for the preparation for operational RO missions. The first operational RO mission will start with the launch of the Metop EUMETSAT Polar Satellite (EPS) around 2005. At that time the EPS Metop will already be part of the Joint Polar system (JPS) with the NPOESS (National Polar-orbiting Operational Environmental Satellite System) satellites, which also will carry GPS receivers (GPSOS) both providing 500 occultations per day since 2009.

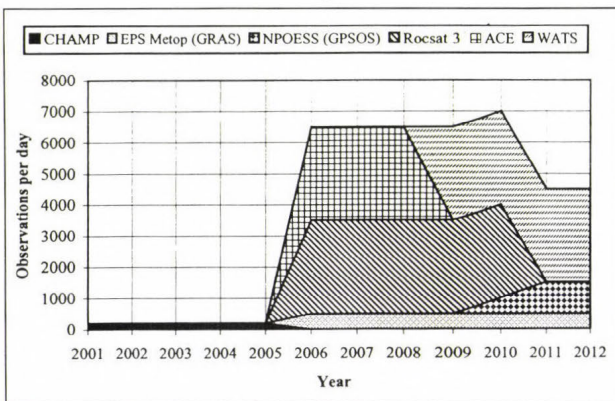


Fig. 1. Predicted radio occultation data sources based on planned and proposed missions (Luntama, 2001).

One of the proposed scientific small satellite missions is the ROCSAT-3 program, which is a collaboration project between UCAR (USA) and National Space Program Office (NSPO) (Republic of China) to develop a constellation of eight low-earth orbiting satellites. The system is called Constellation Observing System for Meteorology, Ionosphere and Climate (COSMIC) (Lee *et al.*, 2001). The program is planned for the 2005–2010 period. Other small satellite programs are the ACECHEM (Atmospheric Composition Explorer for Chemistry and Climate Interaction) with a 6-satellite constellation, proposed operation between 2005 and 2008; and WATS (Water Vapour and Wind in Atmospheric Troposphere and Stratosphere) starting about 2008/2010. Both are candidates of ESA Earth Explorer Core Missions for climate monitoring. The predicted future daily number observations (occultations) are shown in Fig. 1. The figure shows that in the near future the number of the observations may be much more than that obtained from the currently existing radiosonde observation network.

In the literature many papers can be found about GPS/MET validation (Ware *et al.*, 1996; Rocken *et al.*, 1997) and about different meteorological case studies using the GPS/MET observations (Nishida *et al.*, 2000; Kuo *et al.*, 1998). Several papers discuss the opportunity of NWP and climatological application. In the next section another GPS meteorological application is described: GPS data are used in the radiometric temperature and humidity radiometric retrieval method.

5. An example of the application of GPS occultation: a simulation study

The aim of this simulation study was to investigate the effect of combining the radio occultation and radiometric data on temperature and moisture profile retrievals as a possible meteorological application of GPS RO technique. Radiometric retrieval techniques using measurements from polar orbiting IR and MW sounders are used to infer temperature and moisture profiles in the lower and upper troposphere. Combining the two systems better quality of retrieved temperature and humidity profiles is expected as they have complementary characteristics: the radiometric technique has limited skill in the stratosphere and to detect the altitude of tropopause. Also, the measurements have good horizontal resolution, but less good vertical resolution. Since the GPS RO technique has a very good vertical resolution but poorer horizontal resolution, it is capable of deriving very accurate upper tropospheric and stratospheric temperature or refractivity profiles. It lacks skill in the low troposphere (see before). The best characteristic of RO technique for improving the radiometric retrieval method is that it can provide very accurate and detailed information around the tropopause.

5.1 Simulation approach

In our study, temperature and humidity retrievals were performed using a statistical regression approach. For simulating the IR and MW brightness temperatures, GPS refractivity and temperature profiles, and surface-based temperature and humidity observations, the NOAA88 radiosonde dataset was used which contains 7547 radiosonde profiles globally distributed in space and time. The profiles have been interpolated into 42 pressure levels from 0.1 hPa to 1050 hPa.

The simulated IR and MW data represent the NOAA Advanced TIROS Operational Vertical Sounder (ATOVS). It has three instruments: the High-resolution Infrared Radiation Sounder (HIRS) with 19 IR and one visible

channels, mainly used for temperature sounding at a maximum horizontal resolution of 18 km (at nadir point). The second instrument is the Advanced Microwave Sounding Unit-A (AMSU-A) with 15 MW channels, measuring energy within the oxygen absorption bands, so it is temperature sensitive. Its horizontal resolution is 45 km at nadir and 125 km at board. The new five channel microwave humidity sounder (AMSU-B) has a best horizontal resolution of 17 km at nadir. The brightness temperatures of the 19 IR and the 20 MW channels were simulated by using a so-called PFAAST pressure layer model fast algorithm for atmospheric transmittances (*Hannon et al.*, 1996). Microwave surface emissivity is inferred from the AMSU-A 50.3 GHz window channel brightness temperature (*Huang and Li*, 1998). In the simulation nominal instrument plus 0.2 K forward model noise were randomly added to the measurements.

To get ancillary information about tropopause, we simulated the GPS refractivity profiles representing the RO derived measurements from a GPS LEO satellite. The noise and vertical resolution of GPS profiles were estimated by a very detailed simulation study (*Kursinski et al.*, 1997). The GPS profiles were simulated on 16 levels between 5 and 30 km, where the best accuracy was accepted. Below 5 km, the noise became bigger because of the presence of moisture and the limitation of GPS occultation technique (see above). Above 30 km, ionospheric electrons cause increased noise. The vertical resolution is limited by the diffraction: 2 km below about 15 km height and 1.5 km above this level. The noise of refractivity was 0.4% on every level.

Another boundary condition of the radiometric retrieval technique is the specification of the surface. Surface temperature and humidity were defined as the lowest level of the RAOB profiles. 0.5 Kelvin temperature and 10% mixing ratio were added to generate noises.

Retrievals were performed using a statistical regression approach. Regression coefficients were computed from 90% of all RAOB profiles and the remaining 10% were used for verification. Bias and rms errors were computed between the retrievals and RAOB profiles in 1 km layers for temperature profiles and 2 km layers for humidity. Bias and rms errors for humidity were normalized by the true value to get the statistics in percentage.

In the statistical regression scheme, both linear and quadratic terms for brightness temperatures, GPS profiles and surface observations were used. This resulted in an 7.4% (from 24.9% to 17.5%) improvement of rms error in the total precipitable water over using just linear terms of ATOVS and GPS measurements. The main improvements are caused by using the quadratic terms of AMSU-B brightness temperature because humidity is a nonlinear function of brightness temperature in the radiative transfer equation, but a linear function of the refractivity (see equation above).

5.2 Results

To study the impact of the different information sources (ATOVS, GPS, and surface), the following combinations of retrievals were calculated:

- Retrievals using HIRS brightness temperature;
- Retrievals using HIRS data and surface (SFC) temperature and humidity;
- Retrievals using HIRS + SFC and GPS refractivity profiles;
- Retrievals using HIRS + GPS data;
- Retrievals using HIRS + AMSU (ATOVS) brightness temperature;
- Retrievals using ATOVS + SFC data;
- Retrievals using ATOVS + GPS + SFC data, and
- Retrievals using ATOVS + GPS data.

The bias and rms errors were computed between the retrievals obtained from these different combinations of information and NOAA88 radiosonde profiles. These statistics for temperature retrievals are shown in *Fig. 2* and for humidity retrievals in *Fig. 3*.

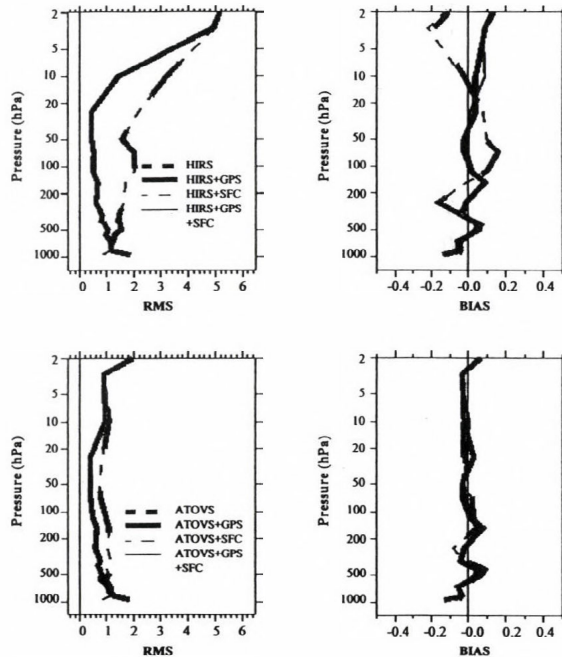


Fig. 2. RMS and BIAS (K) of temperature profiles between NOAA88 radiosonde profiles and the retrievals using different sources of data. Retrievals without AMSU (upper panels) and with AMSU (lower panels) are shown.

The effect of GPS information on HIRS retrievals is an about 1.5 K improvement in the layers above 100 hPa level and more than 0.5 K below down to the 475 hPa pressure level. Note that the HIRS instrument can characterize the GOES sounder as well since its sounder has similar characteristics (18 infrared channel). The effect of GPS refractivity profiles on the ATOVS temperature retrievals is less dramatic (lower panel of Fig. 2). It is a 0.3 K improvement between the 400 and 15 hPa layers with the maximum of 0.48 K in layer 135–85 hPa. The surface temperature and humidity information can improve the retrieval in the surface layer by about 1 K in both (HIRS and ATOVS retrieval) cases. Significant difference (positive effect) between using or not AMSU channel information can be seen above 10 hPa level, where other data were not available. It can be seen that the most powerful combination is when we use all data together (gray narrow solid line on the lower panel of Fig. 2). The rms error of that “best case” is under the 1.2 K between 3 and 920 hPa pressure levels. The biases in all cases were under the ± 0.2 K.

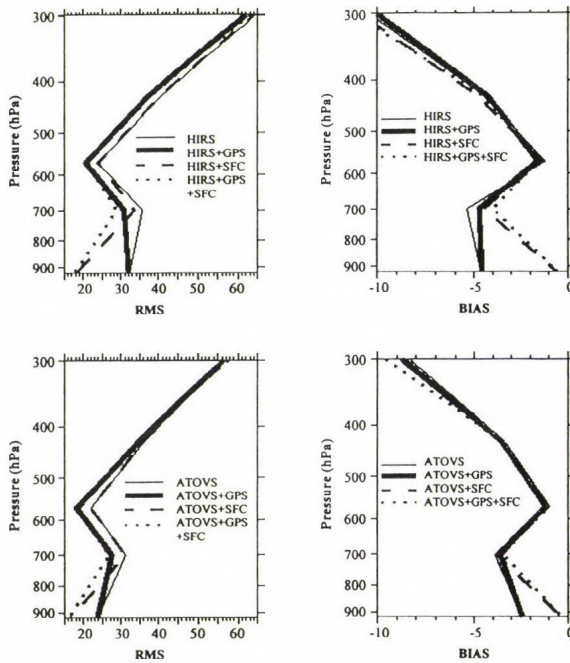


Fig. 3. RMS and BIAS errors of humidity (mixing ratio, in unit %) between NOAA88 radiosonde profiles and the retrievals using different sources of data. Retrievals without AMSU (upper panels) and with AMSU (lower panels) are shown.

It is evident that the effect of GPS refractivity profiles on radiometric humidity retrievals is less important than it was for temperature because the refractivity profiles were derived only above altitude of 5 km where the water vapor content is already very low. The maximum improvement of GPS data on HIRS humidity retrievals is 4.7% in the 780–620 hPa layers, while the impact on ATOVS retrievals is 4.3%. Surface observations are obviously very useful; their effect on ATOVS retrieval in the surface layer is a 7.6% improvement. The biases of humidity retrievals are negative, but using more information sources decreased them.

6. Summary

This paper introduced GPS meteorology with a short history of its development. The advantages and disadvantages of this new meteorological application were mentioned. Further improvements in the proposed future systems suggest that this scientific area is very promising. Several papers discuss the opportunity for NWP and climatological applications, but in this paper another GPS meteorological application is described: the use of GPS data to support the retrieval of temperature and humidity profiles from satellite radiances. In this study we followed a statistical regression approach, using radiometric (IR and MW) and radio occultation data. The test results showed that the RO data improved the IR and MW retrievals of temperature and moisture in the upper troposphere and the temperature retrievals in the stratosphere. The best quality results were obtained by using all of sources of information.

In the future this study will be repeated on real data (RO data from GPS/MET or CHAMP measurements) to do a fully independent validation.

Acknowledgements—This work was supported in part by NOAA Cooperative Agreement NAO7EC0676 and by the Hungarian National Research Foundation (OTKA-T032466).

References

- Allan, D.W., 1996: Harmonizing GPS and GLONASS. *GPS World, May 1996*, 51-53.
- Fjeldbo, G. and Eshleman, V.R., 1968: The atmosphere of Mars analyzed by integral inversion of the Mariner IV occultation data. *Planet. Space Sci.* 16, 1035-1059
- Gorbunov, M.E. and Gurvich, A.S., 1998: Microlab-1 experiment: Multipath effects in the lower troposphere. *J. Geophys. Res.* 103, D12, 13,819-13,826.
- Hannon, S., Strow, L.L., and McMillan, W.W., 1996: Atmospheric infrared fast transmittance models: A comparison of two approaches. *Proc. SPIE*, 2830, 94-105.

- Healy, S. B. and Eyre, J. R., 2000: Retrieving temperature, water vapour and surface pressure information from refractive-index profiles derived by radio occultations: A simulation study. *Quart. J. Roy. Meteor. Soc.* 126, 1661-1683.
- Hocke, K., Pavelyev, A. G., Yakovlev, O.I., Barthes, L., and Jakowski, N., 1999: Radio occultation data analysis by the radioholographic method. *J. Atmos. Soar-Terr. Phys.* 61, 1169-1177.
- Hoffmann-Wellenhof, B., Lichtenegger, H., and Collins, J., 1993: *GPS-theory and Practice*. Springer Verlag, Wien, New York. Second edition.
- Huang, H. L. and Li, J., 1998: Determination of microwave emissivity from Advanced Microwave Sounding Unit measurements. *Proc. of SPIE, The International Society for Optical Engineering*, 3503, 233-237.
- Komjathy, A., Zavorotny, V. U., Axelrad, P., Born, G. H., and Garrison, J. L., 2000: GPS signal scattering from sea surface: Wind speed retrieval using experimental data and theoretical model. *Remote Sensing of Environ.* 73, 162-174.
- Kuo, Y.-H., Zou, X., Chen, S. J., Huang, W., Guo, Y.-R., Anthes, R. A., Exner, M., Hunt, D., Rocken, C., and Sokolovskiy, S., 1998: A GPS/MET sounding through and intense upper-level front. *Bull. Amer. Meteor. Soc.* 79, 617-626.
- Kursinski, E.R., Hajj, G.A., Bertiger, W.I., Leroy, S.S., Meehan, T.K., Romans, L.J., Schofield, J.T., McCleese, D.J., Melbourne, W.G., Thornton, C.L., Yunk, T. P., Eyre, J.R., and Nagatani, R. N., 1996: Initial results of radio occultation observations of Earth's atmosphere using the global positioning system. *Science* 271, 1107-1110.
- Kursinski, E.R., Hajj, G.A., Schofield, J.T., Linfields, R.P., and Hardy, K.R., 1997: Observing Earth's atmosphere with radio occultation measurement using the Global Positioning System. *J. Geophys. Res.* 102, 23,429-23,465.
- Lee, L.-C., Rocken, C. and Kursinski, R., 2001: *Applications of Constellation Observing system for Meteorology, Ionosphere & Climate*. Springer Verlag, Hong Kong Ltd.
- Luntama, J.-P., 2001: Space based GPS Meteorology and GOS. [http://www.wmo.ch/hinsman/CGMS Workshop web/Luntama web/sld015.thm](http://www.wmo.ch/hinsman/CGMS%20Workshop%20web/Luntama%20web/sld015.thm).
- Nishida, M., Shimizu, A., Tsuda, T., Rocken, C., and Ware, R.H., 2000: Seasonal and longitudinal variations in the tropical tropopause observed with the GPS occultation technique (GPS/MET). *J. Meteor. Soc. Japan* 78, 691-700.
- Rocken, C., Anthes, R., Exner, M., Hunt, D., Sokolovskiy, S., Ware, R., Gorbunov, M., Schreiner, W., Feng, D., Herman, B., Kuo, Y.-H., and Zou, X., 1997: Analysis and validation of GPS/MET data in the neutral atmosphere. *J. Geophys. Res.* 102, No. D25, 29,849-29,866.
- Smith, E.K. and Weintraub, S., 1953: The constants in the equation for atmospheric refractive index at radio frequencies. *J. Res. Natl. Bur. Stand.* 50, 39-41.
- Ware, R.H., Exner, M.L., Herman, B. M., Kuo, Y-H., Meehan, T.K., and Rocken, C., 1995: GPS/MET Preliminary Report, July 1995. http://cosmic.cosmic.ucar.edu/gpsmet/over/septsumn_top.html
- Ware, R., Exner, M., Feng, D., Gorbunov, M., Hardy, K., Herman, B., Kuo, Y., Meehan, T., Melbourne, W., Rocken, C., Schreiner, W., and Trenberth, K., 1996: GPS sounding of the atmosphere from low earth orbit: Preliminary results. *Bull. Amer. Meteor. Soc.* 77, 19-40.
- Wickert, J., Reigber, C., Beyerle, G., König, R., Marquardt, C., Schmidt, T., Grunwaldt, L., Galas, R., Meehan, T.K., Melbourne, W.G., and Hocke, K., 2001: Atmosphere sounding by GPS radio occultation: First results from CHAMP. *Geophys. Res. Lett.* 28, 3263-3266.

IDŐJÁRÁS

Quarterly Journal of the Hungarian Meteorological Service
Vol. 105, No. 4 — Vol. 106, No. 1, October 2001 — March 2002, pp. 243-251

High accuracy skin temperature retrieval from spectral data of multichannel IR imagers

Ferenc Miskolczi

*Science Applications International Corporation,
1 Enterprise Pkwy, Suite 300, Hampton, VA 23666, USA
E-mail: f.m.miskolczi@larc.nasa.gov*

(Manuscript received November 14, 2001)

Abstract—The increasing number of IR spectral channels of recent satellite imagers implies the more accurate retrieval of surface skin temperature. In this paper the theoretical accuracy limits as a function of channel numbers, viewing angles and noise equivalent radiances have been studied. Based on LBL computations of the channel radiances regression type relationships have been established between the brightness temperatures and the skin-temperatures. In this study model filter functions of the 7 IR channels of the GLI imager of the ADEOS-I have been used with a large set of temperature profiles. The global and seasonal distribution of temperature profiles were considered by groups of climatologically representative temperature profiles. Standard singular value decomposition program package was used to solve the multivariable linear regression problem. Results show that the accuracy limits of the skin temperature retrievals are depending mainly on the noise equivalent radiances and up to around 60 degree viewing angles remaining in the range of 0.1–0.2 K.

Key-words: remote sensing, skin temperature, ADEOS

1. Introduction

Satellite based remote sensing of the Earth-atmosphere system has an increasing role in climate change detection. Imager instruments have nowadays improved accuracy and more channels allowing the development of better retrieval algorithms for a variety of surface and atmospheric parameters. The first step in the retrieval of the surface temperature is to derive the accurate skin temperature from the radiance measurements. Formerly, with imagers using one or two spectral channels, accuracy was limited. The necessary information on the characteristics and involvement of the H₂O and other molecular species in the windows absorption was unavailable. The Global Imager, (GLI), on board the Advanced

Earth Observing Satellite, (ADEOS 2), offers four window channels and three H₂O channels for better surface temperature detection with a possibility of obtaining information on the initial trend of the moisture profile. In the present paper, the theoretical accuracy limits of the clear-sky skin temperature retrievals using the GLI infrared channels have been established, based on high resolution radiative transfer computations and regression analysis.

2. Method

For a given filter function the average wave number, the effective wave number and the channel radiance are expressed as:

$$v_k^a = \frac{\int_{\Delta v} v \Phi_k(v) dv}{\int_{\Delta v} \Phi_k(v) dv}, \quad (1)$$

$$v_k^e = \frac{\int_{\Delta v} v I(v) \Phi_k(v) dv}{\int_{\Delta v} I(v) \Phi_k(v) dv}, \quad (2)$$

and

$$I_k = \frac{\int_{\Delta v} I(v) \Phi_k(v) dv}{\int_{\Delta v} \Phi_k(v) dv}, \quad (3)$$

where $I(v)$ is the spectral radiance, $\Phi_k(v)$ is the filter function, v is the wave number and the subscript k refers to the serial number of the spectral channel. In *Table 1* the GLI and GOES-8 filter functions are compared. Some GOES-8 channels are close to the corresponding GLI channels, therefore the results and conclusions could also be valid for those filters.

Table 1. Average wave numbers, v_k^a , and half widths, β_k , of the GLI engineering model filter functions and some similar GOES-8 filter functions (units are in cm⁻¹)

No.	GLI		GOES-8	
	v_k^a	β_k	v_k^a	β_k
1	836.47	52.52	835.97	64.18
2	945.83	69.60	934.75	86.06
3	1160.30	72.12		
4	1377.06	94.67		
5	1430.78	97.10		
6	1484.88	113.60	1482.04	122.76
7	2699.92	239.34	2559.44	165.62

Skin temperature retrieval using regression type relationships between the channel scene temperatures and the true radiative temperatures of the surface is very simple:

$$T = \alpha_0 + \sum_{k=1}^N \alpha_k T_k^c, \quad (4)$$

where T is the skin temperature, N is the number of the spectral channels, α_k 's are regression coefficients and T_k^c 's are the estimated scene temperatures. T_k^c 's are computed from the brightness temperatures and they are supposed to be corrected for the shift in the effective wave number with the change in the structure of the spectral radiance. The brightness temperatures are computed from the channel radiances via the inverse Planck function and using the average wave number. The "accurate" scene temperature is computed the same way, but using the effective wave number. In case of an ideal black body radiance spectra, the magnitudes of the brightness temperature corrections at different GLI channels are presented in *Fig. 1*.

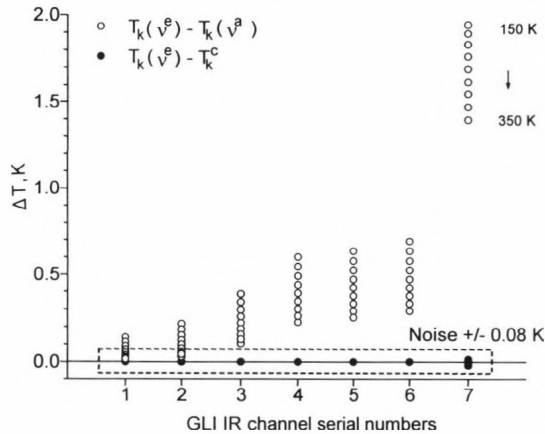


Fig. 1. Brightness temperature corrections using ideal black body functions in the range of 150–350 K. The dashed line is an assumed average noise level of the IR channels.

To perform the corrections there are several methods. NOAA uses linear (or more recently second order polynomial) fit, *Weinreb et al. (1997)*. For the GLI channels we applied a logarithmical fit to express the effective wave number as the function of the channel radiance:

$$T_k^c = B^{-1}(v_k^c, I_k), \quad (5)$$

where

$$v_k^c = c_k^1 + c_k^2 \ln(I_k). \quad (6)$$

In the above equations v_k^c is the estimated effective wave number, c_k^1 and c_k^2 are regression coefficients. Eq. (5) and (6) proved to be more accurate, (not shown here), and uses less coefficients than the NOAA method. Brightness temperature corrections based on ideal black body radiation is not justified when the distribution of the spectral radiance does not follow the Planck's radiation law. In the present work the c_k^1 and c_k^2 regression coefficients were determined using real atmospheric radiance spectra. Obviously, since the degree of modulation of the ideal black body spectra is dependent on the optical path within the atmosphere, for correct scene temperature computations a set of regression coefficients are needed for different viewing angles.

In Fig. 2, the brightness temperature corrections as the function of the channel radiances are plotted for the GLI channel 6. The correction error is the difference between the corrections, $(T_k - T_k^c)$, using ideal black body type or real atmospheric spectra in Eqs. (5) and (6). In this channel, Fig. 2 shows a large (-0.68 K) bias, and actually suggests not to use any corrections based on ideal black body radiance spectra. The situation in the GLI channel 7 is similar, but with a bias of 0.5 K. In channel 1 and 2 the biases remain below the noise level.

In general, the success of the regression scheme given in Eq. (4) is entirely dependent on the accuracy of the computed channel radiances and the statistical representativeness of the atmospheric temperature, water vapor, ozone and other trace gas profiles.

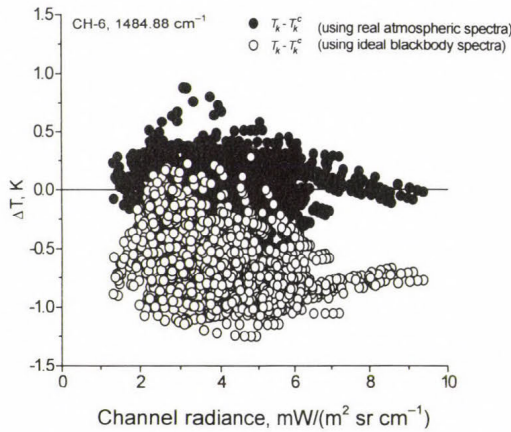


Fig. 2. Scene temperature error in the GLI water vapor channel due to the different brightness temperature correction methods.

3. Regression data set

The present study uses a subset of the TOVS Initial Guess Retrieval (TIGR), database of 1761 radiosonde observations (*Chedin and Scott, 1983*). This data set contains the pressure, temperature, H₂O and O₃ mixing ratio profiles at 40 pressure levels between 0.05 and 1013 hPa. The soundings were collected over both hemispheres and over all seasons from 1976. In *Table 2* the characteristics of the original data set are summarized.

Table 2. Average characteristics of the TIGR subset containing 1761 profiles in 11 classes (*M* is the number of profiles, *u* is in prcm, *T_e* is in K and *p_e* is in hPa)

	Region and season	M	u	T _e	P _e
1	Arctic summer	112	1.0	263	795
2	Arctic winter	295	0.3	250	779
3	North midlatitude summer	57	2.7	281	797
4	North midlatitude fall/spring	88	1.1	266	804
5	North midlatitude winter	332	0.9	263	804
6	North/South tropical	114	3.6	285	816
7	South midlatitude summer	131	1.6	271	808
8	South midlatitude fall/spring	155	1.0	264	805
9	South midlatitude winter	151	1.1	269	823
10	Antarctic summer	157	0.5	255	783
11	Antarctic winter	169	0.3	250	774

To obtain the best retrieval on a global scale, the profiles were classified according to their geographical latitudes and the seasons. Based on the latitudinal and annual distribution, 5 latitudinal belts were selected, and in each belt, one, two or three “seasons” were established, roughly based on the solar climate. Because of the apparent asymmetry in the global and seasonal distribution of the available solar radiation, the northern and southern hemispheres were treated separately. This classification of profiles resulted in 11 groups with a minimum of 57 profiles during the northern midlatitude summer, and a maximum of 331 profiles during the northern midlatitude winter. Further on, for practical reasons, it was necessary to reduce the number of the profiles to a reasonably small number, suitable for detailed line-by-line calculations. Due to the fact that the window channel radiances are affected mainly by the absorption of atmospheric water vapor, the selection of the individual TIGR profiles was based on the total precipitable water, *u*, effective H₂O temperature, *T_e*, and effective H₂O pressure, *p_e*. The effective values were computed by weighting the temperature and pressure profiles with the water vapor column density profile. A pre-selection based on the

statistical characteristics of the 11 groups resulted in 297 profiles. The extreme profiles from each group (profiles closest to the average \pm three standard deviations) have been excluded on the basis that we did not want the regression coefficients to be affected by some statistically insignificant rare cases. After eliminating the redundancies the final set has been reduced to 228 profiles. This set contained approximately 20 profiles in each class and has a similar statistical pattern to the original dataset.

4. Radiative transfer computation

For the radiance computations the High Resolution Radiative Transfer Code (HARTCODE) was used with the GEISA 97 absorption line catalog (Miskolczi *et al.*, 1990). In addition to the H_2O and O_3 , there are nine molecular species that exhibit significant absorption in the GLI IR channels. The volume mixing ratio profiles of these absorbers (CO_2 , N_2O , CH_4 , NO , SO_2 , NO_2 , CCl_4 , F11 and F12) were taken partly from the seasonal standard atmospheres. CCl_4 , F11 and F12 mixing ratio profiles were measured at the Oklahoma ARM site. To create a physically consistent data set, after merging the additional absorbers into the TIGR profiles, a new exponential layering was introduced. The top altitude was set to 61.2 km and the number of the layers were reduced to 32. The new layers have a geometrical thickness of about 100 m at the bottom and 10 km at the top. The outgoing radiances were computed with 1 cm^{-1} spectral resolution in 9 different viewing angles, which makes a total of 2052 high resolution radiance spectra. In the convolution of the radiance spectra with the filter functions, the radiance spectra were interpolated to the higher resolution discrete points of the filter functions. The 1 cm^{-1} resolution was sufficient for the accurate evaluation of channel radiances in Eq. (3). The α_k regression coefficients in Eq. (4) were determined by singular value decomposition. In the present study, the first 6 GLI channels were utilized and in each group of profiles 9 set of regression coefficients were generated for each viewing angle. The reason of using 9 set of coefficients for 9 different viewing angles is in the fact that no uniform limb darkening function exists, even within one group of profiles. The best retrieval results are expected by using interpolated regression coefficients with respect to the viewing angles.

5. Results

According to test computations, the derived α_k regression coefficients were very stable, they were not sensitive to a 0.2 K white noise added to the scene temperatures, therefore, the regression coefficients were assumed to be error free. There

is no effect of the brightness temperature correction on the accuracy of the retrieval. This is expected, since the standard error in a linear regression scheme is invariant for the linear transformations of the variables. However, the use of brightness temperature instead of channel radiance improves the explained variance by about 4 to 5 per cent. It is interesting to note that the conversion of channel radiances into brightness temperatures or scene temperatures is not always beneficial. For example, in retrieving water vapor effective pressure, p_e , it is better to use directly the channel radiance. In *Figs. 3, 4* and *5* the different kinds of errors of the skin temperature retrievals as the function of the viewing angles are displayed. In all cases the computations were based on the estimated scene temperatures using Eqs. (5).

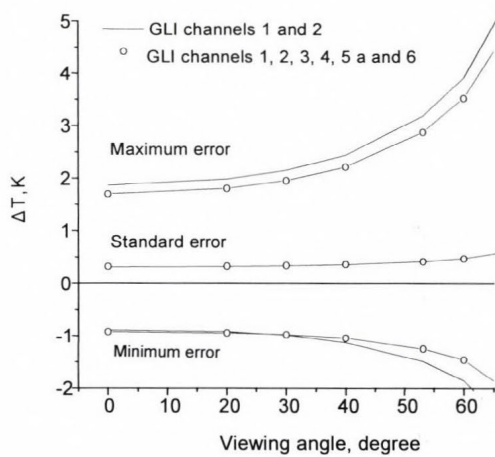


Fig. 3. Skin temperature errors in case of applying two or six spectral channels in the retrievals. (Full data set, no classes, 0.1 K noise.)

Fig. 3. shows the dependence of the errors on the number of the channels involved in the retrieval. In this case all the profiles in the 11 classes were merged into one large group of 228 profiles. It is surprising that adding an additional window channel and the three water vapor channels has no noticeable effect on the standard error, however, the minimum and maximum errors were slightly reduced. Probably there is a better way to use the information content of the excess channels than to include them directly into the regression scheme.

In *Fig. 4* the effect of the grouping of the profiles are presented. Here the retrievals were based on the first 6 channels of the GLI. Apparently the accurate limb darkening corrections by using sets of regression coefficients for the different viewing angles are necessary to achieve an accuracy of around 0.1 K.

Fig. 5 shows the dependence of the errors on the noise equivalent temperatures. In this cases regression coefficients were generated for each class and viewing angle. The scene temperatures were loaded with a zero-mean white noise of different standard deviations. The close to linear degrading effect due to the measurement noise is obvious. The zero-noise curve at around 0.05 K can be regarded as a “theoretical” upper accuracy limit that can be obtained using simple linear regression methods.

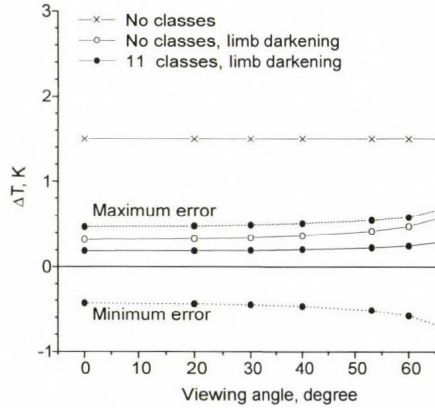


Fig. 4. Skin temperature errors in case of three different grouping. (2052 spectra in 1, 9 or 99 groups, 0.1 K noise.)

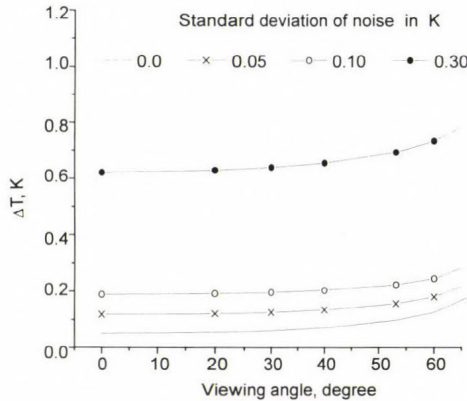


Fig. 5. Skin temperature errors in case of four different load of “white” noise.

6. Conclusions

Accurate skin temperature retrieval on global and annual scales can only be achieved by applying several sets of regression coefficients for the different regions, seasons and viewing angles. Limitations related to the instrument noise have been estimated. For the GLI instrument, assuming an average 0.08 K noise, the 0.3 K accuracy (in the sense of standard errors) is realistic. The target accuracy of the retrieval, using for example the GOES -10 imager, (assuming ~0.3 K noise and using less channels), could be around 0.6–0.8 K. Other conclusion is that sophisticated algorithms for the brightness temperature corrections using ideal black body, or even real atmospheric spectra, have no practical value when applying in a linear regression scheme. Further on, involving more H₂O and window channels into the retrieval will not increase the accuracy significantly. It seems that the only way of improvement is to reduce the noise in the spectral channels to or below 0.05 K.

References

- Chedin, A. and Scott, N., A., 1983: The improved initialization inversion procedure. *First International TOVS Study Conference*, Igls, Austria, August, 1983.
- Miskolczi, F., Rizzi, R., Guzzi, R., and Bonzagni, M, 1990: High-resolution Radiance-Transmittance Code. *Meteor. Environ. Sci. Elsevier Pub. Co.* 743-790.
- Weinreb, M.P., Jamieson, M., Fulton, N., Chen, Y., Johnson, J.X., Smith, B., and Baucom, J., 1997: Operational calibration of geostationary operational environmental satellite imagers asounders. *Applied Optics* 36, 6895-6904.

IDŐJÁRÁS

Quarterly Journal of the Hungarian Meteorological Service
Vol. 105, No. 4 — Vol. 106, No. 1, October 2001 — March 2002, pp. 253-263

On the use of satellite-derived climatological data sets to map global land surface temperature range

Iván A. Csiszár

University of Maryland, Department of Geography
1121 LeFrak Hall, College Park, Maryland 20742 USA
E-mail: icsiszar@hermes.geog.umd.edu

(Manuscript received November 28, 2001)

Abstract—The long data record from operational environmental satellites allows the long-term, large-scale mapping of various characteristics of the Earth. This paper focuses on the diurnal temperature range (DTR) over land. The availability of necessary daytime and nighttime infrared radiation measurements within the various long-term satellite-based data sets is discussed. We conclude that currently the most suitable data sets for global DTR mapping are those that were produced by projects originally designed for the observation of atmospheric parameters: the International Satellite Cloud Climatology Project (ISCCP; mostly geostationary at low and mid-latitudes) and the Pathfinder Atmosphere from AVHRR (PATMOS; polar only). While ISCCP has more frequent sampling of the diurnal temperature cycle, there exists a large data gap over Asia due the lack of geostationary satellites. It is suggested that PATMOS data be used to fill this gap. However, daytime and nighttime PATMOS data need to be corrected for the effects of the local times of observation, which are not coincident with the times of occurrence of the daily maxima and minima. We demonstrate that, over hot surfaces, significant differences exist between coincident PATMOS surface temperatures and those from ISCCP corresponding to the same local time, indicating differences in calibration and/or in deriving surface skin temperature from top-of-the-atmosphere radiances. Residual differences also exist between coincident ISCCP and PATMOS daytime-nighttime temperature differences, suggesting that appropriate ISCCP to PATMOS normalization be made prior to adjusting PATMOS data for diurnal cycle effects to derive DTR maps.

Key-words: satellite data sets, land surface temperature, satellite observing systems

1. Introduction

Diurnal temperature range (DTR) is an important surface characteristic related to thermal inertia (*Price, 1977*). However, the properties of DTR on a global scale have not been investigated in detail. On a global scale, DTR can be

mapped and monitored only from space. Ideally, satellite measurements of the daily minimum and maximum temperatures are needed.

Operational geostationary environmental satellites (GOES, METEOSAT, INSAT, GMS,) have been providing meaningful temperature measurements between $\sim 60^{\circ}\text{S}$ and 60°N latitudes at a high temporal frequency, allowing the accurate estimation of daily temperature minimum and maximum. While thus the temporal sampling is sufficient for DTR mapping, the inter-satellite differences require a careful inter-calibration of the data (*Desormeaux et al.*, 1993).

The Advanced Very High Resolution Radiometer (AVHRR) on board the polar orbiting National Oceanic and Atmospheric Administration (NOAA) satellites has been providing global, near-continuous measurements over the last ~ 20 years. As AVHRR has on-board calibration capability of the infrared channels, in a radiometric sense the AVHRR data is relatively stable. While long-term records of its original 1-km resolution Local Area Coverage (LAC) measurements exist on a regional basis, full global continuous coverage is available only at the 4-km Global Area Coverage (GAC) resolution (*Gutman et al.*, 2001). GAC data are created from the 1-km data by a sampling and averaging procedure (*Kidwell*, 1998). From the six-hourly AVHRR measurements, the daytime (ascending orbit) and nighttime (descending orbit) temperature measurements from the “afternoon” satellites are the most useful for DTR mapping. However, the time of the observations rarely coincides with the occurrence of either the daily minimum or the daily maximum. In general, the inappropriate temporal sampling poses a bigger problem at daytime, when the temperature changes more rapidly over time. (Note that near the poles the overlapping orbits provide a much higher frequency of observations.)

Data from the geostationary and polar satellite systems have been collected and processed into well-documented climate data sets, particularly within the NOAA/NASA (National Aeronautics and Space Administration) Pathfinder Program (*Ohring and Dodge*, 1992). The World Climate Research Programme (WCRP) Global Energy and Water Cycle Experiment (GEWEX) also provides framework for the creation and collection of satellite data sets, in particular within the International Satellite Land Surface Climatology Project (ISLSCP, *Sellers et al.*, 1995) and the International Satellite Cloud Climatology Project (ISCCP, *Schiffer and Rossow*, 1983).

Long-term time series of daytime and nighttime measurements from the various operational geostationary and polar orbiting satellites are available from ISCCP. (Some of the specifications of the ISCCP products were defined at the Meeting on Real-time Satellite-derived Cloud Climatology in Balatonalmádi, Hungary in June 1980.) Although this data set was primarily designed for atmospheric applications, the clear-sky radiances allow the mapping of surface temperatures. This will be the primary data set considered in this paper for DTR mapping.

In principle, satellite-based DTR mapping also can be done by data from the global, long-term data sets that have been constructed from AVHRR data. The various existing data sets were designed to provide information for different applications. In general, surface applications require higher resolution data than atmospheric applications. The major such data sets are: the NASA Pathfinder Land data set (*James and Kalluri, 1994*), the NOAA/NESDIS Global Vegetation Index data set (*Gutman et al., 1995*), Global Inventory Mapping and Modeling Studies (*Los et al., 1994*), and the Global Land 1-km AVHRR data set (*Eidenshink et al., 1994*). A common characteristic of these data sets is that daytime AVHRR data are preprocessed and mapped on a daily basis and then sampled in time into weekly or 10-day composites. Unfortunately, none of them include nighttime measurements and thus their usefulness for DTR mapping is limited.

The only AVHRR-based global, long-term data set that can be used for DTR mapping is the NOAA/NESDIS Pathfinder Atmosphere (PATMOS) data set, which includes daytime and nighttime AVHRR-derived radiance products from 1981 through 2000 on a global 10,000 km² equal-area grid (*Stove et al., 2002*). Although this data set was created primarily for atmospheric applications, its clear-sky long-wave radiance products can be converted into surface temperatures. Thus, in addition to ISCCP, we will analyze PATMOS data for DTR mapping.

Note that surface temperature products are also available from data sets from other instruments on polar orbiting satellites, such as the Pathfinder TOVS (TIROS Operational Vertical Sounder on board the NOAA satellites) or Pathfinder SSM/I (Special Sensor Microwave Imager on board the Defense Meteorological Satellite Program satellites). As in many aspects the DTR mapping from TOVS and SSM/I these data have similar issues with AVHRR, they will not be discussed further in this paper. Also, data from the GOES Pathfinder project will not be discussed because of its limited spatial coverage.

In the remaining sections of this paper we analyze the relative merits of the ISCCP and PATMOS data sets for long-term, global DTR mapping. Description of the data used is provided in Section 2. Section 3 presents an inter-comparison of data from PATMOS and ISCCP, followed by discussion and conclusions in Section 4.

2. The ISCCP and PATMOS data sets

2.1 ISCCP

From the suite of ISCCP products, we used the “mean surface (skin) temperature (T_s) from clear sky composite” product from the ISCCP Monthly Cloud Product D-2 data set from the 1984–1993 period. D-2 is a statistical

summary of the original satellite observations presented as monthly means in eight 3-hour intervals, from 00 through 24 UTC, mapped globally in an equal-area $(280 \text{ km})^2$ projection (Rossow *et al.*, 1996). T_s is derived from clear-sky infrared radiances corrected for water vapor absorption, assuming a surface emissivity of unity. In assigning data to a certain grid cell, data from geostationary satellites are preferred over polar data. Unfortunately, the ISCCP spatial coverage is poor over Central Asia, where only some observations from polar satellites are available due to the lack of coverage from the geostationary INSAT satellite (except for a 1-year period starting in April 1988). *Fig. 1* shows data coverage in July 1993. Note the data gaps at 6 and 9 UTC, the time of the daily skin temperature maximum in that region. (Surface skin temperature very closely follows the solar radiative heating and thus on a cloud-free day daily skin temperature maximum occurs shortly after the local noon.) Missing data at 18 and 21 UTC indicate the lack of information on minimum temperature.

Filling these data gaps is one of the major issues of global DTR mapping. One plausible way is to establish relationships between ISCCP (mostly geostationary) and PATMOS (polar AVHRR) data outside the Asian gap and then use those relationships to estimate DTR within that region. In this context, AVHRR data from PATMOS are preferred to AVHRR data from ISCCP over the Asian gap because of possible effects of PATMOS-AVHRR preprocessing differences and consequent data incompatibility.

To estimate more precisely the daily maximum and minimum temperatures, an hourly global (except for the Asian gap) ISCCP-based surface temperature database was constructed by converting the 3-hour GMT time slots into local times, and interpolating the surface temperatures with cubic splines into a regular 1-hour grid. This database was used to specify daily maximum (T_{\max}) and minimum (T_{\min}) temperatures. DTR was calculated as $\text{DTR} = T_{\max} - T_{\min}$.

2.2 PATMOS

In the current analysis we used monthly mean daytime and nighttime, clear-sky, channel 4 and 5 brightness temperatures (T_{4d} , T_{4n} , T_{5d} and T_{5n}) derived from the corresponding long-wave radiance products and re-projected onto the ISCCP global grid. From the top-of-the-atmosphere brightness temperatures daytime (T_{sd}) and nighttime (T_{sn}) skin temperatures were derived by the split-window equation from *Becker and Li (1990)*:

$$T_{sx} = a + T_{4x} + b(T_{4x} - T_{5x}), \quad x = d, n \quad (1)$$

using updated coefficients for each NOAA satellite by *Czajkowski et al.*

(1998). These formulae assume blackbody (i.e., emissivity=1) surface and thus are compatible with the way ISCCP skin temperatures were derived.

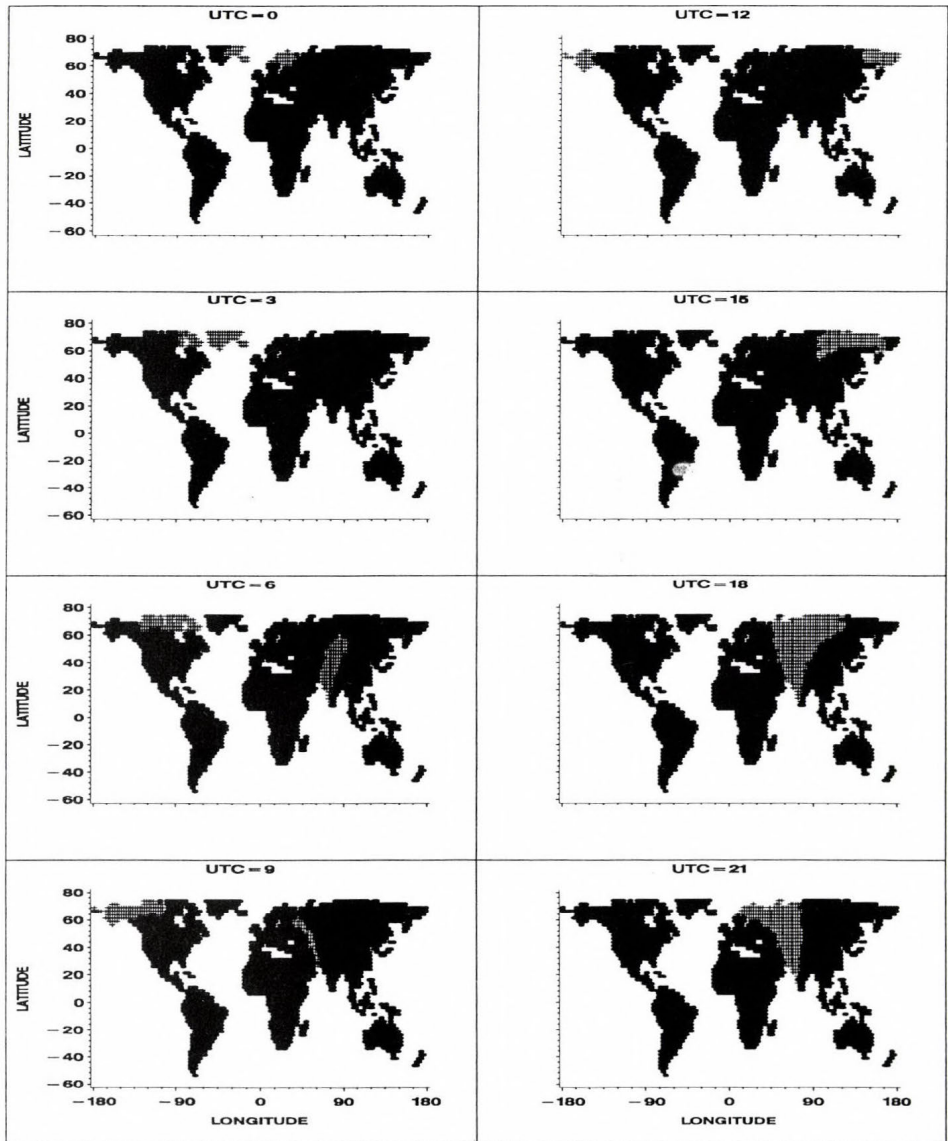


Fig. 1. Coverage of ISCCP D-2 data over land in July 1993.

While the nighttime AVHRR temperature measurements are often near the daily minimum, the daytime measurements are taken in the mid-afternoon, when the surface temperature is usually different from the daily maximum. The problem is aggravated by the orbital drift of the NOAA satellites (*Fig. 2*), which causes several hours of difference in the local time of observation over several years (*Price, 1991*). Additionally, within a given satellite orbit, there is an ~ 90 -minute difference between the local times of observation in the mid-latitudes of the Southern and Northern hemispheres (*Fig. 3*). Thus, careful adjustment of the measurements according to the local time of observation is necessary (*Gutman, 1999*). Note that the monthly mean temperatures used here are averages of temperatures corresponding to $\pm 55.4^\circ$ satellite scan angles, a ~ 2700 km wide swath and an ~ 1.5 hour local time difference therein. In this paper we assume that the monthly averaging compensates for these differences in daily observations and that the monthly mean characterizes the average conditions at nadir view.

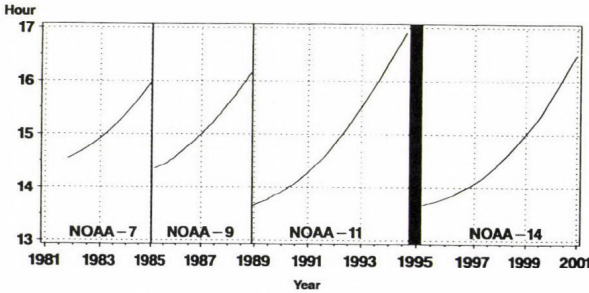


Fig. 2. Equator crossing times of the “afternoon” NOAA satellites.

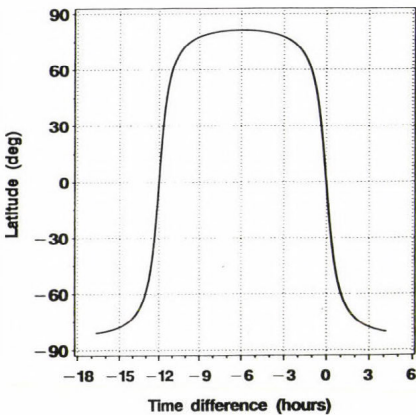


Fig. 3. Time difference between the local time of the equator crossing (ascending) and the local time of observation along a full orbit of a NOAA satellite. Note that the satellite’s actual movement along its orbit corresponds to a movement along the curve from the right towards the left on this figure.

3. Comparison of skin temperatures from ISCCP-D2 and PATMOS

We can consider the daytime-nighttime AVHRR temperature difference as a first-order estimate of DTR and develop corrections to it using ISCCP-derived DTR as training data. The error in the AVHRR-based estimate of DTR is mainly in the decrease of the afternoon temperature with the local time of observation and thus its deviation from the daily maximum. Fig. 4 shows the relationship between the PATMOS and ISCCP temperatures. The PATMOS daytime temperatures (Fig. 4a) deviate considerably from the daily maximum for high temperature values. This can be explained by the strong afternoon decrease of skin temperature in hot, mainly desert areas. The PATMOS nighttime temperatures (Fig. 4b), on the other hand, show good agreement with the daily minima, confirming a lower rate of temperature change in the hours before sunrise. The “daily mean temperature” from PATMOS ($[T_{sd} + T_{sn}]/2$) remains close to that derived from ISCCP daily minimum and maximum values (Fig. 4c), but the PATMOS “daily temperature range” ($T_{sd} - T_{sn}$; Fig. 4d) has a significant error for high values of DTR, driven by the high ($T_{\max} - T_{sd}$) difference.

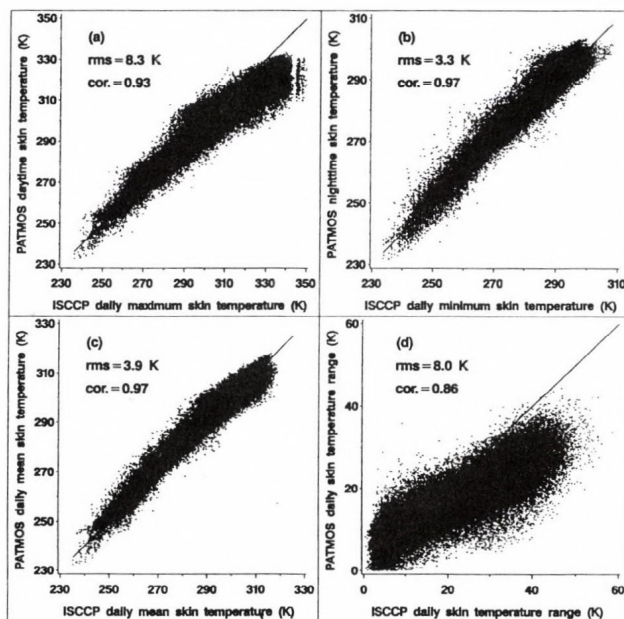


Fig. 4. Comparison of PATMOS daytime and nighttime surface skin temperatures with ISCCP daily maximum and minimum values and the daily means and daily temperature ranges derived from them.

In addition to the differences in the time of observation, some of the scatter of the data is caused by residual cloud effects inherent in both the ISCCP and PATMOS clear sky products, and by preprocessing differences, such as calibration and spatio-temporal sampling.

To analyze the compatibility of ISCCP and PATMOS surface skin temperatures, the data need to be brought to a common time of observation. This was done by selecting the ISCCP temperature values that are nearest to the actual local time of observation of the PATMOS (AVHRR) data by the following procedure:

- The equator crossing time of the NOAA satellite was determined from the year and month of the PATMOS data (Fig. 2).
- The difference between the equator crossing time and the local time of observation was calculated from the latitude of the PATMOS data, separately for the ascending (daytime) and descending (nighttime) parts of the orbit (Fig. 3).
- The actual local time of PATMOS data was calculated.
- ISCCP data corresponding to the nearest hour in local time of the PATMOS data was selected.

The results of the PATMOS-ISCCP match-up are shown in Fig. 5. Daytime temperatures (Fig. 5a) are now somewhat closer than in Fig. 4a, as the better statistics indicate. However, there is still a remarkable difference for warm temperatures, with ISCCP values systematically higher than PATMOS. This confirms that, in addition to differences in the time of observation, other factors also contribute to the ISCCP-PATMOS deviation, such as calibration differences and differences in deriving skin temperature. A significant overestimation of instantaneous AVHRR top-of-the atmosphere brightness temperatures by coincident instantaneous geostationary data has been observed in Australia (*J. Janowiak*, NOAA/CPC, 2001, personal communication) and Africa (*P. Romanov*, NOAA/NESDIS, 2001, personal communication). This suggests that of the two effects mentioned above, calibration is the more important one. In addition, this is an indication that—assuming a more reliable AVHRR calibration—the rigorous geostationary to polar orbiter (AVHRR) calibration normalization procedure within ISCCP (*Brest et al.*, 1998), may have residual errors for warm targets. Detailed analysis of the ISCCP and PATMOS infrared calibration procedures however is beyond the scope of this paper.

Nighttime temperatures, as expected, are again in good agreement. However, one still would expect some improvement in the statistics after the temporal matching of the data. But if we assume that ISCCP indeed overestimates temperatures (particularly warm ones), we should in fact expect a better

agreement between ISCCP daily minimum—with a warm bias—and PATMOS, taken a few hours before the daily minimum and thus being somewhat warmer than the daily minimum. Having just a slightly lower RMS and a somewhat lower correlation in the time-matched nighttime temperatures is thus consistent with our earlier finding; however, as the temperatures in general are lower at nighttime, the differences are not so significant as between Figs. 4a and 5a.

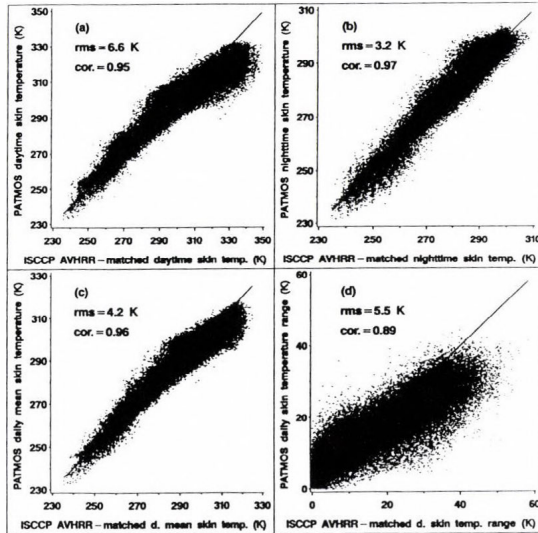


Fig. 5. Comparison of PATMOS daytime and nighttime surface skin temperatures with ISCCP temperatures corresponding to the time of the AVHRR observations within PATMOS. Daily means and daily temperature ranges are also shown.

Note that in this figure (and also in Fig. 4 for PATMOS-derived parameters) the “daily means” and “daily skin temperature ranges” are not the true values because they were not derived from daily minima and maxima, but from temperatures at the times of the AVHRR observations in PATMOS. However, because of the temporal matching, ideally, the plots in Figs. 5c and 5d now should run along the one-to-one line. But the combination of the calibration effects on daytime and nighttime data yields a slightly higher deviation of the “daily mean” values (Fig. 5c) than in Fig. 4c. The “DTR” values (Fig. 5d) show considerably better statistics than in Fig. 4d. However, the ISCCP-PATMOS difference still increases with temperature, but in a clearly more linear fashion than in Fig. 4d. This suggests that diurnal cycle effects—including their dependence on surface type and temperature—have been removed and the

residual error is mostly due to sensor calibration differences, with some scatter of the data because of incompatible cloud screening etc.

4. Summary and conclusions

Currently, the most plausible method of deriving monthly global maps of diurnal temperature range is to use monthly mean clear-sky statistics of daily maximum and minimum temperatures from ISCCP. However gaps in the spatial coverage from geostationary satellites exist particularly over the Central Asian region. To achieve a fully global coverage, ISCCP data need to be combined with other data sets, of which the AVHRR-based PATMOS appears to be the most suitable candidate.

A simple comparison of daily maximum and minimum temperatures from ISCCP, and daytime and nighttime temperatures from PATMOS has shown that there exist significant differences between them that affect DTR mapping. In general, a positive bias in ISCCP calibration for warm targets is suspected. At daytime, this calibration bias and the temperature bias caused by the later local time of the daytime AVHRR observation sum up. At nighttime, however, both effects are smaller and rather tend to cancel each other. Thus, a temporal matching of the ISCCP and PATMOS data decreases the difference at daytime and basically has no effect at nighttime. Residual calibration differences are still visible in the comparison of daytime-nighttime temperature ranges from ISCCP and PATMOS. This suggests that, in using ISCCP as a training database to derive a relationship between DTR values from PATMOS, a two-step procedure needs to be followed. First, an adjustment between ISCCP and PATMOS temperatures needs to be done (presumably rather the normalization of ISCCP to PATMOS than vice versa). Only after this step should one attempt to make adjustments for the diurnal cycle effects inherent in the PATMOS dataset.

The multi-year, monthly maps derived from PATMOS and ISCCP using the principles outlined in this paper will allow the study of the regional characteristics of the annual cycle of DTR and its inter-annual variability. Relationships between DTR and independent observations of surface characteristics (such as vegetation indices) or atmospheric effects (precipitation, cloud cover etc.) can be analyzed.

To derive higher resolution, global DTR maps, considerations need to be made for the more extensive archival and use of nighttime observations from polar orbiting satellites for land surface studies. Current efforts at NOAA and NASA in defining the future strategy of creating satellite-based climate data sets is a good opportunity to take appropriate action towards this goal.

References

- Becker, F. and Li, Z., 1990: Towards a local split window method over land surfaces. *Int. J. Remote Sens.* 11, 369-393.
- Brest, C.L., Rossow, W.B., and Roiter, M., 1997: Update of Radiance Calibrations for ISCCP. *J. Atmos. Ocean. Tech.* 14, 1091-1109.
- Czajkowski, K.P., Goward, S.N., and Ouaidrari, H., 1998: Impact of AVHRR filter functions on surface temperature estimation from the split window approach. *Int. J. Remote Sens.* 19, 2007-2012.
- Desormeaux, Y., W.B. Rossow, C.L. Brest, and C.G. Campbell, 1993: Normalization and calibration of geostationary satellite radiances for ISCCP. *J. Atmos. Ocean. Tech.* 10, 304-325.
- Eidenshink, J.C. and Faundeen, J.L., 1994: The 1 km AVHRR global land data set: first stages of implementation. *Int. J. Remote Sens.* 15, 3443-3462.
- Gutman, G., 1999: On the monitoring of land surface temperatures with the NOAA/AVHRR: Removing the effect of satellite orbit drift. *Int. J. Remote Sens.* 20, 3407-3413.
- Gutman, G., Tarpley, D., Ignatov, A., and Olson, S., 1995: The enhanced NOAA Global Land Dataset from the Advanced Very High Resolution Radiometer. *Bull. Amer. Meteorol. Soc.* 76, 1141-1156.
- Gutman, G., Elvidge, C., Csiszár I., and Romanov, P., 2001: NOAA Archives of Data from Meteorological Satellites Useful for Fire Products. In *Global and Regional Fire Monitoring from Space: Planning a Coordinated International Effort* (eds.: F. Ahern, J. Goldammer and C.O. Justice (SPB Academic Publishing, The Hague, The Netherlands), pp. 257-266.
- Ignatov, A. and Gutman, G., 1999: Monthly mean diurnal cycles in surface temperatures over land for global climate studies. *J. Climate* 12, 1900-1910.
- Rossow, W. and Schiffer, R., 1991: ISCCP cloud data products. *Bull. Amer. Meteorol. Soc.* 72, 2-20.
- James, M.E. and Kalluri, S.N.V., 1994: The Pathfinder AVHRR land data set: an improved coarse resolution data set for terrestrial monitoring. *Int. J. Remote Sens.* 15, 3347-3363.
- Kidwell, K.B. (ed.), 1998: *NOAA Polar Orbiter Data Users Guide*. U.S. Department of Commerce, National Oceanic and Atmospheric Administration, National Environmental Satellite Data and Information Service, National Climatic Data Center.
- Los S.O., Justice, C.O., and Tucker, C.J., 1994: A global $1^\circ \times 1^\circ$ NDVI data set for climate studies derived from the GIMMS continental NDVI data. *Int. J. Remote Sens.* 15, 3493-3518.
- Ohring, G. and Dodge, J., 1993: The NOAA/NASA Pathfinder Program. In *IRS'92: Current Problems in Atmospheric Radiation*. A. Deepak Publishing, Hampton, Virginia, USA, pp. 405-408.
- Price, J.C., 1977: Thermal inertia mapping: a new view of the Earth. *J. Geophys. Res.* 18, 2582-2590.
- Price, J.C., 1991: Timing of NOAA afternoon passes. *Int. J. Remote Sens.* 12, 193-198.
- Rossow, W.B., Walker, A.W., Beuschel, D.E., and Roiter, M.D., 1996: International Satellite Cloud Climatology Project (ISCCP). Documentation of new cloud data sets. World Meteorological Organization, World Climate Research Programme.
- Schiffer, R.A. and Rossow, W.B., 1983: The International Satellite Cloud Climatology Project (ISCCP): The first project of the World Climate Research program. *Bull. Amer. Meteor. Soc.* 64, 779-784.
- Sellers, P.J., Meeson, B.W., Hall, F.G., Asrar, G., Murphy, R.E., Schiffer, R.A., Bretherton, F.P., Dickinson, R.E., Ellingson, R.G., Field, C.B., Huemmrich, K.F., Justice, C.O., Melack, J.M., Roulet, N.T., Schimel, D.S., and Try, P.D., 1995: Remote sensing of the land surface for studies of global change: Models-algorithms-experiments. *Remote Sens. Environ.* 51, 3-26.
- Stowe, L.L., Jacobowitz H., Ohring, G., Knapp K.R., and Nalli, N.R., 2002: The advanced very high resolution radiometer pathfinder atmosphere (PATMOS). Data set. *J. Climate*, in press.

IDŐJÁRÁS

Quarterly Journal of the Hungarian Meteorological Service
Vol. 105, No. 4 — Vol. 106, No. 1, October 2001 — March 2002, pp. 265-278

Observations of three-dimensional radiative effects that influence satellite retrievals of cloud properties

Tamás Várnai¹ and Alexander Marshak

*Joint Center for Earth Systems Technology of University of Maryland,
Baltimore County, and NASA Goddard Space Flight Center*

(Manuscript received October 5, 2001; in final form November 27, 2001)

Abstract—This paper examines three-dimensional (3D) radiative effects, which arise from horizontal radiative interactions between areas that have different cloud properties. Earlier studies have argued that these effects can cause significant uncertainties in current satellite retrievals of cloud properties, because the retrievals rely on one-dimensional (1D) theory and do not consider the effects of horizontal changes in cloud properties. This study addresses two questions: which retrieved cloud properties are influenced by 3D radiative effects, and where 3D effects tend to occur. The influence of 3D effects is detected from the way side illumination and shadowing make clouds appear asymmetric: Areas appear brighter if the cloud top surface is tilted toward, rather than away from, the sun. The analysis of 30 images by the Moderate Resolution Imaging Spectroradiometer (MODIS) reveals that retrievals of cloud optical thickness and cloud water content are most influenced by 3D effects, whereas retrievals of cloud particle size are much less affected. The results also indicate that while 3D effects are strongest at cloud edges, cloud top variability in cloud interiors, even in overcast regions, also produces considerable 3D effects. Finally, significant 3D effects are found in a wide variety of situations, ranging from thin clouds to thick ones and from low clouds to high ones.

Key-words: satellite, solar radiation, cloud property retrievals, inhomogeneous clouds

1. Introduction

Satellite measurements are often used to infer various cloud properties, such as the clouds' water content or particle size. Currently, the calculations assume that when a satellite measures the solar radiation reflected from a particular area of a cloud, the characteristics of this radiation are shaped by the cloud

¹ *Corresponding author address:* Tamás Várnai, Code 913, NASA GSFC, Greenbelt, MD 20771, USA. E-mail: varnai@climate.gsfc.nasa.gov

properties in that area only. In other words, the calculations rely on one-dimensional (1D) radiative transfer theory: They interpret the radiances measured at a particular pixel by assuming that the pixel's surroundings have identical cloud properties, with no changes in horizontal directions. This approach has the advantage of allowing an unambiguous interpretation of the measured radiance values, leading to a single set of estimated cloud properties. In contrast, if the full three-dimensional (3D) radiative transfer were considered (including horizontal interactions between areas that have different cloud properties), the radiances measured at a pixel could correspond to a variety of cloud properties: For example, a thin cloud could be as bright as a thicker cloud that was shaded by an even thicker cloud.

Since the mid-1980s, numerous theoretical studies have indicated that the 1D approximation can cause significant errors in satellite retrievals and that 3D radiative effects must also be considered (e.g., *Davies*, 1984; *Kobayashi*, 1993; *Barker and Liu*, 1995). Simulation results have indicated that, depending on the circumstances, 1D retrievals can yield clouds that are too thin or too thick, too rough or too smooth, artificially anisotropic, and asymmetric (e.g., *Marshak et al.*, 1995; *Zuidema and Evans*, 1998; *Várnai*, 2000). Unfortunately, detecting the influence of 3D effects in actual observations has proven to be a much more elusive task, mainly because of the difficulties in separating the influence of 3D effects from uncertainties in other factors, such as variations in cloud droplet size. The lack of observational evidence made it difficult to tell whether the 3D effects suggested by theoretical results really occur in the atmosphere. The main question has been not whether 3D radiative processes are calculated correctly for the clouds considered in theoretical studies, but whether the simulated clouds have realistic horizontal variability.

The first unambiguous observations of 3D effects emerged in the mid-1990s. First, several studies examining 30 m-resolution Landsat images found that for high sun, the diffusion of radiation inside clouds smoothes out small-scale variability—and so clouds appear more homogeneous than they really are (*Marshak et al.*, 1995; *Davis et al.*, 1997; *Oreopoulos et al.*, 2000). Around the same time, the statistical analysis of satellite data at resolutions ranging from 1 km to 30 km revealed that 3D effects make clouds appear too thick when the sun is very oblique (*Loeb and Davies*, 1996; *Loeb and Coakley*, 1998). In addition, new multiangle satellite measurements revealed that cloud reflection into forward oblique view directions is smaller than expected from 1D theory—and that the reduction can be caused by 3D effects (*Buriez et al.*, 2001; *Ákos Horváth, Iliana Genkova and Roger Davies*, 2001, personal communication). Most recently, *Várnai and Marshak* (2002) found a clear signal of 3D effects for moderately oblique solar illumination: Side illumination and shadowing effects make clouds appear asymmetric, as if clouds were brighter

and thicker on their side facing the sun than on the opposite side. This effect makes it more difficult to combine the satellite data with ground-based or airborne measurements on a pixel-by-pixel basis, distorts the histogram of retrieved cloud properties, and makes clouds appear rougher than they really are. On the positive side, theoretical simulations by *Várnai* and *Marshak* (2002) indicated that the observed asymmetry is closely related to the way 3D effects change the average cloud reflection of large areas—which suggests that one can use the observed asymmetry values to estimate the large-scale retrieval biases due to 3D effects.

The goal of this paper is to analyze observations of apparent cloud asymmetry in order to gain new insights into 3D radiative effects. First, Section 2 describes the satellite data used in this study and briefly discusses how the apparent cloud asymmetry is determined from the observations. Section 3 then analyzes the observations to see which retrieved cloud properties are influenced by 3D effects and to better understand in which clouds 3D effects tend to occur. Finally Section 4 offers a brief summary and a few concluding remarks.

2. Data and methodology

2.1 Satellite data used

This study uses measurements by the Moderate Resolution Imaging Spectroradiometer (MODIS) instrument on board the Terra satellite. Terra was launched on a polar sun-synchronous orbit in December 1999, and it orbits the Earth in 98 minutes with a 10:30 a.m. equatorial crossing time at a 705 km altitude. MODIS is a precursor instrument to the next generation of imagers that will replace the Advanced Very High Resolution Radiometers (AVHRR) on the operational polar-orbiting satellites of the National Oceanic and Atmospheric Administration (NOAA). MODIS takes measurements at 36 wavelengths ranging from 0.4 to 14.4 μm . The spatial resolution at the subsatellite point is 250 m, 500 m, or 1 km, depending on the wavelength. This study uses 1 km resolution data from two wavelengths, 0.86 μm and 11 μm . The 0.86 μm radiances are converted to reflectances (R) using the equation

$$R = \frac{\pi \cdot I}{\cos \Theta_0 \cdot F_0}, \quad (1)$$

where I is the radiance, Θ_0 is the solar zenith angle, and F_0 is the solar constant. The 11 μm radiances are transformed into equivalent brightness temperature values using the Planck formula (e.g., *Thomas and Stamnes*, 1999, p. 94).

Although AVHRR and other instruments also offer measurements at similar wavelengths, MODIS is particularly well suited for this study because of its high radiometric accuracy. Especially important is the sensitivity at 11 μm , because observations of small temperature changes are crucial for the adopted methodology. (MODIS images report temperature changes as small as 0.01 K, and the noise equivalent temperature difference is around 0.05 K (NASA, 2000).)

In addition to using radiance measurements, this study also uses some standard MODIS products freely available at http://daac.gsfc.nasa.gov/CAMPAIGN_DOCS/MODIS/index.shtml. In particular, we used the 1 km-resolution cloud optical thickness, cloud water path, and cloud particle size data; the 5 km-resolution land-water mask; and the solar and viewing zenith and azimuth angles.

MODIS data are distributed in approximately 2000 km by 2000 km segments called granules. This study used the central 450 km-wide portion of 30 granules, where the viewing zenith angle is less than 20° . This restriction eliminates potential difficulties that could arise for oblique views, such as areas being viewed twice or pixel sizes increasing. The 30 granules were taken from three days separated by 10-day intervals: May 14, May 25, and June 4, 2001. The 10-day separation ensures that the images are relatively independent from each other, because the weather systems observed on one day are not likely to still exist 10 days later. Ten granules were taken from each day—essentially all granules that satisfy the following two criteria. First, the central portion of the granule should cover mostly oceanic areas. This is helpful because cloud detection and cloud property retrievals are easier and more accurate over ocean than over land. Second, the sun should be moderately oblique, with solar zenith angles around 60° . (Due to the large size of MODIS images, the actual zenith angles vary between 45° and 75° , but they remain close to 60° most of the time.) Because of the Terra satellite's sun-synchronous orbit, this requirement implies that all granules are around 35°S latitude. Let us note that the images are from a similar season and latitude band as in Várnai and Marshak (2002)—which used images from November 2000 around 40°N latitude—but from the southern hemisphere. The specific granules used in this study are listed in Table 1.

Table 1. Dates and UTC times (hour:minute) that identify the granules used in this study

Date	Time
May 14, 2001	03:20, 05:00, 06:40, 09:55, 11:35, 16:30, 18:10, 19:50, 21:30, 23:05
May 25, 2001	01:25, 03:00, 04:40, 08:00, 11:15, 12:55, 17:50, 19:30, 21:10, 22:50
June 4, 2001	05:15, 06:55, 08:35, 10:15, 13:30, 15:10, 16:50, 18:30, 21:45, 23:25

2.2 Calculation of the apparent cloud asymmetry

This study follows the methodology described in Várnai and Marshak (2002). The method's basic assumption is that if the cloud top surface is not horizontal (as assumed in 1D theory), 3D radiative effects make pixels brighter or darker than they would be in 1D theory. The brightening or darkening is expected to come from changes in the solar illumination, depending on whether the cloud top is tilted toward or away from the sun. For any given $(1 \text{ km})^2$ cloudy pixel—for which the operational MODIS data processing retrieved a nonzero cloud optical thickness—the direction of the cloud slope is determined in two steps. First, Step 1 determines which two neighboring pixels in front and behind are closest to the solar azimuth. Step 2 then compares the $11 \mu\text{m}$ brightness temperatures (T) of these two neighbors. Because temperature tends to decrease with altitude, Step 2 declares that our pixel is on a slope tilted toward the sun if $T_{\text{front}} > T_{\text{behind}}$ and that it is on a slope tilted away from the sun if $T_{\text{front}} < T_{\text{behind}}$. Following Várnai and Marshak (2002), the two kinds of pixels will be identified as *illuminated* (subscript i) or *shadowy* (subscript s), even though no actual shadows are required for a pixel to be designated as shadowy.

Let us note that this designation can be made for pixels at local temperature minima and maxima as well, and even for pixels at cloud edges. The only exception is if both the neighbors in front and behind are cloud free—that is, if a single pixel contains both the illuminated and shadowy sides of a cloud. For such “isolated” pixels, the relationship between T_{front} and T_{behind} has much more to do with conditions at ground level than at the cloud top—and so these pixels are not considered in our calculations. Fortunately, such isolated pixels occur quite rarely: In the examined scenes, fewer than 2% of all cloudy pixels fall into this category.

Once all cloudy $(1 \text{ km})^2$ pixels in a $(50 \text{ km})^2$ area are designated as either illuminated or shadowy, the method compares the mean cloud properties of all illuminated pixels to the mean properties of all shadowy pixels. If the two mean values are close to each other, this indicates that 3D effects do not make much of a difference. If, however, there are large differences (e.g., if illuminated pixels are much brighter than shadowy pixels), then 3D effects are expected to be strong.

The approach described above assumes that the solar azimuth does not influence cloud development, and so the illuminated and shadowy slopes have statistically similar true cloud properties. One can argue that if 3D radiative effects did influence cloud development, the most likely consequence would be the enhancement and reduction in absorption at illuminated and shadowy slopes, respectively. This would make clouds geometrically asymmetric by making the buoyancy conditions different on the opposite clouds sides. The re-

sulting asymmetries in cloud top altitude should then make the brightness temperature fields asymmetric as well. *Fig. 1*, however, indicates that the brightness temperatures of illuminated and shadowy slopes are statistically identical, which suggests that 3D effects did not have a strong influence on the vertical growth of clouds. (Another possible consequence of 3D effects would be that the enhanced absorption in illuminated slopes could reduce droplet size through increased evaporation. Section 3, however, will show that this effect is not very large either.) Naturally, random processes (such as wind shear or the overlap of two cloud layers) can make clouds asymmetric in any particular area, but these effects should even out when a large number of areas are considered. As a result, if we see that the illuminated portions of $(50 \text{ km})^2$ areas are systematically brighter than their shadowy portions, 3D effects must be responsible for the systematic difference.

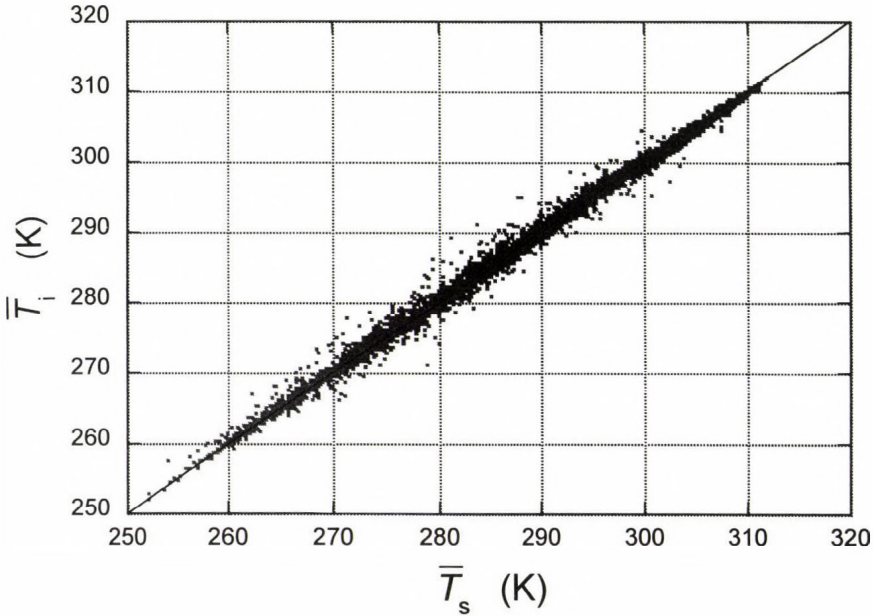


Fig. 1. Comparison of the mean brightness temperatures of illuminated (\bar{T}_i) and shadowy (\bar{T}_s) pixels. The overbar indicates averaging over $(50 \text{ km})^2$ areas, and so each point represents the mean values for a $(50 \text{ km})^2$ area. All figures are based on the 9410 areas in the examined 30 MODIS scenes that have a cloud coverage larger than 10%. (Areas with cloud coverage below 10% were not considered because of the large statistical uncertainties that may arise for them.)

3. Observations of 3D radiative effects

3.1 Analysis of 3D effects in retrievals of various cloud properties

Fig. 2 compares the $0.86 \mu\text{m}$ reflectances observed at illuminated and shadowy slopes. The figure clearly indicates that 3D effects are important in the examined scenes; the illuminated slopes are much brighter than the shadowy slopes. This intuitive tendency is in clear contrast to the behavior of $11 \mu\text{m}$ brightness temperatures in Fig. 1.

Fig. 2. Comparison of the mean $0.86 \mu\text{m}$ reflectances of illuminated (\bar{R}_i) and shadowy (\bar{R}_s) portions of $(50 \text{ km})^2$ areas.

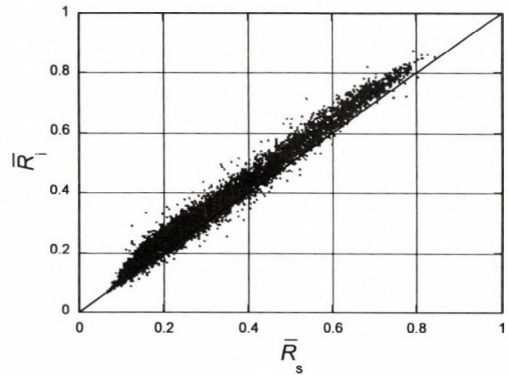


Fig. 3. Comparison of mean optical thicknesses retrieved at the illuminated ($\bar{\tau}_i$) and shadowy ($\bar{\tau}_s$) portions of $(50 \text{ km})^2$ areas.

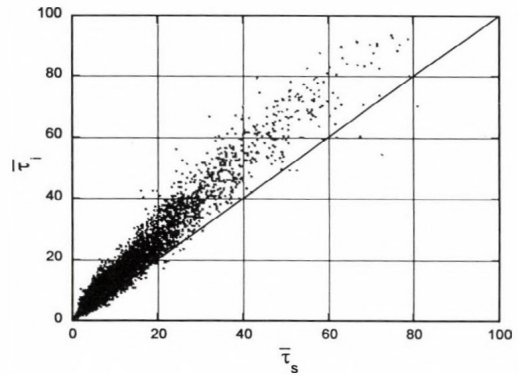


Fig. 3 shows that the 3D effects in Fig. 2 have a strong influence on optical thickness (τ) retrievals, which estimate much larger τ values at slopes tilted toward the sun. It is interesting to note that the asymmetries in Fig. 3 are about twice as strong as in Várnai and Marshak (2002): The median relative

difference between $\bar{\tau}_i$ and $\bar{\tau}_s$ is 26%, as opposed to the 13% in the earlier study. (The mean relative difference is 28%.) The discrepancy is probably related to differences in the distribution of cloud types in the two studies: Flat stratiform clouds that are close to the 1D ideal appear to be more frequent around 40°N in November (in the earlier study), whereas the bumpier convective clouds that cause stronger 3D effects are more frequent around 35°S in May (in this study). The differences indicate large regional or interannual variations in 3D radiative effects, and they highlight the need for comprehensive studies on the climatological distribution of 3D effects.

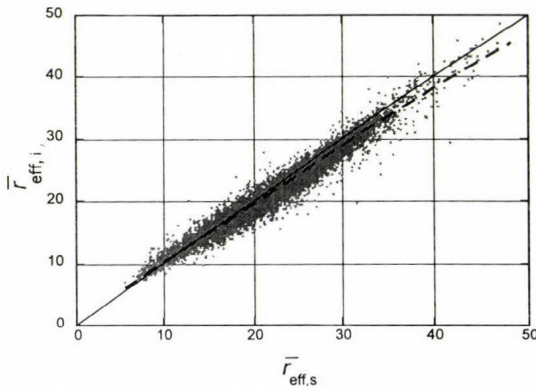


Fig. 4. Comparison of mean effective particle radii retrieved at the illuminated ($\bar{r}_{\text{eff},i}$) and shadowy ($\bar{r}_{\text{eff},s}$) portions of (50 km)² areas. The dashed line indicates a linear fit to the data.

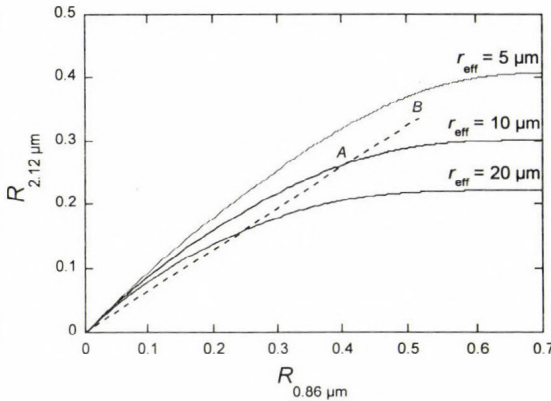


Fig. 5. Illustration of the concept of 1D effective particle radius retrievals. The figure displays the relationship between nadir cloud reflectances at 0.86 μm and 2.12 μm , which was calculated using 1D theory for three different droplet sizes. The sample calculations are for 60° solar zenith angle, completely transparent cloud-free air, and nonreflecting surface.

Fig. 4 indicates that retrievals of the effective particle size (r_{eff}) are influenced much less than, and in the opposite direction from, τ retrievals. The main reason for the opposite behavior is illustrated in Fig. 5, which depicts the

way particle size is retrieved from pairs of reflectance measurements at 0.86 and 2.12 μm . The retrievals use the algorithm of *Nakajima and King (1990)* to take advantage of the fact that absorption, and hence reflectance, depend strongly on droplet size. To explain the asymmetry in Fig. 4, let us assume that if 3D effects enhance the illumination of a pixel on an illuminated slope by a certain percentage, the 0.86 and 2.12 μm reflectances increase by a similar percentage. For example, if the true properties of the pixel put it at point *A* in Fig. 5 according to 1D theory, side illumination moves it to point *B* along the dashed line. The enhanced 2.12 μm reflectance is then interpreted by the 1D retrievals as if cloud absorption were smaller, that is, as if cloud droplets were smaller. On shadowy slopes the retrievals make the opposite error, thinking that the droplets are larger there. This overestimation of droplet size is further strengthened by the fact that absorption allows less 2.12 μm than 0.86 μm radiation to flow from the illuminated to the shadowy side inside the clouds, and so the 2.12 μm reflectance is actually reduced by a larger percentage than the 0.86 μm reflectance in shadowy slopes.

An additional factor contributing to the trend in Fig. 4 may be that—as mentioned in Section 2.2—the enhanced absorption at illuminated slopes strengthens the local radiative heating, and this increase weakens the condensational growth of cloud droplets on these slopes. Because, however, the combined effect of all these factors is quite small (about 1 to 2 μm), neither one of the contributing factors appears to be particularly strong.

After retrieving τ and r_{eff} , the operational MODIS data processing uses the results to calculate the clouds' water content (water path, or WP) from the equation

$$WP = \frac{2}{3} \rho \cdot \tau \cdot r_{\text{eff}}, \quad (2)$$

where ρ is the density of water (*King et al., 1997*). Since Figs. 3 and 4 show that 3D effects have a much stronger influence on retrievals of τ than of r_{eff} , it is not surprising that the water path—which is a product of τ and r_{eff} —shows a behavior similar to that of τ (Fig. 6). The median relative difference between the water path of illuminated and shadowy slopes is 23%.

Because theoretical simulations in *Várnai and Marshak (2002)* indicated that the observed asymmetries are closely related to the area-averaged biases caused by 3D effects, we can conclude that the results discussed above indicate that 3D effects introduce the largest errors in retrievals of τ and WP, whereas the retrievals of r_{eff} are much less affected.

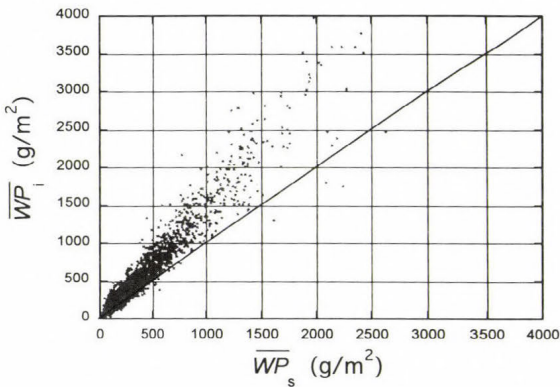


Fig. 6. Comparison of mean water paths retrieved at the illuminated (\overline{WP}_i) and shadowy (\overline{WP}_s) portions of $(50 \text{ km})^2$ areas.

3.2 Examination of where 3D radiative effects occur

Although the possibility of random asymmetries in true cloud properties prevents our technique from locating 3D radiative effects on a pixel-by-pixel basis, the technique can nevertheless yield valuable statistical information on where 3D effects tend to occur. One important question is whether 3D radiative effects are limited to some specific situations, or whether they occur under a wide range of circumstances. To address this question, *Fig. 7* plots the relative difference between the $(50 \text{ km})^2$ average water path values retrieved for illuminated and shadowy pixels, as a function of the mean optical thickness of the $(50 \text{ km})^2$ areas. The figure indicates that the relative difference increases rapidly until about $\tau \approx 5$, as multiple scattering (essential for any 3D effects) becomes more and more important. Once cloud reflection gets dominated by multiple scattering, however, the relative differences remain fairly constant. On one hand, this means that the absolute magnitude of 3D effects increases with cloud reflectance. On the other hand, the results reveal that clouds in a wide range of optical thicknesses are similarly effective in causing 3D radiative effects.

One can also use the available data to examine how 3D effects depend on cloud altitude. For this, *Fig. 8* displays the overall average water path of all $(1 \text{ km})^2$ illuminated and shadowy pixels (combined over all 30 scenes) as a function of cloud top pressure. (This pressure value is reported in the operational MODIS cloud product.) The figure reveals that average cloud thickness tends to increase with altitude—which is consistent with the idea that convective clouds contain more water as they grow taller. Although the absolute magnitude of 3D effects ($WP_i - WP_s$) increases with altitude accordingly, the inset reveals that clouds in a wide range of altitudes are similarly effective in creating strong 3D effects and that low-level clouds in the boundary layer are the most effective ones.

Fig. 7. Dependence of 3D effects on the $(50 \text{ km})^2$ average cloud optical thickness. The relative difference (D_r) is calculated

$$\text{as } D_r = \frac{(\overline{WP}_i - \overline{WP}_s)}{\left(\frac{\overline{WP}_i + \overline{WP}_s}{2}\right)} \cdot 100\% .$$

The solid line shows the local mean values at τ -steps of 2.5, and the error bars indicate the uncertainty of these mean values.

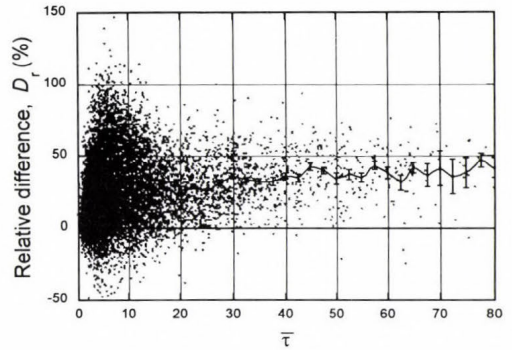
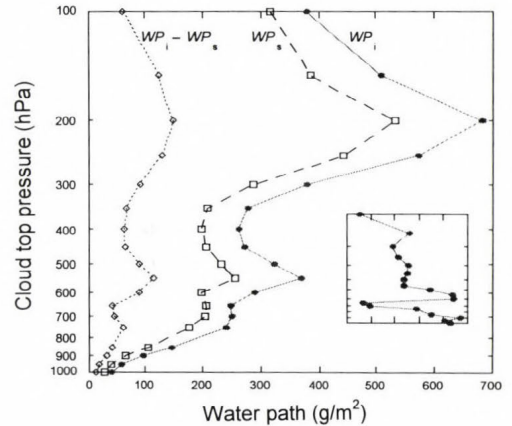


Fig. 8. Dependence of the overall average water path of illuminated (WP_i) and shadowy (WP_s) pixels on cloud top pressure. The dotted line indicates the difference $WP_i - WP_s$. The inset shows the overall average relative difference calculated as $\frac{(WP_i - WP_s)}{\left(\frac{WP_i + WP_s}{2}\right)} \cdot 100\%$ using all cloudy pixels in each cloud top pressure interval.



Finally, let us examine how 3D effects depend on cloud brokenness. For this, Fig. 9 plots the relative difference between the area average values for WP_i and WP_s as a function of the cloud coverage in $(50 \text{ km})^2$ areas. Although the cloud coverage is not a very good indicator of cloud brokenness (for example, 50% cloud coverage can occur not only in truly broken scenes, but also at the edges of large overcast cloud fields), the figure has two interesting features: It shows that 3D effects are quite important even in overcast scenes and that 3D effects become even stronger in broken clouds. These results suggest that cloud edges may be more effective than areas inside the cloud at creating 3D effects, but cloud top variations are also very important. These conclusions are confirmed clearly in Fig. 10, which displays the difference between the overall average WP_i and WP_s values (combined over all 30 scenes) as a function of the cloudy pixels' distance to the closest cloud-free pixel. As expected, the differences are largest right at the cloud edges, but they remain significant even in the interior of clouds.

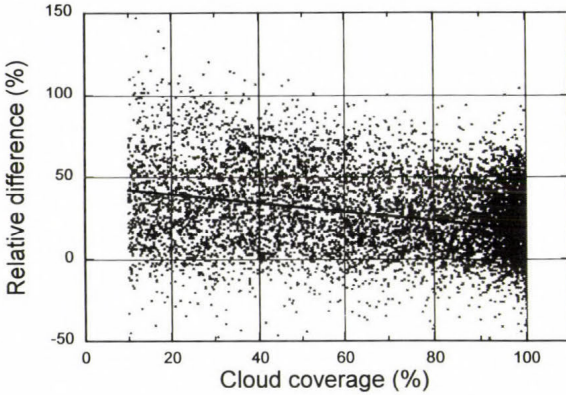


Fig. 9. Dependence of D_r values (defined as Fig. 7) on the cloud over of $(50 \text{ km})^2$ areas.

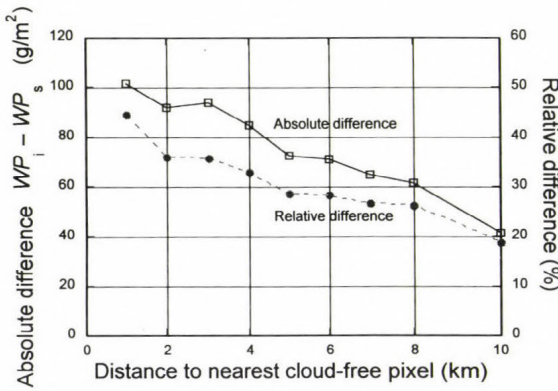


Fig. 10. Dependence of the illuminated-shadowy differences on the distance to the nearest cloud-free pixel. The relative difference is calculated as in Figs. 7 and 8, but combining all $(1 \text{ km})^2$ pixels in all 30 examined scenes (instead of combining only pixels in individual $(50 \text{ km})^2$ areas). The values displayed at a distance of 10 km represent the results for all distances greater than 8 km.

4. Summary

This study examined three-dimensional (3D) radiative effects, which arise from horizontal radiative interactions between areas that have different cloud properties. Current methods of retrieving cloud properties from satellite measurements do not consider these effects, because the retrievals rely on one-dimensional (1D) radiative transfer theory—that is, they treat each pixel as if it were surrounded by identical pixels, without any changes in horizontal directions. Although the 1D approximation has the advantage of allowing an unambiguous interpretation of the radiances measured at a given pixel, numerous studies have argued that not considering 3D effects can cause problems in the retrievals. This paper focused on two particular questions: which retrieved cloud properties are most influenced by 3D radiative effects, and where 3D effects tend to occur.

To address these questions, the study examined 30 images, 2000 km by 450 km each, by the Moderate Resolution Imaging Spectroradiometer (MODIS), which were taken in May and June 2001 over oceans around 35°S latitude. The images were analyzed using the method proposed in *Várnai and Marshak (2002)*. The method's basic idea is that if 3D effects are present in a scene, they make areas tilted toward the sun better illuminated—and consequently brighter—than the areas tilted away from the sun. This can result in systematic differences between the two kinds of areas, causing systematic asymmetries in the retrieved cloud properties. Thus, the method examines 3D effects by first estimating the tilt of cloud top surfaces from thermal infrared images, and then comparing the cloud properties retrieved for the two kinds of slopes.

The results revealed that 3D effects cause quite large uncertainties in the retrievals of cloud optical thickness and cloud water path: The median (and mean) difference between the values retrieved for areas tilted toward and away from the sun was about 25%. This result highlights that there are large regional differences in the importance of 3D effects, because, when *Várnai and Marshak (2002)* examined optical thickness fields, they found 3D effects only about half this strong in a similar season and latitude band in the northern hemisphere. In contrast, the present study found cloud particle size retrievals to be much less influenced by 3D effects: On average, droplet sizes were only about 1 to 2 μm larger on slopes that are tilted away, rather than toward, the sun.

The results also revealed that 3D radiative effects are not limited to some narrow range of situations or cloud types, because 3D effects remained significant over a wide range of cloud thicknesses and cloud top altitudes.

Finally, the results showed that although cloud edges are most effective in causing 3D radiative effects, cloud top variability is nearly as important. Consequently, 3D effects were found to be strongest in broken clouds, but they were quite significant even in large overcast regions.

Overall, the results highlight that the 1D approximation is a significant limitation in current techniques that retrieve cloud properties from shortwave satellite measurements. Because the simulation results of *Várnai and Marshak (2002)* indicate that the observed consequence of 3D radiative interactions (the apparent cloud asymmetry) is closely related to other consequences of 3D effects, the presented results have implications for a wide range of issues, from the interpretation of satellite measurements to the modeling of photochemical processes. The abundance of 3D effects indicates that radiative transfer in cloudy atmospheres is an inherently 3D process, and it highlights the need for new radiative transfer models that can move beyond the 1D framework both in remote sensing and in other applications involving radiative transfer calculations.

Acknowledgments—We appreciate funding for this research from the NASA EOS Project Science Office (under Grant NAG5-6675) and support from project scientist David O’C. Starr. We also thank Laura L. Atwood for proofreading the manuscript and providing helpful suggestions.

* * *

I am very happy to be able to contribute to this special issue honoring *Dr. Major*. I am deeply grateful to him for his support throughout my years at the Hungarian Meteorological Service, and for his help when I applied to graduate school.

Tamás Várnai

References

- Barker, H.W., and Liu, D., 1995: Inferring optical depth of broken clouds from Landsat data. *J. Climate* 8, 2620–2630.
- Buriez, J.-C., Dutriaux-Biucher, M., Parol, F., and Loeb, N.G., 2001: Angular variability of the liquid water cloud optical thickness retrieved from ADEOS-POLDER. *J. Atmos. Sci.* 58, 3007–3018.
- Davies, R., 1984: Reflected solar radiances from broken cloud scenes and the interpretation of satellite measurements. *J. Geophys. Res.* 89, 1259–1266.
- Davis, A., Marshak, A., Cahalan, R., and Wiscombe, W., 1997: The Landsat scale-break in stratocumulus as a three-dimensional radiative transfer effect, implications for cloud remote sensing. *J. Atmos. Sci.* 54, 241–260.
- King, M.D., Tsay, S.-C., Platnick, S., Wang, M., and Liou, K.-N., 1997: *Cloud retrieval algorithms for MODIS: Optical thickness, effective particle radius, and thermodynamic phase*. MODIS Algorithm Theoretical Basis Document No. ATBD-MOD-05, Version 5, NASA.
- Kobayashi, T., 1993: Effects due to cloud geometry on biases in the albedo derived from radiance measurements. *J. Climate* 6, 120–128.
- Loeb, N. G., and Davies, R., 1996: Observational evidence of plane parallel model biases: Apparent dependence of cloud optical depth on solar zenith angle. *J. Geophys. Res.* 101, 1621–1634.
- Loeb, N.G., and Coakley, J. A., 1998: Inference of marine stratus cloud optical depths from satellite measurements: Does 1D theory apply? *J. Climate* 11, 215–233.
- Marshak, A., Davis, A., Wiscombe, W., and Cahalan, R., 1995: Radiative smoothing in fractal clouds. *J. Geophys. Res.* 100, 26,247–26,261.
- Nakajima, T.Y., and King, M.D., 1990: Determination of the optical thickness and effective radius of clouds from reflected solar radiation measurements. Part I: Theory. *J. Atmos. Sci.* 47, 1878–1893.
- NASA, 2000: *MODIS—Moderate Resolution Imaging Spectroradiometer*. Available from http://modarch.gsfc.nasa.gov/MODIS/INSTRUMENT/modis_brochure.pdf
- Oreopoulos, L., Marshak, R., Cahalan, F., and Wen, G., 2000: Cloud 3D effects evidenced in Landsat spatial power spectra and autocorrelation functions. *J. Geophys. Res.* 105, 14,777–14,788.
- Thomas, G.E., and Stamnes, K., 1999: *Radiative Transfer in the Atmosphere and in the Ocean*. Cambridge University Press, 517 pp.
- Várnai, T., 2000: Influence of three-dimensional radiative effects on the spatial distribution of shortwave cloud reflection. *J. Atmos. Sci.* 57, 216–229.
- Várnai, T., and Marshak, A., 2002: Observations of three-dimensional radiative effects that influence MODIS cloud optical thickness retrievals. *J. Atmos. Sci.*, in press.
- Zuidema, P., and Evans, K.F., 1998: On the validity of the Independent Pixel Approximation for the boundary layer clouds observed during ASTEX. *J. Geophys. Res.* 103, 6059–6074.

IDŐJÁRÁS

Quarterly Journal of the Hungarian Meteorological Service
Vol. 105, No. 4 — Vol. 106, No. 1, October 2001 — March 2002, pp. 279-291

Operative cloud classification using Meteosat images

Márta Diószeghy

*Hungarian Meteorological Service, Satellite Research Laboratory,
P.O. Box 39, H-1675 Budapest, Hungary
E-mail: dioszeghy.m@met.hu*

(Manuscript received November 19, 2001; in final form January 31, 2002)

Abstract—Satellite based cloud information is an essential input for the nowcasting system recently developed at the Hungarian Meteorological Service (HMS). This paper describes the cloud classification method used operationally for half-hourly Meteosat images. It was worked out in frame of a co-operation between HMS and Météo-France. A pixel by pixel algorithm is applied using auxiliary data as well such as the actual surface temperature and surface reflectivity. For the classification we use the results of the test runs of clustering type cloud classification methods earlier developed by Météo-France and by HMS separately. The monthly averaged kernels of those clusters are actualized as functions of the surface parameters pixel by pixel and images are classified according to these actual kernels. Verification was made by the forecasters of HMS. We also examined the possibility of applying the method for filtering noisy radar images. The results of a special study comparing the radar and satellite based cloud top height values according to cloud types gave new considerations for the development of the cloud classification method as well.

Key-words: cloud classification, Meteosat, nowcasting, satellite meteorology

1. Introduction

Cloud parameters extracted from satellite imagery became more and more important in the last years at the Hungarian Meteorological Service (HMS) as lots of the synoptic stations were changed for automatic weather stations with less detailed cloud representation. At the Satellite Research Laboratory of HMS we have access for half-hourly images of the geostationary Meteosat and also the AVHRR (Advanced Very High Resolution Radiometer) images of the polar orbiting NOAA (National Oceanic and Atmospheric Administration) satellites 4–6 times a day. The different spatial and spectral resolutions result in different

approaches for deriving cloud parameters. Usually threshold techniques are used for multi-channel NOAA/AVHRR images while statistical or combined methods with auxiliary data for the present geostationary satellite of Europe, the Meteosat-7. The geostationary GOES satellites of the United States have more channels, therefore threshold techniques can be effective for those images. The launch of Meteosat Second Generation (MSG) is planned for July 2002. It will have 12 channels compared to the present 3 of Meteosat, with 15 min time resolution and 3 km spatial resolution in most of the channels. There is a possibility to develop methods for MSG with the help of the already available GOES or NOAA/AVHRR data. International efforts are focusing to develop such algorithms (e.g., *Derrien and Le Gléau, 1999*). NOAA/AVHRR based fog and cloud detection has already been worked out at HMS as well (*Putsay, 2001*), and the results are available operationally for the forecasters. We will use this algorithm for MSG but until then for nowcasting and very short range forecasting, where the good temporal resolution of images is essential, we have to use Meteosat cloud parameters.

An automatic nowcasting system (MEANDER: Mesoscale Analysis Nowcasting and Decision Routines) has been worked out recently at the Hungarian Meteorological Service (*Geresdi and Horváth, 2000*). The analysis runs operationally since the end of 1999, while the nowcasting for 3 hours in 15 min time steps is pre-operational since summer 2001. The scheme makes use of most of the available data like radiosonde, synop and automatic weather station measurements, mesoscale numerical model outputs, radar and satellite images and lightning data. All raw data are interpolated and derived fields are calculated on the nowcasting grid. Decision trees have been defined to derive "present weather codes" and other complex parameters for the grid points. Meteosat derived cloud parameters like cloudiness, cloud top height and cloud types are among the most important elements of the system (*Diószeghy et al., 1999*).

This paper focuses on Meteosat cloud classification as one of the operational procedures of the nowcasting scheme. The cloud classification program package separates and determines the different cloud types on the images. The algorithm was developed in frame of a co-operation with Météo-France, CMS, Lannion (*Brisson et al., 1997*).

Earlier clustering type automatic cloud classification from Meteosat imagery had been developed at both HMS and Météo-France. The cluster analysis was performed on a time cumulated histogram made from the infrared and visible images. The heights of cloud layers are represented by the infrared (IR) measurements, while reflectance values on the visible images (VIS) refer to cloud thickness, therefore, the peaks on the two dimensional histogram present different cloud types. Cluster analysis is a statistical tool to find these peaks automatically on the histogram. The standard deviation fields of the images

were used as well in order to separate cumuliform and layer clouds. The method of CMS was reported by *Bellec et al.* (1992) based on the algorithm of *Seze and Debois* (1987). In this method the standard deviation fields of the infrared data were involved as a third dimension of the histogram. For an attempt to use the method operationally during a test year in 1992, the clusters were automatically assigned to cloud types using thresholds for the kernels of the classes (centers of clusters). At HMS we worked out a method (*Diószeghy and Fejes*, 1995) based on the work of the already referred French authors (*Seze and Debois*, 1987) and also *Porcú and Levizzani* (1992). We used bispectral histograms and used a threshold for the standard deviation field of IR images. We tried to use kernels of multiyear cumulated monthly histograms to determine the clusters as traditional cloud types as they are used in the forecasters' terminology.

The clustering algorithm using visible and infrared data could separate distinct classes of clouds but this statistical approach requires a large amount of data accumulated in time and leads to the mixing of pixels with different surface conditions (temperature and albedo). Besides, the methods for automatically assigning cloud types to the clusters were not reliable enough. Therefore, in the frame of the co-operation with CMS we decided to establish a new cloud classification scheme based on a pixel by pixel approach.

2. Data requirements and collocation

The new method is a combination of the statistical clustering and the threshold methods and as such besides Meteosat IR and VIS images it requires auxiliary data as well.

The spatial resolution of Meteosat images over Hungary is 6–7 km for the infrared and water vapor channels and 3–4 for the visible channel. The mesh size of the nowcasting grid is a variable parameter, but usually it has a smaller resolution than that of the image. Satellite data are transformed to the grid. Pixel values are attributed to the nearest grid point. If more than one pixel found for one grid point then the maximum value is used for the visible and the minimum for the infrared images. This means an overestimation of the cloudiness and cloud development, but it is more appropriate for nowcasting purposes, especially for thunderstorm warning. All the other fields are also transformed to this grid within the MEANDER procedure, so all the input data of the cloud classification are available in the same resolution (*MEANDER*, 1999).

We need surface temperature fields, more exactly the brightness temperature of the surface, mainly for the separation of cloud free areas from low clouds. 2m temperature fields are used and transformed into surface brightness

temperature values according to the function found for NOAA/AVHRR derived brightness temperatures (*Brisson et al.*, 1997). We have to use model forecasts for the real time processing, but the field is corrected with SYNOP data already available at the time of the run of the nowcasting procedure. The used model outputs within MEANDER are from the ALADIN numerical weather prediction model running operationally at HMS (*Horányi et al.*, 1996).

For the surface reflectivity we use monthly surface albedo maps derived from Meteosat visible data (*Brisson et al.*, 1994). These maps were also transformed to the nowcasting grid.

Monthly "kernel library" was built using the centers of clusters of the test year (1992) at CMS. The automatic cloud type assignment to kernels was manually corrected and the average kernels of the months were derived. The values were transformed from the IR-VIS fields to physical parameters as cloud top temperature, variance of temperature and reflectivity values to be comparable to the surface parameters. We can say these kernels are the average cloud characteristics (cloud top temperature, its variance and reflectivity) of the different cloud types for the months. The kernels are given as linear functions of the surface parameters coming from regression analysis in case of surface dependent clouds. This dependence is especially important in the cloud top temperature of low clouds and reflectivity values of very thin cirrus. Different kernels were determined for sea and land cases and also for daytime and night-time classification. The grid of the nowcasting calculations at HMS consists of land points only. Details on the kernel library can be found in *Brisson et al.* (1997).

3. Cloud classification scheme

The flow diagram of the cloud classification algorithm is shown in *Fig. 1*. In this pixel by pixel method the raw visible and infrared counts disseminated by Meteosat are first transformed into physical units. VIS data are calibrated to reflectivity considering the calibration coefficients for the satellite, Sun-Earth distance for the day and illumination conditions. IR data are transformed to cloud top temperature values according to the Planck law. The standard deviation field of the cloud top temperature is derived in 3×3 pixel boxes and logarithmically rescaled in order to be comparable with the scales of the reflectivity and cloud top temperature values on the three-dimensional histogram. These 3 values of the pixel are then compared to the predetermined cloud characteristics, which means they are attached to the nearest kernel representing the average values of a certain cloud/surface type. These kernels are already actualized pixel by pixel as linear functions of the surface temperature and surface reflectivity. At night only the cloud top temperature and its vari-

ance can be used, and from the surface parameters, only the temperature. The kernels are also different at night and do not have reflectivity components. The boundary of the daytime and night-time classification is defined by an 80 degrees threshold applied on the solar zenith angle, thus it can happen that part of the image is classified as daytime classification while the other part as night-time classification. *Brisson et al. (1997)* describe more details on the classification algorithm. The cloud types are listed in *Table 1*.

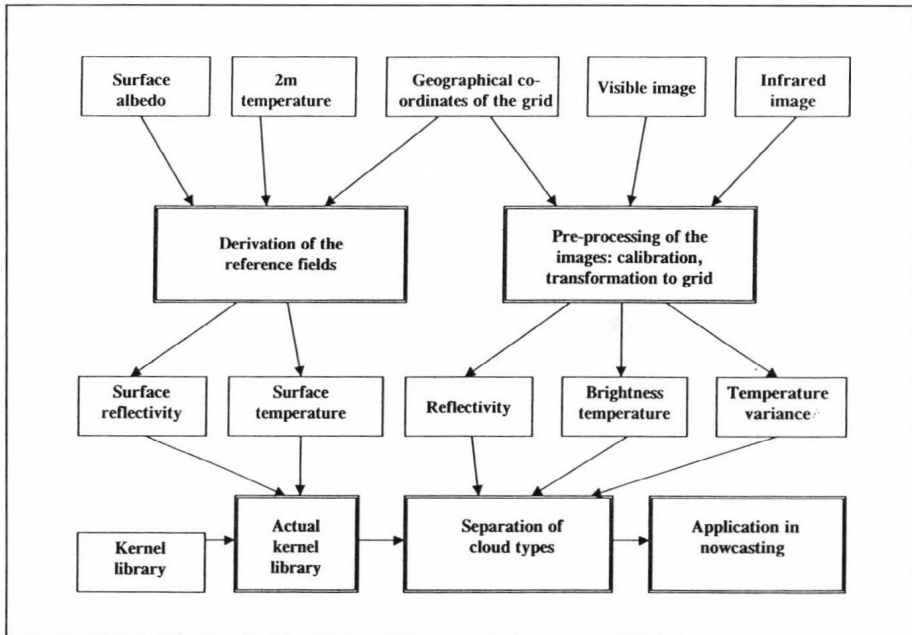


Fig. 1. Flow diagram of the cloud classification algorithm.

The visible channel is important in separating clear sky and cloudy pixels and evaluating cloud thickness. But for different illumination conditions the reflectance of the surfaces (land, sea, clouds) can vary, so it is difficult to compare consecutive images or different areas of the same image. Therefore, we use homogenized visible data for the continuity of the classification results throughout the day and the kernels were also corrected for the illumination conditions.

The usual homogenization procedure (dividing the reflectance values by the cosine of the solar zenith angle and normalizing to a constant angle) overestimates the reflectance values for high solar zenith angles due to anisotropy effects. We used the MODTRAN3.5 radiative transfer model (*Berk et al.*,

1989) for simulating reflectance values for cases representing all the illumination conditions (considering satellite zenith angle and relative azimuth angle as well) detailed enough for a further linear interpolation. We used different built in cloud models of MODTRAN. After the simulations we integrated the radiance values with filter functions of different satellite detectors. The validation was made with NOAA 12, Meteosat and ERB measurements (*Diószeghy et al.*, 1996). We had some difficulties for a limited range of the illumination conditions (forward scattering close to the sunglint case) which might be neglected for the Meteosat B format but will become important for further GOES and NOAA applications. We produced correction tables from the simulations by linear interpolation which can be used directly to measured radiance values. At the moment this correction method is used in the cloud classification scheme of CMS (Météo-France), where it is not in direct operational use, but it is applied for radiation calculations for ocean areas. For the nowcasting system of HMS this correction method would not be fast enough so only the mentioned cosine correction is used at the moment. Attempts are made to use the new analytical correction method of *Manalo-Smith et al.* (1998).

Table 1. Cloud categories of the classification scheme

No.	Cloud type	Abbreviation on figures	Remarks	Dependence on the surface
1	Clear	-		YES
2	Cloud edge	CE1		YES
3	Cloud edge	CE2	only night	YES
4	Thin cirrus	Ci		YES
5	Thick cirrus	Cs		YES
6	Cirrus + other clouds below	Ci+af		NO
7	Nimbostratus	Ns		NO
8	Small cumulus	Cu		YES
9	Cumulus mediocris	CuM	only day	YES
10	Cumulus congestus	CuC	only day	NO
11	Stratus	St		YES
12	Stratocumulus	Sc		YES
13	Altostratus	As		NO
14	Altostratus, Nimbostratus	As+Ns	only day	NO
15	Alto cumulus	Ac	only day	NO
16	Cumulonimbus	Cb	May to October	NO

4. Verification and possibilities of combined use with radar data

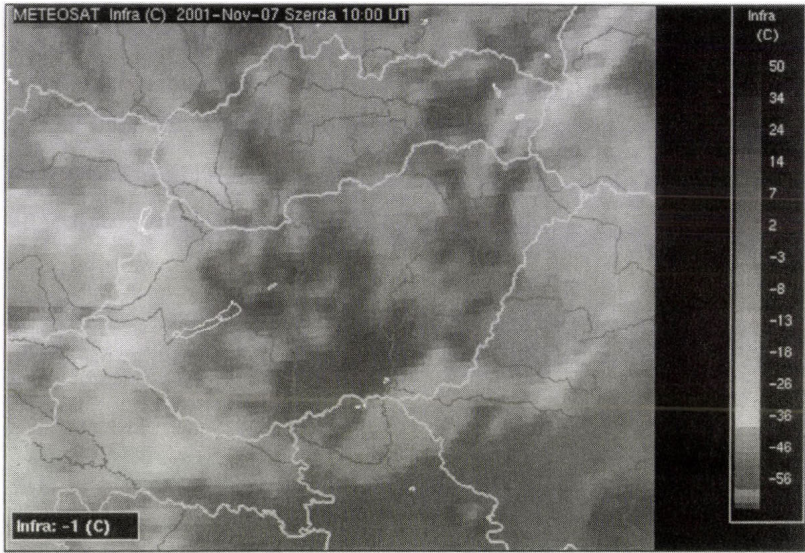
At CMS, Météo-France, we compared the results to the earlier classification. Remarks of skilled nephanalysts were available for the selected test cases of 1992 to help the validation. Also the results of the classification were compared to the NOAA/AVHRR cloud analysis.

At HMS the verification work is done by the Forecasting Division. Two periods, from November 8 to December 31, 2000 and from September 1 to 30, 2001 were tested and all noon images were compared to SYNOP cloud codes. The verification was made within the Hungarian Advanced Weather workStation (HAWK), where it is easy to visualize all available meteorological information together with satellite information (*Diószeghy et al.*, 1999). An example of the cloud classification results together with the IR image is shown in *Fig. 2a* and *b*.

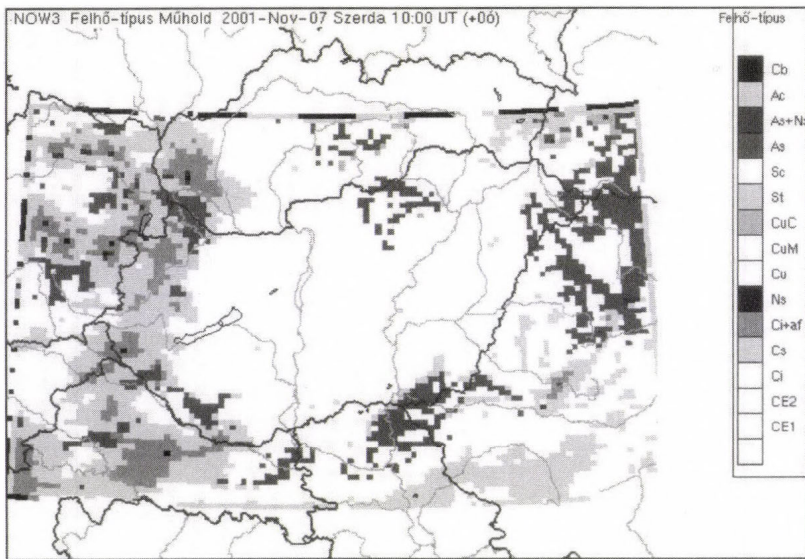
The new scheme allows a homogeneous processing of all individual pixels. Earlier images had to be divided to small zones with different surface characteristics (mountains, etc). Some discontinuity remains however at the boundary of the daytime and night-time cases at sunrise and sunset.

The frontal cloudiness is generally well classified although cloud edges might appear as cirrus clouds. Subpixel cumulus clouds and very thin cirrus might be misclassified and at nighttime, in case of inversion (mainly winter), separation of very low clouds from clear areas is not possible with the only one IR channel of Meteosat. For very large Cb cells sometimes it occurs that the center of the cell is classified as Ns+Ci, as it is very homogeneous and cirrus cloud can cover the Cb (cirrus spissatus cumulonimbogenitus). For the forecasters it is not misleading but in statistics or in an automatic use for decision trees it can cause problems. We should remark that in case of very high Cb clouds, the top of the tower can be tilted with several pixels compared to the cloud base. Thus the position of the maximum of the VIS counts is shifted from the minimum of the IR counts in the image and it is very difficult to properly catch the Cb with a pixel by pixel or any other method (*Anthis et al.*, 1996).

An overestimation of cirrus clouds was reported by the forecasters. It is very difficult to compare the satellite based and surface based (SYNOP) cloud observations because of the different points of view. So it is natural that the satellite can see more high clouds while the observer can see the lower cloud layers. For the same reason it is nearly impossible to work out an objective and automatic verification procedure with SYNOP data. Only one layer cloud types can be compared and one should consider that a visual observer can see the dome of the sky with a 20–30 km radius, so all the satellite pixels within this area should be included in the comparison. At the moment the verification is interactive, but we made automatic statistical comparisons for precipitating cloud types with radar data.

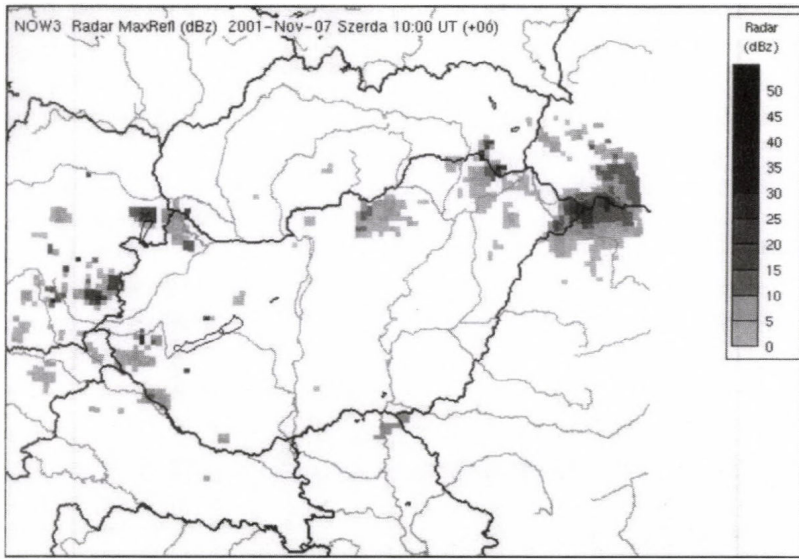


(a)

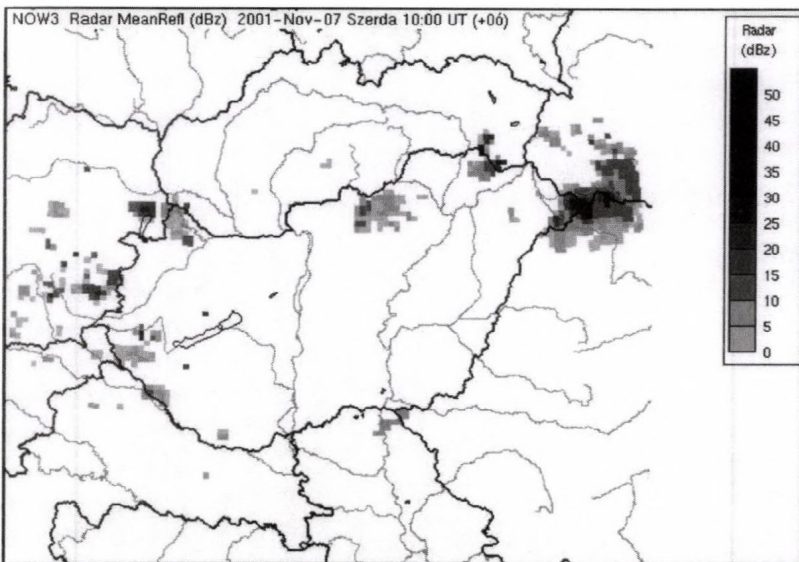


(b)

Fig. 2. Satellite and radar information for 10 UTC, November 7, 2001. (a) Infrared Meteosat image; (b) Cloud classification based on Meteosat data. For the black and white presentation we replaced the 16 colors with a special scale. All non precipitating types are white and the others are darker according to the precipitation possibilities. →



(c)



(d)

(c) Composite radar image made from the data of the three Hungarian radar stations and data from the neighboring countries. A median filter was applied. (d) Radar data after the filter according to non-precipitating cloud types of the satellite based cloud classification.

During a special experiment in summer 2001 we compared satellite and radar based cloud top height (CTH) values for the different cloud types (Diószeghy *et al.*, 2001). The aim of the study was to improve the precipitation and cloud information available for the nowcasting system of HMS as two important input of the different decision trees are the cloud top height and the radar intensity. Besides the radar based cloud top height measurements, an independent product from Meteosat data is available. As described in Randriamampianina *et al.* (2000), the cloud top height is calculated using satellite derived cloud top temperature compared to temperature profiles from numerical weather prediction model (ALADIN). As the radar and the satellite also observe the atmosphere from two different points of view, the reliability of the two methods depends on the cloud types. Results of the Meteosat based cloud classification of the nowcasting system were used to make a statistical comparison of the two cloud top height fields separately for the different cloud types.

From hourly satellite and radar CTH values we calculated difference fields and collected them together with cloud classification results for the summer months, June, July and August of 2001. Histograms of these differences were calculated for the different cloud types for all the data and also separately for night-time and daytime cases. Only those pixels were involved where radar echoes existed. *Fig. 3* shows some of these histograms for 5 selected cloud types.

Only types 5, 6, 7, 10, 13, 14, 16 (as listed on Table 1) have considerable peaks on the histogram as these are the precipitating clouds or precipitating clouds below cirrus clouds. The monthly histograms had different frequency values but the maximum of the peaks were placed at the same difference values, so we can consider this representative.

For most of the cloud types we can say that the satellite gives higher values, since it measures also the cirrus clouds above precipitating clouds. Also for the higher layers of Nimbostratus the echo can be very small and the radar can underestimate CTH. We should remark that in the cloud classification procedure we cannot separate Altostratus (As) and Nimbostratus (Ns) with satellite data alone, in the future we should include radar intensity values as well. A visual observer only calls an As as Ns after the first rain drops has fallen which cannot be determined by the satellite of course.

For Cumulonimbus (Cb) clouds the histogram is very flat and wide as the range of the differences between satellite and radar based CTH values can be very large. When overshooting cloud top occurs the difference is big and the radar measures higher and also more realistic values, since we cannot find equivalent temperatures for the cloud top in the numerical temperature profiles. Here we should notice that this difference value can be very useful for estimating the range of overshooting and from this the status of the develop-

ment and the maximum vertical velocity inside the Cumulonimbus clouds. But for this purpose we should update the cloud classification procedure first in order to have more accuracy in Cb detection.

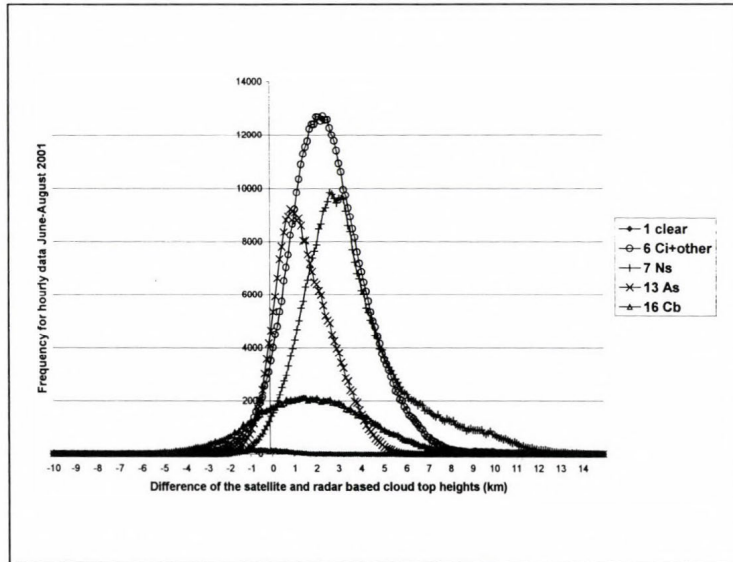


Fig. 3. Histogram of the differences between Meteosat and weather radar derived cloud top height values for different cloud types. All pixel values for hourly data of the period June 1–August 31, 2001.

The results of the comparison with radar data can also be used to determine the precipitating cloud types of the cloud classification to help to filter the radar fields from noise. In case the classification gives clear, cloud contaminated pixel or non raining clouds we can mask out the radar values. An example of this application is shown on Fig. 2c and d. First a median filter is applied to the original radar data (c), involving not only the three Hungarian stations but also the data of the neighbouring countries. Then we mask out the left noise with the cloud types (d). Since this filter is not yet verified the forecasters have access for both the filtered and non filtered data of course. On the figures the case of 10 UTC, November 7, 2001, is shown corresponding to Fig. 2a and b. Some noise around the Nyíregyháza-Napkor radar station of HMS were filtered out with the help of the cloud types. In this case no rain was reported at the neighboring synop stations.

5. Conclusions

- We found the new cloud classification algorithm applicable for operational use and the results are already available for the forecasters half hourly.
- At HMS the most important application of satellite based cloud types is the nowcasting system. It is one of the main inputs for the decision trees calculating “present weather” codes.
- In the future the conclusions of the study comparing radar and satellite based cloud top height values for different cloud types should be integrated in the decision trees of the nowcasting system and further we should make statistics considering the radar intensity values as well and compare them to different CTH values and cloud types.
- We should remark that satellite derived cloud types alone will never be as accurate as visual observations especially for low clouds or subpixel scale cumulus and very thin cirrus, but for frontal cloudiness and multilayer clouds it gives very important information for the forecasters. Combined use with radar data improves this information and the forthcoming MSG satellites will give lots of new possibilities in this field.

Acknowledgements—The cloud classification scheme was worked out in frame of a bilateral co-operation with Centre Météorologic Spatiale, Météo-France, and the essential input fields of albedo values and the kernel library were made available for us in the Hungarian adaptation. I am especially grateful to *Guy Rochard, Pierre Le Borgne, Anne Marsouin* and *Alain Brisson* and the financial support of the French Ministry for Foreign Affairs for the possibility to take part in this project. The study for cloud top height comparisons was partially supported by the Hungarian Scientific Research Foundation (OTKA-T031865).

I am very grateful for the supervising of *Dr. György Major*, for the help of the colleagues at the Satellite Research Laboratory and for the useful validation work of the forecasters of HMS.

References

- Anthis, A.I. and Cracknell A.P.*, 1996: Cloud classification of a typical synoptic situation affecting Greece using Meteosat data. *Proc. of the 1996 Meteorological Satellite Data Users' Conference, Vienna*. Austria, 16-20 Sept. 1996, EUM P19, 203-207.
- Bellec, B., Brisson, A., Le Borgne, P., and Marsouin, A.*, 1992: Operational cloud classification with Meteosat data. *Proc. of the Central Symposium of the ISY Conference*. Munich, 30 March - 4 April 1992, ESA SP-341, 323-327.
- Berk, A., Bernstein, L.S., and Robertson, D.C.*, 1989: *MODTRAN: A Moderate Resolution Model for LOWTRAN 7*. Air Force Geophysical Laboratory, Hanscom AFB, MA 01731, GL-TR-89-0122.

- Brisson, A., Le Borgne, P., Marsouin, A., and Moreau, T., 1994: Surface irradiances calculated from Meteosat sensor data during SOFIA-ASTEX. *Int. J. Remote Sensing* 15, 197-203.
- Brisson, A., Diószeghy, M., Le Borgne, P., and Marsouin, A., 1997: Classification nuageuse Meteosat: experience 1996 (in French). *Technical Report, CMS, Météo-France, Lannion, France.*
- Derrien, M. and Le Gléau, H., 1999: Cloud classification extracted from AVHRR and GOES imagery. *Proc. of the 1999 EUMETSAT Meteorological Satellite Data Users' Conference.* Copenhagen, 6-10 September 1999, EUM P 26, 471-474.
- Diószeghy, M. and Fejes, E., 1995: Cloud classification derived from METEOSAT data involving the standard deviation fields of the brightness values. *Advances in Space Research* 16, (10)33-(10)36.
- Diószeghy, M., LeBorgne, P., Marsouin, A., and Putsay, M., 1996: Sun zenith angle correction applied to Meteosat visible data. *Proc. of the 1996 Meteorological Satellite Data Users' Conference.* Vienna, Austria, 16-20 Sept. 1996, EUM P19, 209-213.
- Diószeghy, M., Horváth, Á., Randriamampianina, R., and Szenyán, I.G., 1999: Applications of Meteosat images in the Hungarian Advanced Weather workstation. *Proc. of the 1999 EUMETSAT Meteorological Satellite Data Users' Conference.* Copenhagen, 6-10 September 1999, EUM P 26, 471-474.
- Diószeghy, M., Horváth, Á., Kerényi, J., Nagy, J., Németh, P., Randriamampianina, R., and Sebők, I., 2001: Cloud and rain information for nowcasting from the combined use of weather radar and Meteosat data. *Proc. of the 2001 EUMETSAT Meteorological Satellite Data Users' Conference.* Antalya, 1-5 October, 2001, in press.
- Geresdi, I. and Horváth, Á., 2000: Nowcasting of precipitation type. Part I. Winter precipitation. *Időjárás* 104, 241-252.
- Horányi, A., Ihász, I., and Radnóti, G., 1996: ARPEGE/ALADIN: A numerical weather prediction model for Central-Europe with the participation of the Hungarian Meteorological Service. *Időjárás* 100, 277-301.
- Manalo-Smith, N., Smith, G.L., Tiwari, S.N., and Staylor, W.F., 1998: Analytic forms of bidirectional reflectance functions for the application to Earth radiation budget studies. *J. Geophys. Res.* 103, D16, 19733-19751.
- MEANDER, 1999: Mesoscale Analysis Nowcasting and Decision Routines (in Hungarian; ed.: Horváth, Á.) Internal Publication of HMS, Budapest.
- Porcú, F. and Levizzani, V., 1992: Cloud classification using Meteosat VIS-IR imagery. *Int. J. Remote Sensing* 13, 893-909.
- Putsay, M., Kerényi, J., Szenyán, I. G., Sebők, I., Németh, P., and Diószeghy, M., 2001: Night-time Fog and Low Cloud Detection in NOAA-16 AVHRR Images and Validation with Ground Observed Synop Data and Radar Measurements. *Proceedings of the 2001 EUMETSAT Meteorological Satellite Data Users' Conference.* Antalya, 1-5 October, 2001, in press.
- Randriamampianina, R., Nagy, J., Balogh, T., and Kerényi, J., 2000: Determination of cloud top height using meteorological satellite and radar data. *Phys. Chem. Earth (B)* 25, 1103-1106.
- Seze, G. and Desbois, M., 1987: Cloud cover analysis from satellite imagery using spatial and temporal characteristics. *J. Climate Appl. Meteor.* 26, 287-303.

IDŐJÁRÁS

Quarterly Journal of the Hungarian Meteorological Service
Vol. 105, No. 4 — Vol. 106, No. 1, October 2001 — March 2002, pp. 293-303

Using observed data for testing the statistical consistency of initial ensemble perturbations

István Szunyogh¹, Györgyi Gyarmati² and Dezső Dévényi³

¹*Institute for Physical Science and Technology and
Department of Meteorology, University of Maryland,
Computer and Space Sciences Building, College Park, MD, 20742-2431, USA
E-mail: szunyogh@ipst.umd.edu*

²*Department of Meteorology, Eötvös Loránd University, Budapest, Hungary*

³*NOAA, Forecast Systems Laboratory and University of Colorado, CIRES, USA*

(Manuscript received February 22, 2002; in final form March 12, 2002)

Abstract—Two random variables are defined, one by an initial ensemble perturbation at a given geographical location, and another by the analysis uncertainty at the same location. The initial ensemble perturbations are said to be statistically consistent with the analysis uncertainty if the probability density functions of the two aforementioned random variables are equal. In this paper, it is shown how observed data can be used to test this statistical consistency. The usefulness of the proposed approach is demonstrated by an application to the global ensemble forecasting system of the National Centers for Environmental Prediction. Targeted dropsonde observations, collected during the 2000 Winter Storm Reconnaissance program, are used to show that increasing the rescaling frequency in the breeding cycle from once a day to four times a day improves the consistency of the initial ensemble perturbations.

Key-words: initial ensemble perturbations, statistical consistency

1. Introduction

The performance of an ensemble prediction system, especially for short forecast lead times, is mainly determined by the representativeness of the initial ensemble perturbations for the analysis uncertainty. Therefore, it is important to verify, whether the initial ensemble perturbations correctly represent the analysis uncertainty defined by the expected difference between analysis and truth. The chief difficulty with this verification is that the analysis

uncertainty cannot be directly determined since the true state of the atmosphere is unknown.

The most frequently used technique to avoid the aforementioned problem is based on Observing System Simulation Experiments (OSSE; *Houtekamer and Derome, 1995; Hamill et al., 2000*), in which the “true state” of the atmosphere is obtained by a model integration. Hence, the analysis error statistics can be directly determined from a sample of the difference between the analysis and the simulated “true state”. While the OSSEs have provided important insights into the strengths and the weaknesses of the different ensemble generation techniques, they cannot be used to measure the performance of an operational ensemble prediction system, whose goal is to predict the true state of the atmosphere.

In the operational practice, the quality of the initial perturbations is usually inferred from the performance of the ensemble at short (6–72 hours) forecast lead times. This approach is based on replacing the true state by its best estimate, the analysis. However, there are two important limitations of this technique. Firstly, the analysis errors are not negligible compared to the short-term forecast errors. Secondly, forecast errors are due not only to growing analysis but also to model errors. This means that the performance of the technique used to generate the ensemble perturbation cannot be separated from the short-term performance of the forecast model.

In this paper, we propose an alternative verification technique, for which the results are not affected by model errors. This technique exploits the opportunity provided by a unique set of targeted dropsonde observations collected during the 2000 Winter Storm Reconnaissance (WSR00) field program over the northeast Pacific. This data set has several favorable features (*Szunyogh et al., 2002*):

- The instrument errors are small for the University Corporation for Atmospheric Research Global Positioning System (UCAR GPS) dropsondes that collected the data.
- The data were collected in regions of significant synoptical features that later had significant impact on the weather over the United States.
- Once assimilated, the data led to significant improvements in the 1–5 days forecasts over the United States. This indicates that the data are capable to detect errors in the analysis cycle that did not assimilate them.

Section 2 explains how observed data can be used to verify the statistical consistency of the initial ensemble perturbations. Section 3 demonstrates the usefulness of the technique by an application to the initial ensemble perturbations generated at the National Centers for Environmental Prediction/National Weather Service (NCEP/NWS) of the United States of America.

2. Verification technique

Let y^t , y^o , y^e , and x^a be random variables that represent, respectively, the true state, the observed state, the observational error, and the analysis at the observational location. These quantities are related through the following equation

$$(y^o - x^a) = (y^t + y^e) - x^a = (y^t - x^a) + y^e. \quad (1)$$

Our goal is to test whether the initial ensemble perturbations are representative for the difference between the true state and the analysis, $(y^t - x^a)$. This goal is achieved by (i) first replacing $(y^t - x^a)$ by the random variable x^p that represents an initial ensemble perturbation at the observational location and then (ii) comparing the two sides of Eq. (1). Since the variables are random, the equality of $(y^o - x^a)$ and $x^p + y^e$ can be verified only in a statistical sense.

Suppose that (i) sufficiently large samples of $(y^o - x^a)$ and x^p are available to estimate their probability density functions (pdfs), $f(z)$ and $h(z)$, respectively; and (ii) an estimate of the pdf of y^e , $g(z)$, is available. Our goal is to verify whether the initial ensemble perturbations are *statistically consistent* with the analysis uncertainty, i.e., whether $h(z)$ can be equal to the probability density function of $(y^t - x^a)$.

If the observations y^o are not used in preparing the analysis, the random variables that represent $(y^t - x^a)$ and y^e become independent. This means that the initial ensemble perturbation represents a random variable, which must be independent of the observational error. Therefore, the initial ensemble perturbation can be consistent with the analysis uncertainty, only if the pdf of $(y^o - x^a)$ is equal to the pdf of $x^p + y^e$; i.e.,

$$f(z) = \int_{-\infty}^{+\infty} h(z - v)g(v)dv. \quad (2)$$

The statistical consistency between the ensemble perturbation and the analysis uncertainty can be verified by the following algorithm:

- Compute the empirical density functions $f(z)$ and $h(z)$ based on a sample of $(y^o - x^a)$ and x^p at the observational locations.
- Choose a probability density function, $g(z)$, to represent the distribution of the observational errors.
- Compute the convolution $c(z)$ of $h(z)$ and $g(z)$:

$$c(z) = \int_{-\infty}^{+\infty} h(z - v)g(v)dv, \quad (3)$$

- Compare $c(z)$ and $f(z)$.

We note that one might (falsely) assume that there exists an alternative verification technique, in which Eq. (3) is applied to the alternative

$$(y^f - x^a) = (y^o - x^a) - y^e \quad (4)$$

form of Eq. (1). This way the pdf of $(y^f - x^a)$ could be directly determined from $f(z)$ and $g(z)$ and compared to $h(z)$. This approach does not work, however, because the two terms on the rhs. of Eq. (4) are not independent random variables; the observation (therefore the difference between the observation and the analysis) is not independent of the error in the same observation.

3. Application

During the WSR00 field program, nearly 300 dropsondes were released over the northeast Pacific on 12 separate flight days. To assess the forecast effect of the data, an additional analysis-forecast cycle was run parallel to the operational cycle. This parallel cycle was identical to the operational one, except no dropsonde data were assimilated (see *Szunyogh et al.*, 2002 for more details). The ensemble initial conditions evaluated in this study were prepared by perturbing analyses from the parallel cycle. This was done to ensure that the difference between the dropsonde observations and the unperturbed analyses is independent of the observational errors.

The computation of the difference between the observations and the analyses at the observational locations required the interpolation of the analysis fields, which were originally available on the Gaussian grid of the spectral NCEP model. The same interpolation was also needed to obtain the initial ensemble perturbations at the observational locations. Statistical samples were collected for the horizontal wind components and the virtual temperature at the 700 hPa, 500 hPa, and 300 hPa pressure level and for the surface pressure. At these levels observations were available from each sonde dropped during the field program. The empirical pdfs were estimated by the average shifted histogram technique (*Scott*, 1985) with using unit bins and shifting the unit-bin histograms twenty times.

The most difficult task was to find a proper statistical model for the observational errors. In this paper, the observational errors are assumed to be normally distributed and results will be shown for two different choices of the standard deviation. One of them is the manufacturer provided instrument error for the NCAR GPS sondes (*Hock and Franklin*, 1999), while the other one is the value assumed by the operational NCEP data assimilation system. The former choice is expected to provide an estimate of the lower bound of the

observational error since beyond the instrument error, the observational error also has an elusive representativeness error component. The observational errors assumed by the operational analysis scheme, on the other hand, include an implicit estimate of the representativeness error, since they are experimentally tuned to provide optimal forecast performance. The problem with this estimate is that the tunable parameter, the assumed observational error, may also be affected by other deficiencies of the analysis scheme (e.g., problems with the background error covariance matrix).

The initial ensemble perturbations were generated by the breeding technique (*Toth and Kalnay, 1993, 1997*), which is the operationally used method at NCEP. The current operational version of the algorithm is explained in detail in *Iyengar et al. (1996)* and *Szunyogh and Toth (2002)*. Here, we provide an alternative explanation of the algorithm, which is more suitable for explaining the results of the present paper.

The purpose of the breeding technique is to mimic the effects of the analysis cycle on the growing analysis error. More precisely, it assumes that errors are growing freely in the direction of the atmospheric instabilities between two analysis cycles and the magnitude of the growing errors is reduced when observed data are assimilated. The operational breeding algorithm takes the analysis uncertainty into account through defining a seasonally varying *mask*, which is also a function of the geographical location. Formally, the *mask* is defined by the rms distance between analyses from two independent and nearly equal quality analysis cycles. That is,

$$mask = \sqrt{\langle (x^{a1} - x^{a2})^2 \rangle}, \quad (5)$$

where x^{a1} and x^{a2} are the two independent analysis and the angled bracket denotes sample mean. The *mask* is also smoothed by a spectral filter, in such a way, that the variability at and below the synoptic scales (above wave number 10) is negligible. The ensemble perturbations, which evolve freely between two breeding cycles, are rescaled so that their magnitude at analysis time becomes equal to the *mask*. Since the *mask* is smooth this rescaling strategy can change only the magnitude, but not the structure, of the perturbations at the synoptic and smaller scales. We note that since the quality of the two analysis cycles is equal, $\langle (y^t - x^a)^2 \rangle$ is the same for both cycles. Making use of the independence of the two cycles, it can be easily shown that

$$mask = \sqrt{2 \langle (y^t - x^a)^2 \rangle}. \quad (6)$$

The *mask* used in operation was computed based on a one-year sample of daily analysis differences. It was prepared by considering one particular state

variable of the atmosphere, the rotational component of the horizontal wind. In the breeding algorithm the same local rescaling factor is applied to all state variables. Strictly speaking, this rescaling strategy assumes that there exists a linear relationship between the rotational wind and the other atmospheric state variables. While this is not an unrealistic assumption (e.g., the linear balance equation can provide the required linear relationship for synoptic and larger scale motions) there can be strong local deviations from this rule in the real atmosphere or in a model based on the primitive equations, such as the NCEP model.

Based on Eq. (6), it can be expected that the initial ensemble perturbations overestimate the analysis uncertainty, on average, by a factor of $\sqrt{2}$. This is not an error in the formulation. The initial analysis uncertainty is overestimated in order to compensate a deficiency of the ensemble: errors in the forecasts grow faster than the ensemble perturbations. Without overestimating the analysis uncertainty, the ensemble would underestimate the forecast uncertainty at all forecast lead times. The $\sqrt{2}$ factor can ensure that the ensemble spread, defined by the standard deviation of the ensemble, is equal to the average error in the ensemble mean at about three-day forecast lead time.

Two sets of initial ensemble perturbations were generated by running breeding cycles (*Toth and Kalnay, 1997*) for the duration of the WSR00 field program. In one of these cycles, the initial perturbations were generated by a replica of the operational breeding cycle. The other cycle was identical, except for that the perturbations were rescaled every six instead of every twenty-four hours. This change was expected to improve the consistency of the initial ensemble perturbations with the analysis uncertainty. In what follows, our verification technique is used to investigate whether this expectation was fulfilled by the experimental ensemble.

The results presented in *Fig. 1* for the surface pressure suggest the following conclusions: (1) the frequency of the large analysis errors is overestimated, while the frequency of the small analysis errors is underestimated by the ensembles, (2) this problem is more serious for the ensemble with 24-hour rescaling frequency, (3) the performance of the ensemble is found to be better when the smaller estimate of the observational error (the instrumental error) is used in the verification.

Interestingly, the above conclusions remain valid regardless of which state variable (temperature or wind) is used, even though the shape of the particular pdf is strongly variable dependent (*Fig. 2–Fig. 4*). The good agreement between the results for the different state variables indicates a systematic problem with the initial perturbations. To further investigate this problem, it is useful to define a measure that can characterize the difference between the

random variables compared by one single number. A straightforward choice is

$$\left(\frac{\sqrt{\langle x^p \rangle}}{\sqrt{\langle (y^o - x^a)^2 \rangle - \langle y^{e2} \rangle}} - 1 \right) \times 100, \quad (7)$$

which shows, in percentages, the extent to which the root-mean-square (rms) of the analysis uncertainty is overestimated by the initial ensemble perturbations. The results summarized in *Table 1* corroborate the conclusions drawn by visually inspecting the estimated probability density functions: the ensemble perturbations, on average, overestimate the analysis uncertainty. The only exception is the wind at the 300 hPa pressure level, but only when the smaller estimate of the observational error is considered.

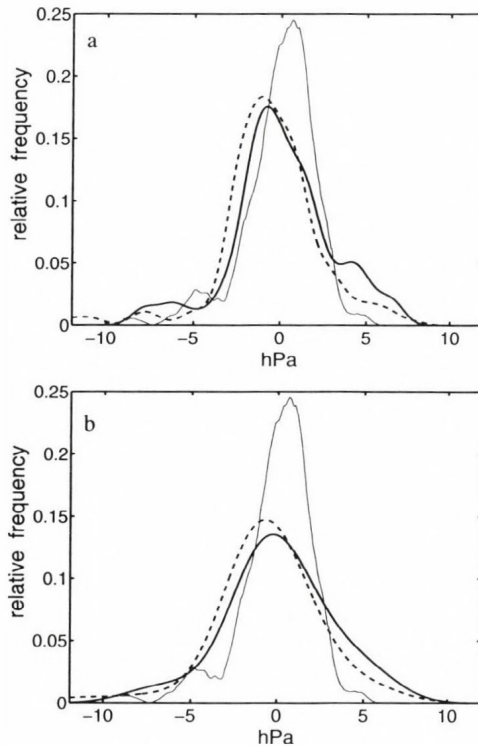


Fig. 1. Probability density functions for the surface pressure. Shown are the pdfs for $y^o - x^a$ (thin solid line), $x^p + y^e$ with 24-hour rescaling (solid line), and $x^p + y^e$ with 6-hour rescaling (dashes). The manufacturer provided instrument error is $y^e = 0.5$ hPa (panel *a*), while the observational error assumed by the data assimilation scheme is $y^e = 1.6$ hPa (panel *b*).

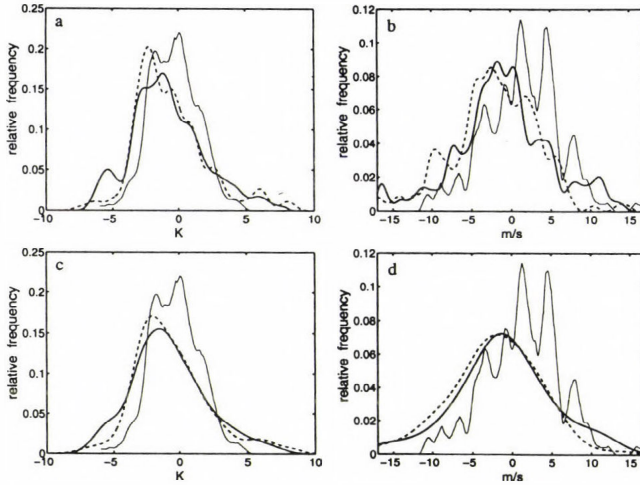


Fig. 2. Probability density functions for the temperature and wind at 700 hPa. Shown are the pdfs for $y^o - x^o$ (thin solid line), $x^p + y^e$ with 24-hour rescaling (thick solid line), and $x^p + y^e$ with 6-hour rescaling (dashes). The manufacturer provided instrument error for the temperature is $y^e = 0.2$ K (panel a), while the observational error assumed by the data assimilation scheme is $y^e = 0.8$ K (panel c). The instrument error for the wind is 0.5 m/s (panel b), and the assumed observational error is 2.4 m/s (panel d).

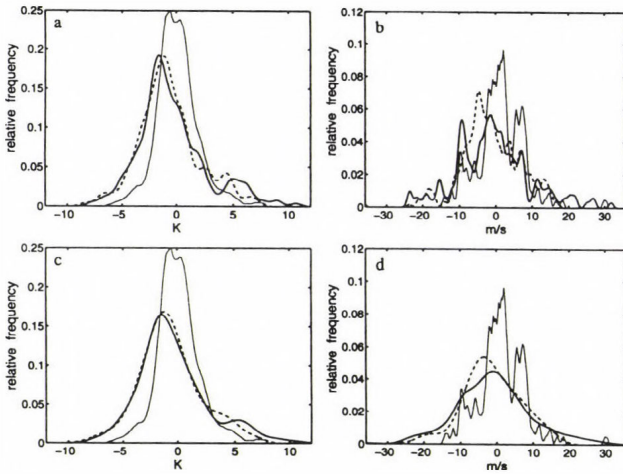


Fig. 3. Probability density functions for the temperature and wind at 500 hPa. Shown are the pdfs for $y^o - x^o$ (thin solid line), $x^p + y^e$ with 24-hour rescaling (thick solid line), and $x^p + y^e$ with 6-hour rescaling (dashes). The manufacturer provided instrument error for the temperature is $y^e = 0.2$ K (panel a), while the observational error assumed by the data assimilation scheme is $y^e = 0.8$ K (panel c). The instrument error for the wind is 0.5 m/s (panel b), and the assumed observational error is 2.8 m/s (panel d).

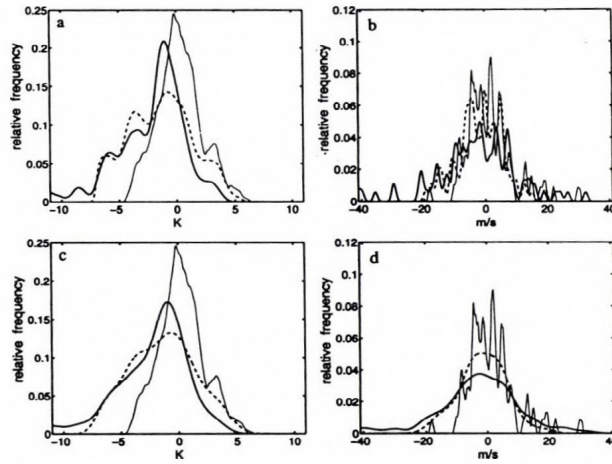


Fig. 4. Probability density functions for the temperature and wind at 300 hPa. Shown are the pdfs for $y^o - x^a$ (thin solid line), $x^p + y^e$ with 24-hour rescaling (thick solid line), and $x^p + y^e$ with 6-hour rescaling (dashes). The manufacturer provided instrument error for the temperature is $y^e = 0.2$ K (panel a), while the observational error assumed by the data assimilation scheme is $y^e = 0.8$ K (panel c). The instrument error for the wind is 0.5 m/s (panel b), and the assumed observational error is 2.8 m/s (panel d).

Table 1. Overestimation of the analysis uncertainty by the initial ensemble perturbations (for definition see Eq. (5)). Shown are the selected state variables (first column), the pressure levels at which the observations were taken (second column), the estimated observational error (third column), overestimates in the 6-hour rescaling cycle (fourth column), and in the 24-hour cycle (fifth column)

Variable	Level	y^e	06-h rms %	24-h rms %
Pressure	Surface	1.6	140	160
Temperature	300	0.8	60	85
Wind	300	2.8	6	84
Temperature	500	0.8	68	93
Wind	500	2.8	35	81
Temperature	700	0.8	68	68
Wind	700	2.4	32	45
Pressure	Surface	0.5	49	61
Temperature	300	0.2	46	69
Wind	300	0.5	-1	71
Temperature	500	0.2	52	75
Wind	500	0.5	22	63
Temperature	700	0.2	52	52
Wind	700	0.5	15	26

As it can be expected by considering the specific form of Eq. (7), the overestimation of the analysis uncertainty is always found to be a less serious problem when the smaller estimate of the observational error is used. What could not be predicted by simply considering Eq. (7) is the fact that the overestimation is always smaller for the more frequent rescaling. Nevertheless, this result is in good accordance with the conclusions drawn based on comparing the pdfs.

The initial ensemble perturbations overestimate the analysis uncertainty, on average, by 38.7% in the 6-hour breeding cycle, and by 67.1% in the 24-hour cycle. (These values were obtained by disregarding the grossly overestimated surface pressure uncertainty and assuming that the results can be averaged for the two different estimates of the observational error.) This result is remarkable considering that the overestimation of the analysis uncertainty by the breeding cycle with 6-hour rescaling (38.7%) is extremely close to the value (about 41%) that can be expected based on Eq. (6). It should be recalled that the *mask* controls the large-scale areal mean of the magnitude of the initial ensemble perturbations, but it has little effect at the synoptic scale, where the energetically dominant baroclinic instabilities are the most intense. Our results, therefore, show that in the regions of atmospheric instabilities, where the observations were collected, the 6-hour rescaling provides perturbations, which are more consistent with the estimates of the analysis uncertainty. (The 24-hour rescaling tends to overestimate the analysis uncertainty in the regions of baroclinic instabilities.)

The relatively large variability of the numbers in Table 1 for the different state variables can be attributed to a couple of possible factors. Firstly, the representativeness error can be different for the different variables. Secondly, as mentioned before, the breeding algorithm rescales all variables with the same factor at a given geographical location, which can lead to inconsistencies in the regions where the linear balance equation is not satisfied.

4. Concluding remarks

In this paper, a new and simple statistical technique was introduced to test the statistical consistency between initial ensemble perturbations and analysis uncertainties. Our study indicates that better statistical consistency can be achieved with the breeding technique when the ensemble perturbations are rescaled every 6 instead of every 24 hours. This result is not surprising considering that the purpose of the breeding technique is to mimic the effects of the analysis cycle on the growing analysis errors. Based on this consideration, the rescaling was done every 6 hours at the time (in 1992) when

operational ensemble prediction was introduced at NCEP. This meant, however, that an extra day of ensemble integration was needed to evolve the initial ensemble perturbations and a 24-hour rescaling was introduced soon to save computer time. In this new setup the regular 24-hour ensemble forecasts were rescaled.

Partly based on the results presented here, NCEP is considering to return to the 6-hour rescaling later this year. The preliminary forecast verification results (not shown in this paper) indicate that increasing the rescaling frequency also improves the skill of the individual ensemble members.

Acknowledgments—We would like to thank the staff of EMC, and in particular *Dr. Zoltan Toth* and *Jack Woollen*, for their support of this work. *Dr. András Horányi* provided helpful comments on an earlier version of the manuscript. The research presented in this paper was partly supported by the *W. M. Keck Foundations*.

References

- Hock, T.F. and Franklin, J.L., 1999: The NCAR GPS Dropwindsonde. *Bull. Amer. Meteor. Soc.* 80, 407-420.
- Hamill, T., Snyder, C., and Morss, R. E., 2000: A comparison of probabilistic forecasts from bred, singular vector, and perturbed observation ensembles. *Mon. Wea. Rev.* 128, 1835-1851.
- Houtekamer, P.L. and Derome, J., 1995: Methods for ensemble prediction. *Mon. Wea. Rev.* 123, 2181-2196.
- Iyengar, G., Toth, Z., Kalnay, E., and Woolen, J.S., 1996: Are the bred vectors representative of analysis errors? *Preprints, AMS Conference on Numerical Weather Prediction*, Norfolk, VA, 64-65.
- Scott, D.W., 1985: Averaged shifted histograms: Effective nonparametric density estimators in several dimensions. *Annals of Statistics* 13, 1024-1040.
- Szunyogh, I. and Toth, Z., 2002: The effect of increased resolution on the NCEP global ensemble mean forecasts. *Mon. Wea. Rev.* 130, 1125-1143.
- Szunyogh, I., Toth, Z., Majumdar, S.J., and Persson, A., 2002: On the propagation of the effect of targeted observations: The 2000 Winter Storm Reconnaissance Program. *Mon. Wea. Rev.* 130, 1144-1165.
- Toth, Z. and Kalnay, E., 1993: Ensemble Forecasting at NCEP: The generation of perturbations. *Bull. Amer. Meteor. Soc.* 74, 2317-2330.
- Toth, Z. and Kalnay, E., 1997: Ensemble forecasting at NCEP and the breeding method. *Mon. Wea. Rev.* 125, 3297-3319.

IDŐJÁRÁS

QUARTERLY JOURNAL
OF THE HUNGARIAN METEOROLOGICAL SERVICE

CONTENTS

Editorial: Academician Rudolf Czelnai is 70	I
<i>Kirill Ya. Kondratyev</i> : Global climate change and the Kyoto Protocol	1
<i>Ágnes Mika, Ferenc Ács, András Horányi and Gábor Radnóti</i> : Sensitivity of the ALADIN weather prediction model to the changes of soil texture	39
<i>Kornélia Radics and Judit Bartholy</i> : Selected characteristics of wind climate and the potential use of wind energy in Hungary. Part II	59
<i>Mónika Lakatos and István Matyasovszky</i> : Specification of multivariate extremity in climatological data	75
News	87

http://omsz.met.hu/irodalom/firat_ido/ido_hu.html

VOL. 106 * NO. 2 * APRIL-JUNE 2002

IDŐJÁRÁS

Quarterly Journal of the Hungarian Meteorological Service

Editor-in-Chief

TAMÁS PRÁGER

Executive Editor

MARGIT ANTAL

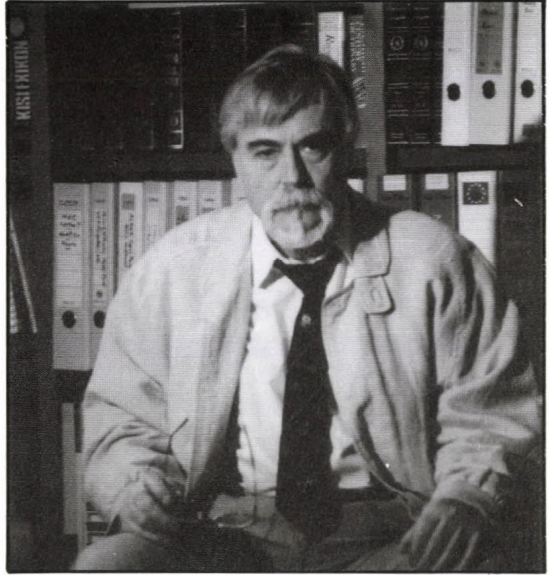
EDITORIAL BOARD

- | | |
|---|---|
| AMBRÓZY, P. (Budapest, Hungary) | MÉSZÁROS, E. (Veszprém, Hungary) |
| ANTAL, E. (Budapest, Hungary) | MIKA, J. (Budapest, Hungary) |
| BARTHOLY, J. (Budapest, Hungary) | MARACCHI, G. (Firenze, Italy) |
| BOZÓ, L. (Budapest, Hungary) | MERSICH, I. (Budapest, Hungary) |
| BRIMBLECOMBE, P. (Norwich, U.K.) | MÖLLER, D. (Berlin, Germany) |
| CZELNAI, R. (Budapest, Hungary) | NEUWIRTH, F. (Vienna, Austria) |
| DÉVÉNYI, D. (Budapest, Hungary) | PINTO, J. (R. Triangle Park, NC, U.S.A.) |
| DUNKEL, Z. (Brussels, Belgium) | PROBÁLD, F. (Budapest, Hungary) |
| FISHER, B. (London, U.K.) | RENOUX, A. (Paris-Créteil, France) |
| GELEYN, J.-Fr. (Toulouse, France) | ROCHARD, G. (Lannion, France) |
| GERESDI, I. (Pécs, Hungary) | S. BURÁNSZKY, M. (Budapest, Hungary) |
| GÖTZ, G. (Budapest, Hungary) | SPÄNKUCH, D. (Potsdam, Germany) |
| HANTEL, M. (Vienna, Austria) | STAROSOLSZKY, Ö. (Budapest, Hungary) |
| HASZPRA, L. (Budapest, Hungary) | SZALAI, S. (Budapest, Hungary) |
| HORÁNYI, A. (Budapest, Hungary) | SZEPESI, D. (Budapest, Hungary) |
| HORVÁTH, Á. (Siófok, Hungary) | TAR, K. (Debrecen, Hungary) |
| IVÁNYI, Z. (Budapest, Hungary) | TÄNCZER, T. (Budapest, Hungary) |
| KONDRATYEV, K.Ya. (St. Petersburg,
Russia) | VALI, G. (Laramie, WY, U.S.A.) |
| MAJOR, G. (Budapest, Hungary) | VARGA-HASZONITS, Z. (Moson-
magyaróvár, Hungary) |

*Editorial Office: P.O. Box 39, H-1675 Budapest, Hungary or
Gilice tér 39, H-1181 Budapest, Hungary
E-mail: prager.t@met.hu or antal.e@met.hu
Fax: (36-1) 346-4809*

Subscription by

*mail: IDŐJÁRÁS, P.O. Box 39, H-1675 Budapest, Hungary
E-mail: prager.t@met.hu or antal.e@met.hu; Fax: (36-1) 346-4809*



Academician Rudolf Czelnai is 70

Academician Rudolf Czelnai celebrated his 70th birthday in May this year. Both me and the President of the Hungarian Meteorological Service, the publisher of Időjárás were thinking that this was an anniversary which should be noted in our Journal. Our feeling was strongly supported by the members of the Editorial Board.

The following is intended to be not just a traditional "laudation" of our highly honoured friend with exact details and dates of his extraordinary scientific career, rather some mixture of the previous and the portrait of the sympathetic personality as we all know him. I would like to wish Academician Rudolf Czelnai in the name of the whole Editorial Board long life full with happiness and successes in his future work for the benefit of our common challenge and mission: meteorology.

Indeed, one can say that Academician Czelnai is the most well-known Hungarian meteorologist all over the world, who gained abiding merits in the development of both domestic and global meteorology. During his scientific career which began in 1954, he achieved important results in very different fields of meteorology, extending almost to the whole range of our science from its theoretical aspects like optimum interpolation or climate research, to very practical ones such as the design and maintenance of instruments and observing systems. He is one of the rare personalities, who has always been interested in every part of meteorology, a person who can be called a "polihistor" in meteorology. He revealed outstanding talents also in university education of our science, and is the author of a number of excellent textbooks. The restitution of training of professional meteorologists in Hungary (at Budapest University) was initiated by him. In the late seventies he compiled the guidelines of a 5 years educational plan for this course which has not been changed in its main features since then, and even in our days is considered as one of the best in Europe.

He became President of the Hungarian Meteorological Service at a relatively young age in 1974. Under his ambitious and talented leadership the Service and meteorological science in Hungary in the whole passed through a little "golden age"; a relative optimum period, restricted, of course, by the large scale political environment of the communist regime. Inside the institution he changed the atmosphere to a more open and friendly one, and maintained a good balance between "theoretical" and "practical work" which was a delicate issue among the employees every time, especially under the communism. This was the basis of the almost unperturbed developments of these years. During the previous 30 years he was the first President who compiled a strategic plan for the HMS on decadal time-scale.

In external relations the main guidelines and outstanding features of his leadership were strong interdisciplinary co-operation with institutions and scientists representing Earth sciences other than meteorology inside Hungary, and lively everyday work contacts with meteorologists from many continents, with the World Meteorological Organisation in the first place. In this activities one could already recognize his extraordinary ability to build up and maintain long-term scientific co-operations and to co-ordinate the views and the work of scientific people from all parts of the world, which is one of the main strengths of his very open and very friendly personality.

It is not incidental, therefore, that he also made a bright career in the WMO serving at first as the Director of Scientific and Technical Programmes in the period 1981–1984, and then, as Assistant Secretary General of the WMO in the years 1985–1992. He supervised a number of global scientific programmes, but with the time going he became the supervisor of core administrative activities, such as technical co-operation of WMO countries, organization of WMO conferences, WMO publications, long-term planning, etc. After these successful, but weary-some years he retired from his position in the WMO, but did not at all retire from the science.

After returning to Hungary, he served for a short while as the President of the Scientific Council of the HMS, and now he plays a very active role in the life of the Hungarian Academy of Sciences. A presentation of Academician Czelnai is always an event for the Hungarian meteorological community. In this context—to explain the reason why people like his presentations—one has to emphasize the global nature and the far-reaching way of thinking which is so characteristic to him, in which he tries to synthesize and analyze the vast complexity of the surrounding world in order to give reasonable and useful answers to the most complicated questions of science and life.

Tamás Práger

IDŐJÁRÁS

*Quarterly Journal of the Hungarian Meteorological Service
Vol. 106, No. 2, April–June 2002, pp. 1–37*

Global climate change and the Kyoto Protocol

Kirill Ya. Kondratyev

*Research Centre for Ecological Safety, Russian Academy of Sciences, and
North-Western International Centre for Cleaner Production,
Nansen International Environmental and Remote Sensing Centre,
Korpusnaya St. 18, 197110 St. Petersburg, RUSSIA
E-mail: kirill.kondratyev@niersc.spb.ru*

(Manuscript received March 12, 2002)

Abstract—In the context of the Third Report of the Intergovernmental Panel on Climate Change (IPCC–2001), failure of the 6th Conference of the FCCC (Framework Convention on Climate Change) parties, and preparations to the World Summit on Sustainable Development (“Rio+10”), the paper discusses unsoundness of the Kyoto Protocol recommendations on greenhouse gas emission reduction and far-fetched “flexible mechanisms” (including “emission trading”) of preventing dangerous changes of the global climate predicted for the 21st century. Analysis of the available observation data and uncertain results of the climate prediction by numerical modeling suggest the need for radically revising the FCCC and rejecting the Kyoto Protocol.

Key-words: global climate change, global warming, Framework Convention on Climate Change, Kyoto Protocol, greenhouse gases, World Summit on Sustainable Development, climate observations, climate modeling

1. Introduction

Recent decades have witnessed the world community’s unprecedented importance attached to climate change problems stirred up by mass media. This, undoubtedly, stimulated both scientific and applied developments through which further progress was achieved in understanding the causes of the present-day climate changes and the regular features in paleoclimate. However, we still need a better vision of climate changes in the future. The reliability of various scenarios and predictions of future climate changes remains doubtful (References). Various speculative exaggerations and apocalyptic prognoses of the men’s climatic impacts were, unfortunately, specifically attracting too much

attention. As a result, the climate change problem, conceptualized as human-induced global warming, became an acute geopolitical issue (*Bohmer-Christiansen*, 1999, 2000; *Hansen et al.*, 2000; *Houghton*, 2000, 2001; *Konratyev*, 1992, 1998a, b, 2001, and many others). Paradoxically, Presidents and Prime Ministers in various countries (e.g., in the USA) enter into discussions on whether the Kyoto Protocol is to be treated as scientifically sound document (*From ...*, 2000). This situation is getting even more complicated, in particular, in the absence of sufficiently clear and uniform terminology. Without focusing on the very complex situation with climate definition (which deserves special discussion), we will remind, that the Kyoto Protocol defined the “climate change” as human-induced climate change. Anthropogenic impact on climate is beyond question, but the contribution made by anthropogenic factors into global climate formation still need to be convincingly assessed, and this is the main problem. In this situation, international documents analyzing the modern climate views unnecessarily apply the term “consensus” to their conclusions. Obviously, science progressed along the pathway of comparing various views and discussing, rather than voting, specific issues. In the climate case, this is dictated not only by the lack of precise definitions for terms being used but also by unclear and vague conceptual assessments for various aspects of climate problems.

The above-said is becoming of particular importance in the context of the World Summit on Sustainable Development to be held in Johannesburg (South African Republic) in September 2002. Unfortunately, the notion of “sustainable development” itself still needs an adequate definition, which is especially pertinent to the Russian version of this term. There is a good reason to believe that “Rio+10” conference will focus specifically on climate problems. In this connection, we will remind that the undeniable success of the Second UN Conference on Environment and Development (Rio de Janeiro, 1992), UNCED, and the Special Session of the UN General Assembly “Rio+5” which was held 5 years later (New York, 1997) consisted only in drawing attention of the Governments and the public to global change and sustainable development problems. Unfortunately, both these world forums were ill-prepared, as most clearly evidenced by their failure to elaborate the “Earth Charter” intended for formulating and substantiating the priorities; instead, a very amorphous and declarative “Rio Declaration” was adopted.

Today, the focus of discussion should be concentrated on three global environmental problems: (1) “global warming”— anthropogenically induced climate change; (2) fate of the ozone layer; and (3) closed nature of global biochemical cycles and the concept of biotic regulation of the environment. The primary importance of the third problem and the secondary significance of the two first-named ones were convincingly substantiated in scientific literature

(Gorshkov, 1990; Gorshkov et al., 2000; Kondratyev, 1990, 1992, 1997, 1998, 1999a, 2000, 2001a). A bitter paradox consists, however, in that despite all this, the UNCED documents show inadequate understanding of the fact that has crucial importance from conceptual viewpoint, namely the sequence of events: socioeconomic development under conditions of the population growth → anthropogenic impact on the biosphere → environmental implications of these impacts (climate, ozone, etc.).

Such misunderstanding advanced the “global warming” problem in the foreground, and this resulted in adoption of the International Framework Convention on Climate Change (FCCC). This is a rather inadequate and misleading document that unjustly treats developing countries; its focus—without good reason—is on anthropogenic origin of the observed global climate change and the recommended reductions of emission of greenhouse gases (GHGs), above all, carbon dioxide.

In December 1997, 160 countries participated in the Third Conference of the FCCC signatory-states, which was held in Kyoto (Japan). There, the possibility of implementing the required 5%—on the average—CO₂ emission reduction by the 2008–2012 period relative to the 1990-year level was the subject of prolonged heated debates. These debates and the so far lacking notable progress in CO₂ emission reduction clearly illustrate the absurd character of the Kyoto decisions. Global emissions tend to increase—not only in developing but also in industrial countries, including USA—and this trend will be preserved in the future. Naturally, the attitude of developing countries is dictated primarily by the highest priority for them, namely, rising the people’s living standard via industrial development rather than curtailment aimed at CO₂ emission reduction. However, specifically the latter item was the FCCC-signing condition laid down by the USA and other “golden billion” countries. The FCCC history is only one example illustrating the giant, primarily bureaucratic activity devouring hundreds of million dollars yearly. According to the GEF data as of July 30, 1998, 1.9 billion USD were assigned for 267 GEF projects (*Project ...*, 1998). In this context, it should be reminded that about 10 thousands participated in the Kyoto Conference only. The recent Hague Conference (November 2000) and Bonn Workshop (July 2001) had also large audiences and entailed large expenditures. The sums absorbed by these useless bureaucratic meetings could have been invested into development of science to a greater benefit of humankind (*Singer*, 1997, 1998).

One can think that the situation outlined stems from poor development of the scientific principles of global change problems. This conclusion is justified only in part, since as early as 1990 the key aspects of global environmental dynamics were discussed, e.g., in monographs (*Kondratyev*, 1990, 1998). *Gorshkov* (1990, 2000) advanced and substantiated the basic concept of biotic

regulation of the environment. *Kondratyev* (1990, 1992, 1998, 2001) demonstrated the fruitlessness of focusing on “greenhouse” aspect of global warming solely and drew attention to the need in studying the climatic system “atmosphere–ocean–land–ice cover–biosphere” taking into account the whole complex of feedbacks among its interactive components. The problem of global observation system was seriously analyzed (*Kondratyev* and *Varotsos*, 2000; *Goody*, 1998, 2001; *Goody et al.*, 2001; *Kondratyev* and *Cracknell*, 2001; *Reconciling ...*, 2000). Special attention is being given to atmospheric ozone variability.

In the problem of human-induced global climate changes, the main uncertainties stem from the following: (1) observation data are incomplete and insufficiently reliable not only for quantitative assessment of the anthropogenic component of the “global warming” but even for its scientifically substantiated identification; (2) uncertainties involved in accounting the climate-forming role of atmospheric aerosol and in introducing the so-called “flux correction” in numerical climate modeling can amount to tens or even 100 W/m² (*Kondratyev*, 1998, 1999), being much more significant than a potential ~ 4 W/m² enhancement of the atmospheric greenhouse effect due to the expected doubling of the atmospheric CO₂ concentration); (3) the results of numerical modeling of climate changes using relevant models differ and cannot be adequately verified; they cannot be used for reliable assessment of the “global warming”, because the results of such calculations depend on adjustment to observation data; and (4) even full accomplishment of the Kyoto Protocol recommendations can ensure only a negligible decrease in the annual average global average near-surface air temperature (SAT), no greater than several hundredth of a degree (*Wigley*, 1999). In this situation, the recommended greenhouse gas emission reductions make no sense, although their implementation can have far-reaching adverse socioeconomic consequences.

Recently, much attention has been given to analyzing the uncertainties (incompleteness) of numerical climate modeling. The major uncertainties, evidently, result from inadequate account of interactive processes in the “aerosol–clouds–radiation” system (*Kondratyev*, 1992, 1998, 2002). The fact that the most complex aspect of climate numerical modeling is taking into account the interactive biosphere dynamics is beyond question. This can be illustrated by two specific examples, which, certainly, only to a small extent reflect the complexity of the problem discussed.

For explaining the decrease in the daily variation of amplitude of the surface air temperature (DTR) by 3–5 K (which was observed during the period 1951–1993) owing to a more rapid rise of the minimal, compared to maximal, temperature, it was suggested that various factors, such as changes in the amount of clouds, water vapor and tropospheric aerosol content, as well as

turbulence and soil moisture should be taken into account. Positive trends in the three first-named factors could be responsible for a global radiation reduction in the daytime and enhancement of the atmospheric longwave radiation (LWD) in the nighttime. At the same time, changes in the turbulent mixing intensity and soil moisture could be responsible for variations of the heat- and moisture-exchange between the surface and the atmosphere, more substantially in the day than in the nighttime.

A fairly pronounced interactivity of the climate-forming processes and inadequate parameterization of them in climate models significantly complicate the task of assessing the contributions from various mechanisms to the DTR decrease. In this connection, *Collatz et al.* (2000) undertook numerical modeling on the response of the daily temperature variation of the vegetation-covered land surface to the changes in the external forcing and biophysical state of the vegetation cover. To this end, those authors used the SiB2 approximate land biosphere model at given meteorological conditions under various scenarios so as to simulate the likely impact of the interactive dynamics of the vegetation cover on the DTR.

The numerical modeling results showed that with increasing LWD the temperature of the air above the vegetation cover, T_m , tends to increase in the nighttime, thus decreasing the DTR. At the same time, changes in T_m or rise of $T_m + LWD$ (this is specifically the case for global warming conditions) favor increases both in the minimal and maximal temperatures making these factors of little importance for DTR. This response is due mainly to the influence of the daily variations of the aerodynamic stability and radiation balance.

Many of climate numerical modeling experiments utilize the global atmosphere circulation models (GCMs) coupled with land surface processes models (LSM). The results of these numerical experiments are essentially dependent on the specific features of interaction between the GCM and LSM models simulating the radiation, momentum, and energy exchanges between the surface and the atmosphere. Striving for covering the diversity of terrestrial ecosystems, LSM models became significantly complicated by introducing submodels, which take into account photosynthesis, vegetation cover dynamics, and biogeochemical cycles thus making the models radically more realistic.

Basing on the Simple Biosphere Model SiB (an LSM version), *Kim et al.* (2001) conducted various numerical modeling sensitivity experiments. They indicated the importance of not only the sensitivity of SiB to many of the morphological parameters of the vegetation cover but also of factors such as the sensitivity of transpiration of high vegetation cover to parameters characterizing the vegetation cover resistance. With improved SiB model those authors took into account the biogeochemical processes governing the water vapor, energy, and carbon dioxide exchange between the surface and the atmosphere.

The results of numerical modeling of the processes, occurring on a rice paddy test plot in Thailand (17°03'N, 99°42'E), using SiB2 and modified SiB2-Paddy models as coupled with mesometeorological model GAME-Tropics (GAME is the monsoon experiment in Asia conducted in the framework of the GEWEX global field experiment on energy and water cycles) were compared with the meteorological data derived in the rain season (September 1–6, 1999).

This comparison showed a good agreement between the results simulated with the two models of interest, on the one hand, and the observed daily variation of the radiation balance and the latent heat flux, on the other. The only exception was the latent heat flux simulated by the SiB2 model. The SiB2-Paddy simulations show a satisfactory agreement with the observed fluxes of latent heat and heat flux in soils, as well as of the carbon assimilation rate, but SiB2 simulations entail major systematic errors. After certain adjustment of the parameters, SiB-Paddy model provides fairly reliable values of the soil, water, and vegetation cover temperatures. The simulations of the radiation balance, as well as of the energy and water balances, latent heat fluxes, and carbon dioxide assimilation rate yielded fairly adequate results. This offers certain promises of adequate account of the biosphere as an interactive component of the climatic system.

De Rosnay et al. (2000) assessed the reliability of the parameterization schemes for the processes occurring on the land surface, which are utilized in general atmosphere circulation models (GCMs), from the viewpoint of agreement between the observed and the calculated annual average energy and water fluxes as dependent on the degree of detail in accounting the vertical structure of soil. The simulations evidence a fairly strong dependence of the fluxes on the vertical resolution. The 11-layer scheme of parameterization of the heat and water transfer in soil proves fairly adequate for a 1-mm-thick upper layer. The possibilities of realizing a scheme with this thin upper layer are unclear. *However, if one takes into account the fact that the horizontal resolution of GCMs is of the order of hundreds of kilometers, finding solution to this kind of problem requires further efforts.*

A major component of the problem of climate numerical modeling is a complex of issues related to the chemistry of atmosphere. It is a well-known fact, e.g., that the concentration field of such a greenhouse gas as tropospheric ozone (TO) under various conditions (city, region, and globe) is strongly affected by various short-lived minor gaseous components (MGCs)—ozone precursors—such as nitrogen oxides ($\text{NO}_x \equiv \text{NO} + \text{NO}_2$), methane (CH_4), as well as many organic compounds, hydrogen, and carbon monoxide (CO). Each MGC has its specific natural (biospheric) and anthropogenic sources.

Since TO is a greenhouse gas, the MGCs emitted can affect indirectly the atmospheric greenhouse effect formation via affecting the TO concentration

field. Also, MGCs-TO precursors affect the hydroxyl concentration field and, thereby, the oxidizing capacity of the troposphere. The hydroxyl concentration distribution in the troposphere, in turn, governs the life-time and, thereby, the global-scale concentration of methane.

All this is responsible for a complex interactivity of the processes responsible for both direct and indirect impacts on the formation of the atmospheric greenhouse effect. *Derwent et al.* (2001) described the global 3-D Lagrangian STOCHEM model which simulates chemical processes taking into account the MGCs transport. This model was used for simulating interconnected TO and methane concentration fields in case of emissions of short-lived precursors of tropospheric ozone such as CH₄, CO, NO_x, and hydrogen. In this case the radiative forcing (RF) of NO_x emissions varies with the emission location, be it near the surface or in upper troposphere, in Northern or Southern Hemisphere. For each short-lived MGC-TO precursor the global warming potential (GWP) was calculated using the data for the reaction between methane and tropospheric ozone under 100-year forcing. *The introduction of GWP means that RF due to emission of 1 Tg of an MGC was estimated (for a 100-year period) as equivalent (in RF) of carbon dioxide emission.* The combined impact of methane and TO led to the GWP of 23.3.

The simulations showed that indirect RF due to changes in the methane and TO content is significant for all the MGCs-TO precursors of interest. In the case of methane the RF is determined primarily by emissions of methane itself, while in the case of TO, by emission of all the MGCs-precursors, especially nitrogen oxides. The tropospheric ozone-induced indirect RF may be so large that MGCs-TO precursors will need to be ranked among the MGCs essential for assessing the likely climate changes and identifying preventive measures.

Despite USA President G. Bush's anti-Kyoto statements, many of the American newspapers of January 2001 published their articles under dramatically strained headings that informed their readers, e.g., about terrible warming predictions of scientists and about the threat of a global catastrophe in this century posed by the accelerating climate shift («Washington Post»), as well as about the Earth warming is generating a new danger signal («International Herald Tribune»), etc. This stemmed from the new climate change scenarios for the 21st century, which predict that the changes will be more significant than expected earlier. The Third Assessment Report of the Intergovernmental Panel on Climate Change (IPCC-2001) states that by the year 2100 the annual average global average surface air temperature (SAT) can increase by 5.8°C relative to the present time (IPCC, 2001) against only 3.5°C according to the estimate of five years' standing (IPCC, 1996).

Kerr (2001b) correctly noted that the widening range of the likely SAT rise compared to earlier estimates has even greater importance. This was not surprising, however, for many of experts in climate numerical modeling, as this field is still in its infancy and, also, numerical modeling has to rely on a limited amount of observation data (even for SAT the data series is about 100 years long only, being not globally complete).

Although the majority of experts tend to attribute the observed global warming to the GHG concentration growth, the range of possible climate change assessments has expanded rather than contracted in certain respects.

The main uncertainties in climate change assessment involve the following three aspects: (1) global warming detection from observation data; (2) global warming attribution to anthropogenic factors; and (3) future climate change prediction. *Kerr* believes (2001b) that owing to the new findings in the IPCC Report–2001, the range of uncertainty with respect to the two first-named aspects of the problem has contracted, but future climate predictions have become still less clear. The IPCC Report–2001 estimated the observed global warming at $0.6^{\circ}\pm 0.2^{\circ}\text{C}$ (at the statistical significance level of 95%), the warming during the recent 50 years being probably (by 66–90%) due to GHG concentration growth. One of the main factors responsible for uncertainties in climate numerical modeling is, as has been mentioned, inadequate account of the climate-forming role of atmospheric aerosols and clouds.

Unfortunately, the IPCC Report–2001 (*IPCC ...*, 2001) did not adequately assess the role of uncertainties in climate numerical modeling, and this specifically motivated the serious criticism towards the Report by many experts (*Han et al.*, 2000; *Kondratyev and Demirchian*, 2001; *Schrope*, 2001; *Singer*, 1997, 1998, 1999; *Soon et al.*, 2000; *Wojick*, 2001; *Woodcock*, 1999, 2000).

In the global change context, assessments of the present-day and the likely future global climate changes are undoubtedly of primary importance. Although the “global warming” concept is still dominating (as evidenced by the IPCC (Intergovernmental Panel on Climate Changes) Third Assessment Report (*IPCC ...*, 2001), new assessments should be treated as due only to mechanical development of the earlier speculations with a far-from-scientific motivation (as convincingly demonstrated by *Boehmer-Christiansen* (1999, 2000). The contradictions inherent in the climate assessments can be illustrated by radically opposite opinions expressed by two Candidates during the President election campaign in the USA (*From ...*, 2000). A. Gore has long been known as an ardent advocate of the “global warming” concept and the Kyoto Protocol, while G. Bush’s opinion can be characterized as follows. He rejects an environmental policy like that corresponding to the Kyoto Protocol, which would result in radical rise in prices for oil, oil products intended for district heating needs, natural gas, and electricity. President G. Bush believes that

such an agreement would expose the USA economy to strongly increased load without properly protecting it against undesirable climate changes. In G. Bush's opinion, the Kyoto Protocol is an inefficient and inadequate document which unjustly treats America, as it excludes from implementation of the Protocol recommendations 80% of the world, including such major population concentration centres as China and India. G. Bush assigns the primary importance to development of new environment friendly technologies and to the use of market mechanisms, including regulation-free electricity and natural gas markets, taxation, and "emission trading". In G. Bush's opinion, natural gas and nuclear energy will play important role in weakening the USA's perilous reliance on petroleum from abroad and in providing the USA with energy resources in the 21st century. While sharing this radical criticism toward the Kyoto Protocol (KP), we will note that G. Bush's opinion of the market mechanisms is specific to the USA, and in the case of "emission trading", disputable.

The unsoundness of the KP is even more clearly evident from the failure of the Sixth Conference of the Parties (COP-6), which was held on November 13–24, 2000, in Hague. It was attended by seven thousands representatives of 182 governments, 323 intergovernmental and non-governmental organizations, and 443 mass media titles. The Congressman J. Barton (Republican, Texas) said that if Bush won (which came true), his advice to Bush will be that USA reject the Kyoto Protocol and start negotiations aimed at setting the USA's economy free from unsound environmental restrictions. Barton said that what they saw at the COP-6 was an extremely useless exercise or making-things-up exercise, at the best. Therefore, in Barton's opinion, nothing from that week's discussion deserved a support by positive voting.

Interestingly—in this connection—the UNEP Executive Director K. Töpfer rejected the suggestion to treat nuclear energy as an important energy prospect, while the USA and Japan delegates in Hague expressed the readiness to support the funding of nuclear energy projects in developing countries with a view to reducing carbon dioxide atmospheric emissions.

An important feature of the Hague discussions was a certain confrontation between the USA and EC member-countries. These latter rejected the American suggestion on making use of various possibilities, including restoration of forests as carbon sink, in the carbon balance and required that the USA follow the general recommendations on carbon dioxide emission reduction (this view has changed later on to start "forest games").

One cannot qualify differently than absurd the recommendations of the COP-6.2 (second part of COP-6) Conference held in July, 2001 in Bonn. These recommendations introduced the notion of "certified emission reduction" (CER), that is, the recommended real emission reduction were replaced

by equivalent intensification of carbon sinks such as forests. This “innovation” permits Japan, Russia, and Canada to accumulate CERs owing to their forests. The absurd character of this recommendation is evident, above all, from the fact that the global carbon cycle problem is still far from solution (*Kondratyev and Demirchian, 2000*), which makes absolutely unrealistic any reliable assessment of the role of CER as a global climate-affecting factor. As to the intensively debated subject of the three “flexibility mechanisms”, namely, joint implementation, emission trading, and clean development mechanism (of technologies), these can be regarded as rhetorical only.

The Bonn recommendations received extremely contradictory opinions. On the one hand, *D. Kennedy* («Science» journal Editor) (2001) was distressed about “going it lonely” by President G. Bush and the USA and qualified the Bonn agreements as “breathing new life” into hopes for progress in solving the problem of global climate change. In *Sherman’s* (2001) opinion, the Kyoto Protocol, in spite of its clear drawbacks, should be regarded as an important milestone in the climate protection history. Sherman argues that the Kyoto Protocol will, probably, exceed any other international agreement, in its effect on the lives of all humans on this planet in the current century. Sherman believes that the success achieved in Bonn is a direct consequence of the dialogue and mutual understanding, as well as of the sense of reconciliation and compromise.

On the other hand, the opinion of a well-known scientist Dr. A. Agrawal [Chairman of the Centre for Science and Environment (India)] was absolutely different (http://www.cseindia.org/html/dte/dte.20010831/dte_edit.htm). To begin with, he said, that the Kyoto Emperor was no more wearing any clothes. Next, Dr. Agrawal characterized the Kyoto Protocol as a tiring and a fairly meaningless agreement on the climate change problem, which was agreed by the world within those two weeks. Dr. Agrawal said that huge scientific uncertainties in assessments of the greenhouse gas emission reduction efficiency made of the Kyoto compromise nothing more than a big shameful invention. This is not, however, surprising, in Dr. Agrawal’s opinion, because climate negotiations concern the economics rather than environmental problems, and each state does its best in protecting its right for environmental pollution. Exactly on the week of the euphoric declarations that the agreement achieved in Kyoto could save the world, the European Community decided to prolong for another 10 years the implementation of its subsidised programme for coal (the most polluting carbon fuel). Dr. Agrawal concluded his statement by saying that the Kyoto compromise would cost the whole world and everyone more than new clothes for the Emperor.

The main point in the global change problem is that while the global climate warming in the 20th century (especially, in its last quarter) is beyond

question, the factors responsible and quantitative estimates of their contributions into global climate change remain the subject of heated debates. This is even more pertinent to climate forecasts taking into account anthropogenic impacts. In this connection, it is symptomatic that the authors of the IPCC Report-2001 abandoned the “climate change” term defined in the FCCC as due to anthropogenic factors only and agreed upon an adequate definition which takes into account both natural and anthropogenic factors responsible for climate change. This correction to the “climate change” term makes senseless the Kyoto processes aimed at emission reduction for preventing undesirable changes because the climate constantly changes due to many factors. To supplement this, such change also contradicts the traditional definition of climate as the phenomenon characterized by 30-years-averaged values of its parameters. Now, we will turn to the question how the IPCC Third Assessment Report affected the views on the causes of climate changes.

2. Observation data

The variance of the present-day climate and climate change studies results primarily from inadequate completeness and quality of the available global archives of observation data. As known, climate can be characterized by numerous parameters such as surface and atmospheric air temperature and humidity, precipitation (liquid and solid); amount, lower and upper boundary altitude, microphysical and optical characteristics of clouds, radiation balance, and its components; microphysical and optical parameters of the atmospheric aerosol, chemical constituents of the atmosphere, and many others. At the same time, the empirical analysis of the climatic data is usually confined to the appeal to SAT observation data, because only in this case the observational series cover a time period of 100–150 years. However, even these series are far-from being homogeneous, which is particularly relevant to the global data file which is the main information source for the “global warming” concept substantiation. It should also be noted that the long-term variations of the annual average SAT rely mainly on imperfect observation data for the sea surface temperature (SST).

In the climate observation diagnostics, the focus must be on analyzing the climate variability, where not just averages but higher order moments are taken into account. Unfortunately, this approach has not been even attempted so far. The same is true of the internal correlation for the observational series. *McKittrick* (2001) analyzed the SAT long-term variations and showed that by subtracting the contribution to the temperature change within several recent decades made by internal correlation (i.e., climate system inertia) one reduces the temperature change virtually to zero. This points only to the fact that natu-

ral factors can affect the temperature, but the main problem still lies in singling out its anthropogenic component. The importance of this problem is dictated by the fact that specifically the global average SAT rise over the last 20–30 years serves the main argument in favor of the dominating anthropogenic contribution to the climate change.

2.1 Surface air temperature

One of the SAT observational series for the period since 1860 showed that the SAT annual average global average value increased by $0.6^{\circ}\pm 0.2^{\circ}\text{C}$. This by $\sim 0.1^{\circ}\text{C}$ exceeds the analogous value from the IPCC Report–1996 (see *Kondratyev*, 1999). The IPCC Report–2001 explains this increase by a higher SAT level over the 1995–2000 period. The observation data are indicative of a very strong spatiotemporal variability of the annual average SAT on the globe (such a variability is a cause of why reliable enough assessment of SAT uncertainties is impossible). For example, the global average SAT change suggests that the climate warming in the 20th century fell primarily on two time periods, namely, 1910–1945 and 1976–2000. Compared to Report–1996, the new version of the global average SAT change in the Northern Hemisphere excludes the warming period of ~ 900 –1200 and the cooling off period of 1550–1900. Only such a revolution in factology allows arguing that the climate warming in the Northern Hemisphere in the 20th century was the strongest over the last thousand of years with the 1990–2000 period as the warmest decade, and the year 1998 as the warmest year. Owing to specifically these arguments, an impression may be created that it is the marked increase in the CO_2 concentration over the last three decades that is specifically responsible for such extreme temperatures. By excluding these, not simulated by numerical models, it is obvious that one can achieve certain adequacy between the modeled and observed temperatures.

The IPCC Report–2001 makes no mention of the previously supposed climate warming enhancement in the Northern Hemisphere high latitudes as a characteristic feature of the human-induced global warming. However, the analysis of the SATs directly measured at the “North Pole” stations over a 30-year period (*Adamenko* and *Kondratyev*, 1999) and the dendroclimatic proxy data for the last 2–3 centuries shows the following. There was no warming enhancement in the Arctic region, and the temperature changes during the last century and recent decades exhibited major spatiotemporal non-homogeneity manifested as the simultaneous formation of climate warming and cooling off regions in the Arctic region (see also *Stafford et al.*, 2000).

Since the 1950s, with a more or less adequate aerological observational network, the trends for the global average SAT and lower troposphere tem-

perature have been almost identical (about $0.1^{\circ}\text{C}/10$ years (Angell, 1999, 2000a, b). According to the satellite-based microwave remote sensing data (over 1979–2000 period), the global average temperature of the lower tropospheric air increased by $\sim 0.036^{\circ}\text{C}/10$ years, i.e., significantly slower compared to SAT ($0.24^{\circ}\text{C}/10$ years). This difference is even more appreciable if one excludes the influence of the sharp temperature rise in 1998 due to the severe El Niño phenomenon. This is evidenced by low trends for the 1979–1997 period, namely, $0.012^{\circ}\text{C}/10$ years for the tropospheric air (that is, cooling according to the microwave remote sensing) and $0.158^{\circ}\text{C}/10$ years for SAT. There is no such a trend difference in the global circulation models that are the main IPCC instruments for understanding climate changes, and this casts serious doubts upon their capabilities. Controversial nature of existing temperature observation data has been convincingly analyzed by *Wojick* (2001).

Sonechkin (1998) has accomplished a study of self-similar and trend-like properties of hemispheric SAT time series as realizations of a fractional Brownian motion by means of the wavelet transform technique. The results obtained indicate a first evidence of a crossover scale that separated the obvious internally-induced, statistically stationary chaotic oscillations from the substantially longer, trend-like SAT variations, which origin is not clear and may be assumed to be extremely forced. The residual trend-like components reveal a single linear warming trend that was started at the beginning of the 20th century. The increment of this trend is equal to $0.59^{\circ}\text{C}/100$ years for both hemispheres. Later on *Sonechkin et al.* (1999) have demonstrated a very strong coupling between long-term SAT variations and Southern Oscillation dynamics. *Datsenko et al.* (2001) have applied similar approach to analyze seven seasonal early instrumental temperature series at various locations in Europe. They emphasized the crucial role of seasonality in the spatiotemporal structure of low-frequency SAT variability.

2.2 Snow and ice cover

These climate characteristics are treated by IPCC as important indirect global warming indicators. The Report says that there was a $\sim 10\%$ snow cover reduction since the late 1960s and a ~ 2 -week reduction of the annual lake and river ice cover in mid- and high-latitudes of the Northern Hemisphere in the 20th century. This was paralleled by retreating of the mountain glaciers in non-polar regions. Also, the Report states that the sea-ice cover in the Northern Hemisphere in spring and summer periods has reduced since the 1950s by 10–15%. It is highly probable that during the last decades (in end summer–early autumn periods) there was a $\sim 40\%$ thinning of the sea-ice cover period in the Arctic region, with a much less significant thinning in the winter period. Since

the 1970s, regular satellite observations have revealed no marked trends for ice cover either in the Arctic or Antarctic regions. Combined with insignificant temperature trends, this allows a conclusion that the ice thickness in the Arctic region is markedly influenced by the ocean currents and the North-Atlantic Oscillation (NAO) dynamics.

2.3 Surface level and heat content of the upper layer of the ocean

These characteristics are also important for IPCC in view of the serious concerns about global consequences of the World Ocean level rise. Because of exclusively fragmentary, intermittent, and unreliable measurement results available, the Report-2001 actually presents the calculation-corrected data. It states that the World Ocean level has risen by 0.1–0.2 m in the 20th century owing to thermal expansion of the sea water and land ice melting due to global warming. The Report says that in the 20th century the World Ocean level rising rate exceeded almost tenfold that over the last 3000 years. Since the 1950s, the ocean surface temperature rising has caused the heat content of the upper ocean layer to increase.

Levitus et al. (2001) analyzed the warming data for individual components of the climate system in the second half of the 20th century. These data were derived from the analysis of the increase in the heat content of the atmosphere and the ocean, as well as the heat consumed by melting of certain components of the cryosphere. The results suggested an increase in the heat content of the atmosphere and the ocean. Over the 1950–1990 period, the increase in the heat content of the 3-km-thick upper ocean level exceeded at least by an order of magnitude those for other components of the climate system. The increase in the heat content of the ocean observed in the 1955–1996 period was estimated at 18.2×10^{22} J, and that in the case of the atmosphere, at 6.6×10^{21} J only. As to latent heat due to phase transformations of water, these were estimated at 8.1×10^{21} J (decrease in the mass of terrestrial glaciers); 3.2×10^{21} J (sea ice cover reduction in Antarctica); 1.1×10^{21} J (melting of mountain glaciers); 4.6×10^{19} J (snow cover reduction in the Northern Hemisphere); and 2.4×10^{19} J (melting of permanent ice cover in the Arctic region).

Levitus et al. (2001) compared the observation data with the results of numerical modeling by the interactive model of the “atmosphere–ocean” system developed at the Geophysical Fluid Dynamics Laboratory (USA). This comparison took into account (1) the radiation effects due to the observed GHG concentration growth and changes in the sulphate aerosol in the atmosphere and extra-atmospheric insolation, as well as volcanic aerosol, and (2) only GHGs and sulphate aerosol. It was found that the observed heat content variations in the ocean can be primarily attributed to the GHG concentration

growth in the atmosphere, although one has to take into account a major uncertainty in assessing the radiative forcing due to sulphate aerosol and volcanic eruptions. The latter fact makes the work by *Levitus et al.* (2001) of insufficient reliability as regards human-induced warming identification. Those authors mentioned major variability of the heat content of the World Ocean from year to year and emphasized the following. They partially attributed the extremal warming of the World Ocean in the 1990s to the multidecadal warming of the Atlantic Ocean and Indian Ocean, as well as to the positive polarity of the possible biannual heat-content fluctuations of the Pacific Ocean. The observed variations of the heat content of the World Ocean can be related to the modes of hemispherical or global variability of the atmosphere from the ocean level to the stratosphere. Gaining insight into the nature of this kind of possible relations is of major importance for understanding the mechanisms governing the global climate.

As has been already mentioned, recent developments on identifying the human-induced climate changes were confined for the most part to analyzing comparatively long series of SAT data. Also, much more limited bodies of information on sea-ice cover variations, vertical temperature profiles (radiosonde data), and satellite microwave remote sensing results were analyzed. On the other hand, numerical modeling results suggest that more representative than SAT should be in this context the extremely scanty data on the amplitudes of the annual and daily temperature variations in winter.

Being the major component of the global climatic system, the World Ocean holds the priority in the variability analysis, especially after *Levitus et al.* (2001) revealed an increase in the heat content of the upper layer of all the oceans within the past 45 years. In this connection, *Barnett et al.* (2001) discussed the results obtained by comparing the numerical modeling and observation data for the heat content of the 3-km-thick upper layer of different oceans. The calculations utilized the "parallel" climate model (PCM) for the "atmosphere-ocean" interactive system (no flux adjustment) and five scenarios of the growth patterns for GHG concentration and sulphate aerosol content in the atmosphere.

The comparison showed that the calculated heat content anomalies (that is, deviations from the data corresponding to the control integration) did not differ from the observed values (for the 1950–1990 period), the statistical significance being at the level of 0.05. The only exception (in the global averaging case) was the data for the 1970s. In this case, the model does not simulate the heat content anomaly observed during this decade. On the whole, the probability of the fact that the heat content anomalies are due to natural variability of the climatic system does not exceed 5%. This makes realistic detection of the anthropogenic signal of the climate changes.

It should be noted, however, that oceans differ substantially in the nature of warming. A typical feature of the Atlantic Ocean (especially of its southern area) is an intensive vertical mixing and rapid propagation of the warming deep into the ocean. In other oceans this process has a much slower rate. The results obtained allow an important conclusion that climate models should simulate not only SAT but also ocean heat content variations. *Barnett et al.* (2001) pointed to certain weak points of the numerical modeling undertaken - in particular, that the natural climate variability was assessed basing on the control numerical modeling data only.

Cai and Whetton (2001) called attention to the fact that the enhancing effect of the “greenhouse” warming on the sea surface temperature (SST) field in the Pacific Ocean tropics can affect significantly the precipitation on the global scale in the future. Studies on these controversial problems with the use of both the observation and numerical modeling data yielded very different results. The climate warming during recent decades was similar in the spatial structure to the El Niño/Southern Oscillation (ENSO) phenomenon. In view of the lack of the data for such a structure over the entire century, it was suggested that the observed warming structure resulted from multidecadal natural climate variability rather than from the greenhouse forcing-induced change.

The first results of the numerical modeling with the use of interactive models of the “atmosphere–ocean” system showed that the warming structure characterized by a zonal SST gradient in the equatorial zone should be similar to El Niño, by contrast to certain theoretical studies which point to a similarity with La Niña. To settle this controversy, *Cai and Whetton* (2000) utilized for climate numerical modeling the interactive model developed at the Australian National Scientific Center (CSIRO Mark 2). They showed that the initially formed spatial structure of the warming is similar to La Niña (the strongest warming in extra-tropical latitudes for weak La Niña which is similar to the structure in tropics), which later on (after the 1960s) transformed to a structure similar to El Niño. Such results were yielded by three versions of numerical modeling (in addition to the control integration over 1000 years) with the GHG concentration growth in the atmosphere prescribed according to the observation data (1880–1990) and the IS92a scenario (1990–2100). These simulations did not take into account the influence of aerosol on climate formation.

The above-mentioned transformation of the spatial structure of the climate warming is due to warm extra-tropical waters that after deep submerging come through subtropics and reach the tropical zone where upwelling arises. This is specifically the reason for climate change. These results can be interpreted as confirming the conclusion that the warming having a characteristic El Niño-like spatial structure, which was observed over recent decades, is at least partly attributable to the human-induced enhancement of the atmospheric greenhouse effect. It was noted, however, that despite the similarity between

effect. It was noted, however, that despite the similarity between the observed and calculated warming structures, the observations carried out before the 1950s are less reliable. Also, conditions similar to La Niña were observed once again recently (in 1995–1996 and 1998–2000).

2.4 Other climate parameters

The observation data suggest a 0.5–1%/10 years precipitation enhancement in the 20th century in most of terrestrial regions in Northern Hemisphere mid- and high-latitudes. This was paralleled by approximately 0.3%/10 years precipitation reduction in most of the subtropical-latitude land regions which, however, weakened in the more recent years. As to the World Ocean, the lack of adequate observation data prevented revealing reliable precipitation trends. Since the middle 1970s, the most stable and intensive phenomena have been those of El Niño/Southern Oscillation (ENSO). Such ENSO dynamics was manifested in the features of the regional variations of SAT and precipitation in most of tropical and subtropical zones. The observation data on the intensity and occurrence of tropical and extra-tropical cyclones, as well as local storms, remain inadequate, which prevents revealing any clear trends (Grigoryev and Kondratyev, 2001).

2.5 Greenhouse gas and anthropogenic aerosol concentration in the atmosphere

The IPCC Report–2001 notes that since 1750 the carbon dioxide concentration in the atmosphere has increased by approximately one third and attained the highest level over the last 420 thousand years (possibly, over the last 20 million years), as evidenced by the borehole data. About two thirds of the CO₂ concentration increase over the last 20 years is accounted for fossil fuel burning emissions (the remainder resulted from deforestation and, to a lesser extent, from cement industry). Interestingly, by the end of 1999 the CO₂ emissions in the USA exceeded the 1990 level by 12%, which figure will further increase by another 10% by the year 2008 (Victor, 2001). At the same time, the Kyoto Protocol requires a 7% emission reduction by 2008 relative to the 1990 level, which implies a total emission reduction by ~25% (which is, certainly, absolutely impossible).

According to the IPCC Report–2001, both the World Ocean and land act now as global sinks of CO₂. In the ocean case, this is due to chemical and biological processes, and in the land case, to enhanced “fertilization” of vegetation due to increasing CO₂ and nitrogen concentrations, as well as to changing land use patterns. The IPCC’s approaches to carbon cycle remained virtu-

ally identical to those in early 1990s, although Report-2001 devoted to this problem a special chapter. From the very beginning, the IPCC was wrong in estimating the forest and land use processes, taking the fossil fuel burning and deforestation as the main sources of CO₂ emissions. In attempts to close the carbon cycle by balance calculations they introduced an undefined “fertilization sink” term which obscures the carbon cycle problem. Emissions due to “carbon burning” by humans when breathing were excluded as a CO₂ source. According to *Wigley* (1998, 1999), about 135 kg of carbon in a year; for 6 billion people this makes about 0.8 Gt, and this is much greater than the cement industry emission which is a “must” in all the Report versions. As shown by *Kondratyev and Demirchian* (2000), an additional, beyond 270 ppm, anthropogenic increase in the CO₂ concentration in parts per million K_a linearly varies with the global population size. According to this dependence, the current CO₂ concentration in the atmosphere can be parameterized as $K \sim 270 + K_a = 270 + 15P$, where P is the population size (in billion). For example, the concentration K of the atmospheric carbon dioxide in the year 2000, when the population size was about 6.1 billion, is equal to $K \sim 270 + 15 \times 6.1 = 361.5$ ppm. This value differs by only 2.2% from that obtained at the Mauna Loa observatory, namely, 369.7 ppm. This inaccuracy is comparable with those for P and K values. When related to the K_a - P linear dependence, the carbon cycle model not only more adequately simulates the processes observed in the carbon cycle, but also (which is more important) more accurately links the forecasted future CO₂ concentration to the only variable, i.e., the population size. For example, basing on this relationship, one can expect that the carbon dioxide concentration in the atmosphere will rise by the year 2100 (with the predicted population size in 2100 of 12 billion) to $K_a = 15 \times 12 = 180$ and $K \sim 270 + 180 = 450$ ppm.

The fact that the CO₂ concentration growth in the 21st century will be due mainly to human activity is beyond question. Basing on the model data, the Report states that the biosphere and ocean will be gradually losing their importance as the concentration rise barrier. In this connection, the Report-2001 presents a probable range of the CO₂ concentrations by the end of century, namely, 540–970 ppm against the pre-industrial and present-day levels of 280 and 369.7 ppm, respectively. The carbon cycle models listed in the Report-2001 assign the primary role in the oceanic sink of carbon to diffusion and chemical processes occurring in water. These models do not take proper account of the processes due to carbon dioxide transport by ocean currents, which is especially relevant to cold water formation regions. Such factors make the carbon dioxide absorbing capability look more optimistic. This is also evidenced by increase in the oceanic sink as stated in the Report. Land use, whose pattern and intensity are governed by the aggregate economic ac-

tivity, can create sinks for carbon. Likewise, deforestation does not necessarily decrease the sink. By making some of the Amazonian large forests a region of zero sink-source carbon balance, one can achieve some positive results. The same role was assigned to lumber industry complexes in the former USSR, where logging was paralleled by creating new forest plantation whose sink significantly increased in time. These and other features of the economic activity make a decisive contribution to the established linear dependence between the increase in the human-induced CO_2 concentration in the atmosphere (K_a) and the population size. The observations and modeling showed that the per capita carbon emissions reached a maximum level by the end of the past century, whereupon they began to decline, which is quite natural in the context of the world economic development situation. It should be noted that the emission declined naturally, not responding to any administrative measures like those recommended by the Kyoto Protocol. All this makes unlikely the forecasts of carbon dioxide concentration above 450–460 ppm.

Since 1750 (indirect data), the atmospheric methane concentration has increased by a factor of 2.5, and now it tends to increase. The annual growth rate of the CH_4 concentration decreased virtually to zero, exhibiting a greater variability in the 1990s compared to the 1980s. Since 1750, the nitrous oxide concentration has increased by 16%. Through implementing the Montreal Protocol recommendations and follow-up measures, the concentrations of a number of halocarbons, acting both as GHGs and ozone-depleting gases, either increased at a lower rate or began to decline. On the other hand, there was a rapid growth of the concentrations of their substitutes and of some other synthetic compounds (e.g., perfluorocarbons PFCs and sulfur hexafluoride SF_6). As to other greenhouse gases, their concentrations expected for the year 2001 widely vary. For example, some experts believe that the tropospheric ozone as a greenhouse gas can become equal in the contribution to methane and will also be important in deteriorating the air quality over the most of the Northern Hemisphere.

The estimated radiative forcing (RF), which characterizes the enhancement of the greenhouse effect in the atmosphere and is due to the concentration growth of the atmospheric mix of minor gaseous components (MGCs), is proved to be 2.42 W/m^2 , into which various minor gaseous components such as CO_2 , CH_4 , halocarbons, and N_2O contributed with 1.46, 0.48, 0.33, and 0.15 W/m^2 , respectively. The decrease in the total ozone concentration observed in the two recent decades could result in a negative RF of -0.15 W/m^2 , which can decline to zero during the present century provided efficient ozone layer-protecting measures be taken. The increase in the tropospheric ozone concentration since 1750 (by approximately one third) could lead to a positive RF about of 0.33 W/m^2 .

Since publication of the IPCC Report–1996, many changes have been made to assess RF as due not only to the previously considered sulphate aerosol but also to other aerosol types. This concerns especially carbon (soot) aerosol which strongly absorbs solar radiation, as well as organic, sea salt and mineral aerosol. Major spatiotemporal variability of the aerosol content in the atmosphere and of its properties significantly complicates assessing the aerosol impact on the climate (*Kondratyev, 1999*). An example to this can be found in the “alternative strategy” proposed by *Hansen et al. (2000)*. These authors assumed the approximate mutual compensation of the climate warming via the CO₂ concentration growth and cooling due to anthropogenic sulphate aerosol. In this situation, more importance is assigned to anthropogenic methane emissions (mainly due to rice paddies) and carbon (absorbing) aerosol. Being acceptable at least for the reason of making unnecessary the Kyoto Protocol, this new strategy—unfortunately—creates a broad scope for political games, now around methane and carbon aerosol.

Another climate-forming factor to be taken into account is the extra-atmospheric solar radiation change. The contribution from this factor to RF over the period since 1750 could have been approximately 20% of that from CO₂, due mainly to enhancement of extra-atmospheric insolation in the second half of the 20th century (the 11-year insolation cycle is important to be taken into account). The fact that the IPCC Report–2001 neglects the phase of the Middle Ages warming and the Little Ice Age indicates that climate experts are still far from understanding the possible mechanisms of enhancement of the solar activity impact on the climate (*Haigh, 2000; Kondratyev, 1998*).

3. Results and reliability of numerical climate modeling

The problem of numerical modeling was analyzed in detail in, e.g., *Bengtsson, 1999; Houghton, 2000, 2001; Kondratyev, 1998, 1999; Schlesinger and Andronova, 2000, 2001; The greenhouse ..., 1999* and many others. Here, we will restrict ourselves to brief comments. The progress in improving the completeness of numerical models of climate which take into account interactively all the components of the climatic system “atmosphere–hydrosphere–cryosphere–biosphere” is beyond question. The interactive simulation of the global carbon cycle in climate models has been started at last. The extreme complexity of climate models and numerous empirical parameterization schemes they utilize for parameterization of various processes hinder assessment of the adequacy of these models, especially from the viewpoint of future climate prediction. This was specifically responsible for very schematic, contradictory, and unconvincing attempts to compare numerical modeling results and observation data.

One is forced to accept the fact that despite all the improvements made, the models in question do not adequately describe the reality. The major drawback of these models is that their adequacy is quantitatively unverifiable. Moreover, the more detailed the simulation of the reality, the more unattainable task of overcoming this drawback in view of the stochastic nature of the processes and models. This makes unconvincing the conclusions concerning, e.g., the long-term change of the annual average global average SAT over the recent 150 years. If, according to the IPCC Report-1996, the observed and calculated (taking into account the CO₂, and sulphate aerosol concentration growth) SAT variations agree well, one has to attach more attention to the methane and carbon aerosol, as proposed by *Hansen et al.* (2000). Unfortunately, in both cases the conclusions rest upon arbitrary opinions, and the agreement between the models and observations is achieved in reality by nothing more than forced fitting. Also, a meaningful comparison of the theory with observations requires consideration of the regional climate changes (not only SAT) and not only average values of the climate parameters but also their variability characterized by higher-order moments. An indication of a necessity to further improve coupled climate models is the controversial conclusion concerning the fate of thermohaline circulation (THC) under conditions of global warming. Due to *Gent* (2001), there will be no THC changes under conditions of global warming. An unsolved problem is the "warming commitment" discussed by *Wetherald et al.* (2001).

According to *Charlson et al.* (2000), anthropogenic aerosols strongly affect the cloud albedo, and the assessment of the global average forcing showed that these values are of the same order of magnitude (though with opposite sign) as those due to GHGs. *Recent studies show that the aerosol forcing can even exceed the predictions.*

The Achilles hill of climate models is parameterization of the biosphere dynamics (*Gorshkov et al.*, 2000; *Kondratyev*, 1998; *Zhang et al.*, 2001). In this context, fairly many numerical experiments were carried out previously with the aim to elucidate how deforestation affects the Amazon river basin. These experiments showed that total deforestation (replacement of rainforest by grass cover) will result in reduction of evaporation from the surface and precipitation, though in a simultaneous rise in the surface temperature. This will be responsible for a rise of SAT within 0.3–3°C. Such changes are due mainly to increase in the surface albedo and decrease in soil moisture. This will cause a decrease in the energy and water vapor fluxes to the atmosphere, a moisture convection decay and latent heat release which, in turn, will be responsible for a decline in the atmosphere warming. This will have a dual effect on the atmosphere circulation: (1) changes in the ascending and descending air flows in tropics and subtropics (Hadley circulation cells) and (2) changes in the

planetary wave generation conditions (Rossby waves) propagating from tropics to mid-latitudes.

To elucidate in more detail how deforestation affects the atmosphere circulation and climate, *Gedney and Valdes (2000)* carried out numerical experiments on simulating the present-day (“reference”) climate and total deforestation conditions for the Amazonian region. To this end they took advantage of a 19-level spectral (T42) general atmosphere circulation model. Deforestation should change the following climate-forming parameters: albedo (13.1→17.7%); roughness (2.65→0.2 m); vegetation cover share (0.95→0.85); leaf area index (4.9→1.9); minimal vegetation cover resistance (150–200 s/m); root zone depth (1.5→1.0 m). All this will change the soil type as well. Numerical modeling revealed statistically significant variations of precipitation in winter period in the north-east area of the Atlantic Ocean, which result from deforestation and propagate further eastwards, toward Western Europe. Such variations are due to changes in large-scale atmosphere circulation in mid- and high-latitudes. Simulation of such variations using the simple model confirmed that they are due to planetary wave propagation. This suggests that the results revealing the interrelation between the processes occurring in the deforestation region and in North Atlantic and Western Europe are independent of the model chosen, with the variation range corresponding to the assessed human-induced climate changes due to increase in the CO₂ and aerosol concentration.

Zhang et al. (2001) carried out a significantly more extensive numerical modeling of the climate implications of tropical deforestation under progressing “greenhouse” warming due to the CO₂ concentration doubling. Those authors utilized the global climate model CCM1-Oz developed at the National Center for Atmospheric Research (USA). Calculations suggest a major decline of evapotranspiration (by ~180 mm/year) and precipitation (by ~312 mm/year), as well as a SAT increase by 3.0 K in the Amazonian region. Similar, though less pronounced changes are observed in South-East Asia (precipitation reduction by 172 mm/year and warming by 2.1 K). Even less pronounced changes are observed in Africa (precipitation increase by 25 mm/year). Energy balance assessments showed that the climate warming is due not only to greenhouse effect enhancement but also to deforestation-induced decrease in evapotranspiration. Statistically significant climate changes are observed in mid-latitudes as well.

The IPCC Report–1996 contains a conclusion that was subject to heated debate, namely, that the balance of evidence suggests a discernible human impact on global climate. Also, the report states that the “anthropogenic signal” is already manifested against the natural climate variability background. The IPCC Report–2001 (*IPCC ...*, 2001) states that detection and attribution studies regularly indicate the presence of the anthropogenic signal in the climate observation data for the last 35–55 years. The nature-induced impacts could play

a role in the warming observed in the first half of the 20th century, but they cannot explain the warming in the second half of the century. This report also indicates, however, that the reconstruction of the climate for the last 1000 years, as well as model estimates demonstrate low probability of that the observed climate changes in the second half of the 20th century could be of completely natural origin. Also, the report emphasizes the high uncertainty of the quantitative estimates for human-induced warming, especially as regards contributions of various warming factors (this holds above all for clouds and atmospheric aerosol). The judgements and conclusions mentioned are so evidently conflicting and unconvincing that we leave them without comments. Certainly, the leading role in substantiating the future climate predictions should belong to integrated models describing the dynamics of the interaction between the socioeconomic development and the nature (Kondratyev, 1999; Prinn et al., 1999; *The Atmospheric ...*, 1998; Victor, 2001). It remains to be seen, however, how realistic the forecasts can be, based on such models with their extraordinary complexity and inadequate input information. It seems likely that at least in the not so distant future integral models will serve for preparing very schematic scenarios only. An important advantage of such models is that they show the regional climate change pattern. However, this pattern (whose adequacy is doubtful) can be obtained only after multiple simulation of climate changes on the global scale, which is very problematic.

New data suggest that with a 1% annual growth of the CO₂ concentration under various scenarios of the economy development and various aerosol compositions, the global average annual average SAT increase during the period 1990–2100 will be 1.4–4.8°C against 1–3.5°C from the IPCC Report–1996. In this connection it is symptomatic that with improving the models and increasing their number, the divergence of this process deepened rather than contracted. Importantly, the SAT values calculated in terms of various models for the same scenario of MGC emissions were virtually identical to those with the same model for various scenarios. As to regional climate predictions, they are still statistically unreliable. However, one can, probably, hold as reliable the conclusion that in many terrestrial regions the warming will be faster than on the global scale, especially, in high-latitudes during the cold half-year. The most substantial (~40% in excess of the global average value) was the calculated climate warming in northern region of Northern America, as well as in the Northern and Central Asia. By contrast, the summer warming in South and South-East Asia and in southern regions of Southern America and the winter warming should be weaker than the global average warming. Numerical modeling data are indicative of the forthcoming enhancement of the water content of the atmosphere as well as precipitation. In particular, there can be precipitation enhancement in Northern Hemisphere mid- and high-latitudes, as well as

in Antarctica in winter. This conclusion is of special importance in the glacier dynamics context. For low latitudes, depending on the MGC emission scenario chosen, both precipitation enhancement and reduction is probable.

Responding to great interest to possible anomalous events, the *IPCC Report (2001)* gives prognostic estimates as correlated with the recent observation data (*Table 1*). This problem has been discussed by *Karl et al. (1999)* and *Grigoryev and Kondratyev (2001)*. The deficient observational data and unreliable results of numerical modeling make the conclusions in the table fairly vague.

Table 1. Observed and predicted anomalous weather and climate changes

Phenomenon	Observations (second half of the 20th century)	Forecast (2050–2100)
Abnormal temperature maxima and number of unusually hot days	Almost all terrestrial regions	Revealed by the majority of models
Enhanced heat index	Many of terrestrial regions	
Abnormally intensive precipitation	Many of Northern Hemisphere mid- and high-latitude regions	
Abnormally high temperature minima and decrease in the number of cold days	Almost all terrestrial regions	Possible, taking into account increase in minimal temperatures
Decrease in the number of frost days		
Decrease in the daily temperature amplitude	Many of terrestrial regions	Almost all models
Summer continent dehydration	Selected regions	
Maximal wind enhancement in tropical cyclones	Not observed, but the number of case studies is scarce	Selected models
Enhancement of medium and maximal precipitation in tropical cyclones	Insufficient data	

Calculations of human-induced (“green-house”) climate changes evidence a possible weakening in the future of thermohaline circulation (THC) in Northern Hemisphere oceans. However, even models revealing such a weakening still reflect the preserved “greenhouse” warming in Europe. It is still unclear

whether the THC collapse can be irreversible and which threshold conditions correspond to this kind of collapse. None of the available models predicts complete cease of THC within the next 60 years.

Numerical modeling of the “global warming” process suggests that there must be further snow and sea ice cover reduction in Northern Hemisphere. Further retreat of glaciers (except for Greenland and Antarctic, including Western Antarctic, ice sheet) is expected in the 20th century. With the given scenarios of the greenhouse gas concentration growth over the 1990–2100 period, the World Ocean level can rise within 0.14–0.8 m (~0.47 on the average), which exceeds 2–4-fold the ocean level rise rate in the 20th century.

IPCC believes that the anthropogenic impact on the global climate will be preserved for a long time, and this will determine the following specific features of the corresponding processes:

- Carbon dioxide emissions have durable impact on the atmospheric CO₂ concentration. Even within several no-emission centuries the fraction of carbon dioxide retained in the atmosphere can reach 20–30% of the total emission level;
- The supposed stabilization of the atmospheric CO₂ concentration requires significant reduction of the carbon dioxide emissions, as well as a more significant decrease in emissions of other greenhouse gases;
- After stabilization of the CO₂ concentration level the global average SAT will also continue to grow for hundreds of years owing to the giant thermal inertia of the ocean (this concerns only 15–25% of the whole increase);
- The ocean level and ice sheets will continue to respond to previous climate changes during thousands of years after the climate stabilization. Model calculations show that in case of warming of 5.5°C, the World Ocean level can rise (owing to the Greenland ice melting) by 3 m within 1000 years. Modern dynamics models for the Western Antarctic ice sheet suggest that the melting can be responsible for the ocean level rising within 3 m during 1000 years, but one should take into account the fact that the possible long-term dynamics of the Western Antarctica cryosphere has not been properly studied.

The conclusions concerning the currently observed and, especially, the likely future climate changes are very uncertain. This concerns both the diagnostics of the present-time dynamics of climate, its simulation models and numerical modeling results. According to the *IPCC Report (2001)*, the priority should be assigned to developments along the following eight directions:

- To stop further degradation of the conventional meteorological observation network;

- To continue research on global climate diagnostics with the aim to obtain long series of observation data with a higher spatio-temporal resolution;
- To attain more adequate understanding of the interaction between the components of the ocean climatic system (including deep-lying layers) in their interaction with the atmosphere;
- To reach more realistic understanding of the long-term climate variability;
- To apply the “ensemble” approach in numerical modeling of global climate in the probabilistic estimation context;
- To develop the integral totality (“hierarchy”) of global and regional models, with a special attention to numerical modeling of regional impacts and extreme changes;
- To substantiate interactive physcobiological climate models and socio-economic development models with the aim to analyze the environment–society interaction dynamics.

This should be supplemented, in particular, by the following:

- For understanding the regular features of the present-day climate, paleoclimatic investigations are essential, especially on sudden—within comparatively short time periods—changes (*Kondratyev, 1998, 1999; Kukla, 2000*);
- Intensive satellite-based remote sensing studies have not yet provided an adequate global information required for climatic system diagnostics, because the existing satellite-based and conventional observation system operate in a far- from-optimum regime. Despite many efforts to and major progress in development of the Global Climate Observation System (GCOS), Global Ocean Observation System (GOOS), Global Terrestrial Observation System (GTOS), and (at a later time) Integrated Global Observation System (IGOS), the task of optimizing the global observation system still remains to be solved. We still need to realize that along with accumulation of long homogeneous observation data series required for climate system diagnostics there is also a need in problem-driven (“focused”) observational experiments. These latter will address problems such as global carbon cycle, anthropogenic impact on the stratospheric and tropospheric ozone, the dynamics of the processes occurring in the “aerosol–clouds–radiation” system, biotic regulation of the environment etc. (*Goody et al., 2001; Kondratyev and Cracknell, 1998; Kondratyev, 1999*);
- The IPCC documents vaguely estimate the levels of anthropogenic impact on global climate. *Reilly et al. (2000)* correctly explain this situation primarily by the lack of quantitative estimates for the uncertainty of the results obtained (this is the case for, e.g., expected rise of SAT by 1.4–5.8°C). Clearly, in such situation the decision-making on environmental policy (e.g., in the case of Kyoto Protocol) relies on views lacking a

icy (e.g., in the case of Kyoto Protocol) relies on views lacking a serious scientific substantiation (see *Soon et al.*, 2000). In this connection, a question arises as to whether predictions for the year 2100 make sense in view of the fact that the prospects for the global socioeconomic development cannot be predicted. The only possible answer to this question suggests itself: One can only prepare entirely conditional scenarios relying on which the political decision-making would be unwise and even fraught with danger. This is even more pertinent to regional scenarios, which have specific of practical interest, rather than global average estimates which can be likened to the "hospital average temperature". Naturally, we cannot accept the attempts by *Allen et al.* (2001) to excuse the lack of quantitative estimates of uncertainties—especially by pleading the fact that in 1990 the IPCC was pressed to make a statement attributing the observed climate changes to anthropogenic impact—on grounds that otherwise it might have been done by anybody else. The opinion by *Wigley and Raper* (2001) defending the IPCC Report–2001 conclusions also cannot be regarded as convincing evidence.

4. Conclusion

The main conclusion following from discussion of the IPCC Reports which have been used to substantiate the need in the entire process of adoption and realization of the Kyoto Protocol is that they are unsuitable as decision-making bases. The gaining insight into characteristic features of the present-day climate system dynamics and especially assessing the likely climate changes in the future are seriously complicated by the lack of reliable estimates of the contribution made by anthropogenic factors to the present-day climate change. We clearly realize that human-induced enhancement of the atmospheric greenhouse effect due to GHGs concentration growth in the atmosphere should be responsible for certain changes in the global climate. But no use of this fact for creating panic and for solving political problems can be tolerated. Unfortunately, many of the leading figures in the IPCC act in accordance with specifically this principle.

For understanding how realistic the climate predictions are, verification of the model adequacy to the currently observed climate changes and paleoclimate dynamics (based on indirect data) has crucial importance. As to the use of modern observation data, the situation seems fairly paradoxical: Such verification is virtually confined to averaged temperatures, while it is evident that one needs all other kinds of information. The paradox consists in that satellite observations provide a giant excess of nonsystematized data, which is paralleled

by the already mentioned degradation of the conventional (in situ) observation network.

Verification of global climate models by comparing the numerical modeling and observation data is an extremely complex task. It has been solved most often by comparing long series of data on the annual average global average SAT, which virtually always yielded the same conclusion (despite substantial—sometimes cardinal—distinctions in accounting climate-forming processes), namely, that calculations agree on the whole with observations. Another feature characteristic of these developments is a conclusion—not adequately substantiated scientifically—of a major (or even dominating) contribution from anthropogenic factors (above all, greenhouse effect) to climate formation. Clearly, this approach to model verification cannot be taken seriously, because (1) modern climate models are still imperfect from the viewpoint of interactive account of the biospheric processes, “aerosol–clouds–radiation” interaction, and many other factors, and (2) the only long-term (100–150-year-long) SAT observation series available is far from being adequate from the viewpoint of calculating annual average global average SAT (not to mention other climate parameters).

Recent developments under GCOS, GOOS, GTOS, and IGOS programmes are undoubtedly useful, but they still do not substantiate the optimal global observation system (this question was discussed in detail in monographs (Kondratyev, 1998; Kondratyev and Cracknell, 1998), and in more recent years, by Goody *et al.* (2001)). This is primarily explained by imperfect climate models intended as the conceptual basis for observation planning to be further improved following the refinement of the models. In this connection we should emphasize the need in analyzing the *divergences* disclosing specific “weak points” of models rather than in making illusory statements treating global climate models as fairly realistic. Clearly, the focus of consideration should be not only on SAT but on the *totality* of the climate parameters. The primary attention should be given to model’s simulation of climate changes (including at least second-order moments).

Paleo data indicate that in the geological past there were strong and sometimes very rapid climate changes. *Alverson et al.* (2000) noted, for example, that the ocean level changed by over 100 m, the stable changing rate being over 1 m within 1000 years. Such changes significantly exceed the supposed human-induced changes corresponding to the doubling of the atmospheric CO₂ concentration, which shows that any concerns about anthropogenic impact on the climate are unjustified. The problem consists not so much in forecasting in detail the climate of the future as in analyzing how sensitive is the modern society and its infrastructures to the likely climate changes. It is worth to mention that for many countries, including Russia and the USA (see *Kondratyev,*

2001), the forecasted warming means advantages rather than danger. In this connection, paleo data are of a greater value for climate prediction than numerical modeling-based schematic scenarios.

As to climate predictions and the atmospheric greenhouse emission reduction recommended by the Kyoto Protocol, the former is clearly need to be interpreted as schematic scenario and the latter, correspondingly, as having no real grounds. This suggests an acute need in revising the Framework Convention on Climate Change (before "Rio + 10") and rejecting unjustified and non-realistic recommendations contained in the Kyoto Protocol that pose threats to socioeconomic development. The collapse of the 6th Hague Conference of the FCCC signatory-countries (November, 2000) suggests that these costly conferences are fruitless and the global climate change problem needs a serious scientific discussion without domination of adepts of "global warming" concept. The real situation consists in that greenhouse emissions continue to increase, and this trend will be preserved, in particular, in the USA, and all the reasonings on the importance of "flexible market mechanisms", "emission trading", etc. are purely rhetorical.

The current status of the climate theory by no means receives only optimistic assessments. In this connection it will be appropriate to mention opinions of American experts (see *Shackley et al.*, 1998). For example, North from Texas University finds it difficult to judge whether climate models have improved over the recent 5 years and believes that the uncertainties are still as large as 20 years ago. Stone from Massachusetts Institute of Technology thinks that the major uncertainties in predictions of present-day climate changes have not decreased at all. Charlson from Washington State University believes that one would be wrong in thinking that one understands the climate. In Kerr's opinion, the information contained in the *IPCC Report (2001)* substantially reduces the uncertainty in solving the problem of detecting the "anthropogenic signal" for climate and supports the conclusion that global climate changes have anthropogenic origin but, at the same time, not only decreases but even extends the range of uncertainties in climate predictions. *Gutzler* from New-Mexico State University says that it seems to him that the solution to the "anthropogenic signal" detection problem has *almost* been found. According to *IPCC Report-2001*, the warming observed during the recent 50 years is, probably (by 66–90%), due *for the most part* to the GHG concentration growth. In this connection, it should be noted that the problem of quantitative estimation of what is "almost" and what is "for the most part" remains to be solved. These vague formulations clearly reflect the degree of uncertainty of the climate numerical modeling results.

Very much to the point was the remark by *Soros (2000)* that at the present time the CO₂ emissions are about 16% above of those in 1990 in the USA, 6% in

the European Community member-countries, 5% in Japan, and 24% in Australia. Thus, in the 1990s there was a rise, rather than stabilization, of atmospheric emissions of carbon dioxide. Also, there is no evidence to suggest any serious emission reduction efforts (the CO₂ emission reduction in Germany and Great Britain have nothing to do with the Kyoto recommendations). *Soros* (2000) was right in voicing a concern about the credibility gap to the Kyoto Protocol and the clear lack of prospect for its ratification by the leading industrial countries.

Tol (2000) mentioned with a good reason that one must not be under misunderstanding that without fossil fuel the world will be like a paradise. Though attractive on small scales, renewable energy sources have unclear prospects on large scales. The limitations of, e.g., hydro energy and wind energy became evident. All this reflects the undoubted truth that one needs to search ways of further development of civilization and to substantiate an adequate environmental policy in the context of the dynamics of the “society–nature” interactive system. Finding solution to this problem will require unprecedented cooperative efforts by experts in natural and social sciences.

References

- Adamenko, V.N. and Kondratyev, K.Ya.*, 1999: Global climate changes and their empirical diagnostics In *Anthropogenic impact on the nature of the North and its ecological implications* (in Russian) (eds.: *Yu.A. Izrael'*, *G.V. Kalabin*, and *V.V. Nikonov*). Kola Scientific Center, Russian Academy of Sciences, Apatity, pp. 17-34.
- Adams, P.J., Seinfeld, J.H., Koch, D., Mickley, L., and Jacob, D.*, 2001: General circulation model assessment of direct radiative forcing by the sulphate-nitrate-ammonium-water inorganic aerosol system. *J. Geophys. Res.* 106, 1097-1111.
- Adequacy of Climate Observing Systems*, 1999. National Academy Press. Washington, D.C.-51 pp.
- Allan, R., Slingo, J., Wielicki, B.*, 2000: Changes in tropical OLR – a missing mode of variability in climate models? *Abstracts. 8th Sci. Assembly IAMAS*. Innsbruck. 10-18 July 2001.
- Allen, M., Raper, S., and Mitchell, J.*, 2001: Uncertainty in the IPCC's Third Assessment Report. *Science* 293, 430, 433.
- Alverson, K.D., Oldfield, F., and Bradley, R.S.* (eds.), 2000: *Past Global Changes and Their Significance for the Future*. Pergamon Press. London. 479 pp.
- Andronova, N. and Schlesinger, M.E.*, 2000: Causes of global temperature changes during the 19th and 20th centuries. *Geophys. Res. Lett.* 27, 2137-2140.
- Angell, J.K.*, 1999: Comparison of surface and tropospheric temperature trends estimated from a 63-station radiosonde network, 1958-1968. *Geophys. Res. Lett.* 26, 2761-2764.
- Angell, J.K.*, 2000a: Tropospheric temperature variations adjusted for El Niño, 1958-1998. *J. Geophys. Res.* 105, 11841-11849.
- Angell, J.K.*, 2000b: Difference in radiosonde temperature trends for the period 1979-1998 of MSU data and the period 1959-1998 twice as long. *Geophys. Res. Lett.* 27, 2177-2180.
- Baliunas, S.L. and Glassman, J.K.*, 2001: Bush is right on global warming. *The Weekly Standard Magazine* 6, N39.
- Barnett, T.P., Pierce, D.W., and Schnur, R.*, 2001: Detection of anthropogenic climate change in the world's oceans. *Science* 292, 270-274.

- Benestad, R.E., 2001: The cause of warming over Norway in the ECHAM4/OPYC3 GHG integration. *Int. J. Climatol.* 21, 371-387.
- Bengtsson, L., 1999: Climate modeling and prediction—achievements and challenges. *WCRP/WMO Publ.*, N 954, 59-73.
- Berger, A. and Loutre, M.-F., 2001: An exceptionally long interglacial ahead?, 2001: In *First Int. Conf. On Global Warming and the Next Ice Age*. Dalhousie Univ., 19-24 Aug., pp. 245-248.
- Boehmer-Christiansen, S.A., 1999: Climate change and the World Bank: Opportunity for global governance? *Energy and Environ.* 10, 27-50.
- Boehmer-Christiansen, S., 2000: Who and how determines the climate change-concerning policy? (in Russian). *Izv. Rus. Geogr. Soc.* 132, 6-22
- Bolin, B., 1998: The WCRP and IPCC: Research inputs to IPCC Assessments and needs. *WCRP/WMO, N904*, 27-36.
- Bradley, R.S., 2001: Many citations support global warming trend. *Science* 292, 2011.
- Brekke, P., 2001: The Sun's role in climate change. In *First Int. Conf. On Global Warming and the Next Ice Age*, Dalhousie Univ., 19-24 Aug. 2001, pp. 241-244.
- Cai, W. and Whetton, P.H., 2000: Evidence for a time-varying pattern of greenhouse warming in the Pacific Ocean. *Geophys. Res. Lett.* 27, 2577-2580.
- Charlson, R.J., Seinfeld, J.H., Nu es, A., Kulmala, M., Laaksonen, A., Facchini, and M.C., 2001: Reshaping the theory of cloud formation. *Science* 292, 2025-2026.
- Chase, T.N., Pielke, R.A., Knaff, J.A., Kittel, T.G.F., and Eastman, J.L., 2000: A comparison of regional trends in 1979-1997 depth-averaged tropospheric temperatures. *Int. J. Climatol.* 20, 503-518.
- Christy, J.R., Spencer, R.W., and Lobl, E.S., 1998: Analysis of the merging procedure for the MSU daily temperature time series. *J. Climate.* 11, 2016-2041.
- Clark, J.S., Carpenter, S.R., Barber, M., Collins, S., Dobson, A., Foley, J.A., Lodge, D.M., Pascual, M., Pielke, R., Jr., Pizer, W., Pringle, C., Reid, W.V., Rose, K.A., Sala, O., Schlesinger, W.H., Wall, D.H., and Wear, D., 2001: Ecological forecasts: An emerging initiative. *Science* 293, 657-660.
- Climate Change 2001: The Scientific Basis*, 2001: (eds.: J.T. Houghton et al.) *Contribution of the WGI to the Third Assessment Report of the IPCC*. Cambridge University Press, 881 pp.
- Collatz, G.J., Bounoua, L., Los, S.O., Randell, D.A., Fung, I.F., and Sellers, P.J., 2000: A mechanism for the influence of vegetation on the response of the diurnal temperature range to changing climate. *Geophys. Res. Lett.* 27, 3381-3384.
- Common Questions About Global Change*. 1997: UNEP / WMO. Nairobi, Kenya, 24pp.
- Crowley, T.J., 2000: Causes of climate change over the past 1000 years. *Science* 289, 270-277.
- Datsenko, N.M., Shabalova, M.V., and Sonechkin, D.M., 2001: Seasonality of multidecadal and centennial variability in European temperatures: The wavelet approach. *J. Geophys. Res.* 106, 12,449-112,461.
- DeFreitas, C., 2001: Is it reasonable for climate scientists to continue to claim that the observed changes in concentration of greenhouse gases in the atmosphere are dangerous? In *First Int. Conf. On Global Warming and the Next Ice Age*, Dalhousie Univ., 19-24 Aug., 2001, p.172.
- Derwent, R.G., Collins, W.J., Johnson, C.E., and Stevenson, D.S., 2001: Transient behaviour of tropospheric ozone precursors in a global 3-D CTM and their indirect greenhouse effects. *Clim. Change* 49, 463-487.
- Dufresne, J.L., Fredlingstein, P., Fairhead, L., Le Treut, H., Ciais, P., and Monfray, P., 2001: Feedback processes between carbon cycle and climate in the IPSLM coupled model. *Abstracts. 8th Sci. Assembly of IAMAS*. Innsbruck, 10-18 July 2001. p. 10.
- Duffy, P.B., Doutriaux, C., Santer, B.D., and Fodor, I.K., 2001: Effect of missing data on estimates of near-surface temperature change since 1900. *J. Climate* 14, 2809-2814.
- Elsaesser, H.W., 2001: *The current status of global warming*. The paper prepared at the request of the Marshall Institute, Washington, D.C., May 2001. 5 pp.

- Erlick, C., Russel, L.M., and Ramaswamy, V., 2001: A microphysics-based investigation of the radiative effects of aerosol-cloud interactions for two MAST Experiment case studies. *J. Geophys. Res.* 106, 1245-1269.
- Ernst, W.G. (ed.), 2000: *Earth Systems. Processes and Issues*. Cambridge Univ. Press, 576 pp.
- Essenhigh, R.H., 2001: Does CO₂ really drive global warming? *Chemical Innovation*, 31, 44-46.
- Fraedrich, K., Gerstengarbe, F.-W., and Werner, P.C., 2001: Climate shifts during the last century. *Climat. Change* 50, 405-417.
- From the Candidates. Gore and Bush address key environmental issues. *Resources*. Fall 2000. Issue 141. Washington, D.C. p. 5-8.
- Fung, K.K. and Ramaswamy, V., 1999: On shortwave radiation absorption in overcast atmospheres. *J. Geophys. Res.* 104, 22,233-22,242.
- Gaffen, D.J., Santer, B.D., Boyle, J.S., Christy, J.R., Graham, N.E., and Ross, R.J., 2000: Multi-decadal changes in the vertical temperature structure of the tropical troposphere. *Science* 287, 1242-1245.
- Godney, N. and Valdes, P.J., 2000: The effect of Amazonian deforestation on the Northern Hemisphere circulation and climate. *Geophys. Res. Lett.* 27, 3053-3056.
- Gent, P.R., 2001: Will the North Atlantic Ocean thermocline circulation weaken during the 21st century? *Geophys. Res. Lett.* 28, 1023-1026.
- Gerholm T.R. (ed.), 1999: *Climate Policy after Kyoto*. Multi-Science Publ. Co. Ltd, Brentwood, U.K., 170 pp.
- Gloersen, P., Parkinson, C.L., Cavalieri, D.J., Comiso, J.C., and Zwally, H.J., 1999: Spatial distribution of trends and seasonality in the hemispheric ice covers: 1978-1996. *J. Geophys. Res.* 104, 20,827-20,835.
- Goldenberg, S.B., Landsea, C.W., Mestas-Nu ez, A.M., and Grey, W.M., 2001: The recent increase in Atlantic hurricane activity: Causes and implications. *Science* 293, 474-479.
- Goody, R., Anderson, J., and North, G., 1998: Testing climate models: An approach. *Bull. Amer. Meteorol. Soc.* 79, 2541-2549.
- Goody, R., 2001: Climate benchmarks: Data to test climate models. *Studying the Earth from Space*, issue 6.
- Goody, R., Anderson, J., Karl, T., Miller, R., North, G., Simpson, J., Stephens, C., and Washington, W., 2001: Why monitor the climate? *Bull. Amer. Meteorol. Soc.* (in print).
- Gorshkov, V.G., 1990: *Biosphere Energetics and Environmental Stability* (in Russian). Itogi nauki i tekhniki, Teoreticheskije. i obshchie voprosy geografii. Vol. 7. Moscow: VINITI, 238 pp.
- Gorshkov, V.G., Gorshkov, V.V., and Makarieva, A.M., 2000: *Biotic Regulation of the Environment. Key Issues of Global Change*. Springer/PRAXIS. Chichester, U.K. 367 pp.
- Grabb, M. with Vrolijk, C., and Brack, D., 1999: *The Kyoto Protocol. A Guide and Assessment*. The Royal Institute of International Affairs. London, 342 pp.
- Grigoryev, A. and Kondratyev, K.Ya., 2001: *Environmental Disasters*. St. Petersburg: Scientific Center, Russian Academy of Sciences. 691 pp.
- Grübler, A. and Nakicenovic, N., 2001: Identifying dangers in an uncertain climate. *Nature* 412, 15.
- Haigh, J.D., 2000: Solar variability and climate. *Weather* 55, 399-407.
- Hall, A. and Manabe, S. 2000: Effect of water feedback on internal and anthropogenic variations of the global hydrologic cycle. *J. Geophys. Res.* 105, 6935-6944.
- Han, Q., Rossow, W.B., Chou, J., and Welch, R.M., 2000: ISCCP data used to address a key IPCC climate issue: An approach for estimating the aerosol indirect effect globally. *GEWEX News* 10, 3-5.
- Hansen, J., Sato, M., Ruedy, R., Lacis, A., and Oinas, V., 2000: Global warming in the twenty-first century: An alternative scenario. *Proc. U.S. Nat. Acad. Sci.* 97, p. 9875-9880.
- Hansen, J.E., 2001: *Statement before the Committee on Commerce, Science and Transportation, United States Senate*. May 1, 2001, 10 pp., ill.
- Hill, D.C., Allen, M.R., and Stott, P.A., 2001: Allowing for solar forcing in the detection of human influence on tropospheric temperatures. *Geophys. Res. Lett.* 28, 1555-1558.

- Houghton J., 2000: The IPCC Report 2001. *Proc. of the 1st Solar and Space Weather Euroconference "The Solar Cycle and Terrestrial Climate"*, Santa Cruz de Tenerife, 25-29 Sept. 2000. – Noordwijk, 2000. – ESA SP ISSN 0379-6566. N463. p. 255-259.
- Houghton, J., 2001: Global climate and human activities. In *Our Fragile World: Challenges and Opportunities for Sustainable Development*. EOLSS Forrunner Volumes 1-2. 13 pp., ill.
- Huang, S., Pollack, H.N., and Shen, P.-Y., 2000: Temperature trends over the past five centuries reconstructed from borehole temperatures. *Nature* 403, 756-758.
- Hu, Z.-Z., Latif, M., Roeckner, E., Bengtsson, L., 2000: Intensified Asian summer monsoon and its variability in a coupled model forced by increasing greenhouse gas concentrations. *Geophys. Res. Lett.* 27, 2681-2684.
- Huber, B.T., MacLeod, K.G., and Wing, S.L., 1999: *Warm Climates in Earth History*. Cambridge University Press. 426 pp.
- Hulme, M., Barrow, E.M., Arnell, N.W., Johns, T.S., and Downing, T.E., 1999: Relative impact of human-induced climate change and natural variability. *Nature* 397, 688-691.
- IPCC Special Report "Land-Use Change, and Forestry", 2000: (eds: R.T. Watson et al.), Cambridge Univ. Press. 377 pp.
- IPCC Third Assessment Report. Vol. 1. 2001: Cambridge University Press.
- Jaworosky, Z., 2000: The global warming. 21st Century. Winter 1999-2000, 64-75.
- Jeptma, C.S. and Munasinghe, M., 1998: *Climate Change Policy: Facts, Issues and Analysis*. Cambridge Univ. Press, 349 pp.
- Jin, F.-F., Hu, Z.-Z., Latif, M., Bengtsson, L., and Roeckner, E., 2001: Dynamical and cloud radiation feedbacks in El Niño and greenhouse warming. *Geophys. Res. Lett.* 28, 1539-1542.
- Johannessen, O.M., Shalina, E.V., and Miles, M.W., 1999: Satellite evidence for an Arctic Sea ice cover in transformation. *Science* 286, 1937-1939.
- Johns, T.C., Gregory, J.M., Stott, P.A., and Mitchell, J.F.B., 2001: Correlations between patterns of 19th and 20th century surface temperature change and Had CM2 climate model ensembles. *Geophys. Res. Lett.* 28, 1007-1010.
- Jones, P.D., New, M., Parker, D.E., Martin, S., and Rigor, I.G., 1999: Surface air temperature and its changes over the past 150 years. *Revs. of Geophys.* 37, 173-179.
- Karl, T.R., Nicholls, N., and Ghazi, A. (eds.), 1999: *Weather and Climate Extremes – Changes, Variations and a Perspective from the Insurance Industry*. Kluwer Acad. Publ., Dordrecht. VI+349 pp.
- Karl, T. and Gleckler, P.J., 2001: Tracking changes in AMIP model performance. *Abstracts. 8th Sci. Assembly of IAMAS*. Innsbruck, 10-18 July, 2001. p. 8.
- Kato, H., Nishizawa, K., Hirakuchi, H., Kadokura, S., Oshima, N., and Giorgi, F., 2001: Performance of Reg CM2.5/NCAR-CSM nested system for the simulation of climate change in East Asia caused by global warming. *J. Meteorol. Soc. Jap.* 79, 99-121.
- Kennedy, D., 2001: Going it alone. *Science* 293, 1221.
- Kerr, R.A., 2001a: World starts taming the greenhouse. *Science*, 293, 583.
- Kerr, R.A., 2001b: Rising global temperature, rising uncertainty. *Science*, 292, 192-194.
- Kim, W., Arai, T., Kanae, S., Oki, T., and Musiaka, K., 2001: Application of the Simple Biosphere Model (SiB2) to a paddy field for a period of growing season in GAME-Tropics. *J. Meteorol. Soc. Jap.* 79, 387-400.
- Kondratyev, K.Ya., 1990: Key Issues of Global Ecology (in Russian). *Itogi nauki i tekhniki. Teoreticheskie i obshchie voprosy geografii. Vol. 9*. Moscow: VINITI, 454 pp.
- Kondratyev, K.Ya., 1992: *Global Climate* (in Russian). Nauka, St. Petersburg, 359 pp.
- Kondratyev, K.Ya. and Galindo, I., 1997: *Volcanic Activity and Climate*. A. Deepak Publ., Hampton, VA. 382 pp.
- Kondratyev, K.Ya., 1998a: *Multidimensional Global Change*. Wiley/PRAxis. Chichester, U.K. 761 pp.
- Kondratyev, K.Ya., 1998b: Environmental risk: real and hypothetical (in Russian). *Izv. Rus. Geogr. Soc.* 130, issue 3, 13-23.
- Kondratyev, K.Ya. and Cracknell, A.P., 1998: *Observing Global Climate Change*. Taylor & Francis, London. 562 pp.

- Kondratyev, K.Ya., 1999a: *Climatic Effects of Aerosols and Clouds*. Springer/PRAXIS. Chichester, U.K. 264 pp.
- Kondratyev, K.Ya., 1999b: *Ecodynamics and Geopolitics. Vol. 1. Global Problems* (in Russian). SRCES RAS, St. Petersburg, 1040 pp.
- Kondratyev, K.Ya. and Varotsos, C.A., 2000: *Atmospheric Ozone Variability: Implications for Climate Change, Human Health, and Ecosystems*. Springer/PRAXIS. Chichester, U.K. 614 pp.
- Kondratyev, K.Ya., 2000: Global changes at the millenium threshold (in Russian). *Vestnik Ross. Akad. Nauk.* 70, 788-796.
- Kondratyev, K.Ya. and Demirchian, K.S., 2000: Global climate changes and carbon cycle (in Russian). *Izv. Rus. Geogr. Soc.* 132, issue 4, 1-20.
- Kondratyev, K.Ya., 2001a: Key issues of global change at the end of the second millennium. In *Our Fragile World: Challenges and Opportunities for Sustainable Development*. EOLSS Vorranner volumes 1-2, p.
- Kondratyev, K.Ya., 2001b: Possible impacts of climate changes on ecosystems and economy of the USA (in Russian). *Izv. Rus. Geogr. Soc.* 133, issue 6, p.
- Kondratyev, K.Ya. and Cracknell, A.P., 2001: Global climate change. Socio-economic aspects of the problem. In Cracknell, A.P.: *Remote Sensing and Climate Change. The Role of Earth Observations*. Springer/PRAXIS. Chichester, U.K, 37-79.
- Kondratyev, K.Ya., 2002a: Aerosol as a climate-forming component of the atmosphere. 1. Chemical composition and optical properties. *Optics of the Atmosphere and Ocean 15*, N1, (in press).
- Kondratyev, K.Ya., 2002b: Aerosol as a climate-forming component of the atmosphere. 2. Direct and indirect climatic impact. *Optics of the Atmos. and Ocean, 15*, N2, (in press)
- Krajick, K., 2001: Tracking icebergs for clues to climate change. *Science* 292, 2244-2245.
- Krapivin, V.R. and Kondratyev, K.Ya., 2002: *Global Environmental Changes: Ecoinformatics* (in Russian). St. Petersburg. 815 pp.
- Kukla, G., 2000: The last interglacial. *Science* 287, 987-988.
- Kukla, G., 2001: Did the last interglacial end with global warming? In *First Int. Conf. On Global Warming and the Next Ice Age*. Dalhousie Univ., 19-24 Aug., 2001, p. 257.
- Kuzelka, R., Seacrest, S., and Leonard, R., 2001: Climate Change: Who is Listening; Who is Planning? In *First Int. Conf. On Global Warming and the Next Ice Age*. Dalhousie Univ., 19-24 Aug. 2001, p.207-210.
- Lempert, R.J., Schlesinger, M.E., Bankes, S.C., and Andronova, N.G., 2000: The impacts of climate variability on near-term policy choices and the value of information. *Clim. Change* 45, 129-161.
- Levitus, S., Antonov, J.I., Wang, J., Delworth, T.L., Dixon, K.W., and Broccoli, A J., 2001: Anthropogenic warming of Earth's climate system. *Science* 292, 267-270.
- Lawrimore, J.H., Halpert, M.S., Bell, G.D., Menne, M.J., Lyon, B., Schnell, R.C., Gleason, K.L., Easterling, D.R., Thiaw, W., Wright, W.J., Heim, R.R. Jr., Robinson, D.A., and Alexander, L., 2001: Climate Assessment for 2000. *Bull. Amer. Meteorol. Soc.* 86, S1- S55.
- Loginov, V.F. and Mikutskii, V.S., 2000: Assessment of the anthropogenic "signal" in city climate (in Russian). *Izv. Rus. Geogr. Soc.* 132, issue 1, 23-31.
- Maier, J., 2001: Climate: last chance in Bonn? Network 2002. July 2001 p. 7,8.
- Mann, M.E., Bradley, R.S., and Hughes, M.K., 1999: Northern Hemisphere temperature during the past millenium: Inferences, uncertainties, and limitations. *Geophys. Res. Lett.* 26, 759-762.
- McKitrick R., 2001: (private communication).
- McNamara, W., 2001: Background on Kyoto Protocol. *The Week That Was*. 14 July 2001, 5-8.
- Meehl, G.A., Washington, W.M., Wigley, T.H.L., Arblaster, J.M., and Dai, A., 2001: Solar and anthropogenic forcing and climate response in the 20th century. *Abstracts. 8th Sci. Assembly of IAMAS*. Innsbruck, 10-18 July 2001, p.12.
- Meleshko, V.P., Katsov, V.M., Sporyshev, P.V., Vavulin, S.V., and Govorkova, V.R., 1999: Sensitivity of the climate model of the Main Geophysical Observatory to atmospheric CO₂ concentration changes. In *Present-day studies of the Main Geophysical Observatory* (in Russian), (eds.: M.E. Berlyand and V.P. Meleshko). Gidrometeoizdat, St. Petersburg. pp. 3-32.

- Michaels, P.J., Knappenberger, P.C., and Davis, R.E., 2001: Integrated projections of future warming based upon observed climate during the greenhouse enhancement. In *First Int. Conf. on Global Warming and the Next Ice Age*. Dalhousie Univ., 19-24 Aug., 2001, 162-167.
- Mo, T., Goldberg, M.D., Crosby, D.S., and Cheng, Z., 2001: Recalibration of the NOAA microwave sounding unit. *J. Geophys. Res.* 106, 10,145-10,150.
- Moss, R.H. and Schneider, S.H., 2000: Uncertainties in the IPCC TAR: Recommendations to lead authors for more consistent assessment and reporting. In *Guidance Papers on the Cross Cutting Issues of the Third Assessment Report of the IPCC* (eds.: R. Pachauri, T. Taniguchi, and T. Tanaka). Word. Meteorol. Organ., Geneva, 33-51.
- Müller, M.J.W., 1997: *Klimälüge? Wissenschaft – Politik – Zeitgeist*. Irene Müller Verlag, ENERI. 256 c.
- Naden, P.S. and Watts, C.D., 2001: Estimating climate – induced change in soil moisture at the landscape scale: An application to five areas of ecological interest in the U.K.. *Clim. Change* 49, 411-440.
- Nicholls, N., 2001: The insignificance of significance testing. *Bull. Amer. Meteorol. Soc.* 82, 981-986.
- O'Neill, B.C., MacKellar, F.L., and Lutz, W., 2001: *Population and Climate Change*. Cambridge University Press.
- Orphan, V.J., House, C.H., Hinrichs, K.-U., McKeegan, K.D., and Delong, E.F., 2001: Methane-consuming archaea revealed by directly coupled isotopic and phylogenetic analysis. *Science* 293, 484-487.
- Pongrácz, R. and Bartholy, J., 2000: Statistical linkages between ENSO, NAO, and regional climate. *Időjárás* 104, 1-20.
- Penner, J.E. and Rotstajn, L., 2000: Indirect aerosol forcing. Response. T.J.Crowley. *Science* 290, 407.
- Pielke, R.A. Sr., Liston, G.E., and Robock, A., 2000: Insolation-weighted assessment of Northern Hemisphere snow-cover and sea-ice variability. *Geophys. Res. Lett.* 27, 3061-3064.
- Prinn, R., Jacoby, H., Sokolov, A., Wang, C., Xiao, X., Yang, Z., Eckhaus, R., Stone, P., Ellerman, D., Melillo, J., Fitzmaurice, J., Kicklighter, D., Holian, G., and Liu, Y., 1999: Integrated Global System Model for climate policy assessment: Feedbacks and sensitivity studies. *Clim. Change* 41, 469-546.
- Project Performance Report. *Global Environmental Facility*. 1998; Washington, D.C.– 89 pp.
- Qian, W. and Zhu, Y., 2001: Climate change in China from 1880 to 1998 and its impact on the environmental condition. *Climate Change* 50, 419-444.
- Reconciling Observations of Global Temperature Change*. 2000: Nat. Acad. Press, Washington, D.C. 85 pp.
- Rees, M., Condit, R., Crawley, M., Pacala, S., and Tilman, D., 2001: Long-term studies of vegetation dynamics. *Science* 293, 650.
- Reilly, J., Stone, P.H., Forest, C.E., Webster, M.D., Jacoby, H.D., and Prinn, R.G., 2001: Uncertainty and climate change assessments. *Science* 293, 430-433.
- Renu, J., 2001: Intercomparison of stationary waves in AMIP-2 GCM's and their maintenance mechanisms. Abstracts. *8th Sci. Assembly by IAMAS*. Innsbruck, 10-18 July 2001. p. 8.
- Ritson, D.M., 2000: Gearing up for IPCC-2001. *Clim. Change* 45, 471-488.
- Robock, A., Vinnikov, K.Y., Srinivasan, G., Entin, J.K., Hollinger, S.E., Speranskaya, N.A., Liu, S., and Namkhai, A., 2000: The global soil moisture data bank. *Bull. Amer. Meteorol. Soc.* 81, 1281-1299.
- de Rosnay, P., Bruen, M., and Polcher, J., 2000: Sensitivity of surface fluxes to the number of layers in the soil model used in GCMs. *Geophys. Res. Lett.* 27, 3329-3332.
- Saloranta, T. M., 2001: Post-normal science and the global climate change issue. *Clim. Change* 50, 395-404.
- Santer, B.D., Wigley, T.M.L., Boyle, J.S., Gaffen, D.J., Hnilo, J.J., Nychka, D., Parker, D.E., Taylor, K.E., 2000: Statistical significance of trends and trend differences in layer-average atmospheric temperature time series. *J. Geophys. Res.* 105, 7337-7356.

- Schlesinger, M.E. and Andronova, N., 2000: Temperature changes during the 19th and 20th Centuries. *Geophys. Res. Lett.* 27, 2137-2140.
- Schlesinger, M.E. and Andronova, N., 2001: Climate sensitivity. *J. Climate.* (in print).
- Schlesinger, M.E., Ramankutty, N., and Andronova, N., 2000: Temperature oscillations in the North Atlantic. *Science* 289, 547.
- Schneider, S.H., 2001: What is "dangerous" climate change? *Nature* 411, 17-19.
- Schröder, W. (ed.), 2000: *Long and Short Term Variability in Sun's History and Global Change.* Science Edition, D-28777 Bremen-Roennebeck, 63 pp.
- Schrope, M., 2001: Consensus science, or consensus politics? *Nature* 412, 112-114.
- Sen, O.L., Bastidas, L.A., Shuttleworth, W.J., Yang, Z.-L., Gupta, H.V., and Sorooshian, S., 2001: Impact of field-calibrated vegetation parameters on GCM climate simulations. *Quart. J. Roy. Meteorol. Soc.* 127. Part B, 1199-1223.
- Senior, C.A. and Mitchell, J.F.B., 2000: The time dependence of climate sensitivity. *Geophys. Res. Lett.* 27, 2685-2688.
- Shackley, S., Young, P., Parkinson, S., and Wynne, B., 1998: Uncertainty, complexity and concepts of good science in climate change modelling: are GCMs the best tools? *Clim. Change* 38, 159-205.
- Sherman, R., 2001: Let the sun rise on the Kyoto Protocol. New York. 2002. September 2001 issue. p. 1, 2.
- Singer, S.F., 1997: *Hot Talk, Cold Science.* Independent Institute, Oakland, Calif., X+110 pp.
- Singer, S.F., 1998: Unfinished business – The scientific case against the Global Climate Treaty. *Energy & Environment* 9, 617-632.
- Singer, S.F., 1999: Human contribution to climate change remains questionable. *EOS*, 80, 183, 186, 187.
- Smith, S.J., Wigley, T.M.L., and Edmonds, J., 2000: A new route toward limiting climate change? *Science* 290, 1109-1110.
- Somerville, R.C.J., 2001: Forecasting climate change: Prospects for improving models. Abstracts. 8th Sci. Assembly of IAMAS. Innsbruck, 10-18 July 2001, p. 9.
- Sonechkin, D.M., 1998: Climate dynamics as a nonlinear Brownian motion. *Int. J. Bifurcation and Chaos* 8, 799-803.
- Sonechkin, D. M., Astafyeva, M.M., Datsenko, N.M., Ivashtchenko, N.N., and Jakubiak, B., 1999: Multiscale oscillations of the global climate system as revealed by wavelet transform of observational data time series. *Theoret. and Appl. Climatol.* 64, 131-142.
- Sonechkin, D.M. and Datsenko, D.M., 2000: Wavelet analysis of nonstationary and chaotic time series with an application to the climate change problem. *Pure Appl. Geophys.* 157, 653-677.
- Soon, W., Baliunas, S., Kondratyev, K.Ya., Idso, S.B., and Postmentier, E., 2000: Calculating the climatic impacts of increased CO₂: The issue of model validation. *Proc. of the 1st Solar and Space Weather Euroconference "The Solar Cycle and Terrestrial Climate"*, Santa Cruz de Tenerife, 25-29 Sept., 2000. – Nordwijk, 2000. – (ESA SP ISSN 0379-6566. N463). – P. 243-254.
- Soon, V., Baliunas, S., Demirchian, K.S., Kondratyev, K.Ya., Idso, S.B., and Postmentier, E.S., 2001: Impact of anthropogenic CO₂ emissions on climate: unsolved problems (in Russian). *Izv. Rus. Geogr. Soc.* 133, issue 2, 1-19.
- Soros, M.S., 2000: *Preserving the atmosphere as a global common.* Environ. Change and Security Project Report. The Woodrow Wilson Center. Washington, D.C., N6, 149-155.
- Stafford, J.M., Wendler, G., and Curtis, J., 2000: Temperature and precipitation of Alaska: 50 year trend analysis. *Theor. and Appl. Clim.* 67, 33-44.
- von Storch, H. and Zwiers, F.W., 1999: *Statistical Analysis in Climate Research.* Cambridge Univ. Press. X+484 pp.
- Stott, P., 2001: External control of 20th century temperature by natural and anthropogenic forcings. Abstracts. 8th Sci. Assembly of IAMAS. IAMAS. Innsbruck, 10-18 July 2001. p. 12.
- Stott, P.A., Tett, S.F.B., Jones, G.S., Allen, M.R., Ingram, W.J., and Mitchell, J.F.B., 2001: Attribution of twentieth century temperature change to natural and anthropogenic causes. *Clim. Dyn.* 17, 1-21.

- Taylor, P.K. (ed.), 2000: *Intercomparison and Validation of Ocean –Atmosphere Energy Flux Fields*. World Clim. Res. Programme/ Wold Meteorol. Organ. N 1036. I-XVI, 303 pp.
- The Atmospheric Sciences Entering the Twenty-First Century*. 1998: National Academy of Sciences. Washington, D.C., 364 pp.
- The Greenhouse Effect and Climate Change. A briefing from the Hadley Centre*. 1999. The Met. Office, Bracknell, U.K., 28 pp.
- The Kyoto Protocol to the Convention on Climate Change*. 1998. Climate Change Secretariat. Bonn. 34 pp.
- The World Meteorological Organization in the Service of Humankind: A vision for the 21st Century*. 2000: *WMO Bull.* 49, N1, 13-16.
- Tol, R.S.J., 2000: International climate policy: An assessment. *IHDP Update*. N3, 11-12.
- Trenbert, K.E., 2001: Climate variability and global warming. *Science* 293, 48-49.
- U.S. National Academy of Sciences Report: Climate Change Science: An Analysis of Some Key Issues*. 2001. Washington, D.C. 28 pp.
- Victor, D.G., 2001: *The Collapse of the Kyoto Protocol and the Struggle to Slow Global Warming*. Princeton University Press. 192 pp.
- Watanabe, M., 2000: *Mechanisms of the Decadal Climate Variability in the Midlatitude Atmosphere – Ocean System*. Center for Climate System Research. University of Tokyo. N12, 157 pp.
- Weatherhead, E.C., 2001: Detecting climate change. In *First Int. Conf. On Global Warming and the Next Ice Age*. Dalhousie Univ., 19-24 Aug. 2001, 168-171.
- Wetherald, R.T., Stouffer, R.J., and Dixon, K.W., 2001: Committed warming and its implications for climate change. *Geophys. Res. Lett.* 28, 1535-1538.
- Wellington, G.M., Glynn, P.W., Strong, A.E., Navarette, A., Wieters, E., and Hubbard, D., 2001: Crisis on coral reefs linked to climate change. *EOS* 82, N 1.p. 1, 5.
- Weyant, J. (ed.), 1999: *The Costs of the Kyoto Protocol: A Multi-Model Evaluation*. Energy Journal Special Issue. June 1999, 448 pp.
- Wigley, T.M.L., 1998: The Kyoto Protocol: CO₂, CH₄ and climate implications. *Geophys. Res. Lett.* 25, 2285-2288.
- Wigley, T.M.L., 1999: *The Science of Climate Change. Global and U.S. Perspectives*. Pew Center on Global Climate Change. Arlington, VA. 48 pp.
- Wigley, T.M.L. and Raper, S.C.B., 2001: Interpretation of high projections for global-mean warming. *Science* 293, 451-455.
- Wilby, R.L., 2001: Cold comfort. *Weather* 56, 213-215.
- Wojick, D.E., 2001: *The UN IPCC artful bias. Glaring omissions, false confidence and misleading statistics in the Summary for Policymakers*. July 2001. 11 pp.
- Woodcock, A., 1999: Global warming – a natural event? *Weather* 54, 162-163.
- Woodcock, A., 2000: Global warming: The debate heats up. *Weather* 55, 143-144.
- Zhang, H., Henderson-Sellers, A., and McGuffie, K., 2001: The compounding effects of tropical deforestation and greenhouse warming of climate. *Clim. Change* 49, 309-338.

IDŐJÁRÁS

Quarterly Journal of the Hungarian Meteorological Service
Vol. 106, No. 2, April–June 2002, pp. 39–58

Sensitivity of the ALADIN weather prediction model to the changes of soil texture

Ágnes Mika¹, Ferenc Ács², András Horányi³ and Gábor Radnóti³

¹Hungarian Meteorological Service, Storm Warning Observatory,
Vitorlás u. 17, H-8600 Siófok, Hungary; E-mail: mika.a@met.hu

²Department of Meteorology, Eötvös Loránd University,
P. O. Box 32, H-1518 Budapest, Hungary; E-mail: acs@caesar.elte.hu

³Hungarian Meteorological Service, P. O. Box 38, H-1525 Budapest, Hungary;
E-mail: horanyi.a@met.hu; radnoti.g@met.hu

(Manuscript received February 6, 2002; in final form June 17, 2002)

Abstract—The sensitivity of ALADIN's forecasts to the changes of soil texture is evaluated. In the experiments different ALADIN versions and soil texture databases are applied. Three ALADIN versions are tested: the 1-dimensional ALADIN, ALADIN with dynamical adaptation, and ALADIN with data assimilation. Two soil texture databases are used: a global soil map and a more detailed Hungarian soil texture map. 48-hour forecasts are analysed. Among forecast variables, the superficial soil water content and the 2m air temperature are chosen. The main results are as follows: the superficial soil water content and the 2m temperature differences increased with increasing soil texture differences. In the case of maximum sensitivity, they reached 2.5 kg m^{-2} and 4.4°C , respectively. The sensitivity was most pronounced for ALADIN with data assimilation.

Key-words: soil texture, superficial soil water content, 2m air temperature, ALADIN limited area model, data assimilation

1. Introduction

The state of the atmosphere is determined in a great extent by surface conditions, via transfer processes of momentum, heat and moisture in the soil–vegetation–atmosphere system (Pitman *et al.*, 1999; Kabat, 1998; Betts and Ball, 1996). Recognising the importance of these interactions, land surface schemes have been developed for use in numerical weather prediction models. The fluxes of momentum, heat and moisture are determined by the properties of the surface, mostly by albedo, roughness length and soil hydraulic

properties. Over ground, the latter parameter depends considerably on the soil texture. For weather prediction purposes, the basic soil properties are usually defined in global datasets, like the FAO (Food and Agricultural Organisation) digital soil map of the world (FAO, 1988).

So far the sensitivity of land surface schemes to the changes of soil texture was investigated using fictitious soil texture data and analysing the changes of near surface fluxes. The sensitivity proved to be strong (Pitman, 1994), especially on climatological scale and it appeared in the annual variation of latent and sensible heat fluxes (Irannejad and Shao, 1998). The sensitivity on a short (several days) time scale was also investigated by Mihailovic *et al.* (1992).

In this paper, the sensitivity of the ALADIN mesoscale limited area numerical weather prediction model to the choice of the soil texture database is analysed. ALADIN's land surface module is ISBA (Interactions Soil Biosphere Atmosphere), a well known and widely tested PILPS (Project for Intercomparison of Land Surface Parameterization Schemes) model (Noilhan and Planton, 1989). The attention is paid to the changes of state variables: the superficial soil water content and the 2m air temperature. In contrary to the previous studies, the experiments are performed using real databases. These databases are the Webb *et al.* (1991) global database and the Hungarian soil texture map.

2. Models

The sensitivity experiments are performed using three versions of the ALADIN mesoscale limited area numerical weather prediction model. They are the operational version of the ALADIN model (using dynamical adaptation), ALADIN using data assimilation, and the one dimensional version of ALADIN, the Single Column Model (SCM). In this chapter a short description of each model version is given along with a short presentation of the ISBA land-surface scheme.

The ALADIN (Aire Limitee Adaptation Dynamique developement InterNational) numerical weather prediction model (Horányi *et al.*, 1996) was developed in the scope of an international collaboration led by Météo France. It is a spectral limited area model. The Hungarian version of the model, ALADIN/HU operates at the limit of the hydrostatic assumption typically at a resolution of 8 km. The model is run at the Hungarian Meteorological Service (HMS) twice a day (using 00 and 12 UTC data). It can make reasonably good short range predictions (up to 48 hours) for the territory of the Carpathian Basin. The lateral boundary conditions for the Hungarian model are taken from the regional ALADIN/LACE model (Brožková, 2001) and the transition

between them is made by relaxation, which means the inclusion of a transition zone between the two model domains (Davies, 1976). The initial conditions are computed from the regional model's analysis fields via horizontal and vertical interpolation. The initial conditions do not include any new information compared to the regional model (ALADIN/LACE), but during the integration at a higher resolution the model is "adapting" to the high resolution surface characteristics. This is the so-called dynamical adaptation.

Objective analysis schemes (optimum interpolation (OI) and 3DVAR) have also been developed for ALADIN to provide the possibility to run the model in data assimilation mode rather than dynamical adaptation. Within the data assimilation cycle the model integration is performed for six hour periods, and in every sixth hour the model state is corrected with observational data. Starting from this modified state, the model is integrated for the next six hours, when new data are used, and so on. In the experiments presented in this paper, the OI scheme (Gandin, 1963) is used and only synoptic surface observations are assimilated.

The 3D operational ALADIN model has a 1D version, called Single Column Model (SCM) (Piriou *et al.*, 1999). With SCM the ALADIN physical parameterization package can be run in an interactive environment, allowing easier understanding and validation of the package. The SCM can be run in two ways: in free mode and in a forced way, when the dynamical forcing (advection terms, adiabatic term from temperature equation, and baroclinic term from wind equation), and the semi-implicit scheme are provided by the 3D model, since these two operators are unavailable in SCM. In forced mode it is possible to replay in an interactive mode the predictions done at a given point of the 3D run, which allows the investigation of the physical package and the observation of the role of dynamic forcings in the forecasts. The free mode run is not designed for prognostic purposes, it can be used for testing the parameterization schemes. The scope of this paper is to observe what effect the altered soil texture has on the temperature and moisture characteristics of the boundary layer. For this purpose the free mode run seems to be the most convenient one. In this case only the initialization of the model is needed (in forced mode boundary conditions from the 3D model are required), which is done by using the 3D model state over a given grid point.

In each model version the air-surface interactions are described by the ISBA land-surface scheme. For a detailed description see Noilhan and Planton (1989) and Noilhan and Mahfouf (1996). The description of the changes made during the implementation in the ALADIN model can be found in Giard and Bazile (2000). The ISBA scheme describes the exchanges of heat and water between the low-level atmosphere, the vegetation and the soil. It has seven prognostic variables: the surface temperature, the deep soil temperature, the

interception water content (the water stored on the leaves), the liquid and frozen part of superficial soil water content (corresponding to a very thin layer of 1cm), and the liquid and the frozen part of the total soil water content.

In ISBA the sand and clay fractions have an effect in controlling the moisture and heat transfer processes through determining the soil thermic and hydraulic coefficients. Hereafter the effect of the soil texture on the soil water content and the 2m temperature is described.

In ISBA the soil water content is computed using the force restore model (Noilhan and Mahfouf, 1996). Its basic concept is the division of the total soil layer into two parts. The thin surface layer (1 cm thick in ISBA) reacts rapidly on atmospheric demands, while the total soil layer, which includes the surface layer too, (with variable depths, roughly from 10 cm for stony areas to 3 m for forests, always including the root zone) makes its contribution on a longer time scale.

The water income for the surface layer is represented by the precipitation, the water dripping down from the leaves (the runoff from the interception reservoir), and the melting of snow and ice. The surface layer loses water through evaporation from the bare ground, runoff, freezing of water, and diffusion of water in the ground. The incomes for the total soil layer water content are the same as for the surface layer. The losses are represented by the bare ground evaporation, transpiration, gravitational drainage, and freezing of water (Giard and Bazile, 2000; Gerard, 2000).

As seen above, all transpiration originates from the deep reservoir, where the roots are situated. Runoff begins when the water content exceeds the saturation value. When the deep soil water content reaches the field capacity, a gravitational drain appears at the bottom.

The sand and clay fractions play their role through three so-called hydraulic coefficients. The first of them appears in the surface layer water content equation. It increases when the soil dries (when hydraulic conductivity is decreasing), thus regulating the amount of incoming water absorbed by the surface layer and its contribution to evaporation. The second coefficient characterizes the speed by which the water profile returns to the equilibrium profile. It increases with hydraulic conductivity and plays part in the formulation of the water diffusion in the ground. The third coefficient is present in the deep layer water content equation, in the formulation of gravitational drainage and it characterizes the speed by which the water profile is relaxed to the field capacity. For the surface and deep soil layer water content equations and for the exact formulation of the hydraulic coefficients see Appendix A.

The 2m temperature is not a prognostic variable, it is interpolated from the surface temperature and the temperature of the lowest model layer. The soil texture has an effect on the 2m temperature through the surface

temperature equation (for detailed formulation see Appendix B). The surface temperature is computed from the energy budget of the following fluxes: surface net radiative energy flux, surface sensible and latent heat fluxes, heat flux between surface and deep ground, snow melting flux and surface freezing flux. A thermic coefficient determines the rate of change of soil temperature with respect to contributing fluxes.

3. Databases

In the operational version of ALADIN the sand and clay fractions used as input data in ISBA are taken from a global database, constructed by *Webb et al.* (1991). In order to show the sensitivity of ALADIN to the soil texture changes, a new database, a Hungarian soil texture map was implemented in the model. In the following section a short description of the two databases is given, followed by the description of the computation of sand and clay fractions based on the Hungarian database and of the differences between the two databases.

3.1 The global database

The Webb et al. database is a standardized global data set of soil horizon thicknesses and textures, compiled from the FAO/UNESCO Soil Map of the World, Vols. 2–10 (1971–81). The very heterogeneous high resolution data were transformed into representative homogeneous information at a much lower resolution. This digital map, with a resolution of 1°, comprises 106 soil types, grouped in 26 major soil units. The textural classes refer to the upper 30 cm of the dominant soil and they reflect the relative proportions of clay (fraction less than 0.002 mm), silt (0.002–0.05 mm), and sand (0.05–2 mm) in the soil. The fraction sizes are in accordance with the USDA classification. Three major textural classes are recognised: coarse, medium and fine. The coarse textures are: sands, loamy sands and sandy loams with less than 18% clay and more than 65% sand. The medium class comprises sandy loams, loams, sandy clay loams, silt loams, silt, silty clay loams, and clay loams with less than 35% clay and less than 65% sand. And finally the fine textures are: clays, silty clays, sandy clays and clay loams, with more than 35% clay. The soil texture and soil depth data can be obtained directly from the database for the ARPEGE/ALADIN model grid.

3.2 The Hungarian database

The Hungarian database is a 1:100.000 scale soil texture map, constructed by the Soil and Agrochemical Research Centre of the Hungarian Academy of

Sciences (HAS). The simplified version of the map can be found in *Várallyay et al.* (1980). The map uses seven soil texture types: sand, sandy loam, loam, clay loam, clay, peat, and coarse fragments. The fraction size limits slightly differ from the limits used in the USDA classification. They are 2–0.02 mm for sand, 0.02–0.002 mm for loam and less than 0.002 mm for clay.

3.3 Computation of sand and clay fractions from the Hungarian database

The computation of sand and clay fractions is performed on the base of the map presented in *Várallyay et al.* (1980). First, the relative coverages of soil texture types are determined for each grid surface. After this, the sand and clay fractions are defined according to the following equations:

$$CF(\%) = CCo RCCo + CMe RCMe + CFi RCFi, \quad (1)$$

$$SF(\%) = SCo RCCo + SMe RCMe + SFi RCFi, \quad (2)$$

where CF and SF are the clay and sand fractions in percent; CCo , CMe , CFi and SCo , SMe , SFi are the clay and sand fractions of the coarse, medium and fine soils in percent, and $RCCo$, $RCMe$ and $RCFi$ are the relative coverages of the coarse, medium and fine soils, respectively. In this study the $CCo=3\%$, $CMe=19\%$, $CFi=58\%$ and $SCo=92\%$, $SMe=43\%$, $SFi=22\%$ values are used, according to those used at Météo France.

Finally, the $RCCo$, $RCMe$ and $RCFi$ parameters are derived as follows:

$$RCCo = RCSa + RCSaCl, \quad (3)$$

$$RCMe = RCLo, \quad (4)$$

$$RCFi = RCCILo + RCCI, \quad (5)$$

where $RCSa$, $RCSaCl$, $RCLo$, $RCCILo$, $RCCI$ are the relative coverages of sand, sandy clay, loam, clay loam, and clay respectively. The sand and clay fractions are not estimated when the grid surface contained peat or coarse fragments.

3.4 Differences between the databases

The differences between the databases are caused first of all by the different resolutions, but also by the fact that there is a difference in the fraction limits used by the two maps. This latter difference is neglected during the computation of sand and clay fractions. On the other hand the parameteriza-

tions used in constructing the data sets are the same, so the differences between the sand and clay fractions can only originate from the differences of the input data (texture and relative coverage).

3.4.1 Clay fraction differences

The largest absolute differences between the two soil texture maps occur in the northeastern part of Hungary (*Fig. 1*). The clay fractions derived from the Webb et al. soil map are about 30% larger than the fractions calculated from the Hungarian database. In some places the differences even exceed 50%. Relatively large (more than 20%) differences can be observed in the north-western part of the country, with the larger values sometimes in the global and sometimes in the HAS database. In the area between rivers Danube and Tisza the Hungarian database contains the larger values, the difference is about 20%. In the south-western part of Hungary the two soil maps are in good agreement, with differences mainly below 20%.

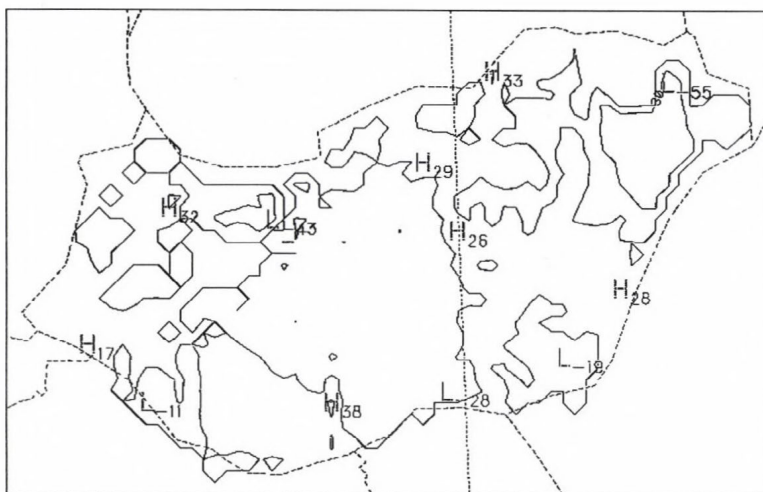


Fig. 1. Clay fraction differences in percent between the global and the Hungarian databases in Hungary (H - high, L - low).

3.4.2 Sand fraction differences

The largest absolute sand fraction differences can be seen in the northeastern part (*Fig. 2*) of the country. Here the Hungarian soil map contains the larger values and the differences exceed 60%, in some places even 70%. In the

western part of the country there are larger values in the Hungarian database, the differences are mainly 30%, but in some places they exceed 60%. In the area between rivers Danube and Tisza the differences are about 30%, with higher values in the Hungarian database. In the southern territory the differences are more than 20%, with larger values in the global database. The sand fractions derived from the two soil maps are in a good accordance in the area to the East of river Tisza except the northeastern part, and in the centre of Transdanubia.

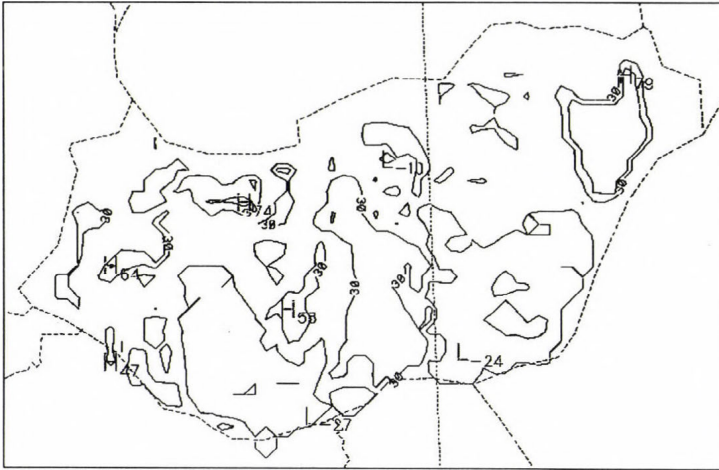


Fig. 2. Sand fraction differences in percent between the global and the Hungarian databases in Hungary (H - high, L - low).

4. Sensitivity tests

Sensitivity experiments are performed with all three versions of ALADIN (presented above). In the following chapter the results obtained from the SCM, operational ALADIN, and ALADIN with data assimilation scheme are presented. The investigated parameters are the superficial soil water content and the 2m temperature.

4.1 Experiments with the SCM

The aim of the experiments conducted with the Single Column Model is to get an idea about the sensitivity of the ALADIN surface physical package to the soil texture during a long integration period.

The model integration is performed for a ten day period, above the grid point with the largest differences between the two databases ($\varphi=48.15^\circ\text{N}$; $\lambda=20.89^\circ\text{E}$). According to the Webb et al. database, in this grid point there is 15% sand and 53% clay, while the Hungarian soil map contains 91% sand and 3% clay. The initial profiles for SCM are computed from the results of the 3D runs. The experiments are performed in free mode, no forcing from the 3D model is supplied into SCM. In these experiments the emphasis is placed on the study of land surface—air interactions and not on the exactness of forecasts. Two model runs are done, starting from the May 22, 1999 and the June 14, 1999 profiles. Due to the fact that the two model runs led to very similar conclusions, only the results of the model integration starting from the June 14, 1999 profile are presented.

The soil water content changes are as expected (*Fig. 3*). The water content curve of the more sandy soil of the Hungarian database is always below the curve representing the results obtained with the global database according to the bigger water conductivity of sand. On the sandy soil a sudden drying can be observed at the beginning of the period as the water content is adapting to the new soil texture. The differences between the results range from 0.6 kg m^{-2} to 1.7 kg m^{-2} .

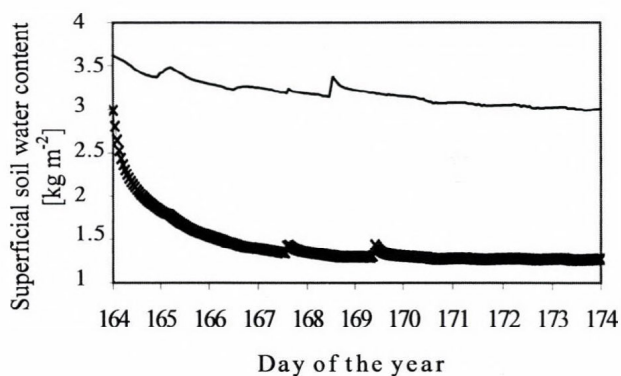


Fig. 3. Soil water content changes in the integration period of ten days. The solid line and the crosses represent the results obtained by the global and the Hungarian databases, respectively.

In the integration period of ten days the greatest difference between the 2m temperatures obtained by the different model runs is 0.8°C . This appears on the fourth day of integration period (*Fig. 4*). The results are in line with the soil texture. Above the sandy soil the temperature maxima are always higher than in the case of the clayey soil. The largest daily temperature oscillations

can be observed above the more sandy soil (the maximum variation here is 6.8°C, while above the clayey soil it is somewhat lower: 6.5°C). The explanation of this phenomenon is the bigger soil water content of the clayey soil, which leads to greater latent heat fluxes, thus moderating the temperature rise during daytime and reducing cooling at night.

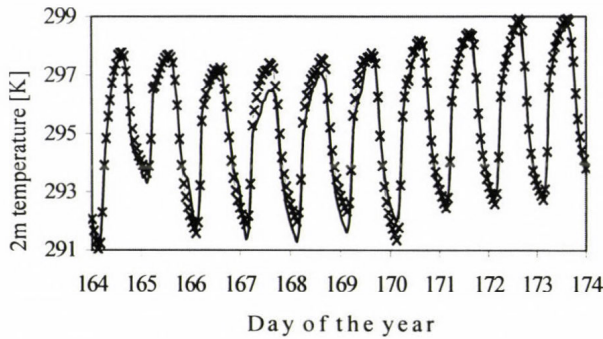


Fig. 4. 2m air temperature changes in the integration period of ten days. The solid line and the crosses represent the results obtained by the global and the Hungarian databases, respectively.

4.2 Experiments with the 3D ALADIN model

Three types of experiments are performed with different versions of the 3D ALADIN model. First, the operational model is run using fictitious soil texture data. In one case this means 100% clay and 0% sand and in the other 100% sand and 0% clay over the whole domain. This highly hypothetical situation is studied in order to get a picture about the maximum sensitivity of ALADIN to the soil texture. Second, experiments are performed with the operational ALADIN, using the two real databases described above. Finally, sensitivity tests are done with the global and the Hungarian databases, using surface data assimilation cycle in ALADIN.

The impact of soil texture on soil water content and especially on 2m temperature is expected to be small. There are lots of effects which can suppress the link between the soil texture and 2m temperature, like precipitation (the convective precipitation is very sensitive to any change of parameters), strong advection, snow cover on the ground, etc. In order to be able to demonstrate the impact, those grid points are investigated for which the effect can be expected to be maximal. Thus four synoptic stations are selected for which the differences between the two databases are the largest. For list of stations see *Table 1*.

One can expect the effect of soil texture on soil water content and 2m temperature to be maximal in such a situation when a wet soil is exposed to a large amount of radiation. Thus, such periods are chosen, based on the daily weather reports, when during the first 24 hours there is precipitation, which is followed by sunshine in the next 24-hour period. Three model runs are done with all model versions using different input data, selected according to the previous criteria. Unfortunately, the forecasts differ from the situation described in the daily weather reports. They predict rain for the last 24 hours too. The results regarding the sensitivity of the model to the databases are similar, so only the 48 hour forecast starting with initial data of the June 14, 1999 is presented.

Table 1. Sand and clay fraction data in percent for the four selected synoptic stations

WMO Nr.	Station name	Latitude	Longitude	Sand fraction		Clay fraction	
				Global	Hungarian	Global	Hungarian
12786	Záhony	48.40°N	22.17°E	21	92	47	3
12815	Mosonmagyaróvár	47.88°N	17.28°E	32	67	35	14
12843	Budapest, Lőrinc	47.43°N	19.18°E	44	72	25	9
12892	Napkor	47.97°N	21.88°E	29	83	34	6

4.2.1 Sensitivity tests with the operational model using fictitious soil texture data

First, the experiments are performed with fictitious soil texture data in order to get a picture about the maximum sensitivity of ALADIN. Two extreme cases are investigated: 100% clay and 100% sand on the whole model domain, respectively. Model runs are performed only with ALADIN using dynamical adaptation. The usage of data assimilation would have led to completely distorted results, due to the fact that information carried by the observations are inconsistent with the fictitious texture data. The model integration is performed for the same period for which the experiments with the real databases are carried out.

The model forecasts predict rain for all four stations. The amount of precipitation during the 48-hour integration time on the sandy soil is between 2.2–6.0 mm, while for the clayey soil between 0.2–3.8 mm. The values are larger above the sandy soil for all stations.

The results for the water content of the surface soil layer can be seen in Fig. 5. The results are as it can be expected on the base of soil texture. The water content of the clayey soil is always higher than that of the sandy soil, in spite of the higher amount of precipitation above the sandy soil. The results show well the great water conductivity of sand. The differences between the results range from 0.1 to 1.6 kg m⁻².

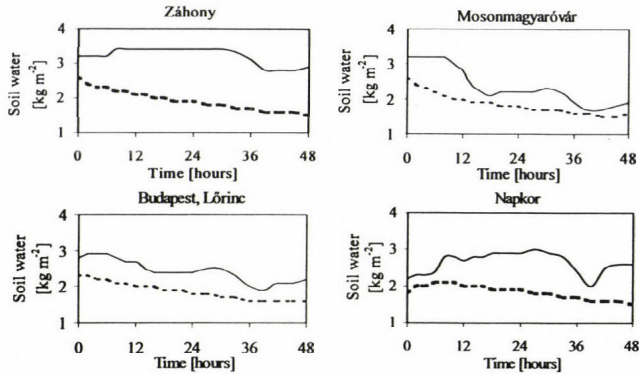


Fig. 5. Soil water content changes in the surface layer in the integration period of June 14–15, 1999. The solid and dotted lines represent the results obtained by the 100% clay, 0% sand and the 0% clay, 100% sand fractions, respectively.

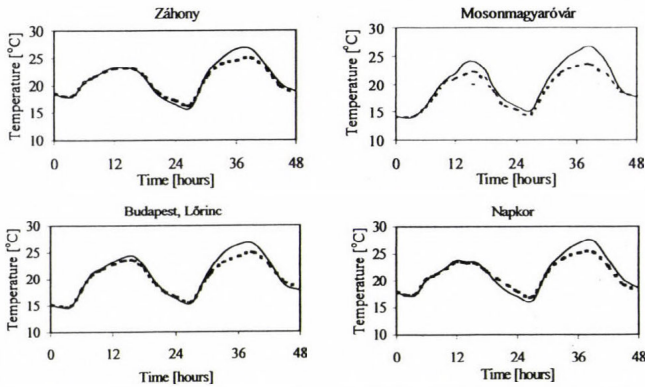


Fig. 6. 2m temperature changes in the integration period of June 14–15, 1999. The solid and dotted lines represent the results obtained with the 100% clay, 0% sand and the 0% clay, 100% sand fractions, respectively.

For 2m temperature predictions see Fig. 6. An unusual result can be observed in the figures, namely that the temperature maxima are higher above

the clayey than above the sandy soil (one could expect the maxima to be higher over sand). The explanation of this surprising result is that above the sandy soil there is a bigger amount of precipitation by 1.6–3.8 mm than above the clayey soil. This increased amount of precipitation can lead to a bigger air moisture content, and thus to a reduced 2m temperature. The differences between the results range from 0 to 3.2°C.

4.2.2 Sensitivity tests with the operational model using real databases

Forecasts with the operational model can be done up to 48 hours, because operationally we have boundary conditions only until that period. In lack of data assimilation the initial soil water content and the initial 2m temperature are not balanced, since they originate from the regional model's analysis fields, which are computed using the global data. The effect of soil texture on the 2m temperature is not as direct as in the case of soil water content (see Appendices A and B), thus one can expect that the 48-hour integration period will not be long enough to allow the occurrence of significant differences between the 2m temperatures computed with the different databases. That's why the experiments were performed using surface data assimilation too.

In the following part the forecasts of superficial soil water content and 2m temperature are presented for the four selected stations.

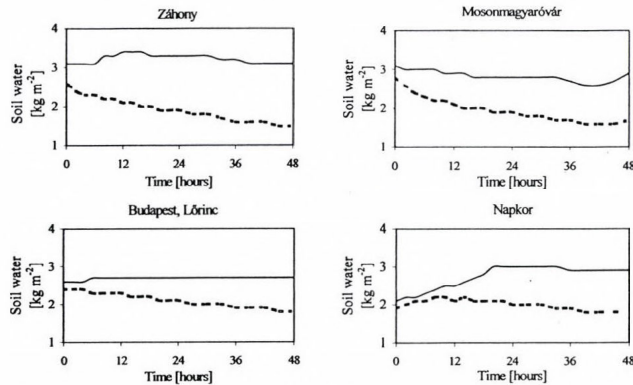


Fig. 7. Soil water content changes in the surface layer in the integration period of 14-15 June, 1999. The solid and dotted lines represent the results obtained by the global and the Hungarian databases, respectively.

The changes of water content of the surface soil layer can be seen in Fig. 7. The soil water content values of the clayey soil of the global database are always higher than those of the sandy soil (by 0.1–1.6 kg m⁻²), because of the

higher hydraulic conductivity of sand. An almost continuous drying of the sandy soil can be observed in spite of the rain (the model gave an amount of precipitation of 1.7–4.5 mm/48 hours for all five stations), while the water content of the clayey soil sometimes increases and sometimes decreases. The differences between the two curves are in general increasing during the integration period for all stations.

The results of 2m temperature forecasts obtained from the model runs with the two databases can be seen in Fig. 8. According to the expectations, the differences between the results are very low, mainly below 0.5°C due to the inconsistency between the values of initial water content and temperature, and the new soil texture. The greatest difference occurred at Záhony: 0.9°C.

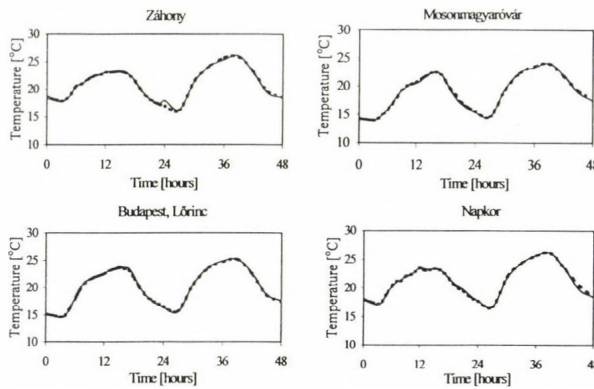


Fig. 8. 2m temperature changes in the integration period of 14–15 June, 1999. The solid and dotted lines represent the results obtained by the global and the Hungarian databases, respectively.

4.2.3 Sensitivity tests with ALADIN using data assimilation

As seen above, the 48-hour integration period is not long enough to demonstrate the effect of soil texture on the 2m temperature, due to the inconsistency between the initial water content and the new soil texture. By using data assimilation we expect greater differences between the results. The data assimilation scheme is run over a three-day period, the model state being corrected with the synoptic data every sixth hour. Afterwards a 48-hour forecast is done. The results for soil water content and 2m temperature are presented below.

The soil water content values can be seen in Fig. 9. The differences between the initial soil water contents have increased compared to the results of the operational model runs, from 0.2–0.5 kg m⁻² to 1.2–2.2 kg m⁻². Due to

the use of the data assimilation, the initial water content is consistent with the texture type. The results are as expected, the water content of the sandy soil is always less than that of the clayey soil. The maximum difference is 2.5 kg m^{-2} .

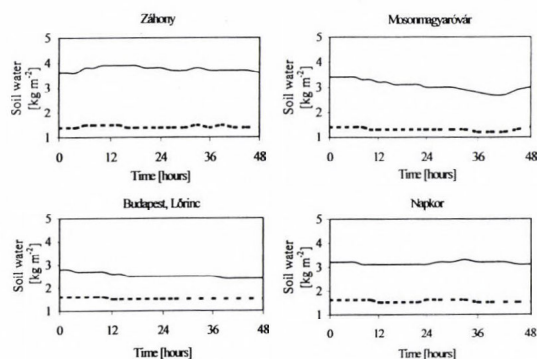


Fig. 9. Soil water content changes of the surface layer in the integration period of 14-15 June, 1999. The solid and dotted lines represent the results obtained by the global and the Hungarian databases, respectively.

The results for the 2m temperature can be seen in Fig. 10. The differences between the results for the two stations where the amount of precipitation exceeded 3.5 mm (Záhony and Napkor) are low. The maximum difference is 0.8°C . This fact illustrates well, how the effect of soil texture on the 2m temperature can be suppressed by precipitation. For the two remaining stations (with less than 3 mm rain) the differences were larger compared to the results of the operational model runs. The maximum difference was 4.4°C .

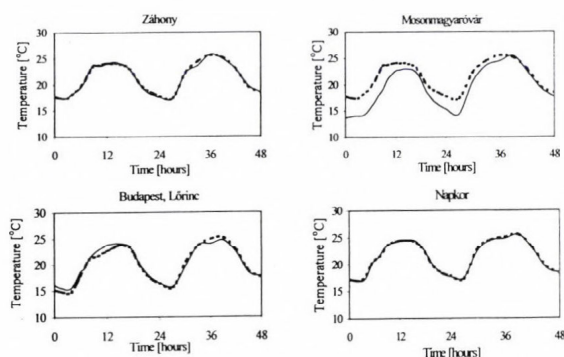


Fig. 10. 2m temperature changes in the integration period of 14-15 June, 1999. The solid and dotted lines represent the results obtained with the global and the Hungarian databases, respectively.

5. Conclusions

The subject of this study was to evaluate the sensitivity of the ALADIN mesoscale numerical weather prediction model to the variation of the soil texture. The sensitivity tests were performed with three versions of ALADIN. They were the one dimensional version of ALADIN, the operational model using dynamical adaptation, and ALADIN with data assimilation. Soil texture data were taken from two databases: the Webb et al. global database and a Hungarian soil texture map. Forecasts were done with all three model versions using the different soil texture data. The sensitivity of soil water content (in the surface layer) and 2m temperature predictions to the changes of soil texture were evaluated in four selected grid points, where the differences between the databases were the largest.

Experiments with SCM were performed for a ten day period. During this time the maximum difference between the soil water contents was 1.7 kg m^{-2} while that for the 2m temperature was 0.8°C .

The operational model was run with fictitious soil texture data first, which meant 0% clay and 100% sand in one case and 100% clay and 0% sand in the other case. The soil water content of the clayey soil was always higher than that of the sandy soil, due to the higher water conductivity of sand. The largest difference was 1.6 kg m^{-2} . In contrast with the expectations, the temperature maxima were higher above the clayey soil, what was caused by the higher amount of precipitation above sand. The maximum difference between the predicted 2m temperatures was 3.2°C .

During the experiments with the operational model using the real databases, the soil water content of the more sandy soil was always less than that of the clayey soil, according to the previous expectations. The largest difference was 1.6 kg m^{-2} . The differences between the predicted 2m temperatures were small, they remained mainly below 0.5°C , with a maximum of 0.9°C , due to the inconsistency between the initial water content, 2m temperature, and the new soil texture.

In order to start the 48-hour forecast from initial conditions consistent with the soil texture, and thus to be able to demonstrate the effect of soil texture on the 2m temperature, a data assimilation cycle was used. The differences between the initial water contents have grown from $0.2\text{--}0.5 \text{ kg m}^{-2}$ to $1.2\text{--}2.2 \text{ kg m}^{-2}$ compared to the results of the operational model runs, due to the use of data assimilation. During the 48-hour integration the greatest difference between the soil water contents was 2.5 kg m^{-2} . The largest difference between the predicted 2m temperatures was 4.4°C . Here it has to be mentioned, that this value is an overestimation of the real sensitivity, due to the fact, that in the data assimilation system no updating of the soil prognostic

variables was included. The use of the same 2m data to constrain the surface would have brought the results somewhat closer.

The differences between the 2m temperatures were larger with increasing texture differences (compare the results of operational model runs with real and fictitious data). The use of data assimilation adjusted the initial conditions to the soil texture, hence the differences between the soil water contents and 2m temperatures grew even larger. The situation considered here wasn't ideal for showing the maximum sensitivity of ALADIN to the soil texture, since the forecasts gave precipitation instead of sunshine for the second 24-hour period. Under ideal circumstances (wet ground exposed to strong radiation) the sensitivity may even prove to be larger.

Further research on this topic should be taken into consideration, running the model with data assimilation and evaluating the results over a long time period. They may even be compared with synoptic data to see whether the forecasts on average can be improved by using a detailed Hungarian soil texture map.

APPENDIX A

Computation of the soil water content

The prognostic equations for the soil water contents of the two layers are the following:

$$\frac{\partial W_s}{\partial t} = \delta_{land} \left[C_1 \left(P_g + F_{evg} + F_{ror} + F_n \right) - F_{wsp} - F_{ros} - F_{si} \right],$$

$$\frac{\partial W_p}{\partial t} = \delta_{land} \left[\left(P_g + F_{evg} + F_{ror} + F_n \right) + F_{tr} - F_{rop} - F_{pi} - F_{si} \right],$$

where

- W_s – superficial liquid soil water content,
- W_p – total liquid soil water content,
- δ_{land} – land fraction within the grid box (1 or 0),
- P_g – precipitation flux at the ground,
- F_{evg} – bare ground evaporation flux,
- F_n – snow melting flux,
- F_{si} – surface freezing flux,
- F_{pi} – deep freezing flux,
- F_{ror} – runoff from the interception reservoir,
- F_{ros} – runoff from the surface reservoir,
- F_{rop} – gravitational drainage (at the bottom of the deep reservoir),
- F_{wsp} – water diffusion in the ground.

Hydraulic coefficients

The C_1 coefficient increases when the soil dries, as hydraulic conductivity is then reduced:

$$C_1 = C_{1sat} \left(\frac{W_{sat}}{W_s} \right)^{\frac{b}{2} + 1},$$
$$C_{1sat} = (5.58 \times CLAY + 84.88) \times 10^{-2},$$
$$w_{sat} = (-1.08 \times SAND + 494.305) \times 10^{-3},$$
$$b = 0.137 \times CLAY + 3.501.$$

The C_2 coefficient characterises the speed by which the water profile returns to the equilibrium profile. It increases with hydraulic conductivity and participates in the formulation of the water diffusion in the ground:

$$F_{wsp} = \frac{C_2}{\tau} (W_s - W_{seq}),$$
$$C_2 = C_{2ref} \frac{F_{Sp}}{1 - F_{Sp} + \varepsilon},$$
$$C_{2ref} = 13.815 \times CLAY^{0.954}.$$

The C_3 coefficient is present in the formulation of gravitational drainage and it characterises the speed by which the water profile is relaxed to the field capacity:

$$F_{rop} = \frac{C_3}{\tau} \max(0, W_p - W_{fc}),$$
$$C_3 = 5.3275 \times CLAY^{-1.043}.$$

Denotation of symbols:

$SAND$ – sand fraction in percentage,

$CLAY$ – clay fraction in percentage,

W_{sa} – water content at saturation,

W_{seq} – superficial water content at equilibrium between gravity and capillarity forces,

τ – the 1 day period (86,400 seconds),

F_{Sp} – the saturated part of the soil,

ε – a small value limiting C_2 at saturation,

W_{fc} – field capacity.

APPENDIX B

Computation of the 2m temperature

The starting equations are the equations for moisture and dry static energy (the sum of enthalpy and geopotential):

$$\begin{aligned} q(z) &= q_s + \alpha_h(z)(q_L - q_s), \\ s(z) &= s_s + \alpha_h(z)(s_L - s_s), \\ s(z) &= c_p T(z) + \phi(z), \\ c_p(q) &= c_{pa} + (c_{pv} - c_{pa})q. \end{aligned}$$

From these the following equation can be derived for the temperature in the z height:

The prognostic equation for the surface temperature is the following:

$$T(z) = \frac{c_p(q_s)T_s + (\phi_s - \phi(z)) + \alpha_h(z) [c_p(q_L)T_L - c_p(q_s)T_s + (\phi_L - \phi_s)]}{c_p(q(z))},$$

$$\frac{\partial T_s}{\partial t} = \delta_{land} C_T (Q_R + Q_{sens} + Q_{lat} - F_{sp} - L_f(F_n - F_{si})).$$

The thermic coefficient for bare ground can be expressed as:

$$C_G = C_{Gsat} (F_{Sp})^{-\frac{b \ln 10}{2}},$$

$$C_{Gsat} = -1.5571 \cdot 10^{-8} \cdot SAND - 1.441 \cdot 10^{-8} \cdot CLAY + 4.70217 \cdot 10^{-6}.$$

For vegetation alone it has a constant value (C_V).

The C_T thermic coefficient for the whole ground-vegetation system can be obtained by weighting the previous contributions by the bare ground and vegetation fractions:

$$C_T = \left[(1 - veg) \frac{1}{C_G} + veg \frac{1}{C_V} \right]^{-1},$$

where

- q – specific humidity,
- s – dry static energy,
- $c_p(q)$ – isobaric specific heat of the wet air as a function of specific humidity,
- c_{pa} – isobaric specific heat for dry air,
- c_{pv} – isobaric specific heat for water vapour,
- T – temperature,
- ϕ – geopotential,
- s – index for the surface,

- L – index for the middle of the lowest model layer,
 z – height,
 α_h – coefficient depending on the atmospheric stability (on the Richardson number),
 $f_h(z)$ – coefficient depending on the atmospheric stability (on the Richardson number),
 Q_R – surface net radiative energy flux,
 Q_{sens} – surface sensible heat flux,
 Q_{lat} – surface latent heat flux,
 F_{sp} – heat flux between surface and deep ground,
 L_f – melting heat,
 veg – vegetation fraction.

References

- Betts, A.K. and Ball, J.H., 1996: The land surface-atmosphere interaction: A review based on observational and global modeling perspectives. *J. Geophys. Res.* 101, 7209-7225.
- Brožková, R., 2001: RC LACE Status Report. *LAM Newsletter*, No. 30, February 2001, pp. 46-52.
- Davies, H.C., 1976: A lateral boundary formulation for multi-level prediction models. *Quart. J. Roy. Meteor. Soc.* 102, 405-418.
- FAO, 1988: *Unesco Soil Map of the World*. Report No. 60, World Soil Resources, Rome.
- FAO/UNESCO, 1971-1981: *Soil Map of the World, 1:1,500,000, Volumes II.-X*. UNESCO, Paris.
- Gandin, L.S., 1963: Objective analysis of meteorological fields. (in Russian) *Gidrometeor. Izd.*, Leningrad, (English Translation by Israel Program for Scientific Translations, Jerusalem, 1965).
- Gérard, L., 2000: Physical parameterizations in ARPEGE-ALADIN. ALADIN internal report.
- Giard, D. and Bazile, E., 2000: Implementation of a new assimilation scheme for soil and surface variables in a global NWP model. *Mon. Wea. Rev.* 128, 997-115.
- Horányi, A., Ihász, I., and Radnóti, G., 1996: ARPEGE/ALADIN: A numerical weather prediction model for Central-Europe with the participation of the Hungarian Meteorological Service. *Időjárás* 100, 277-301.
- Irannejad, P. and Shao, Y., 1998: Description and validation of the atmosphere-land-surface interaction scheme (ALSIS) with HAPEX and Cabauw data. *Global Planet. Change* 19, 87-114.
- Kabat, P., 1998: Land surface data in climate and weather models. The role of the land surface in controlling climate is still underestimated. *Bach News* 6, 8-10.
- Mihailovic, D.T., de Bruin, H.A.R., Jettif, M., and van Dijken, A., 1992: A study of the sensitivity of land surface parameterizations to the inclusion of different fractional covers and soil textures. *J. Appl. Meteor.* 31, 1477-1478.
- Noilhan, J. and Mahfouf, J.-F., 1996: The ISBA land surface parameterization scheme. *Global Planet. Change* 13, 145-159.
- Noilhan, J. and Planton, S., 1989: A simple parameterization of land surface processes for meteorological models. *Mon. Wea. Rev.* 117, 536-549.
- Piriou, J.-M., Bouyssel, F., and Bazile, E., 1999: ARPEGE-ALADIN Single Column Model. Scientific and Algorithmical Aspects. *MÉTÉO-FRANCE, Internal Documentation*.
- Pitman, A.J., 1994: Assessing the Sensitivity of a Land-Surface Scheme to the Parameter Values Using a Single Column Model. *J. Climate* 7, 1856-1869.
- Pitman, A., Pielke, R., Avissar, R., Clausses, M., Gash, J., and Dolman, H., 1999: The role of the land surface in weather and climate: does the land surface matter? *IGBP Newsletter* 39, 4-11.
- Várallyay, Gy., Szűcs, L., Murányi, A., Rajkai, K., and Zilahy, P., 1980: Map of soil factors determining the agro-ecological potential of Hungary (1:100.000) (in Hungarian). II. *Agrókémia és Talajtan* 29, 35-69.
- Webb, R., Rosenzweig, C., and Levine, E., 1991: A global data set of soil particle size properties. *Technical Report 4286*. NASA, GISS New-York.

IDŐJÁRÁS

Quarterly Journal of the Hungarian Meteorological Service
Vol. 106, No. 2, April–June 2002, pp. 59–74

Selected characteristics of wind climate and the potential use of wind energy in Hungary. Part II

Kornélia Radics^{1,2} and Judit Bartholy¹

¹*Department of Meteorology, Eötvös Loránd University,
P.O. Box 32., H-1518, Budapest, Hungary*

²*Meteorological Service of the Hungarian Defence Forces,
H-1885, Budapest, Hungary*
E-mails: nelly@nimbus.elte.hu; bari@ludens.elte.hu

(Manuscript received September 3, 2001; in final form December 20, 2001)

Abstract—Renewable energy resources including especially wind energy are considered important energy sources. Since the early 80's several research projects have investigated new technologies worldwide, others have built wind field models and dealt with the optimal siting of wind power stations. This work is to clarify the possibilities of wind energy utilization in Hungary. In the second part of the paper, first, 20th century wind climate in the country is summarized analysing and comparing wind data of five different sources. Wind profile is analysed using multilevel wind measurements (from 10 m to 115 m) at the Hegyhátsál area. Significant differences are found in wind speed frequency distributions of vertical levels during the year. A case study is carried out using a mesoscale wind model for surroundings of Hegyhátsál (41 km × 41 km) in order to estimate horizontal and vertical cross sections of wind power fields. Height of a given available wind power level is mapped for larger areas (100 km × 100 km) over Trans-Danubia and over the Great Hungarian Plain demonstrating the importance of siting wind power stations.

Key-words: renewable energy resources, wind energy, wind climate, wind profile, statistical time series analysis, wind field modeling

1. Introduction

Conversion of renewable energy is considered a key issue that plays an important role in the life of inhabitants of our planet. Apart from a negligible period relative to historical time scales, renewable energy provided the only energy resources accessible to mankind. Continuously increasing energy need and energy use of human settlements stem from hundreds of years ago, so it is

a persistent problem starting long before the last century (Gipe, 1995). Structure of these complex processes and their interrelations are presented in Fig. 1. The upper part of the figure (using data from Sørensen, 2000) shows the trend of the average rate of energy conversion per capita on a logarithmic time scale, extending backwards from year 1990. Furthermore, it indicates the estimated variation in energy use with dotted and dashed lines representing societies using the largest and the smallest energy amounts, respectively. For the more recent period, data from Darmstadter et al. (1971) and the European Commission (1997) are included. The lower part of the figure presents the dramatically increasing population rate and the quantity of burnt fossil fuel having definitely similar trends.

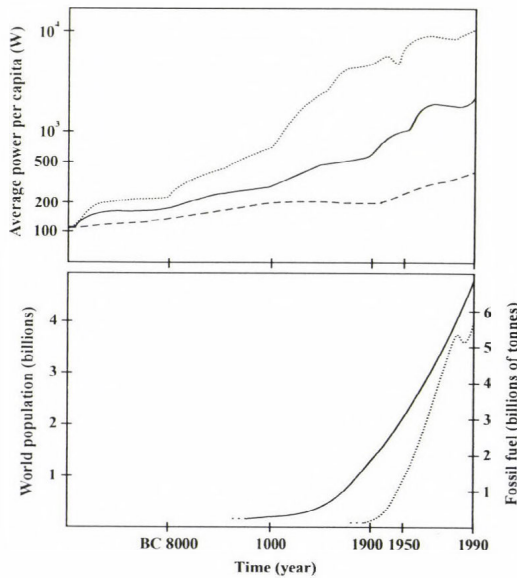


Fig. 1. Trend of the average rate of energy conversion per capita on a logarithmic time scale (up). The estimated variation in energy usage is shown with the dotted and dashed lines representing societies using the largest and the smallest energy amounts, respectively. The dramatically increasing population rate (solid line) and the quantity of the burnt fossil fuel of the world (dotted line) are also indicated (down). (Sources: Sørensen, 2000; Darmstadter et al., 1971; the European Commission, 1997.)

During the entire history of mankind, difference between societies with the highest and the lowest energy consumption has never been so high as nowadays. Increasing energy use of the last millennium is partly due to the

shift in population distribution towards higher latitudes, and to overall increased energy demand (space heating, hot water, lighting, refrigerating, transportation, etc.). Development in the last century is dominated by the energy consumption of the industrialized countries. Evidently, people living in well-organized and mostly urbanized societies use the largest energy amounts.

The difference between the most and the least developed regions of the world, considering energy use as well as infrastructural conditions, seems to continue to widen. Further development of the industrialized part of the world is extremely important because of its dominant share of the total energy used. However, the key factors of the near future trends depend on the other and larger part of the world now using very little energy: whether it will continue to do so or it will increase its energy use.

From a long-term point of view it is suggested that man must base his energy use partly on renewable energy resources. Consequently, there is an urgent need to expand the currently limited technological capacity aimed at utilization of renewable energy, and make such energy conversion technologies more viable than they are at present.

The main purpose of this research project was to consider and review the utilization of potential wind resources of Hungary. In the second part of the paper, first, wind climatologies for Hungary are reviewed, summarizing the results published by several authors in the last century. Then, results of wind profile measurements are presented. Based on the observed time series, errors of wind profile fitting are estimated. Finally, model simulations of wind field are provided to characterize possible wind energy utilization in selected regions of Hungary.

2. *Wind climate*

Nowadays, there is a growing and identified interest to erect wind turbines in order to substitute traditional or environmentally pollutant energy resources. Optimal siting of wind power stations requires the knowledge of detailed topography and wind climate of the studied region. Since climate change can be an important factor as well, wind climate variations of Hungary has been analysed for the last century. Wind climatological data from all available sources have been collected (several authors studied various time periods using sometimes irregular units such as Beaufort scale). For this analysis from the viewpoint of wind energy utilization, the best climate indicators would be the wind climate tables (*Troen and Petersen, 1989; Bartholy and Radics, 2001*). However, measurements that can satisfy the requirements of climatological diagrams are unavailable from the earlier decades of the last century. Therefore, spatial distribution of mean wind speed can be presented summariz-

ing all available information. Selected and corrected data sets have been re-drawn and nine of them are presented in Fig. 2, 3, and 4. Difficulties arose in the comparison because the various sources apply different averaging periods (annual, semi-annual, and monthly averages) and different measuring networks.

Fig. 2 shows the spatial distribution of annual mean wind speed over the country determined from wind observations in 1901–1930. This map was transformed from a similar one (*Bacsó*, 1959) which was given in Beaufort force. For a ten-year-long period (1931–40) *Bacsó et al.* (1953) gave a more detailed semi-annual map-pair for summer and winter half-year (Fig. 3) using data of much more stations than in Fig. 2.

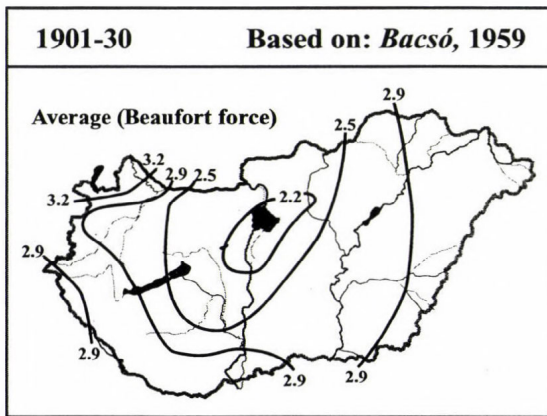


Fig. 2. Spatial distribution of annually averaged wind speed over Hungary.

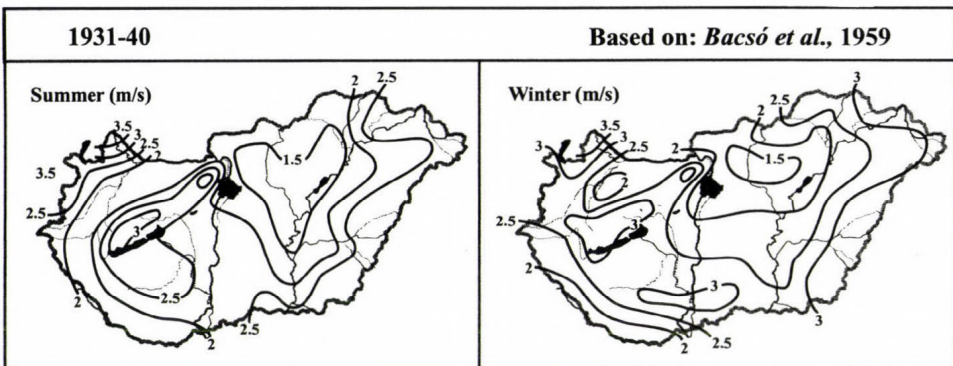


Fig. 3. Spatial distribution of averaged wind speed for winter and summer half-years over Hungary.

Wind energy utilization is the most critical in transition seasons where annual maximum and minimum values occur. Generally, April (in some region March) is the windiest month in the country, while October can be characterized by large spatial variability over different regions of Hungary. Therefore, for the second half of the 20th century—when more observations are available—we chose April and October to represent wind climate. Fig. 4A, B, and C show monthly mean wind speed in April and October for the periods of 1958–1962, 1968–1972, and 1950–1980, respectively (*Kakas, 1967; Tar, 1991; Pécsi, 1989*).

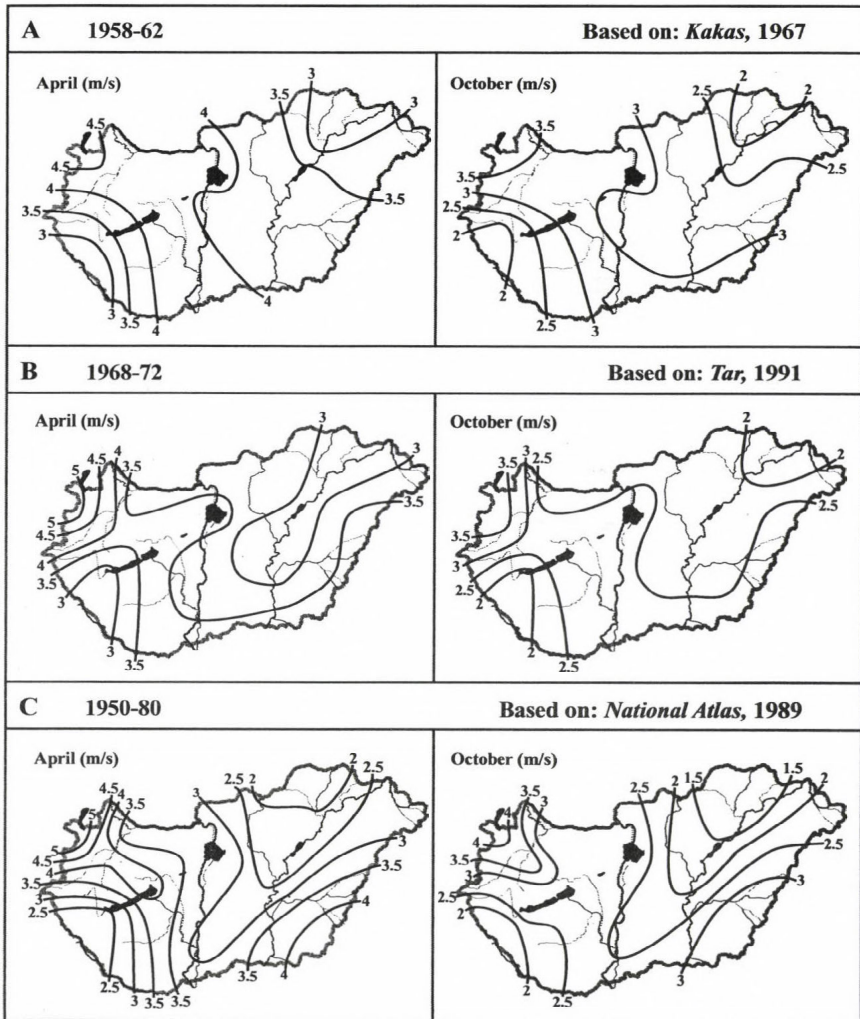


Fig. 4. Monthly wind speed averages of April and October for three different time intervals.

As a summary of Fig. 2, 3, and 4 the following can be drawn. Maximum wind speed values occur in the northwestern corner of the country (around the Dévényi-gate). In general, two minimum wind speed centers appear on the maps, one in the southwestern and the other in the north, northeastern part of Hungary. Average values in Trans-Danubia are higher than in the eastern part of the country. Although, maximum and minimum centers do not show annual moving, values are higher, and the range between the maximum and minimum values are getting also somewhat higher in spring (April) than in autumn (October). Based on the analysed wind speed data no significant changes can be observed during the 20th century, nevertheless for selected areas and shorter periods significant trend was found (Tar *et al.*, 2001).

Because of the inhomogeneity of time series, the changes in measuring techniques and instruments, several replacements of measuring stations and their changing surroundings, the above summary obviously includes some uncertainties. Despite all these factors, it is very unlikely that significant trend would stay hidden in this analysis.

3. Wind profile

Collaborating with the AEROCARB EU-5 framework project (Haszpra *et al.*, 2001), we had the opportunity to carry out wind profile measurements near the village Hegyhátsál, at a site of the northwestern part of Hungary (46.96°N, 16.65°E). Wind speed and wind direction have been observed at four levels from the end of September 1994 (Bartholy and Radics, 2000) on a 117 m tall TV and radio transmitter tower. The measuring station lays at 248 m above sea level, and surrounded mainly by agricultural fields and forest patches. As shown in Fig. 5, the lower part of the tower (56 m) is a 7.75 m diameter cylinder where measurements are recorded at 48 m height in both south and north direction. On the upper cylindrical part (1.82 m diameter) measurements are performed at 82 and 115 m height in north direction. The tower is also a NOAA/CMDL (National Oceanic and Atmospheric Administration/Climate Monitoring and Diagnostics Laboratory) global air sampling network site. In addition, carbon dioxide mixing ratios are continuously monitored, and the atmosphere-surface exchange of CO₂ is measured by eddy covariance (Haszpra *et al.*, 2001).

First, data set of the lowest measuring point (near surface) was analysed. The instrument is placed at 10 m above ground and 70 m away from the tower with the intention to exclude as much as possible shelter effects of the tower. The well-known annual cycle of wind speed can be recognized in the observed data. April is the windiest month in Hegyhátsál area, and October is the least

windy month of the year, as the Hungarian wind climate can be characterized in general. Therefore, relative wind speed frequencies of these months are presented in Fig 6. The first columns represent the relative frequencies of wind calm periods that are relatively low compared to some other regions of Hungary. Certainly, calm periods appear much more frequently in October (9.3%) than in April (5.0%). In both months the most frequent wind speed values are in the 0–4 m s⁻¹ interval. However, wind speed values above the average in April occur more often than in October.

Fig. 5. Structure of the wind profile at the measuring station Hegyhátsál.

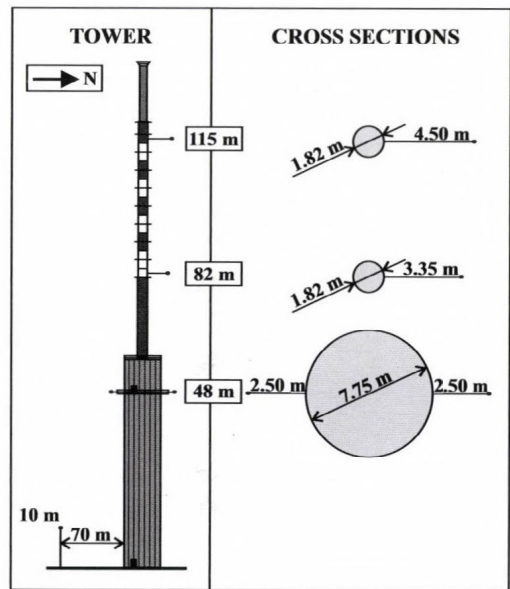
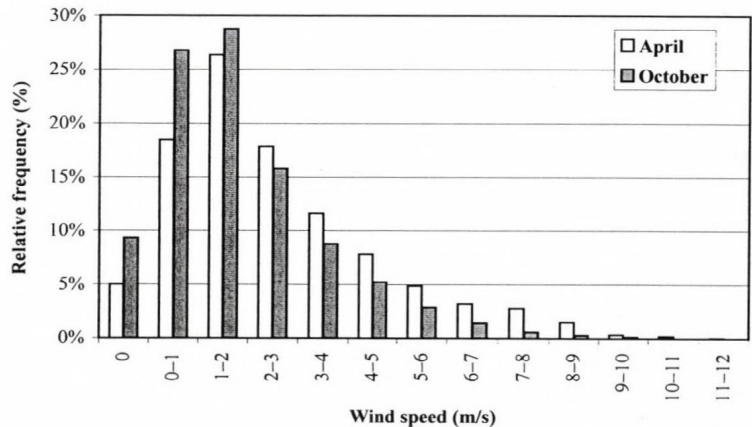


Fig. 6. Frequency distributions of wind speed for April and October at station Hegyhátsál.



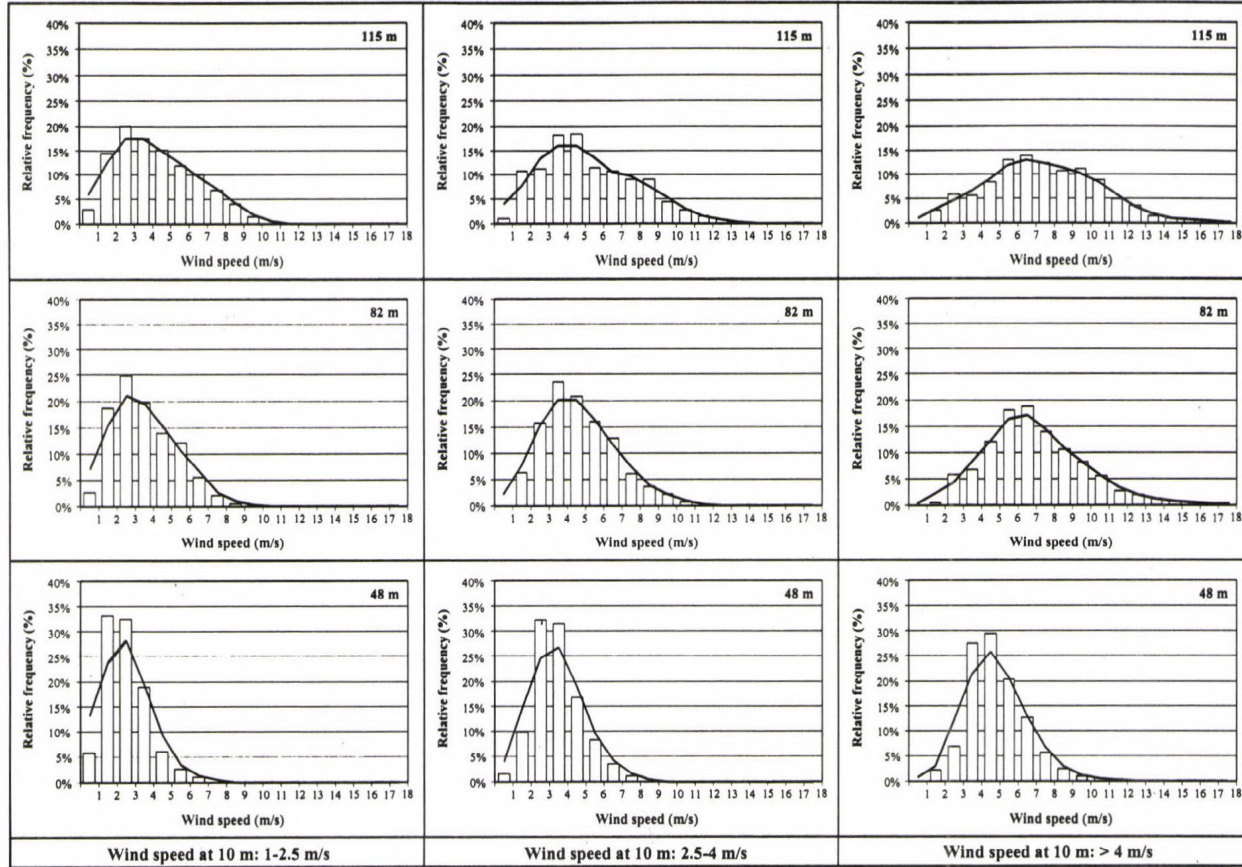


Fig. 7. Relative frequencies of wind speed observed at three levels in April using the tercile classification of April near surface data. Smoothing (running means) is indicated by solid lines.

Multilevel wind speed measuring experiments on towers are suitable to estimate the vertical profiles of wind speed. Although our data set includes errors coming from the shelter and wind field perturbation effects of the specially shaped tower, detailed profile analysis and profile fitting can provide appropriate information about the vertical structure of the flow.

Six-year-long (1995–2000) database measured at four levels was analysed. Classification of wind speed values is based on the near surface time series (observed at 10 m). Periods with wind speed less than 1 m s^{-1} were excluded from the analysis having no significant effect in wind energy production. After determining the tercile values (2.5 m s^{-1} and 4 m s^{-1}) of wind speed time series in April near the surface, ranked data was divided into three groups with equal number of observations (33.3% of data in each group). *Fig. 7* shows the frequency distributions of observations from the higher measuring levels (48, 82, and 115 m) based on the near surface wind speed classification described above. Also the smoothed curves of the distributions are indicated in the figure (where the running mean technique were applied for all consecutive wind speed classes). In order to compare the selected two months, the same threshold values (terciles of April) were used for October leading to an asymmetric distribution (46.9%, 31.8%, and 21.3%, respectively). *Fig. 8* represents the relative frequencies of the above-defined categories in case of October.

In spite of the unequal distribution of the groups of October data, relative frequencies remain smaller than in case of April. However, large differences cannot be observed between April and October wind climate conditions at higher levels. As height and wind speed increase, the range of wind speed frequencies is getting larger resulting in larger errors in wind profile estimation.

4. Wind field estimations

Before estimating extractable wind power or siting wind power stations, it is necessary to map the spatially continuous wind fields. Such maps can be obtained solely by using wind models. The WAsP model (*Mortensen et al.*, 1993) developed at Risø National Laboratory, Roskilde, Denmark has been selected for this reason. It is a linear spectral model for near neutral boundary layer flow over complex terrain. The model can be used to analyse raw time series and estimate the wind climate at any site using digitized topographical, roughness, and shelter maps.

In order to verify the WAsP model for selected regions of Hungary, input data measured at Hegyhátsál at 10 m height have been used to model the wind

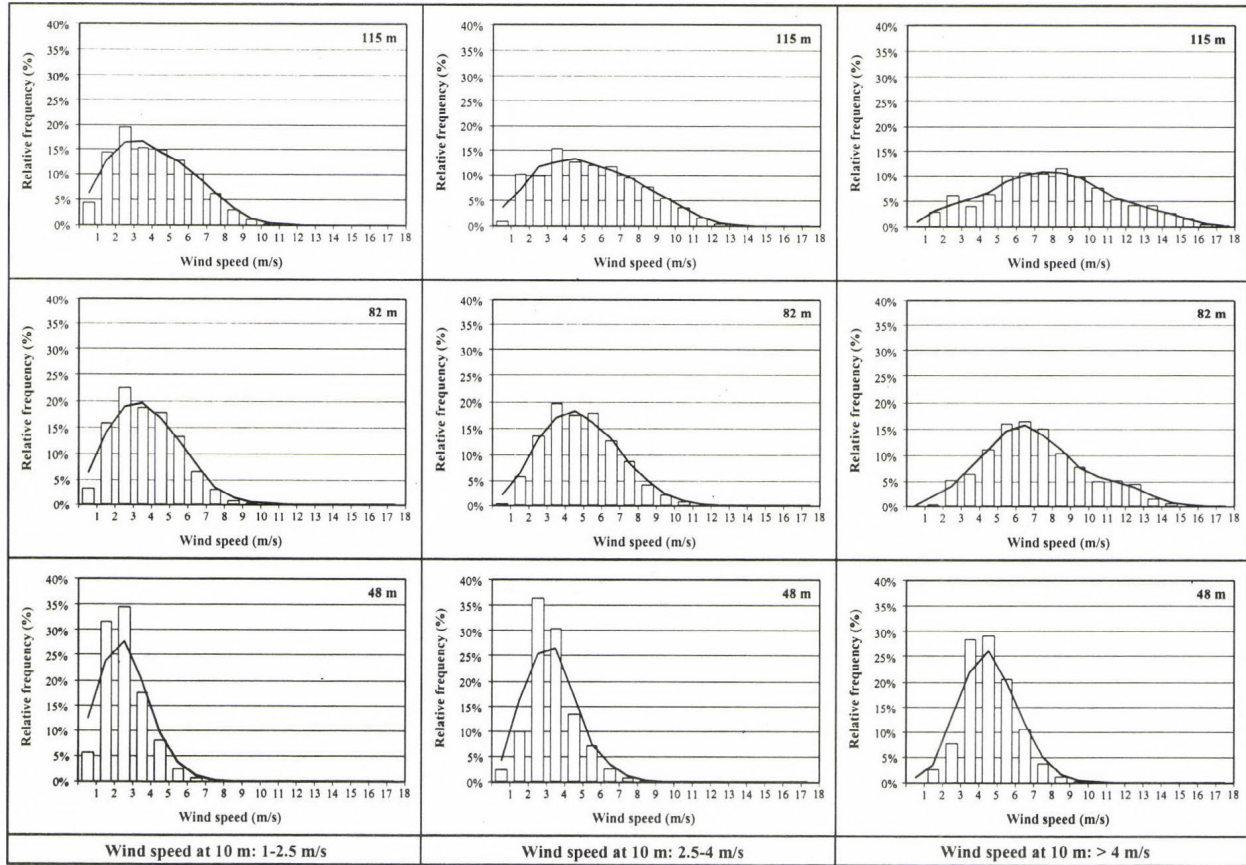


Fig. 8. Relative frequencies of wind speed observed at three levels in October using the tercile classification of April near surface data. Smoothing (running means) is indicated by solid lines.

field over the hilly terrain of 41 km × 41 km area. The topography has been included in WAsP as a height-contour map using 25 m isolines. Roughness length has been set to 1 m, 0.5 m, and 0.1 m for forests and cities, villages and orchards, and shrublands or grasslands, respectively. In case of water bodies, 0.001 m has been chosen. Effects of every obstacle near the station have been taken into consideration. We did not find considerable differences between measured and simulated values; consequently, topography of the hilly terrain does not generate remarkable model errors. Since orography of Hungary does not show large variability in elevation above the sea level, our preliminary results suggest that the WAsP model will provide reasonable output fields (Bartholy and Radics, 2001). Therefore, it is possible to extrapolate wind data of Hegyhátsál simulating mean flow over the surroundings.

After including the orographical characteristics of Hungary into the WAsP model, measured wind data were extrapolated horizontally and vertically. In Fig. 9 a case study for the Hegyhátsál area is presented. First, mean wind speed field was simulated for a 41 km × 41 km area around the measuring place at 18 m height. The model run was based on the fine resolution digital terrain model (DTM 1000) and on the measured wind speed at 10 m height (Fig. 9, top). Then, available wind power fields were estimated and mapped for 18 and 50 m heights, respectively (Fig. 9, middle and bottom). The simulated mean wind speed values, as well as, the topography are in good agreement with the structure of the mean wind power field. Consequently, the case study demonstrates strong dependence on height and topography. Even at siting wind power station with 50 m rotor axis height, the available wind power has 80–130% variability (comparing to the wind power value of Hegyhátsál) depending on terrain modification.

Figs. 10 and 11 present the vertical cross-sections (longitudinal and latitudinal, respectively) of available wind power fields resulted from simulations using the WAsP model. On both diagrams the vertical structure of wind power fields in Hegyhátsál area can be recognized through the run of the 50, 100, 150 and 200 W m⁻² isolines. This kind of figures can provide useful hints in case of siting wind power stations, but three-dimensional information would be the best tool over a larger area.

Results of two case studies are presented in Fig. 12, where height and structure of a given wind power level (180 W m⁻² was selected based on the results of Fig. 9) are mapped for a Trans-Danubian and a Great Hungarian Plain sector (100 km × 100 km each). The upper part of the figure is centred to Pápa (47.36°N, 17.49°E), and the lower part to Kecskemét (46.92°N, 19.75°E). Height of the selected wind power level was calculated by the WAsP model using ten-year-long database of the above mentioned stations.

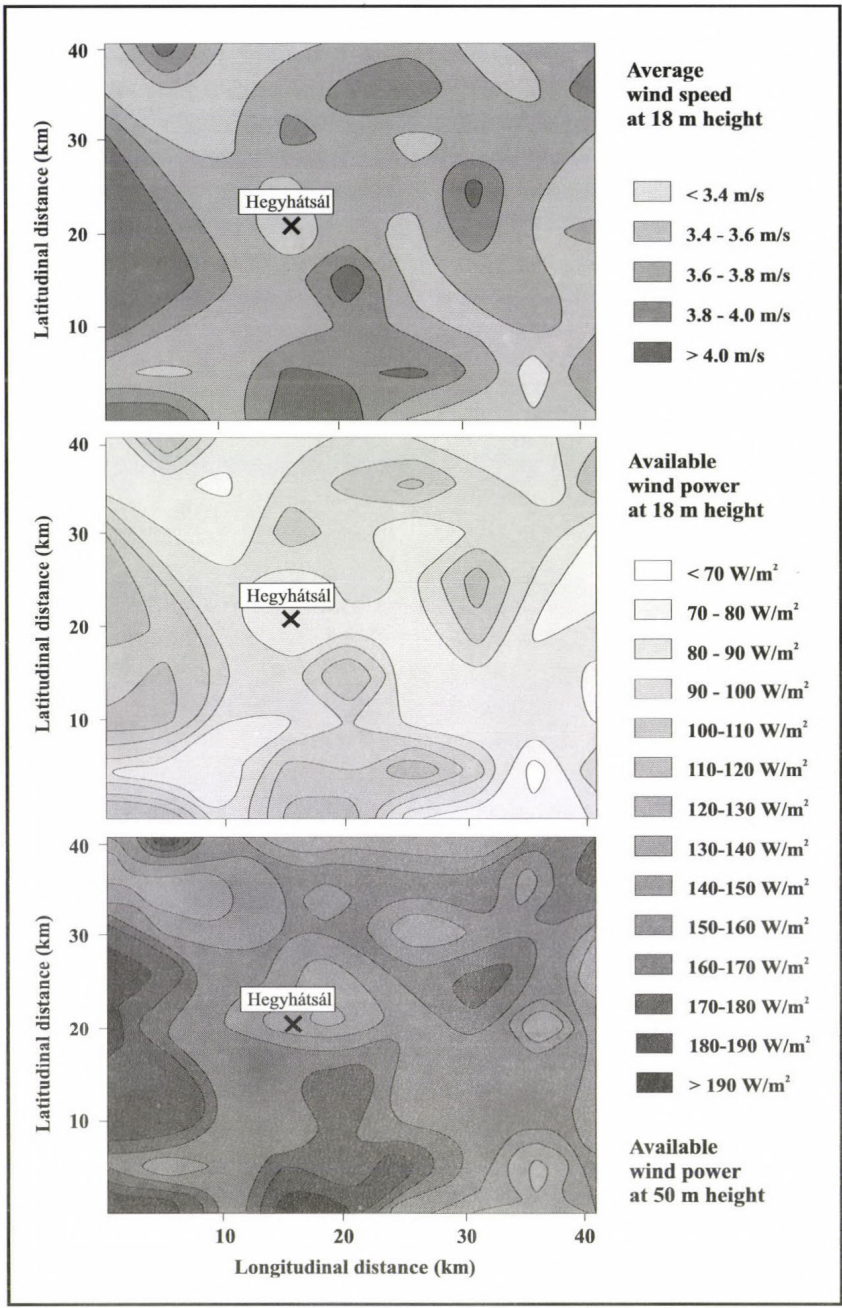


Fig. 9. Average wind speed and available wind power values at different levels around station Hegyhátsál.

Considerable spatial differences are present at both areas (maximum values: 60–70 m, minimum values: 8–10 m) that can be explained partly by topography and roughness, and partly by basic flow patterns of the region. Effects of the complex orography of the Pápa region (including foothills of the Alps, Mountain Bakony, etc.) result in somewhat more variable structure of isolines than the flat terrain of the Kecskemét region (Great Hungarian Plain). The northwestern-southeastern axis dividing the higher and lower height values on the Kecskemét map has good correspondence with the structure of wind climates presented in Figs. 2–4. This type of maps can support the optimal siting of wind power stations. However, the optimal solution would be to construct a map of the entire country using data observed at many more stations and considering more detailed digital terrain models.

Fig. 10. Latitudinal (N-S) vertical cross-section of mean flow demonstrating wind power isolines around station Hegyhátsál.

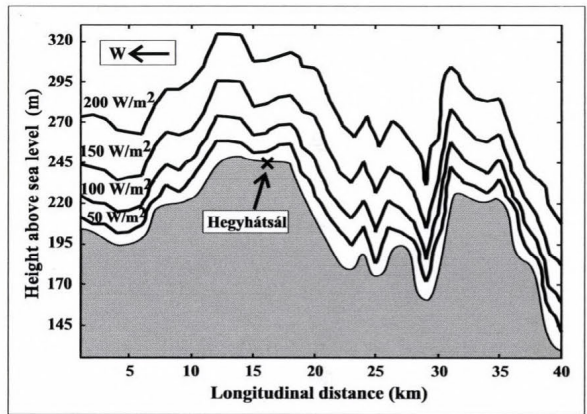
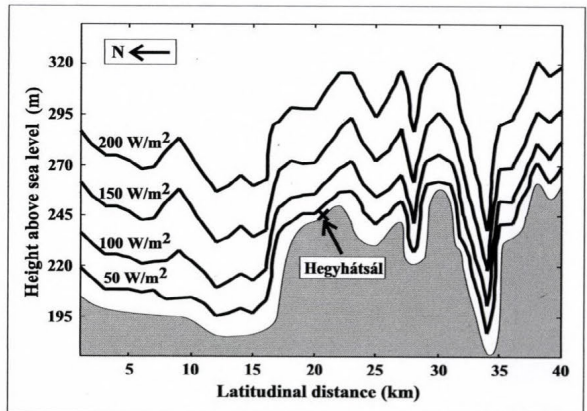


Fig. 11. Longitudinal (W-E) vertical cross-section of mean flow demonstrating wind power isolines around station Hegyhátsál.



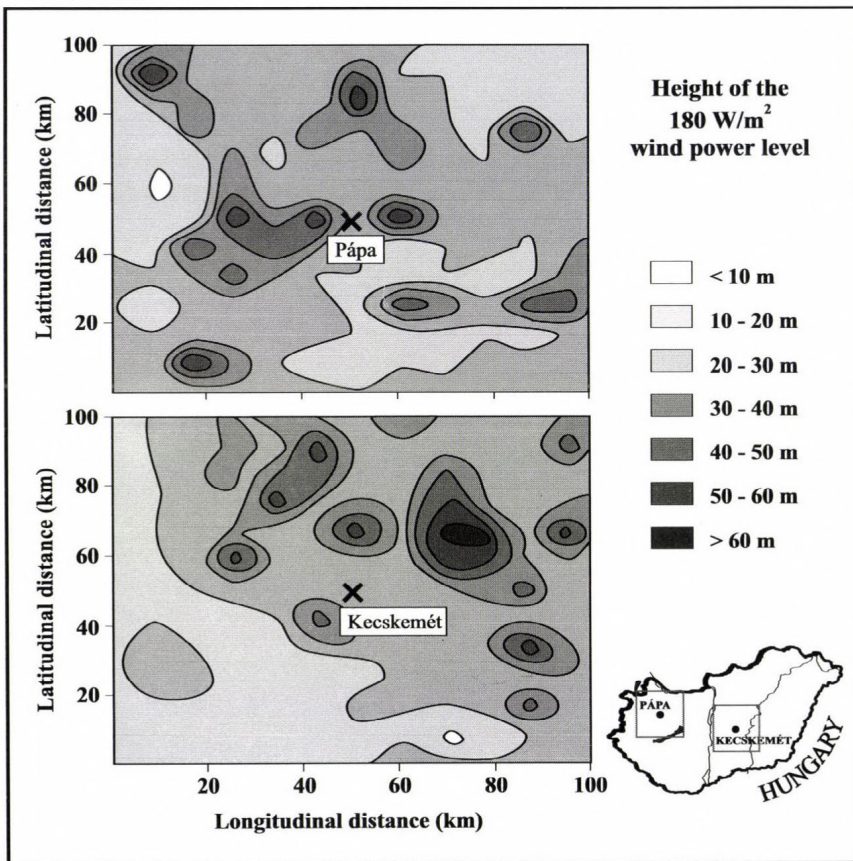


Fig. 12. The height and the structure of 180 W m^{-2} wind power level over Trans-Danubia (up) and the Hungarian Great Plain (down).

5. Conclusions

For wind energy utilization purposes, the second part of the paper begins with summarizing the wind climate information of the 20th century. Maximum wind speed values occur in the northwestern corner of the country, while minimum centers appear in the southwestern and in the north, northeastern part of the country. Although, these centers do not have annual moving, the analysis of transition seasons show that wind speed values are higher, and the range between the monthly extremes is getting also somewhat higher in April than in October. In spite of different error sources (inhomogeneity of data, changes in

observation techniques and measuring instruments, replacements and changing surroundings of measuring stations, etc.), the last century do not show significant changes or variations in mean regional flows.

Wind profile measurements and data analysis was carried out on Hegyhátsál TV transmitter tower, where multilevel wind speed time series are available from the 1994–2000 period. Selecting the windiest (April) and the least windy (October) months of the year, wind speed frequency distributions was analysed. Case classification was based on truncated tercile values of near surface (10 m) data of April. Using the same terciles for October, leading to an asymmetric distribution of group members (46.9%, 31.8%, and 21.3%, respectively), relative frequencies remain smaller than in April. Larger differences can be observed near the surface that seems to become smaller at higher levels.

Instead of discrete estimations of available wind power, we present horizontal and vertical cross-sections of average wind speed and available wind power isosurfaces around Hegyhátsál (41 km × 41 km) using the WASP model. Three-dimensional maps provide more information, where height of the 180 W m⁻² wind power surface is presented for a 100 km × 100 km area of Trans-Danubia and the Great Hungarian Plain. In order to have a complete overview of available wind power of the entire country, further model simulations are necessary using more detailed digital terrain models and wind data from denser measuring network. In the future this type of maps may support the optimal siting of wind power stations in Hungary.

Acknowledgements—The authors wish to thank the *MOWIE* project (Department of Earth Sciences – Meteorology, Uppsala University, Sweden, JOR3–CT98–0254) for the application of the WASP model. We are very grateful to *Dr. L. Haszpra* (Hungarian Meteorological Service) and *Z. Barcza* (Eötvös University, Department of Meteorology) for the wind profile data from Hegyhátsál, to *Dr. T. Weidinger* (Eötvös University, Department of Meteorology) for the digital terrain model, and to the *Meteorological Service of the Hungarian Defence Forces* for the wind database of Kecskemét and Papa. The technical help provided by *R. Pongrácz* (Eötvös University, Department of Meteorology) has been very constructive and is highly appreciated.

Research leading to this paper has been supported by the *Hungarian National Science Research Foundation* under grants T23811, T26629, T25803, T34867 and T38423, also, by the AEROCARB EU-5 framework project (EVK2-CT-1999-00013).

References

- Bacsó, N., 1959: *Climate of Hungary* (in Hungarian). Akadémiai Kiadó, Budapest.
- Bacsó, N., Kakas, J., and Takács, L., 1953: *Climate of Hungary* (in Hungarian). Orsz. Meteorológiai Intézet Hivatalos Kiadványa, XVII.
- Bartholy, J. and Radics, K., 2000: *Possibilities of Wind Energy Usage in the Carpathian Basin* (in Hungarian). Egyetemi Meteorológiai Füzetek, No. 14. ELTE, Budapest.
- Bartholy, J. and Radics, K., 2001: Selected characteristics of wind climate and the potential use of wind energy in Hungary. Part I. *Időjárás* 105, 109–126.

- Darmstadter, J., Teitelbam, P., and Polach, J., 1971: *Energy in the World Economy*. John Hopkins Press, Baltimore.
- European Commission, 1997: *Energy in Europe, 1997 – Annual Energy Review*. DGXII: Science, Research & Development, Special Issue, p. 179.
- Gipe, P., 1995: *Wind Energy Comes of Age*. John Wiley and Sons, Inc., New York.
- Haszpra, L., Barcza, Z., Bakwin, P. S., Berger, B. W., Davis, K. J., and Weidinger, T., 2001: Measuring system for the long-term monitoring of biosphere/atmosphere exchange of carbon dioxide. *J. Geophys. Res.* 106, No. D3, 3057-3070.
- Kakas, J., (ed.), 1967: *Climate Atlas of Hungary*, II. Volume, *Data Base* (in Hungarian). Akadémiai Kiadó, Budapest.
- Mortensen, N. G., Landberg, L., Troen, I., and Petersen, E. L., 1993: *Wind Atlas Analysis and Application Program*. Risø National Laboratory, Roskilde.
- Pécsi, M. (ed.), 1989: *National Atlas of Hungary*, Kartográfiai Vállalat, Budapest.
- Sørensen, B., 2000: *Renewable Energy*. Academic Press, London.
- Tar, K., 1991: *A Complex Statistical Analysis of the Wind Climatology in Hungary* (in Hungarian). OMSZ Kisebb Kiadványai 67. Orsz. Meteorológiai Szolgálat, Budapest.
- Tar, K., Makra, L., Horváth, Sz., and Kircsi, A., 2001: Temporal change of some statistical characteristics of wind speed over the Great Hungarian Plain. *Theor. Appl. Climatol.* 69, 69-79.
- Troen, I. and Petersen, E. L., 1989: *European Wind Atlas*. Risø National Laboratory, Roskilde.

IDŐJÁRÁS

Quarterly Journal of the Hungarian Meteorological Service
Vol. 106, No. 2, April-June 2002, pp. 75-85

Specification of multivariate extremity in climatological data

Mónika Lakatos¹ and István Matyasovszky²

¹Hungarian Meteorological Service, Climate Research Division,
P.O. Box, 38, H-1525 Budapest, Hungary; E-mail: lakatos.m@met.hu

²Department of Meteorology, Eötvös Loránd University,
P.O. Box 32, H-1518 Budapest, Hungary; E-mail: matya@ludens.elte.hu

(Manuscript received November 23, 2001; in final form March 27, 2002)

Abstract—A methodology is presented to determine extreme regions of multivariate climatological data. The term extreme is defined as events having small probabilities at the tails of an underlying probability density function. The traditional parametric procedure to estimate the density does not guarantee that such a model fits the data satisfactorily in areas representing rare events. Therefore, a nonparametric approach is proposed which does not restrict the possible form of the density. Two examples, namely dangerous apparent temperatures and icing conditions are discussed to illustrate the methodology.

Key-words: extremes, multivariate data, kernel density estimator, apparent temperature, icing

1. Introduction

The term “extremes” can be defined in several ways. These include tools such as the average returning period of an occurrence arising from small probabilities, number of exceedances of high or low thresholds, duration below or above these thresholds, and many other choices. These characteristics are closely related to the probability distribution of maximum or minimum of a variable during a specific period. Theory of extreme distributions based on asymptotic formula is well-developed for univariate data (*Gumbel*, 1958; *Leadbetter* et al., 1983). In multivariate case, similar results are available when maxima or minima are considered in every component of multidimensional variables (*Tawn*, 1990). However, special attention is frequently

dedicated to states of multidimensional variables, which are not necessarily extremes in every or even in one dimension, but these states may be called extremes as vectors, because they drastically deviate from the “usual” state.

Therefore, the term extreme is now defined as events having small probabilities at the tails of an underlying probability density function. Consider a multivariate random variable with probability density function $f(x)$. For any ε satisfying $0 < \varepsilon < 1$ an extreme set $T = T(\varepsilon)$ is defined as

$$T : \{x; f(x) < c\} < \varepsilon, \quad \int_T f(x) dx = \varepsilon, \tag{1}$$

where $c = c(\varepsilon)$ (Fig. 1). When the analytical form of f is known, the solution of problem Eq. (1) is straightforward. The traditional procedure for estimating f is the parametric approach, which consists of equipping a prespecified family of density functions with a finite set of parameters. The task is then to estimate these parameters using a sample of data. However, there is no guarantee that such a model fits the data satisfactorily in areas representing rare events, although customary tests do not reject the model.

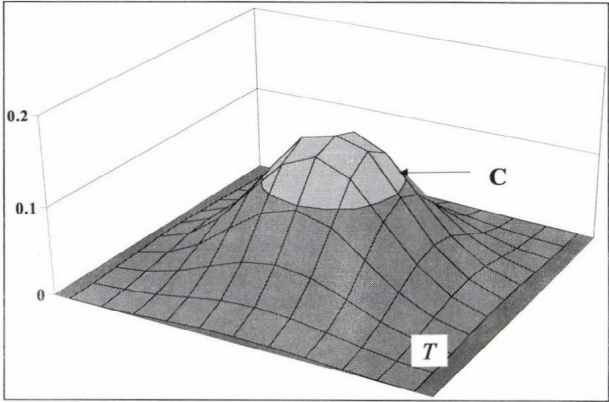


Fig. 1. The extreme set, T , specified by C in two dimensions (see Eq. (1) for explanation).

The present paper proposes another procedure, namely the nonparametric approach to estimate f . The technique does not restrict the possible form of the density function, the estimate is obtained directly from data. In the rest of the paper, Section 2 introduces the methodology to obtain extreme sets with a nonparametric estimator. Two examples for the two-dimensional case are discussed in Section 3.

2. Methodology

2.1 Concept

The idea of nonparametric estimation of univariate probability density functions was introduced by *Rosenblatt* (1956) and *Parzen* (1962). The so-called kernel density estimate $\hat{f}(x)$ from a sample x_1, x_2, \dots, x_n is given by

$$\hat{f}(x) = \frac{1}{nb} \sum_{i=1}^n K\left(\frac{x-x_i}{b}\right), \quad (2)$$

where $K(z)$ is a kernel function satisfying certain properties to provide an appropriate estimate of $f(x)$. An example of appropriate kernel functions is in Eq. (10). Note that Eq. (2) is a sum of elementary densities

$$\frac{1}{nb} K\left(\frac{x-x_i}{b}\right) \quad (3)$$

over sample elements, and the bandwidth b controls how well these elementary densities centre around the observations (*Fig. 2*).

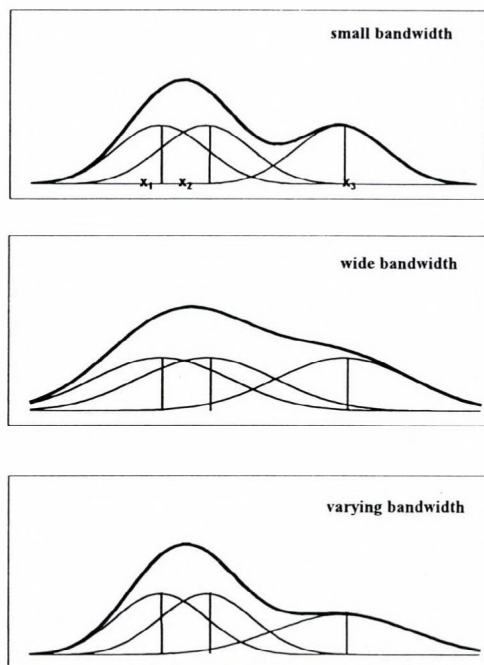


Fig. 2. Role of different bandwidth (b in Eq. (2) and others) choices.

A possibility for choosing the kernel is that $K(z)$ itself is a density function because $K(z)$ is required to integrate to unity. $K(z)$ with support $[-1,1]$ ($K(z)_{[-1,1]}$) is called kernel of order k if the condition

$$\int_{-1}^1 K(z)z^j dz = \begin{cases} 1, & j=0 \\ 0, & 0 < j < k \end{cases} \quad (4)$$

is satisfied.

Under $n \rightarrow \infty; b \rightarrow 0; nb \rightarrow \infty$, Eq. (2) provides an asymptotically unbiased and consistent estimate of $f(x)$ with asymptotic mean square error (MSE)

$$MSE(x) = E\left[(\hat{f}(x) - f(x))^2\right] = u^2(x) + v^2(x), \quad (5)$$

where the asymptotic bias is equal to

$$u(x) = E[\hat{f}(x) - f(x)] = B \frac{h^k}{k!} f^{(k)}(x), \quad (6)$$

and the asymptotic variance is

$$v^2(x) = Var[\hat{f}(x)] = E\left[(\hat{f}(x) - E[\hat{f}(x)])^2\right] = \frac{V}{nb} f(x), \quad (7)$$

while

$$B = \int_{-1}^1 K(z)z^k dz, \quad V = \int_{-1}^1 K^2(z)dz. \quad (8)$$

Symbol E denotes the expectation, and $f^{(k)}(x)$ is the k th derivative which is assumed to be finite. The dependence of the MSE on the density and its k th derivative, the kernel, and the bandwidth is clearly shown by Eqs. (5) to (8). The bias Eq. (6) is higher in areas where $f^{(k)}(x)$ is higher, and the variance Eq. (7) is higher where $f(x)$ is large. The bias term penalizes oversmoothing, and the variance term penalizes undersmoothing. Thus, an optimal bandwidth that recognizes this trade-off must exist. The optimal b minimizing Eq. (5) is

$$b_{opt}(x) = \left(\frac{f(x)V}{(f^{(k)})^2 n B^2} \right)^{1/(2k+1)}, \quad (9)$$

and the convergence rate of $\hat{f}(x)$ to $f(x)$ is proportional to $n^{-2k/(2k+1)}$.

Eq. (9) cannot directly be used in practice because it needs the knowledge of $f(x)$. The bandwidth, therefore, should be estimated from the sample. One could think that the choice of b is not a difficult problem by using the bandwidth which delivers, in some sense, a best fit to the sample available,

while the choice of k and K seems to be quite arbitrary. However, the situation is just the contrary. A class of optimal kernel functions is known, and several simulation and real data studies suggest that a small variability in k does not considerably affect the resulting density. Generally, a small value of k , say $k=2$ can be chosen. In contrast, the bandwidth choice has a great importance.

The selection of kernels is based on asymptotic properties Eqs. (6) and (7). Kernel functions minimizing the asymptotic variance Eq. (7) can be found in Gasser *et al.* (1985). For instance, for $k=2$ and $k=4$, the kernel is $K(z)=1/2_{[-1,1]}$ and $3/8(3-5z^2)_{[-1,1]}$, respectively. One of the most frequently used kernels is

$$K(z) = \frac{3}{4}(1-z^2)_{[-1,1]} \quad (10)$$

having smallest MSE among kernels with $k=2$.

The above functions, however, may be used just in the case when $f(x)$ is defined on the interval $(-\infty, \infty)$, unless the kernels are modified near the endpoints. Müller (1991) has developed a very general formulation to have kernels for any $x \in (m, M)$ and M for any k , where (m, M) denotes the support of $f(x)$. Let $K_+(q, z)$ and $K_-(q, z)$ be functions with support $[0, 1] \times [-1, q]$ and $[0, 1] \times [-q, 1]$, respectively and with some smoothing requirements (Müller, 1991). Then, kernels at a point x are given by

$$K_x = \begin{cases} K_+(1, z), & m+b \leq x \leq M-b \\ K_+((x-m)/b, z), & 0 \leq x < m+b \\ K_-((M-x)/b, z), & M-b < x \leq M \end{cases}, \quad (11)$$

where $K_-(q, x) = K_+(q, -x)$. Eqs. (6) and (7) to calculate asymptotic bias and variance are essentially held, but now B and V depend on q . The boundary kernel Eq. (11) corresponding to Eq. (10) is

$$K_+(q, z) = 6(1+z)(q-z) \frac{1}{(1+q)^3} \left[1 + 5 \left(\frac{1-q}{1+q} \right)^2 + 10 \frac{1-q}{(1+q)^2} z \right]. \quad (12)$$

A natural choice of the bandwidth is to minimize the integrated mean square error

$$\int_m^M (\hat{f}(x) - f(x))^2 dx, \quad (13)$$

which is estimated by the so-called least square cross-validation (LSCV)

$$1/n \sum_{i=1}^n \hat{f}^2(x_i) - 2/n \sum_{i=1}^n \hat{f}_i(x_i), \quad (14)$$

where $\hat{f}_i(x_i)$ is a cross-validated estimate, i.e., an estimate Eq. (2) but with x_i omitted.

The methodology outlined above has serious limitations. Specifically, \hat{b} obtained with the minimization of Eq. (14) is selected globally while Eq. (9) clearly shows the necessity of locally varying bandwidths. The use of local bandwidth $b(x)$ is, however, not practical because the resulting curve does not necessarily integrate to unity. Additionally, the estimated density function may behave poorly at tail areas of the real density, which is crucial when just extremes are in question. In order to remove these difficulties, Eq. (2) is modified according to *Abramson (1982)* as

$$\hat{f}(x) = \frac{1}{nh} \sum_{i=1}^n f(x_i)^{1/2} K\left(\frac{x-x_i}{h} f(x_i)^{1/2}\right). \quad (15)$$

The usefulness of local bandwidths $b(x_i) = hf(x_i)^{-q}$, $q > 0$ obvious, because many sample elements are available where the density function is large, but few observations come from flat regions of the underlying density (see Fig. 2). Such a choice therefore, makes the importance of sample elements more uniform. The exponent $q=1/2$ is optimal in the sense that it eliminates the asymptotic bias of the estimate. The unknown values $f(x_i)$ in Eq. (15) are substituted by their initial estimates $\check{f}(x_i)$ obtained with a global bandwidth. The parameter h is chosen as to minimize

$$1/n \sum_{i=1}^n \hat{f}^2(x_i) - 2/n \sum_{i=1}^n \hat{f}(x_i), \quad (16)$$

where \hat{f} corresponds to Eq. (15) with cross-validated $\check{f}_i(x_i)$ initial estimates.

2.2 Estimation of multivariate densities

Taking a sample $\mathbf{x}_1, \mathbf{x}_2, \dots, \mathbf{x}_n$ for a p -dimensional random vector, the Parzen-Rosenblatt estimator is given by

$$\hat{f}(\mathbf{x}) = \frac{1}{n|\mathbf{B}|} \sum_{i=1}^n K_p(\mathbf{B}^{-1}(\mathbf{x} - \mathbf{x}_i)), \quad (17)$$

where \mathbf{B} represents the bandwidth matrix and $|\mathbf{B}|$ denotes its determinant. The p -dimensional kernel function defined on $S = [-1, 1]^p = [-1, 1] \times [-1, 1] \times \dots \times [-1, 1]$ satisfies

$$\int_S z_1^{j_1} \dots z_p^{j_p} K_p(\mathbf{z}) d\mathbf{z} = \begin{cases} 1, & \sum_{i=1}^p j_i = 0 \\ 0, & 0 < \sum_{i=1}^p j_i < k \end{cases} \quad (18)$$

for every $j_1, j_2, \dots, j_n \geq 0$. A simple choice to specify the estimator is to use products of one-dimensional kernels with the same bandwidth in every dimension resulting in the same amount of smoothing in different directions of coordinates. This choice is not favorable when the variance of the components differs substantially. Therefore, a much more reliable estimate can be obtained by different bandwidths for different directions as

$$\hat{f}(\mathbf{x}) = \frac{1}{nb^p} \sum_{i=1}^n \left[\prod_{j=1}^p \frac{1}{\sigma_j} K\left(\frac{\mathbf{x}_j - \mathbf{x}_{ij}}{b\sigma_j}\right) \right], \quad (19)$$

where j refers to j th component of the vector and σ denotes standard deviation.

The Abramson estimator Eq. (15) in multivariate case becomes

$$\hat{f}(\mathbf{x}) = \frac{1}{nh} \sum_{i=1}^n f(\mathbf{x}_i)^{p/2} K_p\left(\frac{(\mathbf{x} - \mathbf{x}_i)f(\mathbf{x}_i)^{1/2}}{h}\right). \quad (20)$$

Comparing Eqs. (19) and (20), the final form will be

$$\hat{f}(\mathbf{x}) = \frac{1}{nh^p} \sum_{i=1}^n f(\mathbf{x}_i)^{p/2} \left[\prod_{j=1}^p \frac{1}{\sigma_j} K\left(\frac{\mathbf{x}_j - \mathbf{x}_{ij}}{h\sigma_j} f(\mathbf{x}_i)^{1/2}\right) \right]. \quad (21)$$

3. Examples

Daily temperature and relative humidity data observed in Budapest, Hungary, 12 UTC from 1961 to 1990 have been analysed in January and July. The aim is to quantify the probability of extreme warm and dry or extreme cold and wet conditions.

The Abramson density estimator Eq. (21) has been used for this purpose. Since the relative humidity is close to but never larger than 100%, the boundary kernel Eq. (12) has been used at the right boundary. First an initial estimate Eq. (2) was produced with $b=0.58$ for summer and with $b=0.63$ for winter. These global bandwidths were chosen by minimizing Eq. (14) (see Fig. 3). Substituting these initial estimates into Eq. (16), the optimal h is 0.046 for summer and 0.059 for winter.

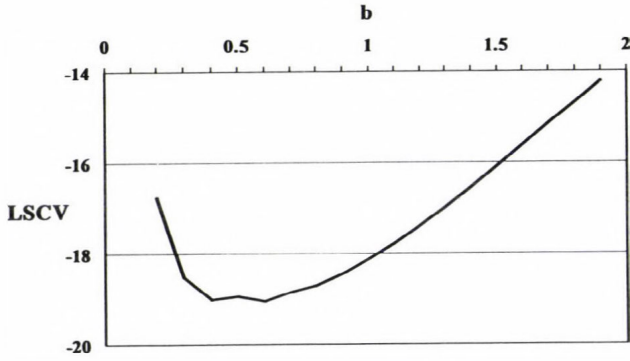


Fig. 3. Quantity of least square cross-validation (LSCV) in case of temperature and relative humidity for July.

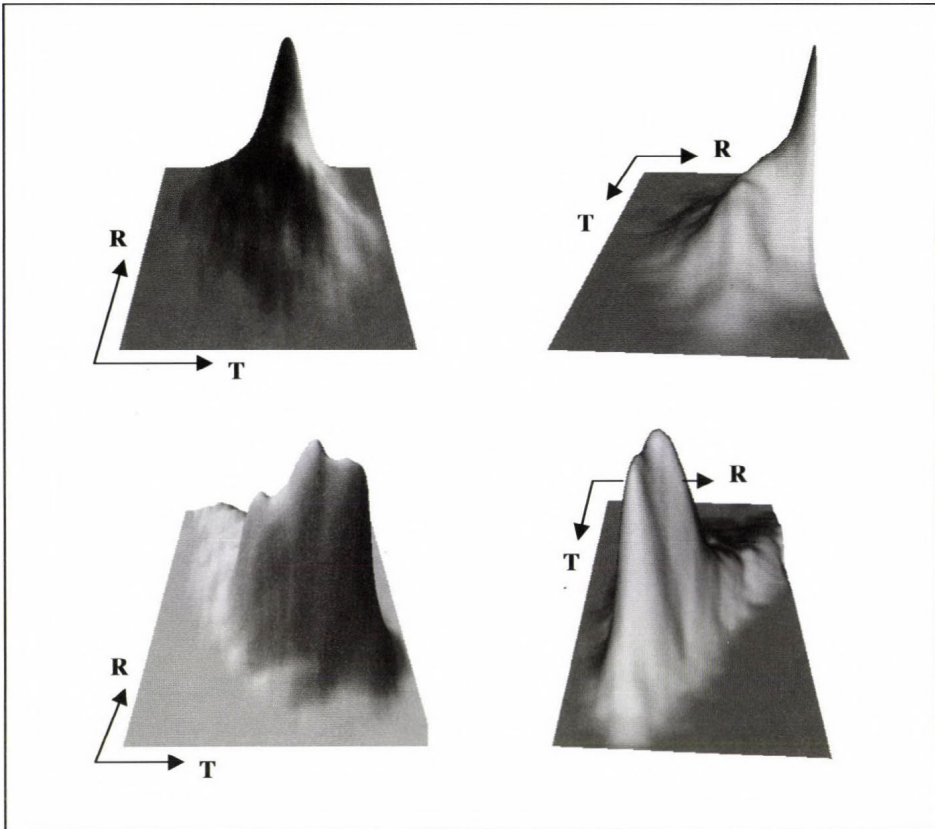


Fig. 4. Two dimensional probability density function of temperature ($T [^{\circ}\text{C}]$) and relative humidity ($R [\%]$) for winter (top) and summer (bottom), as seen from two orthogonal view-points.

Fig. 4 shows the estimated densities from two directions. In summer, the density has a fine structure with a wide maximum area scattered by three local peaks. The main maximum (25.7°C, 45%) does not correspond to average conditions since the means calculated from data are 24.6°C and 49% for temperature and relative humidity, respectively. The difference between the maximum and mean is due to the asymmetry of the density. One of the local peaks is related to cooler and wetter (frequently rainy) days, while the second local peak reflects hot and dry conditions associated with air masses from Sahara. Also, the density has a long tail toward low temperatures and high relative humidities meaning a considerably larger chance for cool and wet conditions than for warm and dry situations. The air is frequently almost saturated in winter. Therefore large values of the density are located at 100% along the temperature axis. The peak is located at (0.15°C, 100%), while the means calculated from data are 0°C and 77% suggesting a substantial asymmetry of the probability distribution of relative humidity.

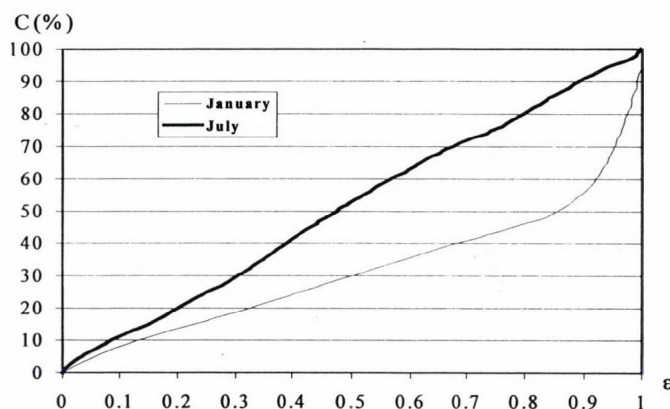


Fig. 5. The relationship between c and ε .

In order to obtain extreme sets $T(\varepsilon)$, the relationship $c=c(\varepsilon)$ has to be established. It can be done by a numerical approximation to the integral in Eq. (1). Cutting the surface of the density function with a horizontal plain at different percentage of the maximum c_{max} of the density, the volume under the dark surface in Fig. 1 gives the probability ε . Correspondence between ε and c/c_{max} is shown in Fig. 5. The curve for January has a larger slope indicating that the density is less concentrated than in summer.

Under normal conditions, temperature and humidity are the most important elements influencing comfort. A special index based on human

physiology was developed to measure of what hot weather feels “like” to the average person. The degree of heat stress may vary with age, health and body characteristics. This index is determined by the actual air temperature and relative humidity, and is called apparent temperature (Quayle and Doehring, 1981). Counterparts of areas surrounded by curves in Fig. 6 define the domains $T(\varepsilon)$ for different probabilities ε . The relationship of air temperature and relative humidity to apparent temperature is also shown here according to four danger categories. The probability of having critical temperature and humidity can be calculated by integrating the density function over the area where corresponding apparent temperatures exceed the critical value of an actual danger category. For instance, if the apparent temperature exceeds 26.6°C (80°F), fatigue is possible with prolonged exposure and physical activity. Under the climate of Budapest, the probability of such an event is 0.249. The probability of events with apparent temperatures exceeding 32.3°C (90°F) is quite small, namely 0.027 in our region. The remaining danger categories when apparent temperature is higher than 40.5°C (105°F) and 54.4°C (105°F) have negligible probabilities.

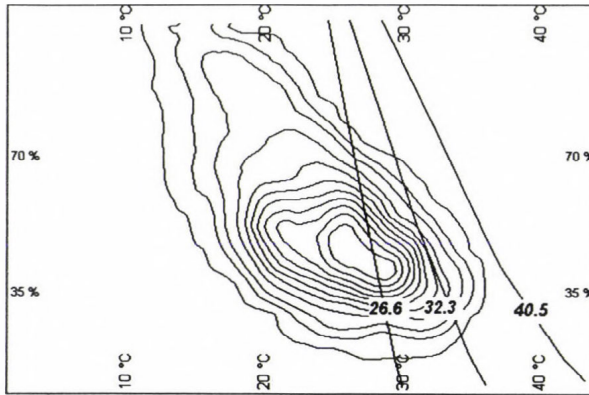


Fig. 6. The heat stress categories defined by the apparent temperatures on probability density function of temperature and relative humidity for July.

There is a chance for icing when the air is close to the saturation and the actual temperature is below zero (Mika et al., 1995). This area is approximately represented by rectangles according to 90% and 95% relative humidities (Fig. 7). Relative frequency of such cases calculated directly from data is 0.126 and 0.062, while integration of the density in Fig. 7 gives 0.146 and 0.076.

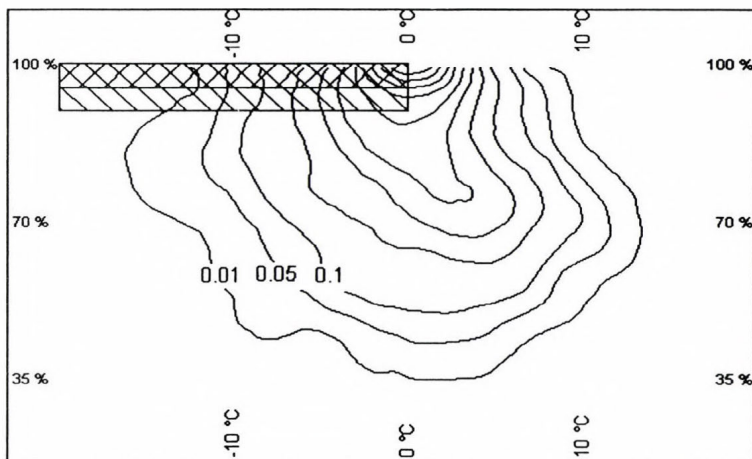


Fig. 7. Conditions preferable for ice formation on probability density function of temperature and relative humidity for January.

Acknowledgements—Research leading to this paper has been supported by KFI 027700-02/2000, grant from Hungarian Science Foundation OTKA T025803, and Bolyai János scholarship of Hungarian Academy of Sciences.

References

- Abramson, I.S., 1982: On bandwidth variation in kernel estimates - a square root law. *Ann. Statist.* 10, 1217-1223.
- Gumbel, E.J., 1958: *Statistics of Extremes*. Columbia Univ. Press, New York.
- Leadbetter, M.R., Lindgren, G., and Rootzen, H., 1983: *Extremes and Related Properties of Random Sequences and Processes*. Springer-Verlag, New York.
- Mika, J., Szentimrey, T., Csomor, M., Kövér, Z., Nemes, C., and Domonkos, P., 1995: Correlation of ice load with large-scale and local meteorological conditions in Hungary. *Atmospheric Research*, 36, 261-276.
- Parzen, E., 1962: On the estimation of probability density function and mode. *Ann. Math. Statist.* 33, 1065-1076.
- Rosenblatt, M., 1956: On some nonparametric estimates of a density function. *Ann. Math. Statist.* 27, 832-837.
- Tawn, J.A., 1990: Modelling multivariate extreme value distributions. *Biometrika* 77, 245-253.
- Quayle, R. and Doehring, F., 1983: Heat stress. *Weatherwise* 64, 120-124.

NEWS

Dr. Iván Mersich winner of a 2001. Dennis Gabor Prize

This highly distinctive prize was established by the NOVOFER Foundation for recognizing outstanding achievements in the field of science and technology. It is given every year to a small number of carefully selected individuals. In the last year one of the seven winners of the prize was *Dr. Iván Mersich*, President of the Hungarian Meteorological Service. The distinction was conferred on him on the 10th of December, 2001 at a solemn ceremony in the presence of many of his friends and colleagues.

The eponym of the prize does not need much introduction. Dennis Gabor—winner of the 1951. Nobel Prize in physics—and been one of the outstanding scientists and innovators of Hungarian origine who substantially contributed to the creation of modern technology. The prize carrying his name was established in 1989. Since that time it was bestowed upon altogether 87 Hungarians and 6 individuals from abroad.

Dr. Iván Mersich is the head of the Hungarian Meteorological Service since the beginning of 1991. Consequently, his term included a particularly difficult period of transition. Under the preceding socialist (planned economy) regime the Meteorological Service had to be—necessarily—a rather inflated autarchic organization quite similar to all other institutions of the Soviet Bloc. From that state this organization had to be radically transformed to become a much leaner, yet more efficient, high-tech service which fits into the array of modern European national meteorological services. Today we may confidently say that the target is achieved and that Dr. Mersich definitely deserves credit for this achievement. The prize was given to him in recognition of his creative, innovative approach to his job and also in appreciation of his untiring drive to get things done.

The Hungarian meteorological community is deeply honoured by the fact that among the excellent individuals, selected from the broadest range of professions, now there is a meteorologist, who deserved this prize and the distinction that goes with it.

R. Czelnai

GUIDE FOR AUTHORS OF *IDŐJÁRÁS*

The purpose of the journal is to publish papers in any field of meteorology and atmosphere related scientific areas. These may be

- research papers on new results of scientific investigations,
- critical review articles summarizing the current state of art of a certain topic,
- short contributions dealing with a particular question.

Some issues contain "News" and "Book review", therefore, such contributions are also welcome. The papers must be in American English and should be checked by a native speaker if necessary.

Authors are requested to send their manuscripts to

Editor-in Chief of IDŐJÁRÁS

P.O. Box 39, H-1675 Budapest, Hungary

in three identical printed copies including all illustrations. Papers will then be reviewed normally by two independent referees, who remain unidentified for the author(s). The Editor-in-Chief will inform the author(s) whether or not the paper is acceptable for publication, and what modifications, if any, are necessary.

Please, follow the order given below when typing manuscripts.

Title part: should consist of the title, the name(s) of the author(s), their affiliation(s) including full postal and E-mail address(es). In case of more than one author, the corresponding author must be identified.

Abstract: should contain the purpose, the applied data and methods as well as the basic conclusion(s) of the paper.

Key-words: must be included (from 5 to 10) to help to classify the topic.

Text: has to be typed in double spacing with wide margins on one side of an A4 size white paper. Use of S.I. units are expected, and the use of negative exponent is preferred to fractional sign. Mathematical formulae are expected to be as simple as possible and numbered in parentheses at the right margin.

All publications cited in the text should be presented in a *list of references*,

arranged in alphabetical order. For an article: name(s) of author(s) in Italics, year, title of article, name of journal, volume, number (the latter two in Italics) and pages. E.g., *Nathan, K.K.*, 1986: A note on the relationship between photo-synthetically active radiation and cloud amount. *Időjárás* 90, 10-13. For a book: name(s) of author(s), year, title of the book (all in Italics except the year), publisher and place of publication. E.g., *Junge, C. E.*, 1963: *Air Chemistry and Radioactivity*. Academic Press, New York and London. Reference in the text should contain the name(s) of the author(s) in Italics and year of publication. E.g., in the case of one author: *Miller* (1989); in the case of two authors: *Gamov and Cleveland* (1973); and if there are more than two authors: *Smith et al.* (1990). If the name of the author cannot be fitted into the text: (*Miller*, 1989); etc. When referring papers published in the same year by the same author, letters a, b, c, etc. should follow the year of publication.

Tables should be marked by Arabic numbers and printed in separate sheets with their numbers and legends given below them. Avoid too lengthy or complicated tables, or tables duplicating results given in other form in the manuscript (e.g., graphs)

Figures should also be marked with Arabic numbers and printed in black and white in camera-ready form in separate sheets with their numbers and captions given below them. Good quality laser printings are preferred.

The text should be submitted both in manuscript and in electronic form, the latter on diskette or in E-mail. Use standard 3.5" MS-DOS formatted diskette or CD for this purpose. MS Word format is preferred.

Reprints: authors receive 30 reprints free of charge. Additional reprints may be ordered at the authors' expense when sending back the proofs to the Editorial Office.

More information for authors is available: antal.e@met.hu

Information on the last issues: http://omsz.met.hu/irodalom/firat_ido/ido_hu.html

Published by the Hungarian Meteorological Service

Budapest, Hungary

INDEX: 26 361

HU ISSN 0324-6329

IDŐJÁRÁS

QUARTERLY JOURNAL
OF THE HUNGARIAN METEOROLOGICAL SERVICE

CONTENTS

- | | | | |
|--|-----|--|-----|
| Editorial | I | <i>I. Orlóci and K. Szesztay:</i> Hydroecological risks of crop production in Hungary .. | 185 |
| Dr. Emánuel Antal's scientific career | II | <i>I. Zima Szalókiné and S. Szalóki:</i> Relationships of water- and nutrient supply, yield and evapotranspiration of maize .. | 197 |
| <i>Z. Varga-Haszonits:</i> Water supply of growing seasons and maize production ... | 89 | <i>Ö. Starosolszky:</i> Impact of the climate change on the hydrological regime. A case study on the Danube River .. | 215 |
| <i>E. Mészáros:</i> Atmospheric wet deposition as a nutrient supply for the vegetation | 103 | <i>B. Nováky:</i> Mapping of mean annual actual evaporation on the example of Zagyva catchment area..... | 227 |
| <i>Gy. Várallyay:</i> Climate change and soil processes | 113 | <i>L. Vermes:</i> International efforts for drought mitigation | 239 |
| <i>M. Hunkár:</i> Agrometeorology of maize – investigation carried out at the Hungarian Meteorological Service .. | 123 | <i>J. Justyák and K. Tar:</i> Characteristics of the economy of water supplies in an oak forest | 248 |
| <i>A. Anda:</i> Slices of plant–water relation in reflection to investigations carried out at Agrometeorological Research Station of Keszthely | 137 | <i>I. Pálfi:</i> Probability of drought occurrence in Hungary..... | 265 |
| <i>G. Szász:</i> Surface energy budget between the atmosphere and the surface in the vegetation period during 1963–1994.. | 161 | <i>F. Ács:</i> On the relationship between transpiration and soil texture | 277 |

http://omsz.met.hu/irodalom/firat_ido/ido_hu.html

IDŐJÁRÁS

Quarterly Journal of the Hungarian Meteorological Service

Editor-in-Chief

TAMÁS PRÁGER

Executive Editor

MARGIT ANTAL

EDITORIAL BOARD

- | | |
|---|---|
| AMBRÓZY, P. (Budapest, Hungary) | MÉSZÁROS, E. (Veszprém, Hungary) |
| ANTAL, E. (Budapest, Hungary) | MIKA, J. (Budapest, Hungary) |
| BARTHOLY, J. (Budapest, Hungary) | MARACCHI, G. (Firenze, Italy) |
| BOZÓ, L. (Budapest, Hungary) | MERSICH, I. (Budapest, Hungary) |
| BRIMBLECOMBE, P. (Norwich, U.K.) | MÖLLER, D. (Berlin, Germany) |
| CZELNAI, R. (Budapest, Hungary) | NEUWIRTH, F. (Vienna, Austria) |
| DÉVÉNYI, D. (Budapest, Hungary) | PINTO, J. (R. Triangle Park, NC, U.S.A) |
| DUNKEL, Z. (Brussels, Belgium) | PROBÁLD, F. (Budapest, Hungary) |
| FISHER, B. (London, U.K.) | RENOUX, A. (Paris-Créteil, France) |
| GELEYN, J.-Fr. (Toulouse, France) | ROCHARD, G. (Lannion, France) |
| GERESDI, I. (Pécs, Hungary) | S. BURÁNSZKY, M. (Budapest, Hungary) |
| GÖTZ, G. (Budapest, Hungary) | SPÄNKUCH, D. (Potsdam, Germany) |
| HANTEL, M. (Vienna, Austria) | STAROSOLSZKY, Ö. (Budapest, Hungary) |
| HASZPRA, L. (Budapest, Hungary) | SZALAI, S. (Budapest, Hungary) |
| HORÁNYI, A. (Budapest, Hungary) | SZEPESI, D. (Budapest, Hungary) |
| HORVÁTH, Á. (Siófok, Hungary) | TAR, K. (Debrecen, Hungary) |
| IVÁNYI, Z. (Budapest, Hungary) | TÁNCZER, T. (Budapest, Hungary) |
| KONDRATYEV, K.Ya. (St. Petersburg,
Russia) | VALI, G. (Laramie, WY, U.S.A.) |
| MAJOR, G. (Budapest, Hungary) | VARGA-HASZONITS, Z. (Moson-
magyaróvár, Hungary) |

*Editorial Office: P.O. Box 39, H-1675 Budapest, Hungary or
Gillice tér 39, H-1181 Budapest, Hungary
E-mail: prager.t@met.hu or antal.e@met.hu
Fax: (36-1) 346-4809*

Subscription by

*mail: IDŐJÁRÁS, P.O. Box 39, H-1675 Budapest, Hungary
E-mail: prager.t@met.hu or antal.e@met.hu; Fax: (36-1) 346-4809*



Dr. Emánuel Antal is 70

Dr. Emánuel Antal recently celebrated his 70th birthday. We wish to celebrate his anniversary with a volume containing articles written by his friends, colleagues. I feel this way of salutation is extremely appropriate in his case, because he was in all his life, and even now continues to be, a man who concentrates his work at building a bridge between meteorology and other sciences. He strongly believes that common, interdisciplinary efforts with well-defined practical aims will give meteorology greater recognition by the state and society. His outstanding scientific and official career is a living example of the successful realization of his ideas. He achieved great scientific and practical results not only in meteorology and climatology, but also in agricultural science, soil science, and hydrology working together with excellent representatives of these sciences. One cannot forget to mention, that his successes were highly recognized by the state through the State Prize and the Schenzl Guidó Prize, and he was a highest-ranking leader of the Hungarian Meteorological Service for a decade.

In the name of the Editorial Board, authors of this issue, and – feeling obliged to do so – the scientific communities of partner disciplines, I would like to send Dr. Emánuel Antal our greetings and wish him continuing successes in his scientific work and personal life.

Dr. Emánuel Antal's scientific career

Dr. Emánuel Antal was born in Jászárokszállás, in 1931. He finished his studies in meteorology at the Eötvös Loránd University of Budapest in 1955, and received his diploma with distinction. Immediately after that, Dr. Antal started to work at the Hungarian Meteorological Institute (which is now the Hungarian Meteorological Service). His scientific interest turned to the problems of micro-meteorology (radiation-, heat-, and water-fluxes in the near-to-the-surface layer of the atmosphere, heat and moisture balance of the surface and the vegetation, plants, etc.) and agrometeorology. He defended his university doctor's thesis very early, in 1960. Just after that, at the age of 31, he was promoted to serve as the Head of Department of Agrometeorological Research. At that time he started his scientific organizational work, which resulted in the re-thinking and re-establishment of Hungarian agrometeorology in the whole or, maybe, the establishment of the applied agrometeorology, as a new interdisciplinary field between agriculture and meteorology. It is impossible to give the whole scope of his extremely significant scientific career in the frame of such a short summary. As examples of the most important milestones of his career, Dr. Antal:

- *successfully defended his CSc thesis in 1968 in the field of agrometeorology, which contained outstanding scientific results, among them the so-called "Antal-formula" for estimation of potential and actual evapotranspiration. In this way, he became one of the rare scientists, who fixed their names in the science of meteorology;*
- *founded the Szarvas Agrometeorological Station in 1963 and the Observatory in 1974, with the aim to investigate the radiation, heat, and moisture exchange in the earth-plant-atmosphere system, and the demand and consumptive use of water by plants;*
- *initiated field research work from 1968 in the Lake Fertő area to explore the heat and water balance of this area rich in natural beauties but, also, extremely vulnerable region;*
- *organized and led, from 1977, the important national agricultural program with the aim to establish a complex decision-making system of growing vegetables the optimum way for the canning industry. For this work he was honoured by the National Prize;*
- *organized and led, from 1987, a common American-Hungarian project to investigate extreme climatic events, such as droughts, etc., which have great and adverse impact on national economy;*
- *served as the meteorological advisor of the Minister of Environment and Regional Policy in the years 1992–1994;*
- *prepared (with a co-author) the booklet "Role of Climate and Climate Change in the Life of Hungary" in 1996, which represented the Hungarian point of view at the Second World Conference on Climate;*
- *served as the elected member of the General Assembly of the Hungarian Academy of Sciences between 1995 and 2001.*

Meanwhile – in his official career – he was promoted to serve as Assistant Director of the Central Institute for Atmospheric Physics (1978), then Vice-President of the Hungarian Meteorological Service (1981), finally President in Charge (1990). He retired from this position in 1991. As the above list of his activities shows, this retirement was only formal, he acts in the same wide range and with the same energy to the present day. At this time he is the highly esteemed chairman or member of several scientific societies in meteorology, agriculture, and hydrology, intensively participates in university education at the Szent István University (Hungary), and follows his extremely fruitful activity in writing and editing scientific books and other publications. He has written more than 100 scientific publications.

IDŐJÁRÁS

Quarterly Journal of the Hungarian Meteorological Service
Vol. 106, No. 3–4, July–December 2002, pp. 89–101

Water supply of growing seasons and maize production

Zoltán Varga-Haszonits

University of West-Hungary, Faculty of Agricultural and Food Sciences
Vár 2, H-9200 Mosonmagyaróvár, Hungary
E-mail: vargahz@mtk.nyme.hu

(Manuscript received March 5, 2002; in final form July 26, 2002)

Abstract—Water is one of the most important factors of plant breeding. The rain water falling from the clouds is stored in the soil. This water is available for the plants. The most significant factor that can reduce the water content of the soil is the evaporation. The water income and the water loss determine the water balance of the soil which shows the quantity of water available for plants.

In agroclimatology, therefore, there is a need to find out a climatic characteristic for representing the water balance of the soil. Such characteristics are aridity indices (ARI) and humidity indices (HI), which can be calculated in a simple way, and they have a clear physical meaning.

These agroclimatic indices may be used for describing the wet or dry character of the years and the vegetation periods. Finally, rather close relationships can be found between the aridity indices and the yield of maize.

The investigations were carried out on the basis of meteorological and yield data collected parallel during the period of 1951–1995.

Key-words: agroclimatology, evaporation, water balance, aridity index, yield, trend function, trend ratio, regression analysis.

1. Introduction

Water is one of the major growing factors for plants. It is necessary for photosynthetic process because plants demand water besides carbon dioxide to produce organic matter. It is also an important element of transport processes since nutrients come to the assimilating organs dissolved in water.

Plants take up water from the soil where it fills the pores together with air. The ratio of the water and air in the pores exert a strong influence on the life of plants. If there is abundance of water, plants suffer the shortage of air since the oxygen is necessary for respiration. If there is a water shortage in the

pores, plants cannot photosynthesize in a normal way because the transpiration process is not able to transport required quantity of water to the organs of assimilation. It is a general demand for plants, therefore, to have certain amount of water in the soil for photosynthesis and a sufficient quantity of air in pores for respiration.

To enable plants to take up water from soil, there is a need for sufficient water in soil pores, a temperature above threshold value that makes possible to take up water by the cells of roots, and continuous transpiration process which is able to transport the water from the soil to plant leaves where the assimilation takes place. Finally, the water not used up by plants goes away to the atmosphere through the stomata.

These phenomena and processes are strongly affected by meteorological factors.

2. Meteorological conditions and the water supply

The water necessary for plants is stored in the soil. The amount of water between field capacity and wilting point is available for plants, and this quantity mainly depends on the precipitation and evaporation. The former is the main source of water income and the latter is the most significant factor of water loss. These are the two meteorological factors by which the atmosphere can control the water amount available for plants.

Other important factors influencing the water content of the soil and the water supply of plants are illustrated in *Fig. 1*. The amount of water in soil is primarily effected by macrometeorological conditions. It is possible that humid air masses arrive at a given place where clouds are forming and significant rain water income occurs. In another case high atmospheric pressure with descending air movements hinders formation of clouds resulting in a clear weather and strong insolation, increasing the water quantity evaporating from the soil.

When the amount of rain water is abundant, the water accumulates in the upper layers of the soil. If the amount of rain water is continuously increasing, the soil fills up slowly with water and finally the water appears on the soil surface. In this case the plants suffer the air shortage.

The first step towards the formation of water shortage is the lack of rain. If this phenomenon is long-lasting accompanied by low air humidity and high temperature, the evaporation from the surface increases gradually.

The soil cultivation can also exert an influence on the water content of the soil.

Finally, the water in the soil has different significance for various plants since their water demand strongly differs (*Varga-Haszonits, 1983*).

In agroclimatology, therefore, there is a need to find out a climatic characteristic for representing the water balance of soil.

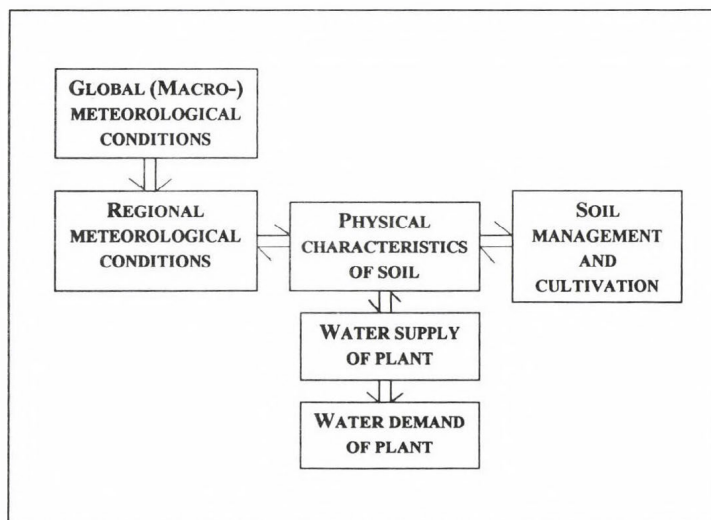


Fig. 1. Factors influencing water demand of plant.

2.1 Agroclimatic index of relative water balance

For characterizing the water balance of a time period at a place, it is practical to use rainfall amount (representing the water income), and the amount of evaporation (representing the water loss) for forming a ratio of two values, which expresses the relative water balance. Using these data we can calculate the relative water balance in the following way (Varga-Haszonits et al., 1996):

$$HI = \frac{P}{E_0} \quad (1)$$

or

$$ARI = \frac{E_0}{P}, \quad (2)$$

where HI is the humidity index, ARI is the aridity index, both are dimensionless, P is the rainfall amount in mm, and E_0 is the evaporative power of air in mm.

The evaporative power of air (E_0) is the amount of water (in mm) evaporated from free water surface, measured by pan „A”. This is a generally used equipment at the meteorological stations. At places, where no evaporation measurements have been made by pan „A”, the evaporative power of air can be determined by using different local formulas developed for the given area (Dunay *et al.*, 1968). Essentially, the evaporative power of air is equal to the potential evaporation.

In Hungary water shortages occur more frequently than water surpluses, therefore, we use the aridity indices for analyzing the humidity conditions of growing seasons. The aridity indices show that how much more water could be evaporated by air than the actual amount of the rainfall in the same period.

2.2 Dry and wet periods of year

Examining the year from the point of view of water balance, we can divide it into two parts. One of these parts is the dry period when the water loss exceeds the water income. The other period is the wet one when the amount of rainfall during the period is higher than the water loss in the same interval. Consequently, the threshold value for separating dry and wet periods is 1, since this shows an equilibrium between water income and water loss. By using this climatic separator value (ARI=1), we can differentiate the periods of different humidity conditions (Varga-Haszonits *et al.*, 1997).

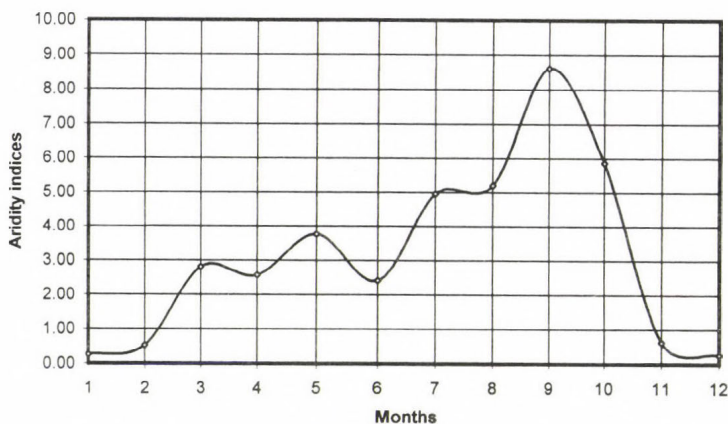


Fig. 2. Annual course of aridity index in Hungary (1951–1955).

The line of annual course of monthly aridity indices intersects the line of aridity index value 1 in February and November (Fig. 2). Between February

and November the values of ARI are higher than 1, so this period is designated as a dry one. While the period from November to February, when ARI falls short of 1, is called wet period.

Looking at Fig. 2 we can see that an increasing dryness becomes dominant in spring finding a moderate decline in June, then the values of ARI begin to grow again to the peak of the curve in September. After the peak the values of aridity indices (ARI) decreases deeply as far as November in which time our country has a secondary maximum of precipitation. As we mentioned earlier, the wet period begins in November and lasts to the end of February.

2.3 Humidity conditions of growing season

Knowledge of meteorological conditions during the growing season is of basic importance for plant breeding (Varga-Haszonits, 1998). Table 1 contains the statistical characteristics and frequency values of ARI during the vegetation periods of years under investigation. The wettest part of the country is the southwestern area (Vas, Zala, Somogy counties) of Transdanubia, where the mean values of ARI fall short of 2. The driest area can be found in central part of the country, in the counties of Pest, Bács-Kiskun, Jász-Nagykun-Szolnok and Csongrád. In this area the average values of ARI vary between 2.75 and 3.10.

Table 1. Distribution of aridity indices in Hungarian counties during the growing season of maize 1951–1995

County	Min.	Aver.	Max.	>1.00	1.01-1.50	1.51-2.00	2.01-2.50	2.51-3.00	3.01-3.50	3.51-4.00	4.01-4.50	>4.00
Győr-Moson-Sopron	1.35	2.43	4.16	3	12	11	9	7	2	1	0	0
Vas	0.74	1.68	3.62	20	18	3	3	0	1	0	0	0
Zala	0.80	1.53	3.34	27	12	3	1	2	0	0	0	0
Somogy	0.92	1.73	3.24	19	14	7	4	1	0	0	0	0
Veszprém	0.93	2.00	3.98	13	12	12	3	2	3	0	0	0
Komárom-Esztergom	0.99	2.21	3.94	6	16	8	8	4	3	0	0	0
Fejér	1.25	2.67	5.68	1	9	14	8	7	2	1	3	3
Tolna	0.99	2.09	4.02	9	14	12	5	2	2	1	0	0
Baranya	1.04	2.28	3.82	7	12	9	9	6	2	0	0	0
Bács-Kiskun	1.32	2.95	6.21	2	8	7	10	8	3	2	5	5
Pest	1.45	3.07	6.42	1	5	8	13	10	0	2	6	6
Jász-Nagykun-Szolnok	1.22	2.78	6.29	2	8	10	10	9	1	2	3	3
Csongrád	1.30	2.86	5.65	3	7	11	8	5	2	4	5	5
Békés	1.35	2.51	4.57	4	7	18	6	5	1	3	1	1
Hajdú-Bihar	0.85	2.44	5.19	8	5	14	8	6	0	1	3	3
Szabolcs-Szatmár-Bereg	1.05	2.45	4.81	5	10	13	5	6	3	1	2	2
Borsod-Abaúj-Zemplén	0.99	2.10	4.66	11	15	8	4	3	2	1	1	1
Heves	1.38	2.70	6.17	4	10	7	10	6	4	1	3	3
Nógrád	0.94	2.21	4.21	6	17	9	5	4	3	1	0	0

The ARI values having a minimum less than 1 are characteristic mainly for the western and northern counties. The growing seasons with ARI under the value 1 can be considered as the wettest ones in our country. This type of vegetation periods, however, does not occur in the middle of the country.

The maximum values of ARI are over 3 in the southwest area, while they vary between 5.5 and 6.5 in the middle of the country.

The frequency values also follow this spatial distribution. Values less than 1.5 are most frequent in the southwestern part of the country. Values between 2.01–2.50 are characteristic for the middle part of the country. Very dry growing seasons occur also in this area.

The humidity conditions of vegetation periods are especially important for the plants sensitive to water supply. It is well known that humidity is one of the most variable meteorological factor which has a significant influence on the yield formation and plays an important role in fluctuations of actual yield from year to year.

The fluctuations of the ARI in successive years are illustrated in *Fig. 3*. The values of ARI during the growing seasons of maize (the ratio of evaporative power of air to rainfall in the time spell from April to September) vary generally between 1.50 and 3.00, that is, the air would be able to evaporate 1.5–3 times more water amount than the actual precipitation in this period.

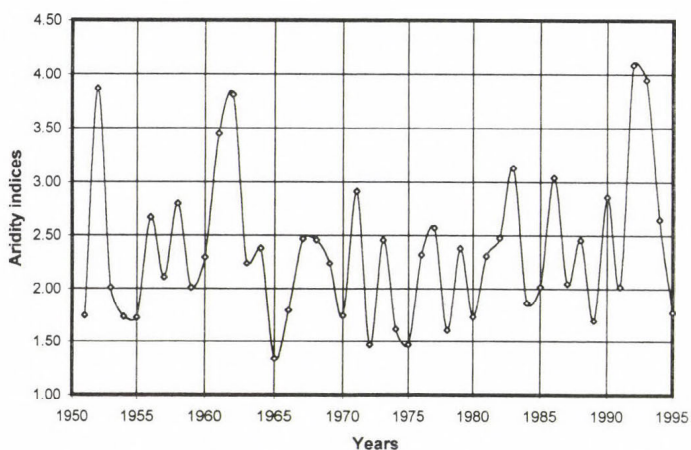


Fig. 3. Temporal fluctuations of aridity indices in Hungary (1951–1995).

There are some extremely dry growing season values some of which exceed the value of 3 and in a single case (in 1992) even 4. In that year the air would have been able to evaporate 4 times more water than the actual amount

of rain water during the growing season. There were 7 years between 1951 and 1995 when the ARI values of vegetation periods were higher than 3. The ARI values went below 1.5 only in 3 years. The minimum value was 1.34 (in 1965).

3. *Agroclimatic analysis of humidity-yield connection*

We used meteorological data collected by the Hungarian Meteorological Service and yield data gathered by the Hungarian Statistical Office as average values for the counties of Hungary. All data belong to a 45 years long period from 1951 to 1995.

Since yield data are referred to a county, we have selected one representative meteorological station in each county for calculating the connections between meteorological and yield data. Knowing the close relationships among neighboring stations, the representativity is self-evident for temperature. The values of precipitation, however, are more variable but showers take place mainly in summer months, when the values of aridity indices are generally high, so the possible errors have no effect on the computation of the relationships. Considering the earlier mentioned facts, the following meteorological stations were selected: Győr, Szombathely, Zalaegerszeg, Kaposvár, Pápa, Tatabánya, Martonvásár, Iregszemcse, Pécs, Kecskemét, Budapest, Szolnok, Szeged, Békéscsaba, Debrecen, Nyíregyháza, Miskolc, Kompolt, and Balassagyarmat.

3.1 *Analysis of yield*

Fig. 4 shows that from early 1960s the yield gradually increased thanks to the introduction of new intensive varieties, as well as more up-to-date fertilizers, and methods of plant protection. It was so till the end of 1980s, when the technological level dropped due to the considerable lack of the rather expensive fertilizers, and the plant protection methods. These variations in technological level can be described relatively well by trend functions. The set of points in Fig. 4 can be determined by third-degree or fourth-degree polinoms. The various trend functions give an approximation with different accuracy.

As we can see in Fig. 4 the actual yield values represented by points are located around the trend curve. It is assumed that the yield is made up of two components, one of the result of technological factors and the other of meteorological factors, that is

$$Y(t) = Y_T(t) \cdot Y_M(t), \quad (3)$$

where $Y(t)$ is the actual yield, $Y_T(t)$ the part of yield caused by technological factors, $Y_M(t)$ is the part caused by meteorological factors, and the t is the time (in this case it is a given year).

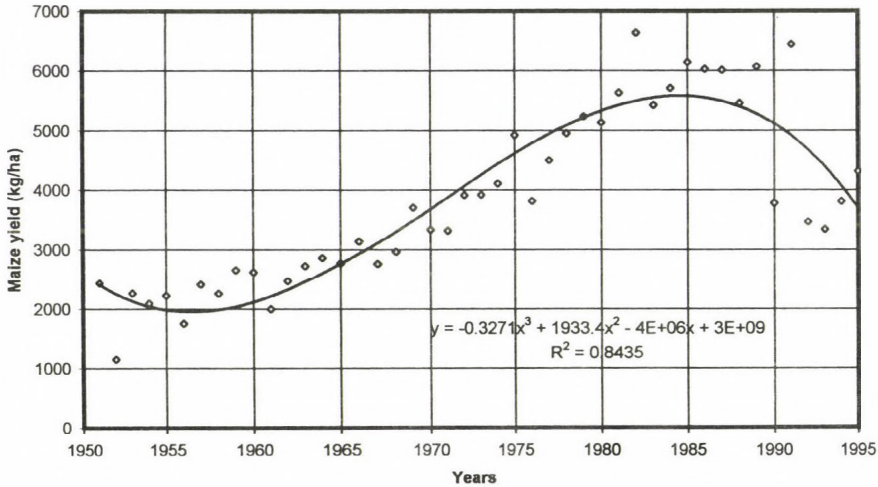


Fig. 4. Average maize yield in Hungary (1951–1995).

From Eq. (3) we can determine the meteorological effect as

$$\frac{Y(t)}{Y_T(t)} = Y_M(t). \tag{4}$$

The actual yield is measured, we can calculate the trend values from actual values, so the left side of Eq. (4) is known and the $Y_M(t)$ can be determined. Using this value, the $Y_M(t)$ expresses the complex effect of all meteorological elements.

It is practical to give the annual fluctuations as deviations from the trend values. The less the annual fluctuations, the more stable the yields are. First, the deviations from trend should be investigated. As Fig. 4 indicates, the fluctuation increases in the case of higher yields, that is the yield stability becomes smaller. If the deviations will be greater with higher yield, the meteorological elements increase or decrease proportionally the part of yield determined by technological factors. That is the reason why Eq. (3) was described in multiplicative form, and the meteorological effect was calculated as a ratio of actual yield to trend value (Eq. 4).

3.2 Complex meteorological effect on yield

Under constant climatic conditions, similar meteorological effects are expected to produce similar yield fluctuations. If it is true, these are considered as additive effects, since the meteorological effects increase or reduce the technological effects to a certain degree, so the meteorological effects are defined by the deviations. As Fig. 4 shows, the yield fluctuations increased in spite of no change in climate. In this case, the meteorological effects can be described by the ratio of the actual yield to the trend value (trend ratio).

Thus we have a possibility to separate technological effects (the effects of hybrids, fertilizers, and plant protection), and meteorological effects influencing the yield.

Trend ratio describes the effects of all meteorological elements, so it is also called index of complex meteorological effects (ICME). In this form it also includes the random effects which only slightly modify the results. We have calculated the trend ratios for each county. The yearly fluctuations of the average trend ratio over the whole country are shown in Fig. 5.

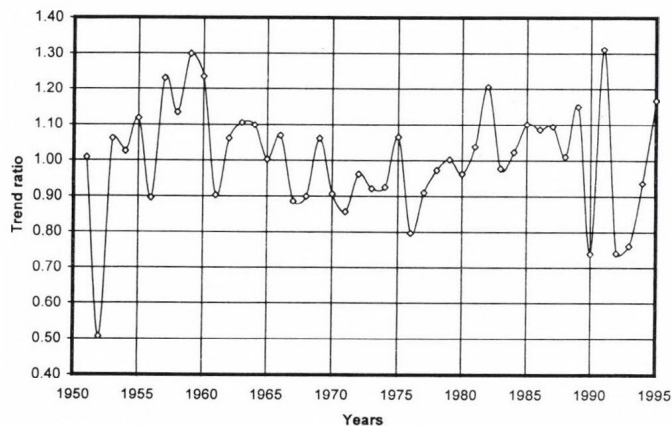


Fig. 5. Yearly fluctuations of the average trend ratio.

Values higher than 1 show that the effect of the weather was favorable for yield in that year. The values equal to 1 represent yields which are in accordance with the technological level, that is the weather neither increase nor reduce the yield. In the event of values over 1, the trend ratio numerically shows to what extent the weather increases the yield, in the case of values less than 1, the trend ratio indicates the extent of yield reduction.

Fig. 5 shows that the highest yield increases induced by the weather vary between 20% and 40%, which indicates a considerable fluctuation. In the period 1951–1995 there are 5 years (1957, 1959, 1960, 1982, 1991) when favorable weather conditions dominated in every county. There were years when positive yield deviations were observed in most counties, and only few counties showed no favorable weather effect.

The most unfavorable meteorological effects vary between 20% and 50%. So they seem to be more intensive. Five years were found (1952, 1976, 1990, 1992, 1993) when the weather conditions were unfavorable in every county, that is the unfavorable effects occurred more often. Most of the years were dominated by unfavorable effects in the greater part of counties, although parallel there could be favorable effects in one or two counties.

The frequency results show that trend ratios between 0.8 and 1.2 add up to 76–84% of all events, i.e., the deviations higher than $\pm 20\%$ account for 16–24% of all events. So approximately in every fifth year the weather may modify the yield by 20% either positively or negatively compared to the technological level.

3.3 Effect of different meteorological elements

The meteorological effects based on various elements can be determined in a particular year (t) in the following way:

$$\frac{Y(t)}{Y_T(t)} = Y_M(t) = f(m_1, m_2, \dots, m_K). \quad (5)$$

Since the values of meteorological elements are measured continuously at numerous places of the country, the only thing we need to know is: which element for which period is to be taken into consideration.

It is well known that green plants as maize require solar radiation for photosynthesis. The water is also an essential element to photosynthesis besides the nutrients dissolved in it and moving from the soil to the organs of assimilation. The speed of biochemical reactions within the plants depends on the temperature. So there are three meteorological elements: photosynthetically active radiation, temperature, and water which have basic importance for plants (Pethő, 1993).

It is practical to choose the precipitation to determine the water amount which is necessary to form unit quantity of yield, and aridity indices for determining the connection between actual yield and humidity factor.

3.4 The time period

We have to make a decision about the time period in which the meteorological elements will be determined. The following obvious time periods can be selected:

- the whole vegetation period,
- phenophases,
- calendar time spell, and
- optional duration of time spell.

In this paper the whole vegetation period was chosen. This is a natural period lasting from planting to ripening, and, therefore, it may be a base of a primary investigation.

3.5 Temporal variations of water used by yield formation

Precipitation amount of growing seasons was used to determine the quantity of water utilized for yield formation. The water use (WU) can be calculated by the following equation (Varga-Haszonits, 1981):

$$WU = \frac{P}{Y_{BIO}}, \quad (6)$$

where P is the precipitation during the vegetation period (in mm), and Y_{BIO} is the biomass. Generally, we know only the economic yield, therefore, the biomass must be calculated. It is known that the economic yield (Y_{ECO}) is a part of total biomass which may be computed as follows:

$$Y_{ECO} = k_{ECO} \cdot Y_{BIO}, \quad (7)$$

where k_{ECO} is a coefficient of economic yield (harvest index). From Eq. (7) we can receive that

$$Y_{BIO} = \frac{1}{k_{ECO}} \cdot Y_{ECO}. \quad (8)$$

So we can calculate the value of biomass by using the value of economic yield. The accuracy of this calculation depends primarily on the value of k_{ECO} .

The results can be seen in *Fig. 6* where the values were averaged for the whole area of the country. *Fig. 6* shows that the water use of maize yield

formation gradually decreased by using new intensive varieties of plants, appropriate doses of fertilizers, and adequate methods of plant protection.

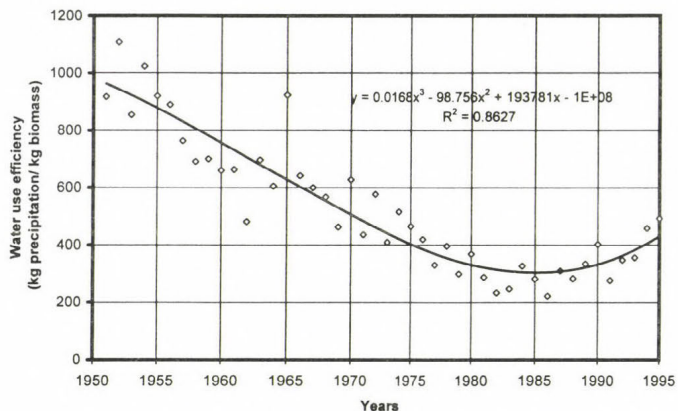


Fig. 6. Temporal changes of water use efficiency of maize in Hungary.

At the end of the 1980s, the application of fertilizers decreased as a consequence of financial problems, so water amount needed for the formation of unit mass of maize yield began to increase again.

For the period 1951–1995 the water use of maize yield can be described by the aim of a third-degree equation.

3.6 Relationship between aridity index and maize yield

We investigated the connection between aridity index and yield in every county by regression analysis (*Varga-Haszonits and Harnos, 1988*). The connection might be described by second-degree equations. The correlation indices are indicated in *Table 2*. As we can see they vary between 0.40 and 0.65. All the values are significant on the 0.1% level of probability.

These values show not only close relationships but also an areal distribution. It is interesting to note that the correlation indices are the highest in the wettest area of the country (Vas, Zala, Somogy, Veszprém counties). It shows that maize yield has a higher sensitivity to the fluctuations of relative water balance in wet areas than in dry ones. In the eastern part of the country (in the eastern border of Hungarian Great Plain) which is a dry area, the correlation indices are the lowest showing less sensitivity of maize yield to the relative water balance.

Table 2. Correlation values (*r* values) of the relationship between aridity index of the growing season and maize yield

County	<i>r</i> values
Győr-Moson-Sopron	0.5591
Vas	0.6306
Zala	0.5771
Somogy	0.6158
Veszprém	0.6158
Komárom-Esztergom	0.6158
Fejér	0.6158
Tolna	0.6158
Baranya	0.6158
Bács-Kiskun	0.5442
Pest	0.5516
Jász-Nagykun-Szolnok	0.4958
Csongrád	0.5002
Békés	0.4626
Hajdú-Bihar	0.4204
Szabolcs-Szatmár-Bereg	0.4354
Borsod-Abaúj-Zemplén	0.5416
Heves	0.5335
Nógrád	0.4798

Acknowledgements—The author expresses his thanks to the Scientific Research Foundation in Hungary (under the number T 034592 of OTKA), and to the Agroecological Project (under the number of OM-3B/0057/2002) for financially supporting this research.

References

- Dunay, S., Posza, I., and Varga-Haszonits, Z., 1968: A simple method for determining evapotranspiration and water content of soil. I. Meteorology of evaporation (in Hungarian). *Öntözéses Gazdálkodás* 6, 2, 39-48.
- Pethő, M., 1993: *Physiology of Agricultural Crops* (in Hungarian). Akadémiai Kiadó, Budapest.
- Varga-Haszonits, Z., 1981: Climatic potential of the yield crops (in Hungarian). *MTA X. Osztályának Közleményei* 14, 2-4, 253-270.
- Varga-Haszonits, Z., 1983: *Agroclimatology and Agrometeorological Forecasting*. International course of meteorology. TESCO-Országos Meteorológiai Szolgálat, Budapest.
- Varga-Haszonits, Z. and Harnos, Zs., 1988: Effect of climate variability and drought on wheat and maize production. In *Identifying and Coping with Extreme Meteorological Events* (eds.: E. Antal and M.H. Glantz). Orsz. Meteorológiai Szolgálat, Budapest, 138-166.
- Varga-Haszonits, Z., Porpáczy, A., and Schmidt, R., 1996: Agroclimatological analysis of natural periods and growing seasons. *Időjárás* 100, 207-218.
- Varga-Haszonits, Z., Schmidt, R., and Buruczky, F., 1997: Dry and wet spells in Hungary and their effect on crop production. *Environmental Protection in Agriculture of the Carpatian Basin*, XXIX., Mosonmagyaróvár.
- Varga-Haszonits, Z., 1998: Climatic variability and crop production. *ICA Summer School*. Pannon University of Agricultural Sciences, Mosonmagyaróvár, 164-170.

IDŐJÁRÁS

*Quarterly Journal of the Hungarian Meteorological Service
Vol. 106, No. 3–4, July–December 2002, pp. 103–111*

Atmospheric wet deposition as a nutrient supply for the vegetation

Ernő Mészáros

*Department of Earth and Environmental Sciences, University of Veszprém
P.O. Box 158, H-8201 Veszprém, Hungary*

(Manuscript received April 4, 2002; in final form July 22, 2002)

Abstract—The chemical composition of precipitation and wet deposition rates of different water soluble substances and metals are presented on the basis of precipitation chemistry programs carried out in Hungary. Data gained by bulk and wet-only collectors are compared and changes in precipitation composition during the last two decades are discussed. Decrease of acidity due to air pollution management and economical changes is emphasized. Hungarian atmospheric metal depositions are compared with other information obtained abroad. It is concluded that atmospheric wet deposition is an important nutrient source of plants in regions where no fertilizers are used.

Key-words: atmospheric precipitation chemistry, wet deposition, soluble matter, heavy metals, Hungary

1. Introduction: remarks on the water cycle

It is a well-known fact that water is an essential compound for life. Thus, the plants on the continents use water molecules, besides carbon dioxide and solar energy, to produce complex carbon species necessary for their metabolism. During this process called photosynthesis, a part of the oxygen is liberated which makes the respiration of animals and men possible. Consequently, the cycle of water in nature is a very important process for ecosystems in continental environment (*Antal and Szesztay, 1996*). The main characteristics of atmospheric water cycle is the fact that the budget in oceanic air is negative. In the atmosphere the balance is transported over the continents, where, due to this excess, the quantity of precipitation is higher than that of evaporation

(actually mainly evapotranspiration). The total yearly continental precipitation amount is equal to about $100 \times 10^3 \text{ km}^3$, while the evaporation is only 70% of this water volume (Manning, 1997). This implies that about 30% of the continental precipitation amount turns back in rivers to the oceans each year. Taking into account the oceanic precipitation amount ($\cong 400 \times 10^3 \text{ km}^3/\text{year}$), as well as the atmospheric water burden ($13 \times 10^3 \text{ km}^3$), a simple calculation shows that the turnover time of water in the atmosphere is equal to 0.026 year, that is about 9 days. This indicates that the quantity of atmospheric water is changed forty times during a year.

The atmospheric turnover of water has a considerable impact on the atmosphere itself. This is due to the fact that aerosol particles imbedded in cloud and precipitation elements and molecules of gases soluble in water are removed from the air during precipitation fall. This so-called *wet deposition* process constitutes an important atmospheric self-cleansing mechanism. Without wet (and dry) deposition the atmosphere would become very dirty in a short time interval owing to the accumulation of trace substances of biogenic and anthropogenic origin. However, due to wet deposition, water soluble trace gases as well as aerosol particles have residence times around 10 days or less in agreement with the turnover time of water in the air. Obviously, species removed from the atmosphere by precipitation are deposited onto the surface, that is the water cycle supplies not only water for continental vegetation, but also a lot of other materials which can be used as nutrients by aquatic and terrestrial ecosystems.

During the last million years of the Earth's history, atmospheric deposition removed exactly such quantity of different trace substances as the amount liberated by natural sources and the vegetation accommodated to the magnitude of this atmospheric input. However, during the last millennia, but mostly during the last century human activities have disturbed this steady state considerably. This is caused by the emission of different pollutants which are removed from the air similarly to biogenic compounds. Consequently, an important concentration increase of different species in precipitation water can be observed. This change alters significantly the atmospheric input into the biosphere which can be dangerous under special circumstances. Thus, the comparison of the nitrate concentration in precipitation water measured in Hungary at the beginning and in the second half of the 20th century shows an increase of seven times, which is obviously due to human activities like transport and energy production (Horváth, 1983).

The aim of this paper is to summarize the results of precipitation chemistry measurements carried out in Hungary during the last decades and to discuss the atmospheric input of different ions and metals into soils and vegetation.

2. Concentration and deposition of different ions

The first Hungarian measuring *network* for precipitation chemistry observations was operated between 1968 and 1970. In this early program precipitation water was collected at eight stations in the country by using *bulk collectors*. These collectors were open continuously, which means that the sedimentation of dust particles was not excluded during the sampling. The results of this program were published by *Kozák* and *Mészáros* (1971) who evaluated the data concerning their agricultural importance. This evaluation indicated that atmospheric deposition of nitrogen (actually ammonium and nitrate) is not an important source for the nitrogen uptake of agricultural plants caused by the magnitude of the nitrogen content of fertilizers. However, in areas where no fertilizers are used (e.g., in forests) the atmospheric input is very important. On the other hand, the wet deposition of sulfur contributes significantly to the sulfur uptake of plants even over agricultural regions. Finally, the potassium deposition is also much smaller than the doses given to the soils as fertilizers. One can speculate, however, that potassium ions reaching the leaves of the plant directly in precipitation water can possibly be taken up by the plants.

The results of the bulk network also demonstrated that the concentration of several ions increased from west to east. An exception was the amount of hydrogen ions which was lower in the eastern part of the country. This finding was interpreted as the effect of dustfall which is obviously more significant over the Great Plain as compared to more hilly western areas covered by denser vegetation. To exclude this problem, in 1977 a new network was organized which consisted of six stations. At these sampling sites precipitation was collected by *wet-only gauges* which opened at the beginning of precipitation fall and closed automatically at the end of precipitation events. The results obtained by this network were presented and discussed by *Horváth* and *Mészáros* (1984) who also compared them with those gained by the earlier bulk network. Among other things, it followed from this comparison that data gained by wet-only collectors did not show the spatial distribution emerged from concentrations obtained by the bulk network, which was previously mentioned.

Data given in *Table 1* are taken from the latter paper referenced. The table shows the average concentrations of different ions analyzed. Wet deposition rates calculated by multiplying mean concentrations by yearly precipitation amounts are also tabulated. In the rows for concentrations the values of specific conductivity, characterizing the total amount of ions, are also given. Further, in the case of hydrogen ions, pH data, defined as the negative logarithm of the concentration, can also be seen. By comparing bulk and wet-only concentrations it is evident that in the bulk network higher concentrations

were measured than by the wet-only collectors. The difference are high in particular for sodium, potassium, and calcium which can be considered as elements typically of surface origin. The ratios of bulk concentration to wet-only concentration for sodium, potassium, and calcium are 2.8, 3.3, and 2.6, respectively. Accordingly, the specific conductivity is two times larger in the case of bulk measurements. It is interesting to note that this ratio is relatively high also for sulfate ions. This involves the possibility that coarse aerosol particles of soil origin contains a large amount of sulfate. Taking into account the high calcium concentration one can speculate that the sulfate is associated with calcium as calcium sulfate which is slightly soluble in water.

Table 1. Average concentrations (C in mg L⁻¹) and wet deposition rates (D in mg m⁻²a⁻¹) according to bulk and wet-only networks. Note that the values of specific conductivity (κ) are expressed in $\mu\text{S cm}^{-1}$ (1 siemens is equal to 1/ohm), while the dimension of the yearly precipitation amount (P) is mm (=L m⁻²).

Network	κ	pH	H	NH ₄ -N	Na	K	Mg	Ca	Cl	NO ₃ -N	SO ₄ -S	P	
Bulk	C	62	4.7	0.02	1.4	1.5	1.1	-	4.4	1.4	0.83	3.7	638
	D	-	-	13	893	957	702	-	2807	893	530	2360	-
Wet-only	C	31	4.5	0.03	1.1	0.54	0.34	0.42	1.7	1.0	0.58	1.9	573
	D	-	-	18	630	309	194	241	974	573	332	1088	-

Considering the deposition rates, it is evident that the dominant elements are calcium and sulfur. The wet deposition rate of sulfur (wet-only network) is about 1 gm⁻² yr⁻¹ which results in a total Hungarian deposition of 93 Gg yr⁻¹ (1 Gg=10⁹g). It is self-evident that this important amount of sulfur deposition is due to sulfur dioxide emission in Hungary and abroad. According to Horváth and Mészáros (1984), the dry deposition of sulfur dioxide was similar to the wet deposition of sulfate (both expressed in sulfur) value at least in the years of the study. It is well documented that the main species responsible for acidic deposition is sulfuric acid. While the concentration of hydrogen ions depends directly on that of sulfate ions (it is speculated that sulfate deposition determines the soil pH), species of soil origin like calcium carbonate tends to decrease the acidity of atmospheric waters. However, we have to take into account that a part of calcium comes from anthropogenic sources (e.g., as fly ash from power plants). This statement is based on our aerosol measurements (Molnár *et al.*, 1993), according to which the enrichment factor of calcium is between 5–10 relative to the average soil composition. Anyway, we can conclude that precipitation in Hungary was rather acidic about twenty years

ago: the hydrogen ion concentration was more than one magnitude higher than the equilibrium value controlled by the absorption of atmospheric carbon dioxide ($\text{pH} \approx 5.7$). A further peculiarity of the precipitation composition based on wet-only network is the fact that the sum of cations expressed in equivalents ($238 \mu\text{eq L}^{-1}$) is higher than the sum of anions ($189 \mu\text{eq L}^{-1}$). This is not surprising, however, since hydrogen carbonate ions were not analyzed in the program. According to a parallel set of analyses, the concentration of these latter ions was found to be $67 \mu\text{eq L}^{-1}$ on an average. Taking into account this value, we can conclude that the sum of anions is equal to the sum of cations which is an absolute necessity of electric neutrality. If we calculate in a first approximation the hydrogen ion concentration as the sum of the amount of sulfate, nitrate, and hydrocarbon ions diminished by the sum of ammonium, calcium, and sodium concentrations (all expressed in equivalents), a pH value of 4.4 is obtained which is similar to the value directly measured (see Table 1).

It is well documented that during the years between 1980 and 1995 sulfur-dioxide emission decreased considerably in Europe (Mylona, 1996) and in Hungary (Bozó, 1998). Generally speaking, air pollution caused by energy production was mitigated significantly. For this reason it seems interesting to estimate changes in precipitation composition during the same time period. In Table 2 the average chemical compositions of precipitation measured between 1977–1980 and 1997–1998 in Hungary are compared (the latter data are kindly provided by the Hungarian Meteorological Service).

Table 2. Chemical composition of precipitation in Hungary collected by wet-only samplers in two time periods. Data are expressed in mg/liter, except those for electric conductivity (κ : in $\mu\text{S cm}^{-1}$) and pH. The table also contains the average yearly precipitation amount (P: mm a^{-1}) observed at the sampling sites.

Period	κ	pH	$\text{NH}_4\text{-N}$	Na	Ca	$\text{NO}_3\text{-N}$	$\text{SO}_4\text{-S}$	P (mm/a)
1977–1980	31	4.5	1.1	0.54	1.7	0.58	1.9	573
1997–1998	20	6.0	0.61	0.63	0.76	0.38	1.0	602

First of all we have to note that the average precipitation amounts were similar in the two periods which makes the comparison reliable (the composition also depends on the amount of precipitation). One can see from data tabulated that an important change occurred between the two time intervals. Thus, the specific conductivity decreased by a factor of 1.5, while precipitation became slightly alkaline, practically neutral (if the effects of carbon dioxide is considered). This is obviously due to the decrease of nitrate,

but mostly of sulfate concentration. At the same time calcium concentration also decreased (decrease of fly ash emission?), while sodium content of precipitation remained the same. This implies that sodium is of soil origin, consequently its concentration is independent of air pollution management. An interesting feature of ammonium is that the concentration of this ion, independent of energy production and industrial activity, also decreased. A similar situation was observed in Eastern Germany in the territory of former German Democratic Republic by *Möller et al.* (1996) who published an ammonium ion concentration decrease of 39% between data gained before 1990 and after the political changes. These authors attributed this change to the decreasing ammonia emission owing to changes in the structure of agriculture after the unification of Germany. In Hungary before and after 1990 the ammonia emission was reduced by a factor of two as discussed in more detail by *Horváth and Sutton* (1998). However, these latter authors stated that this reduction was not reflected in atmospheric ammonia/ammonium concentration. This means that further research is needed in this fields since ammonia (ammonium ions in precipitation) plays an important role in the control of nitrogen deposition and of acidity of atmospheric waters.

As it was previously mentioned, the significance of atmospheric deposition is important in particular for forest ecosystems where no fertilizers are used. For this reason the rate of dry and wet depositions was studied in detail at three forest sites in Hungary (Farkasfa: western Hungary in a hilly area; K-pusztá: central part of the country at the Great Hungarian Plain; Nyírjes: north-east area in the Mátra-mountains) by *Horváth et al.* (1993). Data collected between 1988 and 1992 show that the concentration of sulfur dioxide and nitrogen dioxide as well as acidic deposition rate decreased during this time interval in agreement with our previous discussion. At the same time the importance of nitrogen (actually nitrogen dioxide and nitrate) deposition relative to sulfate-sulfur increased. This is obviously related to the fact that the decrease of the release of nitrogen oxide into the atmosphere was not as drastic as in the case of sulfur dioxide (see *Mészáros*, 2001).

3. Deposition of different metals

Beside essential components like water, nitrogen, and sulfur, the so-called microelements (e.g., metals) play an important role in the control of the life of terrestrial and aquatic ecosystems. The question of microelements has become an important environmental problem since human activities liberate a lot of metals into different domains of the environment including the atmosphere. Briefly, practically each element is needed for the plants. It should be

emphasized, however, that the amount is a very important factor. If a given element is not available for a given plant, this causes deficiency disease. On the other hand, and this is the general case concerning pollution, too high quantities lead to poisoning the vegetation. This explains the great number of projects in the last decades aiming to estimate the atmospheric deposition of different metals onto the surface of continents and oceans.

The Hungarian program, the results of which is published in the literature (in Hungarian: *Mészáros et al.*, 1993; in English: *Molnár et al.*, 1995), was carried out in 1992. In this program precipitation water was collected by wet-only gauges in the country at three sampling sites including K-puszta mentioned above. Special care was made to avoid chemical contamination and transformations during sample storage before chemical analyses. Parallel to wet deposition observations, the concentration and size distribution of different elements in the atmospheric aerosol were also measured for estimating dry deposition rates. It was found, however, that the magnitude of dry deposition was much smaller than wet deposition rates, so they are not included into the following discussion. *Table 3* gives the concentration in precipitation of some environmentally important metals determined on the basis of K-puszta samples. In the tables the wet deposition rates can also be seen as calculated by multiplying the concentrations by the yearly amount of precipitation. For comparison some data from other parts of the world (Sweden, Ontario) are also included (see *Mészáros*, 1999).

Table 3. Concentrations (C in $\mu\text{g L}^{-1}$) and wet deposition rates (D in $\text{mg m}^{-2}\text{a}^{-1}$) of different metals at K-puszta station (Hungary) in 1992, where P gives the yearly precipitation amount expressed in mm. In the table appropriate data for Sweden and Ontario (Canada) are also given.

Parameter	Cd	Cu	Ni	Pb	V	P
C (Hungary)	0.94	3.6	1.8	13	2.4	477
C (Sweden)	0.14	1.4	-	8.8	-	-
C (Ontario)	<0.20	1.3	-	2.4	0.4	-
D	0.45	1.7	0.85	6.2	1.1	-

One has to consider that the elements listed in *Table 3* are practically totally of anthropogenic origin in populated industrial areas like Europe and North America. Briefly, cadmium and copper emissions are due to non-ferrous metal production, although a part of cadmium is liberated into the atmosphere during fossil fuel use and waste incineration. The main nickel source is oil combustion, in a lesser way coal burning. Lead is a notorious product of the

use of leaded gasoline, while atmospheric vanadium is created during oil combustion.

It follows from Tables 1–3 that metal concentrations in precipitation are one or two orders of magnitude smaller than ions concentrations. However, one should keep in mind that depositions calculated from concentration data give essentially the anthropogenic contribution to the atmospheric input into natural and agricultural ecosystems. The deposition rate of copper and lead is high in particular. We have to note, however, that lead emission has certainly decreased considerably during the last decade owing to the introduction of unleaded gasoline (see *Isakson et al.*, 1997). It is a fortunate thing that the deposition of cadmium, very dangerous for life, is relatively low. Finally, one can see from the table that metal concentrations in precipitation are rather high in Hungary as compared to information obtained in other parts of the world. Hungarian concentrations are roughly higher by a factor of 2 relative to those measured in Sweden and North America.

Results of atmospheric budget calculations for Hungary indicate (*Molnár et al.*, 1995) that the emission of cadmium, copper and lead is smaller than the respective depositions. This means that continental wide emission mitigation is needed to control their deposition values. On the other hand, caused by fossil fuel use, in Hungary more nickel and vanadium is emitted than deposited indicating that the country is a net atmospheric source of these elements.

It goes without saying that there is not intention here to discuss the importance of the above metal depositions in the uptake of microelements by plants. Information in Table 3 gives the necessary input data for such an evaluation which is badly needed for estimating the impact of atmospheric pollution on the microelement cycle of natural and agricultural vegetation.

4. Conclusions

On the basis of information presented and discussed in this paper we can conclude that atmospheric wet deposition carries an important amount of material continuously into terrestrial and aquatic ecosystems. Before the industrial era this material input certainly was an important source of different elements necessary for natural vegetation. Nowadays, however, the atmospheric flux is significant first of all in areas where no fertilizers are used (e.g., national parks, forests, and grazing grounds).

During about the last fifty years the wet deposition rate of sulfur and some other materials (e.g., ammonium and calcium) has decreased in a significant way due to economic changes and continental-wide air pollution management. It is a bit surprising that the nitrate deposition has also decreased

in spite of the fact that no important change in nitrogen oxide emissions occurred. Further research is necessary to prove and/or elucidate this finding.

It is an important fact that the acidity of precipitation is lower now than about twenty years ago when acid rains caused important ecological damages in Europe, mostly in forest and lake ecosystems. It is certain that the improvement of the situation is a consequence of substantial decrease in sulfur dioxide emissions.

The comparison of metal depositions of anthropogenic origin in Hungary with those gained elsewhere indicates that Hungarian deposition rates are rather important. The estimation of the impact of these depositions on material budget of plants is an obvious need for further research.

References

- Antal, E. and Szeszty, K., 1996: Climate and water in plant ecology. *Időjárás* 100, 193-206.
- Bozó, L., 1998: Temporal variation of atmospheric sulfur budget over Hungary during 1980-1996. *Időjárás* 102, 141-147.
- Horváth, L., 1983: Trend of nitrate and ammonium content of precipitation water in Hungary for the last 80 years. *Tellus* 35B, 304-308.
- Horváth, L. and Mészáros, E., 1984: The composition and acidity of precipitation in Hungary. *Atmospheric Environment* 18, 1843-1847.
- Horváth, L. and Sutton, M.A., 1998: Long-term record of ammonia and ammonium concentrations at K-puszta, Hungary. *Atmospheric Environment* 32, 339-344.
- Horváth, L., Baranka, Gy., and Führer, E.Gy., 1993: Decreasing concentration of air pollutants and the rate of dry and wet deposition at the three forestry monitoring stations in Hungary. *Időjárás* 97, 179-186.
- Isakson, J., Öbländ, M., Lindgren, S.E., Fridell, M.D., Pacyna, J.M., and Makinen, M., 1997: Perturbations of background aerosol at rural sites in the Nordic countries. *Atmospheric Environment* 31, 3077-3086.
- Kozák, M. and Mészáros, E., 1971: Chemical composition of precipitation waters in Hungary and its agricultural significance (in Hungarian). *Agrokémia és Talajtan* 20, 329-352.
- Manning, J.C., 1997: *Applied Principles of Hydrology*. Prentice Hall, Upper Saddle River, N.J., USA.
- Mészáros, E., 1999: *Fundamentals of Atmospheric Aerosol Chemistry*. Akadémiai Kiadó, Budapest.
- Mészáros, E., 2001: *Regional and global environmental problems (acidification, ozone and climate change) in relation with national sustainable development* (in Hungarian). Report prepared for Ministry of Environmental Protection, Budapest.
- Mészáros, E., Molnár, A., and Horváth, Zs., 1993: Atmospheric deposition of microelements in Hungary (in Hungarian). *Agrokémia és Talajtan* 42, 221-228.
- Molnár, A., Mészáros, E., Bozó, L., Borbély-Kiss, I., Koltay, E., and Szabó, Gy., 1993: Elemental composition of atmospheric aerosol particles under different conditions in Hungary. *Atmospheric Environment* 27A, 2457-2461.
- Molnár, A., Mészáros, E., Polyák, K., Borbély-Kiss, I., Koltay, E., Szabó, Gy., and Horváth, Zs., 1995: Atmospheric budget of different elements in aerosol particles over Hungary. *Atmospheric Environment* 29, 1821-1828.
- Möller, D., Acker, K., Marquardt, W., and Brüggemann, E., 1996: Precipitation and cloud chemistry in the Neue Bundesländer of Germany in the background of changing emissions. *Időjárás* 100, 117-133.
- Mylona, S., 1996: Sulphur dioxide emissions in Europe 1880-1991 and their effects on sulphur concentrations and depositions. *Tellus* 48B, 662-689.

IDŐJÁRÁS

*Quarterly Journal of the Hungarian Meteorological Service
Vol. 106, No. 3–4, July–December 2002, pp. 113–121*

Climate change and soil processes

György Várallyay

*Research Institute for Soil Science and Agricultural Chemistry
of the Hungarian Academy of Sciences, Herman Ottó út 15, H-1022 Budapest, Hungary
E-mail: g.varallyay@rissac.hu*

(Manuscript received February 27, 2002)

Abstract—The changes in the gas composition of the atmosphere may lead to increasing temperature with heterogeneous spatial and time distribution. These changes are reflected in changes of vegetation and land use pattern with considerable impacts on soil formation properties and soil characteristics. These potential changes are discussed in the paper, analysing the impact on soil formation processes, the moisture regime, and soil degradation processes under the influence of four plausible climate scenarios.

Key-words: climatic scenarios, soil formation processes, soil moisture regime, soil degradation processes

1. Introduction

Human activities lead to changes in the global environment at virtually unprecedented rates, with potentially severe consequences to our future life. The study and solution of the problems of global environmental changes require urgent and efficient actions. This crucial task formulates a challenge for science: to describe and understand the interactive physical, chemical, and biological processes that regulate the Total Earth System, the unique environment for life (*Toward...*, 1988).

2. Potential changes in climate

In the last century considerable changes took place in the *gas composition of the atmosphere* due to natural processes and human activities, such as increasing energy consumption, industrialization, intensive agriculture, urban

and rural development. This may lead to a *rise in global temperature* with a rate of 0.1–0.8°C per decade. The spatial and temporal patterns of temperature increases will be heterogeneous on Earth. The changing temperature regime pattern will be followed by considerable changes in *precipitation characteristics*: quantity of rain and snow, their spatial and temporal distribution pattern, rain intensity, etc. Their forecast is even more uncertain (*Scharpenseel et al.*, 1990).

3. *Consequences of climatic change*

Due to the increasing temperature, an increasing part of the mountain glaciers, the permafrost soil zone, and the Polar ice caps will melt. It leads to changes in the water flow dynamics, including flood waves and surface runoff will result in a *rise of the eustatic sea level*. The forecasted 0.20–1.40 m sea level rise will threaten low-lying, man-protected lands, settlements, agricultural areas, and extended seashores with low slope. Another consequence will be the further extension of salt affected territories under the direct effect of temporal sea water inundations or due to the rise of the sea level-connected water table of saline or brackish groundwaters.

The changing climate will result in considerable changes in the *natural vegetation* and in *land use practices* (*Greenland and Szabolcs*, 1993; *Lal et al.*, 1994). The great vegetation zones will move into the direction of the Poles, with a predicted rate of 25–200 km/100 years. Vegetation — in many cases — cannot tolerate and follow this „velocity” and it leads to considerable changes in the species distribution, dynamics, diversity, and production capacity of various ecosystems. *Land use practices* will follow or modify the natural changes, depending on environmental and socio-economic conditions (*Lal et al.*, 1994).

Changes in the vegetation or land use pattern result in a feedback effect on climate, modifying albedo, surface roughness, micro-circulation processes, the heat and energy balance of the near-surface atmosphere, the characteristics of both temperature and precipitation. Vegetation changes will considerably influence the field water cycle and soil formation processes.

4. *Impacts of climate changes on soils and soil processes*

Climate changes and their consequences will result in significant alterations in *soil conditions* (*Brinkman*, 1990; *Greenland and Szabolcs*, 1993; *Lal et al.*, 1994; *Rounsevell and Loveland*, 1994; *Scharpenseel et al.*, 1990; *Tinker and Ingram*, 1994). These impacts and their relationships are summarized in *Fig. 1*

(Várallyay, 1989, 1990a,b, 1994). The figure clearly indicates why the quantitative evaluation of the impact of any climate change on the soil conditions and soil processes is so difficult and far from being satisfactory. The uncertainties in the long-term global temperature and precipitation forecasts are combined here with the complex, integrated influences of changing vegetation and land use pattern and the changing hydrological cycle (Arnold et al., 1990; Toward ..., 1988; VITUKI, 1989).

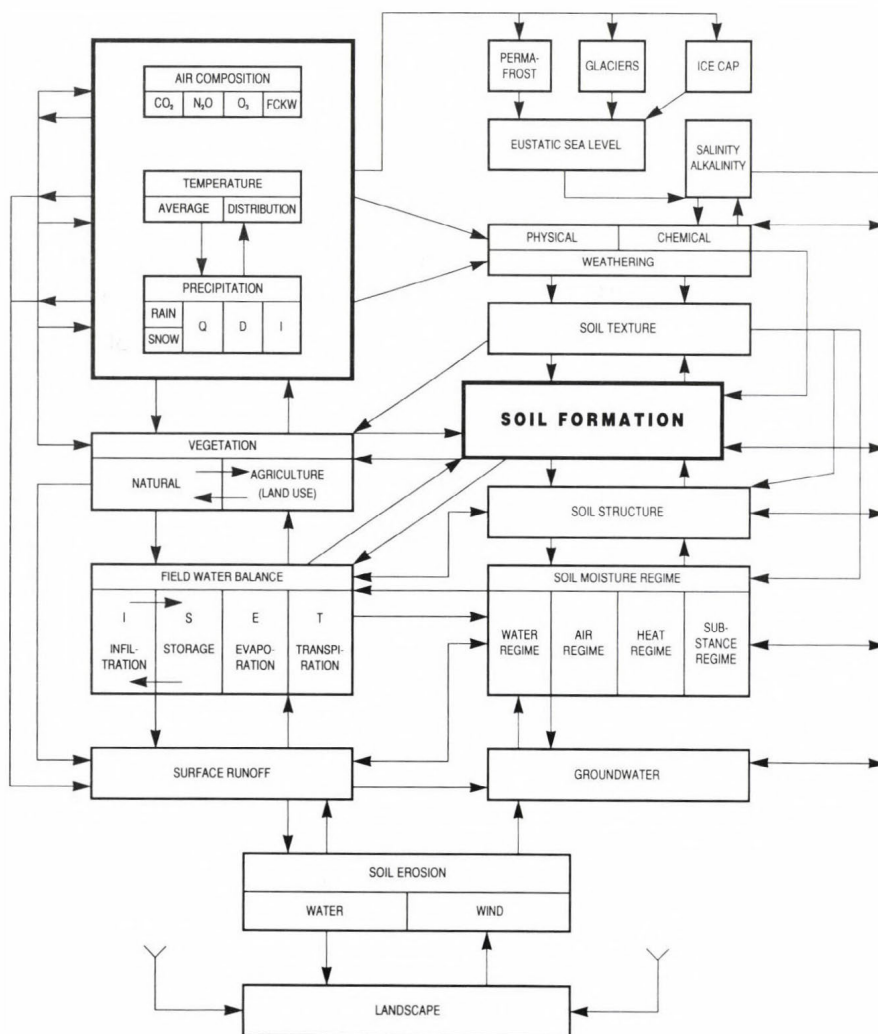


Fig. 1. The potential consequences of climate changes on soil processes.

4.1 Soil formation processes and soil properties

Climate, vegetation, and water regime determine (or at least strongly influence) *soil properties* (Arnold *et al.*, 1990; Brinkman, 1990; Rounsevell and Loveland, 1994; Scharpenseel *et al.*, 1990; Várallyay, 1990a).

Soil texture (particle-size distribution) is a rather constant soil parameter: characteristic response time is $>10^3$ years. *Physical and chemical weathering* are slow processes. Climate changes result in only slight and slow changes in these processes, and only moderately influence the “*biological weathering*”. The influence is more expressed on the texture differentiation within a soil profile and on the organic matter turnover (Arnold *et al.*, 1990).

4.2 Moisture regime

The integral impact of climatic–hydrologic–vegetation–land use changes are reflected by the *field water balance* and *soil moisture regime* (Antal *et al.*, 2000; Várallyay, 1990a,c). Their components and the potential impact of 4 plausible climate change scenarios on these factors are summarized in Fig. 2.

An increase in *precipitation* will be followed by an increase of:

- surface runoff (R) in hilly lands with undulating surfaces and without permanent and dense vegetation, if the infiltration rate, permeability, and water storage capacity of the soil are limited;
- infiltration (I) and water storage (S) within the soil if they are not limited, in flat lands;
- groundwater recharge (G) if the soil has good vertical drainage, permeability is not limited, especially in low-lying areas;
- evaporation (E), if infiltration is limited;
- transpiration (T) in the case of well-developed plant canopies.

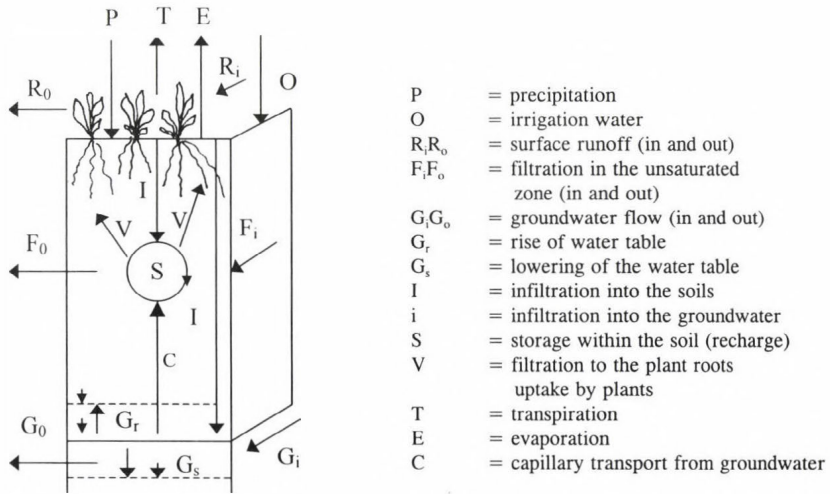
The decrease in precipitation results in adverse changes.

The rise in *temperature*

- increases the potential E and T, if the plant canopy is not suffering from limited water supply due to climatic or soil-induced drought, e.g., low precipitation or limited water storage capacity;
- decreases R, I, S, and G, especially if it is accompanied by low precipitation;
- decreases the intensity (depth) of permafrost; it will modify the geographical boundaries of permafrost, opening possibilities for increasing water storage and water movement, biological activity and soil formation processes within the unfrozen part of the soil.

The decrease in temperature will result in adverse changes.

These general influences are modified with the impact of vegetation characteristics (type, density, dynamics, species composition, biomass production, litter and root characteristics), and depend greatly on the type, intensity, spatial and temporal distribution of atmospheric precipitation. Man's influence is still more complex. Land use, cropping pattern, agrotechnics, amelioration (including water and wind erosion control, chemical reclamation, irrigation, and drainage), and other activities sometimes radically modify the field water balance and its components (Arnold *et al.*, 1990; Lal *et al.*, 1994; Tinker and Ingram, 1994; Toward ..., 1988).



Factors	Cl			
	Cold, wet	Cold, dry	Hot, wet	Hot, dry
P	I	D	I	D
R	I	d,D	I	D
G	i	d	i	D
I	I	d	I	D
I	i	D	(i)	D
S	I	d	(I)	D
E	D	E	E	I
T	D	E	i	I
F	-	-	-	-
G _r	i	-	(I)	-
G _s	-	I	-	I

Fig. 2. Components of the field water balance and soil moisture regime, and the influence of four potential climate scenarios on these factors: *i* and *I*: slight and great increase; *d* and *D*: slight and strong decrease; *E*: no change (equilibrium).

5. Impacts of climate changes on soil degradation processes

Soil degradation is usually a complex process in which several features of soil deterioration can be recognized. Soil degradation may lead to the loss of land or soil; limitations in normal soil functions; decrease in soil fertility and “productive capacity” (Oldeman *et al.*, 1991; Várallyay, 1989). Soil degradation may be the result of natural factors and/or human activities.

For the assessment of soil degradation a world-wide project was initiated by UNEP. In the framework of GLASOD (GLObal Assessment of SOil Degradation), a map was prepared in the scale of 1:10,000,000 on the present status and potential future development of the various human-induced soil degradation processes.

In Fig. 3 an attempt was made to show the potential impacts of the four basic climatic scenarios on the main soil degradation processes. In the figure their main natural and human causative factors were summarized, as well.

	Sign	Climatic scenarios				Causative factors	
		Cold and dry	Cold and wet	Hot and dry	Hot and wet	Natural	Anthropogenic
Soil erosion by water	E	4	1	4	1	1,2,3	9,10,11,12
Soil erosion by wind	D	3	4	4	4	3	9,10,11,12
Acidification	A	3	1	4	1	2,4	13,15
Salinization/Alkalization	S		4	1	4	5,6,8	14
Physical degradation	P	3			1	-	10,12
Extreme moisture regime (water logging)	M	4	1	4		5,6,7	11,12,14
Biological degradation	B	3			1	-	11,16
Unfavourable nutrient regime	N	3			1	(2,6)	13
Soil pollution (toxicity)	T	4	3	3	4	-	16

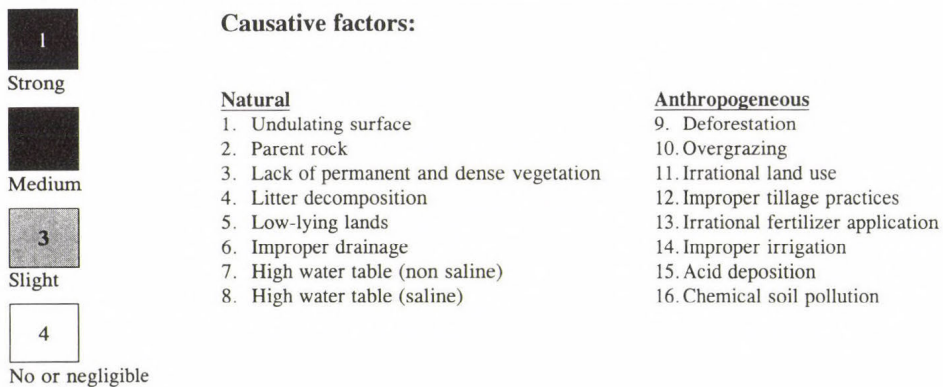


Fig. 3. The influence of four main climatic scenarios on the main soil degradation processes, and their natural and anthropogenic causative factors

(a) Soil erosion

There are no linear relationships between mean annual precipitation, surface runoff, and the rate of denudation/erosion. The rate, type, and extension of *soil erosion* depends on the combined influences of climate (primarily the quantity and intensity of rainfall), relief, vegetation (type, continuity, density), and soil erodability characteristics.

The main impacts of potential climate change on soil erosion are as follows (*Lal et al.*, 1994; *Várallyay*, 1990a):

- higher precipitation may result in an increasing rate of erosion (→ higher runoff), if it is not balanced by the increasing soil conservation influences of better vegetation due to better water supply;
- lower precipitation generally reduces the rate of erosion, but it can be counterbalanced by the less intensive soil conservation influence of poor vegetation due to the non-adequate water supply of plants; this can be the consequence of increasing temperature, as well;
- lower precipitation (or higher temperature) may intensify wind erosion;
- increasing temperature may reduce the erosion hazard moderating the permafrost influence (limited infiltration rate and water storage capacity of the soil); but may considerably increase the erosion-risk reducing the snow: rain ratio in the cold regions and in high mountains.

(b) Acidification

Increasing precipitation may intensify downward filtration and leaching, consequently may help acidification. Climate determines the dominant vegetation types, their productivity, the chemical character and decomposition of their litter deposits, and influences the development of soil reaction in this way (*Brinkman*, 1990; *Scharpenseel et al.*, 1990).

(c) Salinization/alkalization

One of the well-pronounced consequences of the forecasted global “warming up” is the rise of eustatic sea level. Higher precipitation (→ increasing rate of downward filtration → leaching) will reduce, lower precipitation and higher temperature will intensify salinization/alkalization processes: higher rate of evapo(transpi)ration → increasing upward capillary transport of water and water-soluble salts from the groundwater to the root zone + no or negligible leaching (*Rounsevell and Loveland*, 1994; *Várallyay*, 1994).

Similar tendencies characterize the leaching and *accumulation of carbonates*, which may lead to the formation of compact and impervious hardpans, petrocalcic horizons.

(d) Physical degradation (structure destruction, compaction, sealing)

The influence of climate change on the changes in soil structure is a complex process with numerous direct and indirect impacts. The most important direct impact is the aggregate-destructing role of raindrops, surface runoff, and filtrating water. The indirect influences act through the vegetation pattern and land use practices.

(e) Biological degradation

Temperature, precipitation, and vegetation changes all considerably influence biological soil processes, but only a few data are available on these consequences (Arnold *et al.*, 1990; Lal *et al.*, 1994; Tinker and Ingram, 1994, *Toward ...*, 1988).

(f) Unfavourable changes in the biogeochemical cycles and the plant nutrient regime

One part of these changes is connected with changes in the soil moisture regime (the ratio between downward and upward water movement in the unsaturated zone; leaching–accumulation), another part is related to the abiotic and biotic transformation phenomena (fixation, immobilization–release, mobilization; changes in solubility and redox status; etc.) in the chemical-biological cycles of various elements (Scharpenseel *et al.*, 1990). High precipitation helps leaching, filtration losses (→ potential groundwater “pollution”) and reductive processes; low precipitation → dry conditions may reduce the solubility, consequently mobility and availability of less soluble compounds.

6. Conclusion

Because of many uncertainties, more detailed, integrated multidisciplinary studies are required on the quantification of the existing facts and processes in the air–water–soil–geological deposits–plant continuum for a more real environmental forecast and for the rational control of soil processes under various potential and real climate change scenarios.

References

- Antal, E., Járó, Z., Scmogyi, S., and Várallyay, Gy., 2000: The geographical and ecological impacts of the 19th century floods control and water regulations in Hungary. MTA Földrajztudományi Kutatóintézet, Budapest.
- Arnold, R.W., Szabolcs, I., and Targulian, V., (eds.) 1990: *Global Soil Change*. IASA. Laxenburg-Budapest.
- Brinkman, R., 1990: Resilience against climate change? Soil minerals, transformation and surface properties, Eh, pH. In *Soils on a Warmer Earth* (eds.: H.W. Scharpenseel, M. Schomaker, and A. Ayoub). Elsevier, Amsterdam, 51-60.
- Greenland, D.J. and Szabolcs, I. (eds.), 1993: *Soil Resilience and Sustainable Land Use*. CAB International, Wallingford.
- Lal, R., Kimble, J.M., Levine, E., and Stewart, B.A. (eds.), 1994: *Soil Processes and Greenhouse Effect*. CRC Lewis Publishers, Boca Raton.
- Oldeman, R.O., Hakkeling, R.T.A., and Sombroek, W.G., 1991: *World Map of the Status of Human-induced Soil Degradation (GLASOD)*. ISRIC, Wageningen.
- Rounsevell, M.D.A. and Loveland, R.J. (eds.), 1994: *Soil Responses to Climate Change*. NATO ASI Series I: Global Environmental Change. Vol. 23. Springer-Verlag, London.
- Scharpenseel, H.W., Schomaker, M., and Ayoub, A. (eds.), 1990: *Soils on a Warmer Earth*. Elsevier, Amsterdam.
- Tinker, P.B. and Ingram, J.S.I., 1994: Soils and global change: an overview. In *NATO ASI Series, Vol. 23*. Springer-Verlag, London, 3-11.
- Toward an Understanding of Global Change*, 1988. National Academy Press, Washington, D. C.
- Várallyay, G., 1989: Soil degradation processes and their control in Hungary. *Land Degradation and Rehabilitation 1*, 171-188.
- Várallyay, G., 1990a: Influences of climate changes on soil moisture regime, texture and erosion. In *Soils on a Warmer Earth* (eds.: H.W. Scharpenseel, M. Schomaker, and A. Ayoub). Elsevier, Amsterdam, 39-49.
- Várallyay, G., 1990b: Consequences of climate induced change in soil degradation processes. In *Trans. 14th ISSS Congress, Kyoto. V.*, 265-270.
- Várallyay, G., 1990c: Potential impact of climate change on soil moisture regime and soil degradation processes. In *Proc. Int. Sem. Future Research Trends in MAB*, Tokyo, Japan, 20-29 Aug, 1990, 256-267.
- Várallyay, G., 1994: Climate change, soil salinity and alkalinity. In *NATO ASI Series. Vol. 23*, 3-11. Springer-Verlag, London.
- VITUKI, 1989: The influence of climate variability and potential climatic change on the hydrologic cycle and water regime. A Hungarian Case Study. Budapest.

IDŐJÁRÁS

Quarterly Journal of the Hungarian Meteorological Service
Vol. 106, No. 3–4, July–December 2002, pp. 123–136

Agrometeorology of maize — investigation carried out at the Hungarian Meteorological Service

Márta Hunkár

Hungarian Meteorological Service
P.O. Box 38, H-1525 Budapest, Hungary
E-mail: hunkar.m@met.hu

(Manuscript received February 18, 2002; in final form August 1, 2002)

Abstract—Maize is one of the most important agricultural crops in Hungary. The high level of production is due to the introduction of new varieties as well as the proper agrotechnology which is the result of investigation of agro-ecological conditions of Hungary. In this review paper a draft overlook is presented about the works of the Hungarian agrometeorologists concerning the meteorological aspects of maize production. The results of field experiments, statistical investigations are presented as well as the results of the experiments carried out by dynamic simulation model of CERES-Maize. It was demonstrated by all of the methods that shortage in water supply is the critical factor in maize production under the climate of Hungary. The risk of drought varies between 20% and 40% among the different agroclimatological districts of the country.

Key-words: maize production, dynamic simulation model, statistical analysis, evapotranspiration, Hungarian investigations.

1. Introduction

Relationship between climatic elements and agricultural production had been revealed in different ways. Up to the sixties statistical methods were used to estimate yields from weather conditions, e.g., average air temperature and precipitation in various months were related to the final yield (*Berényi, 1945*). In the past decades, mechanistic models have been developed in which crop growth is simulated in relation to observed weather conditions. These models integrate knowledge of the most important effects of weather on individual crop growth processes like global radiation on photosynthesis, air temperature

on development. Using these models it is possible to study the overall effect of weather on crop yield. In our study we use maize as test plant because it is one of the most important agricultural crops in Hungary. The sowing area is about 1 million hectares. Due to the introduction of new hybrids from the early seventies, yield level increased from 3 tons/ha up to 6 tons/ha as a country average. Hybrids can also be categorized according to the length of the vegetation period by FAO numbers. Climate of Hungary is suitable to grow hybrids with FAO number from 200 to 600.

Intensive agrometeorological experiments had been started at the Agrometeorological Research Stations in 1963 to assess the relationship among maize production, development, and climatic elements. The investigated subjects were description of phenological development, water consumption relating to irrigation, and estimation of yield production (*Antal*, 1966a; 1966b).

Investigation on maize production according to methodology belongs to one of the three direction: field experiments, statistical analysis and system analysis.

2. Field experiments

Majority of the field experiments carried out in the frame of the Hungarian Meteorological Service aimed to assess the optimal evapotranspiration and water requirement for irrigation (*Antal and Posza*, 1966; *Antal et al.*, 1971; *Posza*, 1973; *Posza and Tóth*, 1974; *Kádár and Szilágyi*, 1978). In agrometeorological observatories of the Hungarian Meteorological Service at Szarvas, Kecskemét, and Keszthely Thornthwaite type compensation lysimeters (*Antal*, 1966b; 1968) were used to assess the optimal evapotranspiration of maize. The seasonal amounts of maize evapotranspiration varied between 350–680 mm depending on weather conditions and agrotechnics.

The importance of agrotechnics in water regime of plants also manifested in field experiments. The efficiency of fertilisation together with water demand of the plant were studied by *Antal et al.* (1975) and *Dávid* (1977). As a result of investigations of their work could be assessed that the optimal level of fertilization was about 150–200 kg nitrogen/ha, 50 kg potassium/ha, and 50 kg phosphorus/ha in average. When the amounts of nitrogen is higher than the optimum level, water demand increases without a reasonable yield increase.

Description of developmental rate in function of environmental variables was given by *Pletser and Szalai* (1979) for thirty maize hybrids.

3. Statistical analysis

Statistical analysis was used to compare the climatic requirements of different varieties (Ábrányi, 1976; Ábrányi et al., 1977a, 1977b; Ábrányi et al. 1981). Using long time data series of county averages of yield, the probability of yield decrease due to aridity was provided by Varga-Haszonits (1979). The smallest number of years with yield decrease caused by drought was found in Zala county (20%), the largest number of years when yield decrease occurred because of drought was found in Bács-Kiskun, Pest, and Győr-Sopron counties (40%). Stochastic relationships between climatic elements and yield level were found by Kmetykó (1984). The paper of Kmetykó presents the forecasting equations and results of the investigations concerning the relation between the relative yield and climatic conditions required by maize for county Tolna. 22 meteorological variables and indices were investigated as predictors. The statistical method applied by the author is linear regression analysis, the period of investigation is 10 years (1970–1979). The most important meteorological parameters were related to precipitation because this is the limiting factor in maize yield production in Hungary. Different methods of statistical analysis were applied by Magyarits (1981) who applied 19-year long data series of maize yield from the experimental field of Martonvásár. The frequency of “extremely good years” and “unfavorable years” was 20%, and 37%, respectively. According to monthly mean temperatures and precipitation amounts, high level of yield can be expected if the meteorological conditions follow the tendency presented in Table 1.

Table 1. Optimal conditions for high level of maize yield. ΔT – anomaly in monthly mean temperature, ΔP – anomaly in monthly precipitation sum, + above, – below the normal, O-indifferent.

	April	May	June	July	August
ΔT	–	+	–	+	+
ΔP	O	+	+	+	O

4. System analysis

The first efforts to describe biomass and yield production using a system analysis was done by Ábrányi (1976). Later Dunkel (1981), Dunkel and Hunkár (1985), Hunkár (1986), Dunkel et al. (1987), Hunkár (1987, 1990, 1994), Hunkár and Dunkel (1987), Bacsí and Hunkár (1994) used dynamic simulation models to study biomass and yield production of maize. Finally, the

crop model CERES-Maize (Jones and Kiniry, 1986) was adapted and validated by data measured at the Agrometeorological Research Station of the Hungarian Meteorological Service at Keszthely (Hunkár, 1994). A sort of simulation experiments has been carried out for different purposes. The basic principles built into the model are as follows together with the results of the simulation experiments.

4.1 Climatic conditions of phenological development

The base temperature for maize germination is 8–10°C (Ábrányi *et al.*, 1977b). Growing degree days in the sowing-emergence phase are independent from the variety. The length of this phase is determined by soil temperature and moisture content with an average of 10–15 days (Derieux and Bonhomme, 1982). In Hungary the optimum sowing date is between April 20 and May 5.

The length of the vegetative period, from emergence until tasseling is determined by the variety mainly in the beginning of development. During this period leaf area increases, the rate of the increase and the final size of leaf area as assimilatory surface determines the radiation absorption as the source of energy for photosynthesis. Biomass accumulation can be derived directly from radiation absorption. Other environmental variables also influence the intensity of the photosynthesis. The optimum range of temperature for maize is around 30°C (Vong and Murata, 1977). According to the present climate of Hungary, the higher the temperature the faster the ontogenic development. Water demand of plants is the other important factor which has an effect on the development. Lack of water manifests itself as the vegetation period is shortened. The time of tasseling is usually between July 10 and 20. The phase from tasseling to maturity is the period of grain filling. The length of this period also depends on the variety. In general the “early type” varieties of short growing season are matured at the end of August, while the “late type” varieties of long growing season are matured in the middle of October. The length of the whole vegetation period from the emergence until maturity is important from the viewpoint of the potential biomass and yield accumulation. The longer the period the higher the potential yield. A warming climate may cause faster development, higher water demand and both of them may result in yield decrease.

4.2 Yield production of maize

The actual final yield of a crop is determined by many factors: weather, crop variety, fertiliser supply, soil conditions, occurrence of pests and diseases. After Penning de Vries and van Laar (1982) several production levels can be

distinguished. In the potential production level the crop is optimally supplied with water and nutrients and free from pests, diseases, and weeds. Crop growth is only determined by crop factors, temperature, and radiation. In water limited condition when nutrients are in optimum level and the crop is free of pests, diseases, and weeds, yield is limited by the availability of water. The effects of climatic variables on yield can be studied on this second production level.

A crop simulation model must be capable of representing the actual performance of crops grown in any particular region before it can be applied to the prediction of agrotechnology or climatic variation. Crop analysis of maize was carried out at the Agrometeorological Research Station at Keszthely and Szarvas, Hungary in the years 1976–1991, and 1988–1997, respectively (Hunkár, 1994). Measured and simulated data of silking date, maturity date, leaf area maximum, final biomass, and grain yield were compared in *Table 2*. The average differences between the predicted and observed plant characteristics are not more than 4% at Keszthely and 5.6% at Szarvas. The probability, that CERES-Maize model simulation results yield and biomass within 15% error in a given year, is 80%.

Table 2. Results of model validation. Averages and standard deviations of predicted and observed plant characteristics at Keszthely and Szarvas for the periods 1976–1991 and 1988–1997

	Predicted		Observed	
	Average	Standard deviation	Average	Standard deviation
Keszthely				
Silking date (day of the year)	199.7	8.3	199.5	8.0
Maturity date (day of the year)	260.4	14.6	257.0	14.2
Grain yield kg/ha	10,681	2190	10,294	2008
Szarvas				
Silking date (day of the year)	192.2	5.1	192.4	5.2
Maturity date (day of the year)	247.2	17.3	261.9**	13.1
Grain yield kg/ha	8476	4570	8020	4110

** harvesting day

Earlier results have been proven that under the climate of Hungary precipitation is the critical factor of the agricultural crop growing. Simulation model CERES-Maize provides an opportunity to estimate yield with optimal moisture supply. It means that the submodel of water balance is switched off. According to *Penning de Vries and van Laar (1982)* that is the production level No. 1. Simulation experiments had been carried out for Keszthely and Szarvas assuming no water stress during the vegetation season. It is called potential production. In *Fig. 1* the simulated potential production together with simulated actual production are presented for Keszthely, and Szarvas, respectively.

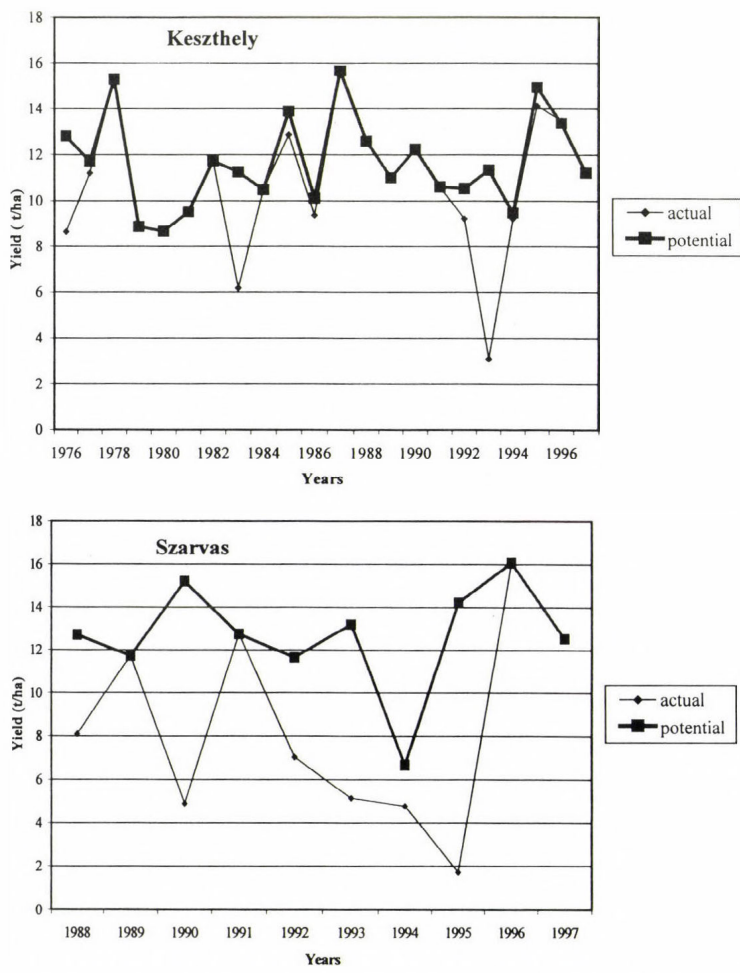


Fig. 1. Simulated yield production of maize with optimal and actual water supply for Keszthely and Szarvas.

The different climate of Keszthely and Szarvas is manifested in the potential production levels as well as in the frequencies of yield decrease due to water shortage. The average of the potential production is 11.7 tons/ha with CV=17%, and 12.7 tons/ha with CV=20% at Keszthely, and Szarvas, respectively. If the actual water supply, i.e., precipitation as driving force is taken into account in the model, there are years when significant yield decrease occurs. Under the climate of Keszthely, water shortage caused significant yield decrease in 14% of the years, while in Szarvas, which has a warmer and drier climate, in 50% of the years. The average yield on the production level No. 2. is 10.7 tons/ha (CV=29%) and 8.5 tons/ha (CV=54%) at Keszthely, and Szarvas, respectively.

It has to emphasize that these results came from simulation experiments, nevertheless they fit the empirical observations. To evaluate the model outputs in a proper way, some details about the plant-water relations have to be considered.

4.3 Behaviour of CERES crop model relating to evapotranspiration

Under the climate of Hungary, moisture supply is a critical and rather risky factor of agricultural crop production. It means that a crop growth model used in Hungarian circumstances must be capable to simulate water relations in satisfactory way. Details about the philosophy of CERES relating to the water balance is given in the *Appendix* after the works of *Ritchie* (1985).

To study the evapotranspiration submodel of CERES crop model a dry and a wet growing season were chosen. The growing season of maize takes from April 1 until September 30 in this relation. In the years 1975–1994 in Keszthely during the growing season, the average amount of precipitation (AVG) was 356 mm (the standard deviation (STD) was 71 mm). The season was assumed to be dry when the amount of precipitation was less than $AVG - STD = 285$ mm, and wet when the amounts of precipitation were above $AVG + STD = 427$ mm.

According to these conditions:

dry seasons	wet seasons
1977 (275 mm)	1975 (488 mm)
1981 (265 mm)	1984 (440 mm)
1982 (274 mm)	1987 (504 mm)
1988 (277 mm)	1989 (432 mm).

Simulation experiments were run for the year 1981 as a dry, and 1987 as a wet year.

Potential evapotranspiration calculated by CERES was compared to the values calculated by the local empirical formula developed by *Antal* (1968), which is widely used in Hungary.

In *Fig. 2* the accumulated potential evapotranspiration is shown. In the dry year CERES gives lower amounts, but in the wet year CERES gives higher amounts of potential evapotranspiration than the amounts calculated by the empirical formula of *Antal*.

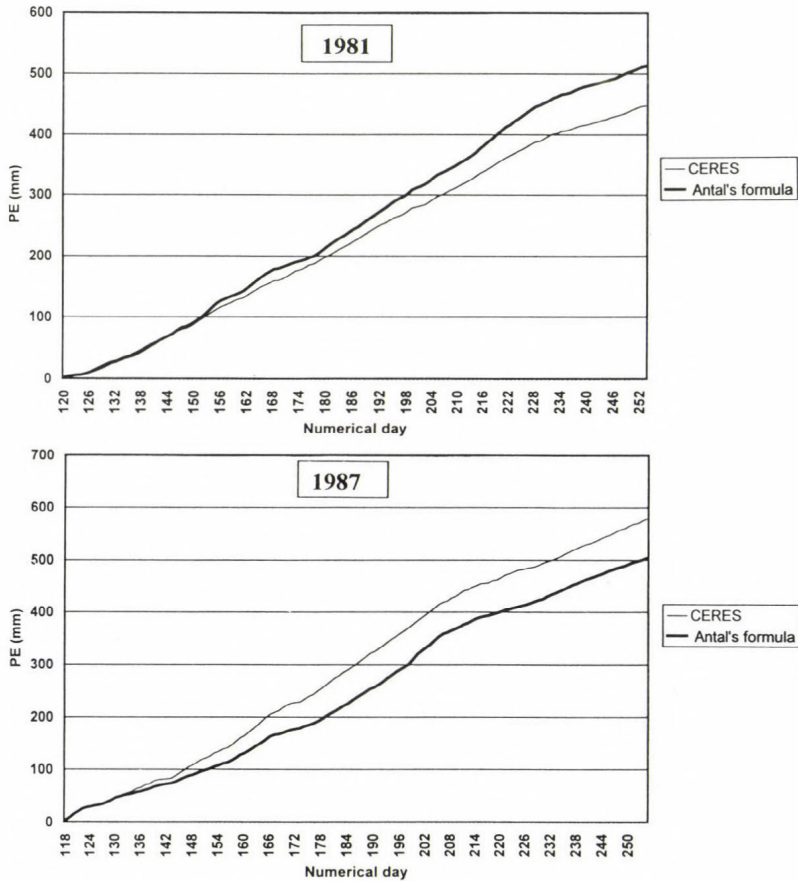


Fig. 2. Accumulated potential evapotranspiration calculated by CERES and *Antal's* formula in a dry (1981) and wet (1987) year at Keszthely.

The actual evapotranspiration simulated by CERES was compared to the measured evapotranspiration. In our case evapotranspiration measurement means that the soil moisture content was determined thermogravimetrically

with about 10 days frequency, and the water balance was followed for those periods:

$$ET = W_1 - W_2 + P,$$

where W_1 , W_2 are soil moisture content in the upper 1 m layer in mm, in the beginning and end of the period, P is the precipitation during the period.

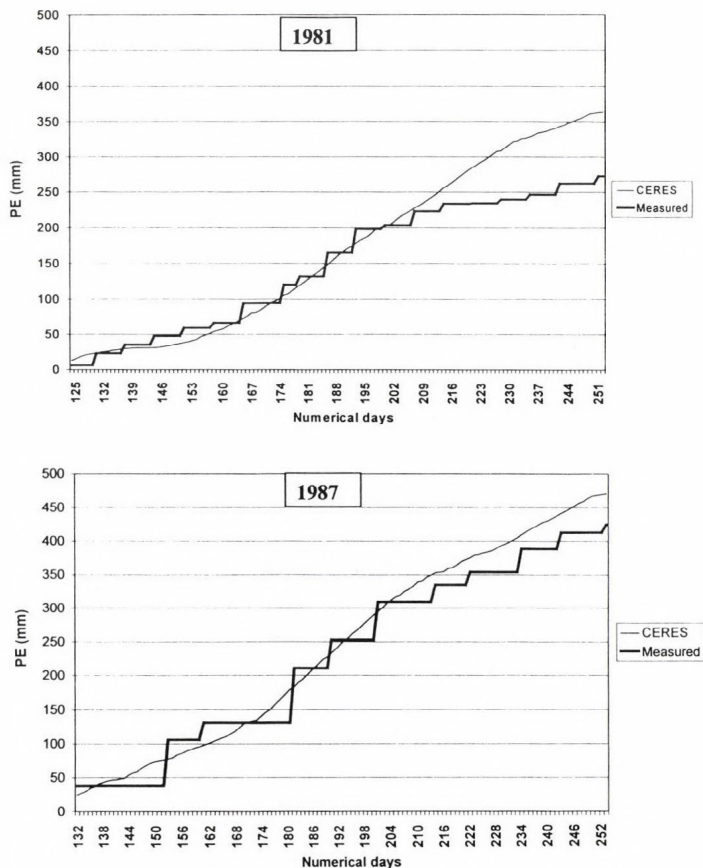


Fig. 3. Accumulation of calculated and measured evapotranspiration in a dry (1981) and wet (1987) year at Keszthely.

The final amounts of evapotranspiration simulated by CERES are higher than the measured ones both in dry and wet years, but the difference is significant only in the dry year. In the wet year the measured and simulated values show a good agreement (Fig. 3).

Considering that the actual evapotranspiration calculated by CERES is less than the potential one only when the amount of available water is below 25% of field capacity at least in one layer, even in a relatively dry soil the crop transpires water without any restriction. In reality the crop transpiration is more sensitive to the soil moisture conditions. Field experiments carried out by *Posza* (1973, 1975) demonstrated that when the amount of plant extractable water is below 50% of the maximum, the resistance against water uptake increases, therefore, the transpiration rate will be reduced. The plant physiological process of adaptation to arid conditions might play important role in water balance of that areas, and there is a need to include this process into crop models as well.

APPENDIX

Philosophy of CERES crop models relating to the water balance

In CERES crop models the submodel of water uptake, evaporation and transpiration is based mainly on the work of *Ritchie* (1985). Hereby a short summary of the concept is given.

Principles:

- The soil is divided into layers. Number of layers are optional, but the depth of the first upper layer is not more than 0.05 m. Number of layers is suggested between 9–15 depending on the maximum root depth which is required to know. Hydrological characterization of the individual layers is needed.
- Daily amounts of precipitation are input data.
- Initial soil moisture status has to be known.
- Equilibrium evapotranspiration rate is governed by the global radiation and daytime temperature:

$$E_q = G(2.04 \times 10^{-4} - 1.83 \times 10^{-4} \cdot \alpha) (T_d + 29),$$

where E_q equilibrium evapotranspiration,

G global radiation,

α albedo,

T_d daytime temperature.

The potential evapotranspiration (*PE*) is calculated from the equilibrium evapotranspiration as a function of daily maximum temperature

(T_{mx}), where the numeric constant 1.1 is used to account for unsaturated air, when T_{mx} is between 5°C and 24°C:

$$PE = 1.1 \times E_q.$$

When T_{mx} is greater than 24°C the constant is increased above 1.1 to account for advection, and

$$PE = E_q [0.05 (T_{mx} - 24) + 1.1].$$

When T_{mx} is less than 5°C, the constant is reduced to account for cold temperature causing an additional decrease in ET :

$$PE = E_q 0.01 \exp (0.18 T_{mx} + 20).$$

- Soil evaporation and plant transpiration are separated.

The potential rate of soil evaporation (PE_S) is then calculated from the leaf area index, LAI . When LAI is less than 1,

$$PE_S = PE (1 - 0.43 LAI),$$

and when LAI is greater than 1,

$$PE_S = E_q \exp (-0.4 LAI).$$

The actual rate of soil evaporation, E_S is limited by a local parameter and depends on the soil moisture of the upper layer.

The potential transpiration rate by the crop (PE_C), since germination is calculated based on the leaf area index (LAI), is

$$PE_C = PE LAI/3,$$

when LAI is less than or equal to 3. When LAI is greater than 3,

$$PE_C = PE.$$

If $PE_C + PE_S$ is greater than PE , then

$$PE_C = PE - PE_S.$$

- Root water absorption provides the water for transpiration. The root water absorption in CERES is calculated using a law of the limiting approach, whereby the soil resistance, the root resistance, or the atmospheric demand dominate the flow rate of water into the roots. All those processes are taking place in each layer of the soil. The number and depth of layers are given by the initialization of the model run.

The actual plant transpiration (E_C) is limited by the potential water uptake values which are determined by the amount of plant extractable soil water in a given layer. The actual evapotranspiration is less than the potential value only in that case, when the model finds less than 25% of the amount of plant extractable water of the field capacity in a soil layer.

Because the actual rate of transpiration is known only after the rate of water uptake by the roots is determined, the actual evapotranspiration rate (ET) is recalculated:

$$ET = E_S + E_C.$$

It has to be mentioned that the “water submodel” of CERES is under the way of a continuous development, and the later versions are more sophisticated in this context.

References

- Antal, E., 1966a: Measurement of maximum water consumption of maize and alfalfa (in Hungarian). Beszámoló az 1964-ben végzett tudományos kutatásokról. Országos Meteorológiai Intézet, Budapest, 60-65.*
- Antal, E., 1966b: Potential evapotranspiration of some agricultural crops (in Hungarian). Öntözéses Gazdálkodás 4, 69-86.*
- Antal, E., 1968: Irrigation schedule on the basis of meteorological data (in Hungarian). CSc. Thesis. Magyar Tudományos Akadémia, Budapest.*
- Antal, E. and Posza, I., 1967: Characteristics of the evapotranspiration of maize (in Hungarian). Beszámoló az 1966-ban végzett tudományos kutatásokról. Orsz. Meteorológiai Intézet, Budapest, 499-509.*
- Antal, E., Posza, I., and Tóth, E., 1971: Relationship of heat- and water regime of maize with the need of irrigation water (in Hungarian). Beszámoló az 1971-ben végzett tudományos kutatásokról. Országos Meteorológiai Szolgálat, Budapest, 142-158.*
- Antal, E., Posza, I., and Tóth, E., 1975: The effect of weather and climate on the effectiveness of fertilization (in Hungarian). Időjárás 79, 95-104.*
- Ábrányi, A., 1978: Meteorological modelling of growth and development of maize (in Hungarian). Beszámoló az 1976-ban végzett tudományos kutatásokról. Országos Meteorológiai Szolgálat, Budapest, 151-156.*
- Ábrányi, A., Pletser, J., and Szalai, D., 1977a: Weather requirements of different maize hybrids (in Hungarian). Beszámoló az 1977-ben végzett tudományos kutatásokról. Országos Meteorológiai Szolgálat, Budapest, 161-169.*

- Ábrányi, A., Pletser, J., and Szalai, D., 1977b: The effect of soil temperature on the early development of maize (in Hungarian). *Beszámoló az 1977-ben végzett tudományos kutatásokról*. Országos Meteorológiai, Budapest, 152-160.
- Ábrányi, A., Pletser, J., and Szalai, D., 1981: The effect of the weather on the maturity process of maize (in Hungarian). *Beszámoló az 1981-ben végzett tudományos kutatásokról*. Országos Meteorológiai Szolgálat, Budapest, 313-320.
- Bacsi, Zs. and Hunkár, M., 1994: Assessment of the impacts of climate change on the yields of winter wheat and maize using crop models. *Időjárás* 98, 119-134.
- Berényi, D., 1945: *Maize Production and Relation to the Weather* (in Hungarian). Tiszántúli Mezőgazdasági Kamara, Debrecen.
- Dávid, A., 1977: The effect of the weather on the yield and development of fertilized maize (in Hungarian). *Beszámoló az 1977-ben végzett tudományos kutatásokról*. Országos Meteorológiai Szolgálat, Budapest, 170-184.
- Derieux, M. and Bonhomme, R., 1982: Heat unit requirements for maize hybrids in Europe: Results of the European FAO subnetwork. *Maydica* 27, 59-77.
- Dunkel, Z., 1981: Dynamic simulation of dry matter accumulation of field crops (in Hungarian). *Beszámoló az 1981-ben végzett tudományos kutatásokról*. Országos Meteorológiai Szolgálat, Budapest, 269-284.
- Dunkel, Z. and Hunkár, M., 1985: Meteorological requirements of crop-yield models. *Proc. of the Symp. on Current Problems of Medium and Long Range Forecast*. Budapest, 1985, 123-126.
- Dunkel, Z., Hunkár, M., and Zárbok, Zs., 1987: Description of development of maize using dynamic simulation model (in Hungarian). *Időjárás* 91, 197-208.
- Hunkár, M., 1986: Growth functions in dynamic models of crop growth (in Hungarian). *Beszámoló az 1983-ban végzett tudományos kutatásokról*. Orsz. Meteorológiai Szolg., Budapest, 111-120.
- Hunkár, M., 1987: Dynamics of biomass production relating to the weather (in Hungarian). *Növénytermelés* 36, 83-90.
- Hunkár, M., 1990: The effect of weather on dry matter production of maize (in Hungarian). *Beszámoló az 1986-ban végzett tudományos kutatásokról*. Országos Meteorológiai Szolgálat, Budapest, 92-98.
- Hunkár, M., 1994: Validation of crop simulation model CERES-Maize. *Időjárás* 98, 37-46.
- Hunkár, M. and Dunkel, Z., 1987: Dynamic simulation of corn growth. *Proc. of the International Symposium on Systems Analysis and Simulation*. Berlin, 229-232.
- Jones, C.A. and Kiniry, J.R. (eds.), 1986: *CERES-Maize A Simulation Model of Maize Growth and Development*. Texas A&M University Press, Texas.
- Kádár, F. and Szilágyi, T., 1978: The optimum evapotranspiration of maize—climatic water shortage and the yields (in Hungarian). *Beszámoló az 1978-ban végzett tudományos kutatásokról*. Országos Meteorológiai Szolgálat, Budapest, 156-166.
- Kmetykó, K., 1984: Prediction of areal average yield of maize on the basis of meteorological parameters (in Hungarian). *Időjárás* 88, 232-237.
- Magyarics, K., 1981: Mathematical analysis of the relationship of maize yield and the weather (in Hungarian). *Beszámoló az 1981-ben végzett tudományos kutatásokról*. Országos Meteorológiai Szolgálat, Budapest, 296-312.
- Penning de Vries, F.W.T. and van Laar, H.H., 1982: *Simulation of Plant Growth and Crop Production*. PUDOC, Wageningen.
- Pletser, J. and Szalai, D., 1979: Early development rate of thirty maize hybrids (in Hungarian). *Beszámoló az 1978-ban végzett tudományos kutatásokról*. Országos Meteorológiai Szolgálat, Budapest, 239-250.
- Posza, I., 1973: Nutrition and evapotranspiration under field conditions (in Hungarian). *Beszámoló az 1973-ban végzett tudományos kutatásokról*. Országos Meteorológiai Szolgálat, Budapest, 162-168.
- Posza, I., 1975: The effect of the ground water level on the evapotranspiration (in Hungarian). *Beszámoló az 1975-ben végzett tudományos kutatásokról*. Országos Meteorológiai Szolgálat, Budapest, 210-218.

- Posza, I. and Tóth, E., 1974: Evapotranspiration of maize in function of nutrition level and moisture supply (in Hungarian). *Beszámoló az 1974-ben végzett tudományos kutatásokról*. Országos Meteorológiai Szolgálat, Budapest, 175-176.
- Ritchie, J.T., 1985: A user oriented model of the soil water balance in wheat. In *Wheat Growth and Modeling. NATO ASI Series*. New York Plenum Publishing Corp., New York.
- Varga-Haszonits, Z., 1979: Agroclimatological conditions of crop production (in Hungarian). *Beszámoló az 1979-ben végzett tudományos kutatásokról*. Országos Meteorológiai Szolgálat, Budapest, 45-51.
- Vong, N.Q. and Murata, Y., 1977: Studies on the physiological characteristics of C3 and C4 crop species. 1. The effect of air temperature on the apparent photosynthesis, dark respiration and nutrient absorption of some crops. *Japanese Journal of Crop Science* 46, 45-52.

IDŐJÁRÁS

*Quarterly Journal of the Hungarian Meteorological Service
Vol. 106, No. 3–4, July–December 2002, pp. 137–160*

Slices of plant–water relation in reflection to investigations carried out at Agrometeorological Research Station of Keszthely

Angéla Anda

*Veszprém University, Georgikon Faculty of Agronomy
P.O. Box 71, H-8361 Keszthely, Hungary; E-mail: anda-a@georgikon.hu*

(Manuscript received February 11, 2002; in final form October 3, 2002)

Abstract—Parallel with theoretical consideration, the investigation conducted at Keszthely Agrometeorological Research Station to study two important counterparts of the plant-water relation is discussed. The first part of the study contains the importance and role of the stomata in balancing plant-environment interaction. Methods of investigations of the stomata are also included. The modeling approach was also applied to justify a new consideration for average resistance estimation of maize. In the second half of the paper, method to assess the plant water supply by using the concept of the crop water stress index (CWSI) is introduced. Suitability of the index adaptation under Hungarian climatic and plant growing conditions for 13 consecutive years was evaluated. We present the influence of such scarcely experienced factor as nitrogen on the formation of determined CWSI.

Key-words: plant-water relation, stomatal resistance, crop water stress index (CWSI), irrigation timing.

1. Introduction

Methods of evaluating the plant watering level to assess irrigation cover a wide range from direct plant observations to theoretical consideration based on energy balance of canopies. Almost the whole plant growing area of Hungary is included in a special network for evapotranspiration determination using compensation lysimeters, which was established in the early 70-es. Operation of these lysimeter-stations for several decades revived a valuable data-set appropriate for producing studies, which contain a wide range of new results about the interactions in the soil-plant-water system. The observations carried

out in the scope of the network include traditional evapotranspiration determinations (*Antal*, 1966a, 1966b, 1968a, 1968b, 1972; *Antal* and *Posza*, 1967, 1970; *Antal* and *Endrődi*, 1972), as well as other experiences on the crop-environment relationships (*Antal et al.*, 1975; *Tóth*, 1978; *Ruzsányi*, 1981, 1990) which highly influence the water balance of plants. Almost the whole range of locally grown arable and horticultural crops (*Kozma* and *Füri*, 1974; *Stollár* and *Gergely*, 1978; *Posza* 1980) were observed at the stations of the network. Results, as they comprise observations for the whole area of Hungary, are unique and irreplaceable on their own. In spite of the newly constructed sophisticated instruments, until now the lysimeters provide valuable information about temporal changes in water loss of plants when the number of studied cropping systems is limited (*Prueger et al.*, 1997; *Tolk et al.*, 1998). From the early 80-es, investigations have been built to the earlier experiments on water balance of plants conducted at Keszthely Agrometeorological Research Station.

In the past three decades, the techniques have greatly developed in sensor accuracy and availability in field use. These instruments combine the latest technology in plant observations and computer know-how into a small, portable, easy to handle unit. Observations by these instrument-units opened a new way in studying the plant-water-atmosphere continuum more precisely than we have ever done it in the past.

The purpose of the study was to present a selection of investigations on plant-water relation carried out at Keszthely Agrometeorological Research Station during the past two decades. Observations, aimed closely at related plant-water connection as irrigation timing and role of stomata, were focused. The study of the role of irrigation scheduling in plant growing has of primary importance, because the weather of the growing seasons became drier in the past decades (*Mika*, 1991). Until now, the stomatal resistance is one of the most popular parameters in investigating the plant-water relation. The paper contains only a few details on the experiments carried out at Keszthely Agrometeorological Station. Only those parts of the theory are partially conferred, which are necessary to understand the explained subject. Detailed description of the applied theory and methodology can be obtained from the cited publications.

2. Material and methods

Field study was conducted at Keszthely Agrometeorological Research Station, on a Ramann type brown forest soil of mean bulk density of 1.5 Mg m^{-3} in the top 1 m of the profile and an available water capacity of 210 mm m^{-1} .

Statistical design of the experiment was in a complete block design, because of the fixed installation of the lysimeters. Data were analysed using combined multiple analysis of variance.

Maize hybrid used was mainly the Norma SC (FAO 380), a dent variety, tolerant to water stress. In stomatal resistance experiment a second maize hybrid, MVNK 480, a dent variety was also grown similarly to Norma. While the hybrid Norma is water stress tolerant, the MVNK 480 is bred for irrigated conditions. More details on different behaviour of the two hybrids are in *Anda* (1998). Both hybrids are commercially grown in Hungary. Plant protection and other agronomic procedures — except of nitrogen fertilizer dosing — were established according to standard agronomic practices for optimum maize production in Hungary, mainly in the surroundings of Keszthely.

The size of the experimental area was 0.7 ha installed with 24 compensation evapotranspirometer pots in the southern edge of the field. The size of plots agreed with the surface area of the lysimeter growing chambers (4 m²). In most of the years, the seed was sown at the end of April or in early May. Plant density was hand-thinned to 7.0 m⁻² in each year. Fertilizer nitrogen applied was 100 kg N ha⁻¹ at planting for the half of the treatments. The other half (controls) were grown without N fertilization. In the irrigation timing trials two experimental factors were investigated: the irrigation process itself, and the influence of nitrogen on *CWSI*. The following abbreviations of the treatments were applied in the figures:

- no N fertilization, C,
- 100 kg nitrogen ha⁻¹, N,
- irrigation, I,
- lysimeter growing chambers, ET,
- rainfed – or control treatments, P.

In the field experiment three watering levels were simulated:

- “Ad libitum” water supply in lysimeter growing chambers,
- rainfed – or control plants,
- irrigated plots by using the values of *CWSI*.

In stomatal resistance observations only crops with non limited watering and the rainfed ones were studied.

Lysimeter provides unlimited water supply from below the bottom of the pots. Surface area of the chambers of Thornthwaite type compensation evapotranspirometers were 4 m², and the depth of them 1 m. We filled the chambers with Ramann type brown forest soil, characteristic soil type of the surroundings. Daily sum of evapotranspiration was given by change in the volume of soil water in the chamber, additional water supply (irrigation) through the compensation pot, and precipitation amounts (*Antal*, 1968a).

Plots were irrigated when the *CWSI* exceeded the limitation value of 0.2–0.25, by using a drip irrigation system. (For easier data-handling we applied tenfold values of *CWSI* in our figures.) The amount of water used per irrigation was between 20 and 40 mm.

Stomatal resistance was measured with transient type porometer. We used a LI-COR 60 version between 1990–1992, and later on an improved model of Delta T Manufacturers, the AP4 type. We constructed a daily change in stomatal resistance by presenting hourly values randomly sampled on clear sky conditions. Two maize hybrids — see above — and three sugar beet varieties, Kawemaya, Gála, and Éva served as test plants. The variety Kawemaya is the most frequent grown sugar beet cultivar in Western Europe. Originally it was bred in Germany. The other two varieties, Gála and Éva are breeding in Hungary. We chose these three cultivars for the study, because they are close to each other in canopy architecture, and there is no literature about the difference in their water-relation. In general, the number of repetitions was 3 to 5. In maize, at the beginning of the seasons (May–June) both abaxial and adaxial leaf sides were sampled. Later on only the lower blade was applied for resistance determinations (amphystomatous plant). In sugar beet we measured the resistance of the lower epidermis only (hypostomatous plant). Daily mean resistance was calculated by averaging the hourly values.

After canopy closure, plant surface temperatures for *CWSI* determinations were resolved by infrared thermometer RAYNGER II. with 2° field of view and an included 8 to 14 μm spectral band filter. The thermometer was hand held 1 m above the plants using an oblique angle of about 30° to the horizontal. The sampling time was 30 seconds with 5 repetitions in each treatment at around solar noon in all measuring days, including holidays. The presumed emissivity of plants was 0.96.

Plant parameters as leaf area and grain yield were also obtained. Weekly assimilation surface size was measured with LI-3000 type portable planimeter, or by using the Montgomery equation on 10 randomly selected sample plants. After harvesting, cobs were taken for dry matter estimation, and they were oven dried at 60°C to a constant weight (5 to 7 days).

3. Results and discussion

3.1 Theoretical introduction of stomata function

All of the water transpired by plants, as well as CO_2 absorbed in photosynthesis pass through the stomata, even though these pores occupy less than 5% of the whole leaf surface. There are two different types of pore on the

epidermis with special capacity of moving: to open and to close. While in the higher plants the elliptical shape is the most common, Gramineae have guard-cells arranged in rows. The stomata are the most frequent on the lower surface of the leaf epidermis, but they may occur on other green tissues as stems, fruits, etc. Crops having stomata on both sides of the epidermis called amphistomatous, and those with stomata restricting to their lower leaf epidermis, hypostomatous plants.

The extreme environmental and physiological sensitivities of the stomata enables them to harmonize the balance between water loss and CO₂ uptake. The size and frequency of the stomata vary on both genetic and environmental conditions. Some examples for variation in frequency of stomata — the number of pores on unique leaf surface area — of different plants are presented in *Table 1*.

Table 1. Values of stomata frequency (number of pores per 1 mm² leaf area) on the two leaf surfaces after summarized data of *Sutcliffe* (1982) and *Jones* (1992)

Plants	Upper (adaxial)	Upper (abaxial) Leaf epidermis
ARABLE AND OTHER CROPS		
	28	105–158
Tomato (high light)	0–2	83
Tomato (high light)	111	131
Tomato (high light)	81–74	242–385*
Soybean (mean of 43 cultivars)	149–158	357–418*
Soybean (watered-stressed)	0	135
Millet (mean of 6 cultivars)	54–98	60–89*
Barley (different cultivars)	52	54–68*
Maize	0	14
Spiderwort	33	14
Wheat	25	23
Oats	85	156
Sunflower	40	281
Bean	0	158
Ivy		
TREES		
	0	170
Carpinus betulus	0	350–600*
Malus pumila (different cultivars)	120	120
Pinus sylvestris	39	39
Picea pungens		

*Results published by more authors. For details see the original literature cited in the title of the table.

The stomatal aperture is linearly related to guard-cell turgor pressure. There are two processes in regulation of the pore movements. The hydro-passive movement of the pores means change in all of the water potential outside the cells, while active variation in osmotic potential of the guard-cells produces the hydroactive term. We should take into account, that both stomata opening and closure are normally active metabolic processes requiring energy of plants.

There are different methods for studying the stomata:

(a) Microscopic observations

Epidermal imprints to characterize the size and frequency of the pores can frequently be applied. In most cases a solution (nail polish) is used to spread over the epidermis, allow it to dry, peel it off, and store for microscopic examination. This method is also suitable for *in vivo* investigations. The imprints sometimes do not produce reliable results, because different modifications may occur in pore apertures during the preparation of the observation.

Diffusion theory enables to derive estimates of the stomatal resistance by using the microscopically measured pore cross-section and diffusion coefficient. The modified version of the above approach can also be used for estimation of resistance of the intercellular spaces as well (*Jarvis and Mansfield, 1981*).

(b) Infiltration method

This approach is only used to study the qualitative differences in pore numbers within one species. To achieve this goal, graded solutions of differing viscosity (various mixtures of liquid paraffin and kerosene) are applied. Viscosity of the solution infiltrating into the pore provides measure of the aperture (*Larcher, 1980*).

(c) Porometry application

The instrument measuring the diffusive transfer of leaf gas exchange is called diffusion porometer. The diffusion porometer provides all of the leaf resistance to water vapor, including any cuticular part and boundary layer resistance in the porometer chamber (*Jarvis and Mansfield, 1981; Idso et al., 1987; McDermitt, 1990*).

The principle of the transit-time instrument is to measure the humidity increase in a closed chamber resulted from the water loss of a given leaf section. The time taken for humidity increase over a fixed interval may be converted into a resistance value using a previously obtained calibration curve. For calibration the leaf is replaced by wet paper. The range of resistance is

simulated by varying the number (size) of precision drilled holes with known resistance values obtained from the resistance theory.

In steady-state porometer air is flowing through a closed chamber — inside the chamber the leaf is also enclosed —, and the transpiration is determined from the flow rate and the water vapor difference in the inlet and outlet airstreams. There are two possible operation modes at using the steady-state porometer. When constant flow rate is applied, the outlet air is uniquely related to leaf resistance (Day, 1977). When the porometer operates in null balance mode, the flow rate is adjusted to give a particular relative humidity (Beardsell *et al.*, 1972). Both of them provide the most precise method in determination of the stomatal resistance in the field.

Among the others, errors in porometer application are discussed in details by Idso *et al.* (1988) and Monteith (1990). Application of diffusive resistance theory for maize under Hungarian climatic conditions is discussed partially in Anda *et al.* (1997) and Anda and Lőke (2002).

3.1.1 Diffusive resistance(s) on the water pathway in the plant-soil-atmosphere continuum

Stomatal resistance (r_s) is the most frequently mentioned counterpart of the diffusive resistances, but not the only component of the total resistance system. Transpiration rate can be expressed in the simplest way by using the Fick's law of diffusion. Complexity of diffusive resistances arising on water pathway from the soil to the open air makes the approach of dominator complicated. Plant water uptake depends on soil resistance, extent of root development, and sap movement of the xylem's vascular system. Roots are thought to offer the largest resistance of the whole soil-plant-atmosphere system, and in most cases they are responsible for the great intra- and interspecific variability (Calveta, 2000). The stem together with leaves nearly match the resistance of the roots (Oke, 1978). In leaves the water vapor diffuses from the wet mesophyll cell walls surrounding the intercellular air spaces to the stomata, allocated between two specialised guard-cells. Resistance of the cuticle is in a parallel circuit with stomatal resistance. When stomata are open, the cuticular resistance is much higher than the stomatal one, and for that most of the researchers ignore it. (Practically, to determine the true cuticular resistance for amphistomatous plants is very complicated, almost impossible). The true stomatal resistance consists of individual, but hardly approachable resistance of mesophyll cell walls and intercellular spaces connected in series. Using a theoretical consideration, the resistance of intercellular spaces is very small comparing to the other counterparts. Neglecting of this component involves about 2–5% error in the total stomatal resistance evaluation (Pearcy *et al.*, 1991).

Determination of the mesophyll cell walls is too difficult, and many uncertainties still exist. Under normal outdoor conditions, the „general” resistance of the mesophyll cell walls was assumed to be about 20 s m^{-1} (another $\sim 5\%$ error in stomatal resistance estimation). Finally, it can be assumed, that nowadays there is no simple way to measure the components of the transfer system distinctly (*Anda and Burucs, 1997*). Constant attempts reveal in the literature to improve the estimation of the actual stomatal resistance. *Kang et al. (2000)* tried to improve the transpiration estimation in maize by applying the ratio of momentary and maximum resistances instead of using the simple stomatal resistance for different soil water status. Others constructed simple model to estimate stomatal conductance — reciprocal of the resistance — over a long term (*Yu et al., 1998*).

The most plants have two evaporating surfaces with different transfer resistances on the abaxial and adaxial leaf surfaces. This difference must also be taken into account at the proper “average” resistance estimation. Theoretical consideration for maize is published by *Anda and Lőke (2002)* and *Anda (2001)*.

Summing the above results, in most investigations we mean stomatal resistance as a measure of the leaf resistance (r_l), but we can measure sum of three — stomatal resistance, resistance of intercellular spaces, and resistance of mesophyll cell walls —, even though four different resistances, as the determined resistance often includes a part of the boundary layer resistance (r_b). Typical values of the most important parts of transfer resistance are totaled in *Table 2* originating and summarizing the data from different literatures (*Oke, 1978*).

Table 2. Typical values of the counterparts of transfer resistance after *Oke (1978)*

Type of diffusive resistances	s m^{-1}
Intercellular spaces (r_i) and mesophyll wall resistance (r_m) together	< 40
Cuticular resistance (r_{cu})	2000–10,000
Stomatal resistance (r_s)	
– minimum for succulents and xerophytes	200–1000
– minimum for mesophytes	80–250
– closed stomata (maximum)	> 5000
Boundary-layer resistance (r_b)	10–100

Although the most meaningful part of diffusive resistance is the stomatal resistance, techniques measuring it separately are not available. In most cases

we measure a resistance mentioned stomatal resistance, but everybody knows, that this is not exactly equivalent to the corresponding resistance.

3.2 Scarcely studied factors influencing the stomata movements: the variety and the nitrogen application

Studying the stomatal behavior in its natural environment is very complicated because of the combination of influencing indoor and outdoor factors. The environment of living crops has great variability, and hardly known interaction exists in the plant-environment response. The stomatal response time can often be longer than the duration of the influencing external — environmental — factor. Large amount of literature was dealing with studying the stomata-environment relationship in the past. These results served as the basis for construction of the soil-vegetation-atmosphere transfer schemes, as for example the SVAT scheme (Franks *et al.*, 1997; Calveta *et al.*, 1998) or others (Gottschalk *et al.*, 2001). Little information is available on such factors like different cultivars or fertilization levels that may influence the stomata function as well. The selected beet varieties are widely used under Hungarian growing conditions. There was significant difference in stomatal resistance of three different sugar beet varieties (Fig. 1). Not only their water demands, but the length of their growing season were close to each other. The beet varieties were similar in their appearance (resembling surface size, leaf orientation, soil covering).

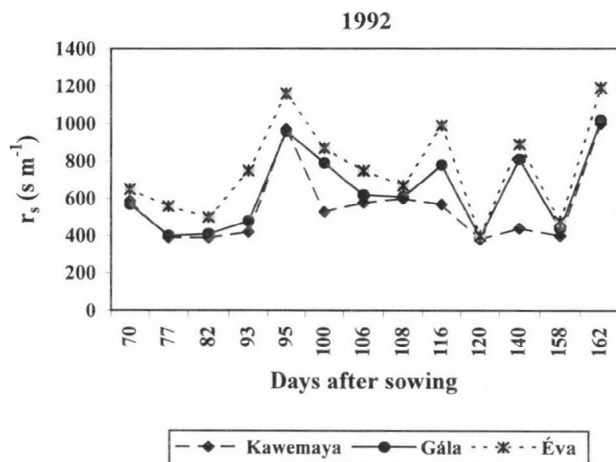


Fig. 1. Influence of the variety on daily average stomatal resistance measured in three different sugar beet cultivars (Kawemaya, Éva, and Gála) on some clear days during the 1992 growing season.

Differences in resistance of altered varieties were manifested during the dry and warm summer of 1992. Results of the stomatal resistance influenced by altered beet varieties are presented by the data measured during this season. The order of resistances measured in different beet cultivars was close to the stomatal resistance published by *Huzulak and Matejka (1992)* for sugar beet grown in Slovakia. The lowest resistance of variety Kawemaya produced the highest transpiration water loss and probably the most effective plant cooling at non limited watering in lysimeter growing chambers. At the end of the season, the sugar-yield of Kawemaya exceeded the sugar production of the other two studied sugar beet varieties (Éva, Gála) with increased stomatal resistance. In this experiment the variation in digestio — the sugar content of the roots in percents —, did not agree with the direction of change in the root production. There was an opposite connection between digestio and root yield of different beet treatments. The sugar beet growing is aimed to achieve the highest sugar yield, the third yield component, which is the multiplication of the digestio and the root yield. Although in 1992 the sugar production of Kawemaya was the highest, seasons of altered weather may revive other production results. As the earlier experiments show, the water level has to be in close connection with beet production, where the varieties may have differences in their sensitivity. There is the obligation of the plant growers to bring into harmony the need of the grown beet variety with the terms of the surrounding environment. The stomatal resistance can help the farmer to choose the best beet variety for his own conditions faster, than the other traditional factors used in the characterisation of the plant-water relation.

Experience of stomatal resistance observations for two maize hybrids was not so unambiguous as it was for sugar beet. In maize hybrids significant difference in stomatal resistance of altered hybrids could not manifested in each period of the investigation. In *Table 3* both the effects of nitrogen fertilization (0 and 100 kg N ha⁻¹) and use of two maize hybrids (Norma and MVNK 480) on daily mean stomatal resistance and evapotranspiration sum are totaled. The size of treatment influence considering the hybrids depends on the time of measurement (phenological development). In the very beginning of the growing season, the hybrid MVNK 480 had higher stomatal resistance than that of hybrid Norma. Later on the resistance determined in Norma increased above the resistance values measured in hybrid MVNK like a tendency. Effect of nitrogen on stomatal resistance was independent of the hybrid, and N always decreased significantly the stomatal resistance. Change in daily sums of evapotranspiration caused by treatment effects was in accordance with stomatal resistance alterations (see also in *Table 3*). Similarly to earlier results of *Howell et al. (1998)*, our investigations confirmed that the nitrogen decreases

the average stomatal resistance in accordance with the increase in plant water loss, independently of the hybrid.

Table 3. Daily averages of stomatal resistance (r_s , s m⁻¹) and daily sum of evapotranspiration (ET , mm day⁻¹) on the same sample days during 1997

Date in 1997	June 28		July 14		July 31		August 7		August 14		September 12	
	r_s	ET	r_s	ET	r_s	ET	r_s	ET	r_s	ET	r_s	ET
	Norma											
Nitrogen	461	5.1	384	5.3	268	5.71	221	5.3	192	6.3	582	5.1
Control	531	4.7	542	3.7	377	4.67	297	3.2	272	4.1	689	4.7
	MVNK 480											
Nitrogen	528	5.3	292	5.3	247	5.31	172	5.9	158	5.6	464	5.3
Control	756	5.0	435	4.4	350	4.15	255	4.0	263	4.2	429	5.0

There is also an endogenous rhythm of pores affecting the stomata movement independently of the current environment. Summarizing the different influencing factors, there are two main systems regulating the stomata, the fluxes of water vapor and CO₂. They need to be controlled and synchronized by pore movements.

3.2.1 Modeling approach of leaf resistance (r_l) evaluation

To test our field stomatal resistance observations, the modified version of Crop Microclimate Simulation Model of *Goudriaan* (1977) was applied. The original model was modified by *Chen* (1984). The basic of assumption of simulation the stomatal resistance is that mass transport processes — both water vapor and CO₂ — occur via stomata, so that the ratio between their resistances is equal to the ratio between their diffusivities. In maize a linear relationship exists between net CO₂ assimilation and inverse leaf resistance (leaf conductance) at constant CO₂ concentration in the sub-stomatal cavity. This connection provided the basis for simulation of leaf resistance, since the net CO₂ assimilation can be deducted precisely from the absorbed visible radiation (*Goudriaan*, 1977). Exceeding the saturation point of CO₂ assimilation (200 J m⁻² s⁻¹ for sunny maize leaves), the leaf resistance approaches the minimum value (*Stieger et al.*, 1977). Rate of net CO₂ assimilation (F , kg CO₂ m⁻² s⁻¹) was considered empirically by *van Laar* and *Penning de Vries* in *Goudriaan* (1977) as follows:

$$F = (F_m - F_d)[1 - \exp(-R_v c / F_m)] + F_d, \quad (1)$$

where F_m is the maximum rate of net assimilation ($\text{kg CO}_2 \text{ m}^{-2} \text{ s}^{-1}$),
 F_d is the dark respiration ($\text{kg CO}_2 \text{ m}^{-2} \text{ s}^{-1}$),
 R_v is the absorbed visible radiation (per LAI) ($\text{J m}^{-2} \text{ s}^{-1}$) and
 c is the slope of photosynthesis-light response curve at compensation point ($\text{kg CO}_2 \text{ J}^{-1}$).

At F_m calculation the influences of leaf age and ambient CO_2 concentration were simplified, and their average values were applied. Leaf temperature was considered to depend on ambient air temperature. Dark respiration was at about -0.1 of F_m (Goudriaan, 1977). To calculate maize leaf resistance, Eq. (1) can be re-written as follows:

$$F = \frac{1.83 \times 10^{-6} (C_e - C_r)}{1.66 r_l + 1.32 r_{b,h}} \Rightarrow r_l = \frac{1.83 \times 10^{-6} (C_e - C_r)}{1.66 F} - 0.783 r_{b,h}, \quad (2)$$

where $r_{b,H}$ is the boundary layer resistance for heat (s m^{-1}),
 1.66 is the ratio between diffusivities (for CO_2 and H_2O),
 1.83×10^{-6} converts CO_2 concentration into $\text{kg CO}_2 \text{ m}^{-2}$ at 20°C ,
 C_e is the external CO_2 concentration (ppm),
 C_r is assumed as „regulatory” CO_2 concentration (ppm),
 1.32 originates from calculation of boundary layer resistance for CO_2 .
The r_l was assumed to be equal to resistance measured by the porometer.

When stomatal resistance samples are taken in maize, the porometer chambers have to be placed on the three-thirds of the leaf blades (Anda, 2001), where the resistance tends to get close to the average of the whole leaf. In our observations this method markedly decreased the great variability of standard deviation of measured resistance values within one maize leaf.

The maize is an amphystomatous plant, having almost the same number of pores on both sides of the leaf blade. In the early phase of the vegetation period, in May and June, the maize stomatal resistance measured on the upper epidermis was about 30% higher than the resistance of the lower leaf side. It might be the special radiation environment attributed by the open canopy structure in spring that lets the radiation penetrative better into the stand decreasing the stomatal resistance. In fully developed canopy, in July and August, a linear relationship in stomatal resistance between adaxial and abaxial leaf surfaces existed (Fig. 2). In most studies the stomatal resistance of maize is only measured in one side of the leaf, assuming that the maize stomatal resistance of the two leaf surfaces are almost the same. In our study difference in resistance between the two leaf sides was registered, mainly at low solar

angles, in early morning and late afternoon. There was hardly enough difference in maize stomatal resistance between the two leaf surfaces at high solar elevation.

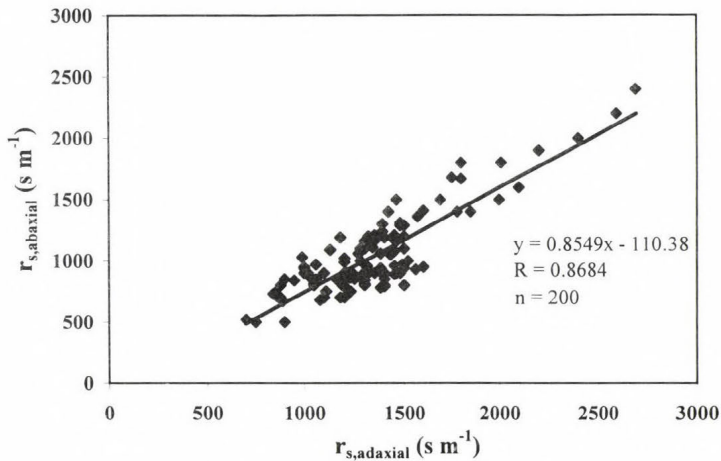


Fig. 2. Relationship in maize stomatal resistance between lower ($r_{s,abaxial}$) and upper ($r_{s,adaxial}$) epidermis. 200 samples (n) were taken at Keszthely, on clear days between 1992 and 1996. Hybrid Norma was applied in investigations.

Earlier results have shown that the influence of illumination exceeds the effects of leaf position or leaf age. We measured the stomatal resistance of totally sunny and shaded leaves separately, and the ratio of sunny (f) and shaded leaf sections were estimated by eyes. The average of the stomatal resistance (r_s) of the whole plant or leaf then will be as follows:

$$r_s = f r_{s,sunny} + (1 - f) r_{s,shaded}, \quad (3)$$

where $r_{s,sunny}$ is the mean stomatal resistance of sunny leaves ($s m^{-1}$),
 $r_{s,shaded}$ is the mean stomatal resistance of shaded leaves ($s m^{-1}$).

Finally the accuracy of estimation of maize average stomatal resistance was tested by using the model of Goudriaan (1977). Diurnal variation of stomatal resistance was simulated using ten soil water potentials from -0.1 to -14.0 bars for a bright summer day in July. At the same time, the lysimeter growing chambers and control field had -0.28 and -4.3 bars soil water potentials, respectively. The soil water potential in the field was measured by

neutron probe. The weather of the sample day was excellent for measuring stomatal resistance. In the two watering levels the resistance values differed and had the highest deviation at around solar noon. Average stomatal resistance of plants grown in lysimeters was 21.1% less than the daily mean of the non-watering control treatments.

Independently of water levels, the measured resistance is below the 1:1 lines, which means that simulation produces higher resistance than the measured one, mainly at around solar noon (Fig. 3). Simulation of maize stomatal resistance at “Ad libitum” watering gave better result than that of the control. While the difference in daily mean resistance at non limited water supply was 8.1%, at control plants it was 12.0%, in favor of simulated values.

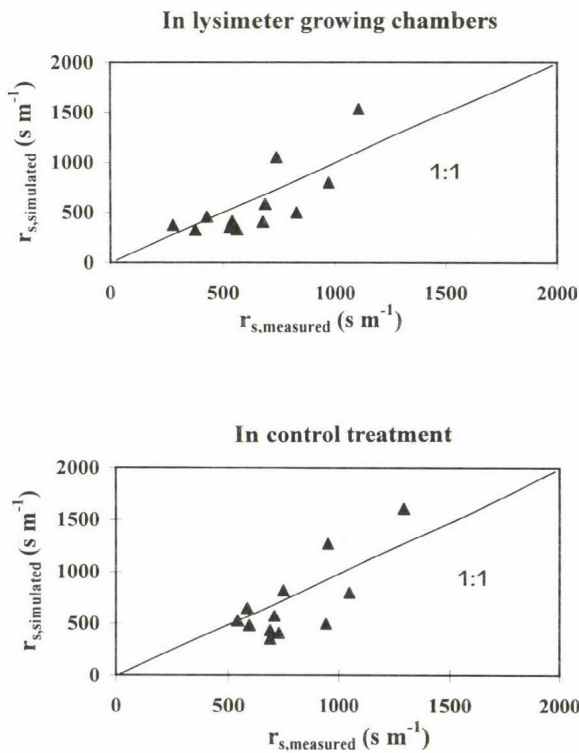


Fig. 3. Results of simulation of leaf resistance, r_l , on July 25, 1996. Samples were taken in hybrid Norma, at Keszthely, using non-limited watering level (lysimeter) and rainfed control stands.

For testing our stomatal resistance estimation, we chose an “ideal” sample day. When the sky was not completely clear, the difference in values of

simulated and measured stomatal resistance increased, and the divergence sometimes exceeded even the 40–50%. These results need further clarifying.

3.3 Considerations of the Crop Water Stress Index (CWSI)

Radiation properties of substances — reflecting, absorbing, and transmitting radiation — vary considerably, thus presenting a method for extracting information about the substances. The infrared thermometer receives the reflected radiation from the surfaces in the direction within the field of view of the thermometer. The instrument yields an integrated temperature, which does not interfere with the plant surface.

The amount of reflected radiation (I , W m^{-2}) can be expressed by the Stefan-Boltzmann blackbody law:

$$I = \varepsilon \delta T^4, \quad (4)$$

where T is the surface temperature (K),

δ is the Stefan-Boltzmann constant ($5.674 \times 10^{-8} \text{ W m}^{-2} \text{ K}^{-4}$),

ε is the emissivity of the substance.

Most infrared thermometers have 8–14 μm wave-band filter, because the peak of blackbody emission at normal temperatures falls within this region, and the water vapor absorption is relatively low here.

Determination of surface temperature is complicated, because the emissivity of different plant surfaces has great variability in time and space. In most investigations emissivity for plant surfaces is adopted from the earliest literature of the subject.

Plant surface or canopy temperature can be a useful parameter in irrigation timing, because meteorological and soil factors indicate when plants may be stressed, as well as plant factors when they are stressed (*Jackson*, 1982). In quantification of plant water supply different indices are widely applied. These stress indices can be grouped into two categories. The combined energy balance-aerodynamic relation (*Penman*, 1948) may be rewritten with surface temperature as a function of net radiation and vapor pressure deficit (*Jackson et al.*, 1981). The second category of stress indices comprises the empirical approach of *Idso et al.* (1981).

3.2.1 Theoretical consideration of the CWSI

The basis of assumption is the energy balance of the plants:

$$R_n = H + \lambda E + G, \quad (5)$$

where R_n is the net radiation (W m^{-2}),

H and λE are sensible and latent heat fluxes (W m^{-2}),

λ is the latent heat of vaporization of the water (J kg^{-1} water),

E is the transpiration intensity ($\text{J s}^{-1} \text{m}^{-2}$),

G is the heat flux into the ground (W m^{-2}).

Similarly to original literature, later on the soil heat flux is neglected.

Monteith (1973) gave detailed discussion and assumption for the members of Eq. (5). At non-limiting watering level, the plants will transpire at potential rate (potential evapotranspiration, *PET*). When there is not adequate water in the soil, the transpiration decreases below potential rate (actual evapotranspiration, *ET*). A measure of the ratio of actual to potential evapotranspiration should result in an index about the plant water status, the crop water stress index, *CWSI*. After expressing the members of Eq. (5), and solving for λE yields, the well known Penman-Monteith equation for *ET*, in terms of canopy (r_c , s m^{-1}) and aerodynamic (r_a , s m^{-1}) resistances is as follows:

$$\lambda E = \frac{\Delta R_n + \rho c_p \{e_s(T_c) - e\} / r_a}{\Delta + \gamma (1 + r_c / r_a)}, \quad (6)$$

where $e_s(T_c) - e$ is the difference in saturation and actual vapor concentrations of the air (hPa),

γ is the psychrometric constant (hPa K^{-1}),

c_p is the heat capacity of air ($\text{J kg}^{-1} \text{K}^{-1}$),

ρ is the air density (kg m^{-3}),

Δ is the slope of saturated vapor pressure-temperature relation ($\text{Pa } ^\circ\text{C}^{-1}$).

In most cases r_c may also be calculated with measurements of stomatal resistance and the leaf area index.

Producing the ratio of actual (λE for any r_c) and potential (λE_p for $r_c = r_{cp}$ measured in lysimeter) evapotranspirations produces:

$$\frac{ET}{PET} = \frac{\Delta + \gamma}{\Delta + \gamma (1 + r_c / r_a)}. \quad (7)$$

Taking into account that plants are going from non-stressed to stress conditions, our index, the *CWSI* will present values from 0 to 1:

$$CWSI = 1 - \frac{ET}{PET} = \frac{\gamma (1 + r_c / r_a) - \gamma^*}{\Delta + \gamma (1 + r_c / r_a)}. \quad (8)$$

The ratio of the resistances can be obtained by re-arranging the energy-balance equation (Eq. 5):

$$\frac{r_c}{r_a} = \frac{\gamma r_a R_n / (\rho c_p) - (T_c - T_a) (\Delta + \gamma) - (e_s(T_c) - e)}{\gamma [(T_c - T_a) - r_a R_n / (\rho c_p)]}, \quad (9)$$

where $T_c - T_a$ is the difference in the plant and air temperatures in °C.

The upper limit at potential transpiration, where $\gamma = \gamma^*$, and r_c is minimal with maximum transpiration:

$$\gamma^* = \gamma (1 + r_{cp} / r_a). \quad (10)$$

The lower limit, where $r_c \Rightarrow \infty$, and $r_{a,H} = r_{a,W} = r_a$ is

$$\Delta = \frac{\lambda E}{H} = \frac{\gamma (r_{a,W} + r_c)}{r_a}, \quad (11)$$

where $r_{a,W}$ is the aerodynamic resistance for water ($s\ m^{-1}$). More details are published in the original literature of *Jackson* (1982).

The empirical procedure in stress index determination suggested by *Idso et al.* (1981) seems to be less complicated than the theoretical one. Following the way of *Idso et al.* (1981), two empirical baselines (canopy and air temperature difference, $T_c - T_a$ versus vapor pressure deficit, *VPD*) are proposed, where the lower baseline can be obtained when water level is unlimited. The upper baseline arises at wilting point, when there is no available soil moisture. The actual water supply of the plants is somewhere between these two bounds presenting a new method of producing stress level of plants (*Fig. 4*). Although this latter method seems to be less complicated, it does not account for changes in net radiation or wind speed. Neglecting of these two important environmental factors, the accuracy of stress evaluation of plants declines.

In the course of our 13-year experiment, both approaches were applied. When we used the *Jackson* (1982) method, the r_c/r_a , the Eq. (9) was determined and substituted into Eq. (8) to get the *CWSI*. To calculate the ratio of Eq. (9), net-radiation, canopy and air temperature difference, humidity (vapor concentrations of the air), wind speeds, and plant height (roughness parameter, displacement height) were measured or counted. In empirical consideration the elements of canopy and air temperature difference and the vapor pressure deficit are the only input parameters.

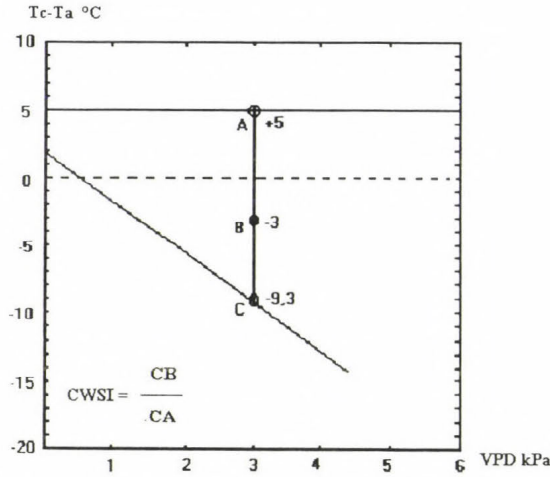


Fig. 4. Relations in plant and air temperature difference (T_c-T_a), vs. vapor pressure deficit (VPD). The lower and upper baselines are presented together with an example of how to calculate the $CWSI$. More details are discussed by *Idso et al.* (1981).

3.2.2 Some examples for practical use of $CWSI$

In our investigations both the empirical and theoretical considerations of $CWSI$ determination were applied. When we calculated the index by using the method of *Idso et al.* (1981), the influence of convective heating on calculated stress index was also taken into account. Parallel investigations on wind and stress index variations were carried out, and a linear relationship between the temporary wind speed (u) and $CWSI$ has been found. If the wind is blowing, the applied $CWSI$ has to be raised with Δy :

$$CWSI' = CWSI + \Delta y, \quad (12)$$

$$\Delta y = 1.11 + 0.27u. \quad (13)$$

More details on the wind- $CWSI$ relation are in *Anda and Ligetvári* (1993).

Seasonal variation of the $CWSI$ depends on the environmental influences, weather, and mainly the amount and distribution of rainfall. The drier the weather of the season, the higher the value of the $CWSI$ is. Our first example represents results in seasonal variation of $CWSI$ during a humid growing season (*Fig. 5*). In 1997 the summer was cool, the seasonal mean temperature was 0.8°C lower than the climatic norm. Distribution of the seasonal rainfall was not very smooth, in August the precipitation was about 15 mm lower than

in most of the years, but in June and July it was 28% higher than the 30-year average. As a result of the excess watering measured in June and July, no irrigation was necessary even in the drier August, during 1997. The tenfold values of *CWSI* never reached the limitation of 2.5 on the rainfed plots. During this humid year, an opposite tendency in *CWSI* appeared in lysimeters, where the excess watering of the chambers and the rainfall together caused increase in stress level of plants. The higher *CWSI* determined for lysimeters derived from the abundant watering of chambers, where the water ousted air from the soil.

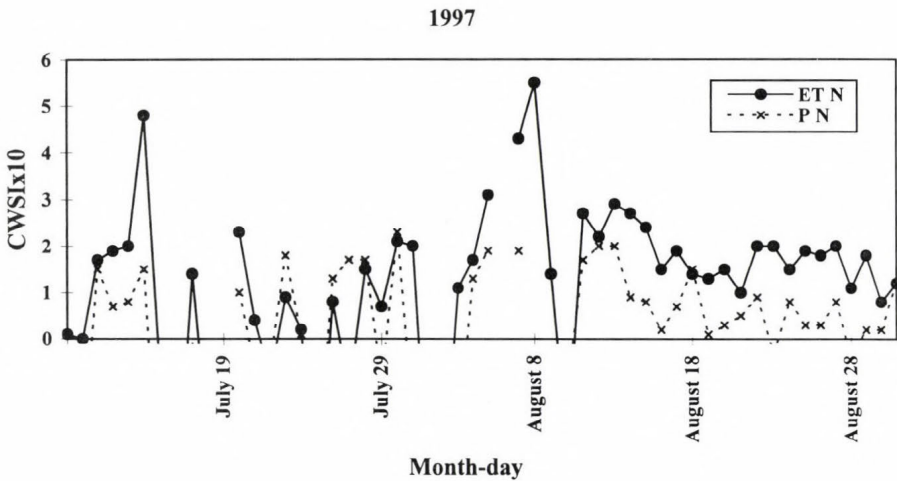


Fig. 5. Seasonal variation of *CWSI* tenfold values of for maize during humid summer of 1997. Continuous line represents indices measured in lysimeter (*ET*), dotted line are for rainfed control (*P*). The abbreviation *N* means nitrogen fertilization.

Traditional and other possibilities in use of *CWSI* are presented by the results determined for 1998. Although the seasonal mean temperature in 1998 was close to the climatic normal, in July and August precipitation was extremely low in the most important period of water stress in maize (Fig. 6). In dry summer of 1998 the seasonal mean of *CWSI* decreased by 131% in irrigated treatment comparing to its non-irrigated rainfed plots. According to the *CWSI* concept, the plants needed irrigation three times in the season (see arrows in Fig. 6). The irrigation produced 14.5% significant grain yield increase during the arid 1998.

Results of irrigation trials carried out at Keszthely by using the canopy temperature based *CWSI* are totaled in Table 4. Our test plant was the maize, duration of the study was 13 consecutive years between 1989 and 2001. We

conclude for maize, that the *CWSI* is a useful tool in scheduling irrigation, but only in arid growing seasons. During humid seasons there is no need for irrigation and for computing the *CWSI*. In semi-humid summers the yield surplus produced by means of irrigation is not enough to cover the extra costs of watering under Hungarian growing circumstances. Other results can be obtained with different crops, mainly with those horticultural plants, which represent higher expense per unit area than the maize. In comparative observations on different types of irrigation timing, the *CWSI* application produced the most economic method with least amount of water and cheapest irrigation cost of all.

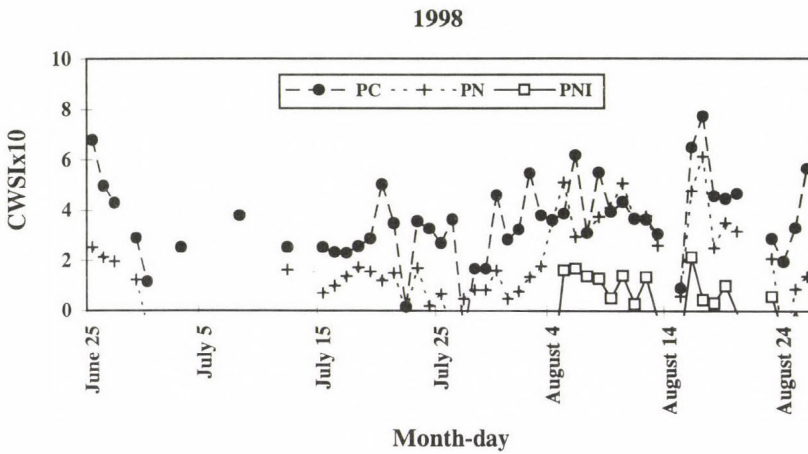


Fig. 6. Changes of tenfold values of *CWSI* in maize during arid 1998 resulted from altered watering (irrigated, *IP*; and non irrigated, *P*, plots) and fertilization levels. *C* and *N* sign the lack of nitrogen and fertilized plots, respectively. The arrows indicate the time of irrigation.

There are other than water problems derived stress factors that may influence the size of the *CWSI*. Effect of these stressors on calculated stress level of maize is demonstrated by artificially simulated N-shortage (Fig. 6). In 1998, the lack of N alone increased the seasonal mean of *CWSI* by 116% in rainfed plots. Surprisingly, the decreased amount of watering together with N limitation hardly increased in the average of *CWSI*. Probably the Liebig minimum-law or the close connection between nutrition and water level of plants might influence the final common stress index. To avoid overflowing the figure, and regarding the similarity of *CWSI* of the treatments without nitrogen, only indices determined for rainfed plots (PC) are presented.

Table 4. Results of the *CWSI* application for maize at Keszthely Agrometeorological Research Station, under different weather conditions between 1989 and 2001

Weather of the season	Arid	Humid	Semi-humid
Number of the seasons	5	3	5
Deviation from the climatic normal			
Average air temperature (°C)	+	-	+ or -
Seasonal rainfall sum (mm*)	-	+	+ or -
<i>VPD</i> at solar noon (kPa)	2.5–3.0 <	< 1.5	< 2.0
Irrigation necessity	Yes	No	Yes
Irrigation water amount (mm)	100–140	No	< 100
Change in <i>LAI</i> (%)	+20 <	No	+8–15
Change in <i>CWSI</i> (%)	-25 <	No	(-10) – (-22)
Change in yield (%)	+10 <	No	~ 5

* Continuous season from April 1 to November 1

Our observations show, that attention should pay on *CWSI* determination, when non water shortage origin stress factors — plant diseases, nutrition or soil problems, etc. — arise. Proper irrigation timing may only be implemented after exclusion of these confusing elements. Neglecting of these influencing factors may lead to application of extra amount of irrigation water.

4. Summary

Field trial was connected to two maize hybrids and three sugar beet cultivars, at Keszthely Agrometeorological Research Station, in the growing seasons between 1989 and 2001. Investigations on two factors influencing the plant-water relation are discussed. The first theme of the study was possibilities in approaching the real stomatal resistance in the field. Theoretical consideration of stomatal resistance among the other counterparts of diffusive resistances was also presented briefly. Widely known, that to determine the value of stomatal resistance under field conditions is very complicated, because of high variability of the factor in both time and space. The modeling approach seemed to be a good assumption in average of leaf stomatal resistance determination. To achieve this goal, the concept of Crop Microclimate Simulation Model of *Goudriaan* (1977) was used. To test the model applicability under Hungarian ecological conditions, maize in lysimeters and rainfed plots was grown. The

accuracy of estimation of mean leaf resistance was 8.1% and 12.0% in rainfed and at non limited watering level, respectively.

The second subject of the paper was the irrigation timing by applying the crop water stress index, the *CWSI* concept. In dry summers the *CWSI* was a useful tool in scheduling irrigation of maize stand. In our trial the watering resulted in about 10% yield surplus during arid seasons. We found that the irrigation with the use of *CWSI* is an economic and environment-friendly way even in maize. Attention should be paid for those non water-shortage origin factors, that might influence the calculated value of *CWSI* (plant diseases, fertilization, etc.).

References

- Anda, A., 1998: Water loss and microclimate of two maize (*Zea Mays L.*) hybrids. *Acta Agronomica Hungarica* 46, 121-133.
- Anda, A., 2001: Micro-meteorological observations in modification of the canopy microclimate (in Hungarian). *D.Sc. Thesis*, Magyar Tudományos Akadémia, Budapest.
- Anda, A. and Ligetvári, F., 1993: Potential use of the scheduler plant stress monitor in soybean. *CATENA Soil Technology* (Special Issue on Irrigation) 1, 137-144.
- Anda, A. and Burucs, Z., 1997: *Relation in Plant and Water in the Soil-Plant-Atmosphere Continuum* (in Hungarian). PATE GMK Nyomda, Keszthely.
- Anda, A. and Lőke, Zs., 2002: Stomatal resistance investigations in maize. *Acta Biol. Szegediensis* 46, No. 3-4, 181-183.
- Anda, A., Páll, J., and Lőke, Zs., 1997: Measurement of mean stomatal resistance in maize. *Időjárás* 101, 275-288.
- Antal, E., 1966a: Measurement of maximum water consumption of maize and alfalfa (in Hungarian). *Beszámoló az 1964-ben végzett tudományos kutatásokról*. Orsz. Meteorológiai Int., Budapest, 60-65.
- Antal, E., 1966b: Potential evapotranspiration of some agricultural crops (in Hungarian). *Öntözéses Gazdálkodás* 4, 69-86.
- Antal, E., 1968a: New method for determination of potential evapotranspiration (in Hungarian). *Beszámoló az 1967-ben végzett tudományos kutatásokról*. Orsz. Meteorológiai Int., Budapest, 452-460.
- Antal, E., 1968b: Irrigation schedule on the basis of meteorological data (in Hungarian). *CSc Thesis*, Magyar Tudományos Akadémia, Budapest.
- Antal, E., 1972: Is plant growth determined by internal water balance and turgor in the cells or by external factors? *Acta Agronomica* 21, *Hungarian Acad. of Sciences*, 458-468.
- Antal, E. and Posza, I., 1967: Characteristics of the evapotranspiration of maize (in Hungarian). *Beszámoló az 1966-ban végzett tudományos kutatásokról*. Orsz. Meteorológiai Int., Budapest, 499-509.
- Antal, E. and Posza, I., 1970: Plants constants of various crops and their variation during the growing period (in Hungarian). *Beszámoló az 1968-ban végzett tudományos kutatásokról*. Orsz. Meteorológiai Intézet, Budapest, 452-460.
- Antal, E. and Endródi, G., 1972: Water demand and irrigation requirement of potatoes (in Hungarian). *Időjárás* 76, 223-233.
- Antal, E., Posza, I., and Tóth, E., 1975: The effect of weather and climate on the effectiveness of fertilization (in Hungarian). *Időjárás* 79, 95-104.
- Beardsell, M.F., Jarvis, P.G., and Davidson, B., 1972: A null-balance diffusion porometer suitable for use with leaves of many shapes. *J. Appl. Ecol.* 9, 677-690.

- Calveta, J.C., 2000: Investigating soil and atmospheric plant water stress using physiological and micrometeorological data. *Agricultural and Forest Meteorology* 103, 3, 229-247.
- Calveta, J.C., Noilhana, J., Roujeana, J.L., Bessemoulina, P., Cabelguenneb, M., Oliosoc, A., and Wigneroc, J.P., 1998: An interactive vegetation SVAT model tested against data from six contrasting sites. *Agricultural and Forest Meteorology* 92, 2, 73-95.
- Chen, J., 1984: Mathematical analysis and simulation of crop micrometeorology. *Ph.D. Thesis*. The Netherlands.
- Day, W., 1977: A direct reading continuous flow porometer. *Agricultural Meteorology* 18, 81-89.
- Franks, S.W., Beven, K.J., Quinn, P.F., and Wright, I.R., 1997: On the sensitivity of soil-vegetation-atmosphere-transfer (SVAT) schemes: equifinality and the problem of robust calibration. *Agricultural and Forest Meteorology* 86, 1-2, 63-75.
- Gottschalk, J.C., Gillies, R.R., and Carlson, T.N., 2001: The simulation of canopy transpiration under doubled CO₂: The evidence and impact of feed-backs on transpiration in two 1-D soil-vegetation-atmosphere-transfer models. *Agricultural and Forest Meteorology* 106, 1, 1-21.
- Goudriaan, J., 1977: *Crop Micrometeorology: A Simulation Study*. Simulation monographs. Pudoc, Wageningen.
- Howell, T.A., Tolk, J.A., Schneider, A.D., and Evett, S.R., 1998: *Evapotranspiration, yield, and water use efficiency of corn hybrids differing in maturity*. *Agronomy J.* 90, 3-9.
- Huzulak, J. and Matejka, F., 1992: Stomatal resistance, leaf water potential and hydraulic resistance of sugar beet plants. *Biol. Plantarum* 34, 291-296.
- Idso, S.B., Allen, S.G. and Kimball, B.A., 1987: The perils of porometry. In *Proc. Int. Conf. on Measurement of Soil and Plant Water Status*, Vol. 2, Utah State Univ., Logan, UT. 10 July 1987, 133-138.
- Idso, S.B., Allen, S.G., and Choudhury, B.J., 1988: Problems with porometry: Measuring stomatal conductance of potentially transpiring plants. *Agricultural and Forest Meteorology* 43, 49-58.
- Idso, S.B., Jackson, R.D., Pinter, P.J., Reginato, R.J., and Hatfield, J.L., 1981: Normalising the stress degree parameter for environmental variability. *Agricultural Meteorology* 24, 45-55.
- Jackson, R.D., 1982: Canopy temperature and crop water stress. *Advances in Irrigation* 1, 43-85.
- Jackson, R.D., Idso, S.B., Reginato, R.J., and Pinter, P.J. Jr., 1981: Canopy temperature as a crop water stress indicator. *Water Resource Research* 17, 1133-1138.
- Jarvis, P.G. and Mansfield, T.A., 1981: The control of transpiration and photosynthesis by stomata. In *Stomatal Physiology* (eds.: P.G. Jarvis and T.A. Mansfield). *Society for Experimental Biology: Seminar Series*, Cambridge University Press.
- Jones, H.G., 1992: *Plants and Microclimate. A Quantitative Approach to Environmental Physiology*. Second Ed., Cambridge University Press.
- Kang, S., Cai, H., and Zhang, J., 2000: Estimation of maize evapotranspiration under water deficits in a semiarid region. *Agricultural Water Management* 43, 1-14.
- Kozma, F. and Fűri, J., 1974: Evapotranspiration of vineyards (in Hungarian). *Beszámoló az 1971-ben végzett tudományos kutatásokról*. Orsz. Meteorológiai Szolgálat, Budapest, 215-226.
- Larcher, W., (ed.) 1980: *Physiological Plant Ecology*. Springer Verlag, Berlin-Heidelberg-New York.
- McDermitt, D.K., 1990: Sources of error in the estimation of stomatal conductance and transpiration from porometer data. *Hort Sci.* 25, 1538-1548.
- Mika, J., 1991: Regional features of a stronger global warming over Hungary. *Időjárás* 95, 265-278.
- Monteith, J.L., 1990: Porometry and baseline analysis: the case for compatibility. *Agricultural and Forest Meteorology* 49, 155-167.
- Oke, T.R., 1978: *Boundary Layer Climate*. Methusen and Co. Ltd., London.
- Pearcy, R.W., Ehleringer, J., Mooney, H.A., and Rundel, P.W., 1991: *Plant Physiological Ecology*. Chapman and Hall, London-New York-Tokyo.
- Penman, H.L., 1948: Natural evaporation from open water, bare soil and grass. *Proc. of the Royal Soc. A*, 193, 120-145.
- Posza, I., 1980: Evapotranspiration of conserved plants (in Hungarian). *Beszámoló az 1978-ban végzett tudományos kutatásokról*. Orsz. Meteorológiai Szolgálat, Budapest, 226-232.

- Prueger, J.H., Hatfield, J.L., Asae, J.K., and Pikul, L., 1997: Bowen ratio comparisons with lysimeter evapotranspiration. *Agron. J.* 89, 730-736.
- Ruzsányi, L., 1981: Influence of irrigation and fertilizers on yield and quality of sugar beet (in Hungarian). *Növénytermelés* 30, 363-370.
- Ruzsányi, L., 1990: Water demand of sugar beet and effect of irrigation (in Hungarian). *Növénytermelés* 39, 423-429.
- Stieger, C.J., Goudriaan, J., Bottemanne, F.A., Birnie, J., Lengkeek, J.G., and Simba, L., 1977: Experimental evaluation of a crop microclimate simulation model for Indian corn (*Zea Mays*). *Agricultural Meteorology* 18, 163-186.
- Stollár, A. and Gergely, I., 1978: Evapotranspiration of a young applecrop (in Hungarian). *Beszámoló az 1976-ban végzett kutatásokról*. Orsz. Meteorológiai Szolgálat, Budapest, 206-215.
- Sutcliffe, J., 1982: *Plants and Water* (in Hungarian). Mezőgazdasági Kiadó, Budapest.
- Tolk, J.A., Howell, T.A., and Evett, S.R., 1998: Evapotranspiration and yield of corn grown on three high plains soils. *Agronomy J.* 90, 447-454.
- Tóth, E., 1978: Evapotranspiration crop yield and water utilisation of maize in the cases of various nutrient supplies and water supplies (in Hungarian). *Beszámoló az 1975-ben végzett tudományos kutatásokról*. Orsz. Meteorológiai Szolgálat, Budapest, 241-256.
- Yu, G.R., Nakayama, K., Matsuoka, N., and Kon, H., 1998: A combination model for estimating stomatal conductance of maize (*Zea Mays*) leaves over a long term. *Agricultural and Forest Meteorology* 92, 9-28.

IDŐJÁRÁS

Quarterly Journal of the Hungarian Meteorological Service
Vol. 106, No. 3–4, July–December 2002, pp. 161–184

Energy budget between the atmosphere and the surface in the vegetation period during 1963–1994

Gábor Szász

Agricultural Center, University of Debrecen
Agrometeorological Observatory
P.O. Box 36, H-4015 Debrecen, Hungary
E-mail: gszasz@helios.date.hu

(Manuscript received April 4, 2002; in final form August 2, 2002)

Abstract—The surface energy budget is characterized by the solar radiation, physical state of the soil, vegetation, sensible and latent heat fluxes, their proportion and periodicity. This paper summarizes the results of measurements carried out on black loam soil covered by natural short grass. The measuring point was located at 47°36'N, 21°36'E, 132 m above the sea level. The surface energy budget is determined mainly by the advective phenomena, however, near the surface plays a significant role. Continuous measurements have been taken at the Agrometeorological Observatory of the University of Debrecen during 1963–1994 for studying the components of the energy budget. Results are summarized by means of monthly mean values for the growing season.

Radiative conditions were examined through global radiation, reflectance of radiation, or albedo, and finally, the radiation balance. Relative distribution of daily values of the global radiation (Fig. 1) representatively indicates the radiation climate of the given area. Albedo is provided by the precipitation and annual course of the sun zenith angle (Table 2). Dynamics of the albedo depends on the soil state. Figs. 2 and 3 illustrate how different soils in wet or dry state modify the value of the albedo or the reflectance spectrum. Decrease of the soil moisture increases the reflectance, to different degrees at different wavelengths (Fig. 4). Ratio of R_n/G can be considered as climatic representative value. Table 3 shows the monthly values of this ratio.

The soil heat flux has a yearly cycle, however, it is only a small part of the radiation balance. Thermophysical layers of the soil differs from the mechanical layers because of the changing moisture content (Table 4). The energy circulation of the examined soil in the growing season is represented by the data of Table 5, showing that the soil heat flux gets the maximum in spring, and continuously decreases after July.

On the examined area, the intensity of the sensible heat flux is controlled mainly by the vertical temperature gradient (Table 6), since the wind speed is 1–4 m/s, and the diurnal fluctuation of the momentum flux is small during the growing season.

The biggest part of the incoming radiation is used for evapotranspiration. Potential evapotranspiration provides a good tool for evaluating the latent heat flux. Table 7

presents the values of the net radiation (R_n) and potential evapotranspiration (PE_0), and their ratio. According to the data, PE_0 gives the 70–90 % of the net radiation. Hourly values of the actual evapotranspiration for the 30 years long measuring experiment are summarized in Table 8 by means of monthly mean values, providing a useful basis for evaluating the time variation of the latent heat. Table 9 contains the values and ratios of the net radiation (R_n), potential (ET_0) and actual evapotranspiration (ET_a), which proves that the character of the budget and the fluctuation of its components are controlled by the water supply, as usual. Table 10 gives a tool for comparing the values of each components and studying their mean time course.

Key-words: energy budget compounds, heat balance in the soil, sensible and latent heat, potential and actual evapotranspiration, microadvection.

1. Introduction

Micrometeorological processes can be considered as interactions between the atmosphere and the surface, described by the components of the energy- and mass balances. Detailed examination of these processes was carried out at the Agrometeorological Observatory of the University of Debrecen in the years of 1964–1993. The measured data base was analyzed on different time scales. This paper presents the resulted characteristics, representing the micrometeorological processes near the surface in the growing season. On the basis of these characteristics, similarly to the climatic standards, a micrometeorological reference parameter system was determined (micrometeorological standards, MS). These standards represent the features of the surface layer (boundary layer) and the physical meanings of the widely used climatic constants. On the basis of the MS, the normality and extremity of the individual elements, as well as the interrelations of the microclimatic processes can be estimated. Climatic radiation and heat balance of Hungary were analyzed firstly by *Bacsó* (1959), on the other hand *Antal* (1974, 1982) presented the monthly values of the radiation-, heat-, and water balance components on the Lake Balaton (1931–1960), as well as Lake Fertő from 1970 to 1979.

During the 40 years history of the observatory all meteorological elements have been measured, from which micrometeorological parameters can be derived. As the technology improved, a digital measuring system with 6 s time scale was implemented giving a tool for more detailed analysis. For performing continuous measurements of the main meteorological elements, a 30 m high measuring tower was built with 8 stories. Turbulent exchange of the air was observed by sonic anemometer. The soil moisture was examined to 8 m depth.

This paper summarizes the resulted monthly values of the energy budget of natural surfaces. The experiments were carried out in Hajdúhát, at the eastern part of Hungary (47°36'N, 21°36'E, 132 m above the sea level), on lime-covered black loam (chernozem) with natural vegetation and agricultural crops.

2. Radiation budget of the natural surface

The only energy source of the surface energy budget is the solar radiation. The basic task is to determine the temporal change of the energy reaching the surface and the transform of the energy kept back by the surface. Another important question is the amount of energy stored in the few meters high layer above the surface, and the amount passed to upper layers. To solve this problem we have to analyze the energy budget of the surface.

2.1 Global radiation

Our study was carried out on short-cut grassland as reference surface. Energy reaching the surface has a major role, in addition to advection, in the micrometeorological processes. Global radiation was analyzed on the basis of the 30 years long data base providing a useful tool to describe the micrometeorological processes. First the mean, daily, and monthly sums of the global radiation were determined using CM-2 and CM-5-6 type Kipp and Zonen radiation measuring instrument. *Fig. 1* shows the empirical distribution of the daily sums of global radiation in monthly figures. The data of this figure are very similar to the results of detailed measurements analyzed by *Takács* (1958) and *Major* (1976). It has to be emphasized that — especially in spring and autumn — the real distribution is a bit different, since the length of daylight modifies the value of the daily sum. Autocorrelation analysis of the daily sums indicates 8–10 days long significant parts, especially in the summer half-year, which is identical with the results of autocorrelation analysis of anticyclonic situations. The maximum of the empirical distribution of daily sums means the radiation sum of a sunny, cloudless day with minimum extinction.

Our study examined the relationship between the global radiation and sunshine duration. It was pointed out that the relation between the daily sum of the radiation and the number of sunny hours is not linear, so the Angström-type formulas overestimate the global radiation when the sunshine duration is low or high, and underestimate in the case of medium number of sunny hours (*Szász*, 1968). To correct this error, we worked out an empirical formula for middle geographical latitudes:

$$G = V \frac{1.163 C \omega G_{\max}}{2}, \quad (1)$$

where G_{\max} is the intensity of the global radiation belonging to the solar zenith angle of the given day, C is a multiplier belonging to the relative sunshine

duration ($C \leq 1.0$), ω is the duration of daytime in minutes, V is the attenuation coefficient ($V=0.88-1.1$). The applicability and accuracy of this formula were evaluated by many researchers (Bohne and Klingebert, 1977). We founded that in the summer half-year, this method estimated the daily sums with 4.3–5.6% error. Comparative analysis of *Hinzpeter* (verbal note) confirmed this estimation. *Table 1* contains the quotient of the measured and calculated values of monthly sums. Correlation coefficient between the measured and calculated values is $r=0.97-0.99$.

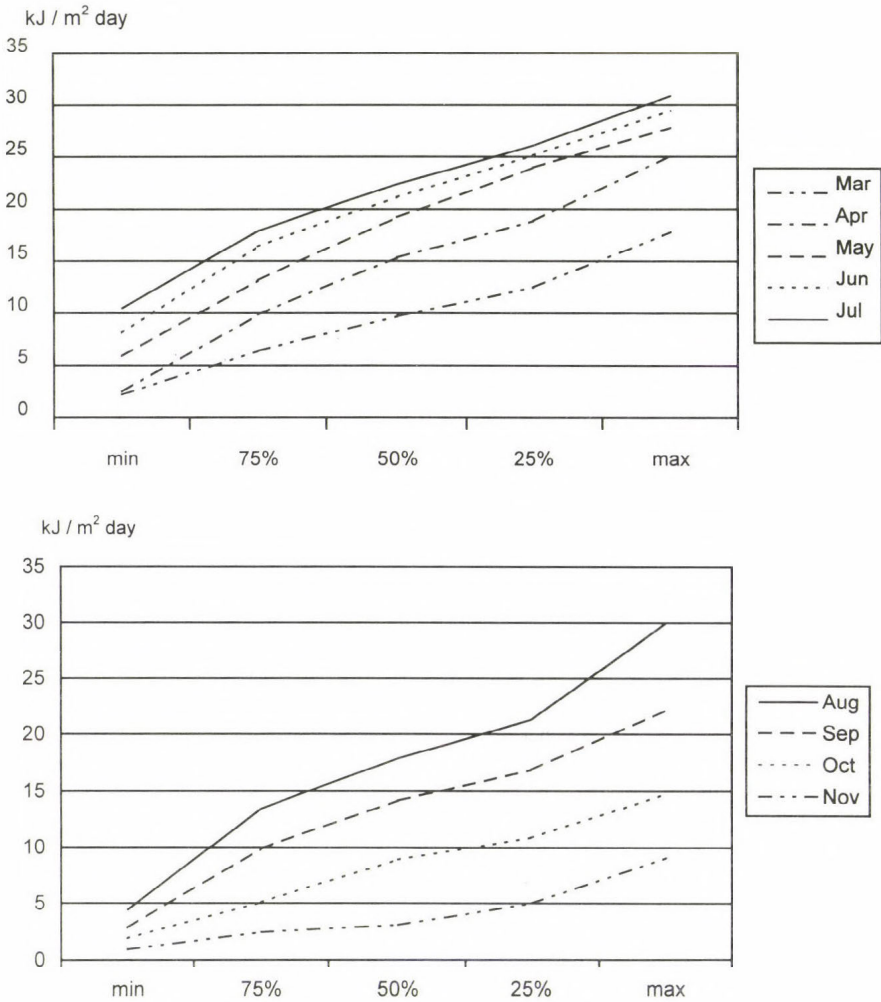


Fig. 1. Relative frequency of daily sums of global radiation in the months of the growing season.

Table 1. Mean values of the attenuation coefficient, V

Month	Jan	Feb	Mar	Apr	May	Jun	Jul	Aug	Sep	Oct	Nov	Dec
V	1.10	1.07	1.12	1.05	0.96	0.95	0.98	0.93	1.00	0.97	0.98	1.06

2.2 Reflection from the surface

Certain part of the radiation reaching the surface is reflected by the ground. The amount of the reflected radiation, relative to the incoming radiation, changes in wide range because of the heterogeneity of the surface. Values of the albedo in Hungary were examined by *Dobosi* (1961) and *Dávid et al.* (1990) providing a general overview, but it is not detailed enough for a particular situation. Our long time data series shows that on the experimental place the moisture content modified the albedo (*Table 2*). Amplitude in the annual course of the albedo is determined by the duration of snow-cover in winter and the precipitation amount in summer. In the vegetation period, the albedo is determined mainly by the vegetation-cover, which depends on the quality and water supply of the soil. Water depletion in the soil — independently from the soil type — increases the albedo. The amount of the reflected radiation is determined by the ratio of the leaf area and the area of the surface, the so called leaf area index. The reflectivity of the surface without vegetation widely varies, it is determined by the volume quotient of the clay in the soil and the soil moisture. The measured spectral distribution of reflection for three main soil structures is shown in *Fig. 2*. Results suggest the conclusion that the reflection increases with raising clay fraction. Another general phenomenon is that the reflectivity of the soil increases with growing wavelengths, independently from the clay- and moisture content. This finding is true for soil structures with few organic matters.

Table 2. Monthly mean values of the albedo of wet and dry soils (%)

Month	Albedo		
	Mean	Dry	Wet
April	16	17	14
May	18	20	16
June	20	23	17
July	22	26	16
August	23	28	15
September	21	24	13
October	18	20	12

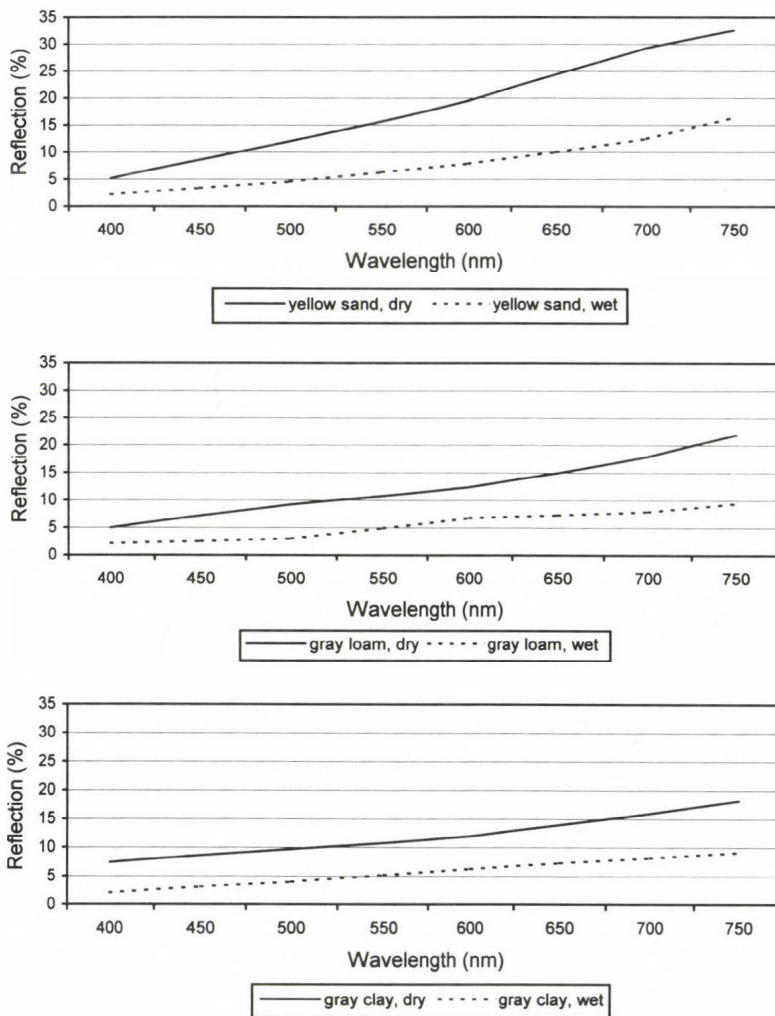


Fig. 2. Spectral distribution of reflection for three main soil structures in the visible range.

Relationship between the intensity of the reflection ($R_{r,\lambda}$) and the wavelength (λ) is as follows, in %:

$$R_{r,\lambda} = 5278 + 0.022 \lambda, \tag{2}$$

where r is the correlation coefficient, $r=0.986$. The high value of the correlation coefficient indicates a nearly linear relation in the 400–1000 nm

range. Bigger clay fraction results in closer linearity. The distribution function can be approached by a parabolic form as well, which makes the formula more accurate, $r=0.985-0.999$. Finally, the general formulas for the main soil structures are as follows, in %:

$$\begin{aligned} \text{Sand:} \quad R_{r,\lambda} &= 5.4 \times 10^{-5} \lambda^2 + 0.124 \lambda - 37.1, \\ \text{Loam:} \quad R_{r,\lambda} &= -3.5 \times 10^{-5} \lambda^2 + 0.091 \lambda - 27.6, \\ \text{Clay:} \quad R_{r,\lambda} &= -0.6 \times 10^{-5} \lambda^2 + 0.036 \lambda - 11.3. \end{aligned}$$

The effect of the moisture content becomes evident in the slope of the linear function fitted into the spectrum. Reflection of sand and clay in wet and dry conditions is illustrated in Fig. 3. The interval between sand and clay is valid for loam soils.

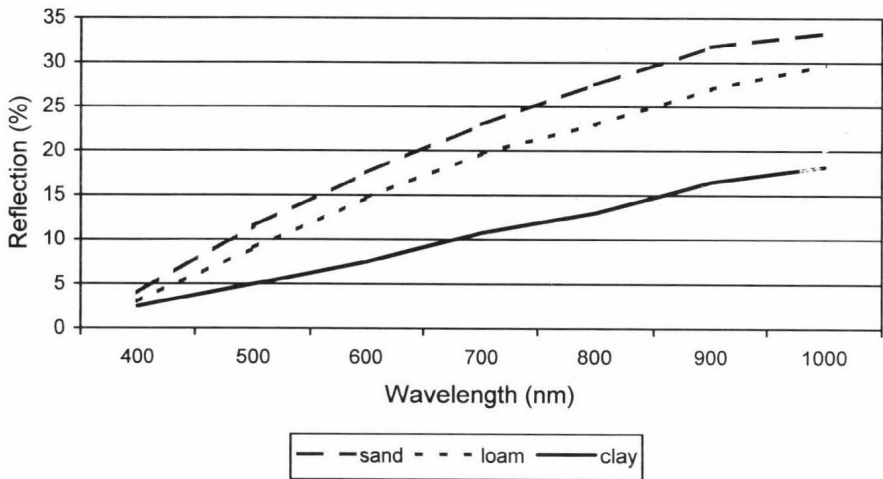


Fig. 3. Reflection of the three main soil structures in the 400–1000 nm range.

Whilst the spectral reflection of the soil linearly increases in the visible range, the reflection of the vegetation is quite different: it is very small in the visible range, then raises to 40–60% in the 750–2500 nm range.

2.3 Effective long wave radiation of the surface

The effective long wave radiation emitted by the surface has the following features:

- (1) The long wave radiation is lower at night than in the daytime during the whole year, because of the local climatic temperature, air humidity, and cloudiness conditions.
- (2) The minimum of the long wave radiation occurs at dawn, and often there is a secondary minimum late at night.
- (3) The main minimum occurs at dawn in the winter half-year and in the evening in summer and autumn. Thermal stratification of the near-surface air layer plays an important role in the temporal variation of the minimum.
- (4) The long wave radiation has its maximum early in the afternoon except the summer months, when the maximum occurs late in the morning because of convective cloud formation.

The long wave radiation strongly depends on the temperature and humidity profiles at night. On the basis of profile measurements we pointed out that there are strong effects modifying the vertical profiles of both temperature and humidity. Measurements, up to 10 m height with lifting technique, indicate horizontal exchange processes, especially late at night. As the inversion is getting stronger at dawn, the exchange processes cease (Szász, 1964b). These effects significantly influence the degree and diurnal variation of the emitted radiation. The lowest mean value of the long wave radiation is not below -25 W/m^2 . The lowest values occur in December at dawn, because at this time the temperature of the surface is the lowest and the stratus clouds become stable. The mean of the highest effective long wave radiation is above 70 W/m^2 , and it can be developed only at the biggest zenith angles in summer.

2.4 The net radiation

The relation between the net- and global radiation is an important question in the study of the micrometeorological processes. The quotient of the net- and global radiation (R_n/R_g) is essential to know, since often we can not calculate the net radiation for lack of necessary data. In that case the net radiation can be calculated from global radiation data, in MJ/m^2 month:

$$R_n = a R_g, \quad (3)$$

where the value of a varies between 0.3–0.6 according to Hungarian authors. *Table 3* presents the published monthly mean values of the a factor. This data well represent the effects determining the net radiation, first of all the effects of cloudiness. Both the mean values and different frequency values can be considered as important parameters of radiation climatology, noting that they

are not valid under other climatic conditions. The values presented by this paper are valid only for the experimental area.

Table 3. Ratio of the monthly mean values of the net radiation and global radiation (*a*)

Author	Mar	Apr	May	Jun	Jul	Aug	Sep	Oct
Bacsó (1959)	0.37	0.42	0.51	0.54	0.59	0.54	0.35	0.22
Major and Tárkányi (1969)	0.33	0.44	0.49	0.50	0.49	0.47	0.39	0.26
Dávid et al. (1993)	0.28	0.46	0.51	0.52	0.50	0.49	0.47	0.40
Szász (1999)	0.35	0.46	0.52	0.53	0.54	0.50	0.42	0.32

The intervals, where the values of the net radiation fluctuate, is not known. For this reason, we calculated the relative distribution of the global radiation and the mean values of the global radiation and net radiation for the days of the summer half-year. It can be concluded that the net radiation on the individual days in the summer months is very variable (*Fig. 4*). Nevertheless, the variability of daily net radiation is smaller than that of daily global radiation.

The curve of the empirical distribution of global radiation has a strong right hand side asymmetry, therefore, days with big radiation energy occur with 15–25% frequency in the months of the summer half-year. Effect of the changing amount of middle layer clouds causes the wide interval of the left hand, downsloping side of the frequency distribution curve. At the same time, in the case of almost total cloudiness, the frequency values steeply decrease. Relative distribution of the daily net radiation — as it seems from data of *Fig. 4* — is considerably shifted to the lower energy ranges. It is worth to emphasize, that frequency distribution of the net radiation is closely symmetrical, and the distribution curve is forced into a much tighter energy range. This phenomenon is caused by the local climatic conditions, therefore, it is representative only for our data base, and can not be generalized. Because of the essential differences of the two distribution curves, the calculation of the net radiation from the global radiation data, using the *a* factors given in *Table 3*, is only a rough estimation. On the other hand, the differences between the calculated and measured daily global radiation data can be considerably big, caused by the very different weather situations. For these reasons, the net radiation was determined by means of measurements.

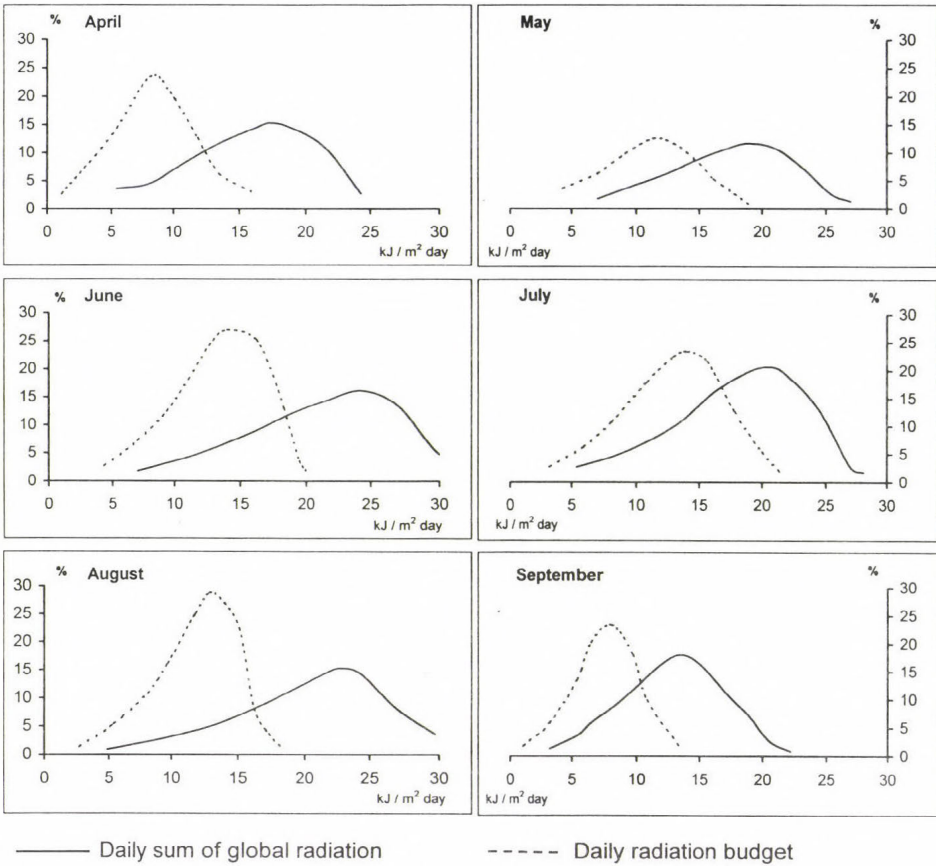


Fig. 4. Frequency distribution of the daily values of global radiation and net radiation.

3. Heat balance in the soil

Heat exchange in the root zone and soil temperature are very important agroecological factors. The soil stores and transports both energy and water. Therefore, there is a close relationship between the water- and heat exchange, where the water content of the individual soil layers deterministically influences the heat exchange.

Analysis of the soil heat flux was based on the Fourier's equation of heat conduction. We determined the most important factors evoking the soil temperature changes of energy gain and loss.

Determination of the soil heat transport is a difficult task, as the heat fluxes not only by molecular conduction, but infiltration of water in the soil.

The amplitude of the diurnal variation of the soil temperature can be derived by Fourier analysis, but only in case of enough effecting factors. Two or three factors are used in practice. Analyzing the weighed spectral distribution of the frequency, we found that the generally used calculation method is only an approaching estimation, because much more factors are needed. The molecular heat conduction can be determined by instrumentally (Szász, 1964b) providing more accurate results. The width of the frequency distribution of the molecular heat conductivity coefficient is 0.3–1.6 W/m² K. The large standard deviation of the coefficient is caused only by the moisture fluctuation. Determination of the heat capacity and conductivity was a much easier task. A representative data base is available about these features, calculated by widely used methods (Szász, 1970).

One of the most important thermophysical parameters describing the soil heat flux is the decline in amplitude (D) of the diurnal variation of the soil temperature with depth. The value of D can be calculated by the formula $D=(2k/\omega)^{0.5}$ (Rose, 1966), where k is the temperature conductivity and ω is the length of the period. There are numerous data measured at our experimental station about the temporal variation of thermal conductivity, molecular heat conductivity (λ), and heat capacity of the soil (Szász, 1970, 1988; Molnár, 1977).

The heat balance in loess soil can be described by soil temperature and moisture data measured by a so-called 'soil heat-flow transducer' instrument during ten years. On the basis of these data, we determined the phase shift of diurnal variation of heat conductivity and temperature, as well as the values of D . Data of each layers were examined and compared to each other, concluding that the soil is thermally anisotropic (Table 4). Searching for the reasons of the differences, above all one can think on the differences in the soil moisture profiles. The thermal anisotropy can be very high, mainly in the soil layer near the surface, nevertheless, there is a significant ratio-gradient in the deeper layers of the examined soil, because at the measuring place the soil water table situates in depth of 10–12 m, from where the water income, raised by capillarity as well as upstreamed by water potential, is very small. It means that the moisture content of the upper soil layers at our experimental station is controlled by the weather only.

Annual variation of thermophysical parameters of the soil is peculiar. Minimal values of the annual variation of the *heat capacity* (2.1 J/cm³ K) occur in the second part of summer caused by summer soil moisture depletion. Maximal values are consequences of snow melting. Annual variation of *heat conductivity* also has only one peak, as it is the function mainly of soil moisture. The *amplitude of temperature* is controlled by the moisture content, too. The diurnal variation of the temperature has a minimum at the end of

June, beginning of July (0.9 m), since the soil is dried up in the following period and the heat conductivity decreases. In spite of the previous variations, the annual variation of *temperature conductivity* can be described by a curve with two peaks. As both the big and small soil moisture contents decrease value of temperature conductivity, its minimum evolves at the time of minimal and maximal soil moisture, while its maximum develops at the beginning of soil moisture depletion and in the period of filling up with precipitation water.

Table 4. Ratios of temperature conductivities in the successive soil layers

Soil layer z/z_{+1}	Temperature conductivity kz/kz_{+1}
2-5/5-10 cm	0.31
5-10/10-20 cm	1.08
10-20/20-50 cm	0.57
50-100/100-150 cm	1.00
100-150/150-200 cm	0.71

Table 5. Values determining the energy budget of the loam soil in different months

(G_M is the daily balance of the heat flux, G_n is the total amount of energy, G^+ is the downward energy, G^- is the daily amount of energy conducted to the surface, G^+/G^- is the ratio of the upward and downward conducted energy amounts, and E_n is the duration of energy uptake)

Month	G_M	G_n	G^+	G^-	G^+/G^-	Unit	E_n
April	561.0	4264.4	2412.7	164.5	14.7	KJ/m ² day	10 ^h 15'
May	641.1	5365.3	3003.2	2362.1	1.3	KJ/m ² day	10 ^h 30'
June	573.6	6386.1	3458.8	2885.1	1.2	KJ/m ² day	12 ^h 00'
July	253.1	7027.2	3640.1	3387.1	1.1	KJ/m ² day	11 ^h 10'
August	-341.7	6592.7	3125.5	3467.2	0.9	KJ/m ² day	9 ^h 50'
September	-164.5	4171.6	2003.6	2168.1	0.9	KJ/m ² day	8 ^h 10'
October	-801.4	4378.3	1796.9	2598.3	0.7	KJ/m ² day	7 ^h 50'
November	-615.8	1577.5	480.9	1096.7	0.4	KJ/m ² day	6 ^h 10'

Table 5 shows an overview of monthly, layer-by-layer soil temperature values in the 200 cm layer. On the basis of the daily balance of soil heat flux, temporal variation of soil temperature can be explained. Table 5 presents the daily average values of the heat balance for different months. The presented data suggests that the soil heat flux plays more important role in the energy

budget mainly in spring and autumn, however, its part is only few percents of the net radiation. In July and August, when the sign of the balance changes, daily balance has a very small share in the energy budget. These values are 4–5% by monthly means, the amount of energy reaching the surface from deep layers compared to the net radiation is significant only in October. The soil heat flux is 12–18 percent of the net radiation, and the main part of it is transferred to the air in the afternoon.

4. Sensible and latent heat balances

As it was mentioned, the soil heat flux shares the sum of the net radiation only in a few percents, the main part of the net radiation is used for maintaining the latent and sensible heat fluxes. Ratio of the sensible and latent heat fluxes is climatically characteristic value, therefore, we analyze these two processes separately.

4.1 The sensible heat flux

Vertical and temporal variations of the temperature, caused by the transform of sensible heat energy are important processes in agroecological point of view. The sensible heat depends on two factors: horizontal advection and the amount of the heat energy transmitted by the surface. It is certain, that only a small part of the sensible heat, transmitted to the air from the surface, remains in the near surface layer, but even this energy causes significant air temperature changes mainly in vertical direction. Approaching the surface, the temperature extremes significantly increase, which can be expressed by the difference between the minimum and maximum temperature values. To prove this fact, *Table 6* presents some measured data. Thermal stratification of the surface air periodically changes during the day in the summer half-year almost without exceptions, day-time lability is changed by night-time stability. The maximal lability is developed at noon, while the maximal stability is observed late in the evening. Cyclic variation of the equilibrium determines the direction of the sensible heat flux in the surface air. It is both theoretical and practical problem, that at the time of the transformation of equilibrium, the inflexion point of the vertical temperature profile falls to the measured height domain, therefore, the profile has an extreme value in this layer. In these cases, the estimation of the heat flux is very difficult, very often impossible. Unfortunately, one of the biggest the disadvantages of the calculations based on gradient method is that the error in the heat flux intensity value is the biggest in the morning and evening when the inversion develops and

disappears. Mainly this is the explanation for the facts, that the vertical temperature difference is small between the two above mentioned layers and the dispersion among the individual days varies in wide range, explained by the different weather features. In the morning, the air temperature gradients change without disturbances, except for the disturbing effects of the clouds caused by the morning lability in the summer half-year. The units and amount of the gradients are expressed by the means of the adiabatic gradient. Thus, the value of the effectively measured gradient is $\Delta T = 0.0098 \times 10^2 / \Delta z$.

Table 6. Daily temperature range on clear days in different heights above surface (°C)

Height (cm)	April	July	September
800	12.4	13.2	12.1
400	12.6	13.7	12.5
200	13.0	14.1	13.0
50	13.6	14.9	13.9

Note: The sample is based on differences of minimum and maximum values of 60 days

The mentioned facts provide only an informative summary, but it can be generalized since the measured data base is extensive. On the basis of the variation of vertical temperature differences, we can conclude that the vertical heat flux varies in very wide range. The change of the sensible heat flux depends mainly on the soil moisture content. When the soil moisture content is big, the heat energy is used for evaporation. In case of smaller soil moisture content, the vertical heat flux is bigger. It can be proved by the next data, calculated for different moisture contents (different values of minimal water capacity in percents) of the upper soil layer:

$$\begin{aligned}
 0.8 W K_{\min}: H/(R_n - G): 15 - 25, \\
 0.5 W K_{\min}: H/(R_n - G): 25 - 40, \\
 0.3 W K_{\min}: H/(R_n - G): 40 - 90,
 \end{aligned}$$

where H is the vertical heat flux, R_n is the net radiation, and G is the heat flux in the soil. These data strengthen the relation between the soil moisture and the vertical heat flux, which is strongest in the summer months. This relation declines with the decrease of global radiation and daily net radiation.

There is a close relation between the vertical sensible heat flux and the turbulent exchange, since the transmitted heat amount is determined by the vertical air temperature gradient as well as the intensity of the exchange processes.

As the wind speed can have very variable values, the sensible heat flux has big fluctuation during the day. Therefore, in addition to soil moisture, the wind speed is an important factor which influences the heat exchange in the air.

Vertical sensible heat fluxes have medium order of magnitude between the magnitude of soil heat exchange and latent heat flux in the energy balance of the surface. Although both have great variability, the distribution curves of the values partly cover each other. The reason of great variability is that the heat exchange with the air depends on many factors. We have pointed out the heat capacity of the upper soil layers, since the warming and cooling of light soils cause intense day-time lability, while late in the evening, when inversion is developed, a strong temporal stability is evolved, which weakens for the night hours. According to our statistical analyses, there is a strong correlation between the daily fluctuation of the soil temperature in the upper 10 cm layer and the vertical heat flux in summer ($r = 0.89$; $n = 95$).

Regarding monthly sums of sensible heat fluxes, the average heat amount passed to the air is generally small in spring because of the moderate amount of radiation energy and the big soil moisture content. In summer, the sensible heat increases with the soil moisture depletion and the increase of the energy reaching the surface. In autumn a smaller part of the radiation balance is shared to the sensible heat amount again, because the exchange processes slow down.

4.2 The latent heat flux

In agroecological point of view, the latent heat flux has great importance, because this is the energy equivalent of the evapotranspiration and dew. Diurnal changes provide useful information in the analysis of daily dynamics in 1–2 hours range. First of all, our purpose was to determine the evaporation loss. For the calculation we used the concept of *Penman* (1956) and *Monteith* (1973). The value of the evaporation has an upper limit, since, supposing that there is no advection, this value should not be greater than the water equivalent of the net radiation. Agroecological researches were carried out on both small and big resolution of temporal variations. Terminology connected to evapotranspiration is as follows:

- *potential* evaporation and -evapotranspiration (ET_0 , in $W\ m^{-2}$, MJ/m^2 units), or its water equivalent;
 - *effective* or *actual* evaporation and -evapotranspiration (ET_a , in W/m^2 , $MJ\ m^{-2}$ units), or its water equivalent;
 - *generally*: the energy used for evaporation of water (evaporation + transpiration – LE , in W/m^2 time, kJ/m^2 time units), or its water equivalent.
- The *Penman-Monteith* method, modified by *Monteith* (1973, 1975), was used in our study:

$$LE = \frac{\Delta(R_n - G) - \rho c_p (e_0 - e)/r_a}{\Delta + \gamma(1 + r_s/r_a)}, \quad (4)$$

where Δ is the value of saturation vapor pressure for 1°C (de_0/dT), R_n is the net radiation, G is the soil heat flux, ρ is the air density, c_p is the specific heat of the air at constant pressure, e_0 is the saturation vapor pressure, e is the real vapor pressure, γ is the psychrometric constant, r_a is the aerodynamic resistance, and r_s is the plant diffusion resistance.

If r_s refers to limited soil moisture exchange, the formula results in the actual evapotranspiration, otherwise, if the water supply in the root zone is near the field capacity the evapotranspiration is potential.

4.2.1 Potential evapotranspiration (ET_0)

In the first period of our investigation we worked out an empirical formula for estimating the potential evapotranspiration (Szász, 1973). It can be used even if daily average air temperature and daily average relative humidity data are available only. The value of the correlation coefficient between the measured potential evapotranspiration and the mentioned air temperature and humidity values is $R = 0.94$ on days without precipitation. On the basis of this close correlation, we could develop a formula which was exact enough for our investigations. The basic relation is: $ET_0 = Y = f(t, R, u)$, where Y is a function of t (temperature in $^\circ\text{C}$), R (relative saturation), and u (wind speed in m/s). Limiting condition of this relation is: $ET_0 = Y = 0$, if $R = 1$. In this case, the function which satisfies the condition and fits the relation is:

$$ET_0 = A(t) (1 - R)^b \rightarrow \log ET_0 = \log A(t) + b \log(1 - R). \quad (5)$$

This relation can be considered linear with good approximation, the slope of the fitting line is independent of the temperature. The value of b is monotonously increasing with the increasing temperature. Accepting the values below 0°C , the reduced determination coefficient of the function fitted to the common b is $r^2 = 0.989$, the common b value is $b = 0.66$. Temperature has a major role in these relations, its computational formula is

$$A = a (t - t_0)^2. \quad (6)$$

Extracting square root of both sides and completing the operation we get: $a = 0.005356$ and $t_0 = 20.89^\circ\text{C} \cong 21^\circ\text{C}$. As final result we get the approaching

equation for the potential evapotranspiration, in the function of temperature and relative humidity, as follows:

$$ET_0 = 0.005356 (t + 21)^2 (1 - R)^{2/3} . \quad (7)$$

There is no linear relation among the daily average values of potential evapotranspiration, temperature, and relative humidity. In this way, this relation differs from the generally used formulas.

Comparing the calculated potential evapotranspiration with the values measured by evaporation pans, it can be concluded that the evaporation of pans is subject to significant microadvective effect. We examined the energy exchange of the evaporation pans in details calculating the values of microadvection. There was no significant difference between the measured potential evapotranspiration, corrected with the microadvection effects, and the calculated values. This empirical relation was controlled by the Penman-Monteith equation, which proved a good agreement in the case of considering microadvective effects. A so-called oasis-effect, a microadvective phenomenon develops in radiation conditions and the summer half-year, which can be both negative and positive, because in the case of a rapid cooling the soil loses its stored heat sooner than the water. On the basis of numerous comparative measurements and computations we determined the numerical value of the microadvective effect, which was integrated into our evapotranspiration estimating model in the following form, in mm/day:

$$ET_0 = c [0.005356 (t + 21)^2 (1 - R)^{2/3}] . \quad (8)$$

The effect of microadvection increasing the evapotranspiration, $c \geq 1$, which can reach the 1.5 mm/day value in summer. This is 35% of the physically real value.

It is worth to compare the water equivalent of net radiation with the daily average values of evapotranspiration (*Table 7*). The ratios presented by the table indicate that the energy remaining for the heat exchange between the soil and air is 26% at the end of spring, about 20% in summer, and 4–10% at the end of the growing season. Furthermore, in the average of the eight months, 85% of the net radiation is shared by the potential evapotranspiration, on our experimental area from March to November. In the agrometeorology and the energy- and water management practice the potential evapotranspiration can be considered as a frame number providing an information about the water shortage and surplus, and their degree. This is the reason for considering potential evapotranspiration as an essential factor in the investigations of water balance. We note, that in irrigation practice the value of potential

evapotranspiration is considered as the upper limit of the water consumptive use of plant stands.

Table 7. Water equivalent and ratio of net radiation and potential evapotranspiration (R_n is net radiation, PE_0 is potential evapotranspiration in mm/day)

	March	April	May	June	July	August	September	October
R_n	1.43	3.34	4.26	4.49	4.89	3.82	2.23	1.27
PE_0	1.34	2.47	3.19	3.67	3.94	3.61	2.01	1.22
PE_0/R_n	0.93	0.74	0.74	0.82	0.81	0.94	0.90	0.96

4.2.2 Actual evapotranspiration (ET_a)

The energy used for the actual evapotranspiration and water consumption of the vegetation is the component taking the biggest part of the heat balance over Hungarian climatic conditions. This part is estimated as 65% in yearly course by the researchers, nevertheless, its daily value can vary between 35–95% depending on weather and vegetation conditions.

For a short period (hours) the actual evapotranspiration is calculated with the aerodynamic method, Bowen-ratio, or Penman-Monteith equation. In the case of calculating daily averages, the following simplified formula can give a reasonable result:

$$ET_a = ET_0 \frac{\Delta + \gamma}{\Delta + \gamma(1 + r_s/r_a)}, \tag{9}$$

where ET_0 is the value computed by Eq. (8), Δ is the slope of the saturation vapor pressure curves in hPa °C unit, γ is the psychrometric constant, and r_s/r_a is the ratio of diffusive resistances of the vegetation and air. When estimating the diffusive resistance of the vegetation, r_s , values concerning xerophilous plants are suitable to use ($r_s > 6$ m/s). r_a is the reciprocal of the exchange coefficient.

Aerodynamical resistance is the function of wind speed and the height of vegetation. In the case of 5–10 cm high grass, its approaching values at different wind speeds are as follows:

u	1	2	3	4	5	m/s
r_a	125	75	60	45	40	s/m

Stomatal resistance can be exactly estimated by *Jarvis'* method (1976). Knowing the daily amounts of evapotranspiration and the mass of the vegetation, we can separate the values of the evaporation from bare soil and the transpiration. In the case of short-cut grass as reference surface, the transpiration is 40–60%, the remaining 60–40% is for the evaporation from bare soil. In the case of agricultural crops, the evaporation from bare soil is 10–30%.

Table 8 shows the hourly average values of evapotranspiration as the average of 21 years of the 1964–84 period in W/m^2 . The hourly average values provide good overview of the dynamics of diurnal variation of evapotranspiration and the amount of used heat energy. According to our calculations, the biggest value of the evapotranspiration is about 0.3–0.4 mm/hour measured in July, but in the most cases the amount of the loss of water is much smaller. The table contains the values of the night-time negative evapotranspiration, i.e., the amount of energy released during dew formation. It is remarkable, that maximum amount of dew is formed at dawn, just before the temperature minimum occurs. Evapotranspiration data given in the table provide a useful overview of every hours of the vegetation period.

On the basis of the data of *Table 9*, diurnal variation of the water equivalents of the potential and actual evapotranspiration and net radiation can be determined. Values in the first column of the table $((R_n - G)/L)$ expresses the amounts of energy, which can be used for evaporation, i.e., the possible maximum values of the daily potential evapotranspiration. Second column contains the measured average values of evapotranspiration, third column shows the ET_a values. An important climatic information is that how large part is the ET_a of the energy usable for evaporation. There is a characteristic dynamics in the changes: in the month following the winter the evaporation becomes large, but for April and May, the water supply significantly decreases, so the energy used for evaporation is only the 40% of the potential amount, then at the time of precipitation maximum, this part is more than 50%, which is continuously increasing in autumn in consequence of atmospheric evaporation.

5. Energy exchange between natural surface and surface air

To describe the interaction between the surface and the atmosphere is possible with analyzing the amount of energy reaching the natural surface and the transport processes of the surface air. The simplest and most certain method of this analysis is to determine the energy balance components. Monthly values can be determined on the basis of the few decades long study. *Table 10*

Table 8. Hourly average values of the actual evapotranspiration (in W/m²), measured at Debrecen, during 1964–1984

Hour	March	April	May	June	July	August	September	October	November
0–1	-18.0	-20.2	-26.9	-37.7	-51.8	-10.8	-6.4	-3.4	-7.1
1–2	-15.7	-19.2	-26.9	-42.4	-42.1	-10.8	-7.2	-28.7	-8.2
2–3	-16.9	-24.5	-40.8	-54.9	-43.3	-8.8	-4.6	-21.2	-7.5
3–4	-12.9	-32.7	-45.6	-35.7	-13.5	-6.0	-17.7	-22.2	-3.9
4–5	-18.8	-11.9	-13.7	-54.2	-6.7	-35.0	-23.8	-30.9	-3.8
5–6	-25.5	-25.7	-0.2	4.2	-5.1	-74.4	-44.0	-43.4	-3.6
6–7	-20.7	16.9	50.1	70.5	85.5	7.6	-20.8	-47.9	-5.7
7–8	10.6	62.8	105.4	112.2	122.7	37.4	20.4	-0.6	-13.9
8–9	65.8	117.8	145.5	144.6	145.1	70.5	52.0	54.0	6.5
9–10	90.1	152.5	191.8	197.5	200.0	106.5	98.6	78.8	30.3
10–11	109.2	182.3	220.4	223.2	232.6	136.2	131.0	99.4	46.4
11–12	129.5	193.9	231.6	229.4	264.0	151.3	149.7	107.1	62.7
12–13	131.8	180.9	203.4	213.4	256.1	163.8	147.3	82.2	52.3
13–14	126.4	175.6	199.2	211.6	245.9	160.6	122.1	80.8	48.1
14–15	103.4	144.4	171.1	174.0	222.4	144.4	118.6	55.9	19.6
15–16	54.5	92.4	139.1	191.0	182.4	111.7	86.1	-20.1	-11.4
16–17	3.9	46.5	127.2	149.6	125.2	87.6	23.5	-24.1	-7.5
17–18	-10.3	8.2	56.4	116.4	36.3	-1.0	-27.0	-16.0	-4.3
18–19	-13.4	-7.1	30.7	8.4	-54.9	-22.7	-4.0	-7.3	-3.9
19–20	-16.4	-10.8	-11.1	-14.0	-17.9	-9.1	-71.0	-7.7	-17.0
20–21	-16.6	-23.5	-8.8	-21.2	-14.9	-8.3	-4.2	-10.2	-17.6
21–22	-16.3	-17.2	-9.4	-21.1	-17.4	-8.3	-8.0	-9.1	-15.3
22–23	-14.4	-18.0	-20.8	-27.4	-17.3	-11.0	-5.4	-4.0	-14.2
23–24	-16.1	-16.6	-25.7	-31.0	-20.1	-11.5	-7.8	-8.2	-14.9

Table 9. Average water equivalents of the potential and actual evapotranspiration and net radiation for the different months

Month	$(R_n-G)/L$ mm/day	ET_0 mm/day	ET_a mm/day	ET_a/ET_0	$(ET_a/R_n-G)/L$
March	1.43	1.34	1.19	0.89	0.83
April	3.34	2.47	1.42	0.57	0.43
May	4.26	3.91	1.78	0.46	0.42
June	4.49	3.67	2.32	0.63	0.52
July	4.89	3.94	2.47	0.62	0.51
August	3.82	3.61	2.32	0.64	0.61
September	2.23	2.01	1.38	0.67	0.62
October	1.27	1.22	0.81	0.66	0.64

Table 10. Average values of the components of energy exchange between the surface and the boundary layer, measured at the Agrometeorological Observatory of Debrecen, during 1961–1993

Components	Mar	Apr	May	Jun	Jul	Aug	Sep	Oct	Nov
R_n (month)	105.6	202.5	298.4	322.9	347.2	291.0	190.8	102.4	-2.1
(day)	3.41	6.75	9.63	10.76	11.2	9.39	6.36	3.30	-0.1
G (month)	3.6	-9.7	-15.0	-20.1	-18.8	-11.1	2.81	11.1	14.5
(day)	0.12	-0.31	-0.50	-0.65	-0.61	-0.36	0.09	0.39	0.48
H (month)	-17.1	-86.0	-145	-128	-136	-99.5	-89.2	-51.5	22.0
(day)	-0.55	-3.24	-4.66	-4.27	-4.39	-3.21	-2.97	-1.66	0.73
LE (month)	-92.1	-107	-139	-175	-192	-180	-104	-63.6	-34.4
(day)	-2.97	-3.56	-4.48	-5.82	-6.20	-5.82	-3.48	-2.05	-1.11
H/R_n	0.16	0.42	0.48	0.40	0.39	0.34	0.47	0.50	-0.10
LE/R_n	0.87	0.52	0.47	0.54	0.55	0.62	0.55	0.62	-
Temperature °C/day	4.8	10.3	17.5	18.4	20.0	19.2	15.2	9.7	3.8
Vapor pressure mbar	6.5	8.5	12.2	15.2	16.2	16.4	13.3	9.7	6.9
Equivalent temperature °C/day	16.3	21.6	30.5	38.0	40.5	41.0	33.3	24.3	14.2
Change of enthalpy kJ/kg day	2.57	.37	5.99	4.52	2.89	-1.34	-5.53	-4.65	-4.31

summarizes the components of the radiation balance and energy exchange in the boundary layer. Theoretically we assume that the components of energy balance are free from advection. This is an acceptable consideration, as the examined area is a plain surface with natural vegetation, and the agricultural crops are farther away. For this reason, the assumption, that surface air represents the friction (planetary boundary) layer suitable for the physical features of the surface, and that the components of the energy balance express the natural conditions of the soil-plants-atmosphere system, seems real.

The first row of Table 10 contains the 30 years averages of the monthly and daily values of the energy balance components. Considering that the examinations were carried out for agroecological reasons, the late autumn and winter months are not represented. Changes in the monthly values of the energy balance components represent the amount of energy transferred by the surface. Ratios of the different components well represent the local climate characteristics of this area.

Temporal change of the components is a useful information, but analyzing their ratios is more interesting. Thus, the share of the sensible and latent heat in the net radiation can be considered as the most important climatic factor. Ratios H/R_n as well as LE/R_n showed in Table 10 are values determined by daily measurements, and they are representative climatic parameters of the observational area. Latent energy shares a big part in the net radiation in the beginning of spring, and then at the end of spring it halved. It alludes to the relatively small amount of soil moisture stored from the winter precipitation, and that it significantly decreases until June in the upper soil layers. At our experimental area the precipitation maximum occurs in June, therefore, the ratio of latent energy increases and becomes stable depending on the precipitation amount, moreover, it can exceed 60% at the end of summer. This later ratio does not mean the increase of the evaporation, but that the decrease of the evaporation is slower than that of the net radiation.

In the average of the three summer months, H/R_n is 51% and LE/R_n is 57%, thus a near equilibrium state is formed between the two ratios. This is a reason for Hungary to be classed among the climatic categories with medium dry summer. It has to be mentioned that there are significant deviations from the average values in the individual years, caused by different prevailing weather conditions of different years.

In the years with Mediterranean weather, when there is a precipitation maximum in winter and a minimum in summer, the mentioned ratio is about 30–40%, and what is more, in extremely dry years it can be considerably decreased below 30%. If cool, oceanic effects influence the year, the value of the LE/R_n ratio can reach 75–80%, thus the fluctuation around the average value is 20%. This ratio and its large fluctuation around the average value are

good evidences of the inclination of the Hungarian climate to have extreme situations. This feature can not be proved by comparison of climatic elements only. Therefore, the study of the ratios provides a useful tool for not only to describe the features of the surface air layer, but it gives exact, considerable data for physical description of the climate.

Summarizing the results, we can state that the systematic, 30 years long research of the energy budget have made numerous important conclusions possible on the fields of climate, micrometeorology, and agroecology.

References

- Antal, E.*, 1974: Heat- and water balance on the area of Lake Balaton (in Hungarian). In *Climate of the Lake Balaton* (eds.: *B. Béll* and *L. Takács*). Országos Meteorológiai Szolgálat, Budapest, 187-273.
- Antal, E., Kozma, F., Kozmáné Tóth, E., Nagyné Dávid, A., and Walkowszky, A.*, 1982: Climate of the Lake Fertő – Radiation- and heat balance (in Hungarian). In *Natural Bases of the Lake Fertő* (eds.: *Z. Kováts* and *E. Tóth Kozmáné*). Északdunántúli Vízügyi Igazgatóság–Orsz. Meteorológiai Szolgálat, Budapest, 44-124.
- Bacsó, N.*, 1959: Climate of Hungary (in Hungarian). Akadémiai Kiadó, Budapest.
- Berényi, D.*, 1964: Microclimatological experiments at Hortobágy in the years 1961 and 1962 (in Hungarian). *Acta Univ. Debreceniensis, Ser. Geogr., Geol. et Meteorol. Tom. IX. Ser. II.*, 3-28.
- Bohne, K. and Klinkenberg, F.*, 1977: Zur Berechnung der Globalstrahlung nach Szász. *Zeitschr. Meteorol.* 27, 162-168.
- Brogmus, W.*, 1959: *Zur Theorie der Verdunstung der natürlichen Erdoberfläche*. Deutsch. Wetterdienst, No. 21. Hamburg.
- Budiko, M.J.*, 1956: *Heat Balance of the Planetary Boundary Layer* (in Russian). Hydrometeorological Press, Leningrad.
- Dávid, A., Takács, O., and Tiringér, Cs.*, 1990: Distribution of the radiation balance in Hungary, in the period of 1951-1980 (in Hungarian). Országos Meteorológiai Szolgálat Kisebbségi Kiadványai, No. 66, Budapest.
- Dobosi, Z.*, 1961: Application of albedo in climatology (in Hungarian). *Időjárás* 65, 354-366.
- Högström, U.*, 1974: A field study of the turbulent fluxes of heat, water, vapour and momentum at a „typical” agricultural site. *Quart. J. Roy. Meteorol. Soc.* 100, 624-639.
- Jarvis, P.G.*, 1976: The interpretation of the variations in leaf water potential and stomatal conductance found in canopies in the field. *Philos. Trans. Roy. Soc. London, Ser. B.*, 273, 593-610.
- Lettau, H.H. and Davidson, B.*, 1957: *Exploring the Atmospheres First Mile*. Vol. 1-2. Pergamon Press, N. Y.
- Major, G.* (ed.), 1977: *Solar Radiation in Hungary* (in Hungarian). Magyarország Éghajlata Sorozat, No. 10. Országos Meteorológiai Szolgálat, Budapest.
- Major, G. and Tárkányi, Zs.*, 1969: Areal distribution of the calculated radiation balance in Hungary (in Hungarian). *Időjárás* 73, 81-85.
- Monin, A.S. and Obukhov, A.M.*, 1954: Basic principles of the turbulent motions in the planetary boundary layer (in Russian). Publications of the Geophysical Institute of the Academy of Sciences, USSR, No. 24, 163-184.
- Molnár, B.*, 1977: Thermophysical examination of loess soil in Hajdúság (in Hungarian). PhD. Thesis, Debrecen.

- Monteith, J.L., 1963: Gas exchange in plant communities. *Proc. Symp. Held Canberra 1962*, Acad. Press, London, 95-112.
- Monteith, J.L., 1973: *Principles of Environmental Physics*. E. Arnold, London.
- Monteith, J.L., 1975: *Vegetation and the Atmosphere*. Acad. Press, London, Vol. I.
- Penman, H.L., 1956: Evaporation – an introductory survey. *Neth. Journ. of Agr. Sci.* 4, K. 9-29.
- Rákóczi, F., 1988: *The Planetary Boundary Layer* (in Hungarian). ELTE University Press, Budapest.
- Rose, C.V., 1966: *Agricultural Physics*. Com. Internat. Libr., Pergamon Press, Oxford.
- Schmidt, W., 1925: *Der Massenaustausch in freier Luft und verwandte Erscheinungen*. H. Grand, Hamburg.
- Sverdrup, H.U., 1936: The eddy conductivity of the air over a smooth snow field. *Geophysiske Publ., Ser. 11*. Nr. 7, 1-69.
- Szász, G., 1964/a: Observations of diurnal variation of soil conductivity (in Hungarian). *Agrokémia és Talajtan* 13, 137-148.
- Szász, G., 1964/b: Bestimmung der nachtlischen Mikroadvektion durch Ausstrahlungsmessungen. *Angew. Meteorol.* 5, 7-12.
- Szász, G., 1968: Calculation methods for global radiation (in Hungarian). *Debreceni Agrártudományi Főiskola Tud. Közleményei*, 239-259.
- Szász, G., 1970: Heat exchange in loess soil at Debrecen (in Hungarian). *Időjárás* 74, 353-392.
- Szász, G., 1973: New method for potential evapotranspiration calculations (in Hungarian). *Hidrometeorológiai Közlemények*, 7, 435-442.
- Szász, G., 1988: *Agrometeorology* (in Hungarian). Mezőgazdasági Kiadó, Budapest.
- Szász, G., 1999: Role of agricultural crops in the surface-atmosphere interactions (in Hungarian). *DSc. Thesis*. Hungarian Academy of Sciences, Budapest.
- Szász, G., 2001: Micrometeorological and energetical problems of flows over heterogeneous surfaces (in Hungarian). *Berényi Dénes Jubileumi Kötet*, Debrecen.
- Szász, G., 2002: Speed extriction of wind over and within plant canopy on heterogeneous surface (in press).
- Takács, L., 1958.: Normalwerte der Globalstrahlung in Budapest. *Időjárás* 62, 65-71.

IDŐJÁRÁS

Quarterly Journal of the Hungarian Meteorological Service
Vol. 106, No. 3–4, July–December 2002, pp. 185–196

Hydroecological risks of crop production in Hungary

István Orlóci and Károly Szesztay

*Water Resources Research Centre,
P.O. Box 27, H-1453 Budapest, Hungary*

(Manuscript received February 1, 2002)

Abstract—It is through hydroecology and the soil moisture regime that water accomplishes her major planetary role: the support of plant and animal life. Within the evolution of terrestrial life forms, nature has elaborated a sophisticated and efficient mechanism for the harmonization of the regulatory processes of the soil-water-vegetation system within the broad framework of the climate-lithosphere-biosphere interaction. Man is now intervening into this regulatory mechanism at a rapidly increasing scale and without a clear and reliable knowledge of the long term consequences of his interventions. The expectable significant and rapid change of climate due to the increasing greenhouse effect is a good, and perhaps the last, opportunity for learning how to restrain our technological and economic capabilities according to the limits set by the carrying capacity of the biosphere. As assessments reveal, the conventional step-by-step analytical research must frequently be supplemented by and combined with management-oriented empirical solutions.

Key-words: soil moisture, evapotranspiration, water balance, irrigation water demand, deforestation, salinization.

1. Hydroecology and crop production

Crop production — lying at the heart of agriculture, food supply, and population growth — can be looked upon in two ways: as the greatest success story of mankind removing the ecological barrier of population size and holding the promise of Paradise for all, or as the largest human intervention into the nature's functioning lying at the hearth of the present environmental crisis and hiding the danger of a catastrophic falldown of our civilization. Both visions are valid and might become our common future pending on motivations, attitudes, and decisions of individuals and governments during the years and decades to come.

History offers ample examples for both, the successful harmonization of crop production with landscape ecology, and an almost total and irreversible deterioration of soil resources and natural ecosystems caused mostly by *complete deforestation* followed by intensive cultivation. Total deforestation can increase the rate of *soil erosion* by a factor of 100 or even 1000 (from 1–20 t km⁻² in the forests to 1000–2000 t in cultivated areas) as documented, e.g., by depositions of the Neolithic agriculture in Europe, as well as the late Bronze age and Roman agriculture in Southern Europe and Britain.

A slower and more subtle form of deforestation-caused soil degradation has been experienced in the flatlands of Hungary. Due to basin-type hydrogeological structure, large parts of this region have an *upwards directed* pressure gradient and *groundwater supply*. The original deep rooted forests “pumped” this slow flow into the atmosphere without its high salt content reaching the soils and the surface. After deforestations (which were accelerated during the wars of the 16th and 17th centuries), the salt content of the upwards moving groundwater reaches the surface and degrades the formerly good quality soils by salinization (*Fig. 1*).

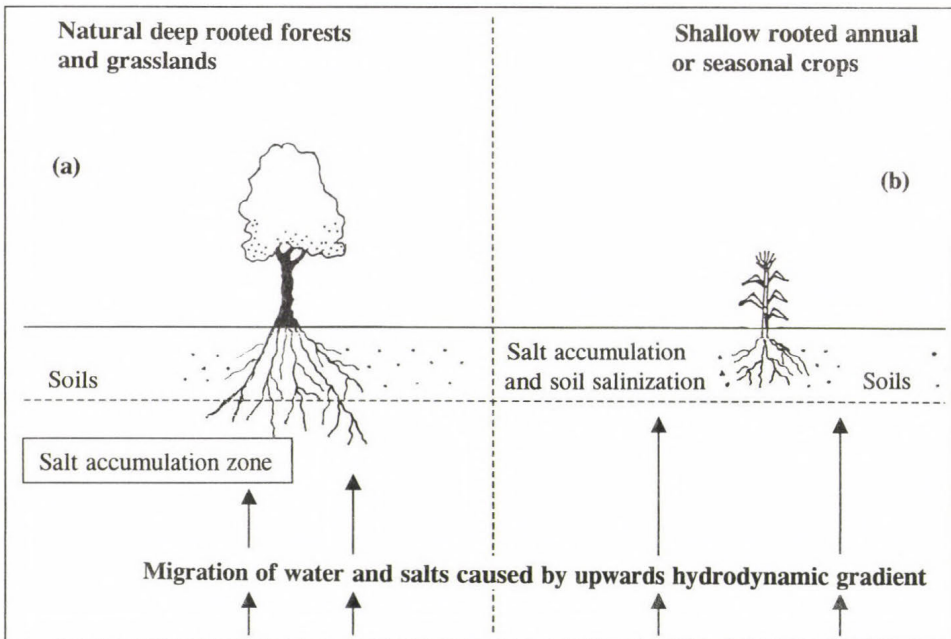


Fig. 1. Salt migration driven by upwards hydrodynamic gradient does not reach the soils in case of deep rooted natural vegetation (panel a), but it reaches the soil and causes salinization in case of shallow rooted crops (panel b).

Within the terrestrial water cycle, hydroecology is structured according to sets of smaller and larger fluvial basins. This integrating role of water manifests itself as the “short”, “long”, and “deep” branches of the subsurface water cycle. The near-surface short and long branches are dominated by climate and can be classified according to the major climatic and vegetational zones. The deep branch of the scheme is governed by the forces and processes of groundwater hydrodynamics, and it gains ecological and economic significance particularly in case of large fluvial basins, such as the Great Plain of Hungary within the Carpathian Basin. Because of the great variability of geohydrological structure within the Great Plain, the deep branches of the water cycle reach large proportions and are of decisive significance for plant ecology and crop production (*Szesztay*, 1991).

2. Analytical planning for integrated water management

In a historical perspective, it is the second time that water is becoming a critical factor of human evolution, the first being of age of fluvial civilizations within which water was a limiting constraint in the form of irrigated agriculture and inland transportation. These ancient constraints were eliminated during the subsequent ages by technological innovations revolutionizing the realms of economic and social development. Today water is becoming a critical factor of human evolution through its integrating roles within and among the technosphere, the biosphere, and the geosphere. The constraints and hazards stemming from these roles can now be overcome through integrated planning of analytical nature supported by improved societal and political water awareness.

The integrated roles of water have a twofold societal implication: within the individual managerial activities, the high level of interrelatedness requires readiness for co-operation and compromises in order to reach mutual advantages, as well as to avoid unnecessary confrontations; in the domain of national and regional policies, the holistic nature of the hydrological cycles urges the legal and economic recognition of water as a fundamental survival factor, as well as the establishment of an informational infrastructure as the basis for expressing and validating the broad public interest within water-related planning and decision-making.

The last decades are frequently labeled as the beginning of the age of information and knowledge. In terms of data handling and modeling capabilities, all technological and computational barriers seem to be overcome in constructing electronic information systems of any scale and complexity. The real bottlenecks of the implementation of societal water awareness seem to

derive from the fragmented nature of our water-related concepts and information. The specific form and content of a holistic knowledge on water is, of course, site and time specific.

The following questions might give, however, a tentative and general indication of a holistic approach (*Orlóci*, 1978; *Orlóci et al.*, 1985):

- What are the socially significant roles (the valued components) of the country's hydrological processes? How can these components be analytically described and quantitatively assessed?
- What are the natural factors and human activities within and outside the country area that have a significant impact on those valued hydrological components?
- What is the role of water in the utilization of land and other natural resources?
- What is the extent of human interventions in the country's water balance and water quality processes, and what are the critical levels of eventual future interventions?
- What are the major social and economic demands for water and water-related services, and what are the major alternatives for satisfying, or influencing these demands?
- What are the major possibilities and modalities for the protection and development of the country's water resources?

The answers to these and other similar questions require (*Fig. 2*):

- (i) a set of basic studies on water-related implications of major policy factors as a point of departure;
- (ii) analytical planning and impact assessment exploring future scenarios with alternative options of human responses and their environmental consequences, and
- (iii) series of carefully designed publications disseminating findings and messages of these studies in easily accessible form and language for the various groups of addressees.

Within the basic studies, water-related implication of present and expectable future technologies deserve particular attention. These preparatory studies should also include a systematic performance analysis of existing water systems and services (*OVK*, 1984).

It should be emphasized that the above advocated ecological orientation of hydrology in no way undermines its relevance and efficiency in supporting water management and hydraulic engineering activities. On the contrary, it shall enhance such applications in several important ways. First of all, improved understanding and modeling of water balance and water quality dynamics offers more reliable and more widely applicable methods for the design and

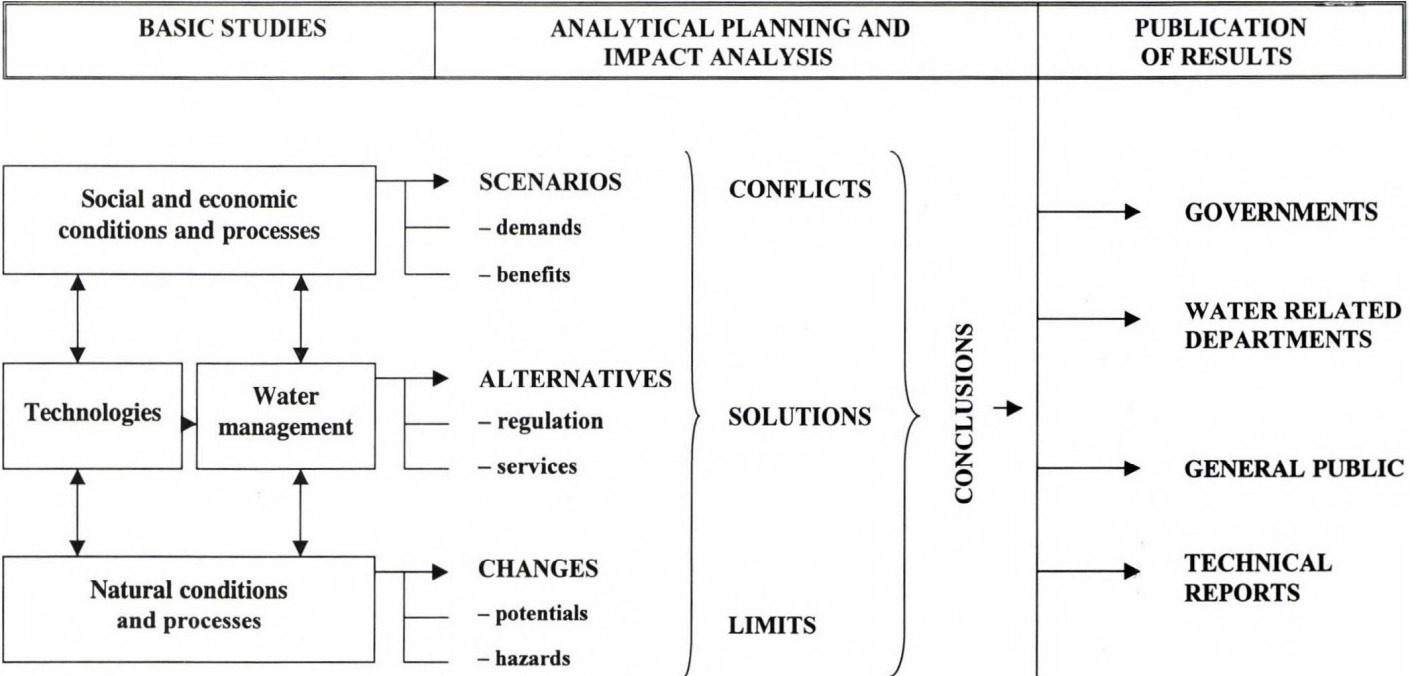


Fig. 2. Formation of programmes and policies for integrated water management (Orlóci, 1978; Orlóci et al., 1985).

operation of engineering projects. In addition, its integration with landscape ecology, crop production sciences, and other aspects of land management enables hydrology to significantly broaden the scope and improve the efficiency of water management through a shift from “runoff and riverflow management” towards “precipitation management”. Such a shift in concept and practice is particularly important for Hungary and other alluvial flatlands of the temperate and semi-arid zone. Under such conditions precipitation is rather unequally partitioned between infiltration and runoff, and groundwater flow is a locally diversified component of the water cycle.

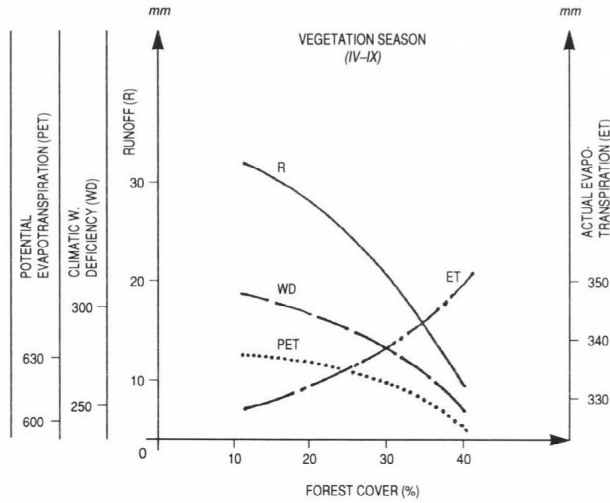
Integration with landscape ecology also opens new perspectives in the assessment of human impacts on water balance and runoff formation. As indicated by data of *Fig. 3a*, relatively slight but opposite changes in potential and actual evapotranspiration (by about 8 to 10%) caused in Hungary by a decrease in forest covered lands from about 40% in the 10th century to about 12% in 1926, gave rise to a substantial change in local climate (as measured by climatic water deficiency) and led to a drastic increase in seasonal runoff (from about 10 mm to 25–30 mm). Water-balance dynamics of the land surface and the unsaturated zone is particularly sensitive to deforestation (and other land use changes) within the Great Plain region. This is reflected by historical changes in the percentages of wetland regions, as well as by the capacity of drainage systems needed for maintaining intensive crop production (*Fig. 3b*).

3. Risk analysis of the soil moisture regime

A water-centric investigation of theoretical and practical questions arising in the broader context of crop production and hydroecology usually leads sooner or later to a comprehensive analysis of the water balance processes taking place in the root zone (*Fig. 4*). Understanding and quantifications resulting from this analysis should be firm and detailed enough to allow the formulation of a *water balance simulation model and procedure* as a basic methodological tool for answering the great number and variety of questions asked by agriculturalists or land use planners.

From point of view of time horizon and practical orientation, these questions tend to fall into two groups. One directed towards longer perspectives of preserving and enhancing the region's soil and other ecological resources and linked usually to the realms of land allocation, regional planning, and nature preservation. The other, generally more privileged under conditions of market economies, considers the root zone primarily through its potentials for crop production and is guided by the principles of achieving an optimal compromise between maximizing incomes and minimizing risks.

(a) COUNTRY AREA AS A WHOLE
FOREST COVER IN 1926 IS 12%; IN THE 10th CENTURY ABOUT 40%



(b) THE GREAT PLAIN REGION
FOREST COVER IN 1980 IS ABOUT 10%; IN THE 10th CENTURY ABOUT 25%

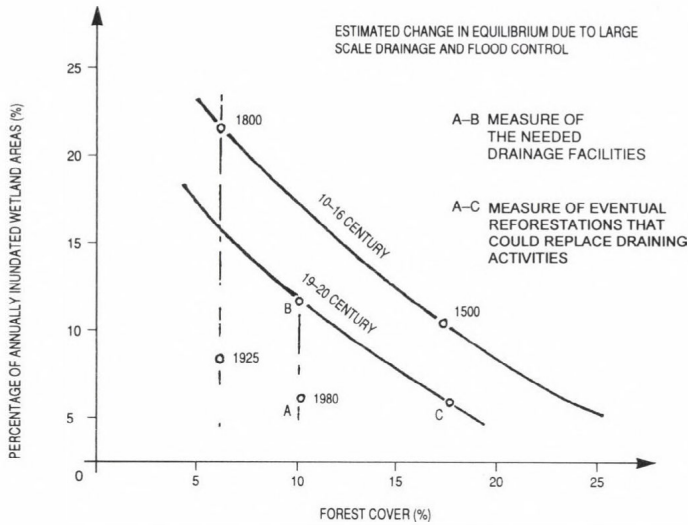


Fig. 3. Tentative relationships describing the effect of deforestations on water balance regime of Hungary (Orlóci et al., 1985). Based on consultant report of Antal (1983) and Pachner (1981) for OVK (1984).

Regarding the results and the outputs of the investigation, the former groups of initiatives usually lead to an ordered set of recommended land use

options. The latter groups of inquiries, linked closely to the motivations and decision problems of the farmer and the agricultural communities, require an ordered set of probability functions describing the expectations for crop-endangering shortages and excesses of water within the root zone, first in terms of hydrological events, then translating these into losses in crop yields — such as elaborated by *Orlóci* and *Pintér* (1981) as part of the 1984 “National Water Plan” (a broadly formulated Water Policy Analysis) for Hungary (*Fig. 5*).

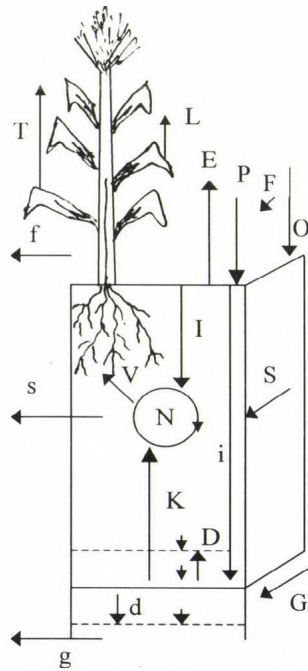


Fig. 4. Water balance components of the root zone (Várallyai, 1987).
(P=precipitation and irrigation; F and f=inflow and outflow through surface runoff; i=infiltration reaching the groundwater; I=infiltration; N=soil moisture storage; V=soil moisture available for plants; T=transpiration; E=soil evaporation; L=wet canopy evaporation; S and s=inflow and outflow through soil moisture flow; G and g=inflow and outflow through groundwater flow; D=rising groundwater level; K=capillary rise of groundwater; d=falling groundwater level)

In fact, these two directions of questioning and problem solving are closely interlinked not only through the water balance simulation as a major tool of methodology, but also in their practical outcomes as no meaningful land use options can be formulated without prior knowledge of the risks and consequences of various potential crop production technologies.

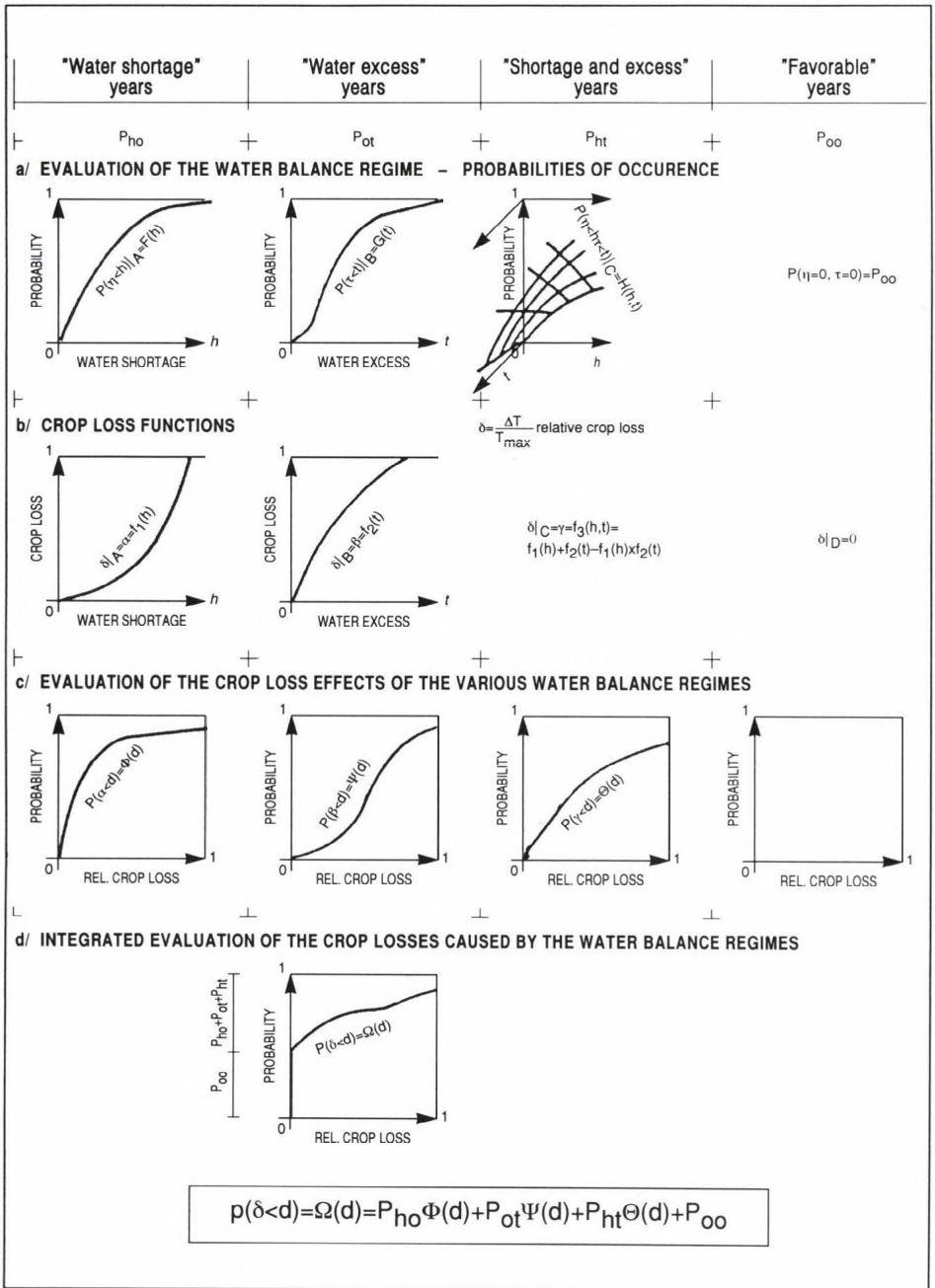


Fig. 5. Evaluation of the crop loss impact of the water balance conditions (Orlóci and Pintér, 1981).

The needs for and the possibilities of water balance simulation stems from the experimentally and theoretically well documented notion that for given climate and soil conditions plant communities tend to evolve according to well defined margins of deficiencies and excesses of heat and water, whereby the extent and frequency of these limiting extremes vary from species to species, and also according to the phenological phases of plant development.

In order to identify these margins and apply them in predictions or planning, one has to quantify the annual and seasonal variability of heat and water availabilities in probabilistic terms. Such quantifications can be made relatively easily for radiation and heat factors on the basis of regular meteorological observations of sunshine and air temperature. For quantifying critical deficiencies and excesses of soil moisture, the required continuing and detailed observational data are, however, not available on a regular basis (Antal, 1988). Modeling and simulation of the soil moisture balance seems to be, therefore, the only feasible solution to this effect (Orlóci *et al.*, 1993).

With regard to possibilities and ways of quantifying evapotranspiration as the key element of the soil moisture balance equation, there seem to be important differences between the water-stress controlled and the heat controlled strategy of plant growth. When soil moisture is unlimited and the system maximizes biomass production under given radiation and heat constraints, the use of water in the form of evapotranspiration can be well approximated for a given plant species and given phase of phenological evolution through atmospheric data alone. The possibility of such approximation is probably a reflection of the coincidence of factors and mechanism guiding stomatal regulation of evapotranspiration with those promoting maximal biomass productivity.

The usual simulation procedure is based on a step by step compilation of the soil moisture balance equation of the root zone for continuous ten days periods. Wherever the soil moisture content drops below the level of unrestricted water availability — which varies widely according to crop type, soil conditions, and the phases of plant growth —, the root zone is hypothetically filled up to field capacity. The amount of irrigation water needed to this effect is registered in the simulation procedure as a measure of natural (climatic) water deficiency event, whereby the accumulated amounts of the hypothetical irrigations provide a quantitative measure of the dry weather events corresponding to the actual local conditions.

For the purposes of the National Water Policy Study for Hungary, some 2000 computerized soil moisture simulations have been made for the country's farmlands according to 13 crop varieties, 7 soil types, 4 categories of ground-water depth, and 3 levels of farming technologies.

The simulations are based on the 1928–1977 data of 23 meteorological stations characterizing climatic differences. The major results were summarized in the form of maps quantifying deficiencies of the soil moisture balance according to major crop types for selected characteristic periods. Water shortages belonging to risk values other than those indicated on the maps, as well as the impact of cultivation intensity (crop yield), soil properties, and groundwater depth are specified by tables or graphs obtainable directly from the simulation results.

The above outlined simulation is not a full description of the natural soil moisture regime. It does not clarify how stomatal regulation minimizes moisture stress within the root zone and it does not quantify the water-controlled evapotranspiration regime. Yet it can provide indirect solution for practical questions as it offers a comprehensive and quantitative description of soil moisture management measures which can keep the soil moisture within the desirable range. In this way the simulation procedure identifies long term equilibrium criteria for the given conditions and it can be envisaged for wide scale use in the allocation of available farmland resources among the required major crops, and in the selection of optimal combination of soil moisture regulation measures and cultivation technologies for given land conditions and crop type.

The proposed methodology could also be applied in climate change assessments by repeating the simulations for various assumed or predicted climates. A more simple solution of assessing hydroecological impacts of climate change can also be implemented by assuming equivalence of the climate differences of various regions and those of various time periods. Based on this assumption, climate dependent changes of irrigation water demands have been recently assessed for the country's agricultural areas by analyzing regional differences in water demands in dependence of the corresponding changes in average temperature and precipitation during the growing season (Szesztay, 1995).

References

- Antal, E., 1983: Water balance conditions of Hungary in historical perspectives with special regard to the role of forests and the impacts of river regulations (in Hungarian). *Consultant Report for OVK-1984*. VIZDOK, Budapest.
- Antal, E., 1988: Comparative analysis of the irrigation water requirement and aridity conditions. In *Identifying and Coping with Extreme Meteorological Events* (eds.: E. Antal and M.H. Glantz). Hungarian Meteorological Service, Budapest, 205-254.
- Orlóci, I., 1978: Principles and guidelines for a new formulation of the National Water Plan and Policy (in Hungarian). Vízgazdálkodási Intézet, Budapest.

- Orlóci, I. and Pintér, Á., 1981: Crop production and the soil moisture regime in Hungary (in Hungarian). *Methodology for OVK-1984*. Vízgazdálkodási Intézet, Budapest.
- Orlóci, I., Pintér, Á., Szalóki, S., and Szesztay, K., 1993: Hydroecological equilibrium and risk analysis for crop production in Hungary. *TEMPUS EWA Ring Postgraduate Seminar, Lecture Notes*. April 1993, Gödöllő, Hungary.
- Orlóci, I., Szesztay, K., and Várkonyi, L., 1985: National infrastructures in the field of water resources. *A contribution to the International Hydrological Programme of UNESCO*, Budapest, Paris.
- OVK, 1984: National plan and policy analysis for water management in Hungary (in Hungarian). Országos Vízügyi Hivatal, Budapest, Hungary.
- Pachner, C., 1981: Climate and water balance conditions of the Carpathian Basin in historical perspectives (in Hungarian). *Consultant Report for OVK-1984*. VIZDOK, Budapest.
- Szesztay, K., 1991: Water related issues of climate change (in Hungarian). *Vizügyi Közlemények*, No. 3-4, Budapest.
- Szesztay, K., 1995: Climate change and irrigation water demands in Hungary (in Hungarian). In *VITUKI Közlemények*, No. 59, Budapest.
- Várallyay, G., 1987: The soil moisture regime (in Hungarian). DSc. Thesis, Hungarian Academy of Sciences, Budapest.

IDŐJÁRÁS

Quarterly Journal of the Hungarian Meteorological Service
Vol. 106, No. 3–4, July–December 2002, pp. 197–213

Relationships of water- and nutrient supply, yield and evapotranspiration of maize

Ildikó Zima Szalókiné and Sándor Szalóki

Research Institute for Fisheries, Aquaculture, and Irrigation
P.O. Box 47, H-5541 Szarvas, Hungary; E-mail: zimai@haki.hu

(Manuscript received February 28, 2002; in final form August 21, 2002)

Abstract—The cycle and utilization of water were examined in lysimeters and on plots in a long-term experiment with four different water- and nutrient supply levels. The given nutrient doses were 100, 200, 300, and 400 kg/ha NPK substance in ratio 2:1:1, and the water-supply levels were rainfall (control), optimum water supply, and two intermediate levels. The given irrigation water levels in average of 18 years were the following: 0, 57, 126, and 173 mm.

It was established that the yield of maize is in close linear correlation both with the amount of precipitation in the growing season (between 150–470 mm), and annual precipitation (between 300–700 mm). The more favorable the nutrient supply, the closer the relationship is between the yield and precipitation. The closest correlation occurred between the evapotranspiration and yield. The irrigation and nutrient supply increased in a larger extent than the evapotranspiration, and the productivity of precipitation and irrigation was improved significantly by the two factors. The amount of water used per 1 kg of grain yield (Q) decreased with the increasing yield by a power function.

The utilization of precipitation is the worst at dry weather, when the evapotranspiration of maize (FAO 400) remains under 350 mm. In such case the yield is raised more than once by 100 to 200 mm supplementary water supply, and the specific water-use (transpiration coefficient) is decreased in an expressive way.

Key-words: evapotranspiration, utilization of irrigation water, utilization of precipitation, yield, maize.

1. Introduction

It is well-known that the yield is influenced by numerous ecological, biological, and agrotechnical factors. Among them the water supply is the most changeable factor. In Hungary the annual precipitation varies between 300–900 mm, while in the growing season it changes between 120–700 mm. 30 days long periods

without precipitation are not rare, and more than 100 mm precipitation is also possible in one day. It often happens that wet and dry periods follow each other during the same growing season. Sometimes there are consecutive droughty or wet periods for several years.

The effect of fluctuation of precipitation is well-known, but the exact quantity relations between the amount and utilization of precipitation and irrigation water are yet missing or they are contradictory.

The increase of precipitation's productivity and rational control of plant water balance have to be examined concerning:

- the water requirement of plants,
- the frequency and yield-limiting effects of water shortage,
- the possibilities of improving precipitation's productivity and moderating the fluctuation of yield,
- the conditions and methods of efficient and environment-friendly water management control,
- the possibilities of harmonization of ecological, biological, and agrotechnical factors.

The report deals with the relations of precipitation, irrigation water, and nutrient supply to the actual evapotranspiration, yield, and productivity of water in maize.

2. Literature overview

The study of ecological needs of plants started with the searching of their water requirement. As early as the end of the 19th century, exact cylinder experiments were carried out to examine the water cycle and transpiration of plants. Measurements of consumptive use of water, namely the evapotranspiration began early in the 20th century (*Blaney, 1954; Thornthwaite and Mather, 1961; Armin, 1969*).

In Hungary the evapotranspiration measurements with compensation lysimeters were started by *László Erdős* (1966) in 1959 and *Emánuel Antal* (1966a, 1966b, 1966c) in 1963. However, in its popularization and wide range application *Emánuel Antal* has the biggest role. His outstanding research activities and personal contribution resulted in building of compensation lysimeters at least in ten different parts of the country within a few years (*Antal, 1968a, 1968b; Petrasovits, 1966; Balogh and Petrasovits, 1970; Possgay, 1983; Fűri, 1968; Posza and Tóth, 1970; Gergely, 1976*), although, only a few pieces of lysimeters (6–12) were built in one place, which were used for establishment of water requirement of plants at quasi-optimal conditions. *Ruzsányi* (1973) studied the water requirement modifying effect of different nutrient supplies at field crops.

Parallel to investigations carried out by the Hungarian Meteorological Service, measurements of actual evapotranspiration have been started by Szalóki (1971) in 188 groundwater lysimeters at the Irrigation Research Institute, Szarvas, Hungary in plants supplied with different levels of water as well as by different ways of water supply. For the purpose of studies of evapotranspiration moderating effect of different agrotechnical factors (variety, plant density, water- and nutrient supply, etc.), a lysimeter station of 320 lysimeters was built in 1971, and this paper is based on the results of experiments carried out at this lysimeter station.

The actual evapotranspiration and water requirement of plants depend on a number of ecological, biological, and agrotechnical factors (Antal, 1968c, 1972; Antal and Posza, 1967; Szász, 1995; Varga-Haszonits and Harnos, 1988). The change in water requirement of plants can be determined — within the potential possibility — mostly by the surface area of plant-stand, and to a lesser extent on its age. There is a connection between the leaf area and the increasing *ET*, which can be characterised by a saturation curve (Szalóki, 1970, 1989), where the evapotranspiration on a unit area of leaves shows a decreasing tendency, even if it is caused by a more favorable water- and nutrient supply. The water requirement is modified by agrotechnical factors, primarily through the effect on surface of plant stand. Besides this, the direct effect of soil cultivation is also indisputable as far as the vegetation does not cover the soil.

Most researchers agree that mostly the nitrogen influences the size of leaf area and yield, and thereby the amount of evapotranspiration and its utilization. Many researchers stated — first of all those making experiments in cylinders — that the yield increase generated by fertilizing required more water only in absolute amount, at the same time the transpiration coefficient decreased (Frank and Hank, 1952; Debreczeni, 1965; Szlovák, 1968; Cselótei, 1977).

In Hungary the relationships of fertilizer, water consumption, and yield of maize were examined by Szalóki (1971, 1989), Ruzsányi (1973), Antal *et al.*, (1975), Szalóki and Németh (1985), and Szalókiné Zima (1992) with regression analyses. It was found that the leaf area — in the case of no other limiting factors — was increased by the improvement of water- and nutrient supplies, and as a result, the evapotranspiration is enhanced by an exponential or saturation curve.

The accumulation of dry matter grows proportionally to the extension of leaf area. At the same time the ratio of dry matter content of grains increases within the total dry matter content, i.e., the harvest-index increases. Coming from the previous statement, the water use per unit of grain yield decreases by a hyperbolic function, i.e., the productivity of water improves (Szalókiné Zima, 1992; Szalókiné Zima and Szalóki, 1998).

It was proven unanimously by the long term fertilizer experiments, that the precipitation (if it is enough) and the irrigation water are utilized better by plants — in case of adequate nutrient supply —, and there is a positive interaction between them (*Debreczeni*, 1994; *Berzsenyi*, 1993; *Ruzsányi*, 1992; *Nagy*, 1994; *Lásztity* and *Csathó*, 1994; *Sárvári*, 1999; *Szalóki*, 1983). Considering the connection between water and nutrient supply, there are contradictory opinions among the researchers.

From the tendentious increase of yield and improving utilization of water some researchers concluded that the enhancing yield does not imply the raising of water consumption (*Klapp*, 1962; *Prenek*, 1967). On the other hand, *de Wit* (1958) has proved that the better water supply increased the water consumption by the same proportion as the quantity of yield, while the utilization of water remained practically the same. Regarding the productivity of irrigation water, it generally agrees with the getting of the diminishing returns, where the utilization of raising irrigation-water is more and more decreased (*Cavazza*, 1963). According to several authors' opinion, the productivity of irrigation water can be higher than that of a small amount of precipitation (*Ruzsányi*, 1975; *Possgay*, 1983; *Szalóki*, 1983).

The relationship between the water shortage and harvest deficiency, and the possibility of its reduction were examined by several authors (*Petrasovits*, 1989; *Ruzsányi*, 1989, 1992; *Szőke Molnár*, 1989; *Szalóki*, 1989; *Varga-Haszonits*, 1989; *Berzsenyi*, 1993). *Szalóki* (1989) found a very close relation between the actual water shortage and the harvest deficiency, which can be characterized by a quadratic equation. *Szalóki and Szőke Molnár* (1981) and *Szőke Molnár* (1989) also completed a simulation model of water shortage and harvest deficiency. Using this model, the probability dispersion curves of potential water shortage and harvest deficiency were determined with lot of plant species and for many different sites.

3. Materials and methods

The experiments have been carried out at the two hectare area of the Lysimeter Station of the former Irrigation Research Institute (now Research Institute for Fisheries, Aquaculture, and Irrigation) Szarvas, Hungary, since 1971, in 320 lysimeters. The experiments have been arranged in five blocks with 64 lysimeters in each. Four different water- and nutrient supplies were applied in 16 treatment-combinations. The number of repetitions was four.

The size of lysimeters was $1\text{ m} \times 1\text{ m} \times 1\text{ m}$ (1 m^3), and they were built into the middle of each plot with 32 m^2 area. The plots and lysimeters got the same treatments. The groundwater level is not kept in lysimeters, which is

characteristic to the Thornthwaite-type lysimeters. The infiltration water is leaching from lysimeters to the dishes placed in cellars by gravitation, the amount of which is measured and its chemical content is analyzed in laboratory conditions.

In the three blocks two-factor long-term experiments have been carried out for 30 years, four repetitions, with the following 16 combinations of treatments.

The water supply in the three main blocks was the following:

I₁ – non-irrigated **control** (natural rainfall),

I₂ – irrigated with **one third** of optimum water supply,

I₃ – irrigated with **two thirds** of optimum water supply,

I₄ – **optimum** water supply (irrigated according to the demand of plants).

The amount of on-demand irrigation means the amount of supplementary water supply which is required for keeping the disposable water content in the active root zone to be higher than 50%.

The soil moisture difference was determined at the beginning and end of the growing season by gravimetric method. The continuous control of soil moisture content during the growing season was carried out by a BWK-Lanze Soil Moisture Meter. Water supply was carried out by drip irrigation through pipes laid on the soil surface, or by a portable plot irrigating device.

The calculation of actual evapotranspiration (ET_a) was carried out according to the following equation:

$$ET_a = P + I^+ - Sm_{diff} - Inf, \quad (1)$$

where P is the precipitation, I is the irrigation water, Sm_{diff} is the soil moisture difference between spring and autumn, and Inf is the infiltration.

Daily evapotranspiration was measured by floating lysimeters supplied with optimum water- and nutrient level. Within the main treatment (water-supply), the nutrient levels were 100, 200, 300, and 400 kg/ha NPK substances in ratio 2:1:1. Type of the soil is chernozem meadow, which is well supplied with phosphorus and potassium, and has a medium nitrogen content. Its natural water capacity is 40 volume percent, half of which is disposable water. Such experiments are carried out in three blocks, in 192 lysimeters, and plots with three plant species. In the other parts of the experimental area different type experiments are run.

Hereafter the results of 18 years long experiments in water balance and water use are evaluated in maize (Volga, Florencia, Columba, Nónius, Reseda).

4. Results and discussion

It is visible from the literature, that there are differences in respect of quantity relations between water and yield, coming from great number of influencing factors. However, it is obvious, that using small amount of water is insufficient, and the precipitation or irrigation water above the water requirement of plants is not utilized, moreover, it may cause depression in yield. As a consequence, it is not advisable to study the effect and productivity of precipitation and irrigation water without considering the requirement of plants and its harmonization to the other factors.

The objectives of the study were realised by examination of results collected in a long-term experiment in maize. In the three blocks of the experiment, the effects of precipitation and three different levels of supplementary water supply on evapotranspiration, yield, and water utilization were investigated in four (same every year) different nutrient supply treatments. Results are demonstrated in *Tables 1* and *2*, and *Figs. 1* to *4*.

Each element of the water balance was measured, so the water consumption could be estimated with reliable accuracy. The moisture content of the soil and its changes were measured in every 10 cm of soil layer as far as 2 m depth at the time of sowing and harvest, but the infiltration into more than 2 m deepness and amount of surface run-off water were not calculated. Based on our observations and calculations, the infiltration under the 2 m soil layer could be significant only at the I_4 treatment.

During the 18 years long experiments, the average precipitation was 297 mm in the growing season, and its extreme values changed between 150–450 mm. The amounts of annual precipitation (October 1–September 30) fluctuated between 300 and 700 mm around an average of 491 mm.

The given irrigation water has also varied not only by treatments but also by years, and in the I_4 treatment it changed between 60–300 mm. In average of 18 years the irrigation water amounts were 57, 126, and 173 mm in each treatment (*Table 1/a*). In the growing season the amount of irrigation water together with the precipitation was 354–470 mm in average, and with the annual precipitation it was between 548–664 mm (*Tables 1/b* and *1/c*). The winter evaporation (E) was averaged around 100 mm (*Table 1/e*).

The infiltration could have been measured only in lysimeters. The amount of infiltration fluctuated between 40–100 mm in a many years average, which occurred mainly early in spring at melting of snow and at the beginning of the growing season (April and May). The amount of infiltration was increased by the precipitation and irrigation and was decreased by the dose of fertilizers (*Table 1/f*).

Table 1. Water balance components in lysimeter- and in plot-experiment in average of 18 years

Treatment	Dimension	Fertilization treatment: NPK 2:1:1				Average	
		100	200	300	400	abs., mm	relative, %
<i>I/a Irrigation water (I)</i>							
I ₁	mm	0	0	0	0	0	0
I ₂	mm	57	57	57	57	57	33
I ₃	mm	126	126	126	126	126	73
I ₄	mm	173	173	173	173	173	100
<i>I/b Precipitation in growing season (P₁) + irrigation water (I)</i>							
P ₁	mm	297	297	297	297	297	100
P ₁ + I ₂	mm	354	354	354	354	354	119
P ₁ + I ₃	mm	423	423	423	423	423	142
P ₁ + I ₄	mm	470	470	470	470	470	158
<i>I/c Annual precipitation (P₂) + irrigation water (I)</i>							
P ₂	mm	491	491	491	491	491	100
P ₂ + I ₂	mm	548	548	548	548	548	112
P ₂ + I ₃	mm	617	617	617	617	617	126
P ₂ + I ₄	mm	664	664	664	664	664	135
<i>I/d Evapotranspiration in growing season in lysimeters (ET_aly)</i>							
ET _a ly ₁	mm	344	356	358	355	353	100
ET _a ly ₂	mm	385	409	408	410	403	114
ET _a ly ₃	mm	436	452	465	464	454	129
ET _a ly ₄	mm	453	476	499	509	484	137
Average	mm	405	423	433	435	424	
<i>I/e Evaporation (E) in lysimeters in winter season</i>							
E ₁	mm	102	94	95	98	97	100
E ₂	mm	105	94	96	97	98	101
E ₃	mm	111	108	104	109	108	111
E ₄	mm	110	102	104	103	105	108
Average	mm	107	100	100	102	102	
<i>I/f Infiltration (Inf.) in lysimeters</i>							
Inf ₁	mm	45	41	38	38	41	100
Inf ₂	mm	58	45	44	41	47	115
Inf ₃	mm	70	57	48	44	55	134
Inf ₄	mm	101	86	61	52	75	183
Average	mm	69	57	48	44	54	
<i>I/g Evapotranspiration in growing season on plots (ET_ap)</i>							
ET _a p ₁	mm	389	397	396	393	394	100
ET _a p ₂	mm	443	454	452	451	450	114
ET _a p ₃	mm	506	509	513	508	509	129
ET _a p ₄	mm	554	562	560	561	559	142
Average	mm	473	480	480	478	478	

The annual actual evapotranspiration (ET_a) of maize varied between 270–600 mm during the analyzed period. During the 18 years of experiments, the average ET_a has been changed between 344–509 mm depending on the applied treatments (*Table 1/d*). The irrigation increased the evapotranspiration, but in the well-watered treatments (I_3 and I_4) it also raised when higher doses of fertilizers were applied (*Table 1/d*). The ET_a of maize was estimated to be between 390–560 mm on plots (*Table 1/g*), on the basis of examination of water balance in the 2 m soil layer. It is worth to mention that the upper 2 m soil layer was saturated several times to water capacity in spring at the I_4 treatment. Presumably, certain infiltration appeared during these years under the 2 m soil layer as well, which has not been taken into consideration in the determination of ET on plots. However, in non-irrigated treatments and at less supplementary water supply, the calculated values of ET are close to the actual values. It is supported not only by the values of average yields, but also the tendency of water productivity.

The average yields of many years are shown in *Tables 2/a* and *2/b*. Comparing the yields in lysimeters with the ones collected on plots shows that the yields are lower in lysimeters than on plots, especially at low water- and nutrient supply levels. The reason is that the lysimeters are only 1 m deep, and significant amount of water and nutrients is released from them.

It is indicated by the about 5 t/ha average yield of non-irrigated maize, that the formation of yield is often strongly limited by water shortage. There were droughty years when there was no grain yield at all in the lysimeters or it was very low. However, in wet years and in treatments with adequate water supply, the yield exceeded 10 t/ha. The increase of fertilizer dose compared to the basic (100 kg/ha NPK) treatment had a depressive effect in the non-irrigated treatments in dry years. In wet years and in treatments with adequate water supply (I_3 ; I_4) the fertilizer also had a good utilization.

The average yield was increased by 3–4 t/ha in lysimeters and 1–2 t/ha on plots in the irrigated treatments, if higher NPK doses were applied and the water supply remained the same. The yield was increased to higher extent by irrigation than by raising of nutrient levels. Nevertheless, the effect of fertilizers was continuously higher in the recent years because of the differences appearing in the nutrient reserve of the soil, and both factors proceeded in a positive interaction with each other.

The correlation between raising yield and water supply is evaluated on the one hand by a regression analysis, and on the other hand by a coefficient expressing the productivity of water.

The relations between the precipitation and yield at different nutrient treatments can be seen in *Figs. 1* and *2* based on the annual data of non-irrigated plots. It also emerges from the data, that the yield of maize has

Table 2. Productivity of precipitation and irrigation water

Treatment	Dimension	Fertilization treatment: NPK 2:1:1				Average	
		100	200	300	400	absolute	relative, %
<i>2/a Yield in lysimeters (Yly)</i>							
Yly ₁	t/ha	4.4	5.0	5.2	4.8	4.9	100
Yly ₂	t/ha	6.0	7.2	7.9	7.9	7.3	149
Yly ₃	t/ha	6.9	9.0	10.6	10.9	9.3	192
Yly ₄	t/ha	8.0	9.7	11.6	12.4	10.5	215
Average		6.4	7.7	8.8	9.0	8.0	164
<i>2/b Yield on plots (Yp)</i>							
Yp ₁	t/ha	6.9	7.0	7.3	7.0	7.1	100
Yp ₂	t/ha	8.9	10.1	10.3	10.2	9.9	139
Yp ₃	t/ha	11.0	12.0	12.7	13.0	12.2	171
Yp ₄	t/ha	11.1	12.3	13.4	13.8	12.7	178
Average		9.4	10.3	10.9	11.0	10.4	
<i>2/c Productivity of the evapotranspiration in lysimeters (Y/ET_a)</i>							
Yly/ET _{a1}	kg/ha/mm	12.8	14.1	14.4	13.7	13.8	100
Yly/ET _{a2}	kg/ha/mm	15.7	17.5	19.4	19.3	18.0	130
Yly/ET _{a3}	kg/ha/mm	15.8	19.8	22.9	23.4	20.5	149
Yly/ET _{a4}	kg/ha/mm	17.8	20.4	23.3	24.3	21.6	156
Average		15.7	18.2	20.4	20.7	18.8	
<i>2/d Productivity of the evapotranspiration on plots (Y/ET_ap)</i>							
Yp/ET _a p ₁	kg/ha/mm	17.7	17.6	18.5	17.8	17.9	100
Yp/ET _a p ₂	kg/ha/mm	20.0	22.2	22.8	22.5	21.9	122
Yp/ET _a p ₃	kg/ha/mm	21.7	23.5	24.8	25.5	23.9	134
Yp/ET _a p ₄	kg/ha/mm	20.0	22.0	23.9	24.6	22.6	127
Average		19.8	21.3	22.5	22.6	21.6	
<i>2/e Productivity of the annual precipitation + irrigation on plots</i>							
Yp/(P ₂ +I ₁)	kg/ha/mm	14.0	14.3	15.0	14.2	14.4	100
Yp/(P ₂ +I ₂)	kg/ha/mm	16.2	18.4	18.8	18.6	18.0	125
Yp/(P ₂ +I ₃)	kg/ha/mm	17.8	19.4	20.6	21.1	19.7	137
Yp/(P ₂ +I ₄)	kg/ha/mm	16.7	18.6	20.2	20.8	19.1	132
Average		16.2	17.7	18.6	18.7	17.8	
<i>2/f Effect of the irrigation (more yield, t/ha)</i>							
I ₂ ly	t/ha	1.6	2.2	3.1	2.7	2.4	49
I ₃ ly	t/ha	2.5	4.0	5.4	5.7	4.4	92
I ₄ ly	t/ha	3.6	4.7	6.4	7.2	5.5	115
I ₂ p	t/ha	2.0	3.1	3.0	3.2	2.8	39
I ₃ p	t/ha	4.1	5.0	5.4	6.0	5.1	71
I ₄ p	t/ha	4.2	5.3	6.0	6.8	5.6	78
<i>2/g Productivity of the irrigation (Y/I)</i>							
I ₂ ly	kg/ha/mm	28.5	37.9	55.0	47.7	42.3	294
I ₃ ly	kg/ha/mm	19.8	31.4	43.2	44.9	34.8	242
I ₄ ly	kg/ha/mm	20.9	27.3	37.2	41.5	31.7	220
I ₂ p	kg/ha/mm	34.6	53.9	51.8	56.0	49.1	341
I ₃ p	kg/ha/mm	32.6	39.4	42.8	47.7	40.6	282
I ₄ p	kg/ha/mm	24.3	30.9	34.9	39.6	32.4	225
Average	kg/ha/mm	26.8	36.8	44.1	46.2	38.5	267

changed between 2–12 t/ha at the same NPK supply depending on weather conditions, and it is in close correlation both with the rainfall in the growing season and annual precipitation. Furthermore, it can be observed that in treatments with low supplementary nutrient supply, the fluctuation of yield was less, as in these treatments nutrient shortage was the limiting factor in rainy years. The degree and closeness of the relation, i.e., the values of regression and correlation factors increase with nutrient levels, which refer to higher utilization of precipitation caused by the fertilizers.

There is an even closer connection between the yield and evapotranspiration than between the yield and precipitation. Regression analysis for the two variables was made using 72 pairs of data of the 18 years and four nutrient- and water supply treatments. Results are shown in *Fig. 3*. It is visible that the correlation between *ET* and grain yield is loose at low NPK level, because in this case the average yield is limited not only by the water shortage but also the shortage of nutrients. The nutrient supply in the soil was highly modified also by the previous crop. At a better nutrient supply, the variability of *ET* and the average yield is more and more determined by the precipitation and irrigation, which is indicated by the increasing regression and correlation factors. The increase of the regression factors means that a yield increase per 1 mm evapotranspiration is got with rising nutrient levels (*Fig. 3*), i.e., the grain yield of maize enhanced to higher extent with the improving water- and nutrient supply than the *ET*, which means that the productivity of water increased and the amount of *ET* per unit of yield decreased. It is shown by functions between the average yield and transpiration coefficient (Q = evapotranspired water per unit of grain yield) in *Fig. 4*.

The results prove definitely that the value of Q depends primarily on the average yield, and it is in a very close negative correlation with the growing yield, which can be characterized by a logarithmic- or hyperbolic curve. Furthermore, it has been established that every factor which increases the yield has a favorable effect on the productivity of water.

Without irrigation the average grain yield is 13.8 kg/ha in lysimeters and 17.9 kg/ha on plots per 1 mm evapotranspiration. At the same time these values increased as high as 24–25 kg/ha in the irrigated treatments.

From the previous observations it is concluded that in case of heavy rainfalls, the productivity of precipitation does not decrease at adequate nutrient supply but increases to some extent. It is supported by the regression factors of *Fig. 2* (i.e., the excess yields per 1 mm increase in rainfall) which are continuously on the rise and exceed the 18 years average of I_1 treatment (*Table 2*). Consequently, not only the average yield but also the productivity of water were increased by the precipitation, as it served the satisfaction of water requirement of plants and improved the other life conditions of plants as well.

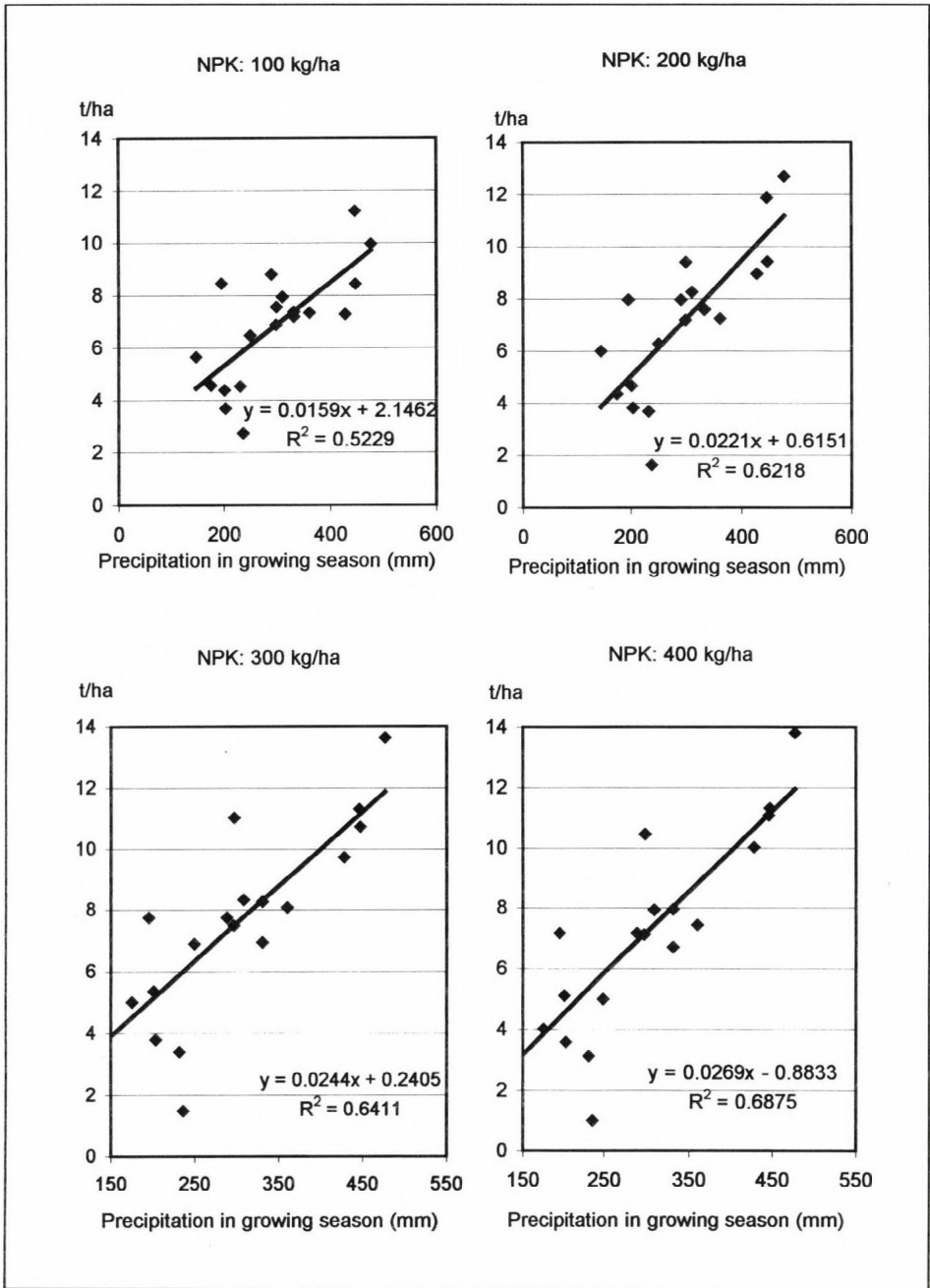


Fig. 1. Relationship between the precipitation and yield during the growing season at different NPK levels in non-irrigated maize.

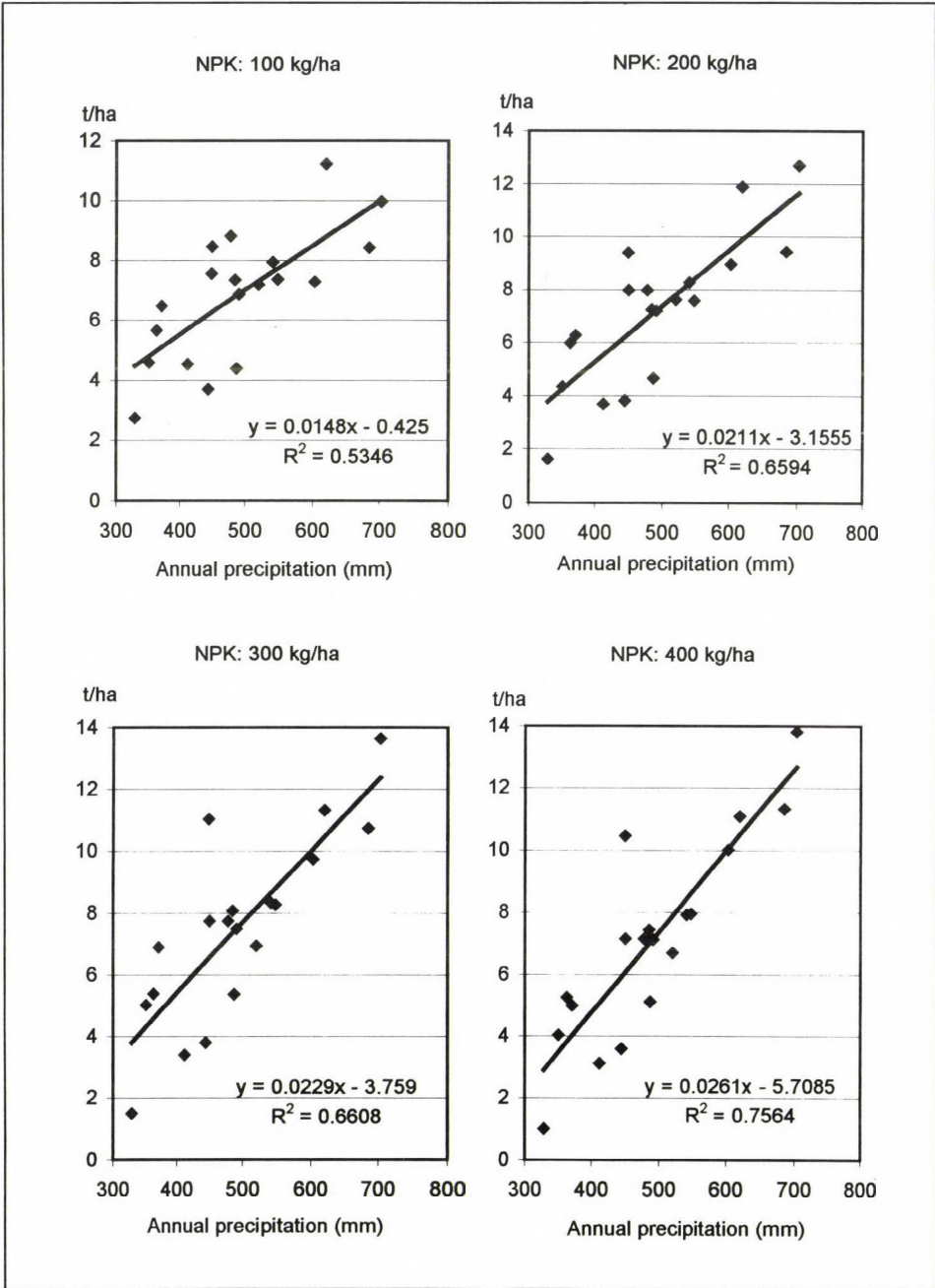


Fig. 2. Relationship between the annual precipitation and yield at different NPK levels in non-irrigated maize.

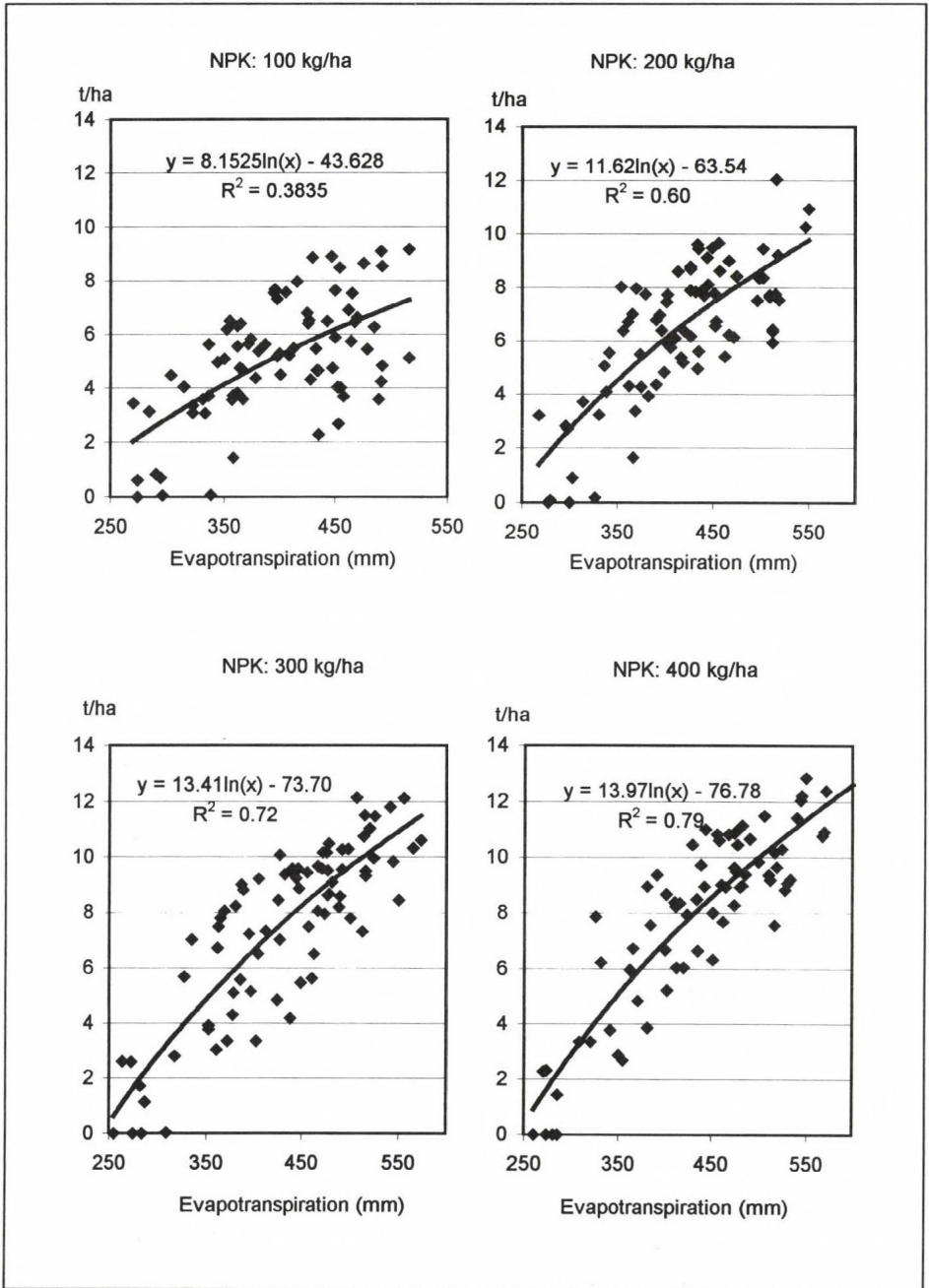


Fig. 3. Correlation between the evapotranspiration of maize and its dry grain yield at different NPK levels.

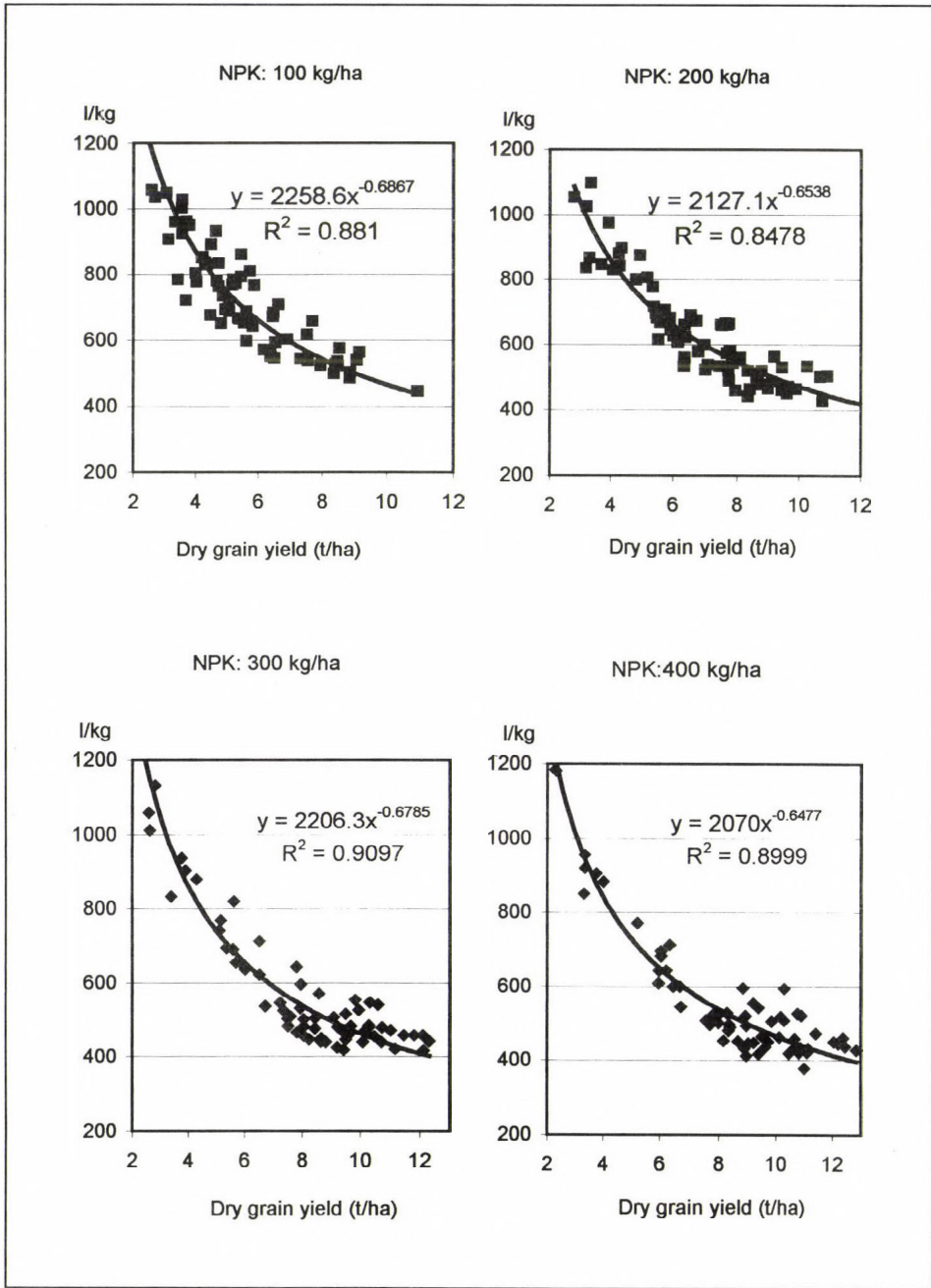


Fig. 4. Correlation between the dry grain yield and the evapotranspiration coefficient of maize at different NPK levels.

Both precipitation and nutrients have weak utilization if the water- and nutrient supplies are insufficient. If adequate and harmonious nutrient and water supply is ensured, the positive interaction of factors predominates, and the yields grow to large extent. Together with the increase of yields the productivity of water also improves. It is demonstrated by the data of the 18 years long experiments as well. The effect of improving water- and nutrient supply of these experiments is presented in Table 2. These data also support the conclusion that with the aid of supplementary water supply the yield was increased on a larger scale than the evapotranspiration, i.e., the utilization of water improved.

The yield increase per 1 mm evapotranspiration, 1 mm precipitation, as well as annual precipitation + irrigation water is also shown in *Tables 2/c, 2/d, and 2/e*. According to the exact measurement data, the utilization was weak at low levels of precipitation which was far behind the requirement of plants (12.8–14.4 kg/mm), especially in lysimeters having shallow productive layer, where even the increase of fertilizer dose was inefficient.

Compared to the above mentioned non-irrigated treatment, the 57 mm supplementary water supply increased the productivity of evapotranspiration to 18 kg/ha, the 126 mm water supply to 20 kg/ha, and finally the 173 mm irrigation water increased the productivity of *ET* to 21.6 kg/ha. The productivity of water also increased on the plots as far as the third level of irrigation.

References

- Antal, E., 1962: Determination of evapotranspiration (in Hungarian). *Beszámoló az 1961-ben végzett tudományos kutatásokról*. Országos Meteorológiai Intézet, Budapest, 131-153.
- Antal, E., 1966a: Potential evapotranspiration of some agricultural crops (in Hungarian). *Öntözéses Gazdálkodás* 4, 69-86.
- Antal, E., 1966b: Agrometeorological and irrigation research station at Szarvas (in Hungarian). *Léghő XI.*, No. 3, 66-70.
- Antal, E., 1966c: Measurement of maximum water consumption of maize and alfalfa (in Hungarian). *Beszámoló az 1964-ben végzett tudományos kutatásokról*. Orsz. Meteorológiai Intézet, Budapest, 60-65.
- Antal, E., 1968a: Über die Änderung des Wasserbedarfs der Kartoffel im Laufe der Vegetationsperiode. *Math. Naturwiss.* 17, Heft 2, Leipzig, 402-403.
- Antal, E., 1968b: A new model for determination of potential evapotranspiration (in Hungarian). *Beszámoló az 1967-ben végzett tudományos kutatásokról*. Országos Meteorológiai Szolgálat, Budapest, 414-423.
- Antal, E., 1968c: Irrigation schedule on the basis of meteorological data (in Hungarian). *CSc Thesis*. Magyar Tudományos Akadémia, Budapest.
- Antal, E., 1972: Meteorological model for the prognostication of irrigation point of time (in Hungarian). *Beszámoló az 1969-ben végzett tudományos kutatásokról*. Országos Meteorológiai Szolgálat, Budapest, 162-173.

- Antal, E. and Posza, I., 1967: Characteristics of evapotranspiration in maize (in Hungarian). *Beszámoló az 1966-ban végzett tudományos kutatásokról*. Országos Meteorológiai Intézet, Budapest, 499-509.
- Antal, E., Posza, I., and Tóth, E., 1975: The effect of weather and climate on the effectiveness of fertilization (in Hungarian). *Időjárás* 79, 95-104.
- Armin, B., 1969: *Evaporation und Evapotranspiration Korrelationsuntersuchungen in einem Bewässerungsgebiet*. Mitteilungen, Leichtweiss Institut, T.U., Braunschweig, Heft 23.
- Balogh, J. and Petrasovits, I., 1970: Evapotranspiration network station and using its measurement data (in Hungarian). *Hidrológiai Közöny* 50, 560-566.
- Berzsenyi, Z., 1993: Effect of N-fertilizer and of weather conditions on yield and N-fertilizer reaction in a long term experiment (in Hungarian). *Növénytermelés* 42, 1, 49-62.
- Blaney, H.F., 1954: Evapotranspiration measurements in Western United States. *Assoc. Internat. Hydrol. Sci.* 3, Bul. 38.
- Cavazza, D., 1963: L'irrigazione fisiologica teoria razionale dell'irrigazione. *L' Italia Agricola, Roma* 100, 115-135.
- Cselótei, L., 1977: Experimental methods to examine the plants' water-consumption. *Int. Comm. on Irrigation and Drainage*. Budapest, Question 2. 2/26. 1-4.
- de Wit, C.T., 1958: Transpiration and crop yield. Versl. Landbouwk. Onderz. Gravenhage, Meded. 59.
- Debreczeni, B., 1994: Connection between the precipitation and fertilisation at different states (in Hungarian). In *Trágyázási kutatások 1960-1990*. Akadémiai Kiadó, Budapest, 371-398.
- Debreczeni, B-né, 1965: Effect of water and nutrient supply on transpiration and nutrient uptake of corn (in Hungarian). *Öntözéses Gazdálkodás* 2, 129-147.
- Erdős, L., 1966: Agrometeorological water balance experiments (in Hungarian). *Habil. Thesis*. Eötvös Loránd University, Budapest.
- Frank, M. and Hank, O., 1952: Connection between the nutrient supply and water consumption at some agricultural plants (in Hungarian). In *ÖTKI Évkönyv*. Mezőgazdasági Kiadó, Budapest, 29-51.
- Füri, J., 1968: The effect of irrigation on the yield and quality of grapes (in Hungarian). *Öntözéses Gazdálkodás* 6, 1, 77-92.
- Gergely, I., 1976: Evapotranspiration of a young apple stand (in Hungarian). *Időszerű Öntözési Kutatások*, VITUKI, Budapest.
- Klapp, E., 1962: Ertragsteigerung und Wasserverbrauch. *Landwirtschaftlich Kulturen. Z. F. Kulturtechnik* 1, 1-5.
- Lásztity, B. and Csathó, P., 1994: Examination of effect of durable fertilisation in wheat-maize biculture (in Hungarian). *Növénytermelés* 43, 157-167.
- Nagy, J., 1994: Evaluation of effect of soil cultivation, fertilisation, stem density and irrigation on the yield of maize (in Hungarian). *DSc. Thesis*, Debrecen.
- Petrasovits, I., 1966: Evapotranspiration experiments with irrigated crop stand (in Hungarian). *Öntözéses Gazdálkodás* 6, 1, 49-68.
- Petrasovits, I., 1989: Integrated struggle against the drought (in Hungarian). In *Aszály. Öntözési Kutató Intézet, Szarvas*, 5-14.
- Possgay, E., 1983: Changes in irrigation utilization in different watering situation (in Hungarian). *Int. Conf. on Water Management and Production Potential in Agriculture*, Szarvas, Hungary. Sections: C, 291-302.
- Posza, I. and Tóth, E., 1970: Changes of potential evapotranspiration, water requirement, actual evapotranspiration and water requirement in Hungary (in Hungarian). *Beszámoló az 1968-ban végzett tudományos kutatásokról*. Országos Meteorológiai Szolgálat, Budapest, 434-451.
- Prenek, J., 1967: Die Bedeutung des Grundwassers für das Wachstum Landwirtschaftlicher Nutzungspflanzen. *Wasser und Boden* 19, 5, 142-146, Hamburg.
- Ruzsányi, L., 1973: Effect of fertilisation on water consumption, water utilization at some field crops (in Hungarian). *Növénytermelés* 23, 249-258.

- Ruzsányi, L., 1975: Examination of evapotranspiration of plant stands at different nutrient supply levels. *CSc Thesis*, Debrecen, Hungary.
- Ruzsányi, L., 1989: Agrotechnical possibilities of mitigation of drought (in Hungarian). In *Aszály. Öntözési Kutató Intézet*, Szarvas, 49-54.
- Ruzsányi, L., 1992: Water requirement, water supply and water utilization (in Hungarian). In *Szántóföldi növénytermesztés* (ed.: E. Bocz). Mezőgazda Kiadó, Budapest, 145-160.
- Sárvári, M., 1999: Effect of production factors on the yield of maize (in Hungarian). In *Magyarország az Ezredfordulón. Növénytermesztés és Környezetvédelem*. Magyar Tudományos Akadémia, Budapest, 117-121.
- Szalóki, S., 1970: Relations of foliage, root yield and water consumption of sugar beet (in Hungarian). *Öntözéses Gazdálkodás* 8, 1, 61-75.
- Szalóki, S., 1971: Relations of yield, evapotranspiration and water utilization (in Hungarian). *Kísérleti Közlemények*, Budapest, 47-63.
- Szalóki, S., 1983: Utilization of precipitation and irrigation in experiments with lysimeters. *Int. Conf. on Water Management and Production Potential in Agriculture*. Szarvas, Hungary. Sections: C, 353-365.
- Szalóki, S. and Németh, S., 1985: Wasserbedarf und Wasserausnutzung des Mais in der Ungarischen VR. Tagungsbericht. *Akad. Landwirtsch.-Wiss.*, DDR, Berlin, Nr. 231, 91-96.
- Szalóki, S., 1989: Water requirement, water utilization and irrigation water requirement of plants (in Hungarian). In *Az öntözés gyakorlati kézikönyve* (ed.: Gy. Szalai). Mezőgazdasági Kiadó, Budapest, 100-154.
- Szalóki, S., 1989: Determination possibilities of frequency of drought (in Hungarian). In *Aszály. Öntözési Kutató Intézet*, Szarvas, 15-27.
- Szalóki, S. and Szőke Molnár, L., 1981: The volume and frequency of water shortage in the more important field plants. *Int. Symposium on Plant Production*. Debrecen, Hungary, Sections 7.
- Szalókiné Zima, I., 1992: Quantity relations between the water and yield in maize (in Hungarian). Diploma work. DATE, Debrecen.
- Szalókiné Zima, I. and Szalóki, S., 1998: Effect of water and nutrient supplies on the water requirement, water consumption and chemical materials of maize (in Hungarian). *Öntözéses Gazdálkodás*, 11-18.
- Szász, G., 1995: Natural productivity of water in the main grown crops in Hungary (in Hungarian). *Éghajlati és Agrometeorológiai Tanulmányok* 3. Orsz. Meteorológiai Szolg., Budapest, 11-31.
- Szlovák, S., 1968: Transpiration coefficient study of maize. *Öntözéses Gazdálkodás* 6, 1, 39-56.
- Szőke Molnár, L., 1989: Increasing danger of harvest deficiency because of drought (in Hungarian). In *Aszály. Öntözési Kutató Intézet*, Szarvas, 63-66.
- Thorntwaite, C.W. and Mather, I.R., 1961: The role of climate in evapotranspiration. *Archiv für Met. Geogh., u. Biokl. Ser. B.* 3, 16-39.
- Varga-Haszonits, Z., 1989: Climatic characteristics of the volume of water supply's degree during the vegetation period (in Hungarian). In *Aszály. Öntözési Kutató Intézet*, Szarvas, 28-41.
- Varga-Haszonits, Z. and Harnos, Zs., 1988: Effect of climate variability and drought on wheat and maize production. In *Identifying and Coping with Extreme Meteorological Events* (eds.: E. Antal and M.H. Glantz). Országos Meteorológiai Szolgálat, Budapest, 138-166.

IDŐJÁRÁS

Quarterly Journal of the Hungarian Meteorological Service
Vol. 106, No. 3–4, July–December 2002, pp. 215–226

Impact of the climate change on the hydrological regime. A case study on the Danube River

Ödön Starosolszky

Water Resources Research Centre,
P.O. Box 27, H-1453 Budapest, Hungary

(Manuscript received February 25, 2002; in final form June 27, 2002)

Abstract—Many Hungarian national studies related to the impact of the climate changes on the stream flow have been published in the last decade. This paper made an attempt to summarize the results on the investigations of potential change of the runoff.

The model system used for operational hydrology data was applied for the climate change study.

The Danube River, its tributaries, and the Hernád River have been investigated. The model system was used for three scenarios of the upper Danube Basin. Some fragments of the studies have been selected as examples for the applicability of the method. The effects of the change in precipitation and temperature on the change of streamflow (runoff) for four scenarios have been applied. The effect of the change in runoff can be predicted particularly. The method is introduced by examples on real observed data (Appendix). The method can be applied for comprehensive studies on the effects of the climate change.

Key-words: case study, climate change, discharge, flood wave, flood, impact modelings, runoff, snow melt, water intakes.

1. Introduction

Hungarian national studies (*Antal and Starosolszky, 1990; Starosolszky, 1989*) on the effects of the climate change go back to the eighties. A comprehensive report covering several aspects was published in 1994 (*Starosolszky, 1994a,b*). In a study for the International Institute for Applied Systems Analysis (IIASA, Laxenburg, Austria), Water Resources Research Centre (VITUKI) submitted a report on the climate change impact covering the upper Danube Basin (*Starosolszky, 1994b*). Another report within the PECO Project of the *European Union* (1997) includes the following items:

- Impact of a potential climate change on long-term discharge data series;
- The expectable impact of the climate change on the characteristic discharges;
- Effects of the temperature change on the catchment over the Nagymaros section and on the flow conditions of the Danube.

The basic aim was the analysis of the regime of the Danube River at Nagymaros. Special emphasis was devoted to the change of temperature in the drainage basin with special regard to snowmelt induced runoff (*Starosolszky, 1989*).

For the studies three periods, each of them covers one year from September 1 to August 31, were selected. The first study for the daily temperatures was fulfilled with (1) observed values, (2) temperatures 1°C higher, and (3) 3°C higher than the observed values all over the periods. The following questions have been tackled:

- seasonal and monthly distribution of runoff;
- changes in the winter low-flow period;
- changes in the peak discharges of floods in winter;
- changes in the peak discharges of the spring snowmelt induced floods.

The calculations with constant temperature rises are oversimplified and can not express the complicated cross-relations among temperature, precipitation and runoff. These aspects have been neglected in the previous studies (*Starosolszky and Gauzer, 1996*).

2. Scenarios

The voluminous data sets are decomposed for selected periods for modeling climatological and hydrological phenomena. The basic changes on the Danube upstream from Nagymaros were selected for temperature, precipitation, and runoff. The data set can cover simulated values originated from the three scenarios as follows:

- UK Meteorological Office equilibrium experiment (UKHI),
- UK Meteorological Office transient experiment (UKTR),
- Canadian Climate Centre high resolution equilibrium experiment (XCCC).

The fourth scenario was based on measured temperature, and precipitation (*Gauzer, 1993a,b*).

Simulated values can be considered in the data sets. The results gained include tables for daily, monthly, and seasonal streamflow data and their graphical presentation.

3. General trends

Climatologists and hydrologists produced some basic data and these studies were described in a special comprehensive publication (*Antal and Starosolszky, 1990*). The higher snowmelt induced winter flood wave occurs, the larger increase in the ratio of the volume of winter runoff to the annual volume can be expected. If no winter flood wave passes on the river, the changes remain insignificant (i.e., under 1–2%).

Changes of a winter flood wave depend on the role of snowmelt. If a winter flood wave induced by liquid precipitation passes on the river, increase of peak discharge remains insignificant (December flood wave in the wet period). In case of mostly snowmelt induced winter flood waves, peak discharges rise significantly (15–30%, December flood wave in the average period).

In case of several spring and early summer snowmelt induced flood waves, the rise of temperature results in an increasing peak discharge for the first flood wave, while consecutive flood waves in such a period pass on the river with decreasing peak discharges (see flood waves in the dry and average period). Peak discharge of a single major snowmelt induced flood wave shows increasing tendency (spring flood in the wet period).

These oversimplified conditions do not follow the realistic cases when temperature changes are combined with precipitation, snowmelt, and the consequence in the change of the runoff. The snowmelt, the rainfall-runoff, the coupled structural stochastic and unsteady flow models have been applied, and observations on rainfall-runoff were used (*Gauzer, 1993a,b*). The so-called EU (*European Union, 1997*) scenarios were selected for the three-year periods and applied in the PECO Project of the EU.

The simulation of the time series is excepted for three periods and the output is summarized for the Nagymaros gauging station on the Danube.

Fig. 1 shows the discharge time series for a selected year. *Fig. 2* demonstrates the monthly average runoff for a selected period using the results of the different scenarios. *Fig. 3* shows the seasonal averages of the observed and simulated values with special attention to the EU simulations.

Monthly average runoff values are tabulated in *Tables 1–3*. The values are variable according to the simulation method. The data originate from the comprehensive study (*VITUKI, 1997*).

Table 2 shows the seasonal average values of runoff. The variations of seasonal values do not show regular character. Similar investigations were executed for a medium size river (gauging station Gesztely, on the Hernád River). Modeling for a smaller river has more difficulties in the simulation grid (Appendix).

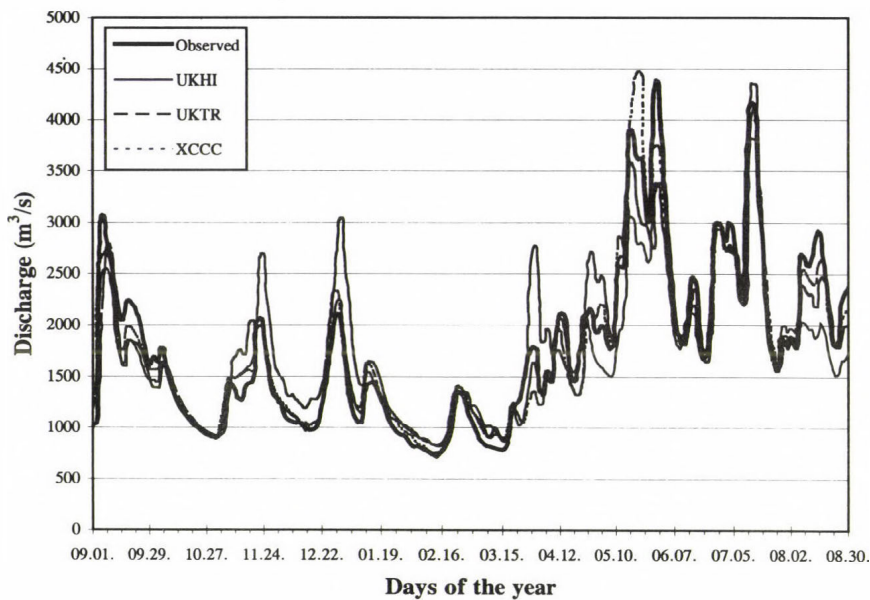


Fig. 1. Runoff simulation for the period 1995-96, at station Nagymaros, Danube River.

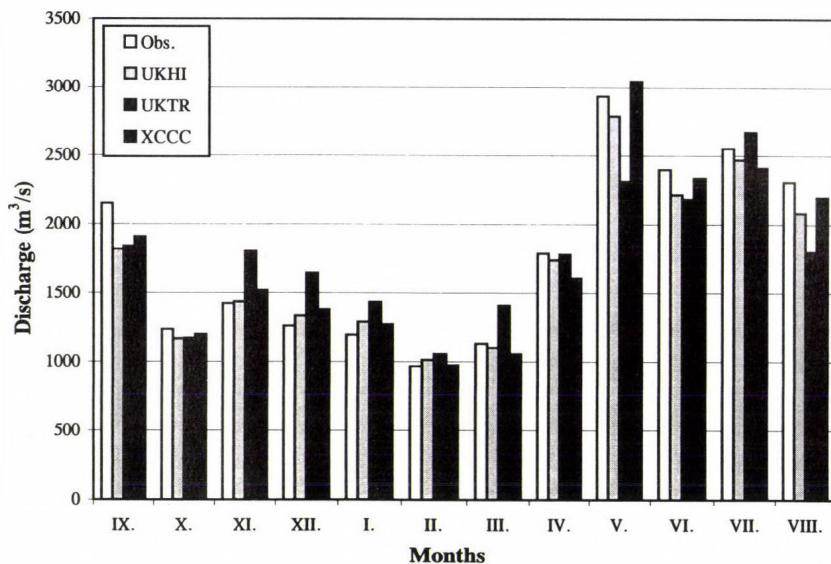


Fig. 2. Monthly average runoff for the period 1995-96, at station Nagymaros, Danube River.

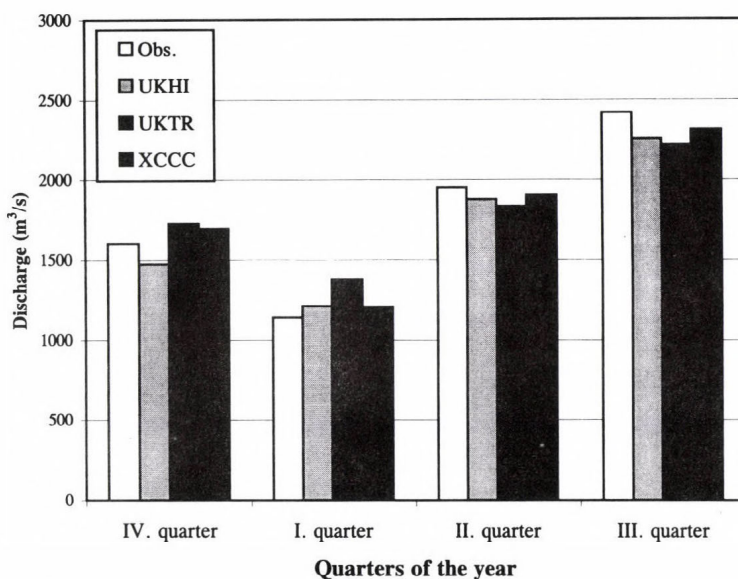


Fig. 3. Seasonal average runoff for the period 1995–96, at station Nagymaros, Danube River.

Table 1. Monthly average values of runoff for cross section of Danube at Nagymaros (m³/s), for the period 1995–96

Scen.	IX.	X.	XI.	XII.	I.	II.	III.	IV.	V.	VI.	VII.	VIII.
Obs.	2151	1234	1424	1263	1195	967	1132	1787	2935	2395	2552	2307
UKHI	1818	1167	1436	1335	1291	1013	1101	1741	2787	2214	2469	2082
UKTR	1838	1170	1801	1644	1435	1054	1410	1779	2311	2182	2669	1800
XCCC	1906	1198	1518	1378	1273	974	1054	1608	3044	2335	2412	2197

Table 2. Seasonal average values of runoff for cross section of Danube at Nagymaros (m³/s), for the period 1995–96

Scenario	IX–XI.	XII–II.	III–V.	VI–VIII.
Observed	1603	1142	1952	2419
UKHI	1474	1213	1876	2255
UKTR	1727	1378	1834	2218
XCCC	1697	1208	1902	2315

Table 3. Statistical characteristics of runoff for cross section of Danube at Nagymaros (m³/s), for the period 1995–96

Scenario	Q _{min}	Q _{max}	Q	σ
Observed	741	4426	1681 (100%)	786
UKHI	798	4032	1707 (102%)	680
UKTR	833	4369	1760 (105%)	651
XCCC	746	4516	1744 (104%)	758

4. Experiences

For the period 1995–96 the following experiences have been gained, as examples: Since air temperatures were not very low during November and December in the observed series representing present day climate, a significant (approximately 5°C) rise of air temperature had a considerable effect on two insignificant floods passed during this period. In spite of the global warming air temperature increase, due to low air temperatures between January and March, changes of runoff remained insignificant. It can be concluded that during this period, due to the low air temperatures, the investigated scenarios have only a slight impact on the safety of power plant operation (Thermal Power Station at Százhalombatta, Nuclear Power Station at Paks).

The number of days gained in the scenarios with discharges higher than those according to the present day climate is 160, 193, and 188, respectively. These are less than values gained by previous periods investigated; this fact is the consequence of slight changes during winter.

The significant decrease of peak discharges of the bi-modal flood for UKHI and UKTR scenarios were the consequence of the earlier snowmelt. Considerable increase of the first peak for the XCCC scenario was produced by smaller air temperature changes.

Since the July flood originated from liquid precipitation, peak discharges were strongly related to the changes of precipitation values.

The decrease of effective precipitation during August was partly compensated by the increase of subsurface inflow as a consequence of higher effective precipitation during winter and spring. As a consequence, 30 percent decrease of precipitation resulted in 20 percent decrease of runoff on the upper catchment.

The rise of the annual average runoff was most significant for the UKTR scenario, due to the most expressed increase of precipitation. The change of standard deviation was influenced by the peak discharge values.

Concluding the present analysis, it is necessary to mention that the simple technique used to transform monthly changes into daily values and also the short data series used may limit the possibility to derive general conclusions from the results received.

Generalization of the results was made for upstream stations for the three selected years. The simulations of the Danube flow regime for three selected periods of one year demonstrated the change in the time series as a consequence of the variation of daily temperature and precipitation. The three scenarios based on global circulation models redistribute the flow time series for the selected periods.

Major changes were found in the freeze and snowmelt periods, thus the flow originated from snowmelt generated runoff was shifted and the spring flows changed characteristically. The minimum and maximum flows were distorted, e.g., minimum flow in the autumn period was further reduced, and maximum flow in springtime was increased.

The simulation of the flow time series offers some general trends in the flow redistribution during the year (e.g., from September 1 to August 31). The arbitrary nature of the selection of the years for the Danube study may hinder the exact generalization of the changes, but some characteristic change could be detected.

The extension of the river basin from the two upstream stations (Pfelling and Wasserburg) downstream to Nagymaros also shows the different nature of the upstream and downstream sub-basins. This is reflected by the smaller runoff coefficients of the catchments located in lower altitudes (like rivers Rába, Morava, Vah). The outputs of the study may be extracted for each gauging station but for the latest (PECO) study at Nagymaros gauging station is considered as reference downstream station (*European Union, 1997*).

5. Climate change and water intakes

Considerations of water intakes on the Danube can be useful for the water management. The crucial question of the Hungarian Danube is the change of the minimum flows at the large cooling water intakes for a thermal (Százhalombatta, rkm 1622) and a nuclear (Paks, rkm 1526) power station. Their pumping stations have been constructed in diversion (intake) canals, considering a design water level for the pumps. Due to water level depletion in the main Danube, the water levels in the derivations can be influenced.

For the sake of simplicity, flow relations have been derived between Nagymaros, and Százhalombatta, and Paks, respectively. A simple linear

correlation was derived for the stations and the effects of the changes of the minimum flows were investigated (Gauzer and Starosolszky, 1997).

The simple flow interrelations are, as follows:

$$Q_{sb} = 104.5 + 0.996 Q_{nm} ,$$

$$Q_{pa} = 20.7 + 0.965 Q_{nm} ,$$

where

Q_{sb} - discharges at Százhalombatta,

Q_{pa} - discharges at Paks,

Q_{nm} - discharges at Nagymaros.

It was concluded that the lowering of the low flows will be transferred to the locations of the intakes, but the reduction of the flow in low water periods will do basically no harm to the water intakes. The effect of the riverbed degradation can be much stronger than the effect of the reduction of low flows.

The changes of the flow due to the climate change expressed by the three temperature and precipitation scenarios can not danger the basic water intakes in Hungary. However a combined effect of low flow reduction and bed degradation can be sensitive for further developments, particularly for new cooling water intakes. It is therefore suggested, that bed degradation due to river morphology and climate change may be simultaneously investigated from the point of cooling water intakes.

For demonstrating the application of the method, an *Appendix* is attached. The river size may limit the applicability. The Hernád River demonstrates a medium size catchment. The Appendix shows the results of modeling climate data according to the three scenarios.

APPENDIX

Application of the model for the simulation over the Hernád River Basin

The Danube study has a regional character. It was obvious to make a study on a tributary representing a medium catchment.

The methodology applied for the Danube catchment over Nagymaros was used for a local study of a subcatchment of the Tisza River, the catchment of the Hernád River (in eastern Slovakia and north eastern Hungary). The total

area exceeds 5359 km², 4300 km² is in Slovakia, and the downstream part of 1013 km² is in Hungary. This can be the minimum size of a catchment where the method is applicable.

The average temperature varies between 8 to 10°C in consequence of the prevailing northeast dry and cool climatic fronts. Interesting to mention that the NE-SW oriented valley sometimes produces a very strange climatic situation, as a dry and hot front from SW direction initiates a sudden temperature rise and low humidity rates in the southern part of the valley. Also these circumstances contribute to the relative low precipitation rate, which amounts to 550 mm/year only in long-term average.

In the Slovakian part, the river drains agricultural areas and some major cities, with Spiska Nova Ves, Presov and Kosice being the three largest ones. The Hungarian part of Hernád is dominated by flood plains. The upper layer of the soil consist of clay, peat land, and in some areas sand.

The average temperature for the coldest month in the Hungarian part of Hernád is approximately -3.5°C, while the warmest month is July with 18–21°C. The rainfall is 530–580 mm/year, and the specific runoff 21 l/s km². The maximum rainfall is during the summer months.

Forests cover 200 km² (20%) of the total catchment area, and grassland extends to 260 km² (26%). The crop area is predominantly tilled, and consists of 410 km² (41%). Built up areas (roads, towns, and villages), water areas, riverbanks, etc. cover 137 km² (13%).

Agriculture is one of the major activities, and the main crops are winter-wheat, maize, sunflower, lucern, rape, potatoes, and barley.

The total population in the river basin is approximately 64,000. There are 72 municipalities within the Hungarian catchment, where the largest villages are Bócs (2643 inhabitants), Encs (6663 inhabitants), Gesztely (2753 inhabitants), Gönc (2378 inhabitants), and Forró (2239 inhabitants). These five villages constitute 26% of the total population, showing that the total numbers of small villages are high. The largest villages are situated along the Hernád River.

The aim of the Hernád study was to demonstrate the applicability of the simulation method for a relatively small catchment of the Danube basin, where the number of the stream gauging stations is rather limited.

The reference periods selected for the simulation are from September 1, 1992 to August 31, 1993 and from September 1, 1995 to August 31, 1996.

For examining the climate change impact, the three selected scenarios UKHI, UKTR, and XCCC were also used. One may note that relatively small figure of the grids involved may influence the accuracy of the simulation. Thus, a refinement of the grid-system would be desirable. The variety of the temperature and precipitation over the catchment may influence the credibility of the simulation.

The results of the simulation are given in tabulated form (*Tables A1–A8*). The effect of the climate change scenarios is rather characteristic for the daily, monthly, and seasonal flows at the gauging station of Gesztely (Hungary).

The conclusion is that the change in flow does not influence heavily the hydropower generation neither at present, nor in the future. Thus, the annual hydropower generation will not be strongly effected.

Changes of air temperature and precipitation according to the scenarios

Table A1. Changes of the monthly air temperature (°C)

	IX.	X.	XI.	XII.	I.	II.	III.	IV.	V.	VI.	VII.	VIII.
UKHI	3.04	3.73	3.59	3.04	1.66	1.52	1.10	1.79	1.93	2.07	1.93	2.62
UKTR	4.20	4.50	7.40	3.70	2.30	1.50	2.30	2.50	3.60	2.50	4.60	5.50
XCCC	1.52	1.66	2.21	1.38	0.97	0.97	1.10	1.10	1.24	1.24	1.38	1.10

Table A2. Changes of the monthly precipitation (%)

	IX.	X.	XI.	XII.	I.	II.	III.	IV.	V.	VI.	VII.	VIII.
UKHI	14.08	23.74	9.38	4.97	1.38	2.35	-0.55	-5.38	-5.80	4.14	4.42	15.04
UKTR	20.30	28.20	45.90	26.00	-5.90	9.00	12.80	-12.8	-3.00	16.50	27.80	31.10
XCCC	9.25	15.18	11.18	9.80	4.00	-0.97	-6.21	0.14	-6.35	0.00	16.84	15.46

Table A3. Calculated monthly maximum flows (m³/s)

	Observed	UKHI	UKTR	XCCC
1992–93	27.213 (July)	27.202 (July)	31.453 (July)	25.523 (July)
1995–96	32.110 (Aug)	31.234 (May)	31.643 (June)	32.282 (May)

Table A4. Calculated monthly minimum flows (m³/s)

	Observed	UKHI	UKTR	XCCC
1992–93	3.311 (Feb)	4.240 (Feb)	4.405 (Feb)	3.881 (Feb)
1995–96	4.121 (Oct)	4.028 (Oct)	4.242 (Oct)	4.026 (Oct)

Monthly mean effective precipitations and discharges according to the selected scenarios

Table A5. Monthly sums of the effective precipitation (mm) (1992/93)

	IX	X	XI	XII	I	II	III	IV	V	VI	VII	VIII
Obs.	26.20	59.40	25.90	13.70	5.10	4.50	15.50	6.60	27.90	36.40	69.40	50.80
UKHI	24.00	62.10	27.30	17.00	6.00	7.50	16.50	6.70	28.60	37.70	68.80	47.50
UKTR	25.10	70.80	34.90	20.00	6.90	7.60	23.50	8.80	26.00	41.30	81.40	42.20
XCCC	24.00	59.60	31.50	16.40	5.50	6.80	18.10	7.30	29.30	35.40	64.40	50.60

Table A6. Monthly sums of the effective precipitation (mm) (1995/96)

	IX.	X.	XI.	XII.	I.	II.	III.	IV.	V.	VI.	VII.	VIII.
Obs.	42.90	2.60	20.40	15.70	19.70	17.20	13.80	41.90	76.50	66.80	44.40	111.5
UKHI	39.20	2.70	21.40	18.60	21.70	22.20	15.00	44.30	77.50	68.30	44.40	104.4
UKTR	41.20	3.30	25.80	22.50	23.20	23.00	21.40	54.30	70.40	74.70	53.20	94.90
XCCC	39.20	2.60	24.80	18.60	21.60	19.70	15.30	47.30	80.00	66.40	40.70	110.7

Table A7. Monthly mean discharges (m³/s) (1992/93)

	IX.	X.	XI.	XII.	I.	II.	III.	IV.	V.	VI.	VII.	VIII.
Obs.	11.17	22.58	17.46	8.158	4.562	3.311	5.505	7.530	7.461	18.17	27.21	21.81
UKHI	10.56	23.25	18.15	9.490	4.939	4.240	6.320	8.003	7.641	18.70	27.20	20.84
UKTR	11.14	26.05	21.82	10.83	5.501	4.405	7.907	10.03	7.228	19.33	31.45	20.28
XCCC	10.60	22.43	19.51	9.402	4.756	3.881	6.402	8.257	7.799	18.20	25.52	21.44

Table A8. Monthly mean discharges (m³/s) (1995/96)

	IX.	X.	XI.	XII.	I.	II.	III.	IV.	V.	VI.	VII.	VIII.
Obs.	18.21	4.121	10.07	6.724	10.49	9.712	6.221	13.47	30.54	29.33	17.95	32.11
UKHI	16.85	4.028	10.43	7.698	11.27	11.33	7.192	14.25	31.23	30.01	18.01	30.57
UKTR	17.66	4.242	12.24	8.984	12.18	11.81	9.059	17.90	30.17	31.64	20.75	29.14
XCCC	16.90	4.026	11.64	7.749	11.40	10.59	6.966	15.17	32.28	29.62	16.99	31.69

References

- Antal, E. and Starosolszky, Ö., 1990: *Role of the Climate and Climate Change in the Life of Hungary* (for the Second World Climate Conference). Hungarian Ministry for Environment and Regional Policy, Budapest.
- European Union, 1997: Contribution to the PECO Project.
- Gauzer, B., 1993a: Effect of temperature change on the flow conditions of the Danube. Part I. (in Hungarian). *VITUKI Report*, Budapest.
- Gauzer, B., 1993b: Effect of temperature change on the flow conditions of the Danube. Part II. Analysing dry and wet periods (in Hungarian). *VITUKI Report*, Budapest.
- Gauzer, B. and Starosolszky, Ö., 1997: The effect of climate change on Danube flow regime. *IAHR Congress*, San Francisco, 1997, 572-577.
- Kuusisto, E., 1994: Climate and water in Europe; some recent issues. *WMO Technical Report*, WG on Hydrology, Helsinki.
- Starosolszky, Ö., 1989: Climatic change and water management (in Hungarian). *Vízügyi Közlemények Vol. 1. LXXI*. No. 3, 465-469.
- Starosolszky, Ö. (team leader), 1994a: Effect of climate change on hydrological and water quality parameters (in Hungarian). (Theme No. 716/90 of the Hungarian NSF). *VITUKI*, No. 59, Budapest.
- Starosolszky, Ö. (ed.), 1994b: Climate change impact on the water management of Hungary including the upper Danube. *IIASA Contract*, No. 94-115.
- Starosolszky, Ö. and Gauzer, B., 1996: Effect of potential air temperature and precipitation change on the flow regime of the Danube. *Időjárás* 100, 219-227.
- VITUKI*, 1979: Effect of precipitation and temperature changes in the catchment upstream of the Nagymaros section on the flow conditions of the Danube (EV5V-CT93-0293), Budapest.
- WMO*, 1989: Conference on Climate and Water. *Report of the Conference*. Helsinki, Finland.

IDŐJÁRÁS

Quarterly Journal of the Hungarian Meteorological Service
Vol. 106, No. 3–4, July–December 2002, pp. 227–238

Mapping of mean annual actual evaporation on the example of Zagyva catchment area

Béla Nováky

Department of Landscape Ecology, Szent István University
Páter Károly u. 1, H-2103 Gödöllő, Hungary
E-mail: novbela@fau.gau.hu

(Manuscript received February 19, 2002; in final form August 5, 2002)

Abstract—A method for the mapping of the mean annual actual evaporation is demonstrated on the example of the Zagyva catchment. For the calculation of the mean annual actual evaporation, the original and modified Turc's formula and two modified types of Budyko's formula were compared. Calculated by the listed formulas, mean annual actual evaporation was compared with its values given by Eq. (1), as a difference between annual precipitation and runoff for drainage areas using, observations within the Zagyva rivershed. The Turc's formula underestimates the evaporation, the best fitting is provided by the modified Budyko's formula (Eq. (10)). Using this formula, the model parameter α was validated by observed runoff data. In the mapping process any drainage area is covered by orthogonal grids, and using the digitized maps of precipitation and temperature, the actual evaporation is calculated for all the grids individually, then step by step a continuous and consistent map of actual evaporation is developed by interpolation between calculated grid values (Fig. 2).

Key-words: mean annual evaporation, Turc's formula, Budyko's formula, water balance, mean annual runoff, grid mapping.

1. Introduction

Some portion of the precipitation over a given area evaporates and returns to the air after a temporal accumulation on land surface or in the soil. The rate of the actual evaporation depends on the capacity of the air to take the vapor, that is, on the potential evaporation and the actual moisture content of soil. The soil moisture content changes mainly with weather conditions, but depends on the soil and vegetation type, too. In many agrometeorological tasks like the calculation of total water demand or irrigation water demand of plants, the soil

and plants play very important role in the actual evaporation, so the calculation of the later needs equations, which take into the consideration those factors. Many methods of such type exist in the world. In Hungary one of the most frequently used formula was proposed by *Antal* (1968). In the calculation of the actual evaporation for larger areas and longer time period (for average year), the climate elements play the main role, probably exceeding the role of the soil and vegetation. This follows from that the soil properties and particularly the vegetation usually are in a good relation with the climate. As the purpose of this paper, to demonstrate the mapping of long term average annual actual evaporation using the formulas based on the climate elements is highly suitable.

The map of the spatial actual evaporation of Hungary was firstly constructed as a difference of maps of mean annual precipitation and mean annual runoff (*Szesztay*, 1957). Later this map was refined using a similar method (*Kardos*, 1975). The mapping is based on the mean annual water balance equation

$$P = ET + R, \quad (1)$$

where P , ET , and R are the mean annual precipitation, actual evaporation, and runoff, respectively.

2. Methods and data

Literary sources suggest many different formulas for the calculation of the actual evaporation. In our investigations the *Turc's* and *Budyko's* formulas were selected.

Using the *Turc's* method (1954), the calculation of the actual evaporation consists of two consecutive steps. Firstly it is necessary to calculate the *EPI*-index expressing the spatial variation of the potential evaporation (EP) by means of the formula

$$EPI = 300 + 25T + 0.051 T^3, \quad (2)$$

which needs to have only temperature data. The second step is the calculation of the actual evaporation by the following equation:

$$ET = P[c + (P/EPI)^n]^{-1/n}, \quad (3)$$

where P is a the precipitation, c and n are the model parameters. Using the observed data of precipitation, temperature, and runoff at the 254 different

catchment areas under various climate conditions, the model parameters were suggested by *Turc* as follows, $c = 0.9$ and $n = 2$, so the specified equation has the form

$$ET = P[0.9 + (P/EPI)^2]^{-0.5}. \quad (4)$$

Application of the *Turc*'s formula in climate conditions of Slovakia, being a neighbouring country to Hungary, showed that the actual evaporation was gradually underestimated using this formula in its proposed form (*Parajka* and *Szolgay*, 1998). Trying to adapt Eqs. (2) and (4) to Slovakian climatic conditions the model parameters were refined. For the calculation of the *EPI*-index and actual evaporation

$$EPI = 237.38 + 40.67 T + 0.0864 T^3, \quad (5)$$

and

$$ET = P[0.9 + (P/EPI)^{2.67}]^{-1/2.67} \quad (6)$$

were proposed. The fact that *Turc*'s formula underestimates the evaporation was shown in Hungarian drainage basins using precipitation and runoff data (*Nováky*, 1991).

The *Budyko*'s (1948) formula was selected for further investigation. The formula is

$$ET = P[1 - \exp(-r/LP)], \quad (7)$$

where r is the net radiation, L is the latent heat, P is the precipitation, and r/LP is the aridity index. The *Budyko*'s formula is the improved version of the relationship between precipitation and runoff discovered by *Schreiber* (1904) nearly 100 years ago. In our investigations the formula was modified, when the net radiation was substituted by the temperature or climate index given by any combination of the temperature and precipitation.

In the first version of the modification, using the equation

$$r/L = P(\ln P - \ln R) \quad (8)$$

given by the rearrangement of the *Budyko*'s formula, the values r/L were calculated for observed drainage areas, and a relationship between calculated

values r/L and the temperature was developed. (The value r/L can be accepted as one of the variant of the *EPI*-index.) This relationship was formulated as follows:

$$r/L = m(T - T_o)^n, \quad (9)$$

where T_o is a threshold temperature, below it the (potential) evaporation can be accepted as it equals to 0, m and n are the model parameters to be validated. In an earlier study for the Rába catchment, these parameters were validated: $m = 15.95$, $n = 1.66$ (Bergman *et al.*, 2001).

The other adapted version of the Budyko's formula was elaborated in the process of mean annual runoff mapping (Nováky, 1985) at the time of the compilation of National Master Plan of Water Management in Hungary (OVH, 1984). The value r/L (practically the net radiation) was substituted in the proposed method by the value of the pan evaporation using a correction factor (α), taking into consideration that both net radiation (r/L) and pan evaporation (E_{pan}) are in close correlation with potential evaporation, consequently also with each other. The relationship between net radiation and pan evaporation is described with equation

$$r/L = \alpha E_{pan}. \quad (10)$$

In the next step, using the observed values of 13 pan evaporation stations under different climatic conditions in Hungary, the relationship between pan evaporation (E_{pan}) and a simple climate index, formulated as the rate of the mean annual temperature to the mean annual precipitation, was developed, as follows

$$E_{pan} = 36,400TP^{-1} + 104 \quad (11)$$

(Nováky, 1985). Substituting the Eqs. (10) and (11) to Eq. (7), a formula

$$ET = P\{1 - \exp[-\alpha(36,400TP^{-1} + 104)P^{-1}]\} \quad (12)$$

is given for the calculation of the actual evaporation. The formula needs the validation of model parameter α . Validating this parameter the calculation of the actual evaporation requires the knowledge only of mean annual precipitation and temperature.

The validation of the model parameter α is possible by the optimisation of values α calculated individually for the observed drainage areas, where the

values of mean annual precipitation, mean annual temperature, and mean annual runoff exist for the same periods of observations used in Eqs. (1) and (12). The optimised value of model parameter α for the whole country without any regionalisation is equal to 2 (Nováky, 1988). While parameter α is in the exponent of Eq. (12), naturally the calculation of the actual evaporation is highly sensitive to its value.

For mapping the actual evaporation, a formula is selected, which allows to calculate its value being best fitted to actual evaporation values calculated as the differences between precipitation and runoff in observed drainage areas.

Besides the model parameter, all formulas for calculation of the actual evaporation need essentially to have two meteorological elements, the precipitation and temperature, so the mapping of the actual evaporation also needs the maps of mean annual precipitation and mean annual temperature. During the process of mapping, all of the catchments are discretized using the net of orthogonal grids. The mean annual precipitation and temperature are determined for all grids separately, that means that continuous maps are digitized according to the space interval of grids. Using the digitized maps of precipitation and temperature, the actual evaporation is calculated for all the grids individually and a continuous and consistent map of actual evaporation is developed by interpolation between these calculated grid values.

Following the calculation of the actual evaporation, the grid runoffs are also calculated as the difference between grid precipitation and evaporation, further by summing up the grid runoffs for the grids belonging to any river section with runoff observations, the catchment runoff is also given. In this process according to the rows and columns of orthogonal grids, a matrix notation can be adopted to identify the grids (*Fig. 1*).

The grid in row i and column j can be denoted by e_{ij} , the calculated runoff by R_{ij} . Let N_{ij} is the set of grids upstream to e_{ij} , so grids belonging to N_{ij} compose the catchment upstream to grid e_{ij} . If a grid e_{kl} belongs to set of grids N_{ij} , the grid runoff R_{kl} reaches the grid e_{ij} , otherwise it does not. The catchment runoff in grid e_{ij} can be calculated as

$$R^* = \sum \sum \delta_{kl} R_{kl}, \quad (13)$$

where δ_{kl} is a Kronecker function, its value is 0, if $e_{kl} \notin N_{ij}$, and 1, if $e_{kl} \in N_{ij}$. Eq. (13) provides a connection between the grid runoff R_{ij} and catchment runoff R^*_{ij} . In the section of observed catchments, the calculated catchment runoff R^* can be compared by its observed value, and on the basis of differences the suitability of the model can be evaluated.

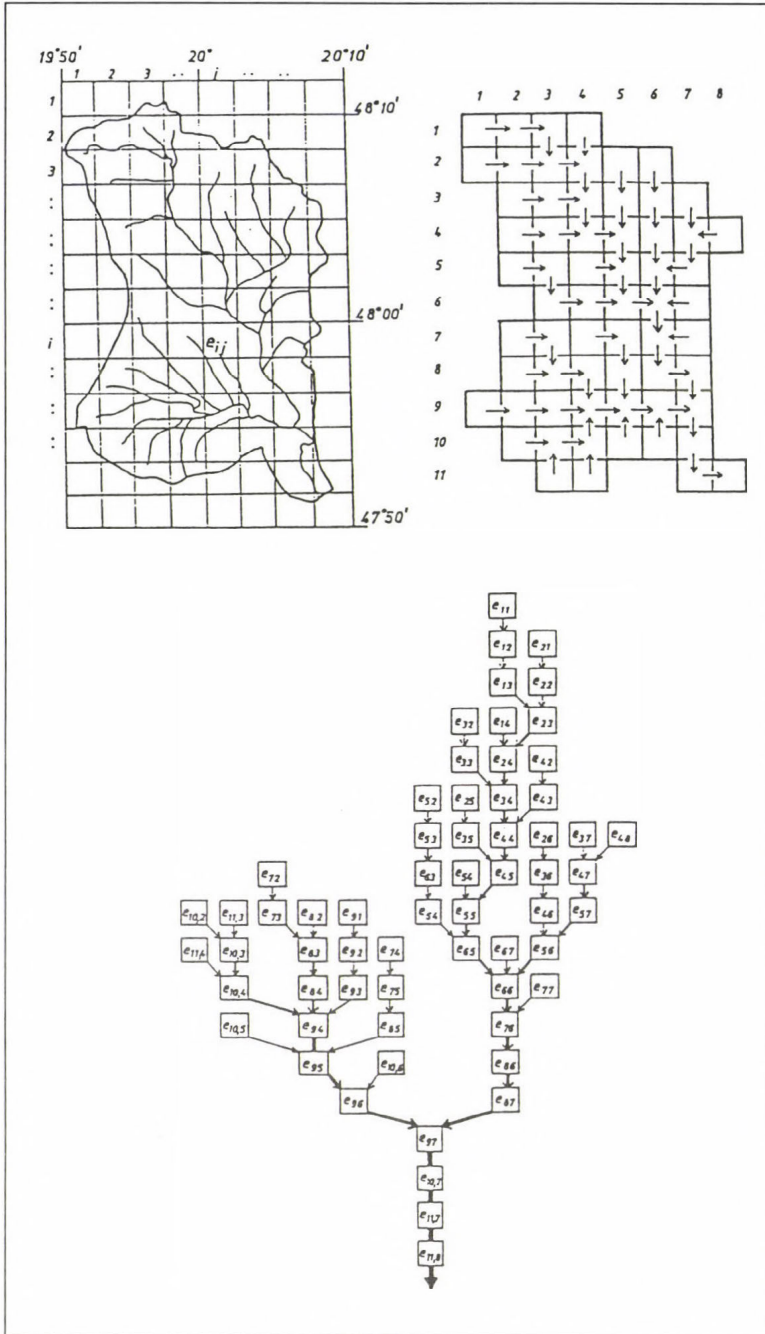


Fig. 1. Spatial discretization of the catchment.

3. Data sources

The map of the actual evaporation was constructed for the Zagyva catchment, where there are some hydrological stations with runoff observation. Using runoff data, the formula mostly available for calculation of actual evaporation can be chosen and its model parameter can be calibrated (Table 1). Runoff data were taken from the study describing hydrological conditions of the Zagyva catchment (Nováky, 1985) compiled in the process of the elaboration the National Master Plan of Water Management in Hungary (OVH, 1984).

Table 1. Mean annual water balance of subcatchments in the Zagyva River basin

Watercourses	Hydrological stations	Catchment area km ²	Precipitation P (mm)	Temperature T (°C)	Runoff R (mm)
Zagyva	Nemti	149	631	8.7	68
	Pásztó	488	636	8.6	94
	Szentlőrincskáta	1955	600	9.1	54
	Jásztelek	4207	605	9.2	56
Tarna	Verpelét	574	645	8.4	79
	Jászdózsa	1810	621	9.1	64
Galga	Galgamácsa	242	585	8.9	54
	Hévízgyörk	416	577	9.0	64
Tápió	Tápiószele	771	562	9.9	44
Bene-patak	Nagyfüged	133	671	8.9	105
Gyöngyös-patak	Jászárokszállás	290	637	9.1	93

In the calculation of mean annual runoff, the period of observation were very different, and its length ranged from 9 (Zagyva, Nemti) to 76 (Zagyva, Jásztelek) years. Therefore, the mean annual precipitation and temperature were calculated for the same period from which the mean annual runoff was originated. Precipitation data before 1970 were taken from the collection of precipitation data compiled by *Hajósy et al.* (1975), and after 1970 from the Hydrographical Bulletins of VITUKI. The mean annual temperature for given periods was taken with appropriate correction from the Climatic Atlas compiled by the Hungarian Meteorological Service (*Kakas*, 1960). The correction factors were calculated using the temperature data of meteorological stations having long term observations.

After selecting the formula mostly available for calculation of actual evaporation, the mapping of the latter was made using digitized maps of precipitation and temperature of the mentioned Climatic Atlas. The grid of the digitization has a size of 6 km × 6 km.

4. Results

To choose the best fitting formula for calculation of the actual evaporation, the original and modified Turc's formulas, also the modified Budyko's formulas were used and compared. Before using the modified Budyko's formula, it was necessary to calibrate the parameters m and n in Eq. (9). Based on the observed data of 11 catchments, the model parameters were calibrated, $m = 10.4$ and $n = 1.85$, so the formula for the calculation of the actual evaporation specified for Zagyva catchment was given as

$$ET = P\{1 - \exp[-10.4(T + 5)^{1.85}P^{-1}]\}. \quad (14)$$

For the calculation of the actual evaporation by Eq. (12), the model parameter α was selected so that the differences between calculated annual evaporation and annual evaporation given by Eq. (1) for the observed catchments were minimal. The calibrated model parameter $\alpha = 2.14$, and the actual evaporation can be calculated by specified formula

$$ET = \{1 - P \exp[-2.14\alpha (36,400TP^{-1} + 104)P^{-1}]\}. \quad (15)$$

The values of the EPI index calculated by Turc's, modified Turc's, two types of modified Budyko's formulas range in order of these formulas in intervals of 540–596 mm, 630–723 mm, 1265–1540, and 1237–1595 mm. In all cases the minimum value is given for the catchment of Tarna at Verpelét and the maximum for Tápió at Tápiószele. The potential evaporation indices given by Budyko's method are significantly higher than values calculated by Turc's formulas. The significant difference can be explained by fact that the EPI index calculated by Budyko's formulas really expresses the energetically possible maximal evaporation, which is formed in case when the whole net radiation energy is directed to evaporation. In fact, in climatic conditions similar to Hungary, only about 70% of net radiation is used for evaporation (Péczely, 1981). Taking into consideration this rate, the values of the EPI index range about between 830–1050 mm, which are higher than values given by Turc's formulas, but are closer to the potential evaporation typical for Hungarian climatic conditions.

The actual evaporation was calculated by four different equations for 11 observed drainage basins (Table 2). The results were compared to the values of actual evaporation given by Eq. (1) as a difference between observed precipitation and runoff. The average error is 21.8% using the original Turc's formula, 8.5% for the modified Turc's formula, and less than 2% for modified Budyko's formulas. A similar order is received when formulas are compared to the errors of calculated runoff, but the errors of runoff calculations are significantly higher (Table 3). The average error is 178% using the original Turc's formula, 69% using its modified version based on Slovakian runoff data, and about 12% using whichever modified Budyko's formula. The Turc's formula significantly underestimates the actual evaporation for Hungarian climatic conditions.

Table 2. Comparison of the formulas for the calculation of actual evaporation

Water-courses	Hydrological stations	Observed actual evaporation mm	Calculated actual evaporation by							
			Turc's formula		Modified Turc's formula		Modified Budyko's formula		Modified Budyko's formula	
			Eq. (4)	Eq. (6)	Eq. (6)	Eq. (14)	Eq. (14)	Eq. (15)	Eq. (15)	
E		E _c	%	E _c	%	E _c	%	E _c	%	
Zagyva	Nemti	563	427	24.1	501	11.0	553	1.8	550	2.3
	Pásztó	542	427	21.2	500	7.7	554	2.2	550	1.5
	Szentlőrincskáta	546	423	22.5	494	9.5	541	0.9	542	0.7
	Jásztelek	549	426	22.4	499	9.1	546	0.5	546	0.5
Tarna	Verpelét	566	427	24.6	500	11.7	554	2.1	550	2.8
	Jászdózsa	557	430	22.8	504	9.5	555	0.3	552	0.9
Galga	Galgamácsa	531	415	21.8	483	9.0	527	0.7	532	0.2
	Hévízgyörk	513	413	19.5	481	6.2	523	1.9	529	3.1
	Tápiószele	518	419	19.1	488	5.8	526	1.5	529	2.1
Bene-patak	Nagyfüged	566	442	21.9	521	8.0	582	2.8	568	0.4
Gyöngyös-patak	Jászárokszállás	544	435	20.3	512	5.9	566	4.0	559	2.8
Mean			21.8		8.5		1.9		1.6	

Table 3. Errors of calculation of mean annual runoff using different formulas for the calculation of mean annual actual evaporation

Water-courses	Hydrological stations	Observed mean annual runoff mm	Mean annual runoff calculated by							
			Turc's formula		Modified Turc's formula		Modified Budyko's formula		Modified Budyko's formula	
			Eq. (3)		Eq. (4)		Eq. (7)		Eq. (10)	
			R _c	%	R _c	%	R _c	%	R _c	%
Zagyva	Nemti	68	204	200.0	130	91.2	78	14.7	81	19.1
	Pásztó	94	209	122.3	136	44.6	82	12.8	86	8.5
	Szentlőrincskáta	54	177	227.8	106	96.3	59	9.3	58	7.4
	Jásztelek	56	179	219.6	106	89.3	59	5.4	59	5.4
Tarna	Verpelét	79	218	175.9	145	83.5	91	15.2	95	20.3
	Jászdózsa	64	191	198.4	117	82.8	66	3.1	69	7.8
Galga	Galgamácsa	54	170	214.8	102	88.9	58	7.4	53	1.8
	Hévízgyörk	64	164	156.2	96	50.0	54	15.6	48	25.0
	Tápiószele	44	143	225.0	74	68.2	36	18.2	33	25.0
Bene-patak	Nagyfüged	105	229	118.1	150	42.8	89	15.2	103	1.9
Gyöngyös-patak	Jászárokszállás	93	202	117.2	125	34.4	71	23.7	78	16.1
Mean			179.6		70.2		12.8		12.6	

The modified Budyko's formula (Eq. (14)) was accepted for mapping the actual evaporation in the Zagyva catchment (Fig. 2). According to the map, the mean annual actual evaporation ranges from 490 to 560 mm. The lowest values are typical for flatland parts of Zagyva close to the mouth of the river, and the highest values are characteristic for mountainous parts of the catchment. The actual evaporation in the Zagyva catchment is determined and limited mainly by the rate of annual precipitation, so the actual evaporation in all catchments is lower than the potential evaporation.

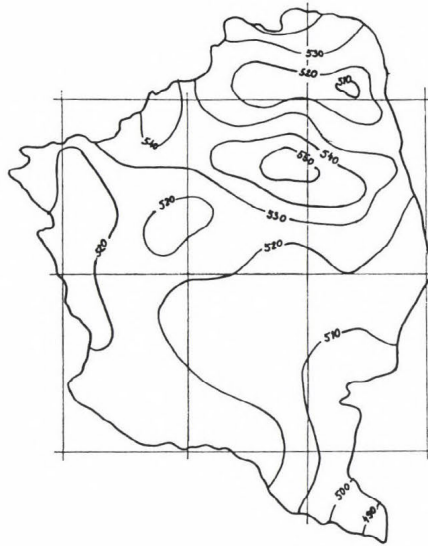


Fig. 2. The map of mean annual actual evaporation for the Zagyva catchment.

5. Discussion

The spatial variation of the actual evaporation reflects the spatial variation of two main meteorological elements, the precipitation and temperature, but does not reflect the mosaic-like spatial variation of land surface properties. For a given locality the map can provide only a first approximation of the actual evaporation, and for a given farm-sized cultivated land, to calculate the actual evaporation, the method proposed by *Antal* (1968) remains as one of the most applicable methods. Nevertheless, there is a possibility for the refinement of the proposed map with taking into consideration at least the spatial differentiation of mean land use categories within the catchment. Further investigations to that direction may lead to the desired results.

References

- Antal, E.*, 1968: Irrigation schedule on the basis of meteorological data (in Hungarian). CSc. Thesis, Budapest.
- Bergman, H., Krainer, R., Krall, E., Domokos, M., Goda, L., Hamza, I., Neppel, F., and Nováky, B.*, 2001: Untersuchungen im Einzugsgebiet der Oberen Raab über Hydrologische folgen einer möglichen Klimaänderung. *Schriftenreihe zur Wasserwirtschaft*, 36, Technische Universität, Graz.
- Budyko, M.*, 1948: *Evaporation in Natural Conditions* (in Russian). Gidrometizdat, Leningrad.

- Hajósy, F., Kakas, J., and Kéri, M., 1975: Monthly and yearly sum of the precipitation in Hungary from the beginning of the observation until 1970 (in Hungarian). Országos Meteorológiai Szolgálat Hivatalos Kiadványai, XLIII., Budapest.
- Kakas, J. (ed.), 1960: *Climatic Atlas of Hungary* (in Hungarian). Akadémiai Kiadó, Budapest.
- Kardos, M., 1975: Water balance of Hungarian part of Danube basin (in Hungarian). *Beszámoló a VITUKI 1972. évi munkájáról*. VIZDOK, Budapest.
- Nováky, B., 1985: Climatic bases of runoff in the water system of rivers Zagyva and Tarna. *Vízügyi Közlemények, LVII., 1., 78-94.*
- Nováky, B., 1988: Methodological problems in the cartographic representation of engineering-hydrologic information. *Hidrológiai Közlöny 68, 4, 193-206.*
- Nováky, B., 1991: Hydrological impacts of climate change (in Hungarian). CSc Thesis, Budapest.
- OVH, 1984: *National Master Plan of Water Management* (in Hungarian). Országos Vízügyi Hivatal, Budapest.
- Parajka, J. and Szolgay, J., 1998: Grid based mapping of the long term mean annual potential and actual evapotranspiration in Slovakia. *IAHS Publ., No. 248, 123-129.*
- Péczely, Gy., 1981: *Climatology* (in Hungarian). Tankönyvkiadó, Budapest.
- Schreiber, P., 1904: Über die Beziehungen zwischen die Niederschlag und der Wasserführung der Flüsse in Mitteleuropa. *Z. Meteorol., Wien, 441-452.*
- Szesztay, K., 1957: Manuals for calculation of actual evaporation (in Hungarian). *Beszámoló a VITUKI 1956. évi munkájáról*. Műszaki Könyvkiadó, Budapest.
- Turc, L., 1954: Le bilan d'eau des sols: Relations entre les précipitations l'évaporation et l'écoulement. *Annales Agronomiques, No. 4, 491-595.*

IDŐJÁRÁS

*Quarterly Journal of the Hungarian Meteorological Service
Vol. 106, No. 3–4, July–December 2002, pp. 239–247*

International efforts for drought mitigation

László Vermes

*Szent István University, Faculty of Horticultural Sciences
Villányi út 35-43, H-1118 Budapest, Hungary
E-mail: vermes@omega.kee.hu*

(Manuscript received April 12, 2002; in final form August 16, 2002)

Abstract—Drought has harmful effects not only on plants and animals, but on all living organisms and the whole human society as well. In the light of this recognition, many organizations and international associations started to deal with the methods of drought mitigation not only in agriculture, but also in wider environment, including socio-economic effects. The paper gives an outlook on some of the most important international and national events concerning drought mitigation in the last few years. Detailed information is given on the activity of ICID European Regional Work Team on Drought (ERWTD) and its guide for drought mitigation strategy. We point out the importance of the construction of the European drought sensitivity map as well as the new evaluation and synthesis of the results of the research work related to different drought effects. For solving all these multi-disciplinary tasks, a well coordinated international co-operation is needed with active participation of the experts of the most interested countries, especially in the frame of the UNCCD.

Key-words: drought mitigation, international co-operation.

1. Introduction

In the last period of time it could be clearly recognized that the rhythm of the changes in the natural and social environment became more and more rapid, and the effects of the changes became increasingly bright, complex, and permanent. All these processes influence the everyday and future human life more and more directly compared to previous time. Dryness and drought are results of the special interaction between natural and social environment. Man and society play active as well as passive roles in this process, which influences the global development of a region. In the last few decades it became also obvious that effects of drought can cause damages not only in

agriculture and plant production, but, at the same time, in all living organisms including domesticated and wild species of plants, animals, microorganisms, and also human beings. Consequently, there is a global need to find out the means and measures against the harmful effects of drought, and to create some variables in space and time for influencing the preparedness of the whole society, including politics, economy, ecology, justice, and ethics, as well as the private and public behavior for the sustainable development of the society (Vermes, 1997).

2. The role and activity of ICID

Recognizing the above mentioned facts, some of the international organizations, especially ICID, the International Commission on Irrigation and Drainage, and its working groups started to deal with drought problems from the year of 1992. ICID — focusing on irrigation, drainage, and flood control questions — is practically active in all problems related to agricultural water management. It has been established as a scientific, technical, professional and voluntary, international non-profit and non-governmental organization, and dedicated inter alia to enhance the worldwide support of food and fiber for all people. ICID strives to achieve this by improving water and land management, and the productivity of irrigated and drained lands through the appropriate management of water, environment, and the application of irrigation, drainage, and flood control techniques. ICID is interested in matters relating to the planning, financing, and economics of the mentioned fields.

In the frame of ICID several working groups are operating, among which two are closely connected with drought problems: (1) the Working group on Irrigated Agriculture under Drought and Water Scarcity (WG-IADWS), and (2) the European Regional Work Team on Drought (ERWTD) in the frame of the European Regional Working Group (ERWG). Hungary is represented in both, but we are more active in the last one, which was established on a Hungarian proposal. This is a task force of the ERWG to help and coordinate member countries interested in the fight against drought damages.

3. An ICID guide on drought mitigation

One of the main tasks of the ERWTD was to compile a guide — entitled *How to Work out a Drought Mitigation Strategy* — for summarizing all the necessary information which is important to drought prevention, which should be taken into consideration during the elaboration of a drought mitigation strategy, and which can be used in the case of the occurrence of drought for

reduction and/or tolerance of the caused damages. The guide was completed on the basis of several earlier initiatives taken and proposals made at former ICID meetings, and by individual experts, members of the ERWTD and other organizations (Vermees, 1998).

In the introductory part of the Strategy, it is important to determine the clear definitions of the relevant concepts concerning drought. There should be distinguished the differences between, e.g., dryness and drought, and here should be formulated the aim of the strategy as well. After this, some drought occurrences have to be quoted from different parts and countries of the world. The ICID guide gives examples from recent drought events from Hungary, Yugoslavia, Romania, and Croatia.

The following part should deal with the drought analysis, examining first the climatic conditions and hydrological factors causing drought, secondly quoting the human made effects, especially the agronomic circumstances, and thirdly analyzing the role of soil types and soil conditions in drought occurrence.

The next part of the Strategy gives the inventory of the harmful impacts and damages of drought, specifically in the given country or region. Among these, in first case the directly effected water users should be introduced and analyzed, namely the different branches of agricultural production, the different branches of industry, especially food industry, and the different services, which mostly suffer from drought. Also the environmental impacts on natural resources, habitats, and ecosystems, natural protected areas, national parks should be determined, and combined environmental effects studied in this part of the Strategy.

Among indirect effects, the trade conditions, especially the import-export relations, financial affairs, and social impacts on public health, on employment/unemployment, on politics and foreign affairs, and on tourism should be evaluated. Some beneficial effects of drought should be examined, too, e.g., mosquito reduction, reduced cost for clearance of snow during winter drought, improvement efficiency in water use and water quality control, and the control of overproduction in agriculture. It has to be strongly pointed out that intensive research work is urgently needed in the field of further beneficial effects of drought.

Also the measures taken so far against harmful impacts of drought damages should be taken into account. In most cases unfounded, not quite well consolidated, highly improvised measures have been taken during — or even after — recent drought events. The steps were mainly succeeding and not preventing the damages, the actions were mainly stop-gap type actions with partial effects. Also the attitude and reaction of the society on drought should be analyzed, which is in most cases strange and not understandable. In this respect the role of the media has to be pointed out as well.

In the most important part of the Strategy the means and methods of the complex fight against drought damages have to be discussed. First the assessment and forecast of drought events should be studied, determining the calculation methods and indices used in the forecasting process. Establishment of a monitoring system in meteorology and water management, as well as in other branches of the economy is an important step. To draw up management plans in agriculture and forestry, it can help to mitigate drought damages in these sectors. Extension services and media programs should be used for increasing awareness of farmers and other professionals on potential drought events. Key question is the determination of prevention methods, damage reduction instruments, and toleration of drought damages. Among prevention methods, supply-oriented and demand-oriented measures, and impact- and losses minimization methods can be distinguished.

The instruments of damage reduction are manifold. There are agricultural methods, like optimum land use, better crop pattern, changes in the elements of agro-technology, complex land reclamation methods, improving plant breeding for better drought tolerant crop varieties, elaborating of authority system for control, regulation and support of drought damaged farmers, determining the sources and means of compensation or disaster aid for those who suffer from great income losses caused by drought, developing special insurance system for drought damages, establishing relief funds and/or guarantee funds for those who lost their yields or properties because of drought, etc.

Toleration means consciously counting on some risk, limitation or losses of yield, or income. Therefore, it is important to determine the tolerable level of losses by risk assessment, to set up priority lists for toleration of deficiencies caused by drought, and to draw up case studies on farm and/or company level for determining toleration, prevention, and reduction measures for damage minimization.

Key questions are the organization and coordination questions, too, among which, first of all, the followings should be answered:

- How to organize the formulation and interpretation of the national drought strategy?
- How to organize the determination of the tasks of different participants?
- How to organize the compilation of the action program on the systems of measures?
- How to establish the National Drought Commission for the realization of the Strategy?

Especially the latest has of great importance, the detailed explanation of which should be included in the Strategy.

As far as the *international cooperation* is concerned, the role of the neighboring countries have to be cleared, where the potential collaboration of the countries concerned should be organized. The contact with international organizations, like UNCCD, ICID, or others, should be determined either.

Also, the needs for research and development, as well as education and training should be analyzed in the Strategy. In most cases new types of research work are needed for summarizing and synthesizing the results gained so far, for systematization of the results and experiences according to a new classification of the themes: ecological, technological, economical, and sociological questions of drought should be differentiated. It is important to find out new sources and funds for financing drought research.

Educational and training programs should be started for better understanding of drought problems among the public, to increase public awareness and preparedness for the coming drought events. Special media awareness program is necessary to convince journalists about drought problems and mitigation possibilities, and long-term educational programs should be established for all groups and economic sectors.

A glossary of terms and indices, and a collection of recommendations for potential risk reduction actions are advised to attach in appendices to the Strategy.

One of the major *future tasks* of the cooperation under the guidance of the ERWTD of ICID could be the preparation of a Network for Central and Eastern European Countries, and to draw up the European drought sensitivity map which can be a good basis of any further actions against harmful drought effects.

4. Fight against drought in the USA

Drought was one of the most underestimated and least understood natural disasters in the United States, too. Based on the recognition, that many of the worst effects of drought can be reduced or even eliminated when proper mitigation measures are introduced in advance of drought events, American climatologists and other scientists in the Institute of Agriculture and Natural Resources at the University of Nebraska-Lincoln decided to establish the *National Drought Mitigation Center* in 1995, and they founded later the *International Drought Mitigation Center* as well (Wilhite, 1998). Both centers are going to help people and institutions develop and implement measures to reduce societal vulnerability to drought. They stress prevention and risk management rather than crisis management. This approach promotes self-reliance to achieve greater resilience to drought, and this way their activities are of great interest for us and give an example to be followed.

In 1998 the Congress of the USA adopted the *National Drought Policy Act* to establish an advisory commission to provide advice and recommendations on the creation of an integrated, coordinated Federal policy designed to prepare for and respond to serious drought emergencies. Main task of the *National Drought Policy Commission* is to conduct a thorough study and submit a report to the Congress on national drought policy in accordance with the duties and tasks determined by the Act (*National...*, 1998).

In the same year the *Western Drought Coordination Council* was organized as an intergovernmental forum that focuses on drought preparedness in the Western United States, especially in New Mexico, Texas, and Colorado. Drought experiences in the West and Southwest in the former years highlighted the need for a long-term, region-wide drought planning and streamlined access to government services. The Western Governors' Association responded to those needs when spearheading it for the Council through a Memorandum of Understanding with representatives of federal, tribal, and local governments. The United States Department of Agriculture (USDA) serves as the lead federal agency, and a Steering Group implements the Council's work plan. The Steering Group oversees four working groups:

- Monitoring, Assessment, and Prediction,
- Preparedness and Mitigation,
- Response, and
- Communications (*Western...*, 1998).

The working groups are staffed by volunteer professionals from federal, state, local, and tribal entities. The Council's purpose is to reduce the effects of future droughts in the Western United States, specifically its goals are

- to foster better intergovernmental coordination and communication on drought planning,
- to help state, local, and tribal governments develop drought preparedness and mitigation plans,
- to contribute an efficient drought monitoring and information delivery system so that decision makers learn about low water supplies and drought prospects as soon as possible, and
- to heighten awareness of drought management issues and promote efficient use of water.

Due to the well organized actions, nowadays most of the States have a drought plan elaborated on certain level, and some of them are even under revision and redesigning.

5. Drought mitigation actions in the United Kingdom

In the frame of the International Decade for Natural Disaster Reduction (IDNDR), the National Committee founded a special working group, the *Drought Mitigation Working Group* (DMWG) in the UK for the organization and coordination of different activities against drought damages and water shortages, and for a more effective and rational use of water resources. The water industry's response to the severe drought events has been to reduce water demands by a mixture of appeals for voluntary restraint, hosepipe bans, and drought order, and to increase supply by bringing forward works which increase the flexibility of supply and allow transfer of water from areas of surplus. The Department of Environment maintained a coordinating role holding monthly meetings with the National Rivers Authority and water companies. Drought orders are issued by the Secretary of State, providing the powers to ban non-essential uses of water, and make changes in abstraction licence conditions. Some conservation bodies, like the Royal Society for Nature Conservation (RSNC), have suggested that legislation should be changed to allow drought orders to be made on environmental grounds (*Dealing with ...*, 1993).

Under a drought order, water companies may first seek to have their conditions of abstractions changed, e.g., a drought order may permit the reduction of the "compensation water" released from reservoirs, allow increased abstraction from some sites, or reduce the minimum river flow above which abstractions are allowed. The National River Authority is unlikely to support such an application unless a hosepipe ban is already in operation.

Other powers which may be sought under the drought order are restrictions on the non-essential use of water, specified by the Secretary of State. These restrictions can include the washing of buildings, watering public gardens, sports grounds, and golf courses, automatic car washes, the filling of swimming pools, ornamental ponds, and the operation of fountains. Drought orders may also be used to change the conditions in discharge consents, but this is not commonly done. The National River Authority also has powers to impose restrictions on abstractions made for spray irrigation — except for greenhouses and container-grown plants. In order to assist farmers, a system of alerts is in operation in the Anglian region, which provides warning of impending partial and total bans of abstraction. Water restrictions are monitored by the Office of Water Services (OFWAT), and form one of the levels of service indicators for the water companies.

6. UN Convention to Combat Desertification and Drought

Because drought and natural processes do not consider political boundaries, the influences from the neighboring territories should be taken into consideration. A good drought strategy deals with international relations and counts on international cooperation in the fight against drought damages. This is promoted even by the United Nations trying to help the countries involved, and call the attention of the states and governments on a better international cooperation in this field. This is declared in the *United Nations Convention to Combat Desertification (UNCCD) in those countries experiencing serious drought and/or desertification, particularly in Africa (United..., 1999)*. The Convention was adopted and open for signing in 1994, Paris, and up till now many countries — altogether 115, including Hungary — joined as full Parties. The main objective of this Convention is to fight against desertification and drought through effective actions at all levels, supported by international cooperation and partnership arrangements, in the framework of an integrated approach which is considered with Agenda 21, with a view to contributing to the achievement of sustainable development in affected areas. Achieving this objective will involve long-term strategies that focus simultaneously, in affected areas, on improved productivity of land, and the rehabilitation, conservation and sustainable management of land and water resources, leading to improved living conditions, in particular at the community level.

Beside of determining the general provisions, the Convention deals in a separate part with *action programmes, scientific and technical cooperation, and supporting measures*, as one of the major fields of implementation of the goals and objectives. All statements and recommendations of the Convention should be taken into consideration and are desired to be built into the national drought strategies and action plans. In the Carpathian Basin the *Fifth Annex of the Convention* is of great interest, adopted in the Conference of the Parties in 2000, which is devoted to the regional implementation of the Convention in the Central and Eastern European countries. Fulfilling the aims of the Convention, Hungary should work actively in the preparation and implementation of national action programmes on drought mitigation.

7. Conclusions

The paper dealt with only some of the very important international and national efforts and events concerning drought mitigation. There was no place to mention all of such efforts, however, in many other countries more and more efforts are made against drought damages, e.g., in Australia, countries in

the far and middle East, as well as the countries in Central and Eastern Europe. In Hungary, the National Drought Strategy is under preparation and the organization of the National Drought Committee was started. All these activities show that a well coordinated, complex work is necessary in all effected countries for an effective fight against drought, and international cooperation is needed either in research work or in practical actions and organizational fields for the minimization of drought damages.

References

- Vermes, L., 1997: What should be the content of a national drought strategy? *Proc. of the Internat. ICID Workshop on Sustainable Irrigation in Areas of Water Scarcity and Drought* (eds.: M.J. de Jager, L.P. Vermes, and R. Ragab). Oxford, England, 221-228.
- Vermes, L. (ed.), 1998: How to work out a drought mitigation strategy? An ICID Guide. ICID ERWG – Kommissionsvertrieb Wirtschafts- und Verlagsgesellschaft Gas und Wasser mbH, Bonn.
- Wilhite, D.A., 1998: The National Drought Mitigation Center. An information package. University of Nebraska-Lincoln
- *Dealing with Drought* (1993). Environmental and Technical Aspects of Water Shortages. The Parliamentary Office of Science and Technology, London.
 - *National Drought Policy Act* (1998). 42 USC 5121 – Public Law 105-199, 112 Stat. 641. 105th Congress of the USA, Washington D.C.
 - *United Nations Convention to Combat Desertification in Those Countries Experiencing Serious Drought and/or Desertification, Particularly in Africa* (1999). Secretariat of UNCCD, Bonn.
 - *Western Drought Coordination Council* (1998). Statement of Accomplishment. Report from the Steering Groups and the Four Working Group. Albuquerque, New Mexico (manuscript).

IDŐJÁRÁS

Quarterly Journal of the Hungarian Meteorological Service
Vol. 106, No. 3–4, July–December 2002, pp. 248–263

Characteristics of the economy of water supplies in an oak forest

János Justyák and Károly Tar

Department of Meteorology, University of Debrecen
P.O. Box 13, H-4010 Debrecen, Hungary
E-mail: tark@tigris.klte.hu

(Manuscript received March 4, 2002; in final form September 19, 2002)

Abstract—The components of the water balance in an oak forest at Síkfőkút were examined in the frame of the *Síkfőkút Project* between 1978 and 1995. The sample site, which has an area of 1 hectare, is situated on a slope of 2–3 degrees in the Bükk Mountains of Hungary at a height of 270–280 meters above sea level. It has a southern exposure. At the beginning of the project, the average height and age of the trees were 21.5 meters and 71 years. The soil is brown forest soil with a vast humus layer. The humus content is 2–5%, field water capacity is about 30 percents. Soil samples were taken by soil strata and decades repeatedly three times. Soil moisture content was determined using gravimetry. In the growing season the soil moisture content decreases in the upper 60 cm layer of the forest soil from April to August. Between 1978 and 1995, soil moisture and precipitation showed a decreasing trend in the sample area. The most humid is the upper layer of the soil (0–5 cm, 4–5% humus). Less water can be found in the next layer between 30–50 cm, since roots take up most of the water in that depth. Moisture content of the upper 60 cm of the soil follows the changes of the amount of precipitation and soil moisture in the growing season. The same is true for the course of mean annual water content of the different horizons of the forest soil. Mean annual interception of the forest is 17%. It is 9% when the trees are leafless and 18% when they are leafy. In the growing season the monthly maxima of actual evapotranspiration are 50–100 mm, while minima are between 30 and 60 mm. The total amount of it is between 297 and 422 mm in the growing season. The Síkfőkút forest consists mostly (84.5%) of sessile oak (*Qercus petraea*), which had decayed dramatically between 1978 and 1995. Possible reasons for this are the decrease of the pH, bacteria, and fungi content of the soil, the decrease of precipitation amount and soil moisture content, and the increase of annual mean temperature. These changes and especially the complex impacts of the chain of these effects have lead to the decay of the trees.

Key-words: effective precipitation, soil moisture, water-balance, surface runoff, actual evapotranspiration.

1. Introduction

Productivity of a forest, condition of the trees, and their resistance to harmful effects from outside depend considerably on the economy of water supplies of the forest. The examinations carried out on the water balance of the Síkfőkút forest are important, because 50% of the sessile oak trees in that forest had decayed between 1978 and 1993. The decay of the forest has decreased and finally stopped only in the previous years due to more precipitation. The simplified water balance equation of the forest,

$$\pm\Delta W = P - ET \pm R - F - I, \quad (1)$$

describes that the change of the moisture content in the root zone ($\pm\Delta W$) is a function of the amount of precipitation reaching the foliage of the forest (P), the evapotranspiration of the forest (ET), the surface runoff ($\pm R$), the infiltration into the deeper layer (F), and the amount of precipitation retained by the whole forest vegetation (trees, shrubs, and undergrowth), the interception (I).

Since during the growing season the forest can gain water from the soil moisture retained in the root zone, it is important to know what kind of changes occur in time in the moisture content of the deep layer of the forest soil within this period.

It is well known that due to global changes that affect the biosphere (acid precipitation, green house effect, etc.), from the beginning of the 80's, interest have been focused on long term biomonitoring researches worldwide. These studies concentrate on the detection and exploration of slow, sometimes hardly traceable processes of ecosystems. In Hungary, this kind of long term biosphere research project, the so-called "Síkfőkút Project", was started by the Department of Ecology of the Kossuth Lajos University of Debrecen in 1972, in the frame of IBP, later the MAB programs (*Jakucs*, 1973, 1985). It was a complex ecological and meteorological study of a climate-zonal Austrian oak-oak joining near the city of Eger. The Department of Meteorology of the Kossuth Lajos University joined the project establishment intensely in 1977. By that time the department had installed a 25 meters tall meteorological tower and a digital data logger with 80 channels (*Justyák*, 1987).

The environmental-biological model site has an area of 1 hectare and it is situated on a slope of 2-3 degrees, with southern exposure. It is placed near the town of Eger in the Bükk Mountains, at a height of 270-280 meters above sea level. It is a brush-wood origin, homogeneous Austrian oak-oak joining. The average height of the trees was 19 meters in 1972, at the beginning of the project. It reached 21.5 meters in 1978. In 1972 the forest was 65 years old. There are a high (3-4 meters) and a low (1-2 meters) shrub level in the forest.

About 60% of the mass of the forest foliage can be found at a height between 15 and 20 meters.

2. Soil moisture

The type of the soil in the model area is lessivated brown forest soil. Its characteristics play an important role in the water balance of the root zone. Its main characteristics are:

- The soil is covered with 2–3 cm thick layer of litter in the forest.
- The 0–10 cm layer (subhorizon A₁) is dark brown loam with 2–3% humus. It is densely laced with the roots of the shrubs.
- The 10–25 cm layer (subhorizon A₂) is brown compact polyederic loam.
- The 25–40 cm layer (subhorizon A-B) is brown compact clay-loam.
- The 40–70 cm layer (subhorizon B₁) is slightly reddish brown compact polyederic loam. It is densely laced with the roots of the trees.
- The 70–90 cm layer (subhorizon B₂) is clay-loam, while horizon C is compact loamy clay without structure.

The pH of the soil is between 4 and 6, hygroscopicity (hy) 3–5%, while humus content is 2–5%. The most important soil characteristics are summarized in *Table 1*.

Table 1. The most important soil characteristics on the area of Síkfökút Project

Depth (cm)	pH		Acidity		hy (%)	Humus (%)
	H ₂ O	KCl	Y ₁	Y ₂		
0–10	6.3	4.6	28.1	1.1	3.1	5.4
10–25	4.7	3.8	38.3	7.2	2.9	2.7
25–40	5.2	4.0	22.0	4.4	3.5	2.2
40–70	6.2	6.0	15.3	–	4.7	1.8

The pH of the different soil layer profiles is characteristic for the lessivated brown forest soil. The values show considerable *acidification*, especially in subhorizon A₂ (10–25 cm), where pH decreases to 4.5. From subhorizon B₁ (40–70 cm), pH increases again.

Bulk density (BD) of the soil increases with the depth from 1.0 to 1.5. *Field capacity* of the soil (FC) is about 30%, while *wilting point* (WP) is between 12 and 18%, therefore the ratio of *available soil water* (AW) is high in the soil. The soil moisture characteristics in the different layers are summarized in *Table 2*.

Bulk density (BD), field capacity (FC), minimal water capacity (WCmin), and wilting point water content (WP) increase with the depth, while saturation water content (SWC) decreases with increasing dept. Bulk density values were taken into consideration when calculating on mm values from soil moisture content.

Table 2. Bulk density (BD), field capacity (FC), and available water (AW) in the soil layers

Depth cm	BD g/cm ³	FC v/v%	FCmax v/v%	FCmin v/v%	AW v/v%
0-10	1.02	38.5	60.1	29.2	12.4
10-25	1.37	42.1	51.0	30.3	11.6
25-40	1.44	40.8	47.6	29.2	14.0
40-70	1.47	42.7	48.2	30.8	18.8

Particle size distribution (%) of samples in the soil profiles are shown in Table 3.

Table 3. Particle size distribution in the soil layers

Depth cm	1-0.25 mm	0.25-0.05 mm	0.05-0.01 mm	0.01-0.005 mm	0.005-0.001 mm	<0.001 mm
0-10	4	3	33	13	26	21
10-25	2	4	30	13	24	27
25-40	2	3	26	11	22	36
40-70	3	2	25	8	19	43

The ratio of the clay fraction is 43% in the depth of 40-70 cm. There is the half of it (21-27%) in the upper subhorizons (0-10 and 10-25 cm), while humus content is higher (Stefanovits, 1985).

Summarizing the above-mentioned facts, it can be stated that the physical characteristics and structure of the soil are important, because the soil of the forest is rich in colloids (clay). The productive layer of the soil is thick and free of stones and pebbles, therefore, if there is adequate amount of precipitation, the soil is able to receive and store a significant amount of water.

In order to determine the soil moisture content, soil samples were taken during the growing seasons between 1978 and 1995 by drilling repeatedly three times from each soil layer from the depths of 0-5, 5-10, 10-20, 20-30, 30-40, 40-50, 50-60 centimeters. Soil moisture content was determined by gravimetric method. Soil moisture content in percentage of the weight of the dry soil was determined for each growing season (from April to October), on

the base of three samples taken by decades (monthly averages are calculated from the values of the three decades).

Soil is able to retain and store a certain amount of water against the force of gravity. This amount of water is called *soil moisture content*. The difference between field capacity and wilting point water content is only a part of this amount, which is available for the trees and shrubs of the forest. This amount of water is usually called *available* or plant extractable *water*. The soil water content will be discussed here as *soil moisture content*.

Mean moisture content of the soil (%) in the Síkfőkút forest for the months and growing seasons are shown in *Table 4*. ($P_{\text{eff. aver.}}$ is the amount of effective precipitation, that reaches the soil falling through the foliage.)

Table 4. Mean soil moisture content (%) and effective precipitation (mm) in the Síkfőkút forest for the months and growing seasons

Years	Apr	May	Jun	Jul	Aug	Sep	Oct	Apr- Oct	$P_{\text{eff.}}$ Apr- Oct
1978	24.2	29.1	25.6	26.9	21.4	17.3	17.0	23.1	376
1979	29.4	25.5	23.3	21.7	19.1	21.6	17.6	22.6	265
1980	30.7	28.5	28.4	27.2	21.9	20.4	21.6	22.5	361
1981	26.8	26.1	22.5	21.1	17.6	19.3	20.9	22.0	288
1982	27.7	26.6	23.4	20.1	15.5	15.0	17.2	20.8	236
1983	27.5	26.7	22.6	15.0	14.7	17.5	17.0	20.1	276
1984	21.3	27.6	26.3	16.0	15.5	15.7	20.2	20.4	319
1985	27.2	27.2	28.5	19.6	18.0	14.5	13.9	21.3	314
1986	25.7	20.8	18.3	15.8	15.6	14.1	14.1	17.8	209
1987	25.9	27.2	22.2	14.7	15.4	14.1	15.9	17.9	270
1988	26.3	24.8	25.6	20.7	15.9	17.2	16.7	21.0	300
1989	26.6	22.6	22.0	15.8	16.4	16.3	16.5	19.5	334
1990	19.2	16.7	16.9	15.9	18.4	18.3	23.4	18.5	290
1991	30.4	29.9	24.0	18.3	19.1	13.4	18.7	22.0	322
1992	27.2	20.1	16.5	14.6	13.7	16.2	18.9	18.2	154
1993	21.9	18.0	14.9	14.9	15.5	20.3	24.3	18.4	233
1994	28.4	21.9	19.8	19.5	14.9	15.6	17.8	19.7	291
1995	24.6	26.6	18.4	13.6	18.3	21.9	12.8	19.5	329
Average	26.2	24.8	21.6	18.2	17.1	17.2	18.1	20.5	285
$P_{\text{eff. aver.}}$	39	55	52	36	43	30	30	-	285

Since the area of the Síkfőkút forest is free of the effects of subsoil water, the soil moisture originates directly from the atmospheric precipitation. It can be seen in *Table 4*, that average monthly moisture content in the upper 60 cm

of the forest soil decreases from April to August by 9.1%. In dry growing seasons, like in 1992 and 1994, the decrease was more than 13%. The soil moisture content, therefore, reaches its minimum in August or September. Monthly average soil moisture contents begin to increase again in October, when weather is cool and the precipitation is more than the evaporation.

The soil moisture content decreases from April to August, because the temperature increases and relative humidity decreases. The growth of the saturation deficit in the air increases the transpiration force on the plants' leaves, while soil moisture content decreases. The difference between the potential and actual evapotranspiration increases in such situation. The energetic background of the process is that higher ratio of the radiation balance is devoted to the warming of the air of the forest with the decrease of soil moisture content, since there is a significant decrease in the amount of energy devoted to evapotranspiration in line with the decrease of soil moisture content. The effective precipitation, which reaches the soil through the foliage in the forest compared to the soil moisture content, does not reflect the increase of the amount of monthly mean precipitation from April to May–July, which is characteristic for Hungary. In other words, the precipitation maximum at the beginning of summer does not appear in the course of soil moisture content, since the forest uses it for increasing biomass production and evapotranspiration.

Moisture content values of the different soil layers are shown in *Table 5*. It can be seen in the table, that the maximum values of soil moisture can be found in the upper soil layer, which contains the most humus. The highest moisture content is found in the topsoil (0–5 cm), since the soil surface is covered with a thick layer of forest litter. For this reason, the soil surface is not dried by the solar radiation and wind. On the other hand, the thick cover of fallen leaves decreases the evaporation from the soil surface. There is less moisture content in the 30–50 cm layer, since it is densely interlaced by the roots of the trees, and the roots take up the most water in this layer. The soil moisture content, its oscillation and standard deviation decreases with the increasing depth. For more details on the soil moisture content in the Síkfőkút forest, see *Justyák and Nagy, 1988, 1990; Antal et al., 1995; Justyák and Vig, 1997; Kiss, 1995*.

Trends of the changes of soil moisture content in the root zone of the forest between 1978 and 1993 were analyzed by the following method. Measured soil moisture data were transformed in order to screen seasonal anomalies in a way, that each value was divided by the 15 years average of its own decade. The set of the transformed data was divided into two heaps for each year. The first contained the data below 1.00 (the decade average), the other contained the values above 1.00. On the basis of the ratio of these heaps

it can be decided for each year, whether the soil of the Síkfőkút forest were dry, wet, or it had average water supply compared to the average of the given period. For annual trend analyses, ratios of the soil moisture content values higher than the decade averages within the whole dataset were taken into consideration (Fig. 1). The decreasing tendency of soil moisture content is clearly visible in the figure.

Table 5. Mean soil moisture content (%) in the growing seasons in the Síkfőkút forest in different depths

Years	0-5 cm	5-10 cm	10-20 cm	20-30 cm	30-40 cm	40-50 cm	50-60 cm	0-60 cm
1978	32.3	26.3	23.1	20.2	19.3	19.9	20.5	23.1
1979	30.0	23.7	21.8	21.9	20.3	18.3	22.2	22.6
1980	38.0	29.8	23.8	21.9	21.3	21.6	21.8	25.5
1981	32.1	24.3	21.5	22.2	18.7	18.9	20.2	22.0
1982	29.1	21.9	20.4	18.6	18.2	18.4	18.8	20.8
1983	28.5	21.5	19.2	17.8	17.8	18.2	18.1	20.1
1984	27.0	23.0	20.7	18.5	17.8	17.8	17.8	20.4
1985	29.5	23.6	20.7	19.7	18.3	18.7	18.6	21.3
1986	20.6	18.9	17.4	16.5	17.2	17.3	17.3	17.8
1987	26.8	20.1	18.2	17.0	17.3	18.0	18.0	17.9
1988	28.2	23.4	21.3	19.8	17.8	18.4	18.3	21.0
1989	25.3	21.2	19.2	17.7	18.0	17.7	16.9	19.5
1990	23.4	20.1	18.6	17.5	16.9	16.2	16.1	18.5
1991	30.2	24.2	21.1	20.4	19.6	19.5	18.8	22.0
1992	22.2	19.9	17.7	16.7	17.5	16.8	16.4	18.2
1993	25.1	22.5	19.0	16.8	15.9	15.3	15.2	18.4
1994	31.1	23.4	17.5	15.9	15.2	15.6	15.5	19.7
1995	27.5	22.2	18.7	18.1	17.1	16.5	15.9	19.5
Average	28.2	22.8	20.0	18.5	18.0	18.0	18.1	20.5
Maximum	38.0	29.8	23.8	22.2	21.3	21.6	22.2	25.5
Minimum	20.6	18.9	17.4	15.9	15.2	15.3	15.2	18.2
Oscilation	17.4	10.9	6.4	6.3	6.1	6.3	7.0	7.3
Standard deviation	4.0	2.5	1.8	1.8	1.4	1.5	2.0	2.1

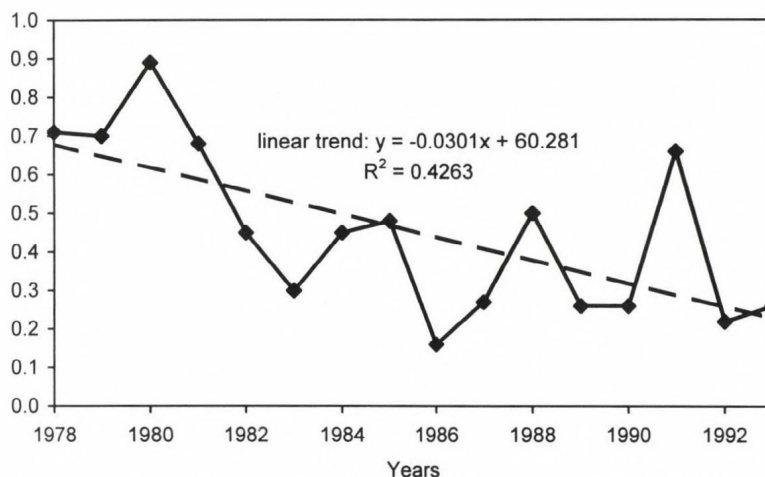


Fig: 1. Ratio of soil moisture content values higher than the average of the decade and total soil moisture content values in the 0–60 cm layer.

3. Water supply

The amount of water could be stored in the soil is determined by the above mentioned physical characteristics of the soil. The supply of water in the forest soil was determined on the basis of soil moisture (%), bulk density (g/cm^3), and thickness of layer (cm), the following way (Szász, 1988):

$$W (\text{mm}) = Sm (\%) \cdot BD \cdot Th / 10, \quad (2)$$

where Sm is the soil moisture content (in percentage of dry soil weight), BD is the bulk density of the soil (g/cm^3), and Th is the thickness of the soil (cm).

Additional information can be obtained by analyzing the monthly water supply (mm) of the soil layers of the forest (Table 6).

Table 6. Annual mean water supply (mm) of the soil layers in the Síkfőkút forest (1978–1995)

Depth (cm)	Apr	May	Jun	Jul	Aug	Sep	Oct	Average
0–10	40	39	34	28	25	25	26	31
10–20	32	30	29	21	20	21	22	26
20–30	29	27	23	20	18	18	19	22
30–40	31	32	28	20	20	21	23	25
40–50	38	30	27	23	24	23	24	27
50–60	23	35	33	30	27	27	27	29
0–60	203	193	174	142	134	135	141	160

It can be seen in the table, that the upper rich humus layer (0–10 cm) and the 50–60 cm deep one, which is not plentiful of living roots, contain the same amount of water. In the other layer, where the root mass of the trees and shrubs can be found, there are only 22–27 mm of water due to the strong water uptake. In line with the soil moisture content, the soil water supply decreases from April to August, which is a consequence of energy transport processes mentioned before, in connection with the soil moisture content.

4. Interceptional water

The difference between the amount of atmospheric precipitation (P) falling onto the foliage of the forest and the amount which reaches the surface falling through the foliage ($P_{\text{eff.}}$) is called *retained water* (P_b). The process of the retention of the precipitation is *interception* (I). Monthly averages of these characteristics are presented in the *Table 7*.

Table 7. Monthly averages of the precipitation characteristics (1978–1995)

Charac- teristics	Apr	May	Jun	Jul	Aug	Sep	Oct	Apr–Oct	Dim.
P	43	68	63	44	54	36	37	345	mm
$P_{\text{eff.}}$	39	55	52	36	43	30	30	285	mm
P_b	4	13	11	8	11	6	7	60	mm
I	9	19	17	18	20	17	19	17	%

(P – atmospheric precipitation, $P_{\text{eff.}}$ – precipitation reaching the surface, P_b – retained water, I – Interception)

It can be seen from the characteristics presented in Table 7, that the forest retained 60 mm of atmospheric precipitation on the average. This interceptional water is not useful for the forest, since it is evaporated into the atmosphere from the trunks, branches, and leafs of the trees. The indirect use of the interceptional water is that it decreases the intensity of transpiration till it evaporates. The annual average *interception* (1978–1995) of the forest during the growing season is 17%. In leafless state it is 9% (April), while in leafy state (May–Oct) it is meanly 18%. These values are characteristic for the forest canopy decayed by 50%. Before forest decay, the average interception of the healthy, closed foliage forest was 21%. In leafless state (April) it was 13% (Szabó, 1985).

The water of abundant rains is conducted to the trunks by the branches, then it flows down on the trunks onto the soil surface. The amount of water flowing down on the trunks in leafy state was 3.4% of the annual average amount of precipitation. In leafless state it was 3.9%, which is not ignorable from the aspect of water balance of the root zone.

Table 8 shows the average interception retained by the Síkfőkút forest in leafy state, in case of different rains, over and inside the forest. It is visible, that the forest can retain higher ratio of small rains and smaller ratio of large rains.

Table 8. Average interception in case of different rains over and inside the forest

Precipitation over the forest (mm)	Precipitation inside the forest (mm)	Water retained by the forest (mm)	Interception (%)
50.0	41.8	8.2	16.4
45.0	35.8	9.2	20.4
38.8	29.3	9.5	24.5
17.5	18.8	4.7	26.9
14.8	10.0	4.8	32.4
7.5	4.7	2.9	37.3
2.5	1.2	1.3	52.0

One hectare of oak forest at Síkfőkút retained 700–2400 m³ water annually depending upon the amount of precipitation over the canopy. Most of it evaporates into the atmosphere. Due to the many influencing factors, this value oscillates within a broad interval. Interception capacity of the Síkfőkút forest was 2300 m³/ha in 1978, and 720 m³/ha in 1982.

In the forest, a part of the precipitation is retained by the litter, while the larger part of it gets into the soil through the litter. When the litter is saturated, the water flows away on the surface, this is the surface runoff. The ratio of the water amounts flowing away and got through the forest is called *surface runoff factor*, which is characteristic for the use of precipitation water. In the Síkfőkút oak forest (on a slope of 3°, intermediately permeable soil), it varied between 0.01 and 0.04 depending on the amount of precipitation. The amount of surface runoff from 1 hectare, from May to November, varied from 40 to 80 m³ (Justyák and Bihary, 1993; Justyák and Vig, 1997).

5. Actual evapotranspiration

Another important component of the water balance in the forest is the *actual evapotranspiration* (AET). The actual evapotranspiration of the forest is determined by the sum of the *transpiration* from leaves and *evaporation* from

the soil surface. The actual evapotranspiration of the forest can be determined using the following simple relationship:

$$AET = P_{eff.} + (W_s - W_f) + I - R, \quad (3)$$

where W_s is for the starting and W_f is for the finishing water supply of the soil (mm), $P_{eff.}$ means the effective precipitation, which reaches the soil and litter falling through the foliage of the forest (mm), I is the interceptional water (mm), and R means the surface runoff (mm).

Mean actual evapotranspiration values from the forest canopy are presented in *Table 9*, where the amount of evaporated interceptional water is taken into consideration as well, while the amount of runoff is ignored.

Table 9. Monthly mean actual evapotranspiration (mm) from the Sikkökút forest canopy during the growing seasons of the 1978–1995 period

Years	Apr	May	Jun	Jul	Aug	Sep	Apr-Sep	$P_{eff.}$ Apr-Sep
1978	60	77	83	88	74	40	422	367
1979	60	59	74	68	80	35	376	239
1980	54	70	97	77	54	42	376	294
1981	44	62	66	82	77	50	381	256
1982	46	63	92	79	58	37	375	236
1983	47	81	69	69	65	38	369	205
1984	47	85	67	62	55	52	368	281
1985	48	87	94	67	70	40	406	309
1986	43	69	70	79	62	39	362	201
1987	57	73	66	63	58	43	360	246
1988	45	80	83	67	79	41	395	291
1989	46	84	97	79	65	36	407	326
1990	55	65	63	69	62	41	355	213
1991	46	78	79	81	66	33	383	267
1992	40	57	50	62	53	35	297	101
1993	50	59	52	60	64	40	325	185
1994	59	71	63	59	75	43	370	250
1995	68	72	85	72	78	46	421	329
Average	51	72	75	70	66	47	374	255
Maximum	68	87	97	88	78	52	421	367
Minimum	43	57	50	59	53	33	297	101
Oscillation	25	30	47	29	25	19	124	166
$P_{eff. aver.}$	39	55	52	36	43	30	255	

During the growing season, the monthly mean actual evapotranspiration increases from April to June and then decreases from July to October in line with the amount of precipitation falling onto the soil surface of the forest. Monthly mean maxima are between 50 and 100 mm. Monthly mean minima are between 30–60 mm. Annual sums of monthly mean evapotranspiration during the growing season are between 297 and 422 mm. Actual evapotranspiration showed a decreasing trend in the examined 18 years period between 1978 and 1995. There were growing seasons (1978, 1995) when a considerable amount of water evaporated (422 and 421 mm). There were few cases as well, when only a small amount of water evaporated (297 mm in 1992).

It is obvious from the data, that the monthly mean actual evapotranspiration is always higher than the effective precipitation, which reaches the soil surface in the forest. The surplus derives from the winter precipitation amounts. The difference originates from the decrement of the soil's water supply and interceptional water. The monthly mean actual evapotranspiration reaches its maximum in May and June (72–75 mm), which is in line with the summer maximum of precipitation. In this period the water uptake of the forest from the root zone increases due to the intense assimilation processes caused by rapid growth of healthy trees and shrubs. The evapotranspiration of the dissolved forest of Síkfőkút is affected by two factors. The *first one* is that the faded trees do not transpire, so the actual evapotranspiration of the forest is lower than that of the healthy forest. The *other factor* is that soil is covered with a 2–3 cm thick layer of litter in the forest, so meteorological elements can affect it only indirectly. The litter layer restricts many water molecules, which are able to get into the air of the forest from the soil. This way the evapotranspiration is decreased by the fading of the trees on one hand and process of evaporation, affected mainly by the characteristics and state of the litter, on the other hand (Justyák, 1987, 1995; Antal *et al.*, 1997).

6. The degree of tree dissolution

At the beginning of the complex environmental-biological studies (1972) in the Síkfőkút forest, there were 816 trees forming the foliage on one hectare area. 84.5% (689 trees) of them were sessile oak (*Quercus petraea*), while 15.5% of them (127 trees) were Austrian oak (*Quercus cerris*). The ratio of tree dissolution in the Síkfőkút forest is presented in Fig. 2. On the left vertical axis of the figure the number of living trees, while on the right vertical axis the number of dead trees are shown (tree fading affected mainly the sessile oak trees). According to Fig. 2, tree dissolution occurred in three main waves in the periods of 1979–80, 1983–86, and 1988–94 (Kiss and O'Heix, 1998).

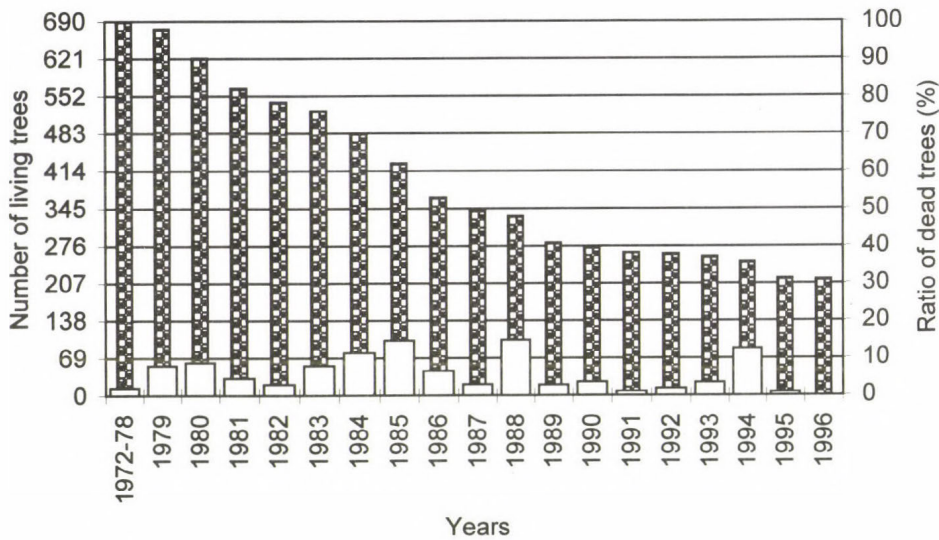


Fig. 2. The degree of fading of sessile oak trees on the 1 hectare sample area of Sikföktü.

Causes of tree dissolution have been studied by many researchers. Some researchers think that the main reason is an epidemic caused by *viruses*. They specify *fungi*, which attack the root trunks of the trees as pathogenic organisms (Redfern, 1973; Rütze and Liese, 1980). Others attribute tree dissolution to soil acidification caused by acidic rain (Ulrich et al., 1979; Ulrich and Pankrath, 1983; Jakucs, 1990). Others again explain the process by the *lack of precipitation* (for instance in the northern mountains in Hungary, where 50% of sessile oak trees have faded due to the lack of precipitation, while in Transdanubia, which gets more precipitation, only 10–20% of sessile oak trees have faded). There are some researchers who believe that the lack of precipitation causes harm to the *mikorrhiza-fungi*, which live in positive symbiosis with thin roots of sessile oak and cause problems in the nitrogen supply of the trees (Berki, 1995).

In connection with tree dissolution, the analysis of Figs. 3 and 4 is interesting. Fig. 3 shows the annual variation and trend of temperature, while Fig. 4 presents the annual amounts and trend of precipitation, the trend equation and correlation coefficient, during the studied period (1978–1994), measured in a treeless area and inside the forest at a height of 2 meters. During the examined 17 years long period, mean temperatures in the forest show stronger increase than those in the treeless area, ratio of steepnesses of the two straights is 1:1.3. Increase of the mean temperature in the forest

during a 10 years period is 1.0°C. It can be explained by several reasons. One reason is that due to the tree fading, density of the forest stand became lower. Other reason could be the consequence of warm weather series of the last 10–20 years. Fading of several trees decreased the shading effect of the foliage, and for this reason the difference between the forest and treeless area has decreased as well (Antal *et al.* 1997).

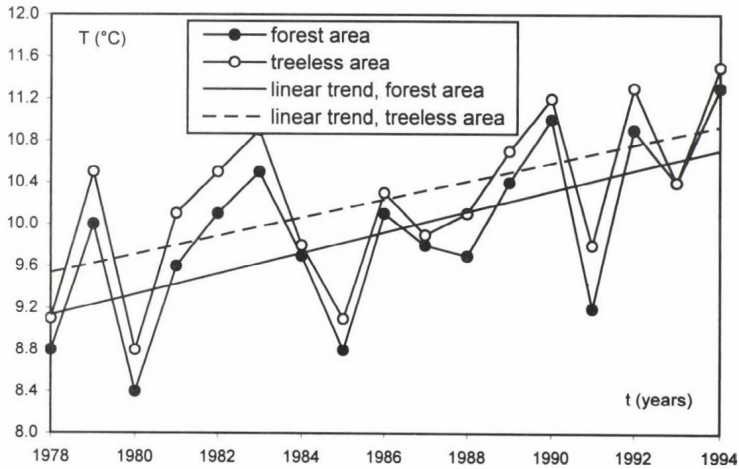


Fig. 3. Annual fluctuation and trend of temperature in the forest and treeless area.

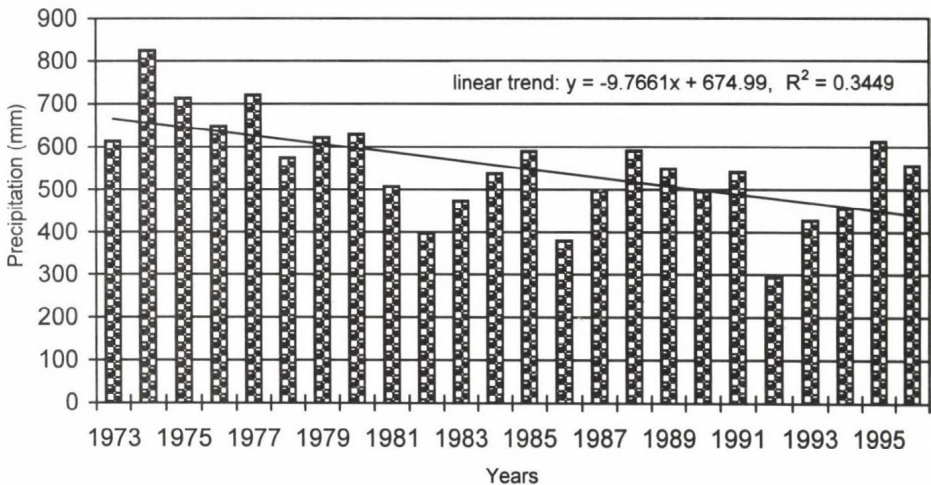


Fig. 4. Annual amounts of precipitation getting into the forest.

In Fig. 4 amounts of annual mean precipitation between 1973 and 1996 are presented. While annual mean temperature has increased, the amount of precipitation shows decreasing trend during the examined period. The annual amount of precipitation decreased yearly by 11.2 mm (with 1% error). Decrease of annual amount of precipitation is in line with decrease of the number of the trees (Fig. 2).

Warmer and drier climate presumably could launch processes, which caused the depreciation of the forest, and in combination with other factors they caused the death of the trees.

It seems however, that since 1995, due to the wetter climate and other factors, tree fading has stopped. These establishments are valid for the Síkfőkút forest only. The deterioration of the forest is in connection with environmental changes, acidification, warming up, decrease of precipitation, damage of root fungi. These changes and the complex effect of these damage-chains could lead to the fading of the trees.

Under natural conditions, the regeneration of the Turkey oak-oak joining requires few decades. Till then, researchers can study the interesting biological and ecological processes of the transformation.

References

- Antal, E., Justyák, J., and Tar, K., 1995: The course of the soil moisture content in the Austrian oak-sessile oak forest stand of Síkfőkút (in Hungarian). *Erdő és Klíma*, Debrecen, 106-117.
- Antal, E., Berki, I., Justyák, J., Kiss, Gy., Tar, K., and Vig, P., 1997: The examination of the heat and water balance of the forest stand of Síkfőkút (in Hungarian). *Department of Meteorology*, Debrecen.
- Berki, I., 1995: Examinations on the reasons of the sessile oak fading in the Northern Hungarian Mountains (in Hungarian). *CSc. Thesis*, Debrecen, Hungary.
- Jakucs, P. (ed.), 1973: "Síkfőkút Project". Environmental biological studies on an oak forest in the frame of the Biosphere Program (in Hungarian). *MTA Biol. Oszt. Közl.* 16., 11-25.
- Jakucs, P., 1985: *Ecology of an Oak Forest in Hungary*, Vol. 1. Akadémiai Kiadó, Budapest.
- Jakucs, P., 1990: Ecological approach to the forest decay in Hungary (in Hungarian). *Fizikai Szemle* 8, 225-234.
- Justyák, J., 1987: Energy balance measurements in a forest oak (Síkfőkút Project). *Időjárás* 91, 131-147.
- Justyák, J., 1995: Actual evapotranspiration of the Síkfőkút forest (in Hungarian). *Berényi Dénes emlékülés*, Debrecen, 34-39.
- Justyák, J. and Nagy, L., 1988: Investigation of available soil water in oak forest and vineyard (in Hungarian). *Léghő* 33, 21-24.
- Justyák, J. and Nagy, L., 1990: Untersuchung des verfügbaren Wassergehaltes des Bodens in Eichenwald und einer Weinbauanlage. *Acta Geogr. Geol. et Meteorol.* Tom. XXVI-XXVII., 131-142.
- Justyák, J. and Bihary, L., 1993: Extent of precipitation run-off in oak forest. *Acta Geogr. Geol. et Meteorol.* Tom. XXX-XXXI., 277-281.
- Justyák, J. and Vig, P., 1997: Microclimate of the forest (in Hungarian). In *Kertészeti és erdészeti meteorológia* (ed.: G. Szász and L. Tőkei). Mezőgazdasági Kiadó, Budapest.

- Kiss, Gy., 1995: Tendencies of soil moisture and temperature in Debrecen and Síkfőkút (in Hungarian). *Berényi Dénes emlékülés*, Debrecen, 136-143.
- Kiss, Gy. and O'Heix, B.C., 1998: Study on temperature and humidity in the vegetation period in the turkey-sessile oak forest at Síkfőkút (1978-1995). In *II. Erdő és Klíma Konferencia*. Kossuth Egyetemi Kiadó, Debrecen, 172-175.
- Redfern, D.B., 1973: Growth and behavior *Armillaria melea* rhizomorpha in soil. *Trans. Brit.Mycol. Soc.* 61, 569-581.
- Rütze, M. and Liese, W., 1980: Biologie und Bedeutung der amerikanischen Eichenwelke. *Forest u. Holzwirtschaft*, Hamburg-Reinbeck, No. 128.
- Stefanovits, P., 1985: Soil condition of the forest. In *Ecology of an Oak Forest in Hungary*, 1 (ed.: P. Jakucs). Akadémiai Kiadó, Budapest, 50-58.
- Szabó, M., 1985: Amount and element content of precipitation reaching the forest soil. In *Ecology of an Oak Forest in Hungary*, Vol. 1. (ed.: P. Jakucs). Akadémiai Kiadó, Budapest, 352-452.
- Szász, G., 1988: *Agrometeorology* (in Hungarian). Mezőgazdasági Kiadó, Budapest.
- Ulrich, B., Mayer, R., and Khanna, P.K., 1979: Deposition von Luftverunreinigungen und ihre Auswirkung in Waldökosystemen in Solling. *Schrift Forstl. Fak. Univ. Göttingen*, 58.
- Ulrich, B. and Pankrath, J. (eds.), 1983: *Effect of Accumulation of Air Pollutants in Forest Ecosystems*. Reidel Publ. Comp., Hingham.

IDŐJÁRÁS

Quarterly Journal of the Hungarian Meteorological Service
Vol. 106, No. 3–4, July–December 2002, pp. 265–275

Probability of drought occurrence in Hungary

Imre Pálfai

*Lower Tisza District Water Authority,
P.O. Box 390, H-6720 Szeged, Hungary
E-mail: vgo@ativizig.hu*

(Manuscript received May 9, 2002; in final form August 2, 2002)

Abstract—The paper gives a brief review on the drought parameters used in the Carpathians' Region, and on the previous investigations of their frequency. It deals with the calculation method of the aridity index (*PAI*) constructed by the author. It contains maps showing the results of a distribution-investigation (the average returning time period of the different severe droughts) of a 70 years long *PAI* data-base determined on 73 meteorological observation stations. Drought is a serious risk factor especially on the Great Hungarian Plain.

Key-words: drought, water scarcity, aridity index, returning time period

1. Introduction

Hungary, situated in Central Europe, belongs to the continental climatic zone, but its weather conditions are influenced sometimes by Atlantic and Mediterranean effects, too. The natural-geographical conditions are favorable for agricultural production from several points of view (about 70 per cent of the total area is cultivated), but drought is a serious risk factor. For making this risk countable, it is necessary to know — among other important factors — the probability of drought occurrence on the different regions of the country. Such an investigation is essential for the elaboration of the national drought strategy (*Harnos, 1993, Vermes, 1998, Vermes et al., 2000*).

However this topic is of high interest, it was relatively neglected in the past home literature. The main reason of this is probably the fact that in Hungary till now there is no consensus in the best indices or parameters usable under home circumstances for the quantification of drought (*Faragó et al.,*

1988, 1990; *Bussay et al.*, 1999; *Domonkos et al.*, 2001). On the other hand, in most cases it is difficult to have long-term data-base for the distribution-investigations at great number of observation stations.

In the years of the 1960-s the probability of the occurrence drought or water scarce situations has been investigated for determining irrigation water demand.

Szesztay (1966) — based on the data observed between April 1 and October 31 of the years 1871–1960 in Debrecen — calculated the water deficit in the summer period as the difference of the potential evaporation and the precipitation, and constructed the probability curve of the 90 years data-base. From this curve the probability of a given water deficit can be read (in average after how many years this water deficit occurs). The value of the potential evaporation has been determined by the sum of number of days with temperature above 10°C (*Szesztay*, 1964).

Antal (1969, 1988) calculated the climatic water deficit for the whole year and also for the cultivation period (April 1–September 30) of the years 1901–1965 at three observation stations (Debrecen, Mosonmagyaróvár, Szombathely), and constructed the probability curves. The potential evaporation was calculated by his own formula, in which the main factors are as follows: the mean daily air temperature, the saturation vapor pressure, and the actual vapor pressure.

The National Master Plan of Water Management (*Varga*, 1984) shows the 80 per cent probability values of the water deficit in the cultivation season on a map-series of different crops. The simulation model-investigation as a basis of the mapping was carried out on 13 groups of plants, for two or three different yield-level of each. The soils have been ranged into four classes according to the water storage capacity of them, and groundwater level has been taken also into consideration. Meteorological effects have been characterized by the 50 years data of the decade heat-sum and precipitation observed in 23 stations. In case of two observation stations (Zalaegerszeg and Kecskemét) the probability distribution-functions of the water deficit in the cultivation season of alfalfa was given as well.

The probability of drought occurrence in the years of the 1980-s has been studied using our own aridity index (*PAI*, see 2.1) which was not quite the same as the present form of the index (*Pálfai*, 1987). Using the data calculated from the values of 1901–1986 years at 67 meteorological stations, first we determined the spatial distribution of the 10 per cent occurrence probability values of the index (values occurring in average every ten years), second the distribution-curves of the national spatial averages were determined according to the Gauss-function. As a result, country-wide drought occurs in every 3.3 years.

Varga-Haszonits (1989) calculated an aridity index as a quotient of the potential evaporation and precipitation data of 1881–1980 years from 25 observation stations, and he determined the frequency values for the vegetation period at each stations. The potential evaporation has been determined by the formulas containing the empirical constants based on the monthly mean air temperature values of the years 1951–1980, differentiated by the counties.

The study of *Dunay and Tölgyesi* (1993) gives the drought frequency data in three classes to nine regions (nine typical observation stations) of Hungary, based on the soil moisture data of the years 1951–1992. As an example, in the region between the Danube and Tisza rivers from the 42 years investigated, 10 years were favorable from the view-point of water supply (it means the soil moisture content did not decreased below 40 per cent of the utilizable water capacity of the soil in the upper 1 m layer), 15 years were classified as droughty (soil moisture content decreased below 20 per cent), and 4 years were severely droughty (soil moisture content decreased below 10 per cent). The frequency of the same categories was found in the western part of Hungary 37, 2, and 0 years, respectively.

Szász (1994) elaborated different formulas for expressing dryness, among which his aridity index is the quotient of the precipitation and potential evaporation, but for certain extent it depends on the value of the winter-spring precipitation and the soil type (water retention capacity of the soil), too. From the average values of the index the Hungarian distribution map has been constructed. Based on the long-term investigations made in Debrecen, it was found that occurrence of dry periods was considerably more frequent in the last decades of the 20th century than at the end of the 19th and beginning of the 20th century. The author intensively evaluated the temperature and precipitation data of the years between 1901–1960 at 15 observation stations, and the connections among them. He determined—among others—the frequency per cents of the occurrence of extremely hot and dry months in the summer period as an indicator of the droughty character of the weather.

An example for the statistical evaluation of the extremely dry periods in the neighboring Vojvodina Province in Yugoslavia can be seen in the paper of *Beric and Neskovic-Zdravic* (1995). A series of maps are showing the length of the water-scarce periods returning in every 2, 5, 10, 20, 50, and 100 years. As a result, the length of these periods is changing between 21 and 72 days.

Another study (*Bussay et al.*, 1999) determined the drought frequency from the relative sum of precipitation, based on the data of the 110 years between 1881 and 1990 of 25 observation stations. According to the recommendations of the WMO, drought has been determined if the monthly relative precipitation values were found below 60 per cent, and the yearly values below 75 per cent. In this case the spatial distribution of the drought

frequency showed surprisingly small variability. The different months were droughty in 30 per cent of the total, while in the whole year investigations the drought frequency remained below 10 per cent.

In the past few years — apart from the Palmer Drought Severity Index (PDSI) —, another index: the Standardized Precipitation Index (SPI) has been used more and more worldwide (*Bussay et al.*, 1999). Both of these indices have been calculated to some Hungarian stations as well (*Domonkos et al.*, 2001).

Vrânceanu et al. (2000) published a map of areas affected by drought, which was constructed by Stanescu and coworkers for the territory of Rumania using our aridity index (*PAI*). The authors gave the average returning time of the drought according to three value-categories of the index, separated on the map.

In the next chapter the calculation method of the *PAI* is given, and the results of the investigations carried out with the index are presented.

2. Method

2.1 Calculation of the Pálfai Aridity Index (*PAI*)

There are indices for the characterization of the severity of an arid situation (dryness) by single digit derived from only few meteorological and/or hydrological parameters. The great advantage of such indices is that long-term data series could be produced by them.

The formula to calculate the base-values of the aridity index has been introduced by *Pálfai* (1984) as follows:

$$PAI_0 = \frac{t_{IV-VIII}}{P_{X-VIII}} \cdot 100, \quad (1)$$

where PAI_0 – base-value of the aridity index ($^{\circ}C/100$ mm),

$t_{IV-VIII}$ – mean value of air temperature of the period of April–August ($^{\circ}C$),

P_{X-VIII} – precipitation depth summed up by the weighed monthly values of precipitation of the period of October–August (mm).

Monthly weights for the precipitation values were based on the conditions of moisture-storage and on the changing general water demand of the crops. Estimates of the weighing factors are the following (with due regard on the overall natural conditions of the Carpathian Basin): 0.1 in October, 0.4 in November, 0.5 from December to April, 0.8 in May, 1.2 in June, 1.6 in July,

0.9 in August. It is evident that month July is the most critical period from the point of view of water supply.

When the values of PAI_0 were compared to the well-known Palmers „drought-index”, strict correlation was founded between them (Pálfai, 1990).

For the more accurate expression of aridity the base-value of PAI_0 should be corrected by the following factors (Pálfai et al., 1995).

Temperature (hot days) correction factor:

$$k_t = 6 \sqrt{\frac{n+1}{\bar{n}}}, \quad (2)$$

where k_t – temperature correction factor, n – number of the hot days ($t_{\max} \geq 30^\circ\text{C}$) in period of June–August (d), \bar{n} – long-term country-wide average of the n value (d); in Hungary this value is 16 days.

Precipitation correction factor:

$$k_p = 4 \sqrt{\frac{\tau_{\max}}{\bar{\tau}_{\max}}}, \quad (3)$$

where k_p – precipitation correction factor, τ_{\max} – the longest precipitation poor period (if the sum of precipitation in the successive days does not exceed max. 5–6 mm) between the middle of June and middle of August (d), $\bar{\tau}_{\max}$ – long-term country-wide average of τ_{\max} (d); in Hungary this value is 20 days.

Groundwater correction factor:

$$k_{gw} = \sqrt{\frac{H}{\bar{H}}}, \quad (4)$$

where k_{gw} – groundwater correction factor, H – mean depth of the groundwater table below ground level in the period of November–August (m), \bar{H} – long-term value of H on the given area (m).

The use of this correction factor is important on plain area. Practically it is the best to use the data of the nearest 2 or 3 groundwater wells in the surrounding of the meteorological station or observation point.

The final value of the aridity index — defined as PAI — is obtained from the base-value (PAI_0) by corrections:

$$PAI = k_t k_p k_{gw} PAI_0, \quad (5)$$

where the correction factors are those described above.

According to the Hungarian experiences, the threshold value of the Pálfai Aridity Index shall be at $PAI=6.0$. Smaller values are for wet years at a particular site, larger values would indicate the different severities of dryness. These may be categorized as follows: $PAI=6-8$: moderate dryness, $8-10$: medium dryness, $10-12$: heavy dryness, >12 : extremely heavy dryness.

2.2 Calculation and statistical evaluation of PAI data-series

The values of the aridity index explained above of the years between 1931–1998 for 68 meteorological stations were published in one of the periodicals of the Hungarian Meteorological Service (*Pálfai et al.*, 1999). Some typing mistakes found in the publications were corrected, plus 5 mountain-stations were included, and the data-base was completed up to 2000. As a typical example, a diagram is given here with the data of Szentes (*Fig. 1*), where — during the 70 years examined — the most severe drought happened in 1952 ($PAI=15.9^{\circ}\text{C}/100\text{ mm}$).

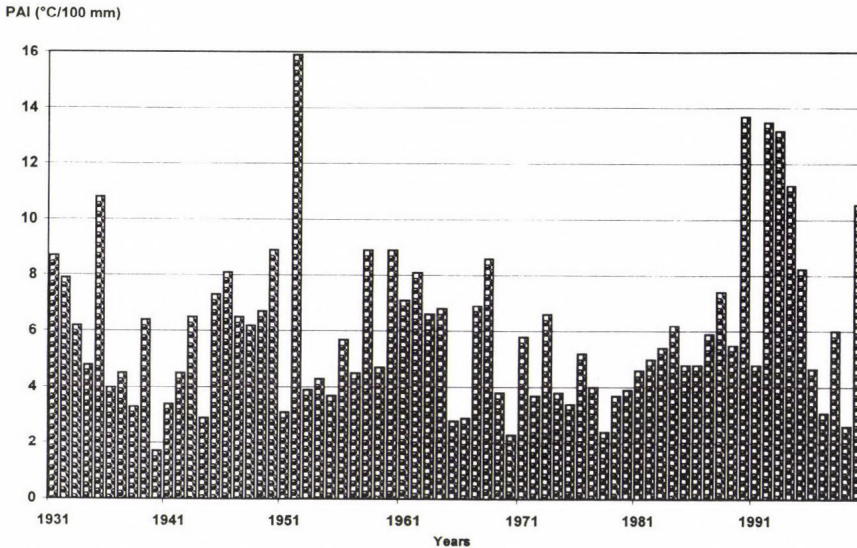


Fig. 1. Values of the Pálfai Aridity Index (*PAI*) between 1931 and 2000 at Szentes station.

Homogeneity of the 70 years data has been investigated by the *Smirnov-Kolmogorov* test. Taking into account the 30 and 70 per cent significancy boundaries, the data-base was taken homogeneous in the majority of the

stations. Inhomogeneity (slightly increasing trend) was observed only in the case of 8 stations, mainly because of the differences in the lower value-categories of the index. Therefore, the data-base was accepted in all stations from the view-point of the determination of drought occurrence probability. Other investigations (Szalai and Szentimrey, 2001) showed much more inhomogeneity.

For the determination of the latest (as the average returning time) the so-called logarithmic Pearson-distribution function has been chosen, because — according to our examinations — this fits best the empirical distribution.

3. Results

The results of the distribution-investigations carried out with the data of the 73 observation stations are given in three figures (Figs. 2, 3 and 4). On these the lines of the returning times of 3, 5, 10, 20, 50, and 100 years are shown for the cases of different severe droughts.

On the spatial distribution of the average returning time of the moderate drought ($PAI \geq 6$) can be stated (Fig. 2), that this type of droughts occurs in every 3 years on the Great Hungarian Plain, which covers the half of the country, while only in 5–20 years on the western and northern part of Hungary (near to the mountain area of the Alps).

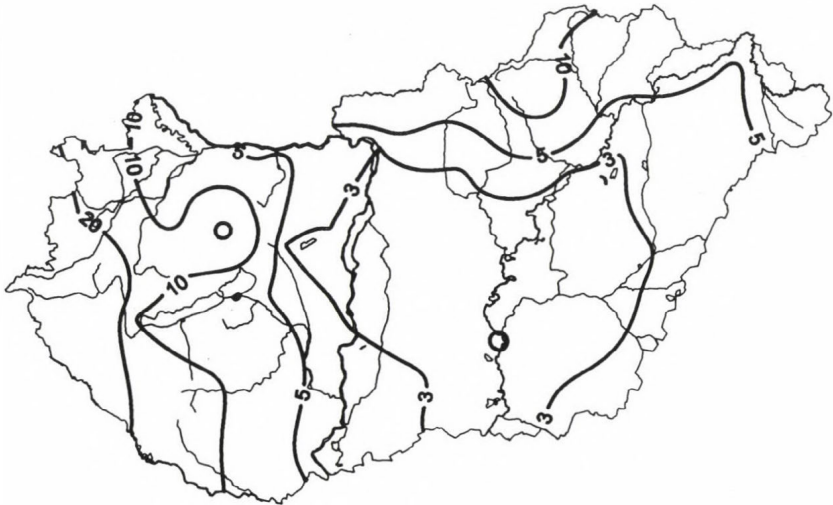


Fig. 2. Spatial distribution of the average returning time of moderate drought ($PAI \geq 6$).

According to *Fig. 3* showing the average returning time of medium drought ($PAI \geq 8$), one can count on this type of droughts in less than 10 years on the Great Hungarian Plain, and about 20–100 years on the western part of Hungary.

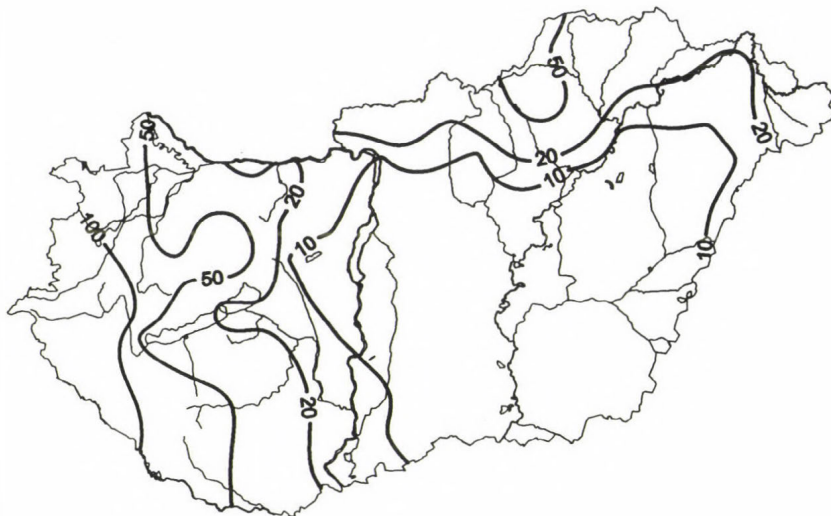


Fig. 3. Spatial distribution of the average returning time of medium drought ($PAI \geq 8$).

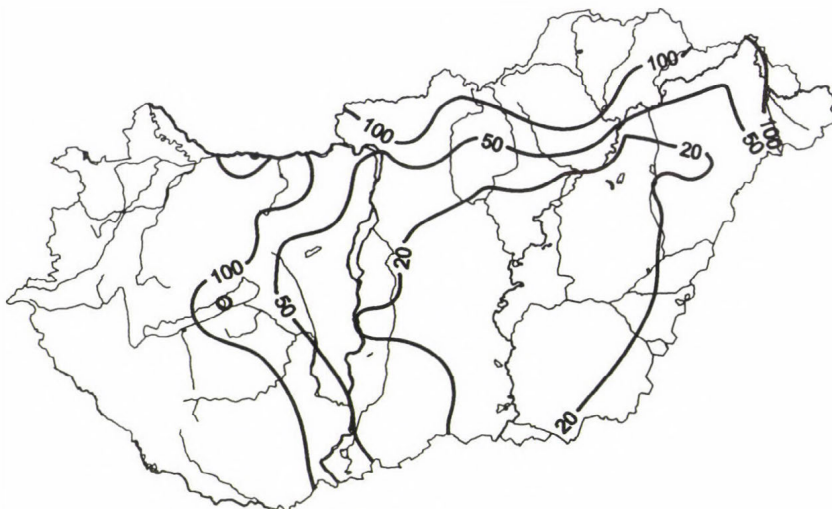


Fig. 4. Spatial distribution of the average returning time of severe drought ($PAI \geq 10$).

As it is seen in *Fig. 4*, severe drought ($PAI \geq 10$) occurs in 10–50 years on the Great Hungarian Plain (except its far eastern part), and 50–100 years on the rest areas of the country.

Extremely severe drought ($PAI \geq 12$) occurred during the 70 investigated years only on the Great Hungarian Plain, therefore the construction of a country-wide map would be illusory. The average returning time of such a drought is about 20–50 years on the middle area, and 50–100 years on the edge of the Plain. In *Table 1* the places and years are listed where and when the PAI -values were higher than 12. In the majority of the stations extremely years 1952 and 1992 occur most frequently. At the stations examined, but not included into the table, the PAI -values did not reached the number 12.

Table 1. Extremely severe droughts in Hungary ($PAI \geq 12$) between 1931–2000

Meteorological stations	Years
Ásotthalom	1952, 1992, 1993, 2000
Békéscsaba	1935, 1950
Budapest	1952, 1992
Cegléd	1952, 1983, 1990, 1992, 1993
Debrecen	1935, 1992
Fegyvernek	1935
Gyöngyös	1992
Hajdúdorog	1952, 1992
Hortobágy	1952, 1990, 1992
Izsák	1952
Jászberény	1992
Kalocsa	1993
Karcag	1952, 1962, 1992
Kecskemét	1952, 1983, 1990, 1992, 1993, 1994
Kiskunfélegyháza	1935, 1952, 1990, 1992
Kistelek	1952, 1993, 2000
Kunszentmiklós	1952
Mezőhegyes	1952, 1992
Örkény	1952, 1983, 1992
Paks	1952
Polgár	1992
Poroszló	1990, 1992
Siófok	1992
Szarvas	1952, 1992, 1993
Szeged	1952, 2000
Szeghalom	1935, 1952, 1992, 1993
Szentes	1952, 1990, 1992, 1993
Szolnok	1992, 1993
Tiszafüred	1992, 1993
Tizsakécske	1952, 1992, 1993
Túrkeve	1935, 1950, 1983

The probability of drought occurrence will be presumably influenced by the future climatic changes. According to several investigations, slight warming up is expected in Hungarian territories, and the probability of precipitation will decrease (Antal, 1997; Bartholy and Mattyasovszky, 1998; Mika, 2002). If this will be the case, the frequency of drought will increase, while the components of the water balance will decrease (Antal, 1992; Domonkos, 1997; Nováky, 2000; Mika, 2002).

4. Conclusions

The results of our investigations interpreted — with the consideration of other factors — give more reliable basis for the analysis of the risks of agricultural production, more precisely of plant production, but even for the examination of some ecological situations and planning of irrigation. Drought is a serious risk factor especially on the Great Hungarian Plain.

Acknowledgements—The author expresses his special thanks to his coworkers, Tamás László Boga and Judit Sebesvári, for their help in gathering and processing of the relevant data.

References

- Antal, E., 1969: Hidrometeorological consideration of the management of irrigation (in Hungarian). *Agrometeorological and Irrigation Problems of the Hungarian Small Plain*. Magyar Meteorológiai Társaság Kiadványa, Budapest, 103-130.
- Antal, E., 1988: Comparative analysis of the irrigation water requirement and aridity condition. *Identifying and Coping with Extreme Meteorological Events* (eds.: E. Antal and M.H. Glantz). Országos Meteorológiai Szolgálat, Budapest, 205-254.
- Antal, E., 1992: Impacts of climate change on drought in Hungary (in Hungarian). *Beszámolók az 1988-ban végzett tudományos kutatásokról*. Országos Meteorológiai Szolgálat, Budapest, 156-164.
- Antal, E., 1997: Climate modifying effect of the regulation of the river Tisza (in Hungarian). *Vízügyi Közlemények* 79, 26-45.
- Bartholy, J. and Mattyasovszky, I., 1998: The changing of the circumstances of the rain and of the temperature in the Carpathians region, in connection with the changing of the climate (in Hungarian). *Az éghajlatváltozás és következményei*. Meteorológiai Tudományos Napok'97. Országos Meteorológiai Szolgálat, Budapest, 117-125.
- Beric, M. and Neskovic-Zdravic, V., 1995: Regional analysis of extreme weather intervals in Vojvodina Province, Yugoslavia. *Proc. of the International Workshop on Drought in the Carpathians' Region* (eds.: L. Vermes and A. Mihályfy). ICID-MTESZ, Budapest, 77-86.
- Bussay, A., Szinel, Cs., and Szentimrey, T., 1999: Investigation and measurements of droughts in Hungary (in Hungarian). *Éghajlati és Agrometeorológia Tanulmányok* 7. (eds.: S. Szalai and S. Dunay). Országos Meteorológiai Szolgálat, Budapest, 9-66.
- Domonkos, P., 1997: Drought and flooded areas in Hungary (in Hungarian). *Léghő* 42, 23-33.
- Domonkos, P., Szalai, S., and Zoboki, J., 2001: Analysis of drought severity using PDSI and SPI Indices. *Időjárás* 105, 93-107.

- Dunay, S. and Tölgyesi, L., 1993: Drought—according to the agrometeorologist (in Hungarian). *Az 1992. évi aszály értékelése* (eds.: I. Pálfi and L. Vermes). FVM-MAE-MHT, Budapest, 17–24.
- Faragó, T., Bézsényi, Á., and Dobosi, E., 1990: The Palmer's surface water balance model and drought index (in Hungarian). *Időjárás* 94, 205–220.
- Faragó, T., Kozma, E., and Nemes, Cs., 1988: Quantifying droughts. *Identifying and Coping with Extreme Meteorological Events* (eds.: E. Antal and M.H. Glantz). Országos Meteorológiai Szolgálat, Budapest, 62–110.
- Harnos, Zs., 1993: The summary of the drought's measurements, conclusions, strategic considerations, challenges in the future (in Hungarian). *Az 1992. évi aszály értékelése* (eds.: I. Pálfi and L. Vermes). FVM – MAE – MHT, Budapest, 69–80.
- Mika, J., 2002: Regional climatic scenarios (in Hungarian). *DSc. Thesis*. Magyar Tudományos Akadémia, Budapest.
- Nováky, B., 2000: The climate effects of the climate's changing (in Hungarian). *A hazai vízgazdálkodás stratégiai kérdései* (ed.: L. Somlyódy). Magyarország az ezredfordulón. Stratégiai kutatások a Magyar Tudományos Akadémián. Budapest, 83–112.
- Pálfi, I., 1984: The drought index (in Hungarian). *MHT V. Országos Vándorgyűlés*, Szarvas. 19–24.
- Pálfi, I., 1987: Dry years in Hungary. *Vízügyi Közlemények* 69, 507–524.
- Pálfi, I., 1990: Description and forecasting of droughts in Hungary. *ICID Fourteenth Congress*. Rio de Janeiro, Q. 43. 151–158.
- Pálfi, I., Boga, T.L., and Sebesvári, J., 1999: Information to Droughts in Hungary 1931–1998 (in Hungarian). *Éghajlati és Agrometeorológia Tanulmányok* 7 (eds.: S. Szalai and S. Dunay). Országos Meteorológiai Szolgálat, Budapest, 67–91.
- Pálfi, I., Petrasovits, I., and Vermes, L., 1995: Some methodological question of the European drought-sensitivity map. *Proc. of the International Workshop on Drought in the Carpathians' Region* (eds.: L. Vermes and A. Mihályfy). ICID-MTESZ, Budapest, 131–142.
- Szalai, S. and Szentimrey, T., 2001: Was the climate warming in 20th century in Hungary (in Hungarian). *Dr. sen Berényi Dénes születésének centenárius jubileumi tudományos ülése* (ed.: G. Szász). Debreceni Egyetem–Magyar Tudományos Akadémia–Országos Meteorológiai Szolgálat.
- Szász, G., 1994: The climate of the Hungary and its changeable (in Hungarian) *Éghajlat, Időjárás, Aszály. I. Az időjárás változékonysága és hidrológiai vonatkozásai* (eds.: L. Cselótei and Zs. Harnos) MTA Aszálybizottság, Budapest, 59–103.
- Szesztay, K., 1964: Irrigation water demand of Hungary and waterhousehold conditions of the Carpathic Basin (in Hungarian). *Beszámoló a Vízgazdálkodási Tudományos Kutató Intézet 1961. évi munkájáról*. Budapest, 274–287.
- Szesztay, K., 1966: Problems in determining irrigation water demands. *Hidrológiai Közöny* 46, 385–395.
- Varga, M. (ed.), 1984: The National Master Plan of Water Management (in Hungarian). *Országos Vízügyi Hivatal*, Budapest.
- Varga-Haszonits, Z., 1989: Climatic parameters of the water deficit in the cultivation season (in Hungarian). In *Aszály* (ed.: V. Hanyecz). Öntözési Kutató Intézet, Szarvas, 28–41.
- Vermes, L. (ed.), 1998: How to work out a Drought Mitigation Strategy. An ICID Guide. *DVWK Guidelines*, 309. ICD-KWVGW mbH, Bonn.
- Vermes, L., Fésüs, I., Nemes, Cs., Pálfi, I., and Szalai, S., 2000: Status and progress of the national drought mitigation strategy in Hungary. *Proc. of the Central and Eastern European Workshop on Drought Mitigation* (eds.: L. Vermes and Á. Szemessy). ICID-MTESZ, Budapest, 55–63.
- Vrânceanu, Al. V., Canarache, A., and Cârstea, S., 2000: State of the art of the National Drought Mitigation Strategy in Romania. *Proc. of the Central and Eastern European Workshop on Drought Mitigation* (eds.: L. Vermes and Á. Szemessy). ICID-MTESZ, Budapest, 91–102.

IDŐJÁRÁS

Quarterly Journal of the Hungarian Meteorological Service
Vol. 106, No. 3–4, July–December 2002, pp. 277–290

On the relationship between transpiration and soil texture

Ferenc Ács

Department of Meteorology, Eötvös Loránd University,
Pázmány Péter sétány 1/A, H-1117 Budapest, Hungary
E-mail: acs@cesar.elte.hu

(Manuscript received March 14, 2002; in final form July 19, 2002)

Abstract—The relationship between microscale transpiration E characteristics and soil texture is analyzed. Microscale means point (few hundred meters \times few hundred meters) and local (few kilometers \times few kilometers) scales. In the analysis, sand and clay is used as soil texture. The point scale transpiration E_p is evaluated by a *deterministic* model, while the local scale transpiration E_l is estimated by a *statistical-deterministic* model. The core of the models is a diagnostic energy balance submodel based on the *Penman-Monteith* concept. The characteristics are considered in terms of analyzing the change of E versus soil moisture content θ , relative frequency distribution of $E(\theta)$, and the aggregation algorithms for estimation of (θ) . The analyses are performed for different atmospheric forcing conditions.

According to the results, the E characteristics for sand and clay show great similarity. They differ from each other only quantitatively. These quantitative differences are extensively discussed. The results obtained can be useful for estimating E for different soil textures.

Key-words: transpiration characteristics, point and local scale, upscaling, sand, clay.

1. Introduction

The soil texture determines indirectly the hydraulic and thermal properties of soil, and also the movement of soil water and the process of evapotranspiration (e.g., *van de Griend et al.*, 1985; *Kondo and Xu*, 1997; *Kim and Entekhabi*, 1998; *Braud et al.*, 1995; *O’Kane*, 1991). These interrelations are investigated experimentally and theoretically. The experimental studies are rare. One of the the most interesting experimental study was performed by *Idso et al.* (1974). The theoretical studies are more widespread. They investigate the chain of the interrelations between the soil hydraulic properties, water movement in the

soil, and the evapotranspiration by numerical experiments. The experiments have been made either in prognostic or diagnostic mode. The former ones are widespread. In most cases they investigated the effect of soil texture on surface fluxes. In general, the experiments are performed in an off-line mode using fictitious data. The sensitivity proved to be strong, especially on the annual scale (*Irannejad and Shao, 1998; Wilson et al., 1987; Pitman, 1994*). The sensitivity on a short (several days) time scale has been shown by *Mihailovic et al. (1992)*, *Ács and Lőke (2001a, b)*. The experiments performed in a coupled mode by a meteorological model are rare (e.g., *Kim and Entekhabi, 1998*). They commonly use fictitious soil physical data but there are also studies dealing with real databases (e.g., *Mika et al., 2002*). In these studies, the sensitivity of meteorological variables is investigated.

In this study, we applied a diagnostic approach to study the relationship between transpiration and soil texture. The objective of this study is to analyse the dependence of microscale transpiration characteristics on soil texture. The characteristics are considered in terms of analyzing the change of E versus soil moisture content θ , relative frequency distribution of $E(\theta)$, and the aggregation algorithms for estimating transpiration on the local scale $E_l(\theta)$. The point (few hundred meters \times few hundred meters) and the local (few kilometers \times few kilometers) scale models are based on the *Penman-Monteith* concept (*Ács and Hantel, 1999; Ács et al., 2000*). To our best knowledge, there is no study investigating the relationship between the soil texture and all the important aspects of microscale transpiration characteristics. In the study, we assumed that there are no advective effects accompanied by occasionally observed internal boundary layers (e.g., *Garratt, 1992; Hupfer and Raabe, 1994*), and there are also no mesoscale circulation patterns induced by surface discontinuities. Then the atmosphere can be assumed to be horizontally homogeneous with constant meteorological boundary conditions above a certain level (*Shuttleworth, 1998*).

2. Models

The two model types used are the *deterministic* model (DM) for diagnosing transpiration on the point scale and the *statistical-deterministic* model (SDM) for estimating transpiration on the local scale.

2.1 Deterministic model

The model does not treat interception. Further, we suppose that the vegetation canopy is completely closed. So the water vapor flux above vegetation is

formed only by transpiration. The model is based on the equation system as follows:

$$H = A_e - \lambda E \quad (1)$$

$$\lambda E = \frac{\Delta \cdot A_e + \rho \cdot c_p \delta e / r_a}{\Delta + \gamma(1 + r_v / r_a)} \quad (2)$$

$$r_a = f_1(u_*, L, \text{constants}) \quad (3)$$

$$u_* = f_2(u_r, L, \text{constants}) \quad (4)$$

$$L = f_3(u_*, H, E, \text{constants}) = \frac{-\rho \cdot T_r \cdot u_*^3}{g \cdot k \cdot \left(\frac{H}{c_p} + 0.61 \cdot T_r \cdot E \right)}, \quad (5)$$

where H and λE are the sensible and latent heat flux, A_e is the available energy of vegetation surface, Δ is the slope of saturated vapor pressure curve, ρ is the air density, δe is the vapor pressure deficit, r_a is the aerodynamic resistance, γ is the psychrometric constant, r_v is the vegetation canopy resistance. r_a depends on the friction velocity u_* , and the stratification expressed by the *Monin-Obukhov* length L . u_r and T_r are the wind speed and air temperature at reference height, c_p is the specific heat of air at constant pressure, g is the gravitational acceleration, and k is the von Kármán constant. The functions f_1 and f_2 depend on the stratification and choice of the universal functions. For *Businger et al.* (1971) functions, their exact form is given, e.g., in *Ács et al.* (2000) or *Ács and Kovács* (2001). But some other functions can also be applied (see e.g., *Antal*, 1962). The available energy flux of vegetation surface can be easily expressed using energy balance equation. r_v is parameterized by *Jarvis* (1976) formula. The moisture availability function F_{ma} is expressed as simply as possible via soil moisture content θ (e.g., see Eq. (35) in *Noilhan and Planton* (1989) or Eq. (35) in *Ács and Hantel* (1998)). Hereinafter this will be referred to as *Theta*-parameterization.

The equation system of five equations contains five unknowns: H , λE , r_a , u_* , and L . The equation system is solved applying an iterative procedure. In most cases, the solution can be easily obtained after 4–5 iterations, but in some physically unreal situations (for instance for strong radiation and weak wind) the procedure does not converge (*Czúcz and Ács*, 1999).

2.2 Statistical-deterministic model

The local scale transpiration is estimated by the *statistical-deterministic* model. It consists of a *deterministic* submodel for estimating transpiration (see section 2.1), a *statistical* submodel for generating θ as a random variable (Wetzel and Chang, 1988), and a submodel for calculating the area-averaged $E(\theta)$. In the following the two latter submodels will be briefly considered.

2.2.1 Modeling soil moisture variability

According to observations of Bell *et al.* (1980) and Hawley *et al.* (1983), area variations of θ on the local scale can be characterized by a normal distribution. According to Wetzel and Chang (1988), the corresponding standard deviation is

$$\sigma_{\theta} = \min (0.08, \theta_m/2), \quad (6)$$

where θ_m is the area-averaged value of soil moisture content. The area variations of θ on the local scale are generated by Monte-Carlo runs applying a standard random number generation algorithm (see Dévényi and Gulyás, 1988) using θ_m and σ_{θ} as inputs.

2.2.2 Calculation of area-averaged transpiration

Since θ is a statistical variable, so are the turbulent heat fluxes H and λE . The statistical distribution of λE or E is analyzed by its relative frequency distribution. The area-averaged value of E is estimated by numerical integration of its relative frequency distribution function $RF(E_j)$ as follows:

$$E_l = \langle E \rangle = \sum_{j=1}^n RF(E_j) E_j, \quad (7)$$

where $\langle E \rangle$ is the area-averaged E , j is the interval number, and E_j is the corresponding E -value for the j th interval. The length of E -interval is chosen as 25 W m^{-2} . The submodel is applied in each step for $0.02 \leq \theta_m < \theta_s$ cycle to obtain the $\langle E(\theta_m, \sigma_{\theta}) \rangle$ curve. θ_s is the saturated soil moisture content.

3. Numerical experiments

The numerical experiments are performed by both the *deterministic* and *statistical-deterministic* models for grass covered surface using sand and clay as soil texture. The simulations are made for different atmospheric forcing

conditions. In this study, we distinguished strong and weak atmospheric forcing conditions. They are presented in *Table 1*. During numerical experiments 2×2 runs are performed using both the *deterministic* and *statistical-deterministic* models. Of course, the computation time of the latter model is much longer with respect to the former one because of the generation of statistical variables.

Table 1. Atmospheric forcing conditions

Variables	Strong atmospheric forcing	Weak atmospheric forcing
Net radiation flux (W m^{-2})	700	300
Air temperature at reference level ($^{\circ}\text{C}$)	25.8	25.8
Vapor pressure at reference level (hPa)	18.0	32.0
Vapor pressure at reference level (hPa)	6.0	2.0

4. Simulation results

Verification of $E(\theta)$ model based on *Theta* parameterization on the point scale is performed on the well known 1987 Cabauw data set (*Beljaars and Bosveld, 1997*). These results are presented in *Ács and Hantel (1998)* and *Ács et al. (2000)*.

The microscale transpiration characteristics are analyzed in terms of the $E(\theta)$ curve (relationship between transpiration and soil moisture content), the relative frequency of $E(\theta)$, and the aggregation algorithm for $E(\theta)$. These features are analyzed for both sand and clay.

4.1 Analysis of transpiration curves

On the point scale, $E(\theta)$ does not show area variations, therefore, it is obtained by running the *deterministic* model. So $E(\theta) = E_p^s(\theta)$ for sand and $E(\theta) = E_p^c(\theta)$ for clay. On the local scale, the area variations of θ are represented by the normal distribution via θ_m and σ_θ . $E(\theta)$ is obtained by running the *statistical-deterministic* model. So, analogously to the point scale transpiration, $E(\theta) = \langle E^s(\theta_m, \sigma_\theta) \rangle = E_l^s(\theta)$ for sand and $E(\theta) = \langle E^c(\theta_m, \sigma_\theta) \rangle = E_l^c(\theta)$ for clay.

$E_p^s(\theta)$, $E_p^c(\theta)$, $E_l^s(\theta)$, and $E_l^c(\theta)$ (including the factor λ) for strong and weak atmospheric forcing are presented in *Figs. 1* and *2*. Inspecting the

curves, it is obvious that the curves obtained for sand ($E_p^s(\theta)$, $E_l^s(\theta)$) and clay ($E_p^c(\theta)$, $E_l^c(\theta)$) are very similar. The similarity between $E_p^s(\theta)$, and $E_p^c(\theta)$ is more pronounced than between $E_l^s(\theta)$ and $E_l^c(\theta)$. The similarity can be analyzed introducing some characteristic soil moisture content values. They are presented in *Table 2* for sand, loam and clay. Note that the corresponding loam-referred curves are not presented here.

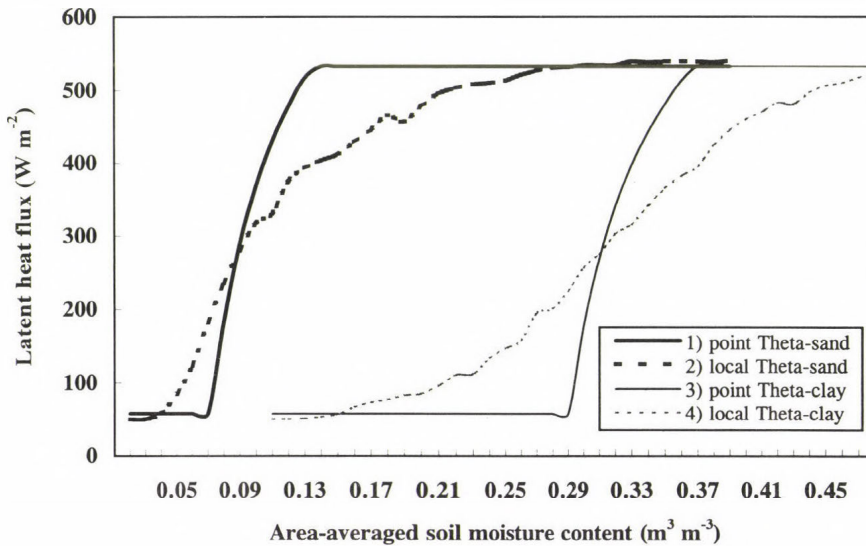


Fig. 1. Transpiration curve as obtained by Theta parameterization (1) on point scale using sand as soil texture (black continuous line), (2) on local scale using sand as soil texture (black dashed line), (3) on point scale using clay as soil texture (grey continuous line), and (4) on local scale using clay as soil texture (grey dashed line). The curves refer to strong atmospheric forcing conditions.

In total there are five boundary values of soil moisture content: the wilting point soil moisture content on the local scale $\theta_{l,w}$, the wilting point soil moisture content on the point scale $\theta_{p,w}$, the θ_c soil moisture content value in the transition region (region between the soil-controlled and the atmospheric-controlled transpiration), namely $E_p(\theta_c) = E_l(\theta_c)$, the field capacity soil moisture content on the point scale $\theta_{p,f}$ and the field capacity soil moisture content on the local scale $\theta_{l,f}$. The shape of $E_p(\theta)$ curves is strongly determined by $\theta_{p,w}$ and $\theta_{p,f}$. In the $0.02 - \theta_{p,w}$ region (the so-called soil-controlled region by low θ

values on the point scale), $E_p^s(\theta) = E_p^l(\theta) = E_p^c(\theta) = \text{const}$. This constant does not depend on the atmospheric forcing conditions. Its value is determined by the parameterization of moisture availability function $F_{ma}(\theta)$. In the $\theta_{p,w} - \theta_{p,f}$ region (the transition region between the soil-controlled and the atmospheric-controlled regions on the point scale), the slope $\partial E_p^s(\theta) / \partial \theta = \partial E_p^l(\theta) / \partial \theta = \partial E_p^c(\theta) / \partial \theta$. Note that the width of the region is about the same (in average about $0.08 \text{ m}^3 \text{ m}^{-3}$) for all three soil textures. Therefore the slope of $E_p(\theta)$ curves is somewhat greater for stronger atmospheric forcing conditions. In the $\theta_{p,f} - \theta_s$ region (the so-called atmospheric-controlled region by high θ -values on the point scale), $E_p^s(\theta) = E_p^l(\theta) = E_p^c(\theta) = \text{const}$. This constant depends only on the atmospheric forcing conditions. In this θ -region, the transpiration is called as potential transpiration. Note that the value of potential transpiration does not depend on the soil texture.

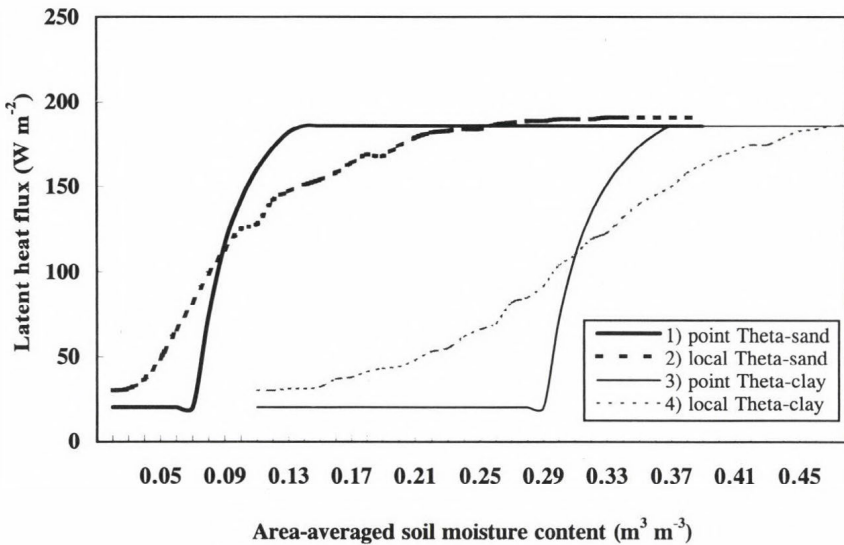


Fig. 2. As in Fig. 1 but for weak atmospheric forcing conditions.

Similar analysis can also be done for $E_l(\theta)$ curves. In the $0.02 - \theta_{l,w}$ region, (the so-called soil-controlled region by low θ -values on the local scale), $E_l^s(\theta) = E_l^l(\theta) = E_l^c(\theta) = \text{const}$. This constant — as in the former case — does not depend on the atmospheric forcing conditions. Since $\theta_{l,w} < \theta_{p,w}$, it is obvious that the parameterization of $F_{ma}(\theta)$ is different on the point and the local scale.

The $\theta_{l,w}-\theta_{l,f}$ region (the transition region between the soil-controlled and the atmospheric-controlled regions on the local scale) has to be separated into two subregions. In the $\theta_{l,w}-\theta_c$ subregion, $\partial E_l^s(\theta)/\partial\theta > \partial E_l^c(\theta)/\partial\theta$ (the slopes $\partial E_l^c(\theta)/\partial\theta$ and $\partial E_l^l(\theta)/\partial\theta$ are about the same, this is not presented here) while in the $\theta_c-\theta_{l,f}$ subregion, $\partial E_l^s(\theta)/\partial\theta \approx \partial E_l^c(\theta)/\partial\theta$. Since $\partial E_l^s(\theta)/\partial\theta > \partial E_l^c(\theta)/\partial\theta$ the $E_l^s(\theta)$ and the $E_l^c(\theta)$ curves are not pronouncedly similar. In the $\theta_{l,f}-\theta_s$ region (the so-called atmospheric-controlled region by high θ -values on the local scale), $E_l^s(\theta) = E_l^l(\theta) = E_l^c(\theta) = \text{const}$. This constant — as in the former case — depends only on the atmospheric forcing conditions. Note that the potential transpiration on the point and the local scale is equal. As in the former case, the value of potential transpiration does not depend on the soil texture.

Table 2. Boundary values of soil moisture content obtained for sand, loam, and clay as soil textures. Symbols: $\theta_{l,w}$ =wilting point soil moisture content on local scale, $\theta_{p,w}$ =wilting point soil moisture content on point scale, θ_c =soil moisture content value in the transition region for which $E_p(\theta_c) = E_l(\theta_c)$, $\theta_{p,f}$ =field capacity soil moisture content on point scale, and $\theta_{l,f}$ =field capacity soil moisture content on local scale

Boundary values of soil moisture content ($\text{m}^3 \text{m}^{-3}$)	Sand	Loam	Clay
$\theta_{l,w}$	0.03	0.08	0.15
$\theta_{p,w}$	0.07	0.15	0.29
θ_c	0.09	0.18	0.31
$\theta_{p,f}$	0.14	0.24	0.37
$\theta_{l,f}$	0.27	0.36	0.47

4.2 Area variations of transpiration

Area variation of $E(\theta)$ is examined analyzing its relative frequency distribution. RF obtained for sand and clay is RF^s and RF^c , respectively. The estimates are performed for strong atmospheric forcing conditions and three different θ_m -values. The characteristic θ_m -values are $\theta_{p,w}$ ($0.07 \text{ m}^3 \text{m}^{-3}$ for sand and $0.29 \text{ m}^3 \text{m}^{-3}$ for clay), θ_c ($0.09 \text{ m}^3 \text{m}^{-3}$ for sand and $0.31 \text{ m}^3 \text{m}^{-3}$ for clay) and $\theta_{p,f}$ ($0.14 \text{ m}^3 \text{m}^{-3}$ for sand and $0.37 \text{ m}^3 \text{m}^{-3}$ for clay). The histograms of RF^s and RF^c for $\theta_{p,w}$ -, θ_c - and $\theta_{p,f}$ -values are presented on Fig. 3a-c, respectively. Obviously the RF^s and RF^c are very similar. They show bimodal distribution.

In dry regime ($\theta_m = \theta_{p,w}$), the RF maximum is on the left-hand side of the spectrum. In wet regime ($\theta_m = \theta_{p,f}$), the RF maximum is on the right-hand side of the spectrum. For $\theta_m = \theta_c$, the peaks on the left-hand side and on the right-hand side of the spectrum are quite large. Since the peaks on left-hand side of the spectrum are larger than the peaks on the right-hand side of the spectrum, the wetness regime represented by θ_c is more dry than wet.

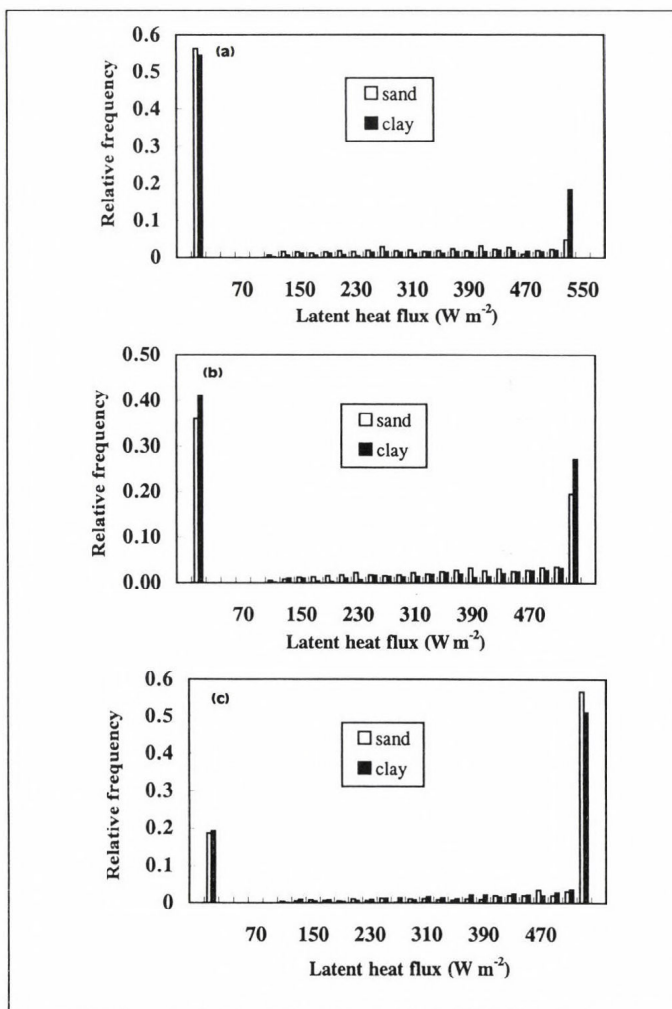


Fig. 3. Relative frequency distribution of latent heat flux from vegetation using sand (light columns) and clay (dark columns) as soil texture for (a) $\theta_{p,w}$, (b) θ_c , and (c) $\theta_{p,f}$. The results are obtained for strong atmospheric forcing conditions.

4.3 Aggregated soil moisture content

The aggregated soil moisture content θ_{ag} is defined by

$$E(\theta_{ag}) = \langle E(\theta_m, \sigma_\theta) \rangle, \quad (8)$$

where $E(\theta_{ag})$ is the area-averaged transpiration calculated by the *deterministic* model using θ_{ag} and $\langle E(\theta_m, \sigma_\theta) \rangle$ is the area-averaged transpiration calculated by the statistical-deterministic model using θ_m and σ_θ . θ_{ag} obtained for sand and clay is θ_{ag}^s and θ_{ag}^c , respectively. The relationship between θ_{ag} and θ_m can be obtained comparing $E_p(\theta)$ and $E_l(\theta)$ curves (see Figs. 1 and 2). The change of θ_{ag}^s and θ_{ag}^c versus θ_m for strong and weak atmospheric forcing conditions is presented in Fig. 4. The plots obtained for sand and clay are similar. The relationship between θ_{ag}^s and θ_m can be treated as linear, while the relationship between θ_{ag}^c and θ_m can be characterised as slightly non-linear. But it has to be noted that in the dry regime ($\theta_m < \theta_c$), the relationship can also be characterized as linear. Further, the relationship between θ_{ag}^s and θ_m does not depend on the atmospheric forcing conditions. In spite of this, the relationship between θ_{ag}^c and θ_m weakly depends on the atmospheric forcing conditions. In dry regime ($\theta_m < \theta_c$) this dependence is very small. In the wet regime ($\theta_m > \theta_c$), the more wet the surface, the more atmospheric-dependent is the θ_{ag}^c/θ_m relationship. This is in accordance with simulation results of *Shao et al.* (2001) made by a mesoscale atmospheric model. Summarizing, the θ_{ag}/θ_m relationship for sand and clay can be characterized by regressions as follows:

$$\theta_{ag}^s = 0.30 \cdot \theta_m + 0.06, \quad r^2 = 0.98 \quad (9)$$

and

$$\theta_{ag}^c = 0.93 \cdot \theta_m^2 - 0.32 \cdot \theta_m + 0.32, \quad r^2 = 0.99, \quad (10)$$

where r^2 is the correlation coefficient. Eq. (10) refers to weak atmospheric forcing conditions.

4.4 Upscaling strategies

The results obtained for $E_p(\theta)$, $E_l(\theta)$ and θ_{ag} determine the possible upscaling procedures of transpiration from point to local scale. Since there is a pronounced similarity between $E_p^s(\theta)$ and $E_p^c(\theta)$, $E_l^s(\theta)$ and $E_l^c(\theta)$ and θ_{ag}^s and θ_{ag}^c , the upscaling strategies for sand and clay will be also very similar. The upscaling procedures to be used are determined by the wetness regime.

In extremely dry (between 0.02 and $\theta_{l,w}$) and wet (between $\theta_{l,f}$ and θ_s) conditions (see Table 2), $E_p(\theta)$ is equal to $E_r(\theta)$, so there is no need for upscaling $E(\theta)$. In the transition region (between $\theta_{l,w}$ and $\theta_{l,f}$) between the extremely dry and wet conditions, the upscaling procedure depends on the characteristics of the θ_{ag}/θ_m relationship. The upscaling of $E^s(\theta)$ is to be performed by Eqs. (8) and (9). In this case, the procedure does not depend on the atmospheric forcing conditions. Analogously, the upscaling of $E^c(\theta)$ is to be performed by Eqs. (8) and (10). In contrast to the former case, the procedure slightly depends on the atmospheric forcing conditions.

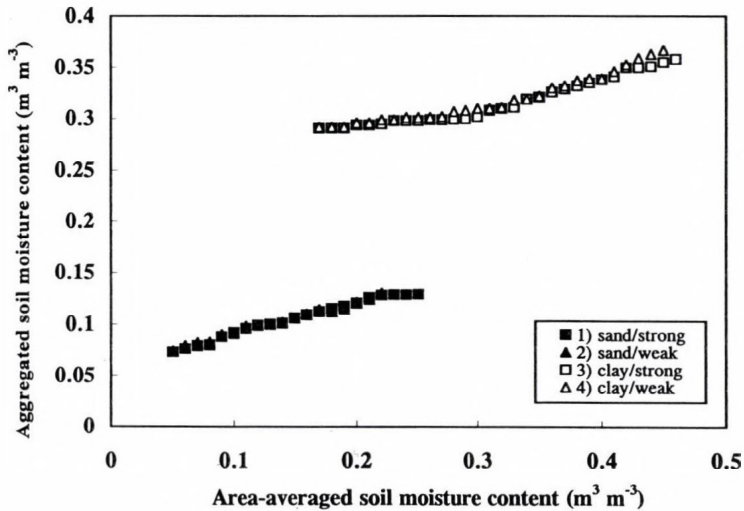


Fig. 4. Aggregated versus area-averaged soil moisture content for (1) sand using strong atmospheric forcing conditions (dark squares), (2) sand using weak atmospheric forcing conditions (dark triangles), (3) clay using strong atmospheric forcing conditions (light squares), and (4) clay using weak atmospheric forcing conditions (light triangles).

5. Conclusions

The relationship between microscale transpiration characteristics and soil texture is analyzed. Microscale means point and local scale transpiration. In the analysis sand and clay are used as soil textures. The point scale transpiration is estimated by a *deterministic* model, while the local scale transpiration is simulated by a *statistical-deterministic* model. The deterministic E_p -model is based on the *Penman-Monteith* concept (Ács and Hantel, 1999), that is, transpiration is determined by the *Penman-Monteith*

equation, and the sensible heat flux is obtained as residual component from the energy balance equation. The *statistical-deterministic* E_T -model consists of an E_p -submodel, a statistical submodel for generating θ as random variable, and a submodel for calculating the area-averaged $E_l(\theta)$. The transpiration characteristics are considered in terms of analyzing transpiration E versus soil moisture content θ , relative frequency distribution characteristics of $E(\theta)$, and the aggregation algorithms for its estimation. The analyses are performed for different atmospheric forcing conditions. The results can be briefly summarized as follows:

- $E_p^s(\theta)$ and $E_p^c(\theta)$ curves are pronouncedly similar to each other. They can be treated as parallel curves translated to each other. The soil texture does not determine the value of E_p in the soil-controlled and atmospheric-controlled regimes, and the slope of E_p ($\partial E_p(\theta)/\partial \theta$) in the transition region. $E_l^s(\theta)$ and $E_l^c(\theta)$ curves are also similar to each other. They are translated but not parallel to each other. The greatest deviation between them is in the $\theta_{l,w}-\theta_c$ region. Similarly to the former case, the soil texture does not determine the value of E_l in the soil-controlled and atmospheric-controlled regimes.
- Normally distributed soil moisture variations produced bimodal RF^s and RF^c . Relative frequencies depend strongly on the wetness regime. According to the expectations, RF^s - histograms obtained for $\theta_{p,w}^s$, θ_c^s , and $\theta_{p,f}^s$ are very similar to RF^c -histograms obtained for $\theta_{p,w}^c$, θ_c^c , and $\theta_{p,f}^c$.
- The relationship between θ_{ag}^s and θ_m is linear. In spite of this, the relationship between θ_{ag}^c and θ_m is non-linear. It has to be noted that in the dry regime ($\theta_m < \theta_c$), this latter relationship can also be characterized as linear. Furthermore, the relationship between θ_{ag}^s and θ_m does not depend on the atmospheric forcing conditions. However, the relationship between θ_{ag}^c and θ_m weakly depends on the atmospheric forcing conditions. In dry regime ($\theta_m < \theta_c$), this dependence is very small. In wet regime ($\theta_m > \theta_c$), the wetter the surface, the more atmospheric-dependent the θ_{ag}^c/θ_m relationship is. This is in accordance with simulation results of *Shao et al.* (2001) using a mesoscale atmospheric model.
- Since there is a pronounced similarity between $E_p^s(\theta)$ and $E_p^c(\theta)$, $E_l^s(\theta)$ and $E_l^c(\theta)$, and θ_{ag}^s and θ_{ag}^c , the upscaling strategies for sand and clay will be also very similar. The upscaling procedures to be used are determined by the wetness regime. In extremely dry (between 0.02 and $\theta_{l,w}$) and wet (between $\theta_{l,f}$ and θ_s) conditions (see Table 2), $E_p(\theta)$ is equal

to $E_l(\theta)$, so there is no need to apply a procedure for upscaling $E(\theta)$. In the transition region (between $\theta_{l,w}$ and $\theta_{l,f}$) between the extremely dry and wet conditions, the upscaling procedure depends on the characteristics of θ_{ag} / θ_m relationship. A crucial aspect is whether the relationship between θ_{ag} and θ_m depends on the atmospheric forcing conditions. If this relationship is simple (there is no atmospheric dependence or this dependence is weak), the upscaling procedure to be applied is also simple (Eqs. (8) and (9) for sand and Eqs. (8) and (10) for clay). If the relationship is complex, for instance, it depends on the atmospheric forcing conditions, the construction of a simple $E_l(\theta)$ formula seems to be unlikely.

It has to be mentioned that soil moisture characteristics on the point scale ($\theta_{p,w}$, $\theta_{p,f}$) presented in Table 2 refer to soils of North-America (Cosby *et al.*, 1984). Obviously, the soil moisture characteristics on the local scale and the microscale transpiration characteristics refer also to the soils of North-America. The extension of the method to Hungarian soils is in process. Of course, these results are valid only — as mentioned in the introduction — when there are no advective effects and mesoscale circulation patterns. In the latter cases the transpiration characteristics and its upscaling strategy are more complex.

Acknowledgement—This study is partly financially supported by the Hungarian Ministry for Culture and Education via OTKA Foundation, project number T-029358.

References

- Antal, E., 1962: Determination of the rate of evapotranspiration (in Hungarian). *Beszámoló az 1961-ben végzett tudományos kutatásokról*. Országos Meteorológiai Intézet, Budapest, 131-153.
- Ács, F. and Hantel, M., 1998: Land-surface hydrology parameterization in PROGSURF: Formulation and test with Cabauw data. *Időjárás* 102, 109-127.
- Ács, F. and Hantel, M., 1999: The Penman-Monteith concept based land-surface model PMSURF. *Időjárás* 103, 19-36.
- Ács, F., Hantel, M., and Unegg, J.W., 2000: Climate diagnostics with the Budapest-Vienna Land-Surface Model SURFMODE. *Austrian Contribution to the IGBP. Vol. 3, National Committee for the IGBP, Austrian Academy of Sciences*.
- Ács, F. and Kovács, M., 2001: The surface aerodynamic transfer parameterization method SAPA: description and performance analyses. *Időjárás* 105, 165-182.
- Ács, F. and Lőke, Zs., 2001a: Simulation of the impact of soil texture on the surface soil moisture changes (in Hungarian). *Agrokémia és Talajtan* 50, 457-468.
- Ács, F. and Lőke, Zs., 2001b: Biophysical modeling in agrometeorology. *Légkör* 46, No. 3, 2-8.
- Bell, K.R., Blanchard, B.J., Schmugge, T.J., and Witzak, M.W., 1980: Analysis of the surface moisture variations within large field sites. *Water Resour. Res.* 16, 796-810.
- Beljaars, A.C.M. and Bosveld, F.C., 1997: Cabauw data for the validation of land surface parameterization schemes. *J. Climate* 10, 1172-1193.
- Braud, I., Dantas-Antonino, A.C., and Vauclin, M., 1995: A stochastic approach to studying the

- influence of soil hydraulic properties on surface fluxes, temperature and humidity. *J. Hydrol.* 165, 283-310.
- Businger, J., Wyngaard, J., Izumi, Y., and Bradley, E., 1971: Flux-profile relationships in the atmospheric surface layer. *J. Atmos. Sci.* 28, 181-189.
- Czúcz, B. and Ács, F., 1999: Parameterization of unstable stratification in land-surface model PMSURF: An examination of the convergence by empirical methods. *Léggör* 44, No. 2, 2-6.
- Cosby, B.J., Hornberger, G.M., Clapp, R.B., and Ginn, T.R., 1984: A statistical exploration of the relationships of soil moisture characteristics to the physical properties of soils. *Water Resour. Res.* 20, 682-690.
- Dévényi, D., and Gulyás, O., 1988: Mathematical statistical methods in meteorology (in Hungarian). *Tankönyvkiadó*, Budapest.
- Garratt, J.R., 1992: The internal boundary layer-A review. *Bound.-Layer Meteor.* 50, 171-203.
- Hawley, M. E., Jackson, T. J., and McCuen, R.H., 1983: Surface soil moisture variation on small agricultural watersheds. *J. Hydrol.* 62, 170-200.
- Hupfer, P. and Raabe, A., 1994: Meteorological transition between land and sea in the microscale. *Meteor. Z.* 3, 100-103.
- Idso, S.B., Reginato, R.J., Jackson, R.D., Kimball, B.A., and Nakayama, F.S., 1974: The three stages of drying of a field soil. *Soil Sci. Soc. Proc.* 38, 831-837.
- Irannejad, P. and Shao, Y., 1998: Description and validation of the atmosphere-land-surface interaction scheme (ALSIS) with HAPEX and Cabauw data. *Global Planet. Change* 19, 87-114.
- Jarvis, P.G., 1976: The interpretation of the variations in the leaf water potential and stomatal conductance found in canopies in the field. *Philos. Trans. Roy. Soc. London, Ser. B.* 273, 593-610.
- Kim, C.P. and Entekhabi, D., 1998: Impact of soil heterogeneity in a mixed-layer model of the planetary boundary layer. *Hydrological Sciences-Journal-des Sciences Hydrologiques* 43, 633-658.
- Kondo, J. and Xu, J., 1997: Seasonal Variations in the heat and water balances for nonvegetated surfaces. *J. Appl. Meteor.* 36, 1676-1695.
- Mihailovic, D.T., de Bruin, H.A.R., Jetric, M., and van Dijken, A., 1992: A study of the sensitivity of land surface parameterizations to the inclusion of different fractional covers and soil textures. *J. Appl. Meteor.* 31, 1477-1478.
- Mika, Á., Ács, F., Radnóti, G., and Horányi, A., 2002: Sensitivity of the ALADIN weather prediction model to the changes of soil texture. *Időjárás* 106, 39-58.
- Noilhan, J. and Planton, S., 1989: A simple parameterization of land surface processes for meteorological models. *Mon. Wea. Rev.* 117, 536-549.
- O'Kane, J.P., 1991: Implications for remote sensing of natural switching from atmosphere-controlled to soil-controlled evaporation or infiltration. In *Land-surface Evaporation: Measurement and Parameterization*. (eds.: T.J. Schmugge and J.-C. André). Springer Verlag, New-York, Berlin, Heidelberg, 371-381.
- Pitman, A. J., 1994. Assessing the sensitivity of a land-surface scheme to the parameter values using a single column model. *J. Climate* 7, 1856-1869.
- Shao, Y., Sogalla, M., Kerschgens, M., and Brüher, W., 2001: Effects of land-surface heterogeneity upon surface fluxes and turbulent conditions. *Meteorol. Atm. Phys.* in press.
- Shuttleworth, J.W., 1988: Macrohydrology-the new challenge for process hydrology. *J. Hydrol.* 100, 31-56.
- van de Griend, A.A., Camillo, P.J., and Gurney, R.J., 1985: Discrimination of soil physical parameters, thermal inertia, and soil moisture from diurnal surface temperature fluctuations. *Water Resour. Res.* 21, 997-1009.
- Wetzel, P.J. and Chang, Y.T., 1988: Evapotranspiration from nonuniform surfaces: A first approach for short-term numerical weather prediction. *Mon. Wea. Rev.* 116, 600-621.
- Wilson, M.F., Henderson-Sellers, A., Dickinson, R.E., and Kennedy, P.J., 1987: Sensitivity of the Biosphere-Atmosphere Transfer Scheme (BATS) to the inclusion of variable soil characteristics. *J. Climate Appl. Meteor.* 26, 341-362.

GUIDE FOR AUTHORS OF *IDŐJÁRÁS*

The purpose of the journal is to publish papers in any field of meteorology and atmosphere related scientific areas. These may be

- research papers on new results of scientific investigations,
- critical review articles summarizing the current state of art of a certain topic,
- short contributions dealing with a particular question.

Some issues contain "News" and "Book review", therefore, such contributions are also welcome. The papers must be in American English and should be checked by a native speaker if necessary.

Authors are requested to send their manuscripts to

Editor-in Chief of IDŐJÁRÁS

P.O. Box 39, H-1675 Budapest, Hungary

in three identical printed copies including all illustrations. Papers will then be reviewed normally by two independent referees, who remain unidentified for the author(s). The Editor-in-Chief will inform the author(s) whether or not the paper is acceptable for publication, and what modifications, if any, are necessary.

Please, follow the order given below when typing manuscripts.

Title part: should consist of the title, the name(s) of the author(s), their affiliation(s) including full postal and E-mail address(es). In case of more than one author, the corresponding author must be identified.

Abstract: should contain the purpose, the applied data and methods as well as the basic conclusion(s) of the paper.

Key-words: must be included (from 5 to 10) to help to classify the topic.

Text: has to be typed in double spacing with wide margins on one side of an A4 size white paper. Use of S.I. units are expected, and the use of negative exponent is preferred to fractional sign. Mathematical formulae are expected to be as simple as possible and numbered in parentheses at the right margin.

All publications cited in the text should be presented in a *list of references*,

arranged in alphabetical order. For an article: name(s) of author(s) in Italics, year, title of article, name of journal, volume, number (the latter two in Italics) and pages. E.g., *Nathan, K.K.*, 1986: A note on the relationship between photo-synthetically active radiation and cloud amount. *IDőjárás* 90, 10-13. For a book: name(s) of author(s), year, title of the book (all in Italics except the year), publisher and place of publication. E.g., *Junge, C. E.*, 1963: *Air Chemistry and Radioactivity*. Academic Press, New York and London. Reference in the text should contain the name(s) of the author(s) in Italics and year of publication. E.g., in the case of one author: *Miller* (1989); in the case of two authors: *Gamov* and *Cleveland* (1973); and if there are more than two authors: *Smith et al.* (1990). If the name of the author cannot be fitted into the text: (*Miller*, 1989); etc. When referring papers published in the same year by the same author, letters a, b, c, etc. should follow the year of publication.

Tables should be marked by Arabic numbers and printed in separate sheets with their numbers and legends given below them. Avoid too lengthy or complicated tables, or tables duplicating results given in other form in the manuscript (e.g., graphs)

Figures should also be marked with Arabic numbers and printed in black and white in camera-ready form in separate sheets with their numbers and captions given below them. Good quality laser printings are preferred.

The text should be submitted both in manuscript and in electronic form, the latter on diskette or in E-mail. Use standard 3.5" MS-DOS formatted diskette or CD for this purpose. MS Word format is preferred.

Reprints: authors receive 30 reprints free of charge. Additional reprints may be ordered at the authors' expense when sending back the proofs to the Editorial Office.

More information for authors is available: antal.e@met.hu

Information on the last issues: http://omsz.met.hu/irodalom/firat_ido/ido_hu.html

Published by the Hungarian Meteorological Service

Budapest, Hungary

INDEX: 26 361

HU ISSN 0324-6329

IDŐJÁRÁS

VOLUME 106 * 2002

EDITORIAL BOARD

- | | |
|---|---|
| AMBRÓZY, P. (Budapest, Hungary) | MÉSZÁROS, E. (Veszprém, Hungary) |
| ANTAL, E. (Budapest, Hungary) | MIKA, J. (Budapest, Hungary) |
| BARTHOLY, J. (Budapest, Hungary) | MARACCHI, G. (Firenze, Italy) |
| BOZÓ, L. (Budapest, Hungary) | MERSICH, I. (Budapest, Hungary) |
| BRIMBLECOMBE, P. (Norwich, U.K.) | MÖLLER, D. (Berlin, Germany) |
| CZELNAI, R. (Budapest, Hungary) | NEUWIRTH, F. (Vienna, Austria) |
| DÉVÉNYI, D. (Budapest, Hungary) | PINTO, J. (R. Triangle Park, NC, U.S.A.) |
| DUNKEL, Z. (Brussels, Belgium) | PROBÁLD, F. (Budapest, Hungary) |
| FISHER, B. (Chatham, U.K.) | RENOUX, A. (Paris-Créteil, France) |
| GELEYN, J.-Fr. (Toulouse, France) | ROCHARD, G. (Lannion, France) |
| GERESDI, I. (Pécs, Hungary) | S. BURÁNSZKY, M. (Budapest, Hungary) |
| GÖTZ, G. (Budapest, Hungary) | SPÁNKUCH, D. (Potsdam, Germany) |
| HANTEL, M. (Vienna, Austria) | STAROSOLSZKY, Ö. (Budapest, Hungary) |
| HASZPRA, L. (Budapest, Hungary) | SZALAI, S. (Budapest, Hungary) |
| HORÁNYI, A. (Budapest, Hungary) | SZEPESI, D.J. (Budapest, Hungary) |
| HORVÁTH, Á. (Siófok, Hungary) | TAR, K. (Debrecen, Hungary) |
| IVÁNYI, Z. (Budapest, Hungary) | TÄNCZER, T. (Budapest, Hungary) |
| KONDRATYEV, K.Ya. (St. Petersburg,
Russia) | VALI, G. (Laramie, WY, U.S.A.) |
| MAJOR, G. (Budapest, Hungary) | VARGA-HASZONITS, Z. (Moson-
magyaróvár, Hungary) |

Editor-in-Chief
TAMÁS PRÁGER

Executive Editor
MARGIT ANTAL

BUDAPEST, HUNGARY

AUTHOR INDEX

Anda, A. (Keszthely, Hungary)	137
Ács, F. (Budapest, Hungary)	39, 277
Bartholy, J. (Budapest, Hungary)	59
Csiszár, I. (Maryland, USA)	*253
Dévényi, D. (Boulder, USA)	*293
Diószeghy, M. (Budapest, Hungary)	*279
Gyarmati, Gy. (Budapest, Hungary)	*293
Horányi, A. (Budapest, Hungary)	39
Hunkár, M. (Budapest, Hungary)	123
Justyák, J. (Debrecen, Hungary)	248
Kondratyev, K.Ya. (St. Petersburg, Russia)	1
Lakatos, M. (Budapest, Hungary)	75
Marshak, A. (Maryland, USA)	*265
Matyasovszky, I. (Budapest, Hungary) ...	75
Mészáros, E. (Veszprém, Hungary)	103
Mika, Á. (Siófok, Hungary)	39
Miskolczi, F. (Hampton, USA)	*243
Nováky, B. (Gödöllő, Hungary)	227
Orlóci, I. (Budapest, Hungary)	185
Pálfai, I. (Szeged, Hungary)	265
Radics, K. (Budapest, Hungary)	59
Radnóti, G. (Budapest, Hungary)	39
Starosolszky, Ö. (Budapest, Hungary)	215
Szalóki, S. (Szarvas, Hungary)	197
Szász, G. (Debrecen, Hungary)	137
Szesztay, K. (Budapest, Hungary)	185
Szunyogh, I. (Maryland, USA)	*293
Tar, K. (Debrecen, Hungary)	248
Varga-H., Z. (Mosonmagyaróvár, Hungary)	89
Várallyai, Gy. (Budapest, Hungary)	113
Várnai, T. (Maryland, USA)	*265
Vermes, L. (Budapest, Hungary)	239
Zima Szalókiné, I. (Szarvas, Hungary) ...	197

* In Vol. 105 No. 4-Vol. 106 No. 1 joined issue

TABLE OF CONTENTS

I. Papers

<p><i>Anda, A.</i>: Slices of plant-water relation in reflection to investigations carried out at Agrometeorological Research Station of Keszthely..... 37</p> <p><i>Ács, F.</i>: On the relationship between transpiration and soil texture 277</p> <p><i>Csiszár, I.A.</i>: On the use of satellite-derived climatological data sets to map global land surface temperature range..... 253</p> <p><i>Diószeghy, M.</i>: Operative cloud classification using Meteosat images..... 279</p> <p><i>Hunkár, M.</i>: Agrometeorology of maize - investigation carried out at the Hungarian Meteorological Service 123</p> <p><i>Justyák, J.</i> and <i>Tar, K.</i>: Characteristics of the economy of water supplies in an oak forest..... 248</p> <p><i>Kondratyev, K.Ya.</i>: Global climate change and the Kyoto Protocol..... 1</p> <p><i>Lakatos, M.</i> and <i>Matyasovszky, I.</i>: Specification of multivariate extremity in climatological data 75</p> <p><i>Mika, Á., Ács, F., Horányi, A.</i> and <i>Radnóti, G.</i>: Sensitivity of the ALADIN weather prediction model to the changes of soil texture..... 39</p>	<p><i>Mészáros, E.</i>: Atmospheric wet deposition as a nutrient supply for the vegetation .. 103</p> <p><i>Miskolczi, F.</i>: High accuracy skin temperature retrieval from spectral data of multichannel IR imagers 243</p> <p><i>Nováky, B.</i>: Mapping of mean annual actual evaporation on the example 227</p> <p><i>Orlóci, I.</i> and <i>Szesztay, K.</i>: Hydroecological risks of crop production in Hungary . 185</p> <p><i>Pálfai, I.</i>: Probability of drought occurrence in Hungary..... 265</p> <p><i>Radics, K.</i> and <i>Bartholy, J.</i>: Selected characteristics of wind climate and the potential use of wind energy in Hungary. Part II..... 59</p> <p><i>Starosolszky, Ö.</i>: Impact of the climate change on the hydrological regime. A case study on the Danube River 215</p> <p><i>Szász, G.</i>: Surface energy budget between the atmosphere and the surface in the vegetation period during 1963-1994..... 161</p> <p><i>Szunyogh, I., Gyarmati, Gy.</i> and <i>Dévényi, D.</i>: Using observed data for testing the statistical consistency of initial ensemble perturbations..... 293</p>
--	--

<i>Varga-Haszonits, Z.</i> : Water supply of growing seasons and maize production ...	89	cloud properties	265
<i>Várallyay, Gy.</i> : Climate change and soil processes	113	<i>Vermes, L.</i> : International efforts for drought mitigation	239
<i>Várnai, T. and Marshak, A.</i> : Observations of three-dimensional radiative effects that influence satellite retrievals of		<i>Zima Szalókiné, I. and Szalóki, S.</i> : Relationships of water- and nutrient supply, yield and evapotranspiration of maize	197

II. News

Czelnai, R.: Dr. Iván Mersich winner of a 2001. Dennis Gabor Prize

SUBJECT INDEX

A

agroclimatology 89
 agroecology 161
 Antal's formula 130, 228, 237
 aridity index 89, 265
 atmospheric precipitation chemistry 103

B

Budyko's formula 227

C

case study 215
 clay 277
 climate change 215
 climatic characteristic 89
 climatic scenarios 113
 crop water stress index CWSI 137
 cultivation period 265

D

Danube 215
 Debrecen 161
 deforestation 185
 discharge 215
 drought mitigation 265, 239

E

energy budget compounds 161
 Europe
 - drought sensitivity map 239
 evaporation 89
 - mean annual 227

evapotranspiration 185, 123, 137, 197
 - actual 161, 248
 - potential 161

F

flood 215
 flood wave 215
 forest cover 185

G

grid mapping 227
 growing season 89, 161

H

heat
 - exchange between soil and surface air 161
 - sensible and latent in boundary layer 161
 heavy metals 103
 holistic approach 185
 human impact 185
 humidity index 89
 Hungary 89, 185, 123, 197, 161, 248, 215, 103
 hydroecology 185

I

international co-operation on drought mitigation 239
 irrigation

- timing 137
- utilization of irrigation water 197
- water demand 185

K

Keszthely 137

L

lysimeter 137, 197

M

- maize 89, 123, 137, 197
- microadvection 161
- microscale transpiration 277
- model
 - deterministic point scale transpiration
- model 277
 - dynamic simulation model CERES-Maize 123
 - impact modeling 215
 - statistical-deterministic local scale
- transpiration model 277

N

nutrient supply 197

O

oak forest 248

P

- planetary boundary layer 161
- plant - water relation 137
- plant water supply 137
- point and local scale 277
- precipitation
 - effective 248
 - utilization 197

R

- radiation balance 161
- regression analysis 89
- returning time period 265
- runoff 215
 - mean annual 227

S

- salinization 185
- sand 277
- snow melt 215
- soil
 - degradation 113, 185
 - formation processes 113
 - heat exchange 161
 - moisture 185, 161, 248
 - moisture regime 113
 - texture 277
 - water content 89
- soluble matter 103
- statistical analysis 123
- stomata 137
- stomatal resistance 137
- sugar beet 137
- surface runoff 248

T

- transpiration characteristics 277
- trend
 - function 89
 - ratio 89
- Turc's formula 227

U

- United Kingdom 239
- United Nations 239
- United States of America 239
- upscaling 277

W

- water
 - balance 89, 185, 227, 248
 - deficit 265
 - intake 215
 - plant - water relation 137
 - scarcity 265
 - storage capacity 265
 - supply 123, 248
- wet deposition 103

Y

yield 89, 197

Z

Zagyva catchment 227